

PATENT  
Attorney Docket No.: 9113-2-DI1

IN THE UNITED STATES PATENT AND TRADEMARK OFFICE

In re: Patent application of  
Randell L. Mills

Serial No.: 08/467,911

Filed: June 6, 1995

For: ENERGY/MATTER CONVERSION  
METHODS AND STRUCTURES

Group Art Unit:  
2204

Examiner:  
H.E. Behrend

**EXHIBITS 15 THROUGH 19, VOLUME III OF IV, SUPPORTING**  
**DECLARATION OF RANDELL L. MILLS, M.D.,**  
**UNDER 37 C.F.R. 1.32**

CERTIFICATE OF MAILING  
UNDER 37 C.F.R. 1.8(a)

I hereby certify that this paper, along with any paper referred to as being attached or enclosed, is being deposited with the United States Postal Service on the date indicated below, with sufficient postage, as first class mail, in an envelope addressed to: Commissioner of Patents and Trademarks, Washington, D.C. 20231.

BY Dynne Wilt  
DATE: 15 November 1996

Testing Facility, Publication, or Reviewing Organization	Independent Test Facility	Report Date	Calorimetry Proof	Hydrino Proof	Dihidrino Proof	Mills Exhibit
HPC Recent Experimental Work	yes	Aug. '96	yes	-	-	1
HPC and Franklin and Marshall College Report for Atlantic Energy Corporation	yes*	Jul. '96	yes	yes	yes	2
Pennsylvania State University Report for HPC	yes	Jun. '96	yes	-	--	3
Pennsylvania State University Report for HPC	yes	Jan. '96	yes	--	--	4
NASA Lewis Research Center Technical Memorandum	yes	Feb. '96	yes	--	--	5
Mills et al., 28 Fusion Technology 1697	--	Nov. '95	yes	yes	yes	6
Jonathan Phillips 37 CFR 1.132 Declaration	yes	Jan. '95	yes	--	--	7
MIT Lincoln Laboratories Final Report (ACC Project)	yes	Apr. '95	yes	--	--	8
Mills et al., Analysis of MIT Lincoln Laboratories Data	--	Jan. '95	--	--	yes	9
Pennsylvania State University Report for HPC	yes	Sep. '94	yes	--	--	10
Thermacore's Final Report for Aero Propulsion and Power Directorate, Wright Laboratory, Air Force Material Command	yes	May '94	yes	yes	--	11
Westinghouse STC Report	yes	Feb. '94	yes	--	--	12
HPC Comments as to the Westinghouse STC Report	--	Feb. '94	yes	--	--	13
Thermacore Report, Hydrino Analysis by Lehigh University	yes	Mar. '94	yes	yes	--	14
Charles Evans & Associates XPS/ESCA Results	yes	Nov. '94	--	yes	--	15
Charles Evans & Associates TOF-SIMS Results	yes	Mar. '94	--	yes	--	16
Mills et al., 25 Fusion Technology 103	yes*	Jan. '94	yes	yes	yes	17
Idaho National Engineering Laboratory (INEL) XPS Report	yes	Nov. '93	--	yes	--	18

Testing Facility, Publication, or Reviewing Organization	Independent Test Facility	Report Date	Calorimetry Proof	Hydrogen Proof	Dihydrogen Proof	Mills Exhibit
Lehigh University XPS Report, Zettlemoyer Center for Surface Studies, Sinclair Laboratory	yes	Nov. '93	--	yes	--	19
Idaho National Engineering Laboratory (INEL) Excess Heat and XPS Report	yes	Jan. '93	yes	yes	--	20 18
Atomic Energy Of Canada Ltd., Chalk River Laboratories Study	yes	Nov. '93	yes	--	--	21
Moscow Power Engineering Institute, Appl. No. '845 Affidavit	yes	Feb. '93	yes	--	--	22
Testimony for Subcommittee on Energy of the Committee on Science, Space and Technology of U.S. Congress	--	May '93	yes	--	--	23
Shaubach and Gernert Affidavit Thermacore Testing Facility	yes	Aug. '92	yes	--	--	24
Noninski, 21 Fusion Technology 163, Franklin and Marshall College Laboratory	yes	Mar. '92	yes	--	--	25
Mills et al., 21 Fusion Technology 65	--	Aug. '91	yes	--	--	26
Brookheaven National Laboratory, Department of Applied Science Letter	yes	Oct. '91	yes	--	--	27
Discovery Documents from Arbitration No. 14 T 199 00196 H/J between HPC and AECL	--	Mar. '93	--	--	--	28
R.T.Bush, 22 Fusion Technology 301	--	Sep. '92	--	--	--	29
Jones et al., 99 J. Phys. Chem. 6973	--	Apr. '95	--	--	--	30
Notoya et al., Proc. of the Int'l Conf. on Cold Fusion, 421-426	--	Oct. '92	--	--	--	31
* - conducted by Thermacore and HPC						

# CHARLES EVANS & ASSOCIATES

SPECIALISTS IN MATERIALS CHARACTERIZATION

FACSIMILE COMMUNICATION • FACSIMILE COMMUNICATION • FACSIMILE COMMUNICATION

COMPANY: Hydrocatalysis Power REF NO: 69942  
ATTENTION: Stev Bollinger DATE: November 3, 1994  
DESTINATION PAGE 1 OF 7  
FAX NO: (610) 651-4940 CE&A REPLY FAX  
FROM: Dr. A.Y. Craig NO: (415) 369-7921  
SUBJECT: XPS/ESCA Results (CEA #44545)

Please find attached typical results for your samples. A 2 mm x 0.8 mm analysis area was selected for this work.

Elements C, O, N, Si, Cl, S, Ni, Zn, Sn, K, Ca, Mg and Cr are detected at the surface for the Nickel Cathode Sample #A. The concentration for C is approximately 52 at%, while that for Ni is approximately 9 at%. The concentrations for Ca (approximately 0.1 at%) and Mg (approximately 0.2 at%) are considered maximum values due to the noisy spectra.

Elements C, O, N, Si, S, Ni, Zn, Sn, Mg and Cr are detected at the surface for the Nickel Cathode Sample #B. The concentration for C is approximately 41 at%, while that for Ni is approximately 13 at%.

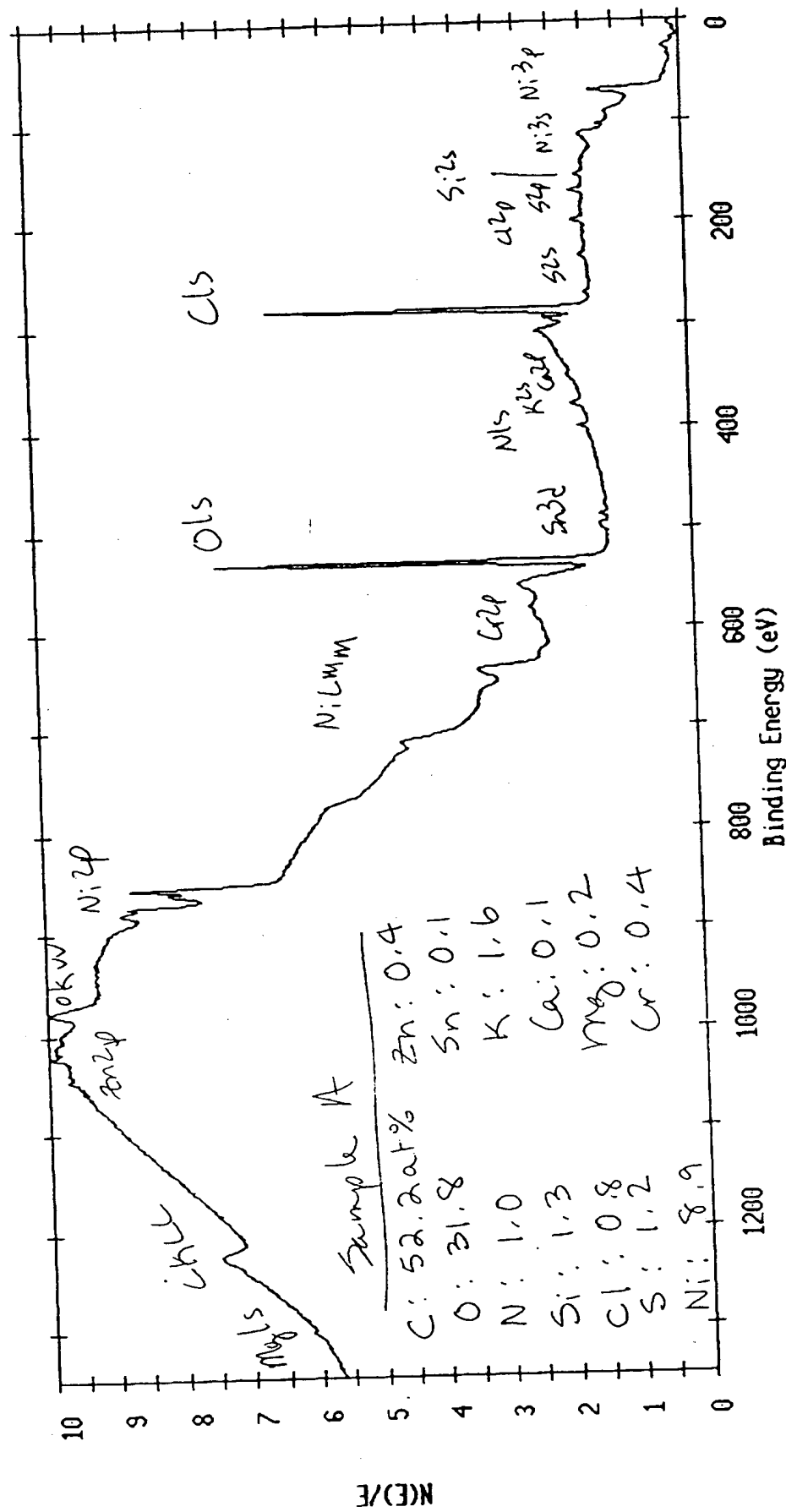
This analysis involved approximately 8 hours of instrument time. You will be invoiced for 6 hours (\$1800.00), as quoted. If you have any questions regarding this work, please call me.

Sincerely,

Angela Y. Craig

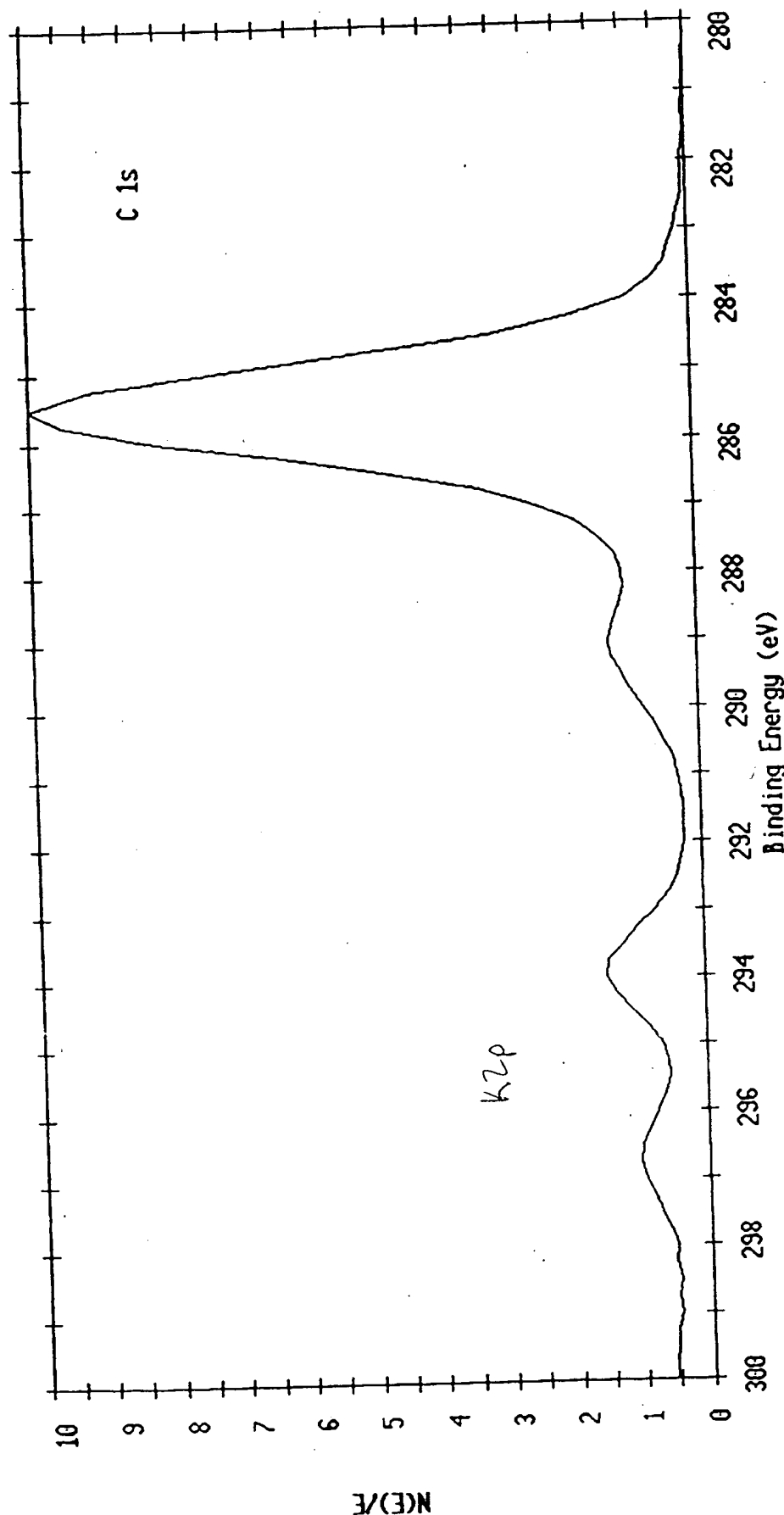
(2)

ESCA Survey 1 Nov 94 Angle: 45 degrees Acquisition Time: 29.82 min  
 File: HYDROCAT10 SAMPLE A  
 Scale Factor: 29.950 kC/s Offset: 7.175 kC/s Pass Energy: 187.850 eV Aperture: 5 A1 450 W



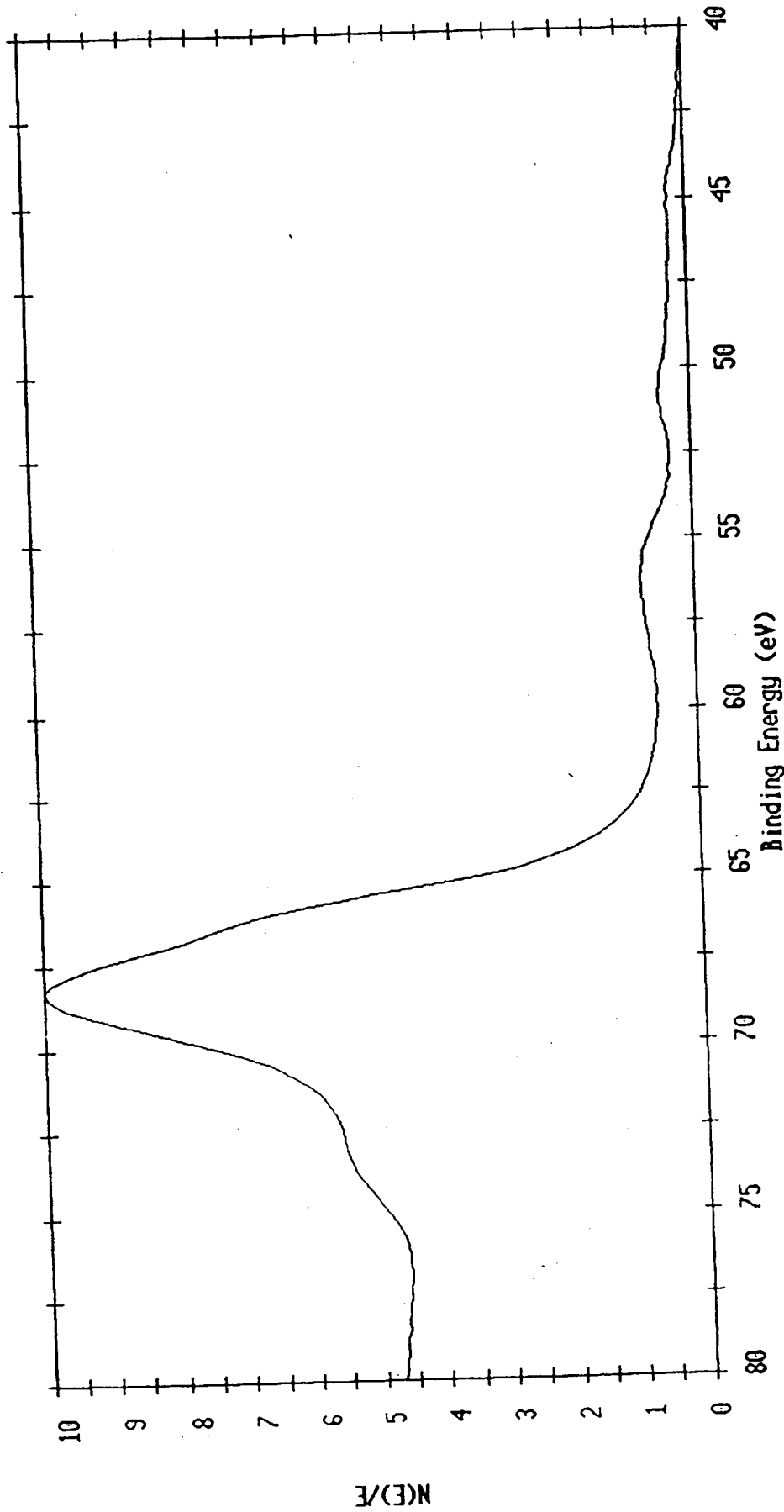
(3)

ESCA Multiplex 1 Nov 94 Species: C1 Region: 1 Angle: 45 degrees Acquisition Time: 2.09 min  
File: HYDROCAT11 SAMPLE A  
Scale Factor: 6.336 kc/s Offset: 13.449 kc/s Pass Energy: 58.700 eV Aperture: 5 Al 450 μ



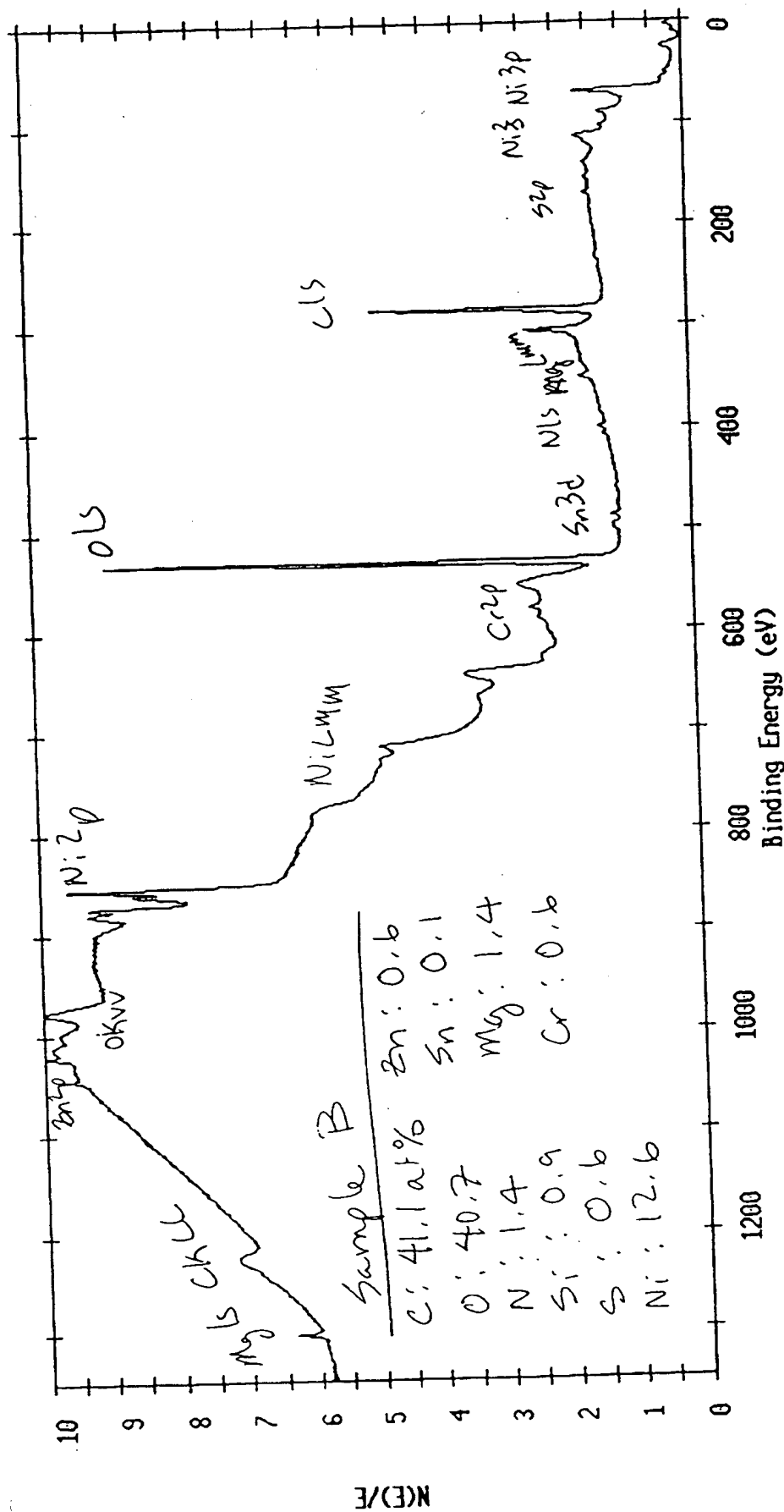
(4)

ESCA Multiplex 1 Nov 94 Species: Fe3 Region: 2 Angle: 45 degrees Acquisition Time: 116.46 min  
File: HYDROCAT11 SAMPLE A  
Scale Factor: 1.290 kc/s Offset: 3.150 kc/s Pass Energy: 58.700 eV Aperture: 5 A1 450 W

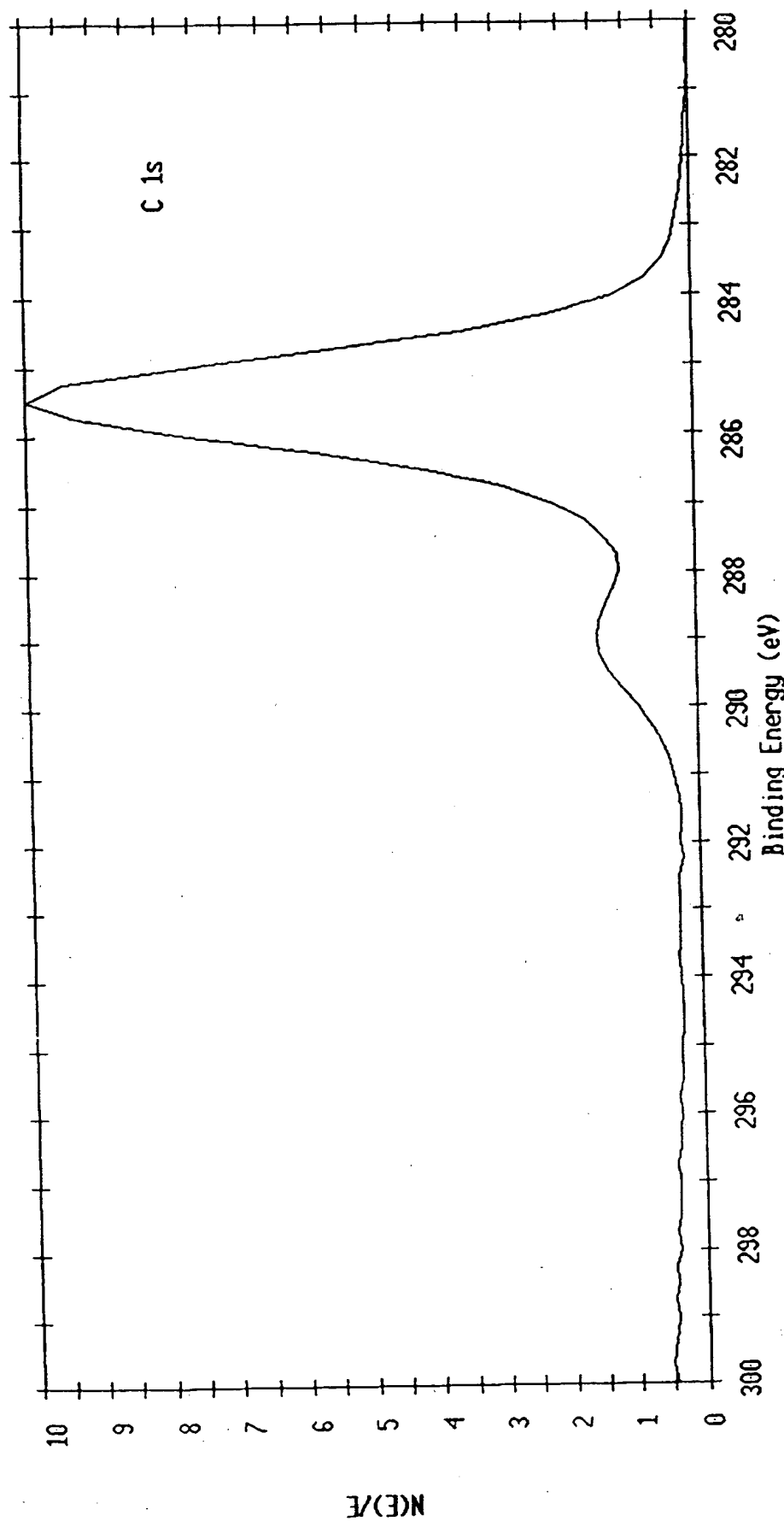


(5)

ESCA Survey 1 Nov 94 Angle: 45 degrees Acquisition Time: 29.82 min  
 File: HYDROCAT20 SAMPLE B  
 Scale Factor: 30.190 kC/s Offset: 6.971 kC/s Pass Energy: 187.850 eV Aperture: 5 Al 450 μ

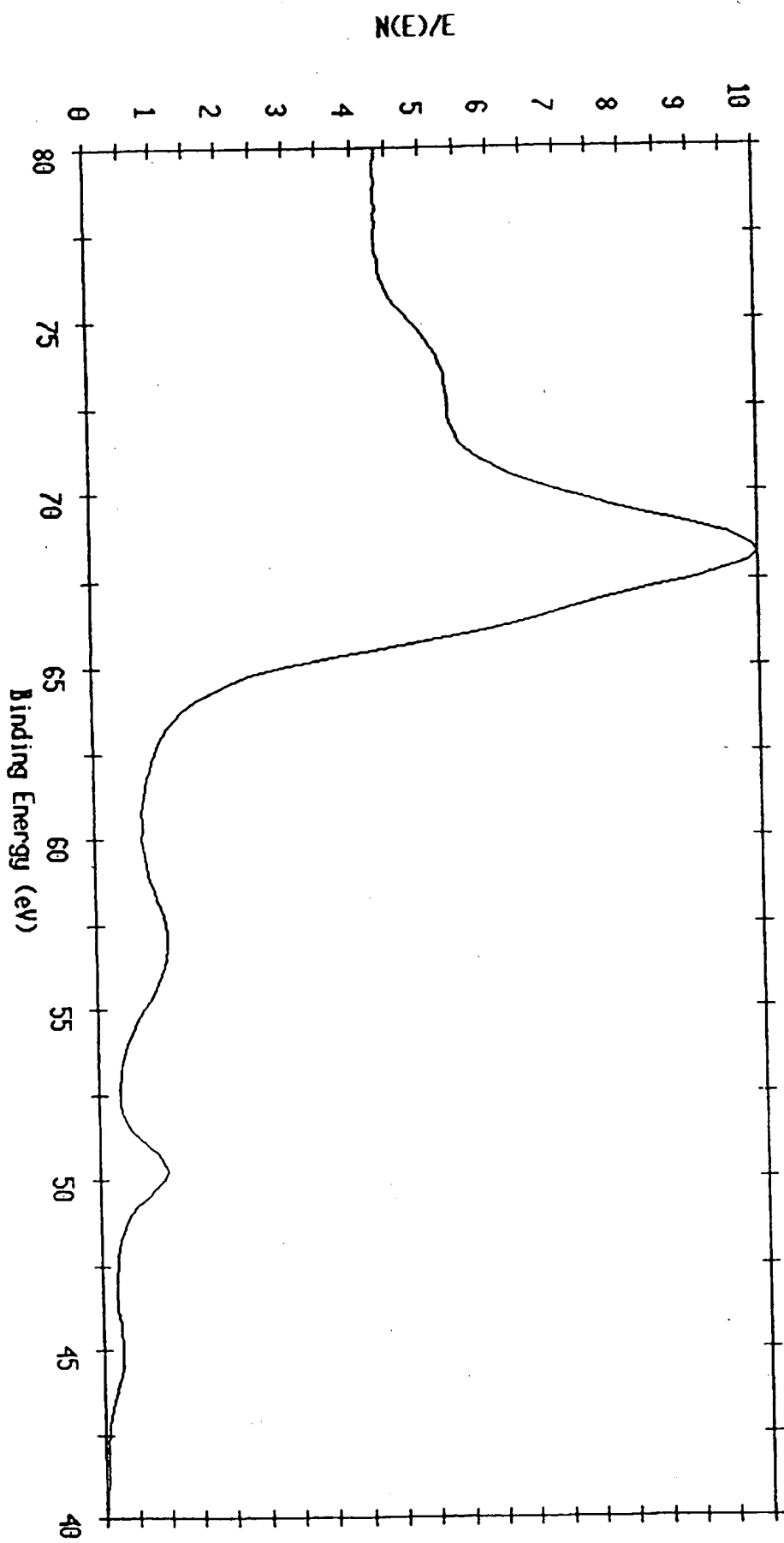


ESCA Multiplex 1 Nov 94 Species: C1 Region: 1 Angle: 45 degrees Acquisition Time: 2.09 min  
File: HYDROCAT21 SAMPLE B  
Scale Factor: 4.695 kc/s Offset: 12.191 kc/s Pass Energy: 58.700 eV Aperture: 5 Al 450 μm



ESCA Multiplex 1 Nov 94 Species: Fe3 Region: 2 Angle: 45 degrees Acquisition Time: 116.46 min  
File: HYDROCAT21 SAMPLE B  
Scale Factor: 1.536 ke/s Offset: 2.987 ke/s Pass Energy: 58.700 eV Aperture: 5 Al 450  $\mu$

(7)



# CHARLES EVANS & ASSOCIATES

Time of Flight-Secondary Ion Mass Spectroscopy Report

**CONFIDENTIAL**

## Company's Summary of the Charles Evans Results

Lehigh University has conducted an extensive investigation of the cathodes from heat producing as well as those from control cells and has determined that the results lend some support to Mills' theory. See Exhibit 6- Lehigh University XPS Report.

The XPS results were confirmed at National Laboratory A followed by Time of Flight-Secondary Ion Mass Spectroscopy (TOF-SIMS) analysis of the nickel surface. Iron and lithium were the only remaining atoms which were in question by Lehigh University and National Laboratory A as the source of the 54.6 eV XPS peak. The Charles Evans TOF-SIMS results demonstrate that iron and lithium were not the source of this peak. TOF-SIMS is orders of magnitude more sensitive in the identification of the presence of a given atom as compared to XPS. TOF-SIMS of Samples #1, #2, #3, #4 showed that no lithium was detected. TOF-SIMS of Sample 1# and Sample #2 showed that iron was at the detection limit which was far less than the amount required for an observable signal by XPS. TOF-SIMS of Sample #3, the control virgin nickel tube, contained six times the iron as Sample #4, but no 54.6 eV XPS peak was observed in the case of Sample #3. Therefore, iron was eliminated as the source of the 54.6 eV XPS peak of Sample #4. See Exhibit 7-Charles Evans Time of Flight-Secondary Ion Mass Spectroscopy Report.

The descriptions of the samples sent to Charles Evans & Associates by National Laboratory A are as follows:

### Sample #1

This sample is Sample # 9 of Lehigh University shown in Figure 34 of the Lehigh University XPS Report which is attached. The XPS was also performed on this sample at National Laboratory A. The survey spectrum is shown as Nitest21 which is attached. The spectrum in the region of 55 eV is shown as Nitest20 which is attached.

### Sample #2

Electrolysis followed by XPS was performed at National Laboratory A. The cathode comprised approximately 60 cm of 0.38 mm diameter nickel wire (99 % Alfa # 10249, cold drawn, clean Ni wire) that was cleaned by placing it in a beaker of 0.57 M K<sub>2</sub>CO<sub>3</sub> /3% H<sub>2</sub>O<sub>2</sub> for 10 hours and then rinsing them with distilled water. The anode comprised a 5 cm by 5 cm platinized titanium mesh. The electrolyte solution was 0.57 M aqueous K<sub>2</sub>CO<sub>3</sub> (Aldrich K<sub>2</sub>CO<sub>3</sub> \*  $\frac{3}{2}$  H<sub>2</sub>O 99+%). Electrolysis was performed with a constant current of 8 millamps which corresponded to approximately 0.5 millamp per square centimeter for 24 hours. The cathode was removed and rinsed with distilled water followed by XPS analysis. The spectrum in the region of 55 eV is shown as Nitest50 which is attached.

### Sample #3

This sample was the virgin nickel tubing of the gas permeation cell fabricated and tested by Thermacore, Inc. which produced 50 watts of power at 300 °C having a nickel surface area of only 300 cm<sup>2</sup>. See Exhibit 13- Shaubach, R., Gernert, N. J., "Measurement of excess heat from nascent hydrogen with potassium carbonate on nickel without electrolysis", Phys. Letts. A, in progress. The XPS spectrum performed at Lehigh University is shown in Figure 4 which is attached. The same spectrum of this sample was also obtained at National Laboratory A.

### Sample #4

This sample was the nickel tubing following the production of energy of the gas permeation cell fabricated and tested by Thermacore, Inc. The cell produced 50 watts of power at 300 °C having a nickel surface area of only 300 cm<sup>2</sup>. See Exhibit 13- Shaubach, R., Gernert, N. J., "Measurement of excess heat from nascent hydrogen with potassium carbonate on nickel without electrolysis", Phys. Letts. A, in progress. The XPS spectrum performed at Lehigh University is shown in Figure 4 which is attached. The same spectrum of this sample was also obtained at National Laboratory A.

# CHARLES EVANS & ASSOCIATES

SPECIALISTS IN MATERIALS CHARACTERIZATION

March 18, 1994

Michael Jacox  
EG&G Idaho, Inc.  
Bldg. CF-601  
Idaho National Engineering Laboratory  
Scoville, Idaho 83415

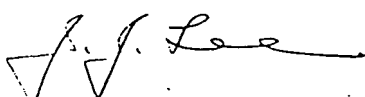
Subject: TIME-OF-FLIGHT SECONDARY ION MASS SPECTROMETRY (TOF-SIMS)  
SURFACE ANALYSIS REPORT  
CE&A Number: 40150  
Purchase Order Number:

Dear Mr. Jacox:

Enclosed is the original copy of the fax report that was sent to you. I believe that the color images in this orginal copy will be more useful to you.

If you have any questions please do not hesitate to contact me.

Sincerely,



Jang-Jung Lee, Ph.D.  
Staff Analyst  
Organic Surface Analysis

Enclosures

# CHARLES EVANS & ASSOCIATES

SPECIALISTS IN MATERIALS CHARACTERIZATION

FACSIMILE COMMUNICATION • FACSIMILE COMMUNICATION • FACSIMILE COMMUNICATION

COMPANY:	EG&G Idaho Inc.	REF NO:
ATTENTION:	Michael Jacox	DATE: March 18, 1994
DESTINATION		PAGE <u>1</u> OF <u>16</u>
FAX NO:	(208) 526-2061	CE&A REPLY FAX
FROM:	J.J. Lee	NO: (415) 369-7921
SUBJECT:	TOF-SIMS Analysis	(CE&A No. 40150)

Here are the results from your Time-of-Flight Secondary Ion Mass Spectrometry (TOF-SIMS) analysis.

Purpose: To obtain mass spectra from two Ni wires, Sample # 1 and 2, and two Ni tubes, Sample # 3 and 4. Elemental contamination in the near surface layer (< 30 nm) is of interest.

Experimental: TOF-SIMS mass spectra were acquired on the Charles Evans and Associates TFS system. Spectra were obtained using a gallium liquid metal ion gun (LMIG) primary ion source. The instrument was operated in an ion microprobe mode in which the pulsed primary ion beam was rastered across the sample's surface, permitting the imaging mode analysis of small features. Typical primary ion doses were on the order of  $10^{12}$  ions/cm<sup>2</sup>.

Results: The data are reported as mass spectra and ion images. Spectra are plotted as the number of secondary ions detected (Y-axis) versus the mass-to-charge ( $m/z$ ) ratio of the ions (X-axis). The ion counts are displayed on logarithmic or linear intensity scales, and probable empirical formulae for a number of the peaks are labeled on the plots. Ion images present the integrated intensities of mass selected ions within the field of view as a function of picture element, or pixel, position.

General material about the interpretation of TOF-SIMS spectra is included at the end of the report.

Discussion: The positive ion spectra of the four samples are included in Figures 1 to 10. Figures 4 to 10 contain expanded plots for various mass ranges to delineate different elemental ion peaks. In each page the spectra from the top panel are for Samples #1, #2, #3 and #4. All the spectra were acquired after a short sputter clean to remove possible surface contamination.

The spectrum of Sample #1 contains peaks for Na<sup>+</sup> (Figs. 1, 4), Si<sup>+</sup> (1, 5), K<sup>+</sup> (1, 6), Ni<sup>+</sup> (1, 9), Mg<sup>+</sup> (4), Al<sup>+</sup> (5), Mn<sup>+</sup> (8) and polydimethylsiloxane (PDMS at  $m/z$  73, 147, 207, 221, etc., Figs. 1, 2 and 3). There may be very low intensity Cr<sup>+</sup> and Fe<sup>+</sup> (possible interference by Si<sub>2</sub><sup>+</sup>) in Figures 7 and 8. PDMS is a commonly found surface contamination (see attachment). The sputter clean process may have reduced the PDMS amount in the analytical area.

Sample #2 contains Na<sup>+</sup> (Figs. 1, 4), Si<sup>+</sup> (1, 5), K<sup>+</sup> (1, 6), Ni<sup>+</sup> (1, 9), Mg<sup>+</sup> (4) and Al<sup>+</sup> (5). Low level Mn<sup>+</sup> ion may be present (8).

Sample #3 shows peaks for Na<sup>+</sup> (Figs. 1, 4), Si<sup>+</sup> (5), K<sup>+</sup> (1, 6), Ni<sup>+</sup> (1, 9), Mg<sup>+</sup> (4), Al<sup>+</sup> (1, 5), Pb<sup>+</sup> (3), Ca<sup>+</sup> (6), Mn<sup>+</sup> (8) Cr<sup>+</sup> (1, 7) and Fe<sup>+</sup> (1, 8).

Sample #4 contains Na<sup>+</sup> (Figs. 1, 4), Si<sup>+</sup> (5), K<sup>+</sup> (1, 6), Ni<sup>+</sup> (1, 9), Mg<sup>+</sup> (4), Al<sup>+</sup> (5), Cr<sup>+</sup> (7) and Fe<sup>+</sup> (8).

Regarding the H detection from the four samples, ion intensities for NiH<sup>+</sup> and H<sup>+</sup> are normalized to Ni<sup>+</sup> and listed in Table 1.

In summary, various elemental ion species were found in the near surface analyses of the four samples. A few ion images acquired from Samples #1, #2 and #4 are included in Images 1 to 3 respectively. It appears that the ion distributions are not uniform in the 18  $\mu\text{m}$  by 18  $\mu\text{m}$  analytical fields. The non-uniformity in distributions are clearly shown in the ion images of Ni<sup>+</sup> and K<sup>+</sup> which are the most dominant ions.

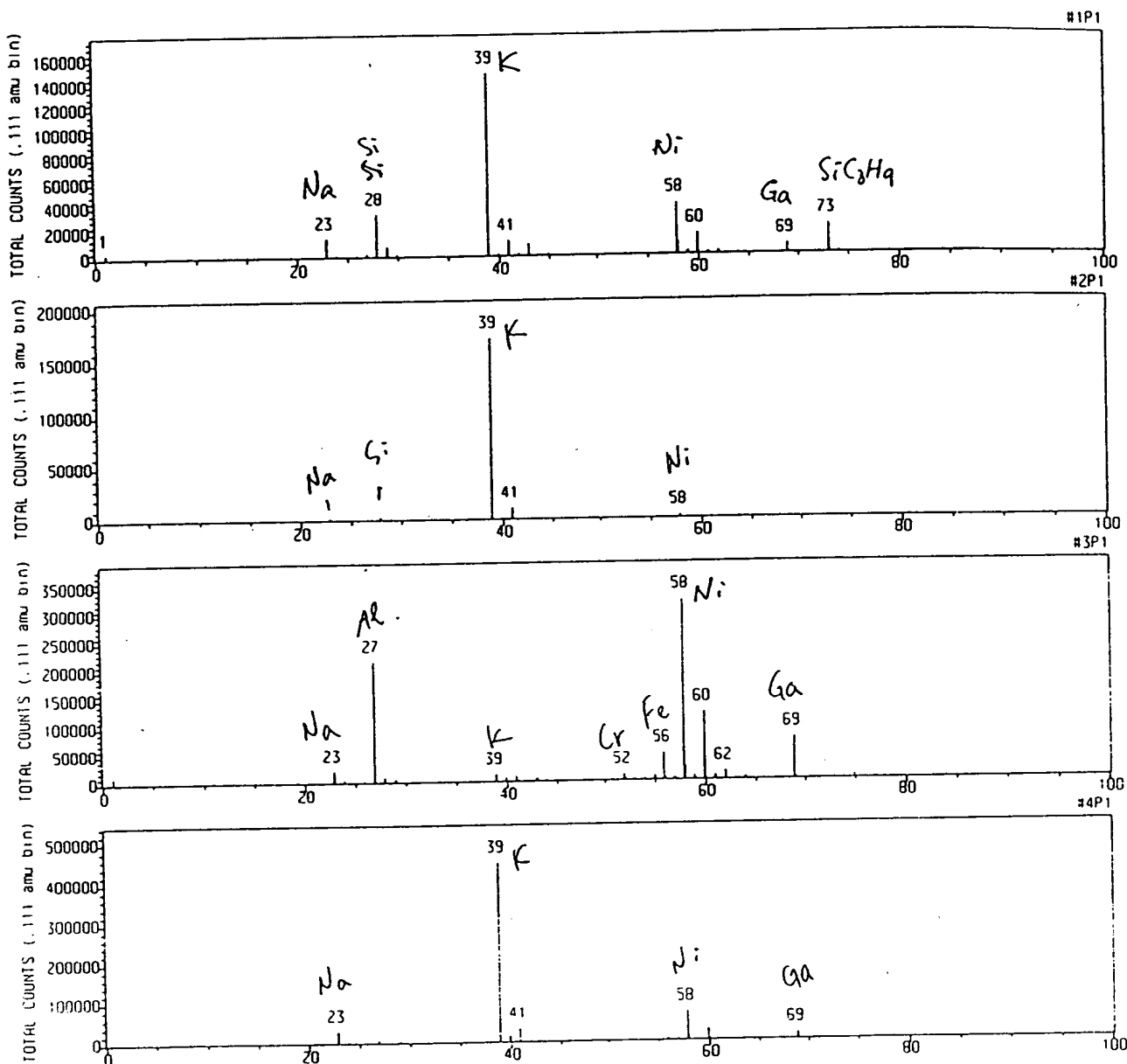
This analysis required 4 hours of instrument time at \$375.00 per hour. The total charge of \$1,500.00 will be invoiced against your purchase order. Please send us a purchase order number if you have done so. If any questions arise about these data, please feel free to contact me.

Table 1. Relative intensities of NiH<sup>+</sup> and H<sup>+</sup> (normalized to Ni<sup>+</sup>).

Samples	Ni <sup>+</sup> ion counts	H <sup>+</sup>	NiH <sup>+</sup>
#1	50230	8.2%	6.4%
#2	3331	20%	2.1%
#3	344508	3.7%	2.7%
#4	83481	4.6%	5.5%

CHARLES EVANS & ASSOCIATES

301 Chesapeake Drive  
Redwood City, CA 94063 USA  
Phone: (415) 369-4567; FAX: 369-7921



FILE NAME: #1P1 DATE : 15 Mar 94 13:21 ACQUISITION TIME: 21.2 MIN. TOTAL INTEGRAL : 464864

+ IONS PRIMARY GUN: Cesium TIME RECORDER: 1-Stop TDC X-Y SOURCE: Raster TIME PER CHANNEL: 156  
DATA SET: 1 Spectra; 3 Image(s) RASTER SIZE: 31 $\mu$ m RASTER TYPE: Full I 4-Fold

FILE NAME: #2P1 DATE : 15 Mar 94 14: 6 ACQUISITION TIME: 15.0 MIN. TOTAL INTEGRAL : 230893

+ IONS PRIMARY GUN: Cesium TIME RECORDER: 1-Stop TDC X-Y SOURCE: Raster TIME PER CHANNEL: 156  
DATA SET: 1 Spectra; 3 Image(s) RASTER SIZE: 31 $\mu$ m RASTER TYPE: Full I 4-Fold

FILE NAME: #3P1 DATE : 15 Mar 94 10:15 ACQUISITION TIME: 15.1 MIN. TOTAL INTEGRAL : 1240561

EG&G/JACOX, #3;  
+ IONS PRIMARY GUN: Cesium TIME RECORDER: 1-Stop TDC X-Y SOURCE: Raster TIME PER CHANNEL: 156  
DATA SET: 1 Spectra; 2 Image(s) RASTER SIZE: 31 $\mu$ m RASTER TYPE: Full I 4-Fold

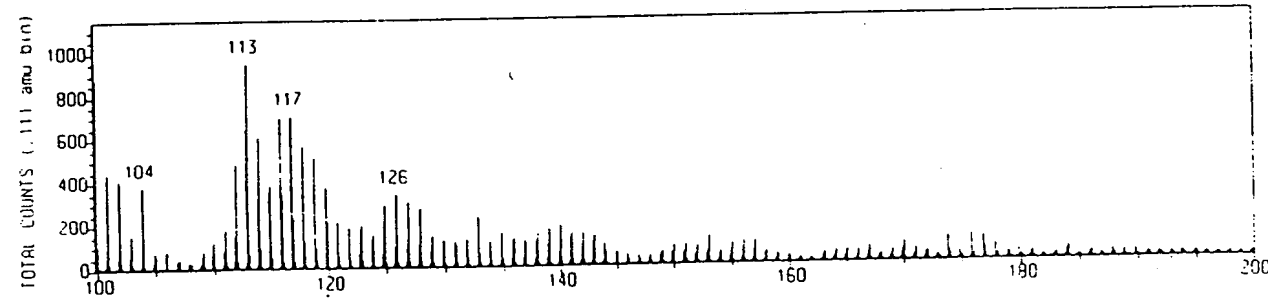
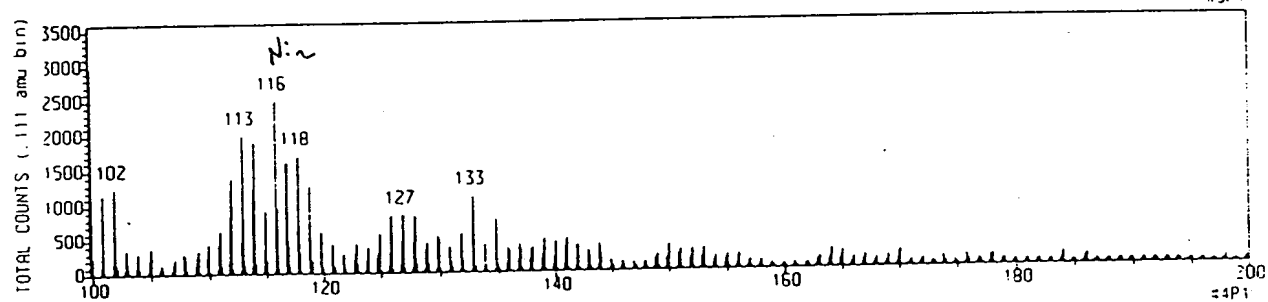
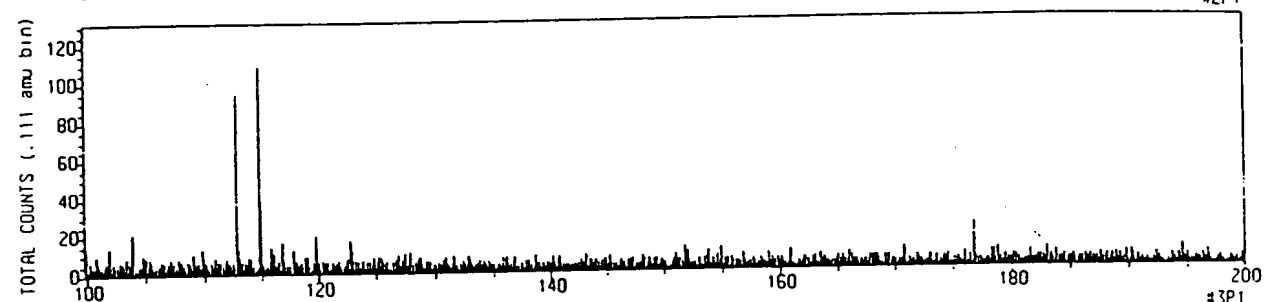
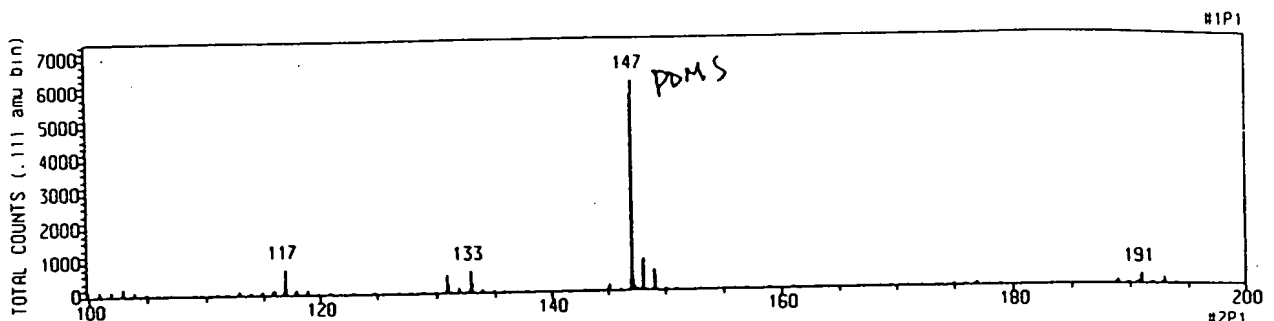
FILE NAME: #4P1 DATE : 15 Mar 94 10:50 ACQUISITION TIME: 14.8 MIN. TOTAL INTEGRAL : 824811

EG&G/JACOX, #3;  
+ IONS PRIMARY GUN: Cesium TIME RECORDER: 1-Stop TDC X-Y SOURCE: Raster TIME PER CHANNEL: 156  
DATA SET: 1 Spectra; 6 Image(s) RASTER SIZE: 31 $\mu$ m RASTER TYPE: Full I 4-Fold

FIGURE 1

CHARLES EVANS & ASSOCIATES

301 Chesapeake Drive  
Redwood City, CA 94063 USA  
Phone: (415)-369-4567; FAX: 369-7921



FILE NAME: #1P1 DATE : 15 Mar 94 13:21 ACQUISITION TIME: 21.2 MIN. TOTAL INTEGRAL 454864

+ IONS PRIMARY GUN: Cesium TIME RECORDER: 1-Stop TDC X-Y SOURCE: Raster TIME PER CHANNEL: 15s  
DATA SET: 1 Spectra; 3 Image(s) RASTER SIZE: 31μm RASTER TYPE: Full I 4-Fold

FILE NAME: #2P1 DATE : 15 Mar 94 14: 6 ACQUISITION TIME: 15.0 MIN. TOTAL INTEGRAL : 230893

+ IONS PRIMARY GUN: Cesium TIME RECORDER: 1-Stop TDC X-Y SOURCE: Raster TIME PER CHANNEL: 15s  
DATA SET: 1 Spectra; 3 Image(s) RASTER SIZE: 31μm RASTER TYPE: Full I 4-Fold

FILE NAME: #3P1 DATE : 15 Mar 94 10:15 ACQUISITION TIME: 15.1 MIN. TOTAL INTEGRAL : 1240561  
EG&G/JACOX, #3:

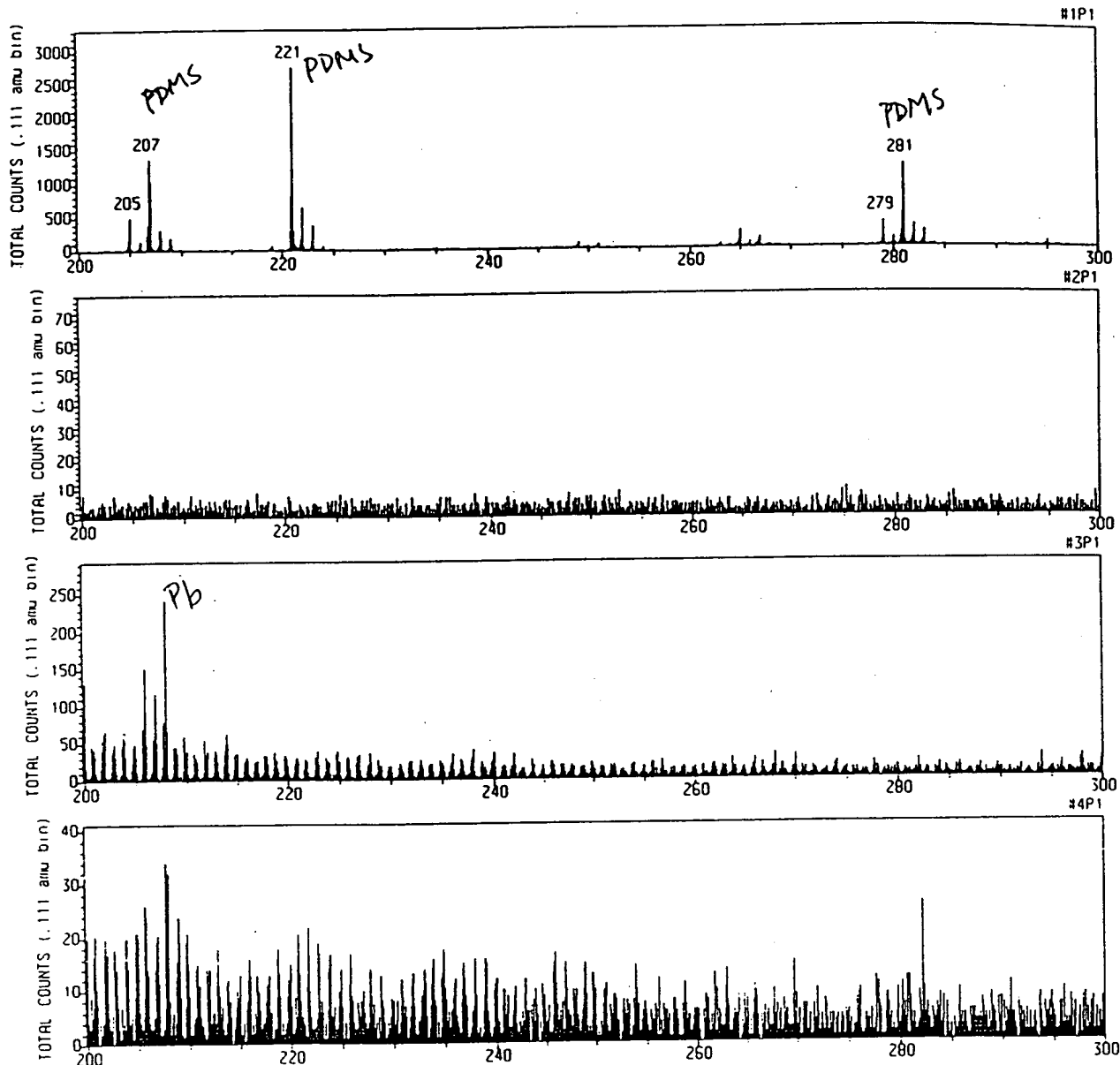
+ IONS PRIMARY GUN: Cesium TIME RECORDER: 1-Stop TDC X-Y SOURCE: Raster TIME PER CHANNEL: 15s  
DATA SET: 1 Spectra; 2 Image(s) RASTER SIZE: 31μm RASTER TYPE: Full I 4-Fold

FILE NAME: #4P1 DATE : 15 Mar 94 10:50 ACQUISITION TIME: 14.8 MIN. TOTAL INTEGRAL : 824811  
EG&G/JACOX, #3:  
+ IONS PRIMARY GUN: Cesium TIME RECORDER: 1-Stop TDC X-Y SOURCE: Raster TIME PER CHANNEL: 15s  
DATA SET: 1 Spectra; 6 Image(s) RASTER SIZE: 31μm RASTER TYPE: Full I 4-Fold

FIGURE 2

CHARLES EVANS & ASSOCIATES

301 Chesapeake Drive  
Redwood City, CA 94063 USA  
Phone: (415) -369-4567; FAX: 369-7921



FILE NAME: #1P1 DATE : 15 Mar 94 13:21 ACQUISITION TIME: 21.2 MIN. TOTAL INTEGRAL : 464864

+ IONS PRIMARY GUN: Cesium TIME RECORDER: 1-Stop TDC X-Y SOURCE: Raster TIME PER CHANNEL: 156  
DATA SET: 1 Spectra; 3 Image(s) RASTER SIZE: 31μm RASTER TYPE: Full I 4-Fold

FILE NAME: #2P1 DATE : 15 Mar 94 14: 6 ACQUISITION TIME: 15.0 MIN. TOTAL INTEGRAL : 230893

+ IONS PRIMARY GUN: Cesium TIME RECORDER: 1-Stop TDC X-Y SOURCE: Raster TIME PER CHANNEL: 156  
DATA SET: 1 Spectra; 3 Image(s) RASTER SIZE: 31μm RASTER TYPE: Full I 4-Fold

FILE NAME: #3P1 DATE : 15 Mar 94 10:15 ACQUISITION TIME: 15.1 MIN. TOTAL INTEGRAL : 1240561

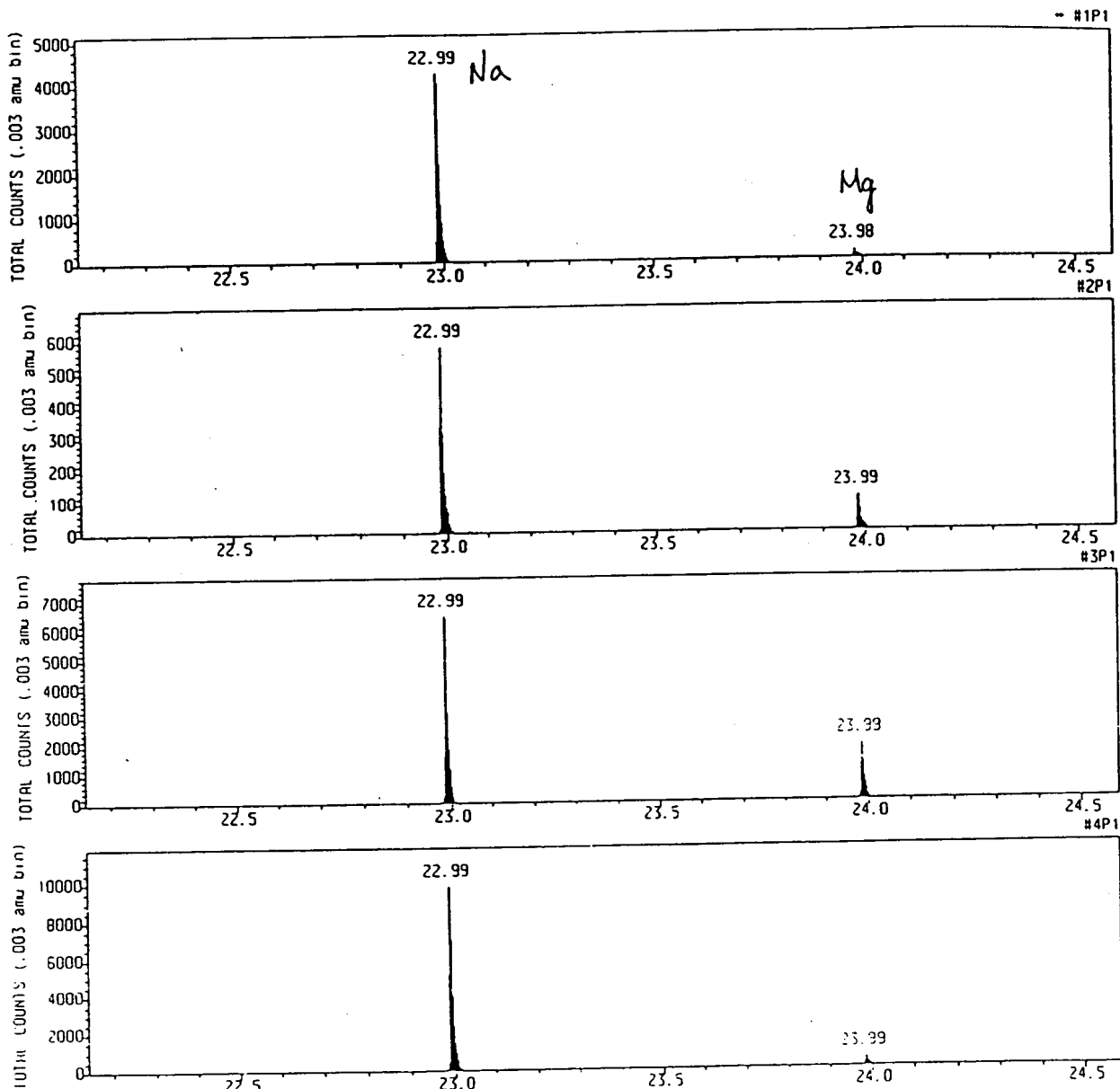
EG&G/JACOX, #3;  
+ IONS PRIMARY GUN: Cesium TIME RECORDER: 1-Stop TDC X-Y SOURCE: Raster TIME PER CHANNEL: 156  
DATA SET: 1 Spectra; 2 Image(s) RASTER SIZE: 31μm RASTER TYPE: Full I 4-Fold

FILE NAME: #4P1 DATE : 15 Mar 94 10:50 ACQUISITION TIME: 14.8 MIN. TOTAL INTEGRAL : 824811

EG&G/JACOX, #3;  
+ IONS PRIMARY GUN: Cesium TIME RECORDER: 1-Stop TDC X-Y SOURCE: Raster TIME PER CHANNEL: 156  
DATA SET: 1 Spectra; 6 Image(s) RASTER SIZE: 31μm RASTER TYPE: Full I 4-Fold FIGURE 3

CHARLES EVANS & ASSOCIATES

301 Chesapeake Drive  
Redwood City, CA 94063 USA  
Phone: (415) 369-4567; FAX: (415) 369-7921



FILE NAME: #1P1 DATE : 15 Mar 94 13:21 ACQUISITION TIME: 21.2 MIN. TOTAL INTEGRAL : 464864

+ IONS PRIMARY GUN: Cesium TIME RECORDER: 1-Stop TDC X-Y SOURCE: Raster TIME PER CHANNEL: 155  
DATA SET: 1 Spectra; 3 Image(s) RASTER SIZE: 31 $\mu$ m RASTER TYPE: Full I 4-Fold

FILE NAME: #2P1 DATE : 15 Mar 94 14: 6 ACQUISITION TIME: 15.0 MIN. TOTAL INTEGRAL : 230893

+ IONS PRIMARY GUN: Cesium TIME RECORDER: 1-Stop TDC X-Y SOURCE: Raster TIME PER CHANNEL: 155  
DATA SET: 1 Spectra; 3 Image(s) RASTER SIZE: 31 $\mu$ m RASTER TYPE: Full I 4-Fold

FILE NAME: #3P1 DATE : 15 Mar 94 10:15 ACQUISITION TIME: 15.1 MIN. TOTAL INTEGRAL : 1240561  
EG&G/JACOX, #3:

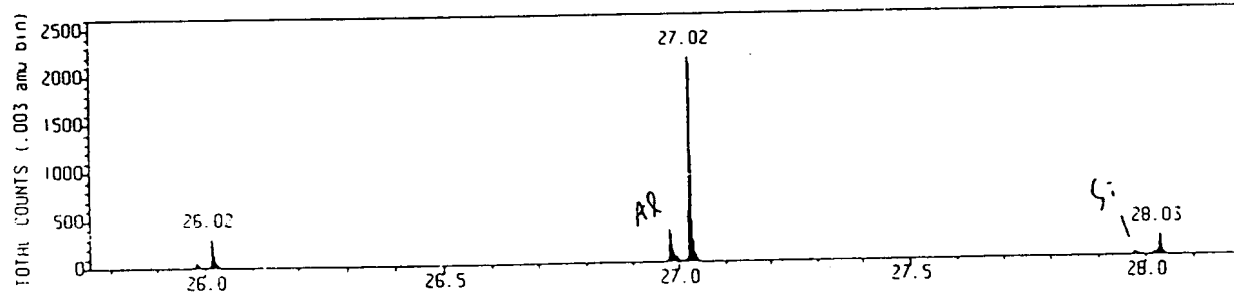
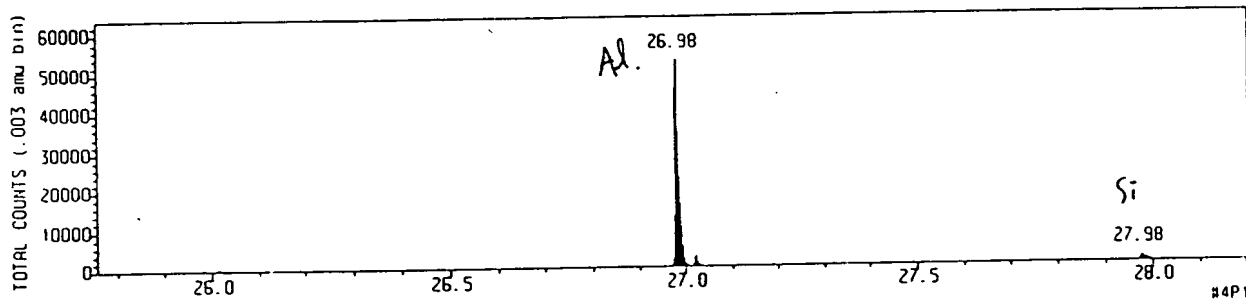
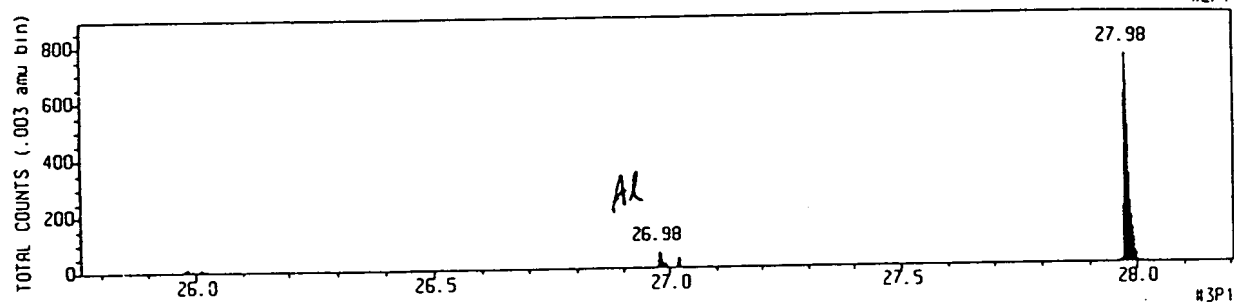
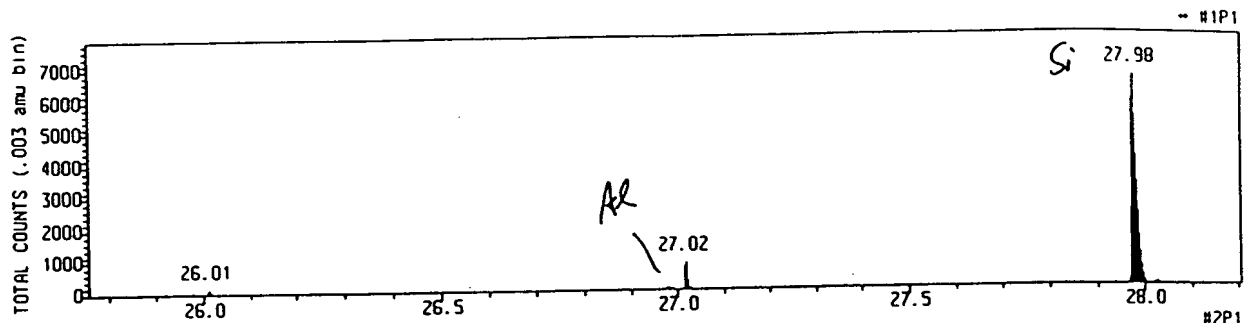
+ IONS PRIMARY GUN: Cesium TIME RECORDER: 1-Stop TDC X-Y SOURCE: Raster TIME PER CHANNEL: 155  
DATA SET: 1 Spectra; 2 Image(s) RASTER SIZE: 31 $\mu$ m RASTER TYPE: Full I 4-Fold

FILE NAME: #4P1 DATE : 15 Mar 94 10:50 ACQUISITION TIME: 14.8 MIN. TOTAL INTEGRAL : 824811  
EG&G/JACOX, #3:  
+ IONS PRIMARY GUN: Cesium TIME RECORDER: 1-Stop TDC X-Y SOURCE: Raster TIME PER CHANNEL: 155  
DATA SET: 1 Spectra; 6 Image(s) RASTER SIZE: 31 $\mu$ m RASTER TYPE: Full I 4-Fold

FIGURE 4

CHARLES EVANS & ASSOCIATES

301 Chesapeake Drive  
Redwood City, CA 94063 USA  
Phone: (415) 369-4567; FAX: (415) 369-7921



FILE NAME: #1P1 DATE : 15 Mar 94 13:21 ACQUISITION TIME: 21.2 MIN. TOTAL INTEGRAL : 454864

+ IONS PRIMARY GUN: Cesium TIME RECORDER: 1-Stop TDC X-Y SOURCE: Raster TIME PER CHANNEL: 156  
DATA SET: 1 Spectra; 3 Image(s) RASTER SIZE: 31 $\mu$ m RASTER TYPE: Full I 4-Fold

FILE NAME: #2P1 DATE : 15 Mar 94 14: 6 ACQUISITION TIME: 15.0 MIN. TOTAL INTEGRAL : 230893

+ IONS PRIMARY GUN: Cesium TIME RECORDER: 1-Stop TDC X-Y SOURCE: Raster TIME PER CHANNEL: 156  
DATA SET: 1 Spectra; 3 Image(s) RASTER SIZE: 31 $\mu$ m RASTER TYPE: Full I 4-Fold

FILE NAME: #3P1 DATE : 15 Mar 94 10:15 ACQUISITION TIME: 15.1 MIN. TOTAL INTEGRAL : 1240561  
EG&G/JACOX, #3;

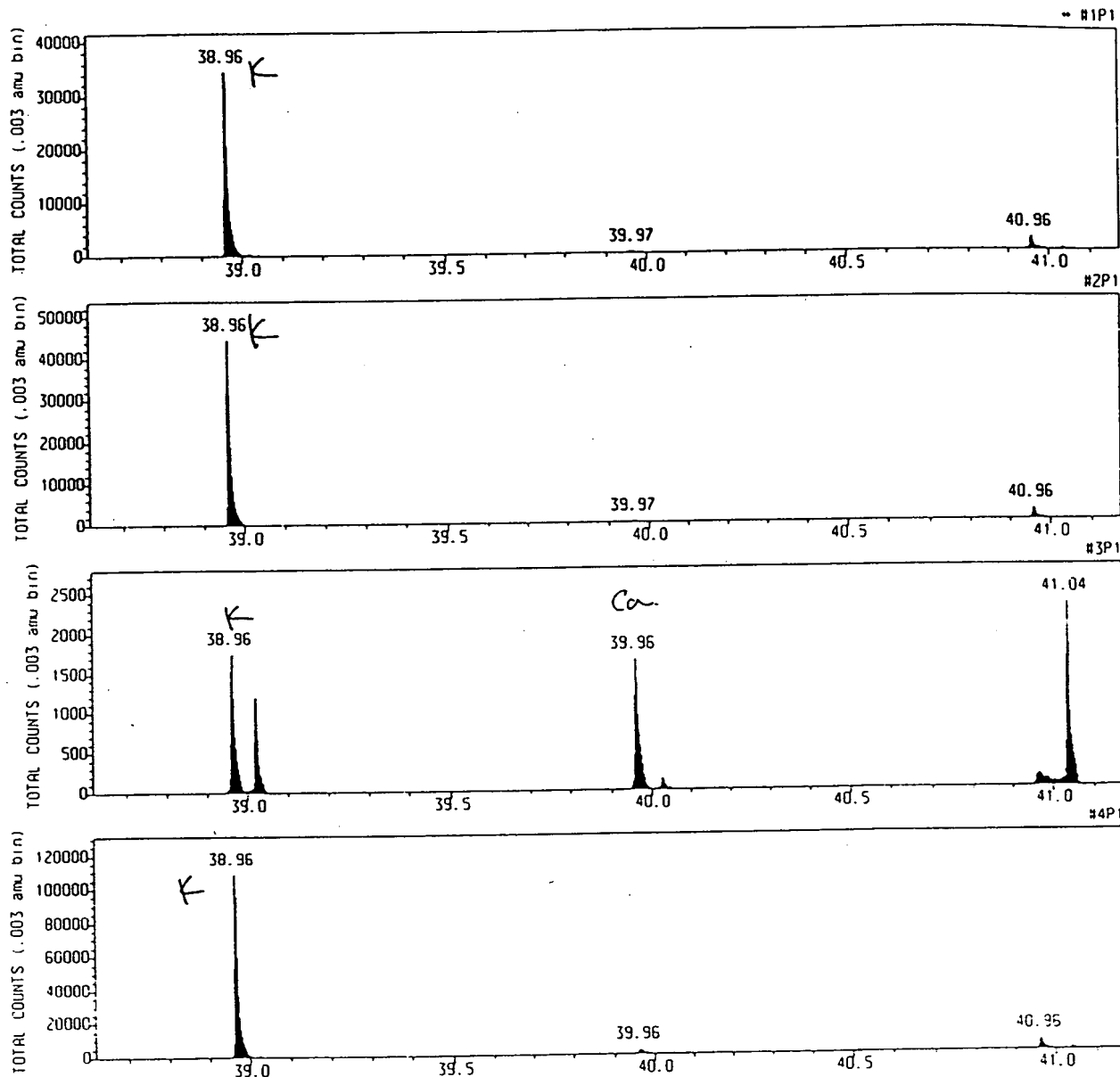
+ IONS PRIMARY GUN: Cesium TIME RECORDER: 1-Stop TDC X-Y SOURCE: Raster TIME PER CHANNEL: 156  
DATA SET: 1 Spectra; 2 Image(s) RASTER SIZE: 31 $\mu$ m RASTER TYPE: Full I 4-Fold

FILE NAME: #4P1 DATE : 15 Mar 94 10:50 ACQUISITION TIME: 14.8 MIN. TOTAL INTEGRAL : 824811

EG&G/JACOX, #3;  
+ IONS PRIMARY GUN: Cesium TIME RECORDER: 1-Stop TDC X-Y SOURCE: Raster TIME PER CHANNEL: 156  
DATA SET: 1 Spectra; 6 Image(s) RASTER SIZE: 31 $\mu$ m RASTER TYPE: Full I 4-Fold FIGURE 5

CHARLES EVANS & ASSOCIATES

101 Chesapeake Drive  
Redwood City, CA 94063 USA  
Phone: (415) 369-4567; FAX: (415) 369-7921



FILE NAME: #1P1 DATE : 15 Mar 94 13:21 ACQUISITION TIME: 21.2 MIN. TOTAL INTEGRAL : 454854

+ IONS PRIMARY GUN: Cesium TIME RECORDER: 1-Stop TDC X-Y SOURCE: Raster TIME PER CHANNEL: 156  
DATA SET: 1 Spectra; 3 Image(s) RASTER SIZE: 31 $\mu$ m RASTER TYPE: Full I 4-Fold

FILE NAME: #2P1 DATE : 15 Mar 94 14: 6 ACQUISITION TIME: 15.0 MIN. TOTAL INTEGRAL : 210893

+ IONS PRIMARY GUN: Cesium TIME RECORDER: 1-Stop TDC X-Y SOURCE: Raster TIME PER CHANNEL: 156  
DATA SET: 1 Spectra; 3 Image(s) RASTER SIZE: 31 $\mu$ m RASTER TYPE: Full I 4-Fold

FILE NAME: #3P1 DATE : 15 Mar 94 10:15 ACQUISITION TIME: 15.1 MIN. TOTAL INTEGRAL : 1240561  
EG&G/JACOX, #3;

+ IONS PRIMARY GUN: Cesium TIME RECORDER: 1-Stop TDC X-Y SOURCE: Raster TIME PER CHANNEL: 156  
DATA SET: 1 Spectra; 2 Image(s) RASTER SIZE: 31 $\mu$ m RASTER TYPE: Full I 4-Fold

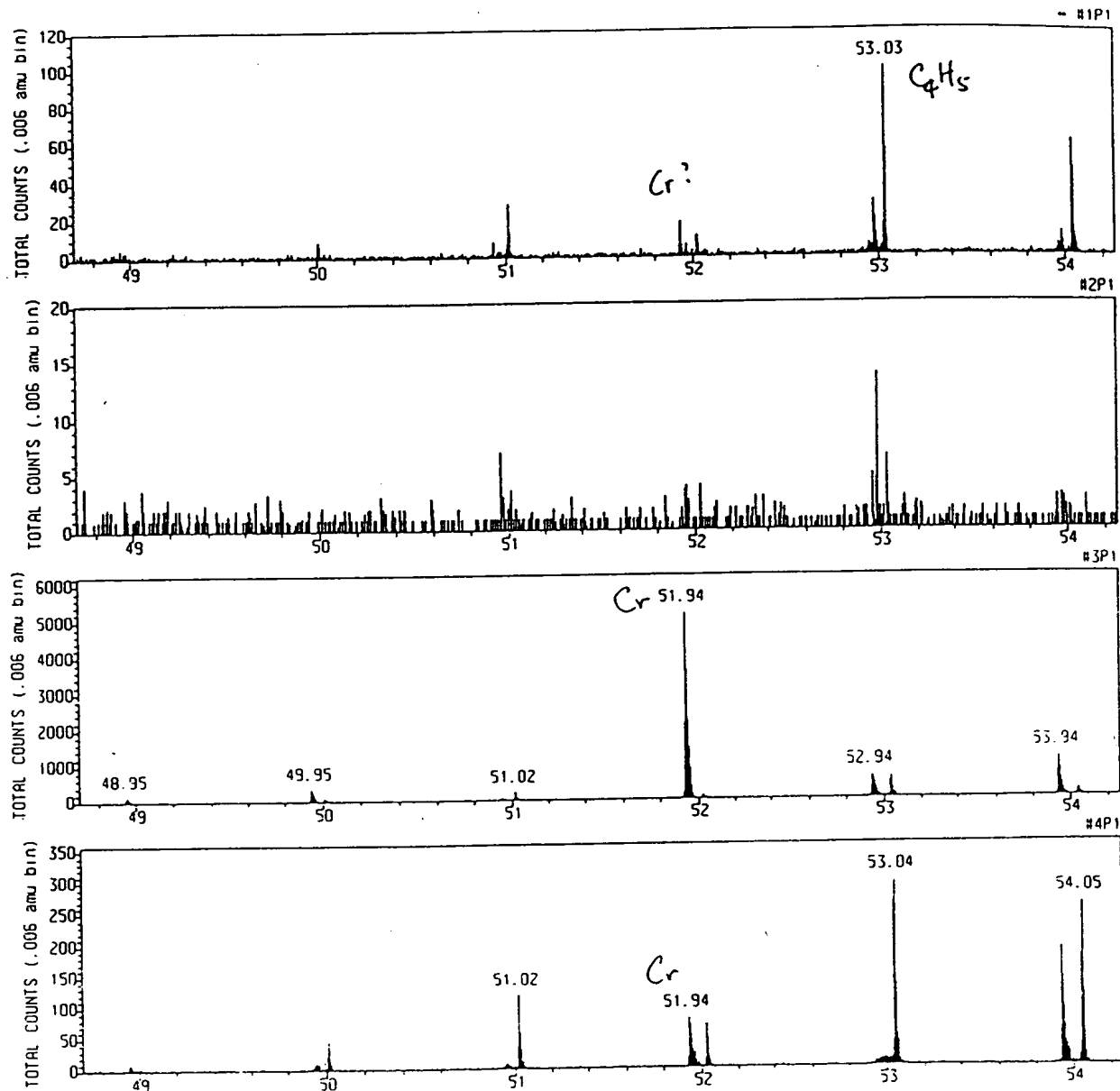
FILE NAME: #4P1 DATE : 15 Mar 94 10:50 ACQUISITION TIME: 14.8 MIN. TOTAL INTEGRAL : 824811

EG&G/JACOX, #3;  
+ IONS PRIMARY GUN: Cesium TIME RECORDER: 1-Stop TDC X-Y SOURCE: Raster TIME PER CHANNEL: 156  
DATA SET: 1 Spectra; 6 Image(s) RASTER SIZE: 31 $\mu$ m RASTER TYPE: Full I 4-Fold

FIGURE 6

CHARLES EVANS & ASSOCIATES

301 Chesapeake Drive  
Redwood City, CA 94063 USA  
Phone: (415) 369-4567; FAX: (415) 369-7921



FILE NAME: #1P1 DATE : 15 Mar 94 13:21 ACQUISITION TIME: 21.2 MIN. TOTAL INTEGRAL : 464864

+ IONS PRIMARY GUN: Cesium TIME RECORDER: 1-Stop TDC X-Y SOURCE: Raster TIME PER CHANNEL: 156  
DATA SET: 1 Spectra; 3 Image(s) RASTER SIZE: 31 $\mu$ m RASTER TYPE: Full I 4-Fold

FILE NAME: #2P1 DATE : 15 Mar 94 14: 6 ACQUISITION TIME: 15.0 MIN. TOTAL INTEGRAL : 230893

+ IONS PRIMARY GUN: Cesium TIME RECORDER: 1-Stop TDC X-Y SOURCE: Raster TIME PER CHANNEL: 156  
DATA SET: 1 Spectra; 3 Image(s) RASTER SIZE: 31 $\mu$ m RASTER TYPE: Full I 4-Fold

FILE NAME: #3P1 DATE : 15 Mar 94 10:15 ACQUISITION TIME: 15.1 MIN. TOTAL INTEGRAL : 1240561  
EG&G/JACOX, #3;

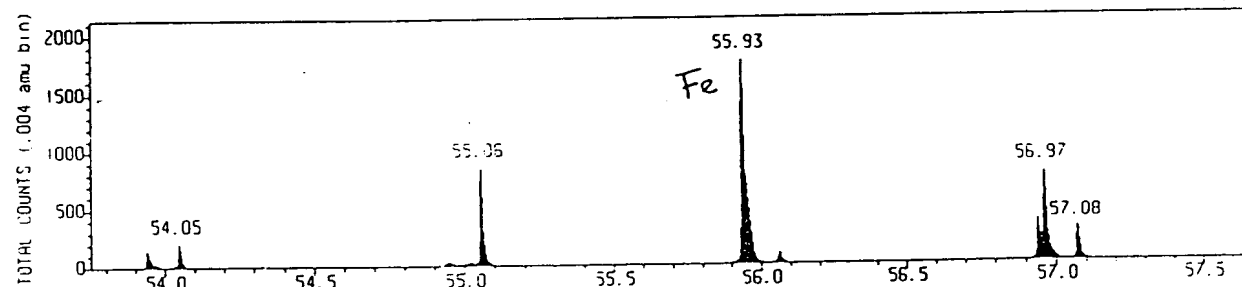
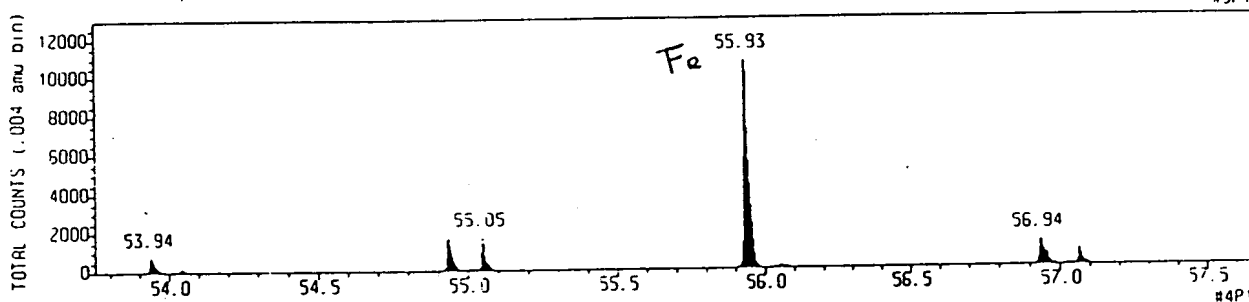
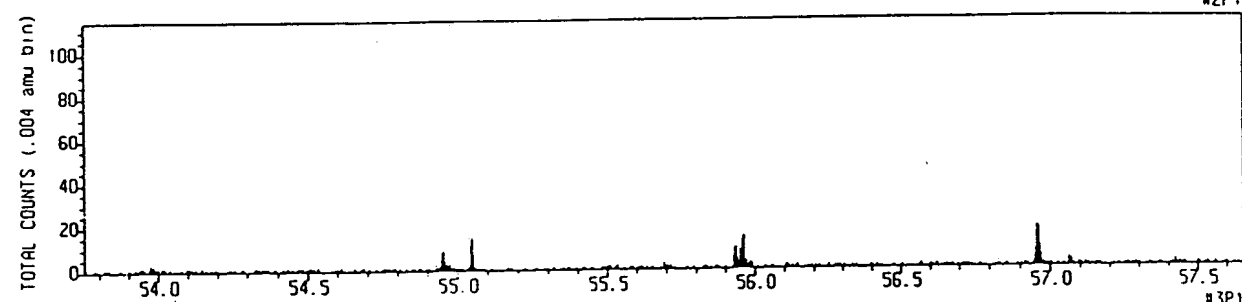
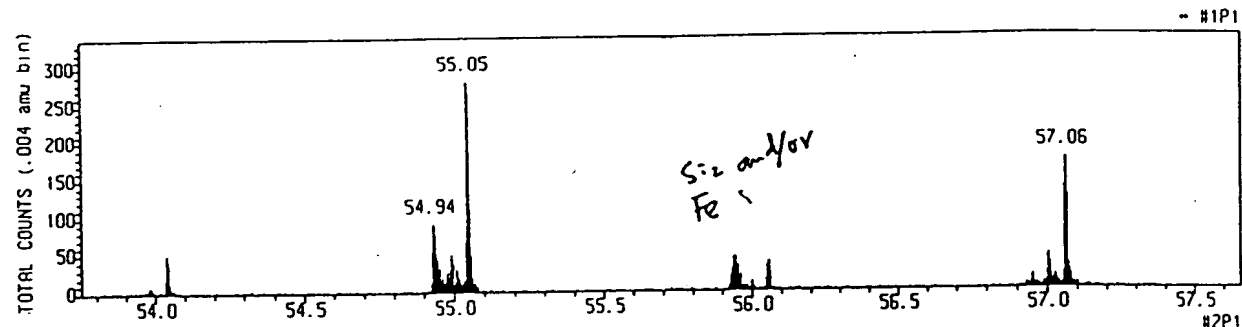
+ IONS PRIMARY GUN: Cesium TIME RECORDER: 1-Stop TDC X-Y SOURCE: Raster TIME PER CHANNEL: 156  
DATA SET: 1 Spectra; 2 Image(s) RASTER SIZE: 31 $\mu$ m RASTER TYPE: Full I 4-Fold

FILE NAME: #4P1 DATE : 15 Mar 94 10:50 ACQUISITION TIME: 14.8 MIN. TOTAL INTEGRAL : 824811  
EG&G/JACOX, #3;  
+ IONS PRIMARY GUN: Cesium TIME RECORDER: 1-Stop TDC X-Y SOURCE: Raster TIME PER CHANNEL: 156  
DATA SET: 1 Spectra; 6 Image(s) RASTER SIZE: 31 $\mu$ m RASTER TYPE: Full I 4-Fold

FIGURE 7

CHARLES EVANS & ASSOCIATES

101 Chesapeake Drive  
Redwood City, CA 94063 USA  
Phone: (415) 369-4567; FAX: (415) 369-7921



FILE NAME: #1P1 DATE : 15 Mar 94 13:21 ACQUISITION TIME: 21.2 MIN. TOTAL INTEGRAL: 444354

+ IONS PRIMARY GUN: Cesium TIME RECORDER: 1-Stop TDC X-Y SOURCE: Raster TIME PER CHANNEL: 156  
DATA SET: 1 Spectra; 3 Image(s) RASTER SIZE: 31μm RASTER TYPE: Full I 4-Fold

FILE NAME: #2P1 DATE : 15 Mar 94 14: 5 ACQUISITION TIME: 15.0 MIN. TOTAL INTEGRAL : 230293

+ IONS PRIMARY GUN: Cesium TIME RECORDER: 1-Stop TDC X-Y SOURCE: Raster TIME PER CHANNEL: 156  
DATA SET: 1 Spectra; 3 Image(s) RASTER SIZE: 31μm RASTER TYPE: Full I 4-Fold

FILE NAME: #3P1 DATE : 15 Mar 94 10:15 ACQUISITION TIME: 15.1 MIN. TOTAL INTEGRAL : 1240561

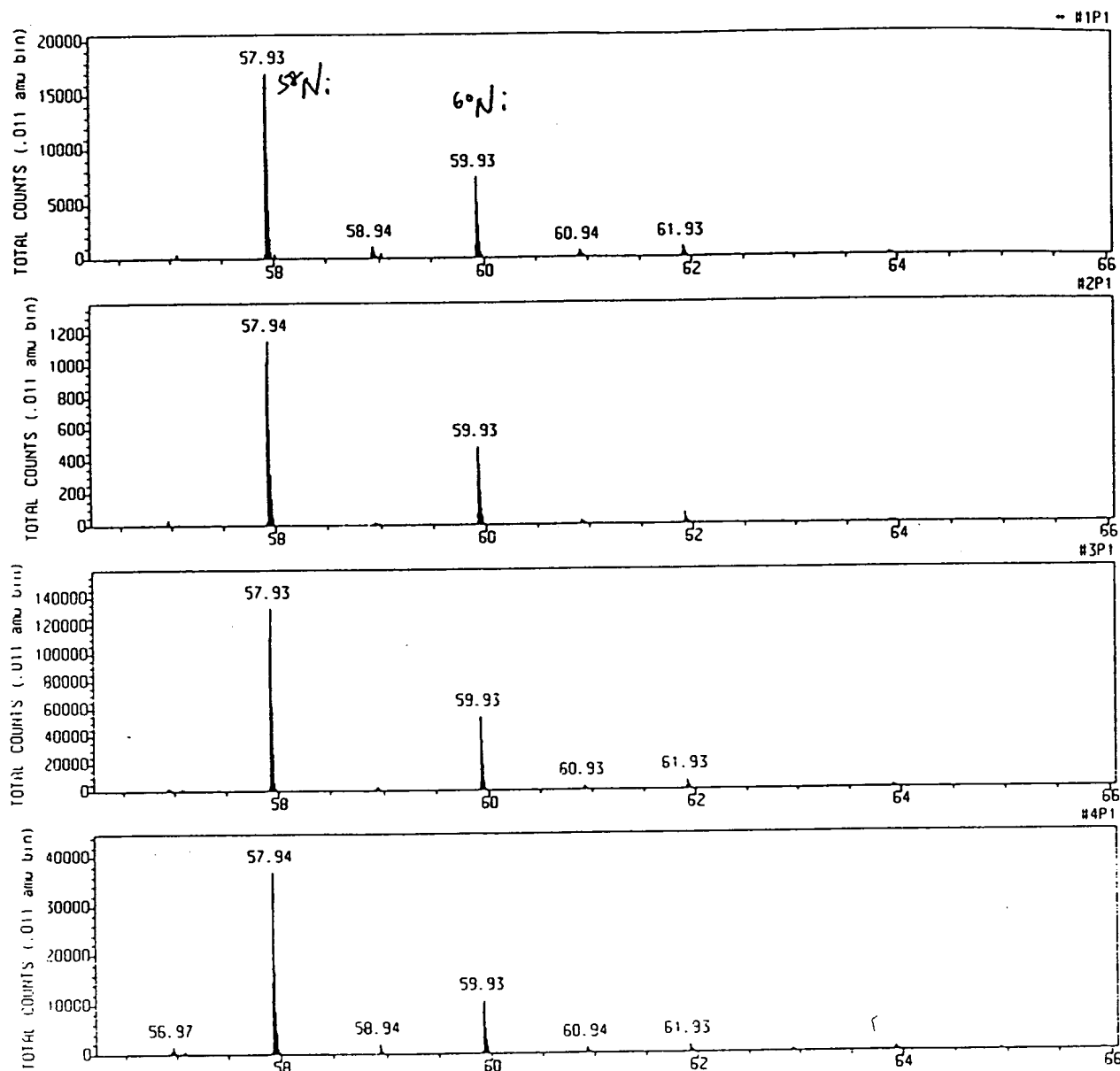
EG&G/JACOX, #3;  
+ IONS PRIMARY GUN: Cesium TIME RECORDER: 1-Stop TDC X-Y SOURCE: Raster TIME PER CHANNEL: 156  
DATA SET: 1 Spectra; 2 Image(s) RASTER SIZE: 31μm RASTER TYPE: Full I 4-Fold

FILE NAME: #4P1 DATE : 15 Mar 94 10:50 ACQUISITION TIME: 14.8 MIN. TOTAL INTEGRAL : 824811

EG&G/JACOX, #3;  
+ IONS PRIMARY GUN: Cesium TIME RECORDER: 1-Stop TDC X-Y SOURCE: Raster TIME PER CHANNEL: 156  
DATA SET: 1 Spectra; 6 Image(s) RASTER SIZE: 31μm RASTER TYPE: Full I 4-Fold FIGURE 8

CHARLES EVANS & ASSOCIATES

301 Chesapeake Drive  
Redwood City, CA 94063 USA  
Phone: (415) 369-4567; FAX: (415) 369-7921



FILE NAME: #1P1 DATE : 15 Mar 94 13:21 ACQUISITION TIME: 21.2 MIN. TOTAL INTEGRAL : 154354

+ IONS PRIMARY GUN: Cesium TIME RECORDER: 1-Stop TDC X-Y SOURCE: Raster TIME PER CHANNEL: 156  
DATA SET: 1 Spectra; 3 Image(s) RASTER SIZE: 31 $\mu$ m RASTER TYPE: Full I 4-Fold

FILE NAME: #2P1 DATE : 15 Mar 94 14: 6 ACQUISITION TIME: 15.0 MIN. TOTAL INTEGRAL : 230893

+ IONS PRIMARY GUN: Cesium TIME RECORDER: 1-Stop TDC X-Y SOURCE: Raster TIME PER CHANNEL: 156  
DATA SET: 1 Spectra; 3 Image(s) RASTER SIZE: 31 $\mu$ m RASTER TYPE: Full I 4-Fold

FILE NAME: #3P1 DATE : 15 Mar 94 10:15 ACQUISITION TIME: 15.1 MIN. TOTAL INTEGRAL : 1240561  
EG&G/JACOX, #3:

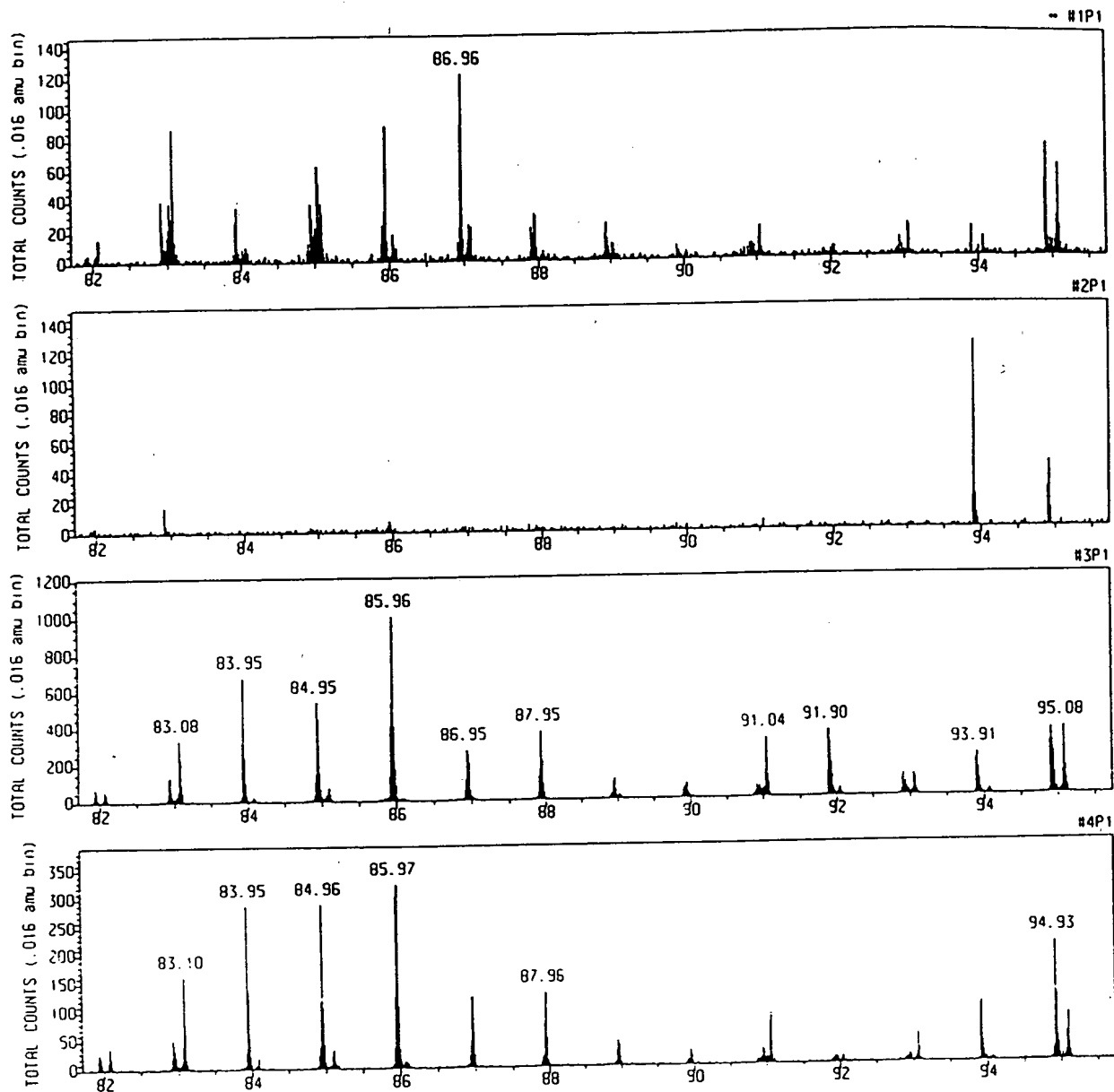
+ IONS PRIMARY GUN: Cesium TIME RECORDER: 1-Stop TDC X-Y SOURCE: Raster TIME PER CHANNEL: 156  
DATA SET: 1 Spectra; 2 Image(s) RASTER SIZE: 31 $\mu$ m RASTER TYPE: Full I 4-Fold

FILE NAME: #4P1 DATE : 15 Mar 94 10:50 ACQUISITION TIME: 14.8 MIN. TOTAL INTEGRAL : 824811  
EG&G/JACOX, #3:

+ IONS PRIMARY GUN: Cesium TIME RECORDER: 1-Stop TDC X-Y SOURCE: Raster TIME PER CHANNEL: 156  
DATA SET: 1 Spectra; 6 Image(s) RASTER SIZE: 31 $\mu$ m RASTER TYPE: Full I 4-Fold

CHARLES EVANS & ASSOCIATES

301 Chesapeake Drive  
Redwood City, CA 94063 USA  
Phone: (415) 369-4567; FAX: (415) 369-7921



FILE NAME: #1P1 DATE : 15 Mar 94 13:21 ACQUISITION TIME: 21.2 MIN. TOTAL INTEGRAL : 464864

+ IONS PRIMARY GUN: Cesium TIME RECORDER: 1-Stop TDC X-Y SOURCE: Raster TIME PER CHANNEL: 156  
DATA SET: 1 Spectra; 3 Image(s) RASTER SIZE: 31 $\mu$ m RASTER TYPE: Full I 4-Fold

FILE NAME: #2P1 DATE : 15 Mar 94 14: 6 ACQUISITION TIME: 15.0 MIN. TOTAL INTEGRAL : 230893

+ IONS PRIMARY GUN: Cesium TIME RECORDER: 1-Stop TDC X-Y SOURCE: Raster TIME PER CHANNEL: 156  
DATA SET: 1 Spectra; 3 Image(s) RASTER SIZE: 31 $\mu$ m RASTER TYPE: Full I 4-Fold

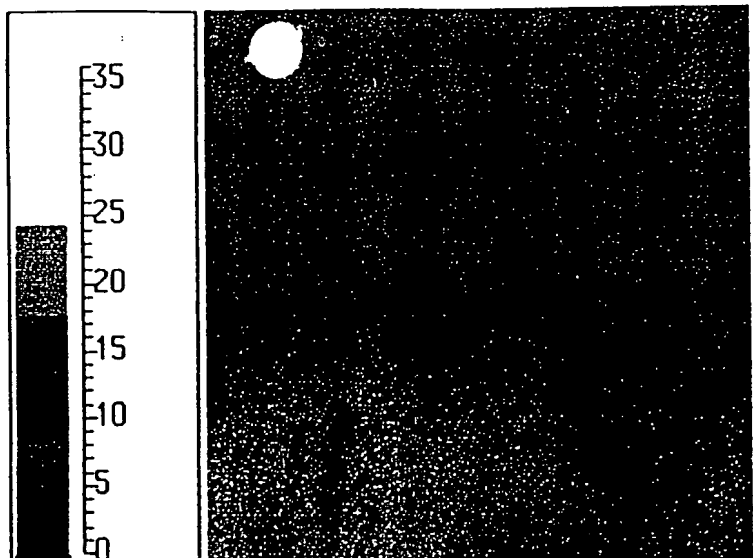
FILE NAME: #3P1 DATE : 15 Mar 94 10:15 ACQUISITION TIME: 15.1 MIN. TOTAL INTEGRAL : 1240561  
EG&G/JACOX, #3;

+ IONS PRIMARY GUN: Cesium TIME RECORDER: 1-Stop TDC X-Y SOURCE: Raster TIME PER CHANNEL: 156  
DATA SET: 1 Spectra; 2 Image(s) RASTER SIZE: 31 $\mu$ m RASTER TYPE: Full I 4-Fold

FILE NAME: #4P1 DATE : 15 Mar 94 10:50 ACQUISITION TIME: 14.8 MIN. TOTAL INTEGRAL : 824811

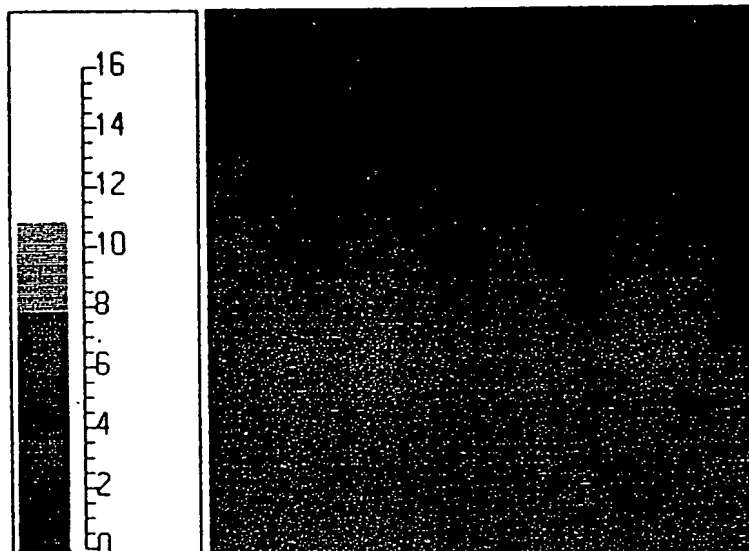
EG&G/JACOX, #3;  
+ IONS PRIMARY GUN: Cesium TIME RECORDER: 1-Stop TDC X-Y SOURCE: Raster TIME PER CHANNEL: 156  
DATA SET: 1 Spectra, 6 Image(s) RASTER SIZE: 31 $\mu$ m RASTER TYPE: Full I 4-Fold

FIGURE 1D



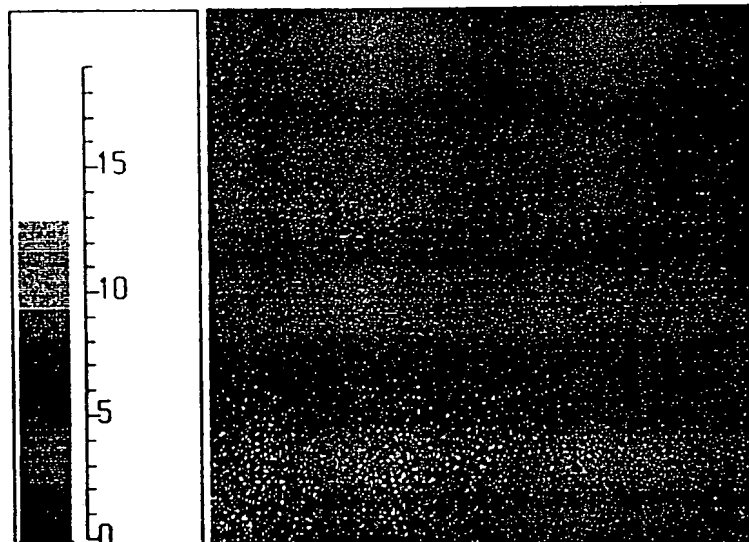
File Name:  
TOFIM708  
Mass:  
Lo: 0.0000  
Hi: 1000.0000  
Status:  
Saved On Disk  
Spectrum:  
#1P1  
Image Scale:  
5 μm

Comments: TOTAL + IONS, #1



File Name:  
TOFIM709  
Mass:  
Lo: 57.7334  
Hi: 58.1468  
Status:  
Saved On Disk  
Spectrum:  
#1P1  
Image Scale:  
5 μm

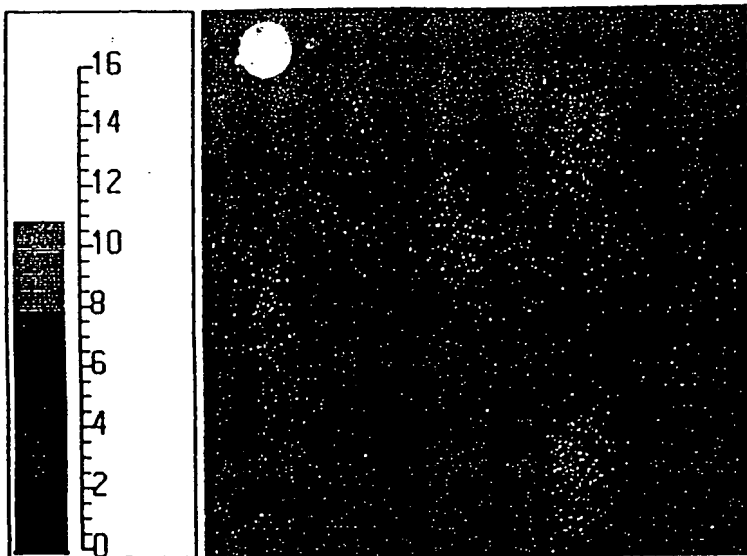
Comments: Ni + IONS, #1



File Name:  
TOFIM710  
Mass:  
Lo: 38.7570  
Hi: 39.1704  
Status:  
Saved On Disk  
Spectrum:  
#1P1  
Image Scale:  
5 μm

Comments: K+ IONS, #1

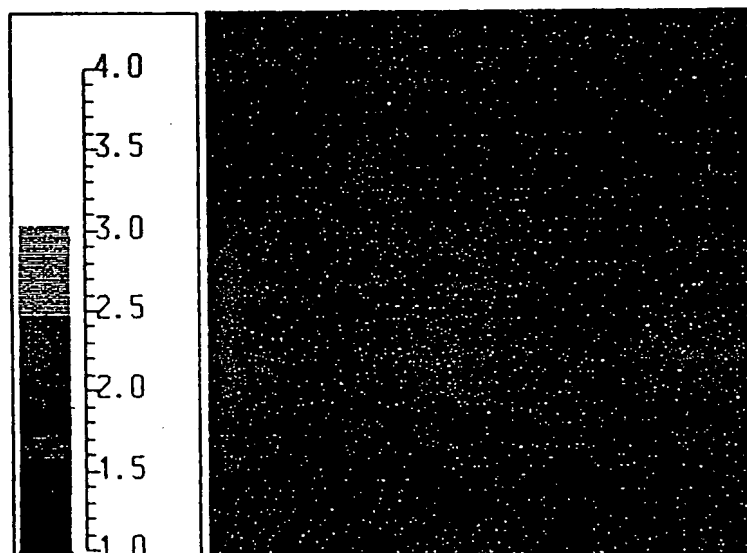
Image 1  
FIGURE



File Name:  
TOFIM765  
Mass:  
Lo: 0.0000  
Hi: 1000.0000  
Status:  
Saved On Disk  
Spectrum:  
#2P1  
Image Scale:

5 μm

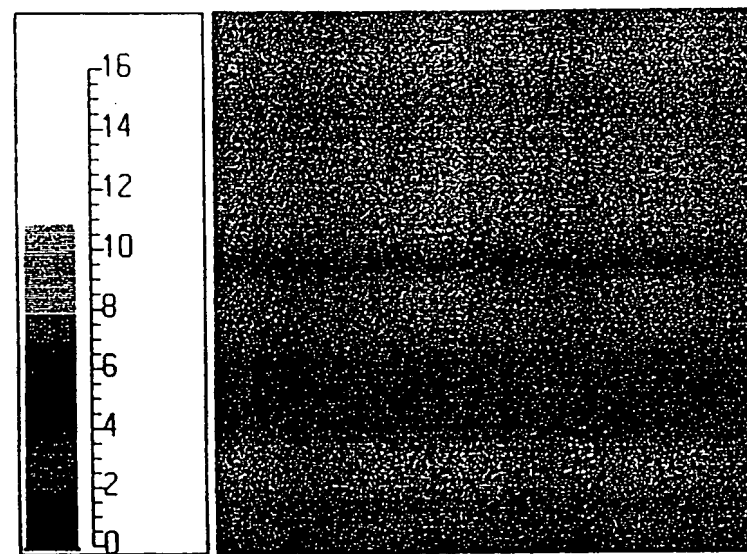
Comments: TOTAL + IONS, #2



File Name:  
TOFIM766  
Mass:  
Lo: 57.7334  
Hi: 58.1468  
Status:  
Saved On Disk  
Spectrum:  
#2P1  
Image Scale:

5 μm

Comments: Ni+ IONS, #2

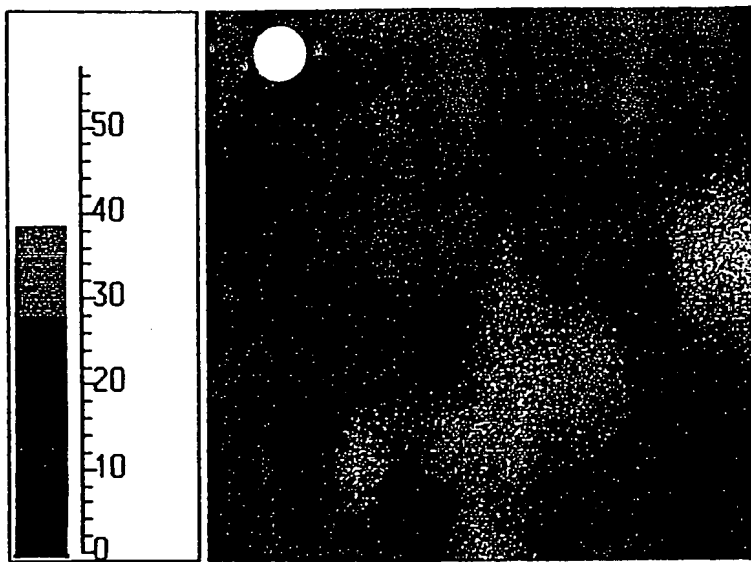


File Name:  
TOFIM767  
Mass:  
Lo: 38.7570  
Hi: 39.1704  
Status:  
Saved On Disk  
Spectrum:  
#2P1  
Image Scale:

5 μm

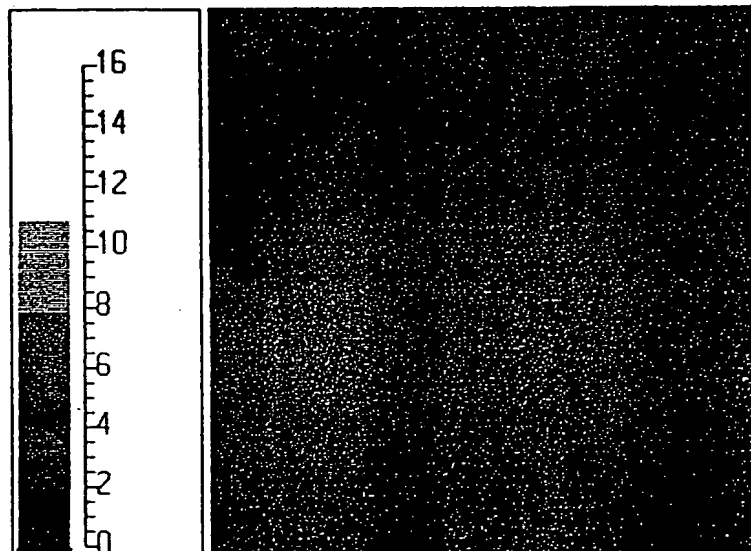
Comments: K+ IONS, #2

Image 2  
FIGURE



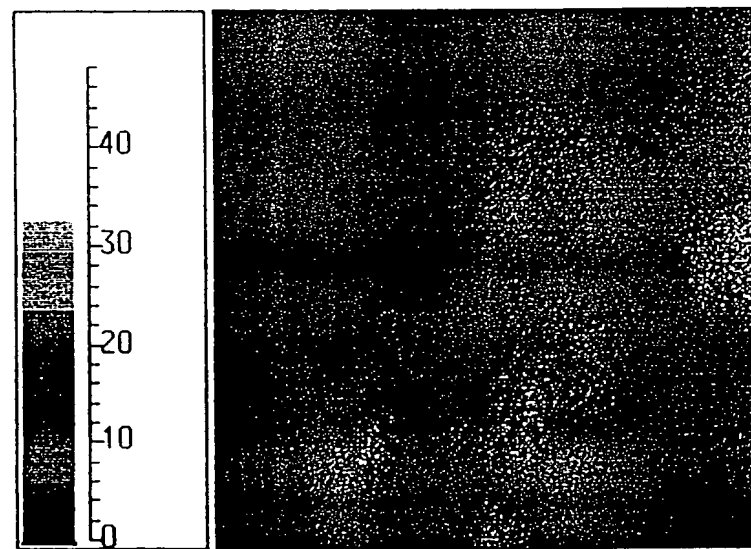
File Name:  
TOFIM636  
Mass:  
Lo: 0.0000  
Hi: 400.0000  
Status:  
Saved On Disk  
Spectrum:  
#4P1  
Image Scale:  
5  $\mu\text{m}$

Comments: TOTAL + IONS, #4



File Name:  
TOFIM637  
Mass:  
Lo: 57.7308  
Hi: 58.2193  
Status:  
Saved On Disk  
Spectrum:  
#4P1  
Image Scale:  
5  $\mu\text{m}$

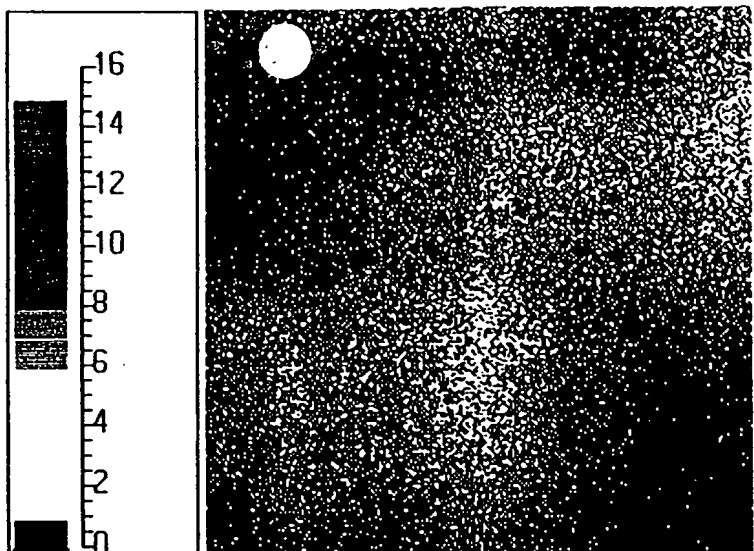
Comments: Ni+ IONS, #4



File Name:  
TOFIM638  
Mass:  
Lo: 38.9553  
Hi: 38.9730  
Status:  
Saved On Disk  
Spectrum:  
#4P1  
Image Scale:  
5  $\mu\text{m}$

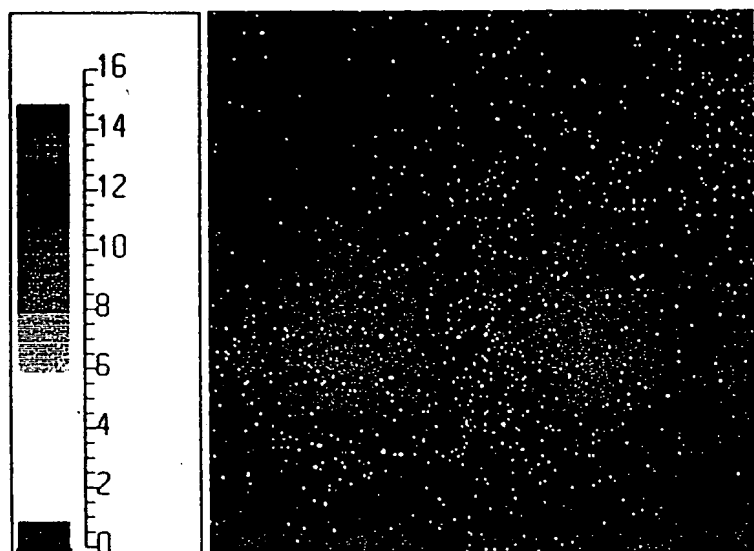
Comments: K+ IONS, #4

Image 3  
FIGURE



File Name:  
TOFIM640  
Mass:  
Lo: 22.9581  
Hi: 23.0214  
Status:  
Saved On Disk  
Spectrum:  
#4P1  
Image Scale:  
 $5 \mu\text{m}$

Comments: Na<sup>+</sup> IONS, #4

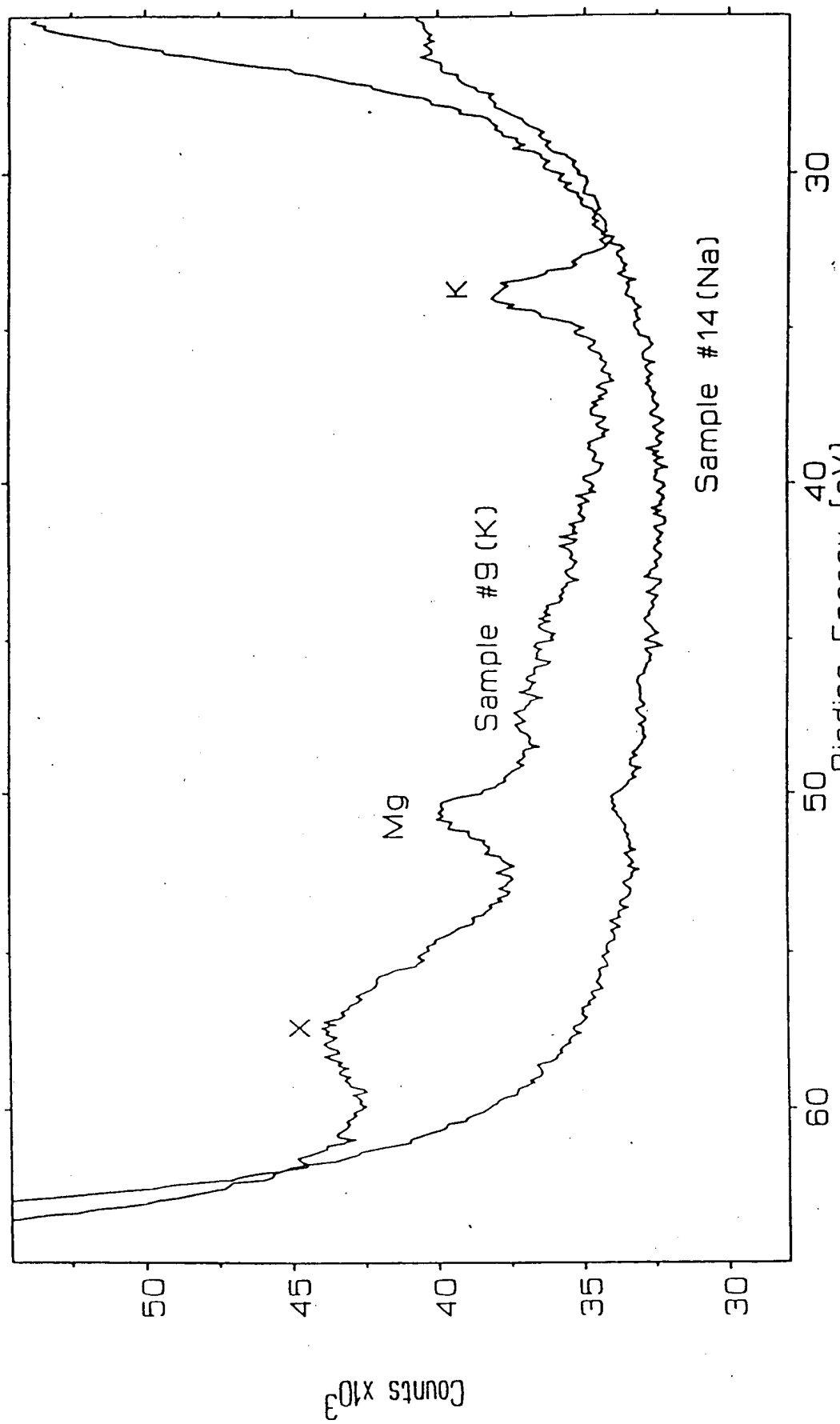


File Name:  
TOFIM641  
Mass:  
Lo: 23.9534  
Hi: 24.0166  
Status:  
Saved On Disk  
Spectrum:  
#4P1  
Image Scale:  
 $5 \mu\text{m}$

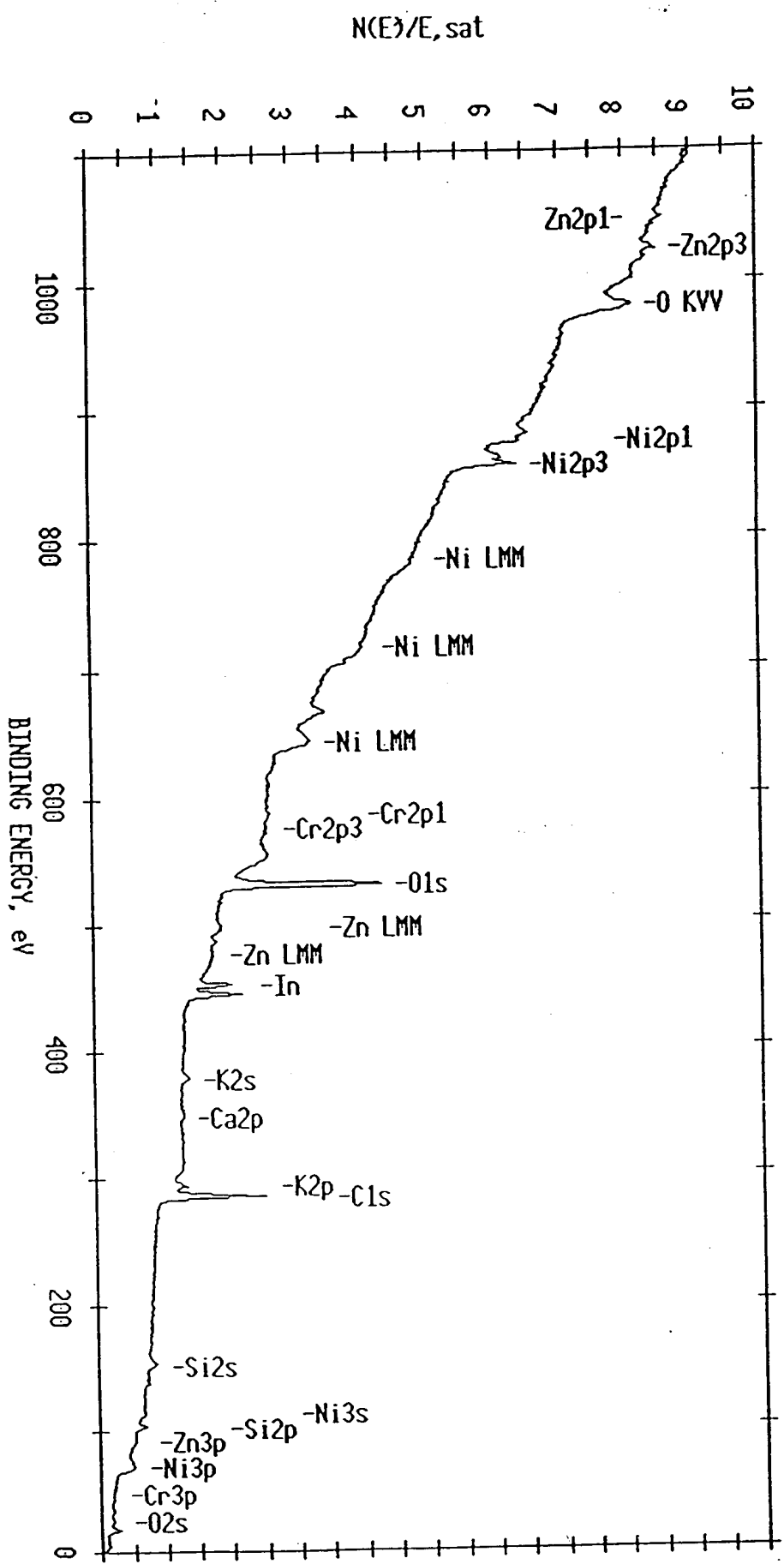
Comments: Mg<sup>+</sup> IONS, #4

Image 3  
FIGURE

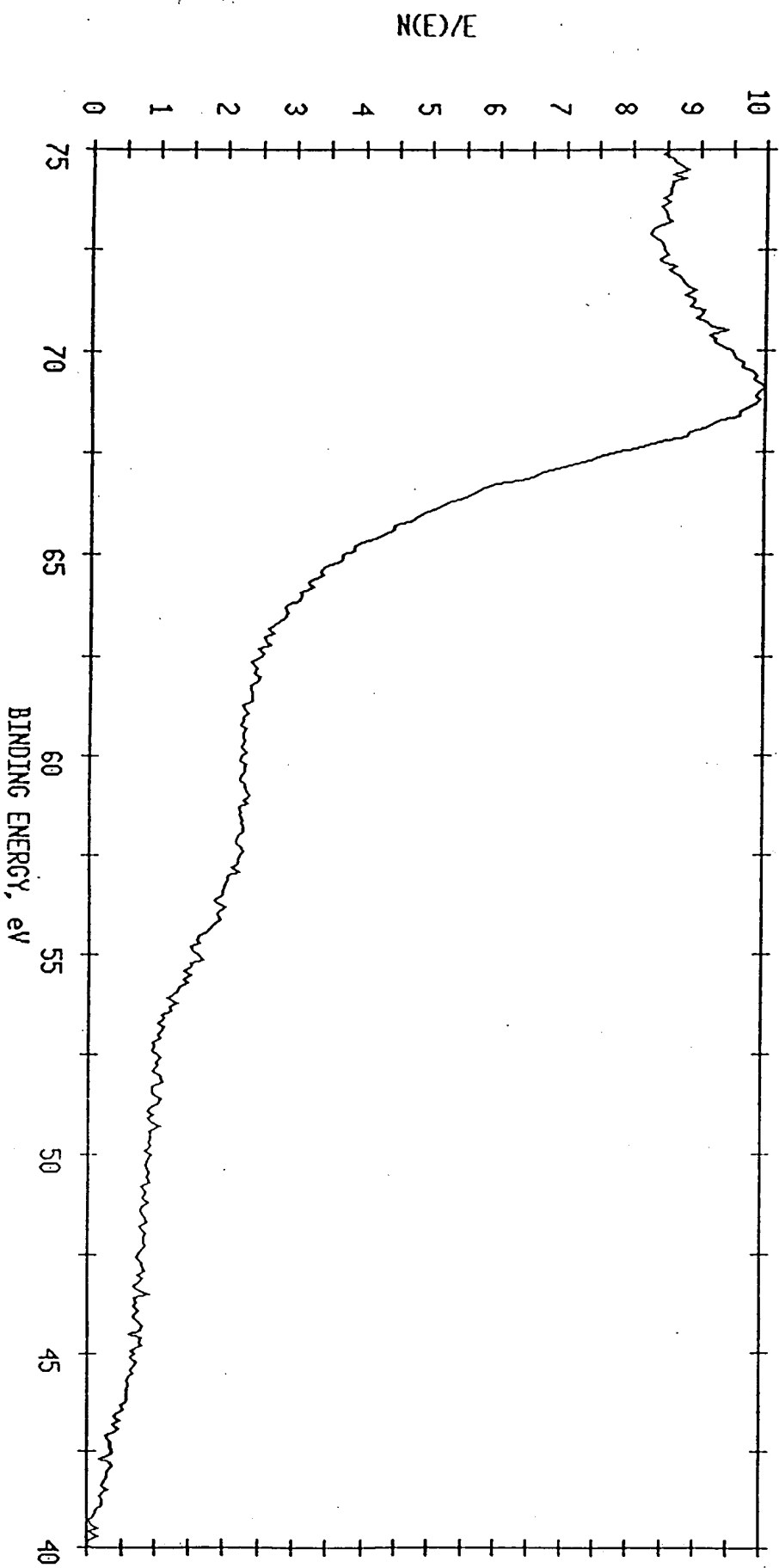
Figure 34



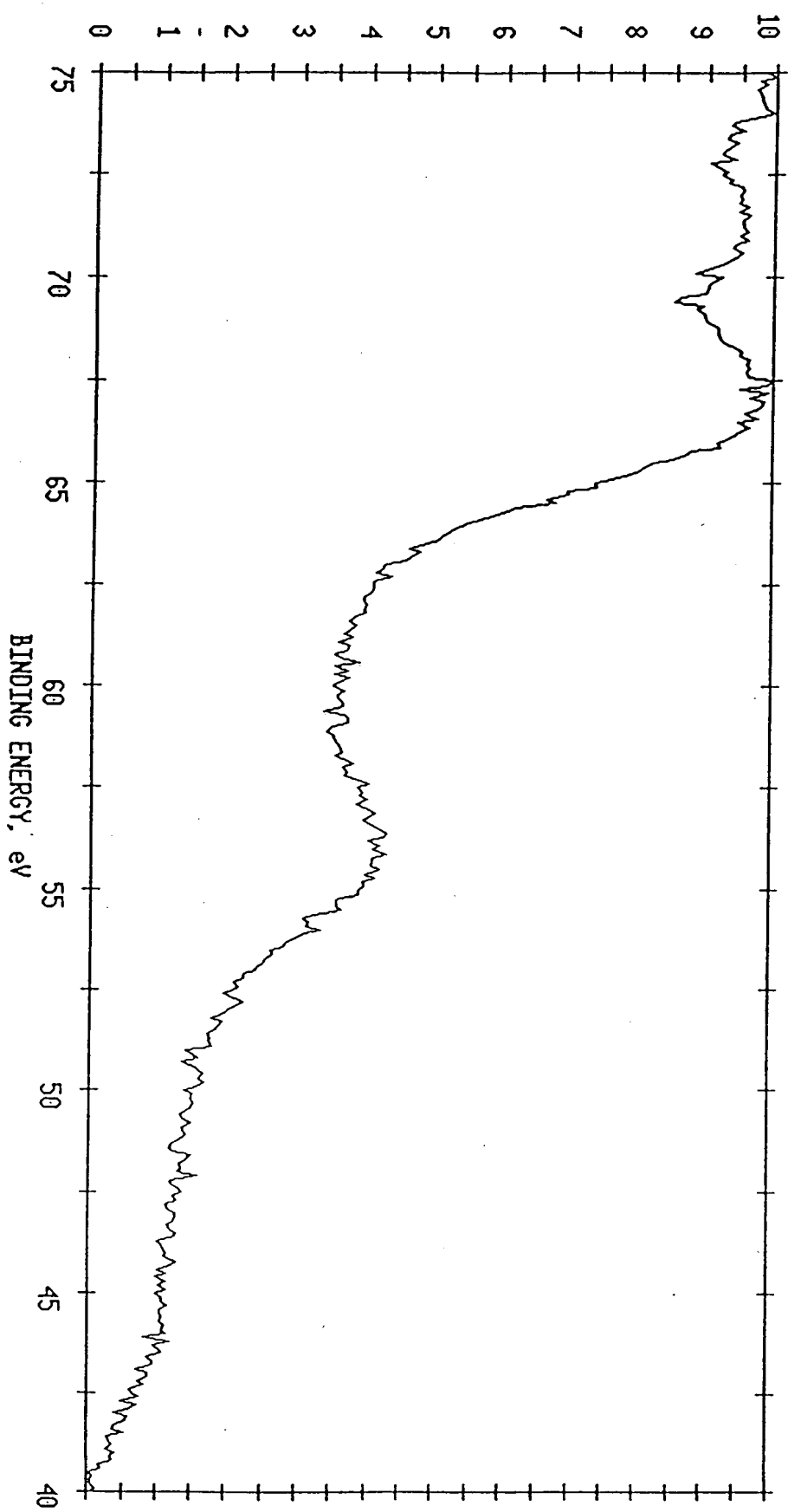
ESCA SURVEY 11/18/93 ANGLE= 15 deg ACQ TIME=29.36 min  
FILE: Nitest21 Ni wire processed in lab. as received.  
SCALE FACTOR= 12.496 k c/s, OFFSET= 1.542 k c/s PASS ENERGY=178.950 eV Al 400 W



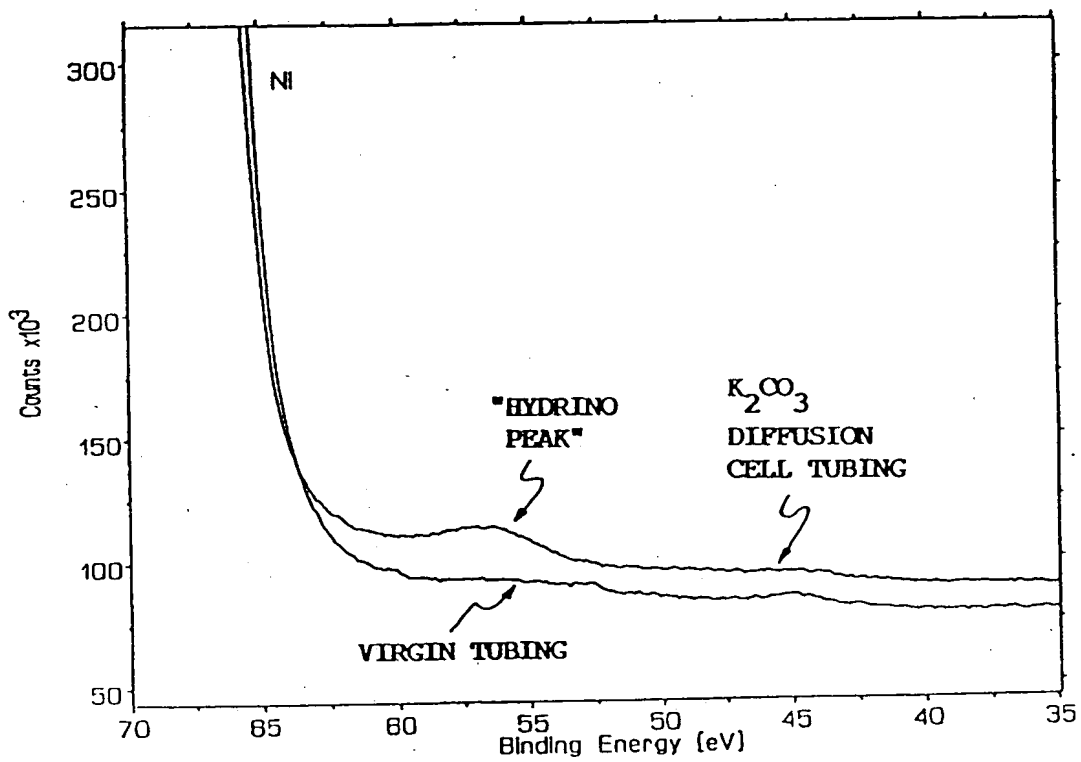
ESCA MULTIPLEX 11/18/93 EL= REG 2 ANGLE= 15 deg ACC TIME=67.28 min  
FILE: Nitest20 Ni wire processed in lab. as received.  
SCALE FACTOR= 0.301 k c/s, OFFSET= 2.742 k c/s PASS ENERGY=143.050 eV AI 400 W



$N(E)/E_{sat}$



ESCA MULTIPLEX 11/24/93 EL= REG 2 ANGLE= 15 deg ACQ TIME=114.08 min  
FILE: Nitest50 Ni wire treated overnight at IRC.  
SCALE FACTOR= 0.095 k c/s, OFFSET= 1.036 k c/s PASS ENERGY=143.050 eV Al 400  $\mu$



# DIHYDRINO MOLECULE IDENTIFICATION

RANDELL L. MILLS and WILLIAM R. GOOD

HydroCatalysis Power Corporation, Greenfield Corporate Center  
1860 Charter Lane, Lancaster, Pennsylvania 17601

ROBERT M. SHAUBACH Thermacore, Inc.  
780 Eden Road, Lancaster, Pennsylvania 17601

NUCLEAR REACTIONS  
IN SOLIDS

KEYWORDS: calorimetry, mass spectroscopy, new hydrogen molecule

Received June 16, 1993

Accepted for Publication July 27, 1993

*Three sets of heat production and "ash" identification data are presented. An exothermic reaction is reported wherein the electrons of hydrogen and deuterium atoms are stimulated to relax to quantized potential energy levels below that of the "ground state" via electrochemical reactants K<sup>+</sup> and K<sup>+</sup>; Pd<sup>2+</sup> and Li<sup>+</sup>; or Pd and O<sub>2</sub> of redox energy resonant with the energy hole that stimulates this transition. Calorimetry of pulsed current and continuous electrolysis of aqueous potassium carbonate (K<sup>+</sup>/K<sup>+</sup> electrocatalytic couple) at a nickel cathode were performed. The excess output power of 41 W exceeded by a factor >8 the total input power given by the product of the electrolysis voltage and current. The product of the exothermic reaction is atoms having electrons of energy below the ground state, which are predicted to form molecules. The predicted molecules were identified by their lack of reactivity with oxygen, by separation from molecular deuterium by cryofiltration, and by mass spectroscopic analysis.*

tions. Rather than invoking a postulated boundary condition,  $\psi \rightarrow 0$  as  $r \rightarrow \infty$ , which leads to a purely mathematical model, we derived the boundary condition from Maxwell's equations<sup>1</sup>: *For nonradiative states, the charge-density function must not possess space-time Fourier components that are synchronous with waves traveling at the speed of light.*

Application of this physical boundary condition leads to a physical model that is consistent with classical physics. The novel theory<sup>2</sup> unifies Maxwell's equations, Newton's laws, and Einstein's general and special relativity. Theoretical predictions conform with experimental observations. The closed-form calculations of a broad spectrum of fundamental phenomena contain fundamental constants only. Equations of the one-electron atom are derived that give four quantum numbers, the Rydberg constant, the ionization energies, the results of the Stern-Gerlach experiment, the electron g factor, the spin angular momentum energies, the excited states, the results of the Davisson-Germer experiment, the parameters of pair production, and the hyperfine structure interval of positronium. Ionization energies of two- and three-electron atoms are given as well as the bond energies, vibrational energies, and bond distances of molecular hydrogen and the molecular hydrogen ion. From the closed-form solution of the helium atom, the predicted electron scattering intensity is derived. The closed-form scattering equation matches the experimental data, whereas calculations based on the Born model of the atom "utterly fail" at small scattering angles. The implications for the invalidity of the Schrödinger and Born models of the atom and the dependent Heisenberg uncertainty principle are discussed. The atomic equations of gravitation are derived from which the gravitational constant and the masses of the leptons and the neutron and proton are derived. The magnetic moments of the nucleons are derived. The beta decay energy of the neutron and the binding energy of deuterium are calculated. Also, the theory predicts exactly the spectral observations of the extreme ultraviolet background emission from interstellar matter, which characterizes dark matter; it

## HYDROCATALYSIS POWER CORPORATION THEORY

Quantum mechanics based on the Schrödinger equation assumes that atomic-sized particles obey different physical laws than macroscopic objects, which behave classically. To overcome the shortcomings of quantum mechanics, physical laws that are exact on all scales were sought. Rather than endowing the electron with a wave nature as suggested by the Davisson-Germer experiment and fabricating a set of associated postulates and mathematical rules for wave operators, we derived a new theory from first principles. In both theories, solutions to the classical wave equation were sought, and the solution of the equation of the electron is time harmonic. But, the novel theory departs from the usual theory in the solutions of the spatial func-

provides a resolution of the solar neutrino paradox, and it provides a basis to produce heat in electrolytic cells that represents an endless supply of cheap, clean energy.

A novel model of the electron<sup>2</sup> describes a bound electron by a charge-density (mass-density) function that is the product of a radial delta function [ $f(r) = d(r - r_n)$ ], two angular functions (spherical harmonic functions), and a time-harmonic function. Thus, an electron is a spinning, two-dimensional spherical surface, called an electron orbitsphere, that can exist in a bound state only at specified distances from the nucleus.

### PHOTON-INDUCED STATES OF THE ONE-ELECTRON ATOM

It is well known that resonator cavities can trap electromagnetic radiation of discrete resonant frequencies. A bound electron is a resonator cavity and can trap photons of discrete frequencies. The relationship between an allowed radius and the electron wavelength is

$$2\pi(nr_1) = 2\pi r_n = n\lambda_1 = \lambda_n , \quad (1)$$

where

$$n = 1$$

$$n = 2, 3, 4, \dots$$

$$n = \frac{1}{2}, \frac{1}{3}, \frac{1}{4}, \dots$$

$\lambda_1$  = allowed wavelength for  $n = 1$

$r_1$  = allowed radius for  $n = 1$ .

Higher and lower energy states are equally valid. The photon standing wave in both cases is given as a solution of Laplace's equation in harmonic coordinates:

*excited-state photon:*

$$\begin{aligned} \hat{\epsilon}_r^i \text{ photon } n, l, m &= \frac{e(na_0)^l}{4\pi\epsilon_0} \frac{1}{r^{(l+2)}} \\ &\times \left( -1 + \frac{1}{r} \operatorname{Re} \{ i[Y_l^m(\phi, \theta) \right. \right. \\ &\quad \left. \left. + Y_s^{m_s}(\phi, \theta)] \} \right) , \end{aligned} \quad (2)$$

for

$$n = 2, 3, 4, \dots$$

$$l = 1, 2, \dots, n - 1 ,$$

and

$$m_l = -l, -l + 1, \dots, 0, \dots, +l ;$$

*below-ground-state photon:*

$$\begin{aligned} \hat{\epsilon}_r^i \text{ photon } n, l, m &= \frac{e}{4\pi\epsilon_0} \frac{\left(\frac{a_0}{n}\right)^l}{r^{(l+2)}} \\ &\times \left[ -1 + n[Y_l^m(\phi, \theta) + Y_s^{m_s}] \right] , \end{aligned} \quad (3)$$

for

$$n = 2, 3, 4, \dots$$

$$l = 1, 2, \dots, n - 1 ,$$

and

$$m_l = -l, -l + 1, \dots, 0, \dots, +l .$$

From energy conservation, the resonance energy hole of a hydrogen atom that excites resonator modes of radial dimensions  $a_0/(m + 1)$  is

$$m \times 27.2 \text{ eV} ,$$

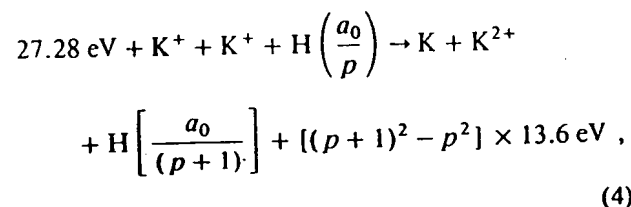
where

$$m = 1, 2, 3, 4, \dots$$

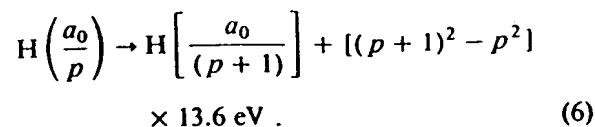
After resonant absorption of the hole, the radius of the orbitsphere  $a_0$  shrinks to  $a_0/(m + 1)$ . After  $p$  cycles of resonant shrinkage, the radius is  $a_0/(mp + 1)$ .

In other words, the radial ground-state field can be considered as the superposition of Fourier components. The removal of negative Fourier components of energy  $m \times 27.2 \text{ eV}$ , where  $m$  is an integer, increases the positive electric field inside the spherical shell by  $m$  times the charge of a proton. The resultant electric field is a time-harmonic solution of LaPlace's equations in spherical coordinates. In this case, the radius at which force balance and nonradiation are achieved is  $a_0/(m + 1)$ , where  $m$  is an integer. In the decay to this radius from the ground state, a total energy of  $[(m + 1)^2 - 1^2] \times 13.6 \text{ eV}$  is released. The potential energy well of the hydrogen or deuterium atom is shown in Fig. 1. The exothermic reaction is referred to as hydrogen emission by catalytic thermal electronic relaxation.

An efficient catalytic system that hinges on the coupling of three resonator cavities involves potassium. For example, the second ionization energy of potassium is 31.63 eV. This energy hole is obviously too high for resonant absorption. However,  $K^+$  releases 4.34 eV when it is reduced to K. The combination of  $K^+$  to  $K^{2+}$  and  $K^+$  to K, then, has a net energy change of 27.28 eV:



And, the overall reaction is



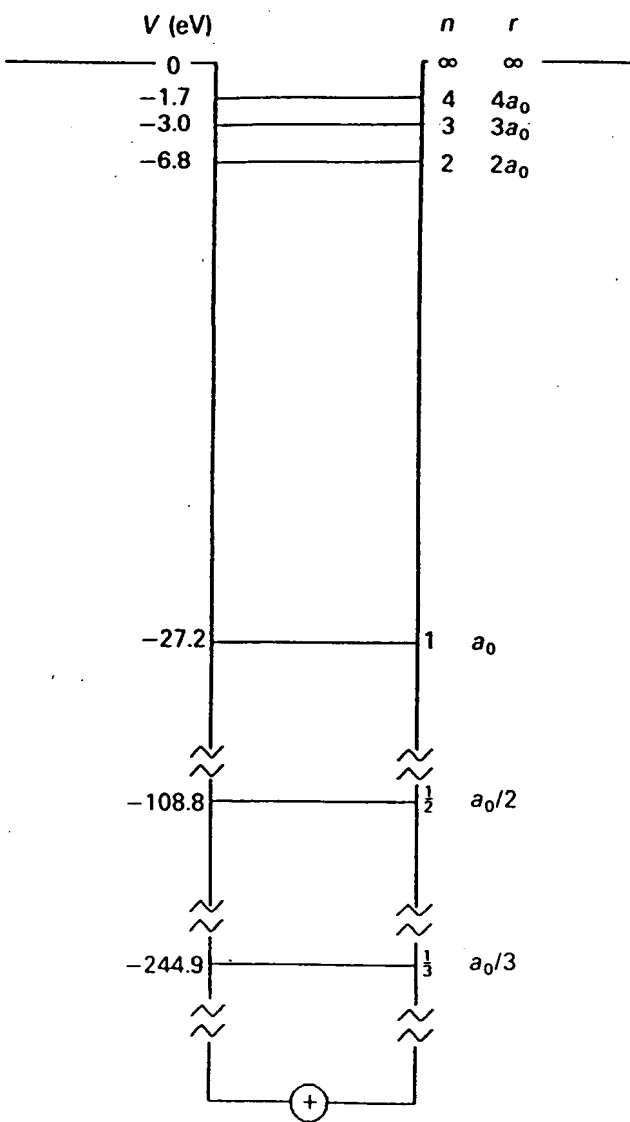
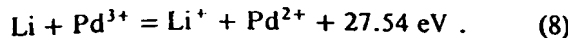
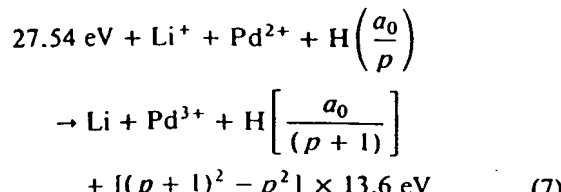
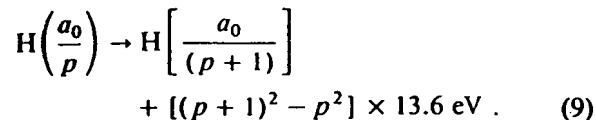


Fig. 1. Potential energy well of a hydrogen atom.

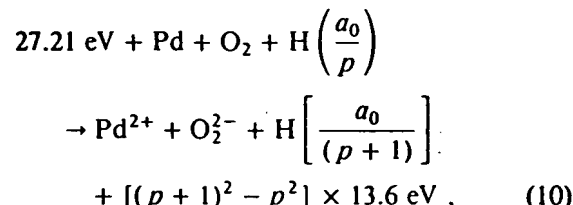
Other less efficient catalytic systems that hinge on the coupling of three resonator cavities exist. For example, the third ionization energy of palladium is 32.93 eV. This energy hole is obviously too high for resonant absorption. However,  $\text{Li}^+$  releases 5.392 eV when it is reduced to Li. The combination of  $\text{Pd}^{2+}$  to  $\text{Pd}^{3+}$  and  $\text{Li}^+$  to Li, then, has a net energy change of 27.54 eV:



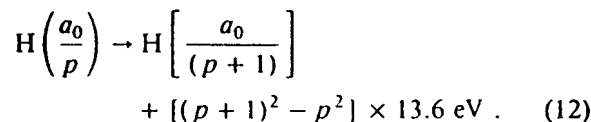
And, the overall reaction is



A catalytic system that hinges on the transfer of two electrons from an atom to a molecule involves palladium and oxygen. For example, the first and second ionization energies of palladium are 8.34 and 19.43 eV, respectively, and the first and second electron affinities of the oxygen molecule are 0.45 and 0.11 eV, respectively. The energy hole resulting from a two-electron transfer is appropriate for resonant absorption. The combination of Pd to  $\text{Pd}^{2+}$  and  $\text{O}_2$  to  $\text{O}_2^{2-}$ , then, has a net energy change of 27.21 eV:

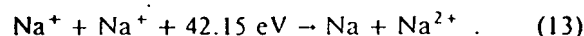


And, the overall reaction is



Additional atoms, molecules, or compounds that could be substituted for  $\text{O}_2$  are those with first and second electron affinities of ~0.45 and 0.11 eV, respectively, such as a mixed oxide ( $\text{MnO}_x$ ,  $\text{AlO}_x$ , or  $\text{SiO}_x$ ) containing oxygen to form  $\text{O}^{2-}$  or  $\text{O}_2$  to form  $\text{O}_2^{2-}$ .

For sodium or sodium ions, no electrocatalytic reaction of ~27.21 eV is possible. For example, 42.15 eV of energy is absorbed by the reverse of the reaction given in Eq. (5) where  $\text{Na}^+$  replaces  $\text{K}^+$ :



## NEW HYDROGEN MOLECULE

According to HydroCatalysis Power Company (HPC) theory, a hydrino atom, a hydrogen atom with its electron in a lower-than-ground-state energy level corresponding to a fractional quantum number, has an unpaired electron and would bind to the nickel cathode. Bound hydrogen atoms demonstrate a high degree of mobility as shown by electron energy loss spectroscopy.<sup>3</sup> Hydrino atoms are predicted to possess high mobility that permits the possibility of subsequent shrinkage reactions and dihydrino-molecule-forming reactions. The hydrino must form muon-like molecules, as indicated by the trace tritium production during the electrolysis of a  $\text{K}_2\text{CO}_3$  heavy water electrolyte with a

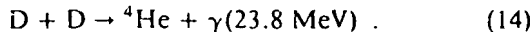
nickel cathode.<sup>2</sup> Dihydrino molecules are evolved from the cathode and are found in the effluent electrolysis gas.

A preferred method to identify the dihydrino molecule is via cryofiltration followed by a search for mass spectroscopic anomalies.

## EXISTING EVIDENCE FOR HYDRINO ATOMS AND DIHYDRINO MOLECULES

Hydrogen transitions to electronic energy levels below the  $n = 1$  state have been found in the spectral lines of the extreme ultraviolet background of interstellar space. This assignment resolves the paradox of the identity of dark matter. It also accounts for other celestial observations such as the facts that diffuse H $\alpha$  emission is ubiquitous throughout the galaxy and widespread sources of flux shortward of 912 Å are required to account for this emission.<sup>2,4</sup>

The dihydrino molecule can be identified by mass spectroscopy. Miles and coworkers<sup>5-8</sup> and Chien et al.<sup>9</sup> report  ${}^4\text{He}$  production as identified by mass spectroscopy of the cryofiltered gases evolved from an electrolysis cell comprising a palladium cathode and a LiOD/D<sub>2</sub>O electrolyte. According to Miles et al.,<sup>7</sup> the intensity of the helium peak maintained an approximate correspondence to the amount of excess power or heat observed in electrochemical calorimetric cells. The samples for helium analysis were analyzed "blindly" by mass spectroscopy. That is, the spectroscopist did not know whether a given sample produced excess heat or not.<sup>10</sup> According to Miles et al.,<sup>7</sup> "ignoring the helium/heat relationship (Table I of Ref. 7), the simple yes/no detection of helium in 7/7 experiments producing excess heat and the absence of helium in 6/6 experiments not producing excess heat (1 in D<sub>2</sub>O, 5 in H<sub>2</sub>O) implies a chance probability of  $(\frac{1}{2})^{13} = \frac{1}{8192}$  or 0.012%." The fusion reaction proposed by the authors is as follows:



Miles et al.<sup>8</sup> report the production of  ${}^4\text{He}$  at a rate of  $\sim 10^{11} \text{ } {}^4\text{He}/\text{s}$ . The associated gamma emission from this proposed fusion corresponds to a 10-Ci 23.8-MeV source. Secondary X rays must also be present as well as neutrons and charged particles in the correct ratios.<sup>11</sup> No neutrons were observed, and no significant radiation above background was observed.<sup>12</sup> Numerous identical heat-producing experiments failed to produce fusion products within 13 orders of magnitude of that necessary to account for the heat.<sup>13</sup> According to Rees,<sup>13</sup> "even if a new fusion process were occurring, there ought to be x-rays produced. It is hard to believe that you could lose over 20 MeV in a single event and see nothing at all coming out."

We feel that the data are not consistent with a fusion reaction as the source of the excess heat or the mass 4 peak. The mass 4 peak is incorrectly assigned as  ${}^4\text{He}$ .

The correct assignment is D<sub>2</sub><sup>\*</sup>, the dideutrino molecule. These molecules form from deutrino atoms on the surface of the palladium cathode. The deutrino atoms form according to the exothermic reaction given by Eqs. (7), (8), and (9), which is the source of the observed excess heat.

The dideutrino molecule is predicted to be spin paired, to be of comparable size to the helium atom, and to have a higher ionization energy and a lower liquefaction temperature than D<sub>2</sub>. Thus, cryofiltration of the gases of an electrolytic cell having an electrolyte of one or more electrocatalytic couples that induce transitions of deuterium atoms to energy levels below the ground state to release excess heat energy followed by mass spectroscopic analysis would appear to be producing  ${}^4\text{He}$ . In fact, the mass spectroscopic separation of  ${}^4\text{He}$  and D<sub>2</sub><sup>\*</sup> would be difficult. And, Miles et al.<sup>10</sup> used the higher ionization potential of the mass 4 peak as a criterion to make its assignment as  ${}^4\text{He}$  rather than D<sub>2</sub>.

The dideutrino molecule can also be identified by high-resolution quadrupole mass spectroscopy. Yamaguchi and Nishioka<sup>14</sup> reported high-resolution (0.001 amu) quadrupole mass spectroscopic data of the gases released from deuterium- or hydrogen-loaded palladium sheets coated on one side with a hydrogen-impermeable gold layer and coated on the other surface with an oxide coat (MnO<sub>x</sub>, AlO<sub>x</sub>, or SiO<sub>x</sub>). Heat was observed from light and heavy hydrogen only when the mixed oxide coat was present. The mass spectroscopic data of the gases released when a current was applied to a deuterium-loaded (99.9%), MnO<sub>x</sub>-coated palladium sheet indicate the presence of a large shoulder on the D<sub>2</sub> peak.

Yamaguchi and Nishioka's<sup>14</sup> control D<sub>2</sub> peak is shown in Fig. 2. A shoulder on the D<sub>2</sub> peak is shown in Figs. 3 (Ref. 14) and 4 (Ref. 15). The anomalous peak of Fig. 3 was assigned to HT ( ${}^1\text{H}-{}^3\text{H}$ ) by Yamaguchi and Nishioka. Tritium is produced by nuclear fusion, and this (HT) peak grows with time as heat evolves. However, no such peak is possible because no  ${}^1\text{H}$  was present, as demonstrated in the control spectrum, and the proposed HT peak was larger than the D<sub>2</sub> peak. The observed heat, including that observed from light hydrogen, is inexplicable from the proposed observed nuclear products. We assert that the data are not consistent with a fusion reaction or with the assignment of the anomalous mass 4 peak as HT. The correct assignment is D<sub>2</sub><sup>\*</sup>, the dideutrino molecule. These molecules form from deutrino atoms on the surface of the palladium sheet, and the deutrino atoms form according to the exothermic reaction given by Eqs. (10), (11), and (12), which is the source of the observed excess heat.

After cryofiltration or combustion, the dihydrino molecule can be distinguished from normal molecular hydrogen by mass spectroscopy. The branching ratio to form  $m/e = 1$  relative to  $m/e = 2$  that is observed for the dihydrino molecule is different than the ratio that

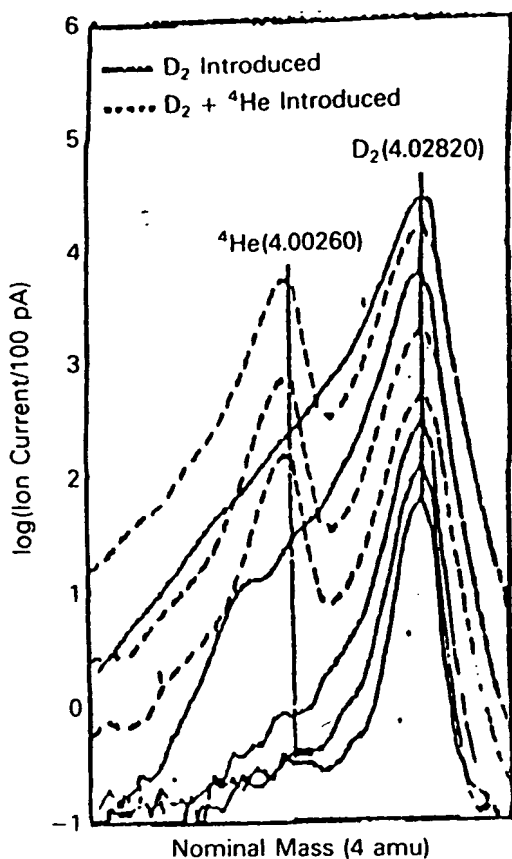


Fig. 2. Yamaguchi and Nishioka's<sup>14</sup> control high-resolution mass spectrum of helium and hydrogen.

is observed for normal molecular hydrogen. Mass spectroscopy will further distinguish a sample containing dihydrino molecules from a sample containing H<sub>2</sub> by showing a different ion production efficiency as a function of ionization potential and a different ion production efficiency at a given ionization potential for the two samples.

#### LIGHT WATER CALORIMETRY EXPERIMENTS

##### Methods

A search for excess heat during the electrolysis of aqueous potassium carbonate (K<sup>+</sup>/K<sup>+</sup> electrocatalytic couple) was conducted by using single-cell, silver-coated, vacuum-jacketed dewars and noninsulated plastic vessels. To simplify the calibration of these cells, they were constructed to have primarily conductive heat losses. Thus, a linear calibration curve was obtained. Two methods of differential calorimetry were used to determine the cell constant that was used to calculate the excess enthalpy. First, we calculated the cell constant during the experiment (on-the-fly calibration) by turning an internal resistance heater off and on and infer-

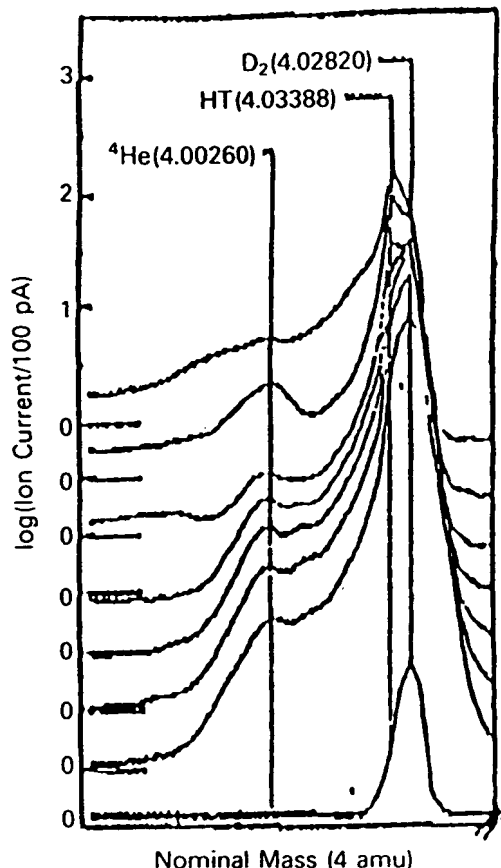


Fig. 3. Yamaguchi and Nishioka's<sup>14</sup> high-resolution mass spectroscopic data of the gases released when a current was applied to a deuterium-loaded (99.9%), MnO<sub>x</sub>-coated palladium sheet, indicating the presence of a large shoulder on the D<sub>2</sub> peak that increases with time.

ring the cell constant from the difference between the losses with and without the heater. Second, we determined the cell constant with no electrolysis processes occurring by turning an internal resistance heater off and on for a well-stirred cell and inferring the cell constant from the difference between the losses with and without the heater. This method overestimates the cell constant because there is no gas flow (which adds to the heat losses).

The general form of the energy balance equation for the cell in steady state is

$$0 = P_{appl} + Q_{htr} + Q_{xs} - P_{gas} - Q_{loss}, \quad (15)$$

where

$P_{appl}$  = electrolysis power

$Q_{htr}$  = power input to the heater

$Q_{xs}$  = excess heat power generated by the hydrogen "shrinkage" process

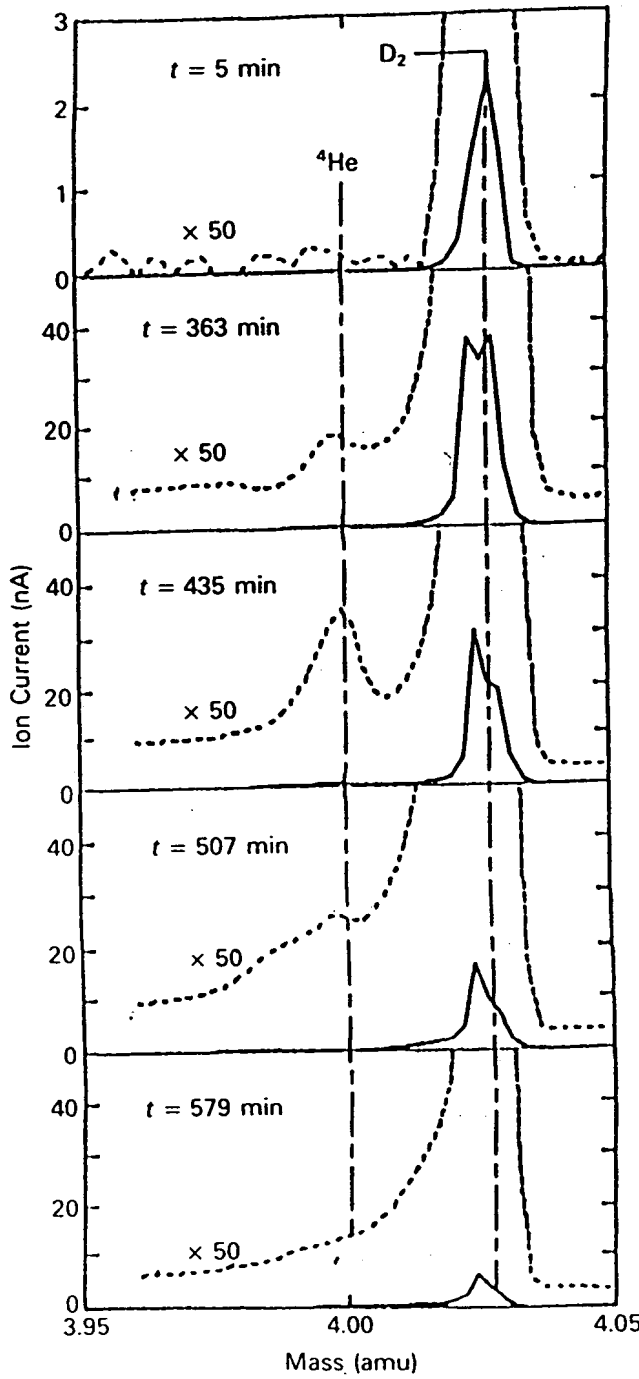


Fig. 4. Yamaguchi and Nishioka's<sup>15</sup> high-resolution mass spectroscopic data of the gases released when a current was applied to a deuterium-loaded (99.9%), MnO<sub>x</sub>-coated palladium sheet, indicating the presence of a large shoulder on the D<sub>2</sub> peak that increases with time.

$P_{gas}$  = power removed as a result of evolution of H<sub>2</sub> and O<sub>2</sub> gases

$Q_{loss}$  = thermal power loss from the cell.

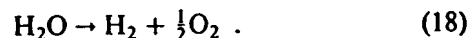
When an aqueous solution is electrolyzed to liberate hydrogen and oxygen gases, the electrolysis power  $P_{appl}$  ( $= E_{appl} I$ ) can be partitioned into two terms:

$$P_{appl} = E_{appl} I = P_{cell} + P_{gas} . \quad (16)$$

An expression for  $P_{gas}$  ( $= E_{gas} I$ ) is readily obtained from the known enthalpy of formation of water from its elements:

$$E_{gas} = \frac{-\Delta H_{form}}{\alpha F} \quad (17)$$

( $F$  is Faraday's constant), which yields  $E_{gas} = 1.48$  V for the reaction



The net faradaic efficiency of gas evolution is assumed to be unity; thus, Eq. (16) becomes

$$P_{cell} = (E_{appl} - 1.48 V)I . \quad (19)$$

We calibrated the cell for heat losses by turning an internal resistance heater off and on while maintaining constant electrolysis and by inferring the cell conductive constant from the difference between the losses with and without the heater where heat losses were primarily conductive losses through the top of the dewar or through the surfaces of the plastic vessel. When the heater was off, the losses were given by

$$c(T_c - T_b) = P_{appl} + 0 + Q_{xs} - P_{gas} , \quad (20)$$

where

$c$  = conductive heat loss coefficient

$T_b$  = ambient temperature

$T_c$  = cell temperature.

When a new steady state is established with the heater on, the losses change to

$$c(T'_c - T_b) = P'_{appl} + Q'_{htr} + Q'_{xs} - P'_{gas} , \quad (21)$$

where the primes indicate values that changed when the heater was on. When we assume

$$Q_{xs} = Q'_{xs} , \quad P_{appl} = P'_{appl} , \quad \text{and} \quad P_{gas} = P'_{gas} , \quad (22)$$

the cell constant or heating coefficient  $a$ , the reciprocal of the conductive loss coefficient  $c$ , is given by the result

$$a = \frac{T'_c - T_c}{Q_{htr}} . \quad (23)$$

In all heater power calculations, we used the following equation:

$$Q_{htr} = E_{htr} I_{htr} . \quad (24)$$

In the case of intermittent square-wave electrolysis with current only during the high-voltage interval of the cycle, the  $P_{appI}$  value of Eq. (16) is calculated as the product of the peak voltage, the peak current, and the duty cycle  $Dc$ , which is the pulse length divided by the period:

$$P_{appI} = (E_{appI} I) Dc = (P_{cell} + P_{gas}) Dc . \quad (25)$$

In the case of intermittent square-wave electrolysis with current only during the high-voltage interval of the cycle and where the net faradaic efficiency of gas evolution is assumed to be unity,  $P_{cell}$  of Eq. (19) becomes

$$P_{cell} = [(E_{appI} - 1.48V) I] Dc . \quad (26)$$

### HPC Experiments 1, 2, and 3

These experiments were carried out by observing and comparing the temperature differences,  $\Delta T_1 = T(\text{electrolysis only}) - T(\text{blank})$  and  $\Delta T_2 = T(\text{resistor heating only}) - T(\text{blank})$  referred to unit input power, between two identical cells. Each cell consisted of a 350-ml silver-coated, vacuum-jacketed dewar (Cole Palmer model 8600) with a 7-cm opening covered with a 0.75-in.-thick Styrofoam stopper lined with Parafilm. One calorimeter dewar of the same configuration, containing the same amount of electrolyte and the same electrodes (nickel cathode and platinum anode), resistor-heater, and thermistor, stirred at the same speed, was used as the blank. In this dewar, neither electrolysis nor heating by the resistor was carried out. Experiments were also carried out by using the blank dewar from a previous experiment as the working dewar and vice versa. This exchange was done to ensure that the effect is not due to any difference in the thermal properties of the two specific dewars used. The experimental apparatus for the differential calorimetry used for these studies is shown in Fig. 5.

The heating coefficients were calculated from

$$\alpha = \Delta T_1 / P_{cell} \quad (27)$$

and

$$\alpha = \Delta T_2 / Q_{htr} . \quad (28)$$

The outsides of the cells were maintained at ambient air temperature, which was monitored. Ambient temperature fluctuations over 24 h were typically  $<0.5^\circ\text{C}$ .

The cathode was 24 m of 0.127-mm-diam nickel wire (99% Alfa 10249, cold drawn) that was coiled about the central platinum anode. We cleaned the cathode by placing it in a beaker of 0.57 M  $\text{K}_2\text{CO}_3$ /3%  $\text{H}_2\text{O}_2$  for 30 min and then rinsing it with distilled water. The leads were inserted into Teflon tubes to ensure that no recombination of the evolving gases occurred.

The anode was a 10-cm  $\times$  1-mm-diam spiraled plat-

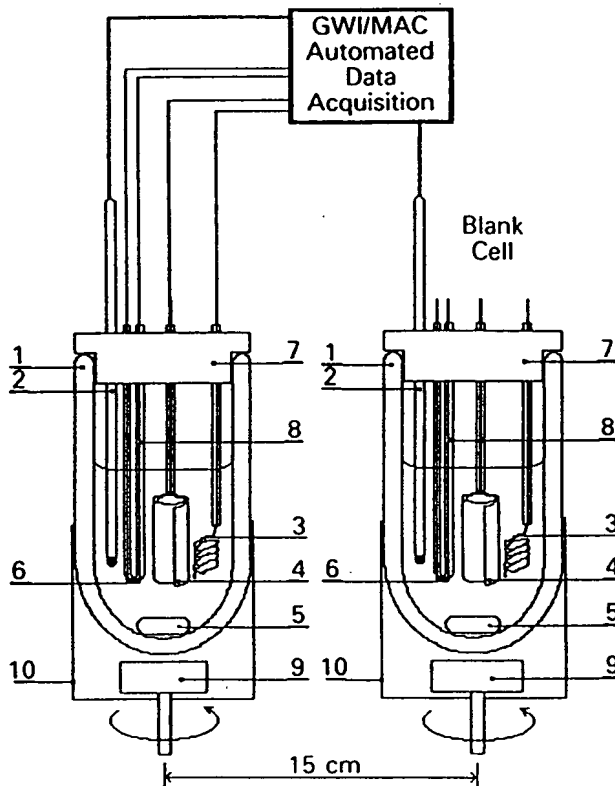


Fig. 5. Experimental calorimeter setup: (1) vacuum-jacketed dewar, (2) thermistor, (3) platinum anode, (4) nickel cathode, (5) magnetic stirring bar, (6) resistor-heater, (7) Styrofoam stopper lined with Parafilm, (8) Teflon tubing, (9) magnetic stirrer, and (10) aluminum cylinder.

inum wire (Johnson-Matthey) with a 0.127-mm platinum lead wire. The leads were inserted into Teflon tubes to prevent recombination, if any, of the evolving gases. The cathode-anode separation distance was 1 cm.

As usual in electrochemistry, measures were taken to avoid impurities in the system, especially organic substances. We note here the known problems with the reproducibility of the hydrogen overpotential that can be overcome only by ensuring the lowest possible level of impurities. The following procedures were applied in order to reproduce the excess heat effect. Before starting the experiment, the electrolysis dewar was cleaned with Alconox and 0.1 M nitric acid and rinsed thoroughly with distilled water to remove all organic contaminants. The platinum anode was mechanically scoured with steel wool, soaked overnight in concentrated  $\text{HNO}_3$ , and rinsed with distilled water. The nickel cathode was removed from its container with rubber gloves, and cut and folded in such a way that no organic substances were transferred to the nickel surface. The nickel cathode was dipped into the working

solution under electrolysis current and was never left in the working solution without electrolysis current.

In experiments 1 and 2, the electrolyte solution was 200 ml of 0.57 M aqueous  $K_2CO_3$  (Aldrich  $K_2CO_3 \cdot \frac{1}{2}H_2O$  99+%); in experiment 3, the electrolyte solution was 200 ml of 0.57 M aqueous  $Na_2CO_3$  (Aldrich  $Na_2CO_3$  ACS primary standard 99.95+%).

The resistance heater used during calibration and operation was a 10- $\Omega$ , 1% precision metal oxide resistor in a 2-mm-o.d. Teflon tube. The heater was powered by a variable direct current voltage power source ( $\pm 0.5\%$ ). The heating power was calculated by Eq. (24).

The electrolyte solution was stirred with a 7-mm  $\times$  2-cm prolate spheroid magnetic stirring bar that was spun by a 6-cm-long open magnet mounted on an open shaft revolving at 750 rpm under the dewar. The shaft was that of an open mixing motor (Fisher Flex-a-Mix model 76).

Erroneous attribution of the effect to temperature gradients was prevented by testing for minute spatial variations of the temperature over time. Three thermistors were positioned  $\sim 2.5$  cm apart from each other at the bottom, middle, and upper parts of the electrolyte. No difference was observed (within the limit of detection,  $\pm 0.01^\circ C$ ).

Voltage ( $\pm 0.5\%$ ), current ( $\pm 1\%$ ), and temperature ( $\pm 0.1^\circ C$ ) data were acquired by a data acquisition system consisting of an Apple Mac II SI 5/80 with an NU bus adapter and the following GW Instruments hardware: GWI-625 data acquisition board, GWI-J2E multiplexer, GWI-ABO analog breakout system, and GWI-4W ribbon cable. The value of  $P_{appl}$  was given by Eq. (16) as the product of the voltage and the constant current, and  $P_{cell}$  was given by Eq. (19).

The current voltage parameters for experiment 2 were a periodic square wave having an offset voltage of 1.60 V, a peak voltage of 1.90 V, a peak constant current of 47.3 mA, a 36.0% duty cycle, and a frequency of 600 Hz. Peak voltage measurements were made with an oscilloscope (BK model 2120), and the time-average current was determined from a multimeter voltage measurement ( $\pm 0.5\%$ ) across a calibrated resistor ( $1\ \Omega$ ) in series with the lead to the cathode. The waveform of the pulsed cell was a square wave. Since there was current only during the peak voltage interval of the cycle,  $P_{appl}$  was given by Eq. (25), and  $P_{cell}$  was given by Eq. (26).

The faradaic efficiency of gas production by a potassium cell was studied. Comparing this result with the sodium system allows the accuracy of the analysis to be seen. A closed cell was fashioned from a 150-ml round-bottom flask, a 2-cm  $\times$  2-mm prolate spheroid stir bar, a glass "Y" adapter, glass tubing bent into the shape of one cycle of a square wave, a 150-ml beaker, and a 0.01-ml graduated buret. The cell was set up to mimic the calorimetry tests as closely as possible. A constant current ( $\pm 0.1\%$ ) supply was used to supply the power for the electrolysis. Current measurement was

done with a Heathly multimeter ( $\pm 0.1\%$ ). Gas was collected and measured in the buret. Several experiments were run to ensure that the cell was sealed tightly.

#### Thermacore Experiment 4

The cell was a 10-gal (33-  $\times$  15-in.) Nalgene tank (model 54100-0010). Two 4-in.-long  $\times$   $\frac{1}{2}$ -in.-diam terminal bolts were secured in the lid, and a cord for a calibration heater was inserted through the lid.

The cathode was a 5-gal polyethylene bucket with  $\frac{1}{2}$ -in. holes drilled over all surfaces at  $\frac{3}{4}$ -in. spacings of the hole centers, which served as a perforated (mesh) support structure, and 5000 m of 0.5-mm-diam clean, cold-drawn nickel wire (NI 200, 0.0197-in., HTN36-NOAG1, Al Wire Tech). The wire was wound uniformly around the outside of the mesh support as 150 sections of 33-m length. The ends of each of the 150 sections were spun to form three cables of 50 sections per cable. The cables were pressed in a terminal connector that was bolted to the cathode terminal post. The connection was covered with epoxy to prevent corrosion. A central cathode was made from 5000 m of the 0.5-mm-diam nickel wire. The wire was wound in a toroidal shape with three cables, each pressed into a terminal connector that was bolted to the cathode terminal post and coated with epoxy. The central cathode was inserted into an cylindrical perforated polyethylene container that was placed inside the outer cathode with the anode array between the central and outer cathodes.

The anode was an array of 15 platinized titanium anodes (ten of Engelhard platinum-titanium mesh, 1.6  $\times$  8 in., with a  $\frac{3}{4}$ -  $\times$  7-in. stem attached to the 1.6-in. side plated with 100 U series 3000; and five of Engelhard 1-in.-diam  $\times$  8-in.-long titanium tubes with a  $\frac{3}{4}$ -  $\times$  7-in. stem affixed to the interior of one end and plated with 100 U platinum series 3000). A  $\frac{1}{4}$ -in.-wide tab was made at the end of the stem of each anode by bending it at a right angle to the anode. A  $\frac{1}{4}$ -in. hole was drilled in the center of each tab. The tabs were bolted to a 12.25-in.-diam polyethylene disk (Rubbermaid JN2-2669) equidistantly around the circumference. Thus, an array was fabricated that had 15 anodes suspended from the disk. The anodes were bolted with  $\frac{1}{4}$ -in. polyethylene bolts. Sandwiched between each anode tab and the disk was a flattened nickel cylinder also bolted to the tab and the disk. The cylinder was made from a 7.5-  $\times$  9-cm-long  $\times$  0.125-mm-thick nickel foil. The cylinder traversed the disk, and the other end of each was pressed about a 10 AWG/600 V copper wire. The connection was sealed with shrink tubing and epoxy. The wires were pressed into two terminal connectors and bolted to the anode terminal. The connection was covered with epoxy to prevent corrosion.

Before assembly, the anode array was cleaned in 3 M HCl for 5 min and rinsed with distilled water. The cathode was placed in a tank of 0.57 M  $K_2CO_3$ /3%  $H_2O_2$  for 6 h and then rinsed with distilled water. The anode was placed in the support between the central

and outer cathodes, and the electrode assembly was placed in the tank containing 28 l of 0.57 M  $K_2CO_3$  (Alfa  $K_2CO_3$ , 99%). The power supply was connected to the terminals with battery cables.

The cell assembly is shown in Fig. 6.

The heater was a 57.6- $\Omega$ , 1000-W Incoloy 800-jacketed Nichrome heater that was suspended from the polyethylene disk of the anode array. It was powered by a constant power ( $\pm 0.1\%$ ) supply (Invar model TP 36-18). The voltage ( $\pm 0.1\%$ ) and current ( $\pm 0.1\%$ ) were recorded with a digital multimeter (Fluke 8600A). The current ( $\pm 0.5\%$ ) was read from an Ohio Semitronics CTA 101 current transducer. The heating power was calculated by using Eq. (24).

Electrolysis was performed at 50-A constant current with a constant current ( $\pm 0.02\%$ ) power supply (Kepco model ATE6-100M). The value of  $P_{appl}$  was given by Eq. (16) as the product of the voltage and the constant current, and  $P_{cell}$  was given by Eq. (19).

The temperature ( $\pm 0.1^\circ C$ ) was recorded with a microprocessor thermometer (Omega HH21) using a type K thermocouple that was inserted through a  $\frac{1}{4}$ -in.

hole in the tank lid and anode array disk. To eliminate the possibility of temperature gradients, the temperature was measured throughout the tank. No position variation was found to within the detection of the thermocouple ( $\pm 0.1^\circ C$ ).

The temperature rise above ambient [ $\Delta T = T(\text{electrolysis only}) - T(\text{blank})$ ] and electrolysis power were recorded daily. The heating coefficient was determined on the fly by the addition of 20 W of heater power to the electrolytic cell every 72 h; 24 h was allowed for steady state to be achieved. The temperature rise above ambient [ $\Delta T_2 = T(\text{electrolysis + heater}) - T(\text{blank})$ ] was recorded as were the electrolysis power and heater power.

In all temperature measurements, the blank consisted of 28 l of water in a 10-gal (33- x 15-in.) Nalgene tank with lid (model 54100-0010). The stirrer was a 1-cm-diam x 43-cm-long glass rod to which an 0.8- x 2.5-cm Teflon half-moon paddle was fastened at one end; the other end was connected to a variable-speed stirring motor (Talboys Instrument model 1075C). The stirring rod was rotated at 250 rpm.

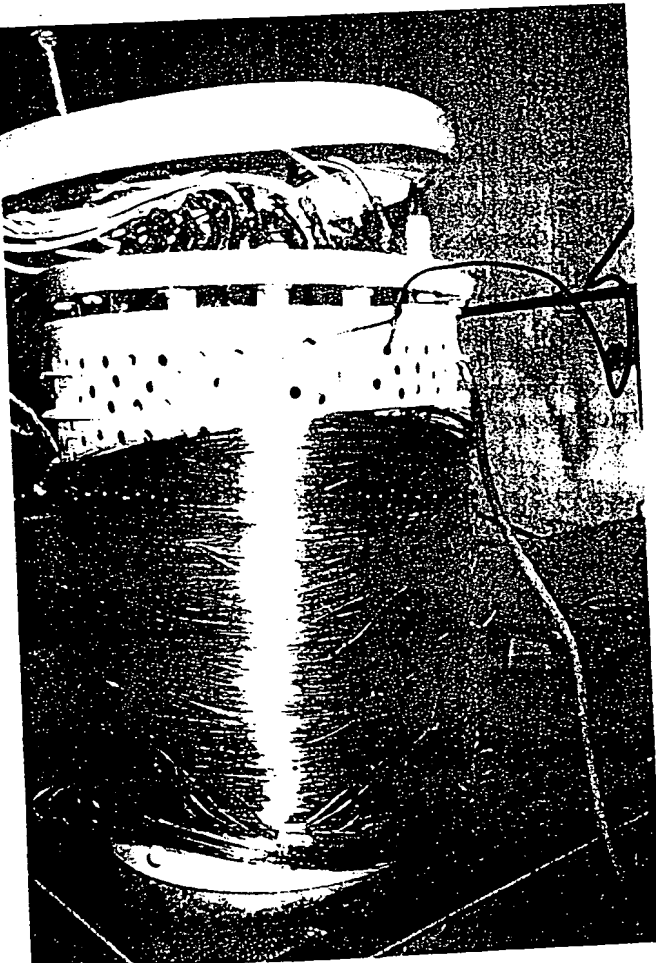
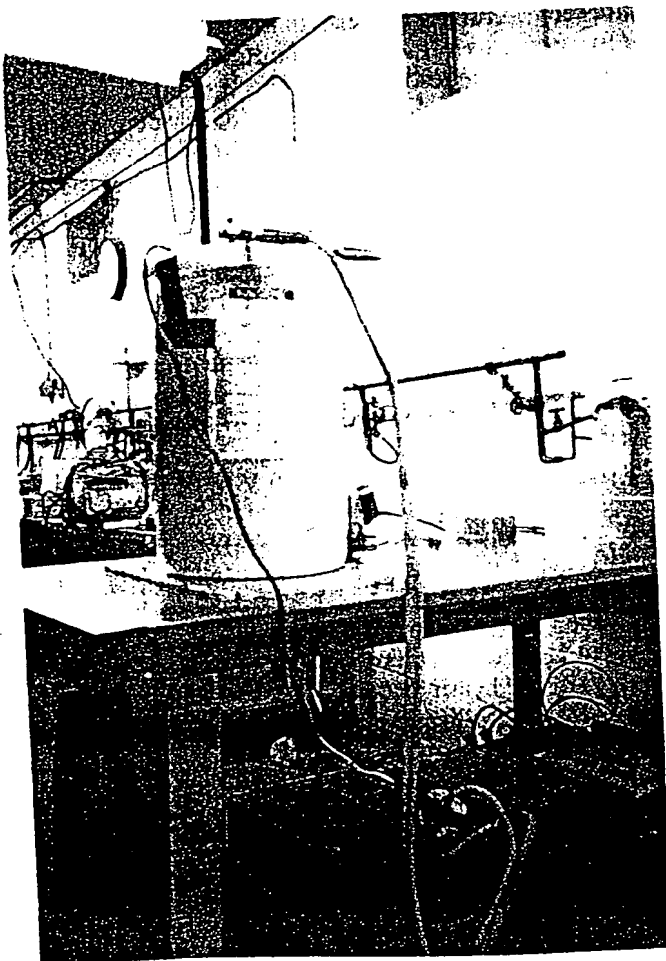


Fig. 6. Cell assembly of experiments 4 through 14.

The blank (nonelectrolysis cell) was stirred to simulate stirring in the electrolytic cell by gas sparging. The 1 W of heat from stirring resulted in the blank cell operating at 0.2°C above ambient.

The temperature ( $\pm 0.1^\circ\text{C}$ ) of the blank was recorded with a microprocessor thermometer (Omega HH21) that was inserted through a  $\frac{1}{4}$ -in. hole in the tank lid.

### Thermacore Experiments 5 Through 13

The electrolytic cell was the same as in experiment 4. Intermittent square-wave electrolysis was performed at 2 Hz at the duty cycles listed in Table I. A constant current supply (Kepco ATE-100M) was programmed at 101-A peak current ( $\pm 0.05\%$ ) and driven by a function generator (BK Precision Dynascan model 3011). Duty cycle measurements were made with an oscilloscope (BK model 2120), and the peak current was determined from the voltage measurement ( $\pm 0.1\%$ ) across an Ohio Semitronics CTA 101 current transducer. The waveform of the pulsed cell current was a square wave. Since there was current only during the peak voltage interval of the cycle,  $P_{appl}$  was given by Eq. (25), and  $P_{cell}$  was given by Eq. (26).

The peak voltage ( $\pm 0.1\%$ ) was recorded with a digital multimeter (Fluke 8600A). The temperature ( $\pm 0.1^\circ\text{C}$ ) was recorded with a microprocessor thermometer (Omega HH21) that was inserted through a  $\frac{1}{4}$ -in. hole in the tank lid and anode array disk. To eliminate the possibility of temperature gradients, the temperature was measured throughout the tank. No position variation was found to within the detection limit of the thermocouple ( $\pm 0.1^\circ\text{C}$ ).

The temperature rise above ambient [ $\Delta T = T(\text{electrolysis only}) - T(\text{blank})$ ] and electrolysis power were recorded at least every 24 h. In all temperature measurements, the blank was the same as for experiment 4.

The electrolytic cell was calibrated by applying electrical power to the 1000-W heater with electrolysis

power set to near zero. The cell temperature rise above ambient [ $\Delta T = T(\text{heater only}) - T(\text{blank})$ ] and heater power were recorded daily. The heating coefficient was determined on the fly by the addition of 40 W of heater power every 72 h; at least 24 h was allowed for steady state to be achieved. The heating power was calculated by Eq. (24).

### Thermacore Experiment 14

The electrolytic cell was the same as in experiments 5 through 13. Intermittent square-wave electrolysis was performed at 1 Hz, 20% duty cycle, by programming a constant current supply (Kepco ATE-50M) at 10-A peak ( $\pm 0.5\%$ ) driven by a function generator (BK Precision Dynascan model 3011). Data were recorded by the apparatus described for experiments 5 through 13. Since there was current only during the peak voltage interval of the cycle,  $P_{appl}$  was given by Eq. (25), and  $P_{cell}$  was given by Eq. (26).

### LIGHT WATER CALORIMETRY RESULTS

Mills's theory<sup>2</sup> predicts that the exothermic catalytic reaction whereby the electrons of hydrogen atoms are each stimulated to relax to a lower energy level corresponding to a fractional quantum state by providing an energy hole resonant with this transition will occur during the electrolysis of  $\text{K}_2\text{CO}_3$ /light water solutions but will not occur during the electrolysis of  $\text{Na}_2\text{CO}_3$ /light water solutions. The results of the electrolysis with a nickel wire cathode at 83-mA constant current and heater run of  $\text{K}_2\text{CO}_3$  appear in Fig. 7 and Table II. The heating coefficient of the heater run (calibration) was 41°C/W, whereas the heating coefficient of the electrolysis run was 87°C/W. The production of excess enthalpy is observed. The higher the heating coefficient is, the more heat is released in the process.

The results of the electrolysis of a  $\text{K}_2\text{CO}_3$  electrolyte with a nickel cathode and a periodic square-wave having an offset voltage of 1.60 V, a peak voltage of 1.90 V, a peak constant current of 47.3 mA, a 36.0% duty cycle, and a frequency of 600 Hz appear in Fig. 8 and Table II. The output power was 16 times the ohmic input power.

The results of the electrolysis at 81-mA constant current and heater run of  $\text{Na}_2\text{CO}_3$  appear in Fig. 9 and Table II. The heating coefficient of the electrolysis run was 47°C/W, whereas the heating coefficient of the heater run (calibration) was 46°C/W. The production of excess heat is not observed.

The data of the faradaic efficiency of the production of gas by a potassium cell and a control sodium cell appear in Table III.

Almost all electrolysis experiments will be similar to the case of  $\text{Na}_2\text{CO}_3$ . Only a few combinations of electrolytes and electrodes, such as the  $\text{K}_2\text{CO}_3$  case, will yield excess heat.

TABLE I  
Duty Cycles for Experiments 5 Through 13

Experiment	Duty Cycle (%)
5	3
6	4
7	5
8	6
9	7
10	10
11	15
12	20
13	25

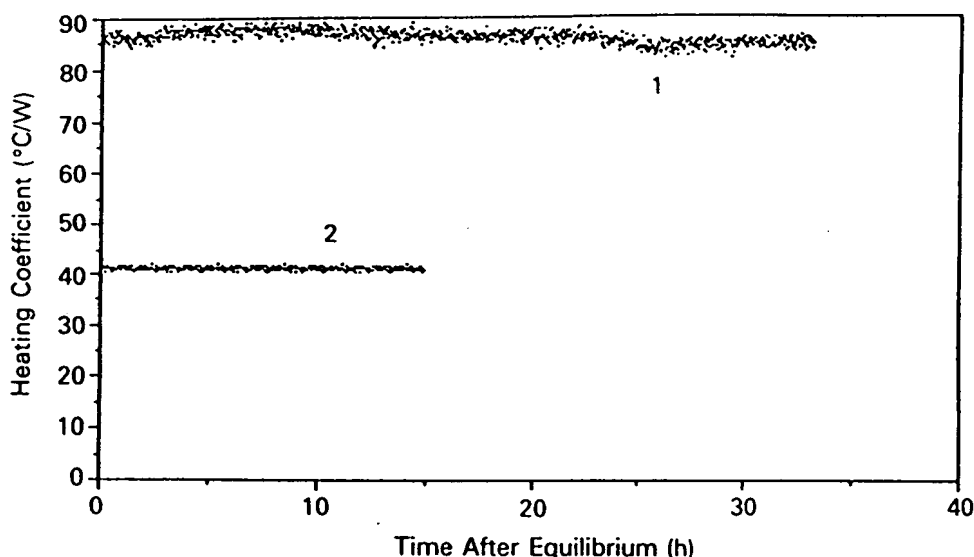


Fig. 7. Experiment 2: plot of the heating coefficients over time: (1) electrolysis with a nickel wire cathode at 0.083 A in  $K_2CO_3$  and (2) resistor working in  $K_2CO_3$ .

TABLE II  
Power Input and Output Parameters of Experiments 1 Through 14

Experiment Number	V (V)	Duty Cycle (%)	I (A)	VI Power (W)	(V - 1.48)/I Input Power (W)	Output Power (W)	Excess Power (W)	Output Input (%)
1	3.05	100	0.083	0.253	0.130	0.275	0.145	212
2 <sup>a</sup>	1.90	36	0.0473	0.032	0.007	0.114	0.107	1630
3	3.51	100	0.081	0.284	0.164	0.167	0.003	102
4	3.25	100	49.9	162	88.3	137	48.2	155
5 <sup>a</sup>	4.13	3	101	12.5	8.03	31.0	21.5	386
6 <sup>a</sup>	4.04	4	101	16.3	10.3	43.5	33.2	422
7 <sup>a</sup>	4.00	5	102	20.4	12.9	54.7	41.8	424
8 <sup>a</sup>	3.95	6	102	24.2	15.1	63.2	48.1	419
9 <sup>a</sup>	3.89	7	101	27.5	17.0	70.0	53.0	412
10 <sup>a</sup>	3.88	10	102	39.6	24.5	58.3	60.8	348
11 <sup>a</sup>	3.88	15	101	58.8	36.4	105.5	69.1	290
12 <sup>a</sup>	3.85	20	101	77.8	47.9	118.1	70.2	247
13 <sup>a</sup>	3.83	25	101	96.7	59.3	135	75.7	228
14 <sup>a</sup>	2.37	20	10.5	4.98	1.87	41.0	39.1	2193

<sup>a</sup>Output is greater than VI.

TABLE III  
Faradaic Efficiency of Gas Production by a  $K_2CO_3$  Cell and a  $Na_2CO_3$  Control Cell

Electrolyte	Faraday's Gas (mmol)	Calculated Volume (ml)	Measured Volume (ml)	Efficiency (%)
0.57 M $K_2CO_3$	1.961	49.91	51.30	102.8
0.57 M $Na_2CO_3$	1.955	49.69	49.86	100.3

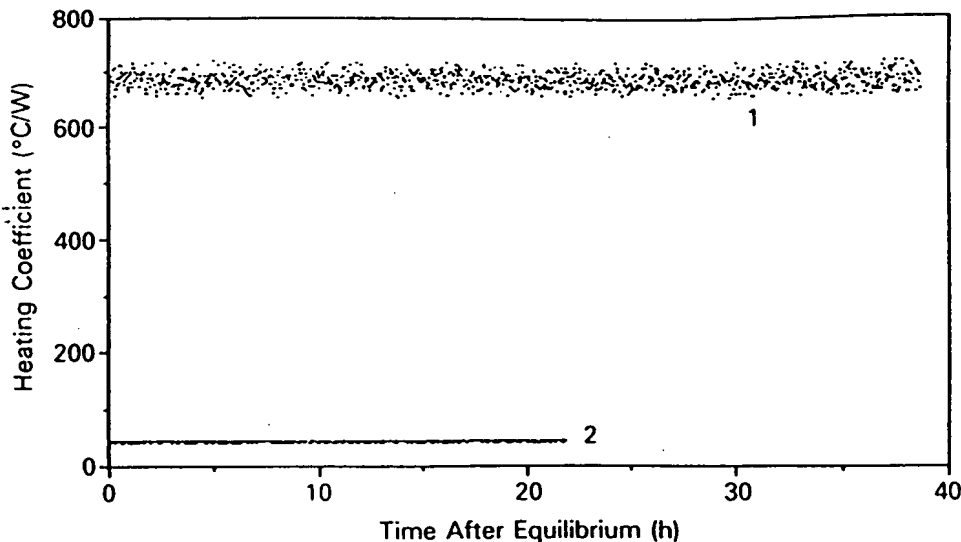


Fig. 8. Experiment 2: plot of the heating coefficients over time: (1) electrolysis with a nickel cathode and a periodic square wave having an offset voltage of 1.60 V, a peak voltage of 1.90 V, a peak constant current of 47.3 mA, a 36.0% duty cycle, and a frequency of 600 Hz in  $K_2CO_3$ , and (2) resistor working in  $K_2CO_3$ .

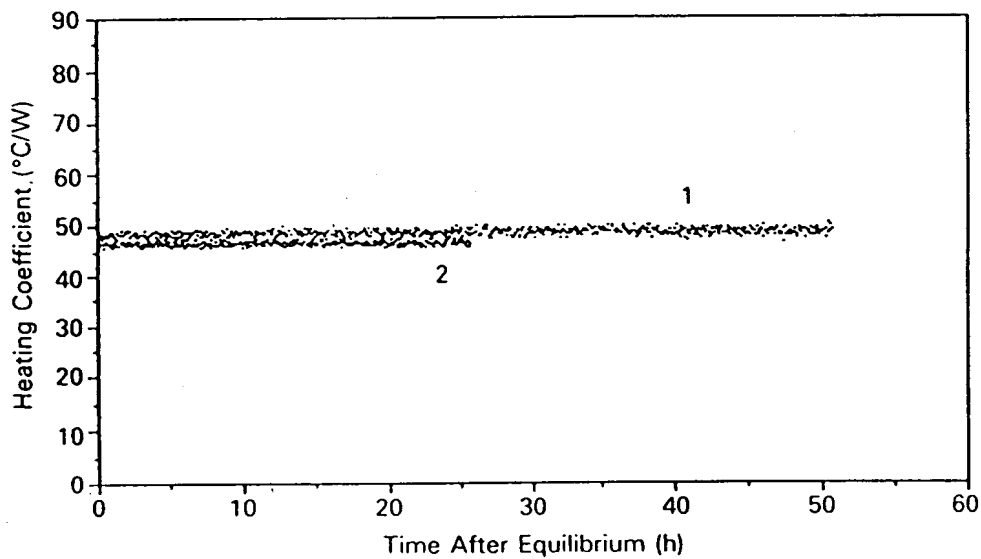


Fig. 9. Experiment 3: plot of the heating coefficients over time: (1) electrolysis at 0.081 A in  $Na_2CO_3$ , and (2) resistor working in  $Na_2CO_3$ .

Data from experiment 4 were recorded over a 29-day period. The voltage remained relatively constant at 2.35 V, and the electrolyte temperature was  $\sim 23^\circ C$  above the temperature of the blank. The parameters at day 27 are given in Table II. The on-the-fly calibration curve of experiment 4 as well as the integral calibration curve for the matched blank cell are shown in Fig. 10.

The on-the-fly heating coefficient of the electrolytic cell was  $(0.17 \pm 0.01)^\circ C/W$ . The intercept at zero in-

put power for the integrally calibrated electrolytic cell was  $8.2^\circ C$ , which indicates 48.2 W of excess heat.

It was observed that gas sparging in the electrolytic cell provides sufficient mixing in the absence of stirring so that temperature gradients were not observed to within their detection limit ( $\pm 0.1^\circ C$ ). The calibration (nonelectrolysis cell) was stirred at 250 rpm to compensate for the lack of stirring by gas sparging. It was determined that the stirring power increased the blank

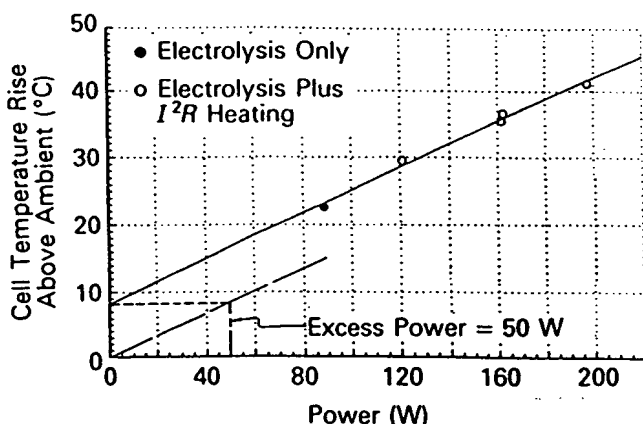


Fig. 10. A graphical determination of the excess power of experiment 4.

temperature  $0.20^{\circ}\text{C}$  above the ambient temperature, and this power was not subtracted from the blank temperature in the temperature measurements. Accounting for this temperature rise would increase the experimentally determined electrolytic cell excess energy by  $\sim 1.2$  W.

From the condensed evolving water vapor, the evaporative losses from experiment 4 were measured to be 6.5 ml per 24 h, and 402 ml of water was added to the cell per 24 h to maintain a constant fill level. The volume consumed by Faraday losses is calculated to be 403 ml. Thus, the evaporative and Faraday losses equaled the maintenance water volume to within 1%.

Elemental analysis and scanning electron microscopy of metallurgical samples of the nickel cathode taken before operation and at day 56 of continuous operation were identical, indicating that the nickel cathode had not changed chemically or physically. Elemental analysis data of a sample of the nickel cathode taken at day 56 of continuous operation are shown in Table IV. Photomicrographs of a sample of the nickel cathode taken at day 56 of continuous operation are shown in Fig. 11.

The cell was disassembled and inspected after 23

TABLE V  
Chemical Analysis of the Potassium Carbonate  
Electrolytic Solution of Experiment 4  
After 42 Days of Operation

Flame emission spectrographic analysis  
Mainly potassium  
Slight trace (100 to 1000 ppm) sodium  
Very slight trace (<10 ppm) magnesium  
Specific gravity = 1.072  
Concentration =  $0.63\text{ M K}_2\text{CO}_3$   
Solution pH = 11.5

days of continuous operation. This inspection showed no visible signs of a reaction between the electrodes and the electrolyte. The cell was reassembled, and it continued to operate with an excess power production of  $\sim 50$  W for an additional 19 days, after which time the voltage and current parameters of experiment 5 were initiated.

The pH, specific gravity, concentration of  $\text{K}_2\text{CO}_3$ , and elemental analysis of the electrolyte sample taken after 42 days of continuous operation were unchanged from the values obtained for the electrolyte sample before operation. These data are shown in Table V.

The results of the gas chromatographic analysis of the evolving electrolytic gases showed two-thirds hydrogen, one-third oxygen, and trace amounts of nitrogen. No significant quantities of CO or  $\text{CO}_2$  were found, confirming that the  $\text{K}_2\text{CO}_3$  electrolyte was not degraded during operation.

Measurements of neutrons were considered unnecessary since light water was used rather than deuterium oxide. Scintillation counter and photographic film measurements show no radiation above background was detected, indicating that nuclear reactions did not occur.

Data from experiments 5 through 13 were recorded over a 135-day period as the duty cycle was increased from 3 to 25%. The input and output powers are listed in Table II as a function of duty cycle. A comparison of cell temperature rise above ambient and power with the calibration curve is shown in Fig. 12. The comparison for experiment 9 shows  $\sim 53$  W of excess energy at a 7% duty cycle. This corresponds to an output over input power ratio of  $\sim 4.12:1$ .

Data from experiment 14 were recorded over a 240-day period at an operating condition of 1 Hz, 10 A, and 20% duty cycle. Data for day 120 are recorded in Table II and show 41 W of output with an output-to-input ratio of  $\sim 22$  assuming 100% Faraday efficiency. Actual Faraday efficiency at these low-current levels (2 A on average) has not been established. If the Faraday efficiency were zero (100% recombination), then the output-to-input ratio would be 8.2:1.

TABLE IV

Chemical Analysis of the Nickel Wire of Experiment 4  
After 56 Days of Operation

Mainly nickel  
Trace (0.1 to 1.0%) copper  
Slight trace (100 to 1000 ppm) magnesium  
Very slight trace (10 to 100 ppm) aluminum and manganese  
Very, very slight trace (<10 ppm) chromium, titanium, silver, tin, iron, silicon, boron, and phosphorus

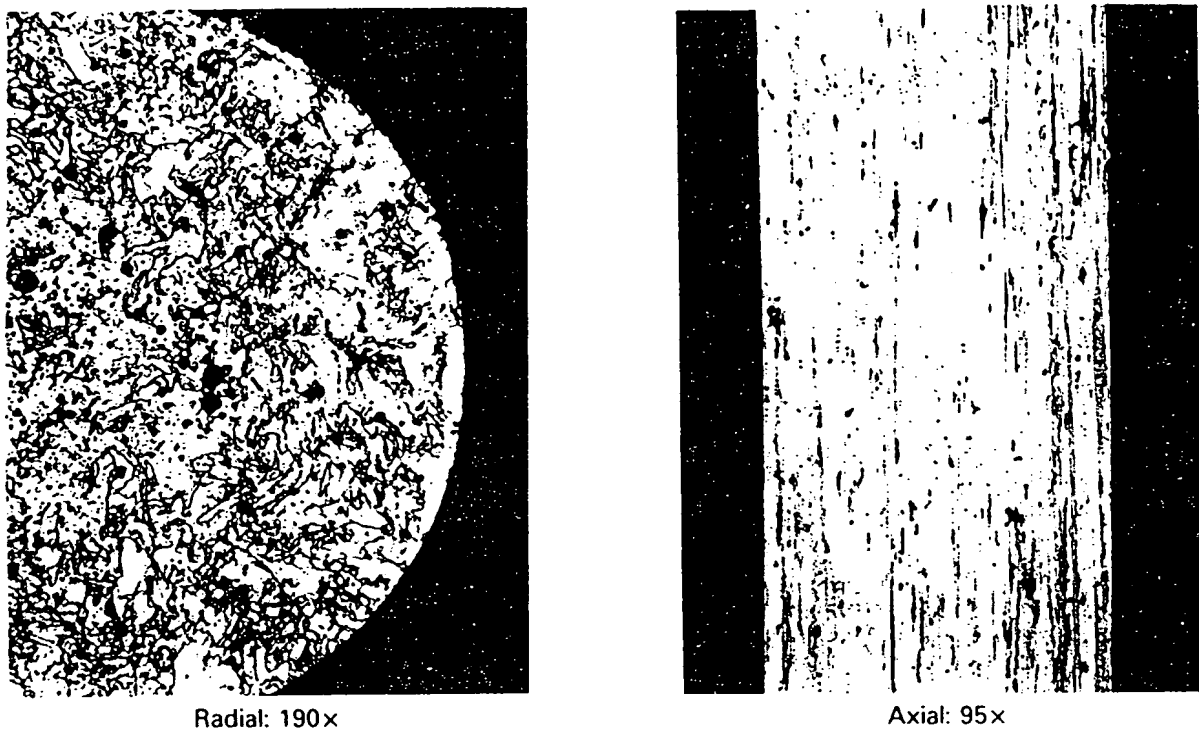


Fig. 11. Photomicrographs of metallurgical samples of the nickel cathode taken at day 56 of continuous operation.

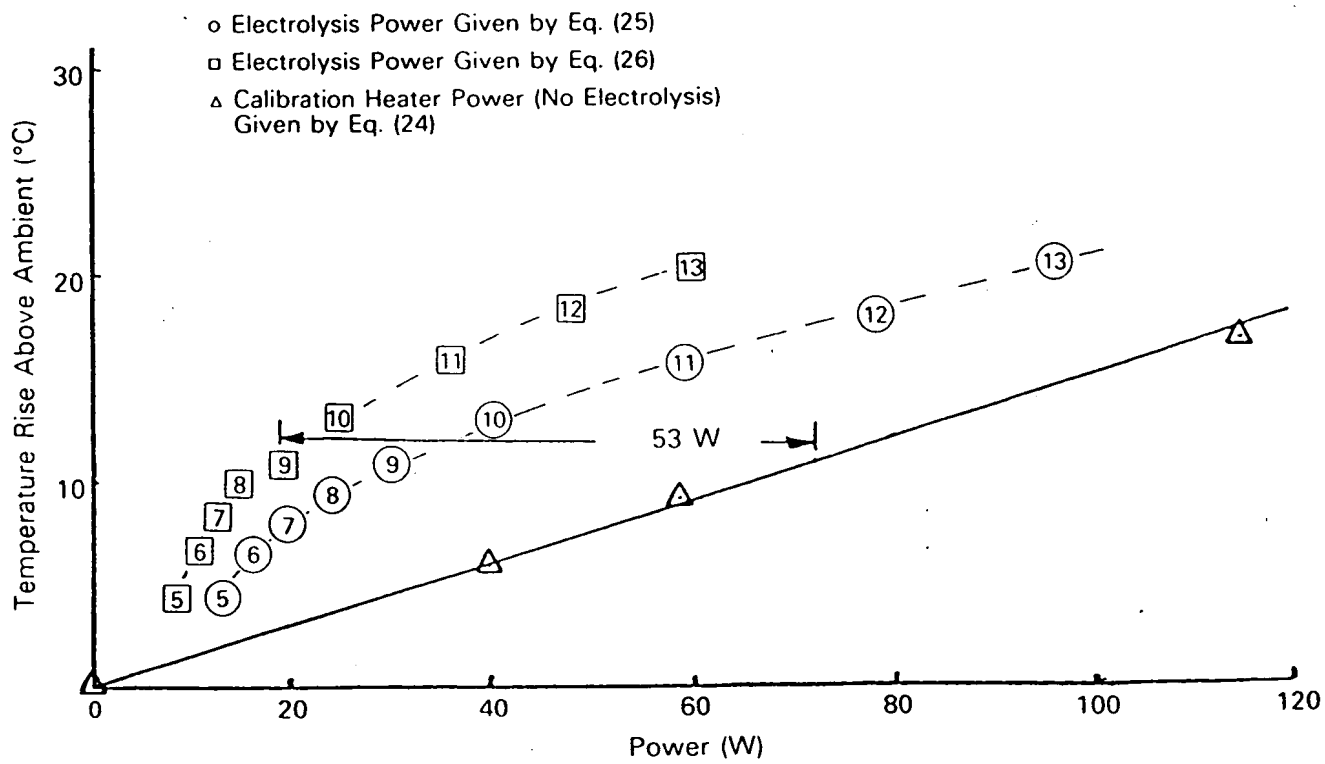


Fig. 12. Comparison between cell temperature rise above ambient for electrolysis power and for heater power for experiments 5 through 13.

## EXPERIMENTAL IDENTIFICATION OF THE DIHYDRINO MOLECULE

The dihydrino molecules would be stable to combustion relative to molecular hydrogen, and the dihydrino molecule could be detected by mass spectroscopy with the presence of a  $m/e = 2$  peak with a different branching ratio to form  $m/e = 1$  relative to  $m/e = 2$ . To test this premise, we collected in an elastomer bladder 1650 ml of the electrolysis gases from experiment 14, which produced 39.1 W of excess power according to the exothermic reaction given by Eqs. (4), (5), and (6). The bladder contained a spark plug that was activated, causing an explosion of the gas contents. The volume of the bladder following combustion was 70 ml. Samples of the pre- and postcombustion electrolysis gases as well as hydrogen and water-saturated air were analyzed by mass spectroscopy.

The dihydrino molecule,  $H_2^+$ , has a higher ionization energy than  $H_2$ . Mass spectroscopy of the postcombustion electrolysis gas sample was performed whereby the intensity of the  $m/e = 1$  and  $m/e = 2$  peaks was recorded while the ionization potential of the mass spectrometer was varied.

The results of the mass spectroscopic analysis of gases evolved from experiment 14 before and after combustion are given in Table VI; of room air saturated with water, in Table VII; of the standard hydrogen sample, in Table VIII; and of the postcombustion electrolysis gas sample whereby the intensity of the  $m/e = 1$  and  $m/e = 2$  peaks was recorded while the ionization potential of the mass spectrometer was varied, in Table IX.

## DISCUSSION

From Table VI, the  $m/e = 18$  and  $m/e = 32$  peak intensities, respectively, demonstrate that both the pre-

and postcombustion electrolysis gas samples contained the same percentage of water vapor and of  $O_2$ . The predicted percentage for the precombustion electrolysis gas sample is one-third, as given by Faraday's law for the electrolysis of water. The oxygen signal for the postcombustion electrolysis gases is higher than can be due to atmospheric contamination.

From Table VI, the  $m/e = 28$  peak intensity demonstrates that the pre- and postcombustion electrolysis gas samples contained the same percentage of nitrogen. The nitrogen was present in trace amounts in both gas samples as demonstrated by the  $m/e = 28$  peak intensities from Table VI and the volume change with combustion. From the volume change, nitrogen represented <4% of the precombustion gas sample, and the  $m/e = 28$  peak intensity of the postcombustion gas

TABLE VII  
Mass Spectroscopic Analysis of Room Air  
Saturated with Water  
( $IP = 70$  eV)

Mass/Charge ( $m/e$ )	Intensity ( $\times 10^{-7}$ )
1	0.24
2	0.040
18	43.0

TABLE VIII  
Mass Spectroscopic Analysis of Hydrogen  
( $IP = 70$  eV)

Mass/Charge ( $m/e$ )	Intensity ( $\times 10^{-7}$ )
1	2.0
2	300.0
3 HD	0.12
3 H <sub>3</sub>	2.0

TABLE IX  
Mass Spectroscopic Analysis with Varying Ionization Potential of Gases Evolved from the Cell of Experiment 14 Following Combustion

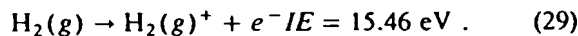
Ionization Potential (eV)	Intensity of Signal Mass-to-Charge Ratio	
	( $m/e = 1$ )	( $m/e = 2$ )
20	$0.007 \times 10^{-8}$	$0.03 \times 10^{-8}$
70	$1.8 \times 10^{-8}$	$1.8 \times 10^{-8}$

sample was only a factor of 2.4 of that of the precombustion electrolysis gas sample. No hydrogen is anticipated following combustion.

The data are consistent with the remaining two-thirds of the postcombustion electrolysis gases comprising the dihydrino molecule,  $H_2^*$ , which does not undergo combustion with oxygen. The stoichiometric ratio of two-thirds  $H_2^*$  to one-third  $O_2$  gives the correct mass balance. The  $m/e = 2$  peak for the postcombustion electrolysis gases is ten times the intensity of the peak from water [given by the product of the ratio of  $m/e = 2$  to  $m/e = 18$  of the water-saturated air mass spectrum times the intensity of the  $m/e = 18$  peak ( $H_2O$ ) of the postcombustion electrolysis gas sample]. Thus, the  $m/e = 2$  peak is assignable to  $H_2$  or to  $H_2^*$ .

The assignment to  $H_2^*$  is made as follows. The  $m/e = 1$  peak of the postcombustion electrolysis gas sample is significantly more intense than that predicted by production from water [given by the product of the ratio of  $m/e = 1$  to  $m/e = 18$  of the water-saturated air mass spectrum times the intensity of the  $m/e = 18$  peak ( $H_2O$ ) of the postcombustion gas sample]. The additional contribution to the  $m/e = 1$  peak predicted with the assignment of the  $m/e = 2$  peak to hydrogen (given by the product of the ratio of  $m/e = 1$  to  $m/e = 2$  of the hydrogen mass spectrum times the intensity of the  $m/e = 2$  peak of the postcombustion electrolysis gas sample) is insufficient to explain the intensity of the  $m/e = 1$  peak. Thus, the species giving rise to the  $m/e = 2$  peak must have a different  $m/e = 1$  to  $m/e = 2$  production efficiency than  $H_2$ . Therefore, the  $m/e = 2$  peak is assigned to  $H_2^*$ .

The dihydrino molecule,  $H_2^*$ , has a higher ionization energy than  $H_2$ . This was observed by measuring the intensity of the  $m/e = 1$  and  $m/e = 2$  peaks while the ionization potential of the mass spectrometer was varied. The ionization reaction of  $H_2$  is



The ionization energies of water are 12.61, 14.8, 18.8, and 32 eV. The data of Table IX demonstrate that no  $m/e = 2$  peak is present at an ionization potential above the threshold for the ionization of molecular hydrogen, but a  $m/e = 2$  peak that is too intense to be attributed to water ionization is present at a significantly higher ionization potential. The data are consistent with the assignment of  $m/e = 2$  to  $H_2^*$ , the dihydrino molecule.

## CONCLUSION

We review and present three sets of heat production and product identification data including the work of HydroCatalysis Power Corporation (experiments 1, 2, and 3) and Thermacore, Inc. (experiments 4 through 14). We report here experimental evidence supporting the HPC theory that an exothermic reaction occurs wherein the electrons of hydrogen and deuterium atoms

are each stimulated to relax to a quantized potential energy level below that of the ground state via electrochemical reactants  $K^+$  and  $K^+$ ;  $Pd^{2+}$  and  $Li^+$ ; or  $Pd$  and  $O_2$  of redox energy resonant with the energy hole that stimulates this transition. Calorimetry of pulsed current and continuous electrolysis of aqueous potassium carbonate ( $K^+/K^+$  electrocatalytic couple) at a nickel cathode was performed. The excess output power of 41 W exceeded the total input power given by the product of the electrolysis voltage and current by a factor of  $>8$ . The product of the exothermic reaction is atoms having electrons each of energy below the ground state, and they are predicted to form molecules. The predicted molecules were identified by their lack of reactivity with oxygen, by separation from molecular deuterium by cryofiltration, and by mass spectroscopic analysis.

The combustion of the gases evolved during the electrolysis of a  $K_2CO_3$ /light water electrolyte ( $K^+/K^+$  electrocatalytic couple) with a nickel cathode was incomplete. The mass spectroscopic analysis of uncombusted gases demonstrated that the species predominantly giving rise to the  $m/e = 2$  peak must have a different  $m/e = 1$  to  $m/e = 2$  production efficiency than hydrogen. The further mass spectroscopic analysis of the  $m/e = 2$  peak of the uncombusted gas demonstrated that the dihydrino molecule,  $H_2^*$ , has a higher ionization energy than  $H_2$ .

The mass spectroscopic analysis of the cryofiltered gases evolved during the electrolysis of a heavy water  $LiOD$  electrolyte ( $Pd^{2+}/Li^+$  electrocatalytic couple) with a palladium cathode demonstrated that the dideutriino molecule,  $D_2^*$ , has a higher ionization energy than  $D_2$ .

Palladium sheets coated on one side with a hydrogen-impermeable gold layer and on the other surface with an oxide coat ( $MnO_x$ ,  $AlO_x$ , or  $SiO_x$ ) were loaded with deuterium or hydrogen. Heat was observed from light and heavy hydrogen only when the mixed oxide coat was present ( $Pd/O_2$  electrocatalytic couple). The high-resolution (0.001 amu) quadrupole mass spectroscopic analysis of the gases released when a current was applied to a deuterium-loaded (99.9%),  $MnO_x$ -coated palladium sheet indicate the presence of a large shoulder on the  $D_2$  peak that is due to the dideutriino molecule,  $D_2^*$ .

Further experiments are planned to demonstrate that this lower energy form of hydrogen is the product of heat-producing cells. Following cryofiltration of the electrolysis gases, the dihydrino molecule is distinguished from normal molecular hydrogen by mass spectroscopy. The branching ratio to form  $m/e = 1$  relative to  $m/e = 2$  that is observed for the dihydrino molecule is different from the ratio that is observed for normal molecular hydrogen. Mass spectroscopy further distinguishes a sample containing dihydrino molecules from a sample containing  $H_2$  by showing a different ion production efficiency as a function of ionization potential and a different ion production efficiency at a

given ionization potential for the two samples. High-resolution mass spectroscopy shows two peaks for a mixture of H<sub>2</sub> and H<sub>2</sub><sup>+</sup>.

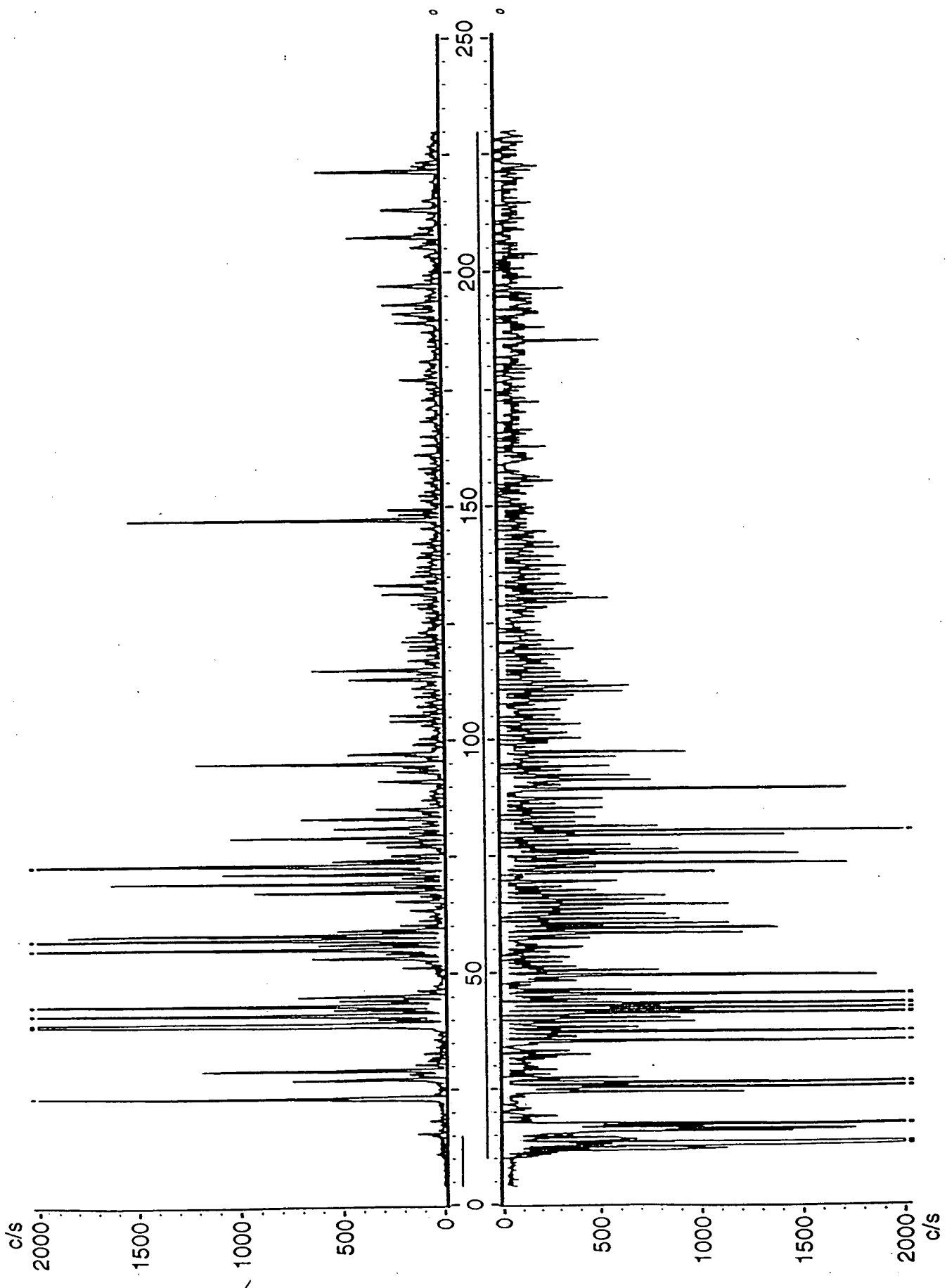
#### ACKNOWLEDGMENTS

Special thanks to J. Farrell for technical support, papers, discussions, and review of this manuscript and to D. Parees, of Air Products Corporation, who performed the mass spectroscopy.

#### REFERENCES

1. H. A. HAUS, "On the Radiation from Point Charges," *Am. J. Phys.*, **54**, 1126 (1986).
2. R. MILLS, *Unification of Spacetime, the Forces, Matter, and Energy*, Technomics Publishing Company, Lancaster, Pennsylvania (1992).
3. R. NIEMINEN, "Atoms Band Together," *Nature*, **365**, 289 (1992).
4. J. FARRELL, W. GOOD, and R. MILLS, "An Alternative Explanation of Extreme Ultraviolet Emissions from Dark Matter," submitted to *Astrophys. Lett. Communications* (1993).
5. M. H. MILES, B. F. BUSH, G. S. OSTROM, and J. J. LAGOWSKI, "Helium Production During the Electrolysis of D<sub>2</sub>O in Cold Fusion Experiments," *J. Electroanal. Chem.*, **304**, 271 (1991).
6. R. DAGANL, "New Evidence Claimed for Nuclear Process in Cold Fusion," *Chem. Eng. News*, 31 (Apr. 1, 1991).
7. M. H. MILES, B. F. BUSH, G. S. OSTROM, and J. J. LAGOWSKI, "Heat and Helium Production in Cold Fusion Experiments," *Proc. Conf. The Science of Cold Fusion*, Como, Italy, June 29-July 4, 1991, p. 363, T. BRESSANI, E. DEL GIUDICE, and G. PREPARATA, Eds., SIF (1991).
8. M. H. MILES, R. A. HOLLINS, B. F. BUSH, J. J. LAGOWSKI, and R. E. MILES, "Correlation of Excess Power and Helium Production During D<sub>2</sub>O and H<sub>2</sub>O Electrolysis Using Palladium Cathodes," *J. Electroanal. Chem.*, **346**, 99 (1993).
9. C. C. CHIEN, D. HODKO, Z. MINEVSKI, and J. BOCKRIS, "On an Electrode Producing Massive Quantities of Tritium and Helium," *J. Electroanal. Chem.*, **338**, 189 (1992).
10. B. F. BUSH, Department of Chemistry, University of Texas, Austin, Personal Communication (1993).
11. S. JONES, Newsgroups: sci.physics.fusion (Mar. 3, 1993).
12. M. H. MILES and B. F. BUSH, "Search for Anomalous Effects Involving Excess Power and Helium During D<sub>2</sub>O Electrolysis Using Palladium Cathodes," *Proc. 3rd Int. Conf. Cold Fusion*, Nagoya, Japan, October 21-25, 1992, p. 189.
13. B. REES, "Cold Fusion: What Do We Know? What Do We Think?" *J. Fusion Energy*, **10**, 1, 111 (1991).
14. E. YAMAGUCHI and T. NISHIOKA, "Direct Evidence for Nuclear Fusion Reactions in Deuterated Palladium," *Proc. 3rd Int. Conf. Cold Fusion*, Nagoya, Japan, October 21-25, 1992.
15. E. YAMAGUCHI and T. NISHIOKA, "Helium-4 Production from Deuterated Palladium at Low Energies," NTT Basic Research Laboratories and IMRA Europe S.A., Personal Communication (1992).

All Data Displays - w/o Peak Picking



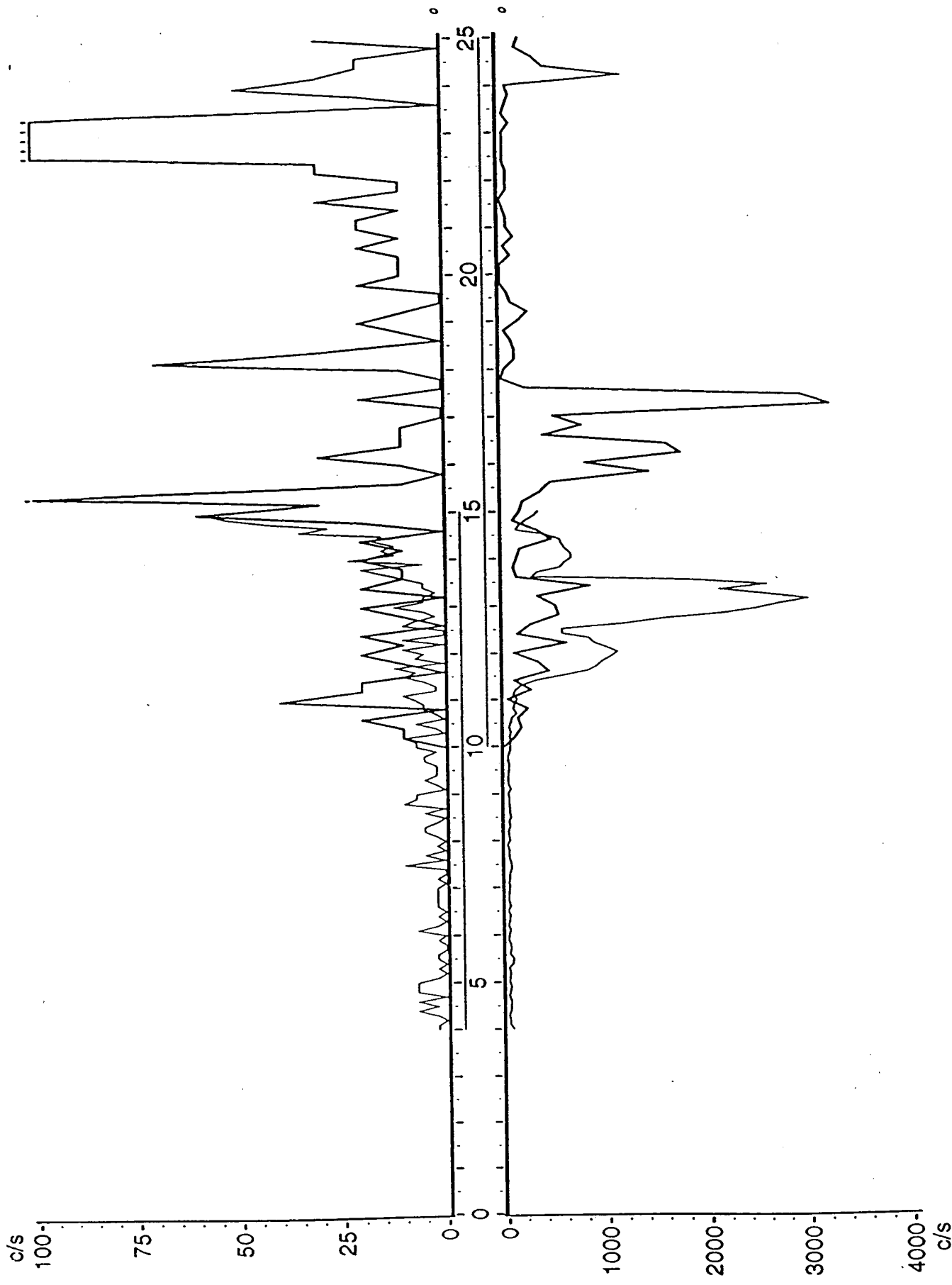
08:57:30 11/18/1993 08:57:30

C:\MASSDEMO\DATA\111893B.DAT Record: 1

08:28:08 11/18/1993 08:31:32

C:\MASSDEMO\DATA\111893A.DAT Record: 1

All Data Depth / No Peak Picking)  
Wine - November 18, 1993



06:57:30 11/18/1993 06:57:38

C:\MASSDEMO\DATA\111663B.DAT

06:28:08 11/18/1993 06:31:32

C:\MASSDEMO\DATA\111663A.DAT

Record: 1

Record: 1

**Cursor**

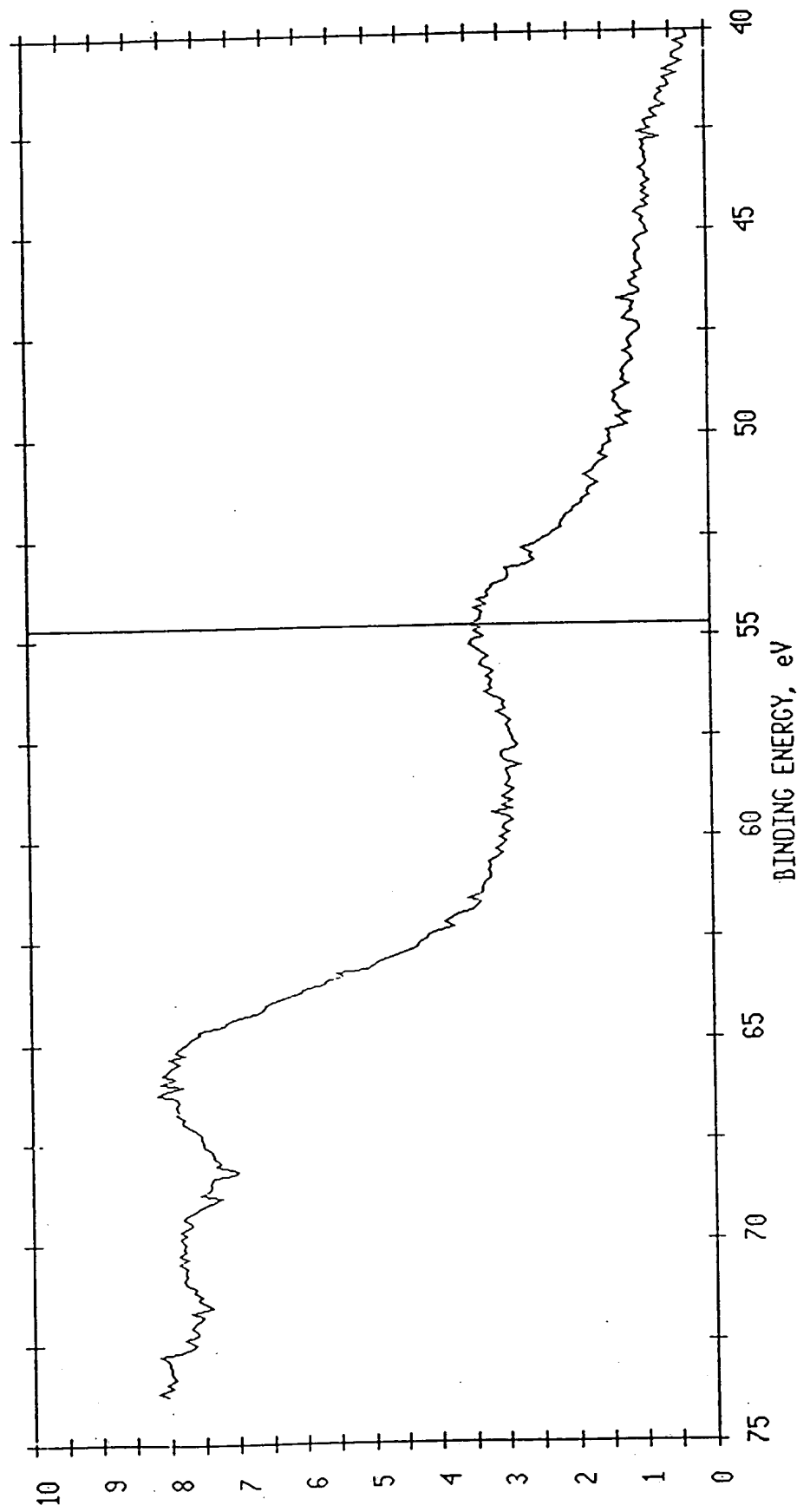
**Energy (eV)**

**54.700**

**Counts**

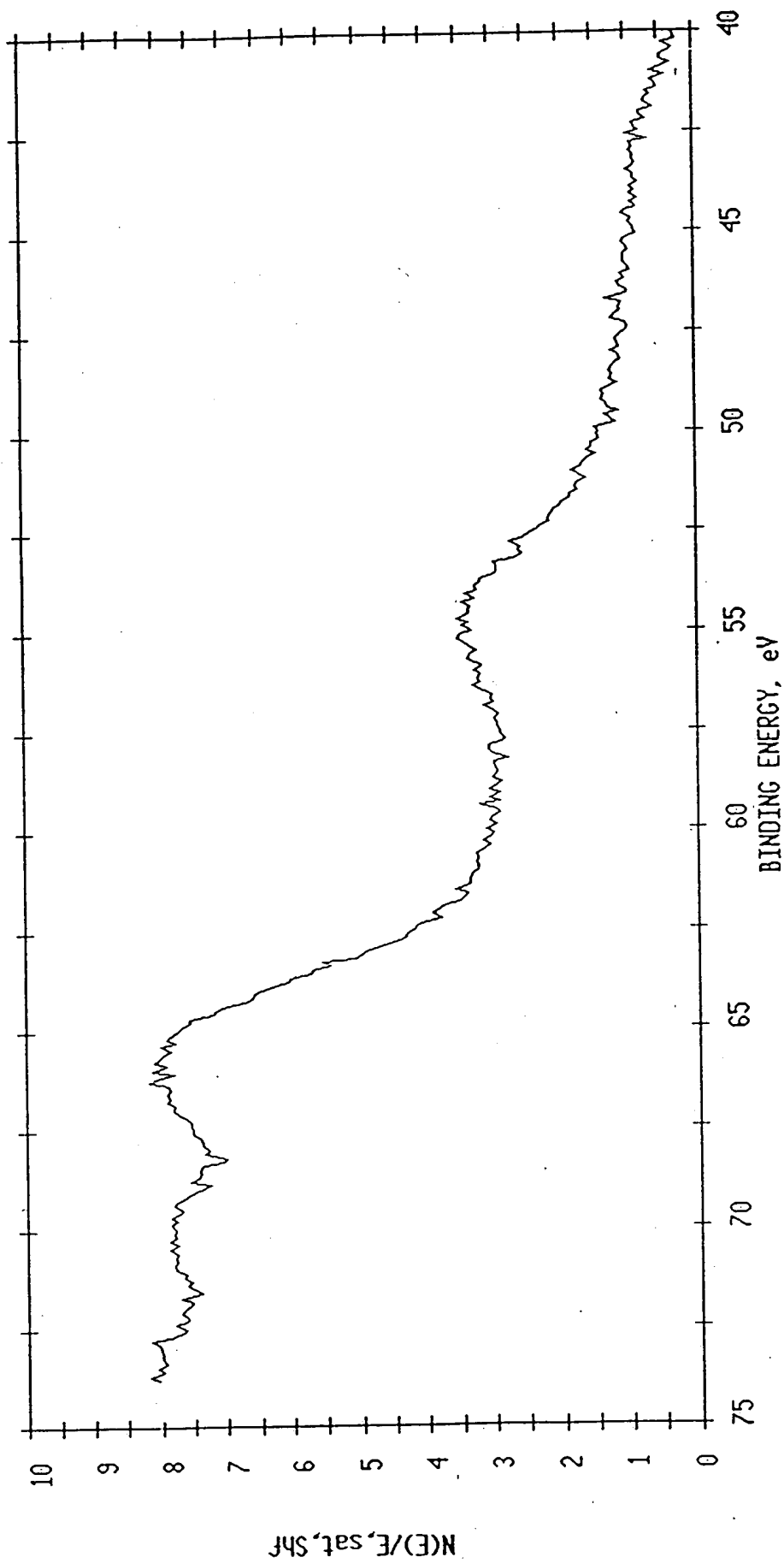
**28173 Counts/Sec**

**1445**

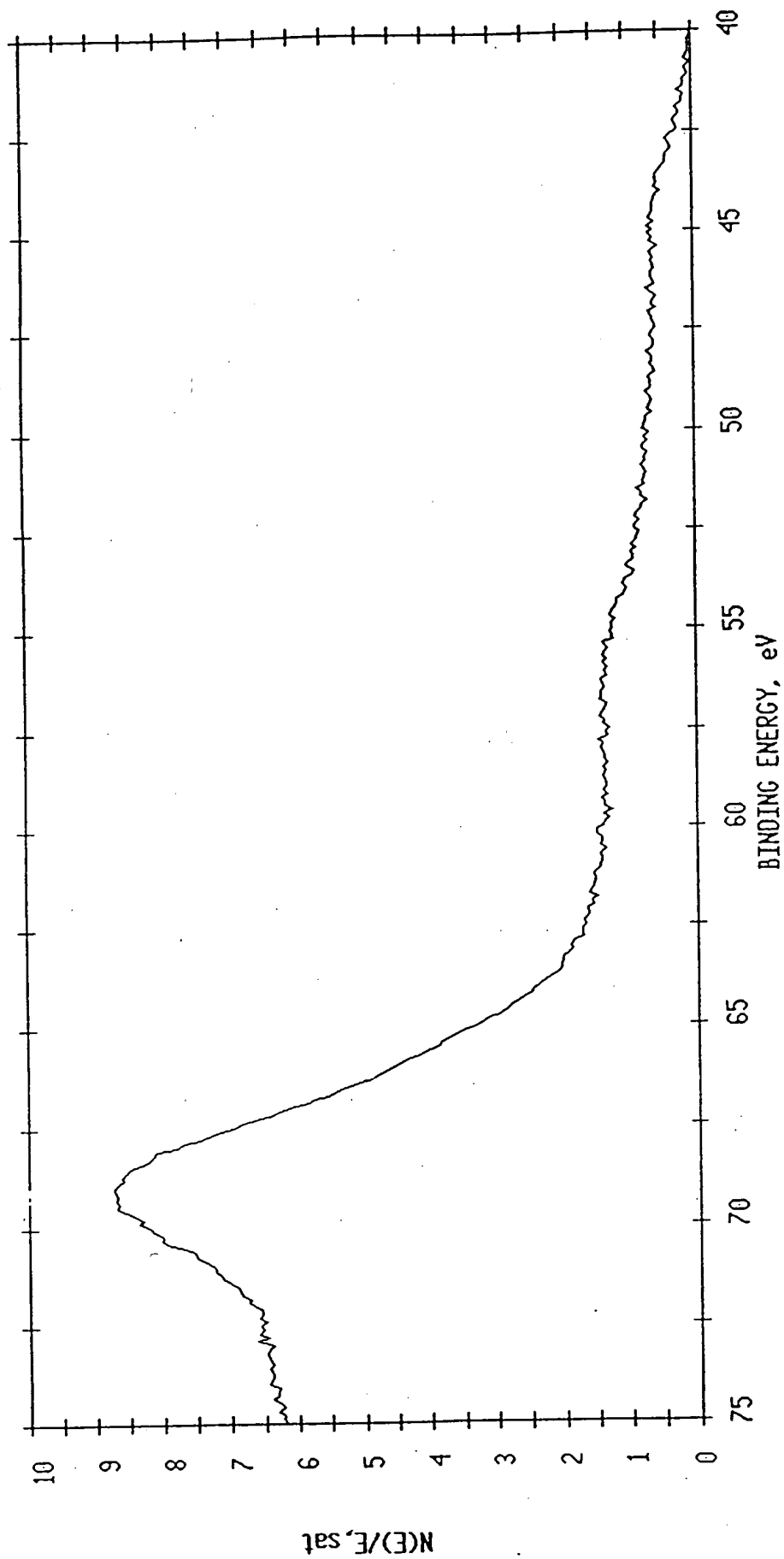


**N(E)/E, sat, Shf**

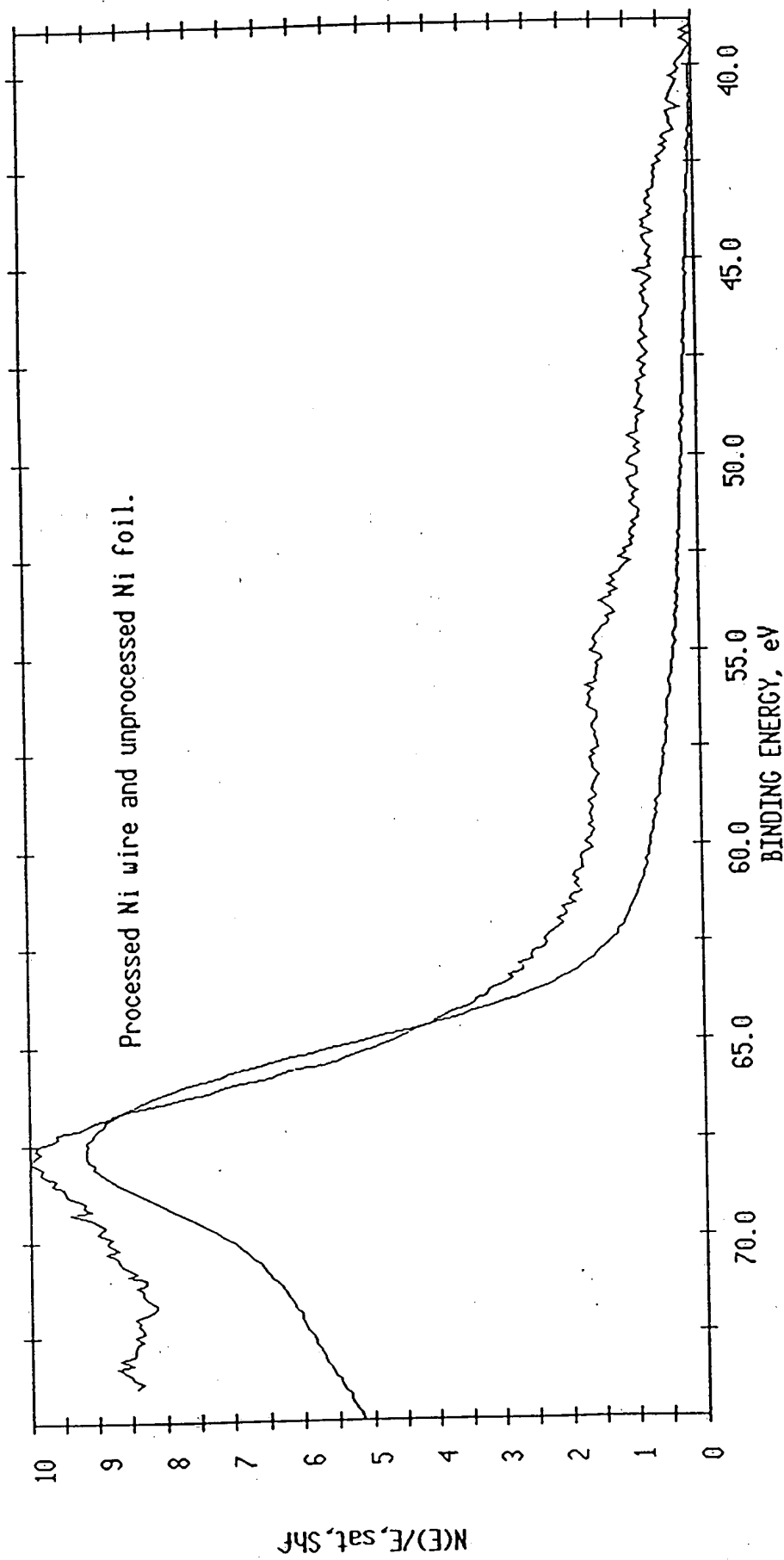
ESCA MULTIPLEX 11/24/93 EL= REG 2 ANGLE= 15 deg ACQ TIME=114.08 min  
FILE: Nitest50 Ni wire treated overnight at IRC.  
SCALE FACTOR= 0.116 k c/s, OFFSET= 1.036 k c/s PASS ENERGY=143.050 eV AI 400 W



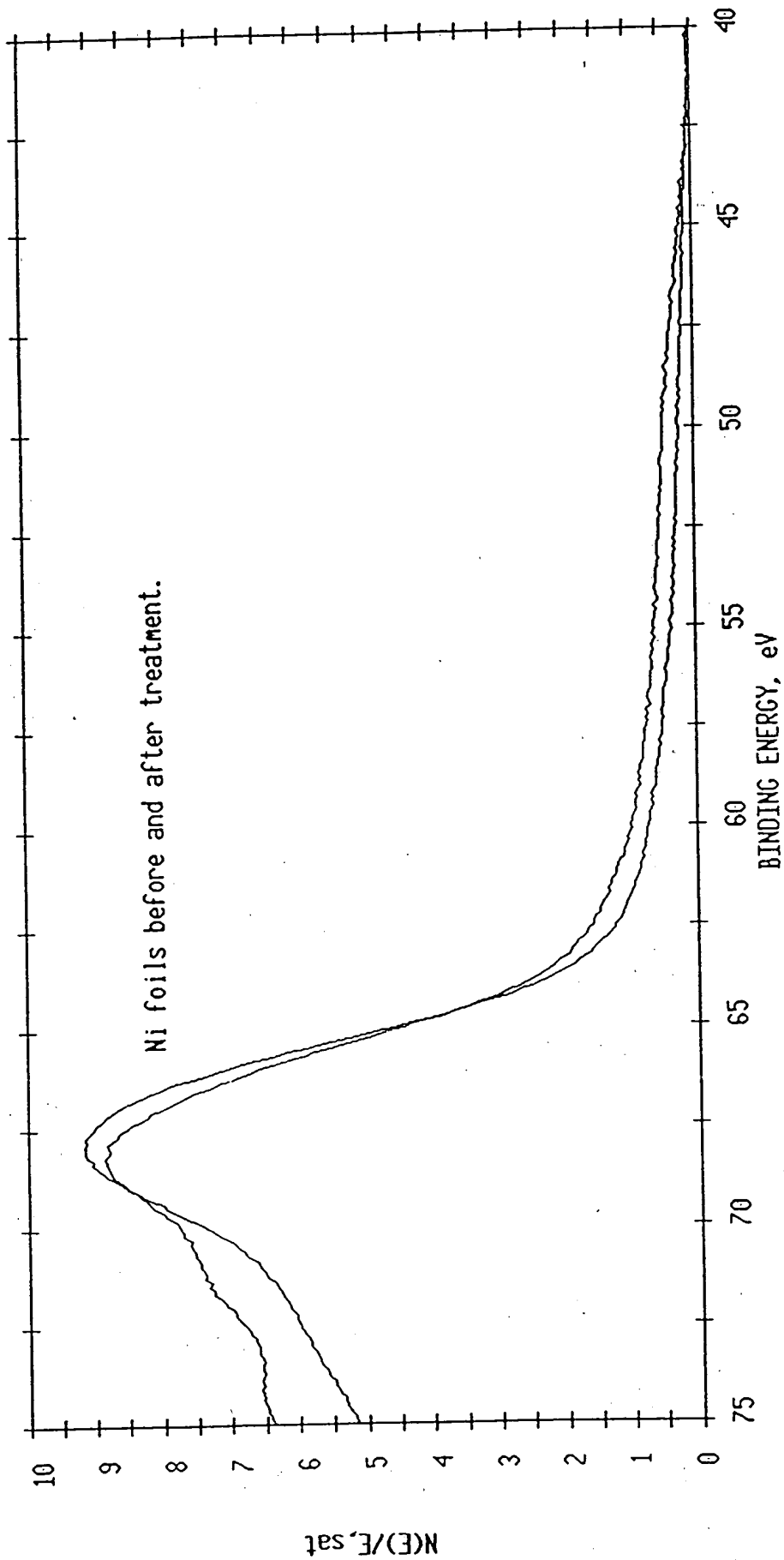
ESCA MULTIPLEX 11/22/93 EL= REG 2 ANGLE= 15 deg ACQ TIME=96.53 min  
FILE: Nitest32 2nd Ni wire treated prior to IRC.  
SCALE FACTOR= 0.274 k c/s, OFFSET= 1.580 k c/s PASS ENERGY=143.050 ev A1 400 W



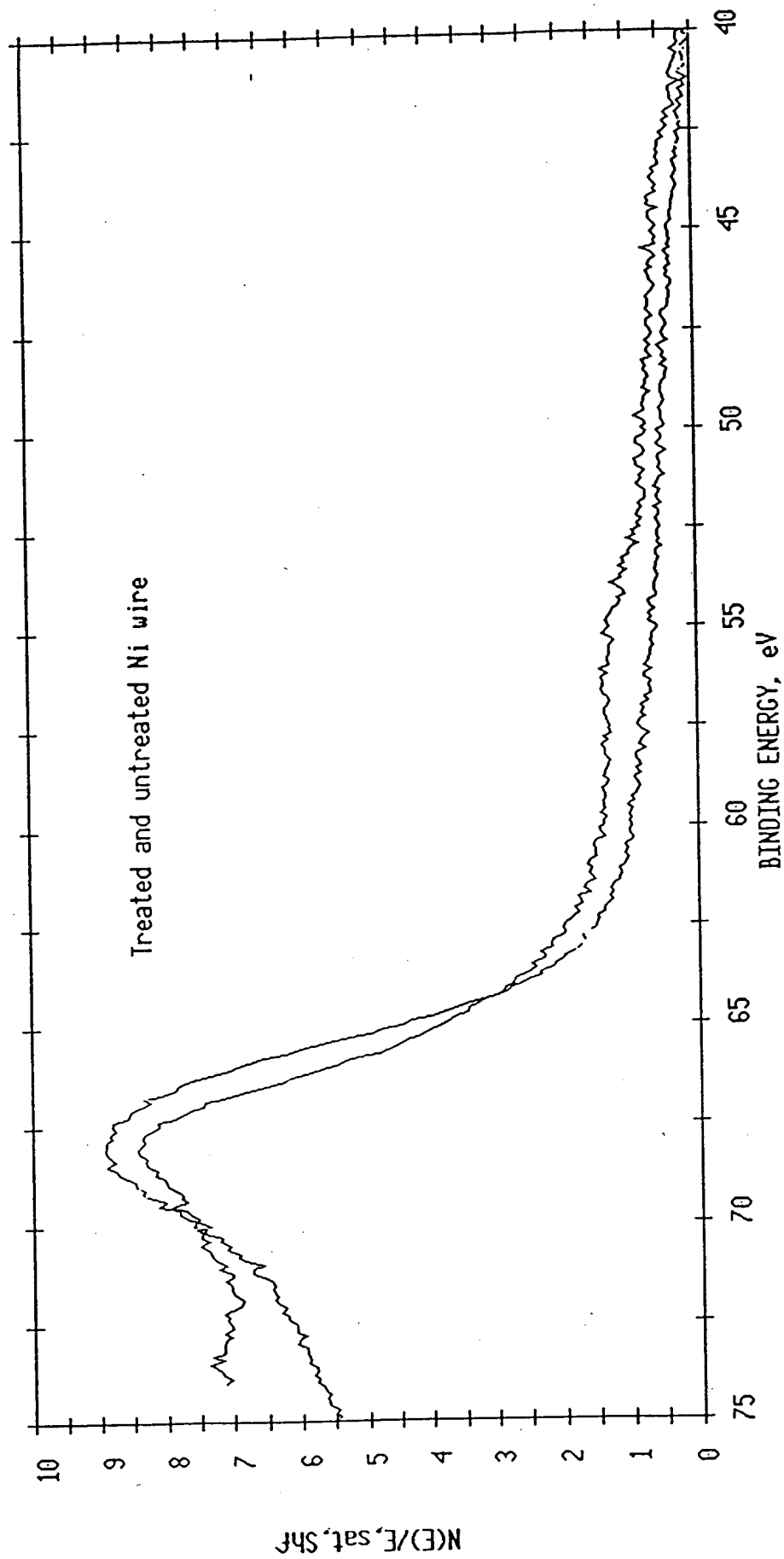
ESCA MULTIPLEX 11/18/93 EL= REG 2 ANGLE= 15 deg ACO TIME=76.05 min  
FILE: Nitest22 Ni foil untreated. as received.  
SCALE FACTOR= 3.401 k c/s, OFFSET= 9.545 k c/s PASS ENERGY=143.050 eV Al 400 W



ESCA MULTIPLEX 11/19/93 EL= REG 2 ANGLE= 15 deg ACQ TIME=84.83 min  
FILE: Nitest25 Ni foil treated in lab for 24 hr. As received.  
SCALE FACTOR= 1.920 k c/s, OFFSET= 8.515 k c/s PASS ENERGY=143.050 eV Al 400  $\mu$



ESCA MULTIPLEX 11/18/93 EL= REG 2 ANGLE= 15 deg ACQ TIME=67.28 min  
FILE: Nitest20 Ni wire processed in lab. as received.  
SCALE FACTOR= 0.331 k c/s, OFFSET= 2.436 k c/s PASS ENERGY=143.050 eV Al 400 W



ESCA MULTIPLEX 11/19/93 EL= REG 2 ANGLE= 15 deg ACQ TIME=61.43 min  
FILE: Nitest27 Ni wire untreated (base line) using Al X-Ray's.  
SCALE FACTOR= 0.326 k c/s, OFFSET= 1.491 k c/s PASS ENERGY=143.050 eV Al 400 K

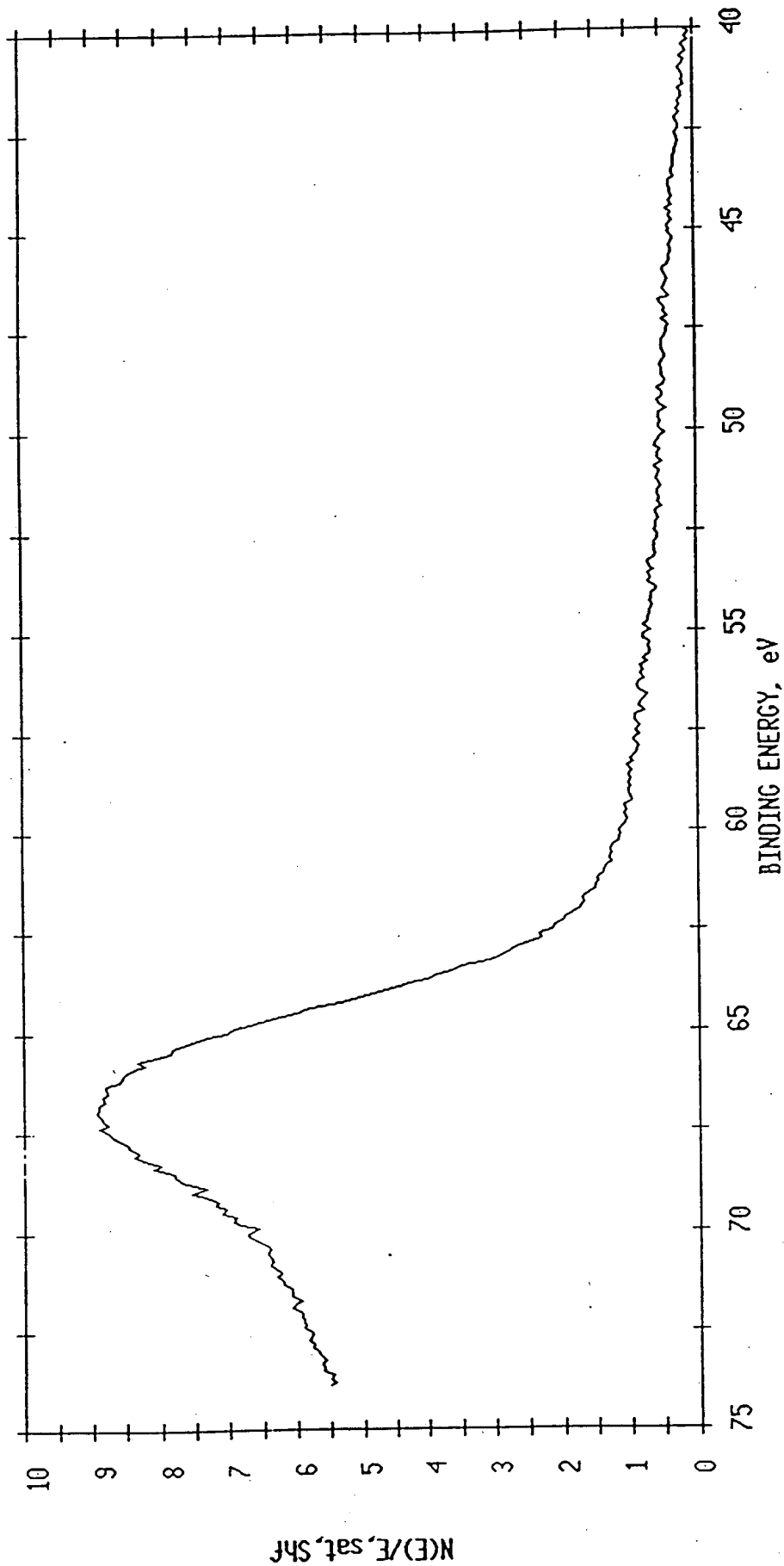
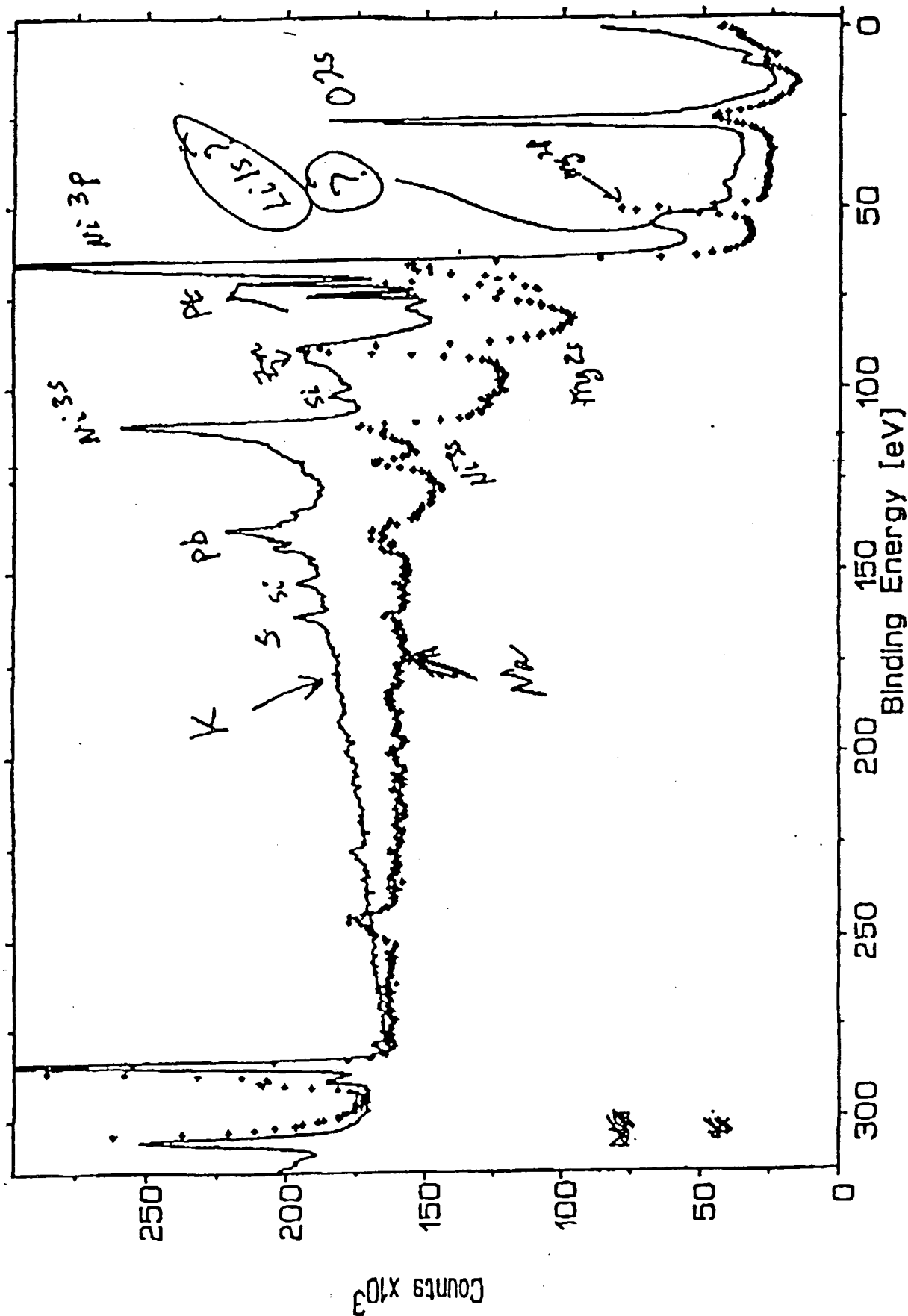


Figure 4 A



Several examples of different energy holes effecting shrinkage and the corresponding effective nuclear charges, total energy released, and final radii of the orbitspheres going from infinity to the final radius,  $a_0/(m + 1)$  are given in Table 20.1.

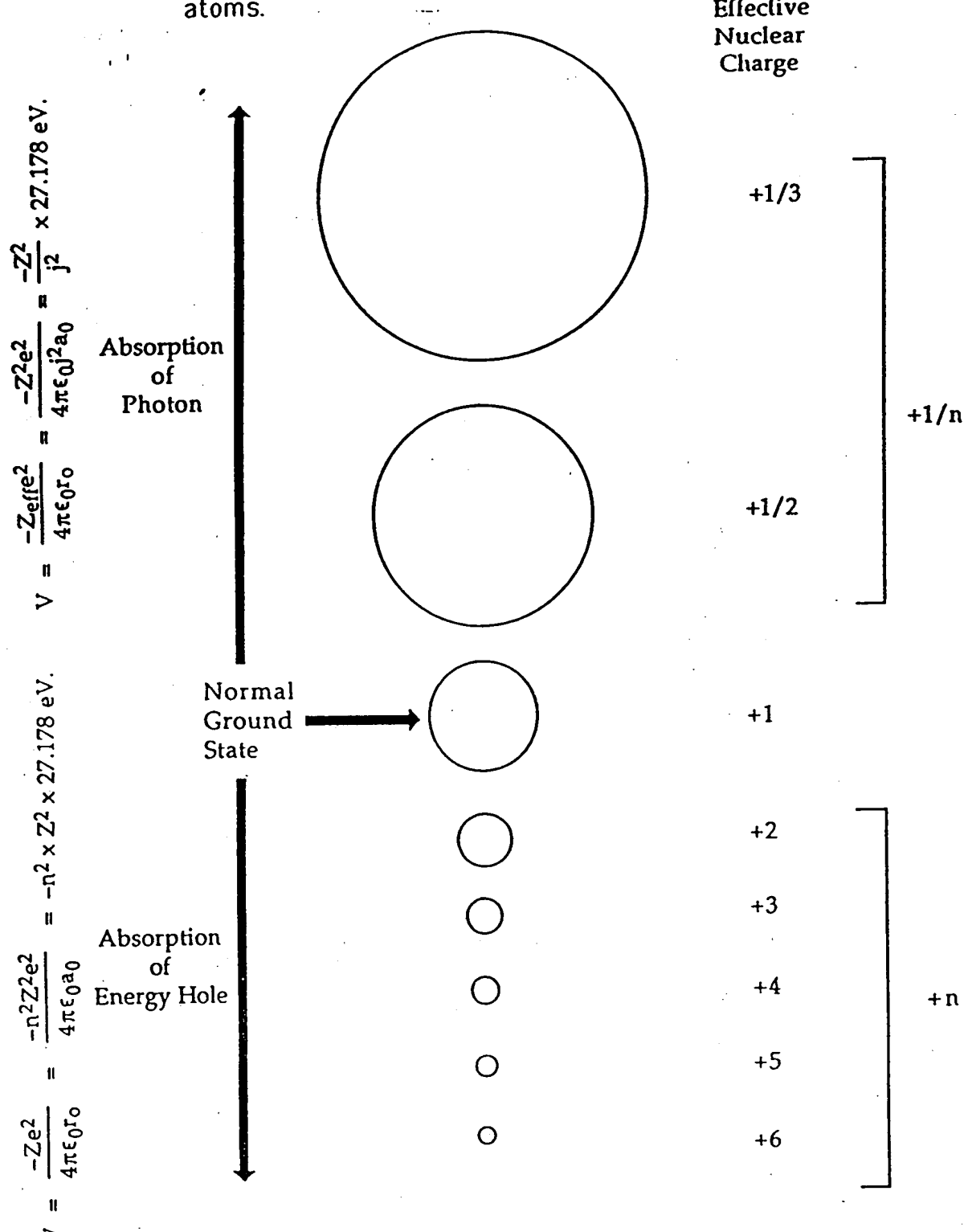
Table 20.1. Radii, energies, energy holes, and energy released for several states of hydrogen or deuterium.

n	R	V(eV)	T(eV)	Zeff	energy hole (eV)	total energy released (eV) $r = \infty$ to $r = R$
-	$a_0$	-27.2	13.6	1	-	13.6
1	$a_0/2$	-108.8	54.4	2	27.2	54.4
2	$a_0/3$	-244.9	122.4	3	54.4	122.4
3	$a_0/4$	-435.4	217.7	4	81.6	217.7
4	$a_0/5$	-680.2	340.1	5	108.8	340.1
5	$a_0/6$	-979.6	489.6	6	136.1	489.6
6	$a_0/7$	-1333.3	666.4	7	163.3	666.4
7	$a_0/8$	-1741.4	870.4	8	190.5	870.4
8	$a_0/9$	-2204.0	1101.6	9	217.7	1101.6
9	$a_0/10$	-2721.0	1360.5	10	244.9	1360.5

Energy released for any transition is given by  $\Delta E_{\text{final}} (\infty \text{ to } R) - \Delta E_{\text{initial}} (\infty \text{ to } R)$

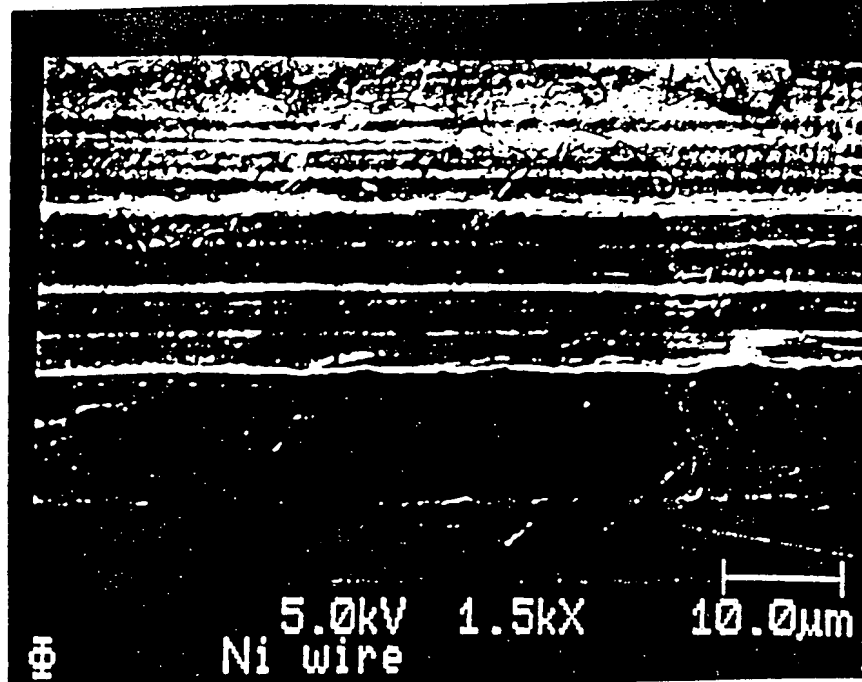
The size of the electron orbitsphere as a function of potential energy is given in Figure 20.2.

Figure 20.2. Quantized sizes and energies of hydrogen or deuterium atoms.



**CAF**  
The electric potential  $V_n$  where  $n = 1, 2, \dots, \infty$  is given by  $V_n = -\frac{Z^2 e^2}{4\pi \epsilon_0 r_n}$ , where  $r_n$  is the separation between the nucleus and the electron. For example, the potential of a muon to electron separation is  $V_{\mu-e} = -\frac{Z_{\mu} Z_e e^2}{4\pi \epsilon_0 r_{\mu-e}}$ . The potential of a deuterium nucleus to an electron is  $V_{D-e} = -\frac{Z_D Z_e e^2}{4\pi \epsilon_0 r_{D-e}}$ . The potential of a proton to an electron is  $V_{p-e} = -\frac{Z_p Z_e e^2}{4\pi \epsilon_0 r_{p-e}}$ . The potential of a deuteron to an electron is  $V_{D-e} = -\frac{Z_D Z_e e^2}{4\pi \epsilon_0 r_{D-e}}$ . The potential of a triton to an electron is  $V_{T-e} = -\frac{Z_T Z_e e^2}{4\pi \epsilon_0 r_{T-e}}$ . The potential of a helium-3 nucleus to an electron is  $V_{He-3-e} = -\frac{Z_{He-3} Z_e e^2}{4\pi \epsilon_0 r_{He-3-e}}$ . The potential of a helium-4 nucleus to an electron is  $V_{He-4-e} = -\frac{Z_{He-4} Z_e e^2}{4\pi \epsilon_0 r_{He-4-e}}$ . The potential of a helium-3 nucleus to a deuteron is  $V_{He-3-D} = -\frac{Z_{He-3} Z_D e^2}{4\pi \epsilon_0 r_{He-3-D}}$ . The potential of a helium-4 nucleus to a deuteron is  $V_{He-4-D} = -\frac{Z_{He-4} Z_D e^2}{4\pi \epsilon_0 r_{He-4-D}}$ . The potential of a helium-3 nucleus to a triton is  $V_{He-3-T} = -\frac{Z_{He-3} Z_T e^2}{4\pi \epsilon_0 r_{He-3-T}}$ . The potential of a helium-4 nucleus to a triton is  $V_{He-4-T} = -\frac{Z_{He-4} Z_T e^2}{4\pi \epsilon_0 r_{He-4-T}}$ . The potential of a deuteron to a triton is  $V_{D-T} = -\frac{Z_D Z_T e^2}{4\pi \epsilon_0 r_{D-T}}$ .

Hydrogen ground state is a proton. In photons.



Φ

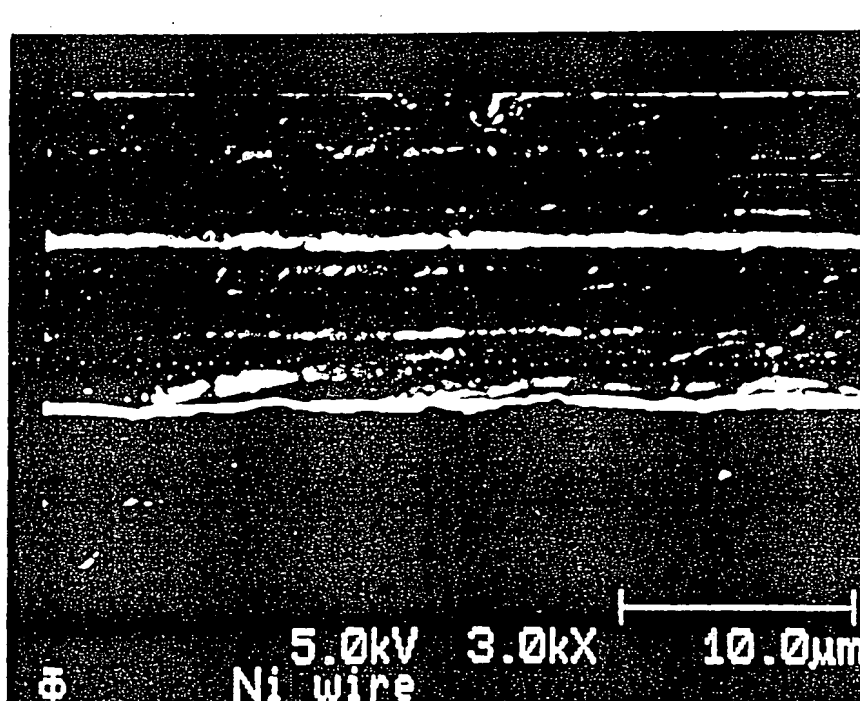
Ni wire

5.0kV

1.5kX

10.0μm

File N-test 104



Φ

Ni wire

5.0kV

3.0kX

10.0μm

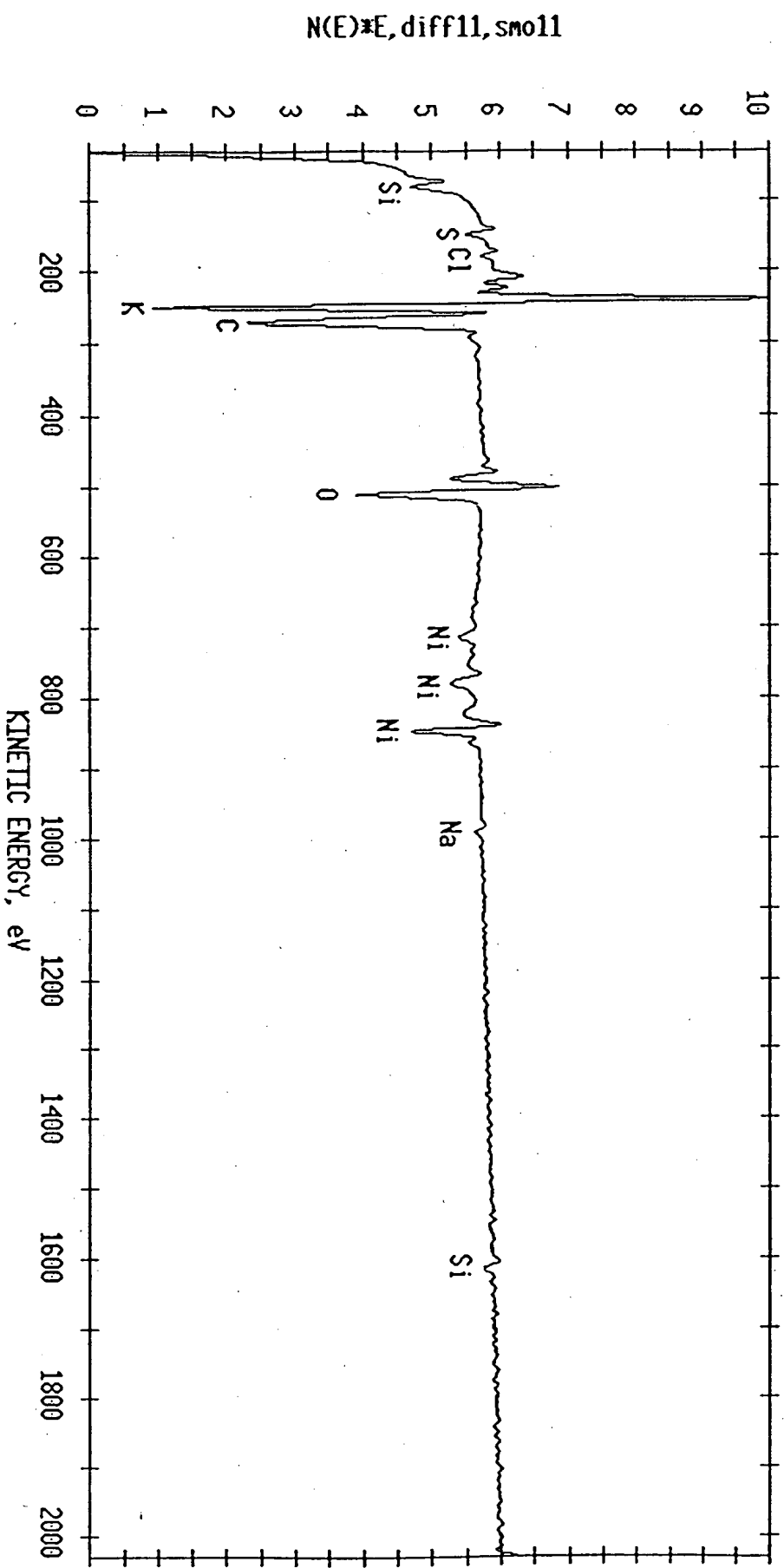
N-test 104

AES SURVEY WF 11/29/93 AREA 1 ACQ TIME=13.34 MIN.

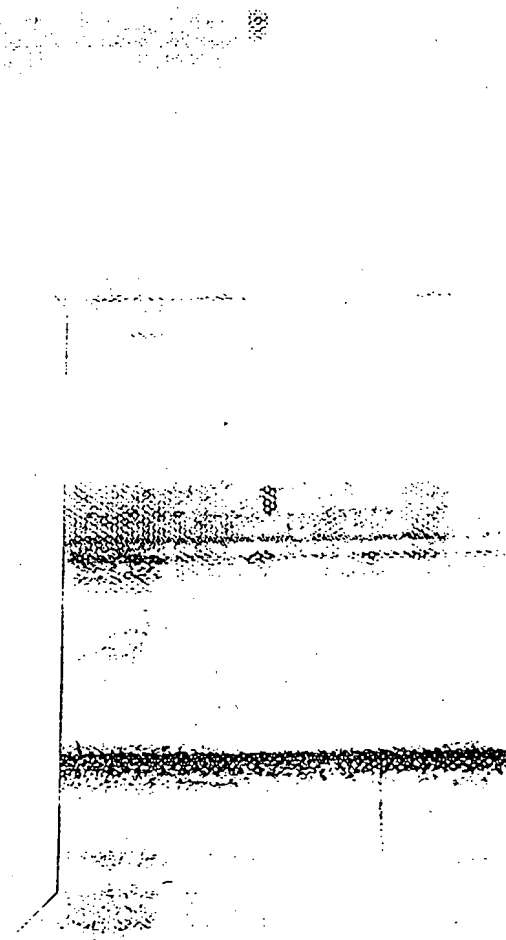
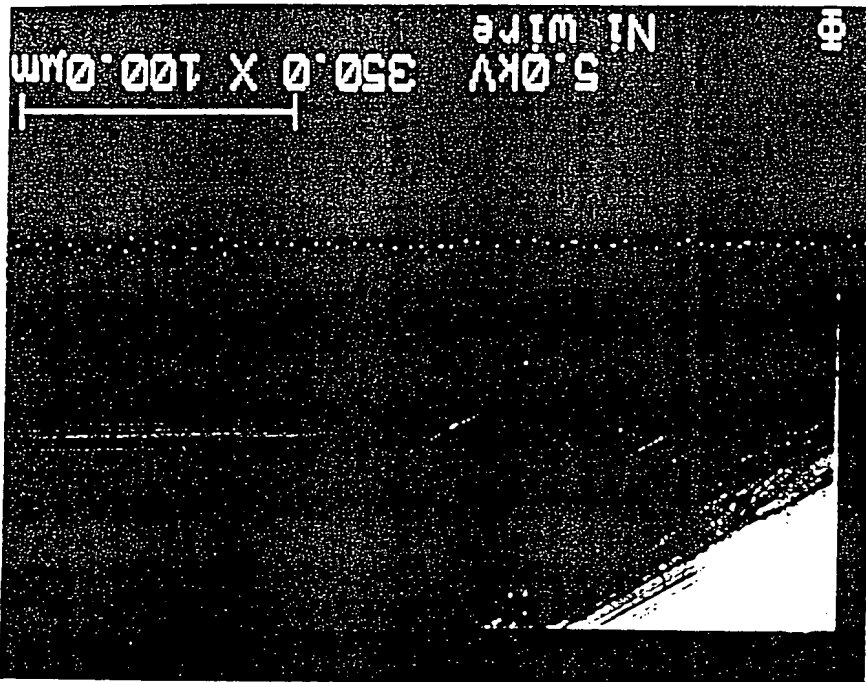
FILE: Nitest104 Ni wire treated for 24 Hr at the IRC.

SCALE FACTOR= 47.398 k c/s, OFFSET= 118.853 k c/s

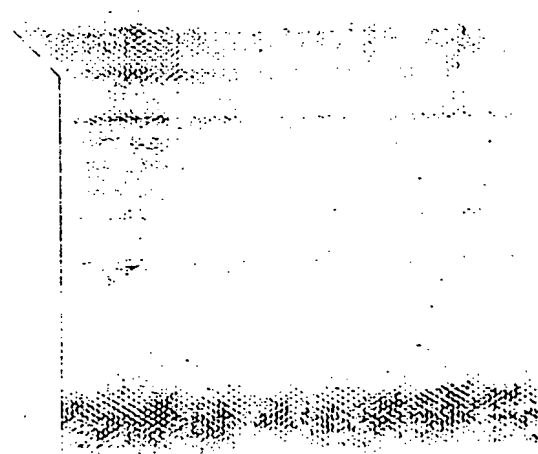
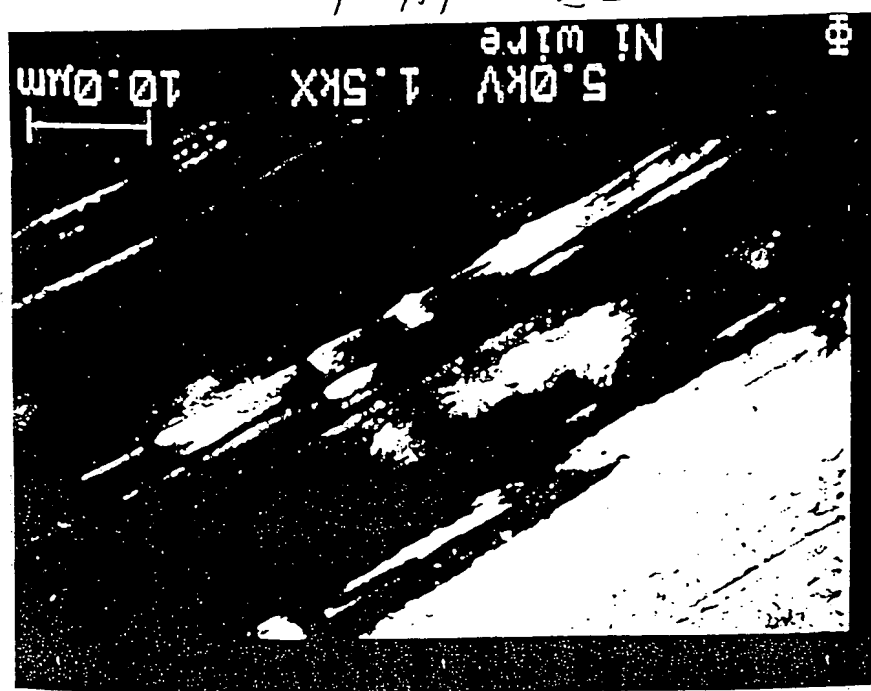
BW=5.00KV BI=0.2793uA



FZC Ni<sub>47</sub>Cr<sub>33</sub>+103



FZC Ni<sub>47</sub>Cr<sub>33</sub>+103

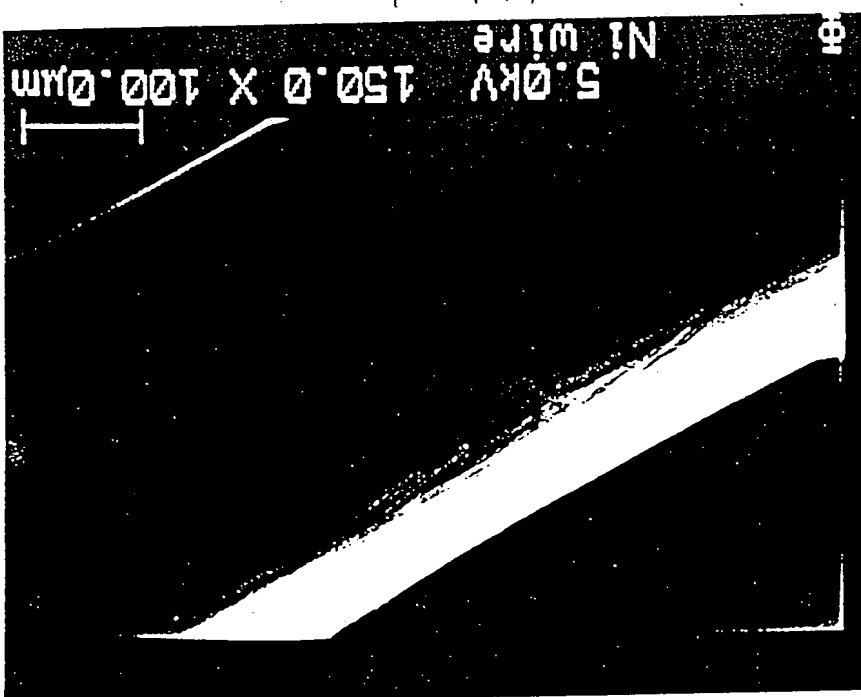


501 + 53 + 103

Ni wire

5.0KV 150.0 X 100.0 mm

Φ



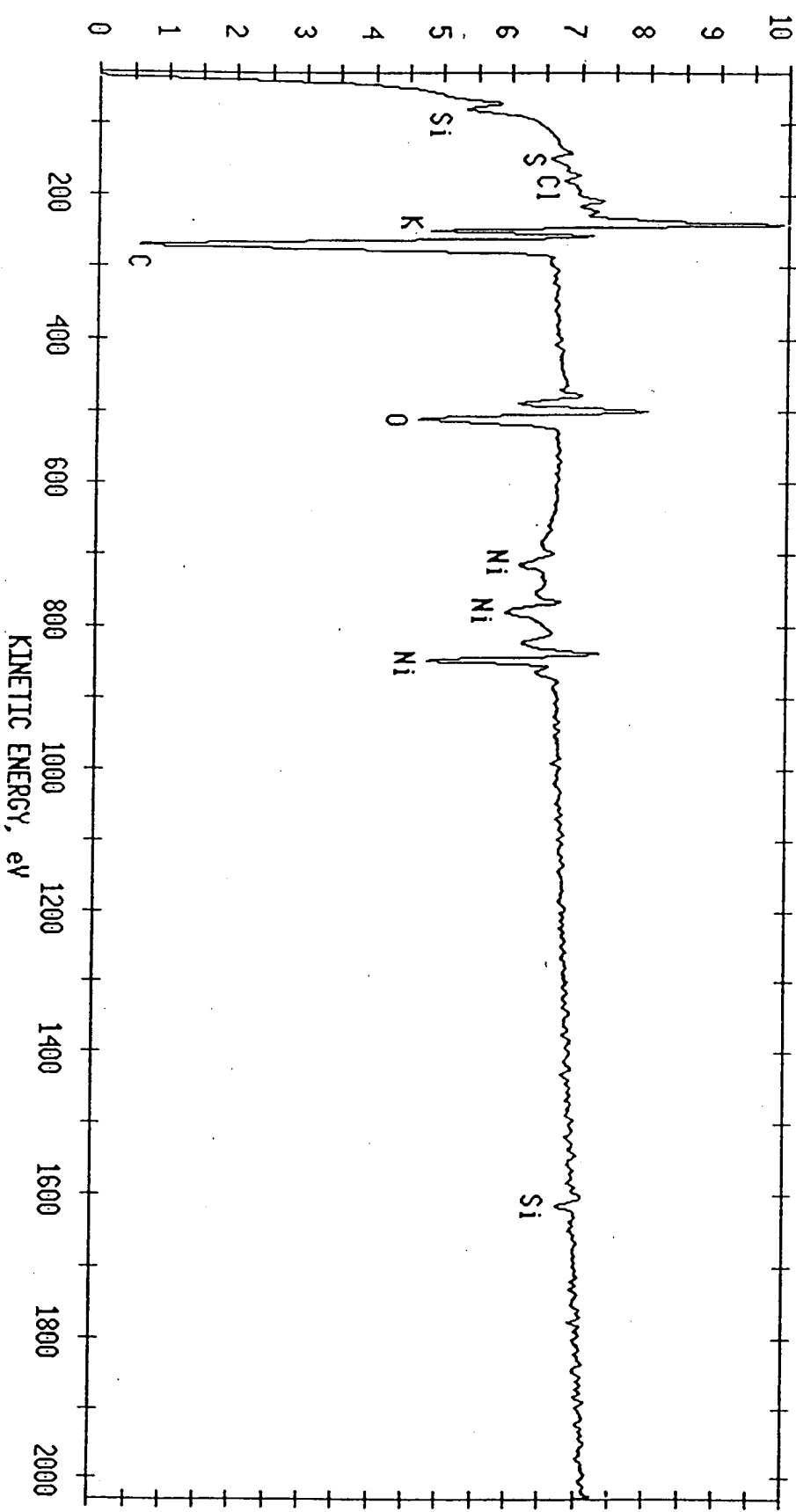
AES SURVEY V/F 11/29/93 AREA 1 ACQ TIME=6.67 MIN.

FILE: Nitest103 Ni wire treated for 24 Hr at the IRC.

SCALE FACTOR= 35.917 k c/s, OFFSET= 331.575 k c/s

BV=5.00kV BI=0.2793uA

N(E)\*E, diff11, sm11



30-Nov-1993 09:39:41

Ni-AR-1

Raster

Accelerating voltage 20.0 KeV  
Beam - sample incidence angle 90.0 degrees  
Xray emergence angle 35.0 degrees  
Xray - window incidence angle 0.0 degrees

STANDARDLESS EDS ANALYSIS  
(ZAF CORRECTIONS VIA MAGIC V)

ELEMENT & LINE	WEIGHT PERCENT	ATOMIC PERCENT*	PRECISION 2 SIGMA	K-RATIO**
Al KA	1.89	4.00	0.09	0.0059
Si KA	0.69	1.41	0.07	0.0029
Mn KA	0.08	0.08	0.02	0.0009
Fe KA	0.10	0.10	0.02	0.0013
Ni KA	97.24	94.41	0.42	0.9699
TOTAL	100.00			

ITERATIONS 6

\*NOTE: ATOMIC PERCENT is normalized to 100

\*\*NOTE: K-RATIO = K-RATIO x R  
where R = reference(standard)/reference(sample)

NORMALIZATION FACTOR: 1.000

30-Nov-1993 09:41:17

Ni-AR-2

Spot

Accelerating voltage 20.0 KeV  
Beam - sample incidence angle 90.0 degrees  
Xray emergence angle 35.0 degrees  
Xray - window incidence angle 0.0 degrees

STANDARDLESS EDS ANALYSIS  
(ZAF CORRECTIONS VIA MAGIC V)

ELEMENT & LINE	WEIGHT PERCENT	ATOMIC PERCENT*	PRECISION 2 SIGMA	K-RATIO**
Al KA	2.22	4.66	0.10	0.0070
Si KA	0.80	1.62	0.07	0.0034
Mn KA	0.05	0.05	0.02	0.0006
Fe KA	0.05	0.05	0.02	0.0007
Ni KA	96.88	93.61	0.45	0.9660
TOTAL	100.00			

ITERATIONS 6

\*NOTE: ATOMIC PERCENT is normalized to 100

\*\*NOTE: K-RATIO = K-RATIO x R  
where R = reference(standard)/reference(sample)

NORMALIZATION FACTOR: 1.000

30-Nov-1993 09:47:39

Ni-AR-4

Raster

Accelerating voltage 20.0 KeV  
Beam - sample incidence angle 90.0 degrees  
Xray emergence angle 35.0 degrees  
Xray - window incidence angle 0.0 degrees

STANDARDLESS EDS ANALYSIS  
(ZAF CORRECTIONS VIA MAGIC V)

ELEMENT & LINE	WEIGHT PERCENT	ATOMIC PERCENT*	PRECISION 2 SIGMA	K-RATIO**
Al KA	4.11	8.52	0.10	0.0130
Mn KA	0.09	0.09	0.02	0.0011
Fe KA	0.07	0.07	0.02	0.0010
Ni KA	95.73	91.31	0.39	0.9535
TOTAL	100.00			

ITERATIONS 7

\*NOTE: ATOMIC PERCENT is normalized to 100

\*\*NOTE: K-RATIO = K-RATIO x R  
where R = reference(standard)/reference(sample)

NORMALIZATION FACTOR: 1.000

30-Nov-1993 09:42:46

Ni-AR-3

Sp. +

Accelerating voltage 20.0 KeV  
Beam - sample incidence angle 90.0 degrees  
Xray emergence angle 35.0 degrees  
Xray - window incidence angle 0.0 degrees

STANDARDLESS EDS ANALYSIS  
(ZAF CORRECTIONS VIA MAGIC V)

ELEMENT & LINE	WEIGHT PERCENT	ATOMIC PERCENT*	PRECISION 2 SIGMA	K-RATIO**
Al KA	3.17	6.61	0.12	0.0100
Si KA	0.71	1.42	0.06	0.0030
Mn KA	0.05	0.05	0.01	0.0005
Fe KA	0.08	0.08	0.02	0.0010
Ni KA	95.99	91.85	0.44	0.9561
TOTAL	100.00			

ITERATIONS 7

\*NOTE: ATOMIC PERCENT is normalized to 100

\*\*NOTE: K-RATIO = K-RATIO x R  
where R = reference(standard)/reference(sample)

NORMALIZATION FACTOR: 1.000

30-Nov-1993 09:57:31

Ni-T-2

576+

Accelerating voltage 20.0 KeV  
Beam - sample incidence angle 90.0 degrees  
Xray emergence angle 35.0 degrees  
Xray - window incidence angle 0.0 degrees

STANDARDLESS EDS ANALYSIS  
(ZAF CORRECTIONS VIA MAGIC V)

ELEMENT & LINE	WEIGHT PERCENT	ATOMIC PERCENT*	PRECISION 2 SIGMA	K-RATIO**
Al KA	3.80	7.90	0.12	0.0120
K KA	0.34	0.49	0.04	0.0029
Mn KA	0.04	0.04	0.01	0.0005
Fe KA	0.06	0.06	0.02	0.0008
Ni KA	95.75	91.50	0.43	0.9537
TOTAL	99.99			
ITERATIONS	6			

\*NOTE: ATOMIC PERCENT is normalized to 100

\*\*NOTE: K-RATIO = K-RATIO x R  
where R = reference(standard)/reference(sample)

NORMALIZATION FACTOR: 1.000

30-Nov-1993 09:54:39

Ni-T-1

Raster

Accelerating voltage                    20.0 KeV  
 Beam - sample incidence angle        90.0 degrees  
 Xray emergence angle                 35.0 degrees  
 Xray - window incidence angle       0.0 degrees

STANDARDLESS EDS ANALYSIS  
 (ZAF CORRECTIONS VIA MAGIC V)

ELEMENT & LINE	WEIGHT PERCENT	ATOMIC PERCENT*	PRECISION 2 SIGMA	K-RATIO**
Only ~1½-2% probably	Al KA      6.47	13.07	0.16	0.0208
	K KA       0.35	0.48	0.04	0.0030
	Mn KA      0.08	0.08	0.02	0.0009
	Fe KA       0.06	0.06	0.02	0.0008
	Ni KA       93.04	86.32	0.39	0.9247
TOTAL	100.00			

ITERATIONS                            7

\*NOTE: ATOMIC PERCENT is normalized to 100

\*\*NOTE: K-RATIO = K-RATIO x R  
 where R = reference(standard)/reference(sample)

NORMALIZATION FACTOR:    1.000

30-Nov-1993 10:00:28

Ni-T-3

Spot

Accelerating voltage                    20.0 KeV  
 Beam - sample incidence angle        90.0 degrees  
 Xray emergence angle                 35.0 degrees  
 Xray - window incidence angle       0.0 degrees

STANDARDLESS EDS ANALYSIS  
 (ZAF CORRECTIONS VIA MAGIC V)

ELEMENT & LINE	WEIGHT PERCENT	ATOMIC PERCENT*	PRECISION 2 SIGMA	K-RATIO**
Al KA	6.00	12.18	0.17	0.0193
K KA	0.38	0.53	0.04	0.0032
Mn KA	0.08	0.08	0.02	0.0009
Fe KA	0.07	0.06	0.02	0.0009
Ni KA	93.47	87.14	0.41	0.9293
TOTAL	100.00			

ITERATIONS                    7

\*NOTE: ATOMIC PERCENT is normalized to 100

\*\*NOTE: K-RATIO = K-RATIO x R  
 where R = reference(standard)/reference(sample)

NORMALIZATION FACTOR:        1.000

30-Nov-1993 10:02:41

Ni-T-4

Raster

Accelerating voltage 20.0 KeV  
Beam - sample incidence angle 90.0 degrees  
Xray emergence angle 35.0 degrees  
Xray - window incidence angle 0.0 degrees

STANDARDLESS EDS ANALYSIS  
(ZAF CORRECTIONS VIA MAGIC V)

ELEMENT & LINE	WEIGHT PERCENT	ATOMIC PERCENT*	PRECISION 2 SIGMA	K-RATIO**
Al KA	1.46	3.12	0.09	0.0045
K KA	0.25	0.36	0.03	0.0021
Mn KA	0.09	0.09	0.02	0.0010
Fe KA	0.09	0.09	0.02	0.0012
Ni KA	98.11	96.33	0.42	0.9795
TOTAL	100.00			

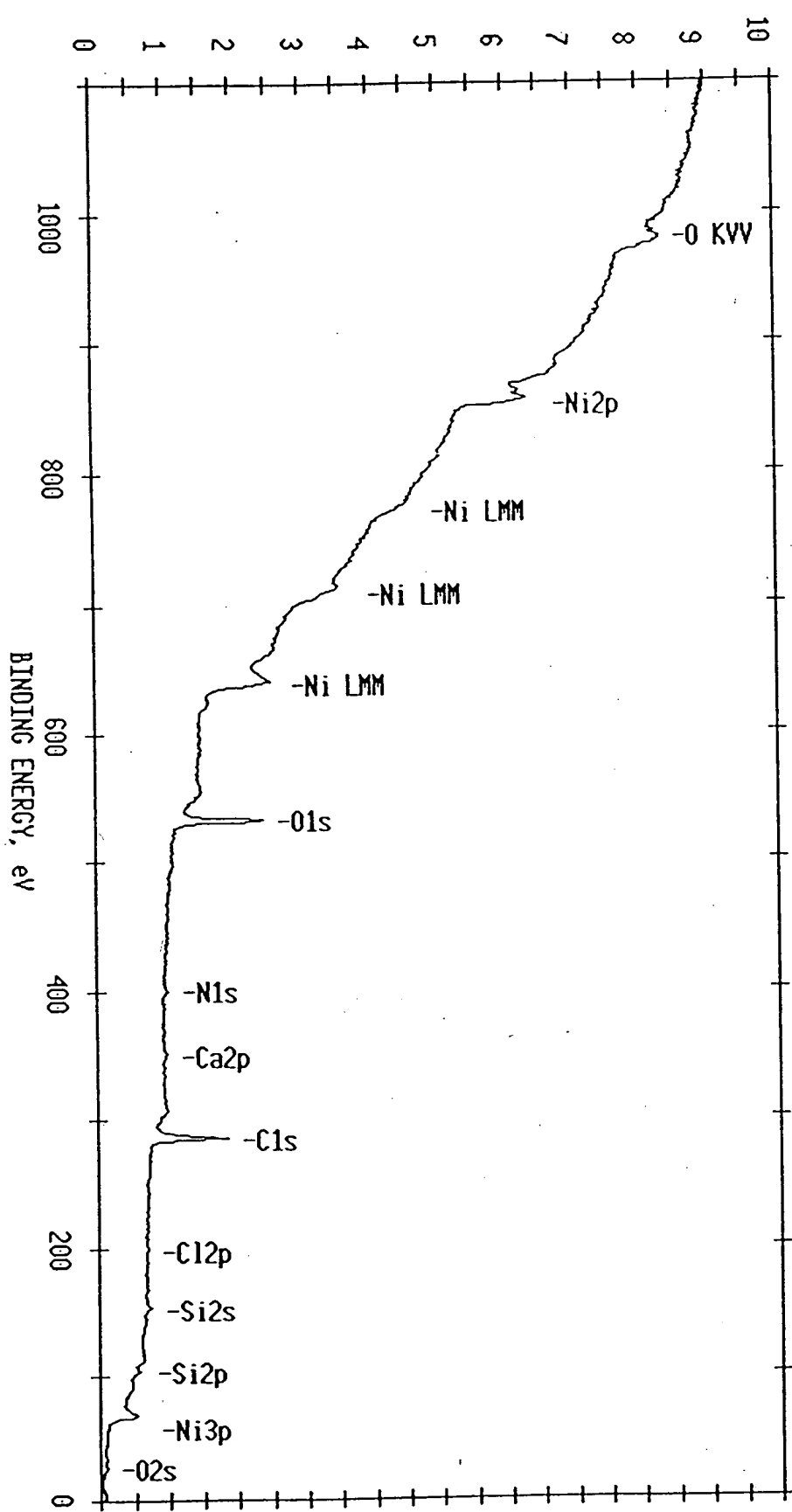
ITERATIONS 6

\*NOTE: ATOMIC PERCENT is normalized to 100

\*\*NOTE: K-RATIO = K-RATIO x R  
where R = reference(standard)/reference(sample)

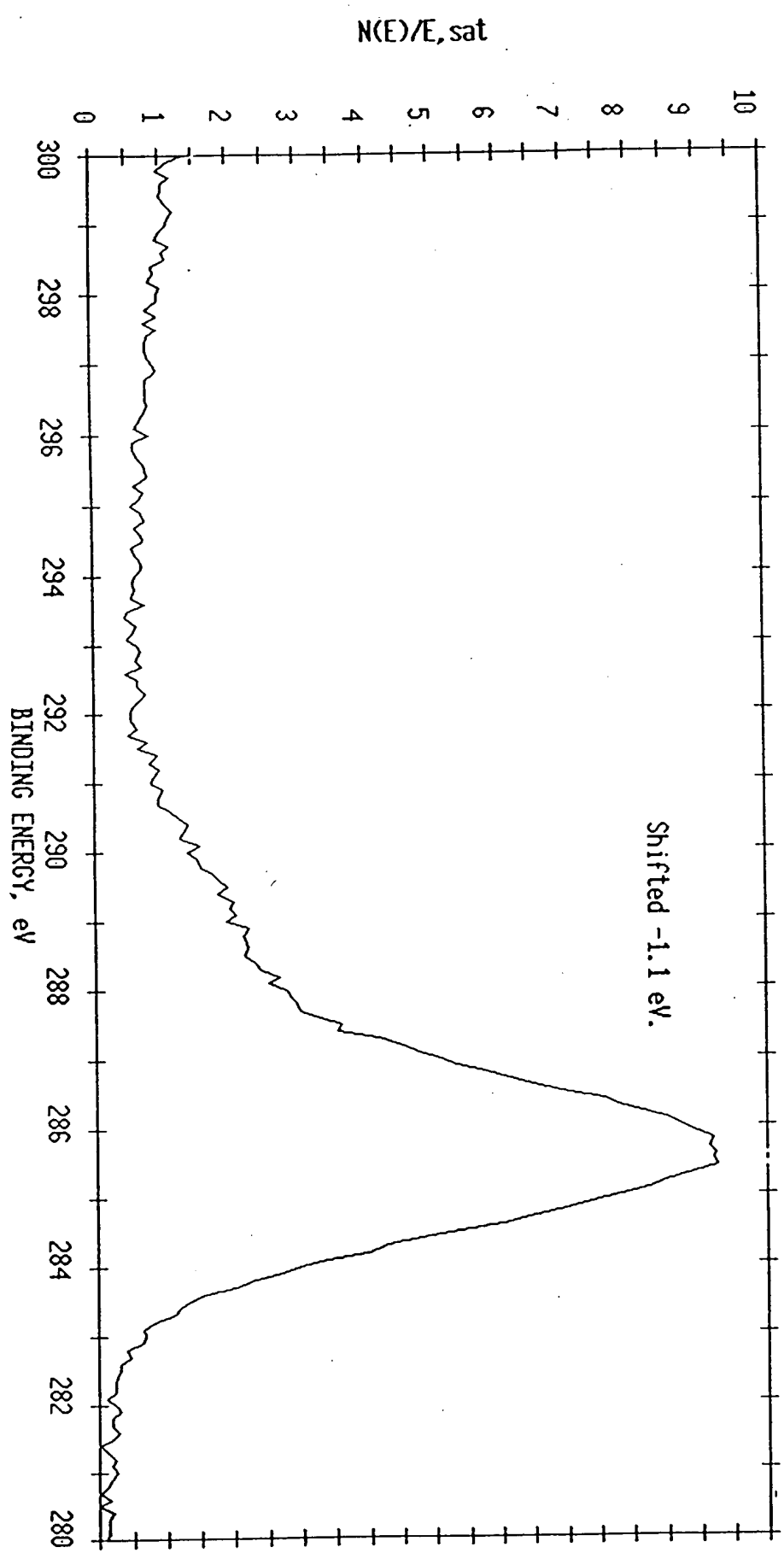
NORMALIZATION FACTOR: 1.000

N(E)/E<sub>sat</sub>

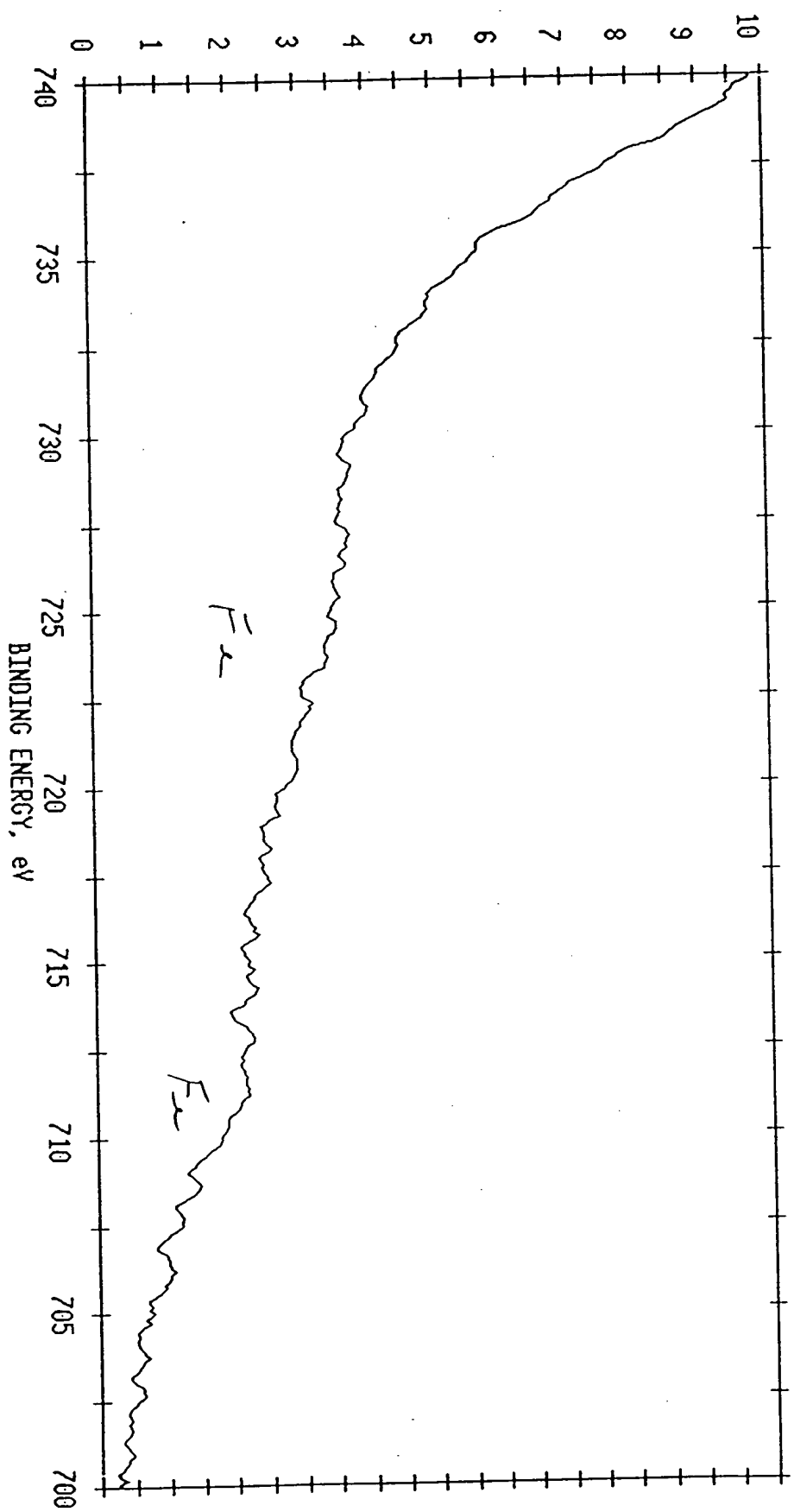


ESCA SURVEY 11/19/93 ANGLE= 15 deg ACQ TIME=29.36 min  
FILE: Nitest28 Ni wire untreated (base line) using Al X-Ray's.  
SCALE FACTOR= 10.010 k c/s, OFFSET= 1.574 k c/s PASS ENERGY=178.950 eV Al 400  $\mu$

ESCA MULTIPLEX 11/19/93 EL=C1 REG 1 ANGLE= 15 deg ACQ TIME=4.19 min  
FILE: Nitest27 Ni wire untreated (base line) using Al X-Ray's.  
SCALE FACTOR= 0.928 k c/s, OFFSET= 5.646 k c/s PASS ENERGY=143.050 eV Al 400  $\mu$



$N(E)/E_{sat}$ , sm011



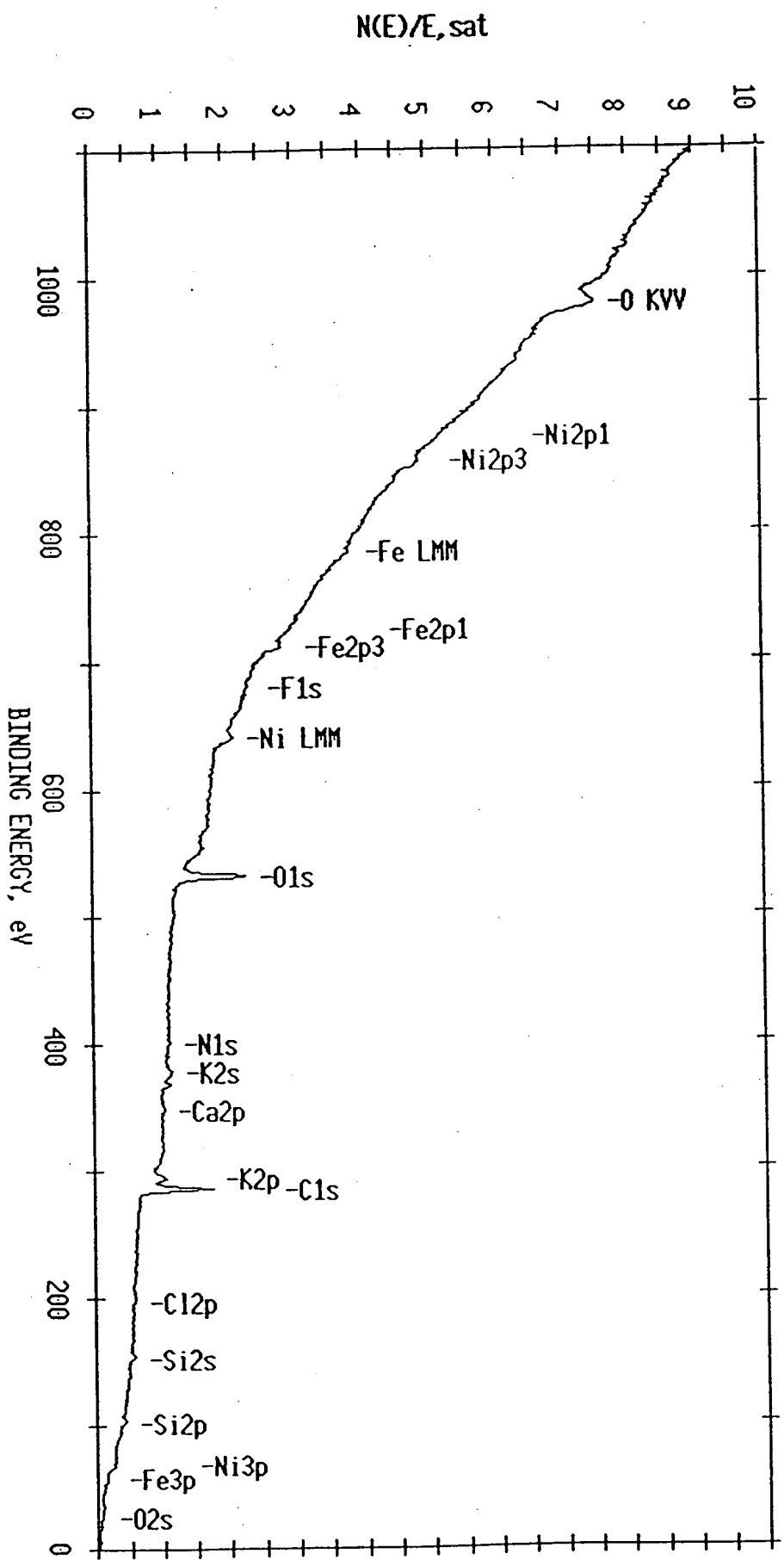
ESCA MULTIPLEX 11/29/93 EL=Fe1 REC 1 ANGLE= 15 deg ACQ TIME=116.96 min  
FILE: Nitest55 More Fe spectra of Ni wire treated overnight at the IRC  
SCALE FACTOR= 0.134 k c/s, OFFSET= 9.937 k c/s PASS ENERGY=143.050 ev

Mg 300  $\text{\AA}$

ESCA SURVEY 11/24/93 ANGLE= 15 deg ACQ TIME=29.36 min

FILE: Nitest51 Ni wire treated overnight at IRC.

SCALE FACTOR= 7.011 k c/s, OFFSET= 0.979 k c/s PASS ENERGY=178.950 eV Al 400  $\mu$



1993.05.29

242AP04/05

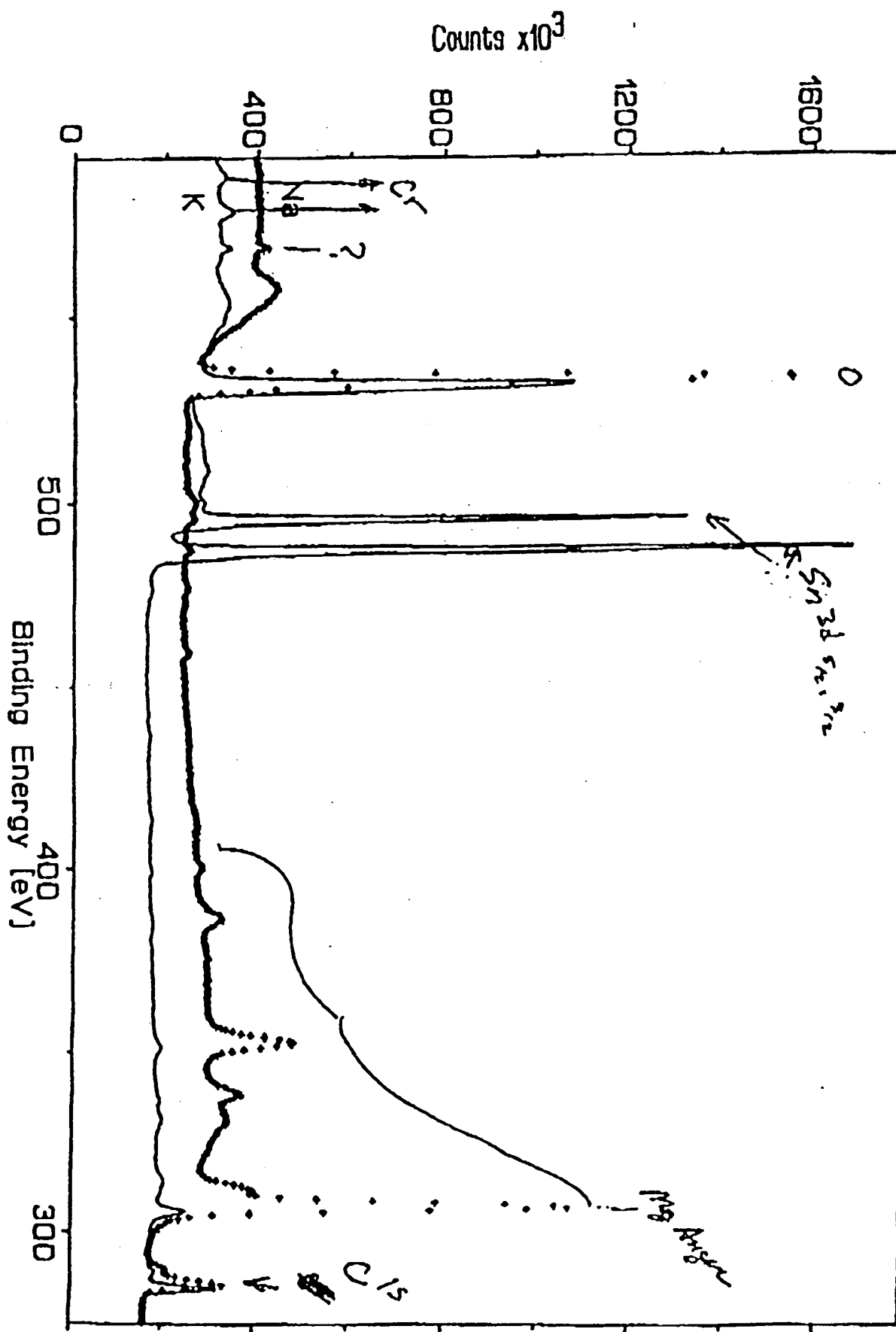


Figure 4c

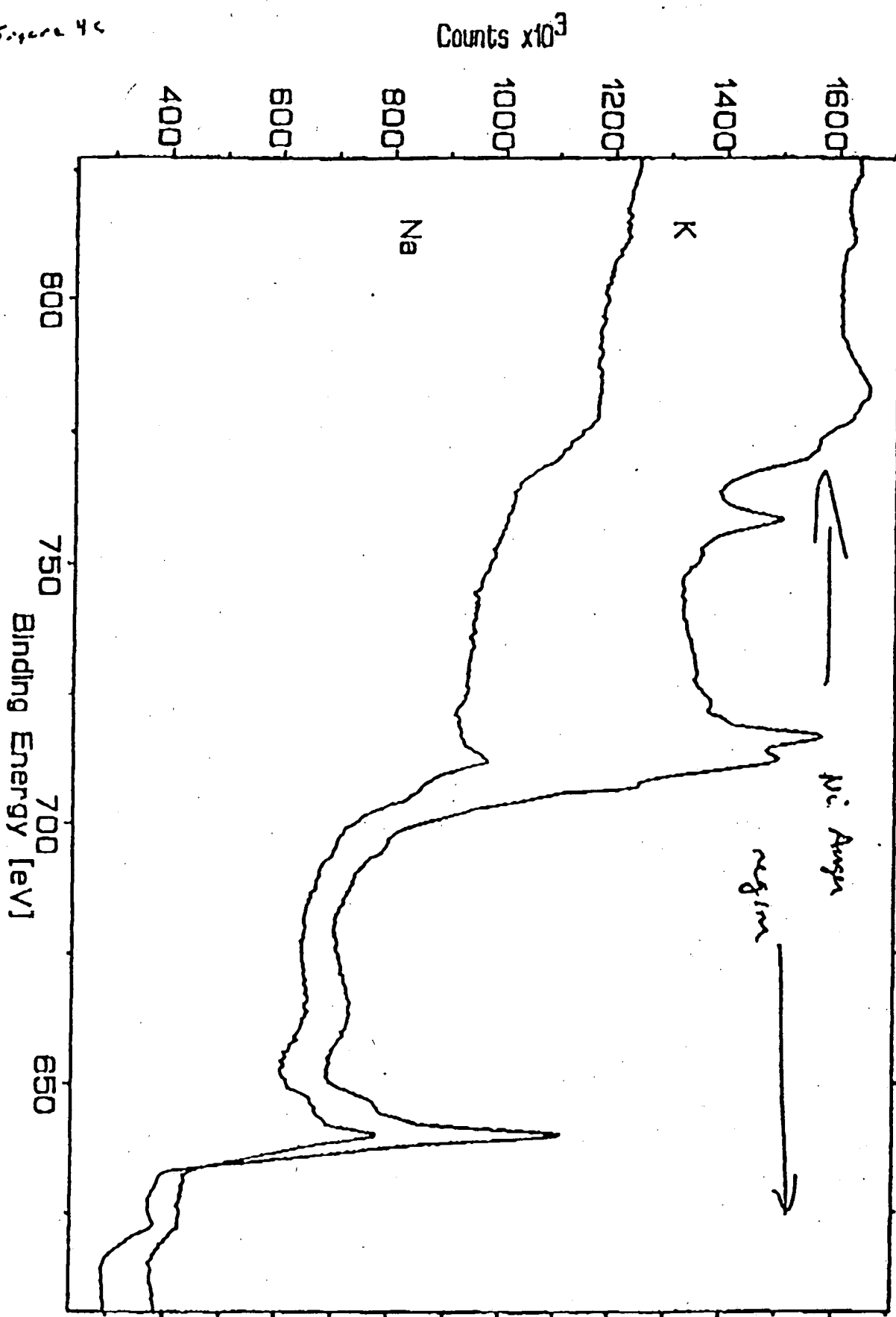
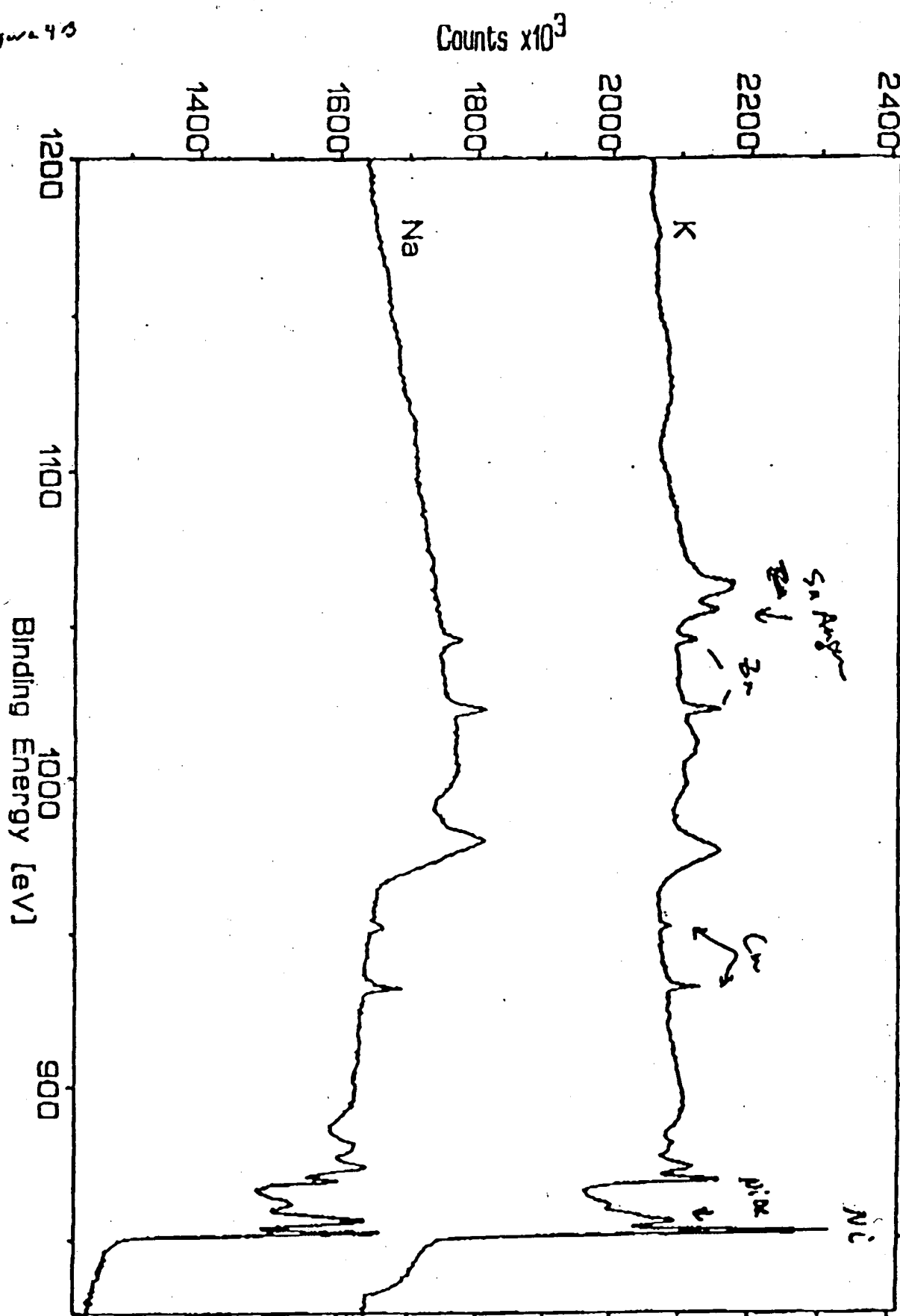
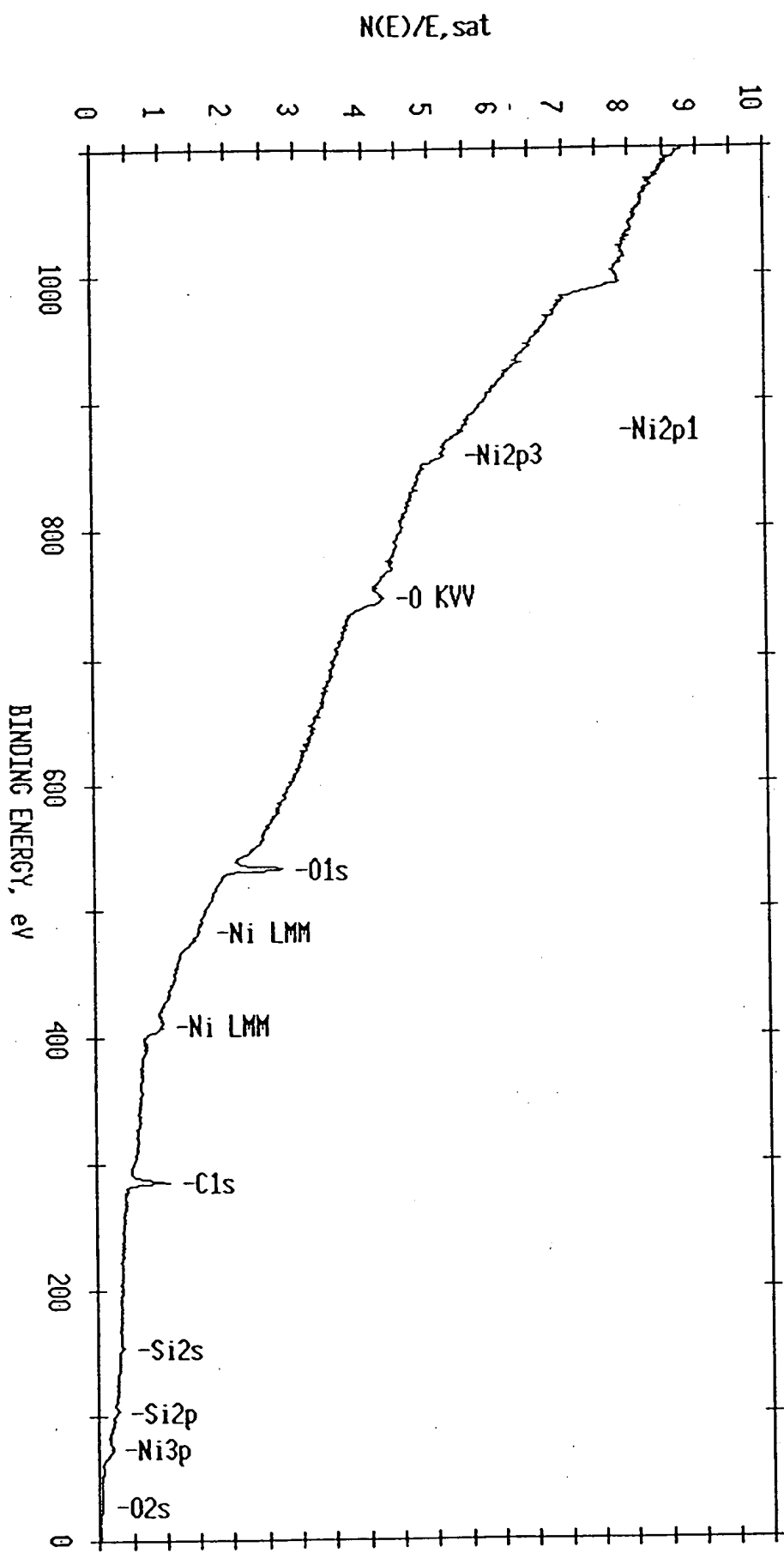


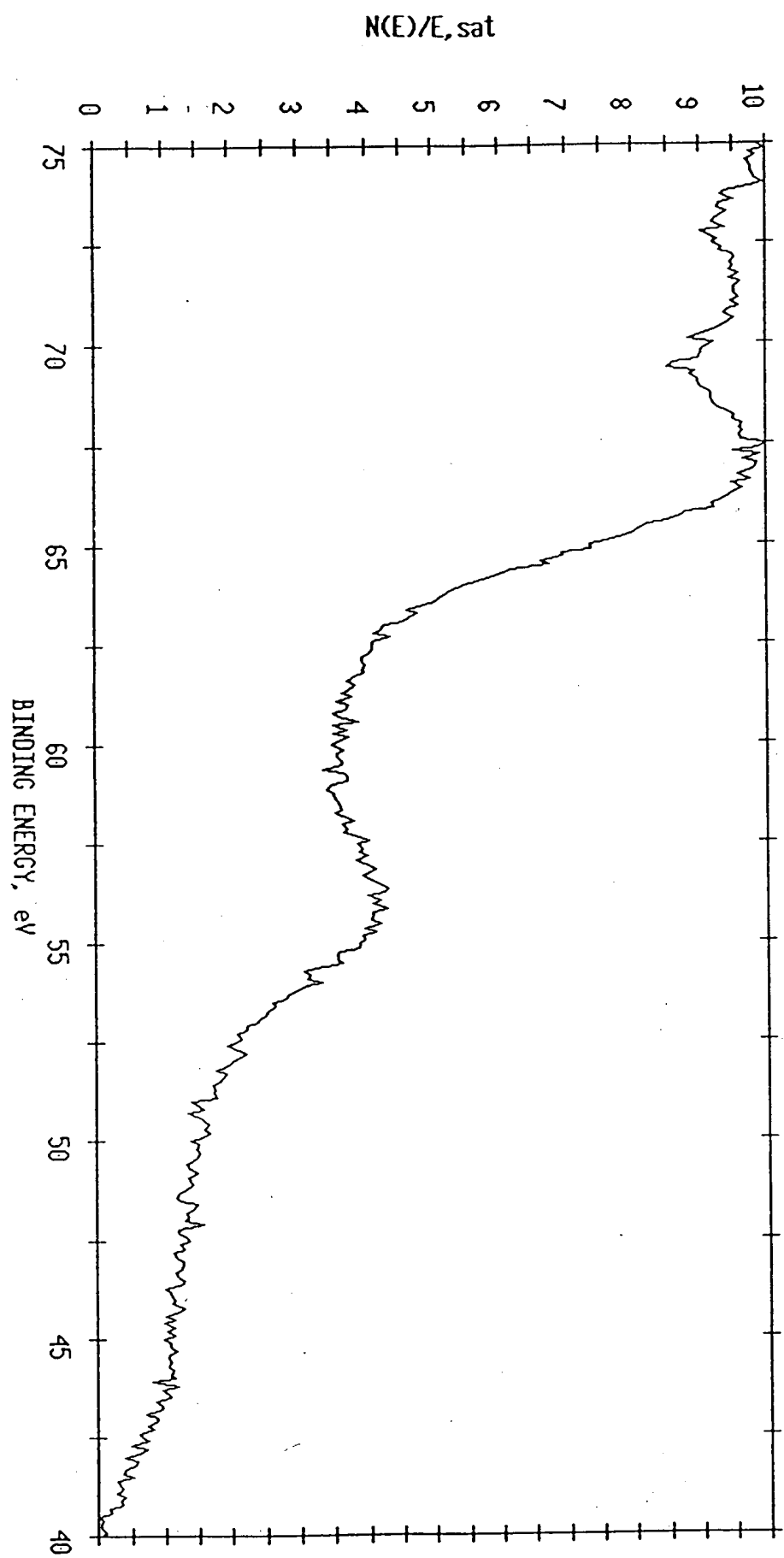
Figure 40



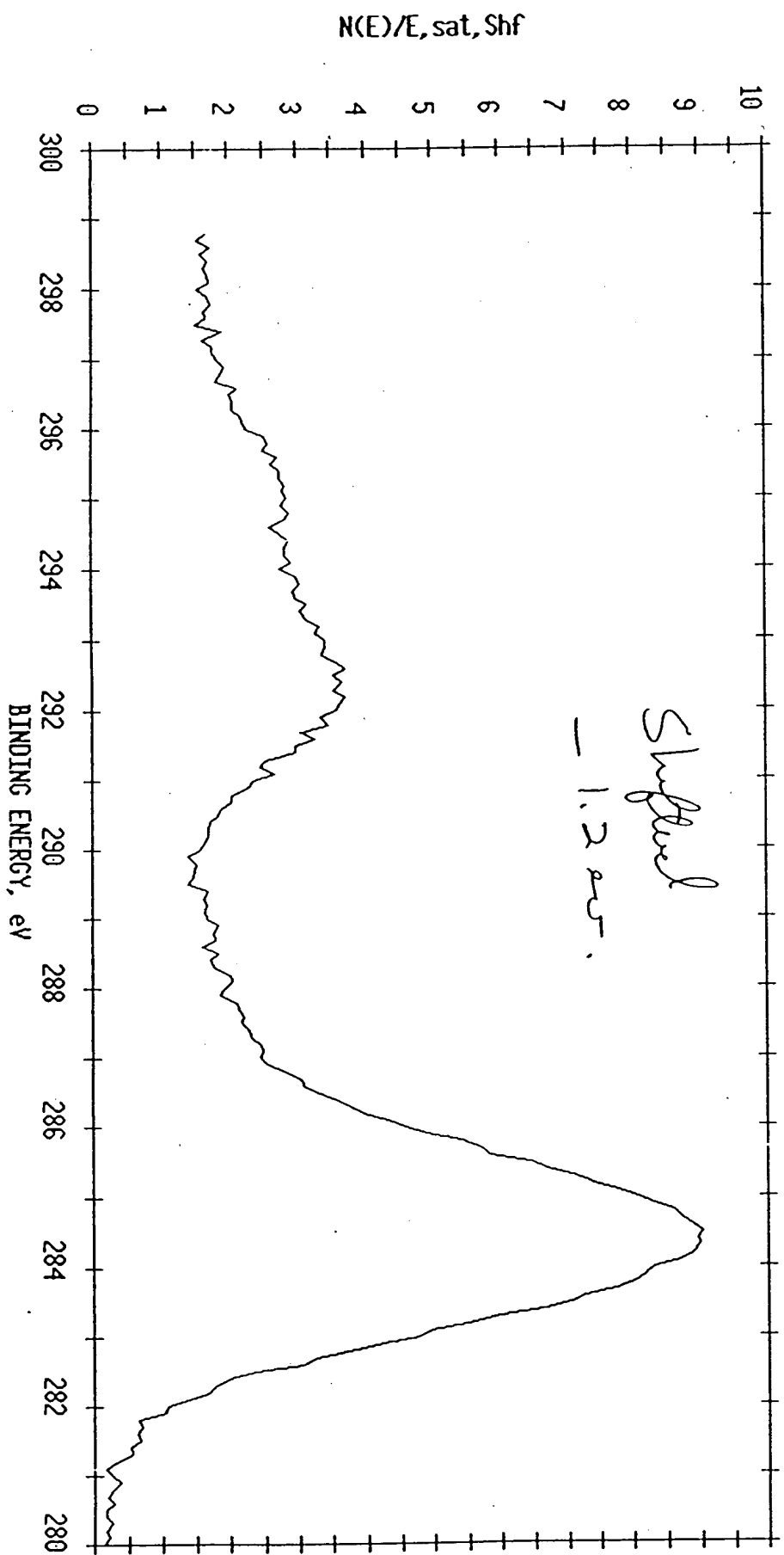
ESCA SURVEY 11/29/93 ANGLE= 15 deg ACC TIME=29.36 min  
FILE: Nitest56 Ni wire treated over Thanksgiving weekend.  
SCALE FACTOR= 4.822 k c/s, OFFSET= 0.306 k c/s PASS ENERGY=178.950 eV Mg 300 W



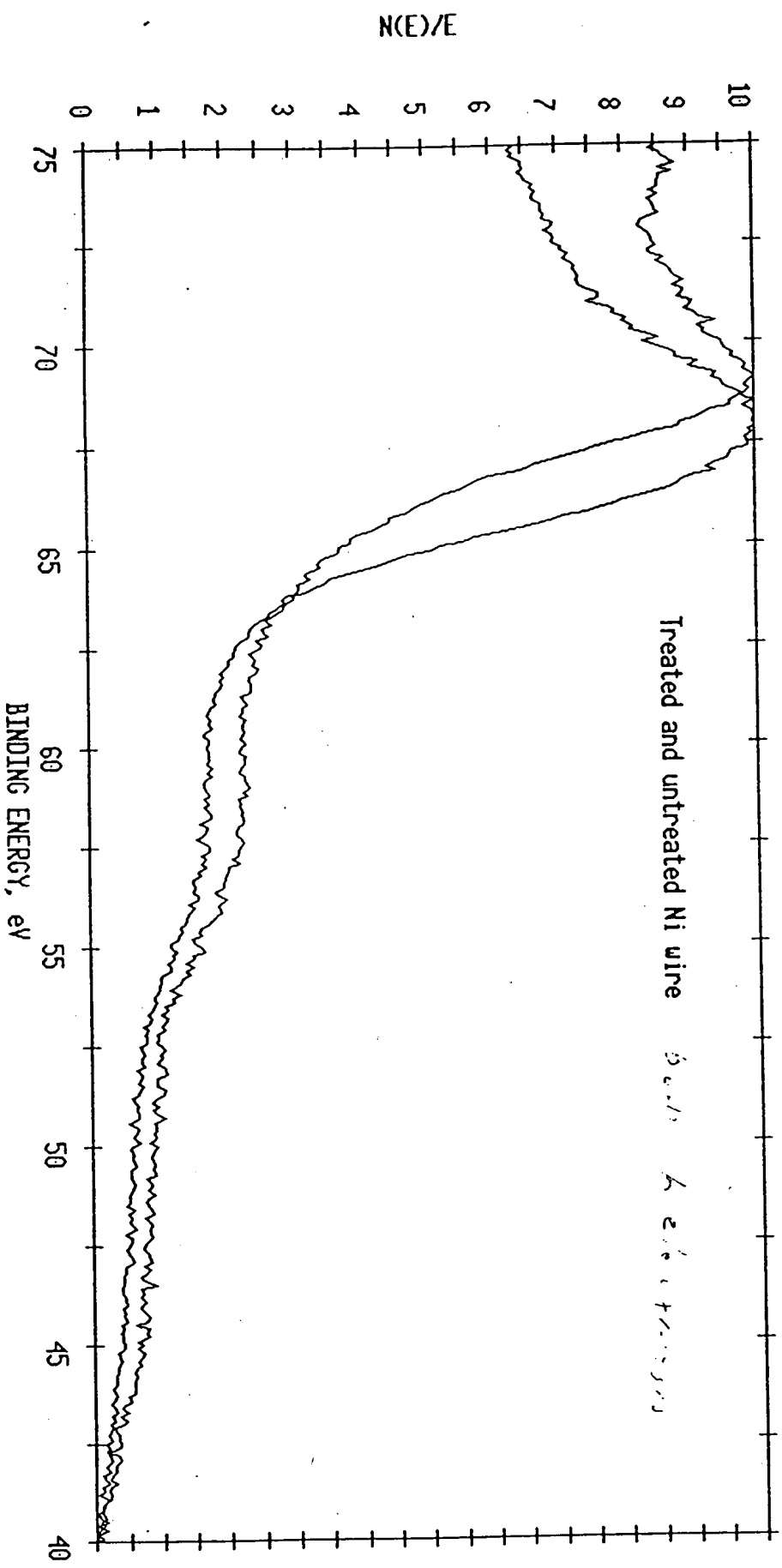
ESCA MULTIPLEX 11/24/93 EL= REG 2 ANGLE= 15 deg ACC TIME=114.08 min  
FILE: Nitest50 Ni wire treated overnight at IRC.  
SCALE FACTOR= 0.095 k c/s, OFFSET= 1.036 k c/s PASS ENERGY=143.050 eV Al 400 W



ESCA MULTIPLEX 11/24/93 EL=C1 REG 1 ANGLE= 15 deg ACQ TIME=7.54 min  
FILE: Nitest50 Ni wire treated overnight at IRC.  
SCALE FACTOR= 0.569 k c/s, OFFSET= 3.655 k c/s PASS ENERGY=143.050 eV Al 400 W



ESCA MULTIPLEX 11/19/93 EL= REG 2 ANGLE= 15 deg ACQ TIME=61.43 min  
FILE: Nitest27 Ni wire untreated (base line) using Al X-Ray's.  
SCALE FACTOR= 0.307 k c/s, OFFSET= 1.683 k c/s PASS ENERGY=143.050 eV Al 400  $\mu$





**SPACE and ADVANCED PROGRAMS UNIT  
P. O. BOX 1625  
IDAHO FALLS ID 83415**

To: Mike Hawkins

Company/Org: \_\_\_\_\_

Fax No: \_\_\_\_\_

Verify No: \_\_\_\_\_

From: Mike Tracy

Company/Org: \_\_\_\_\_

Phone No: \_\_\_\_\_

Fax No: 1-208-526-2061 (FTS) 8-208-526-2061

No. of pages including the cover page: 2

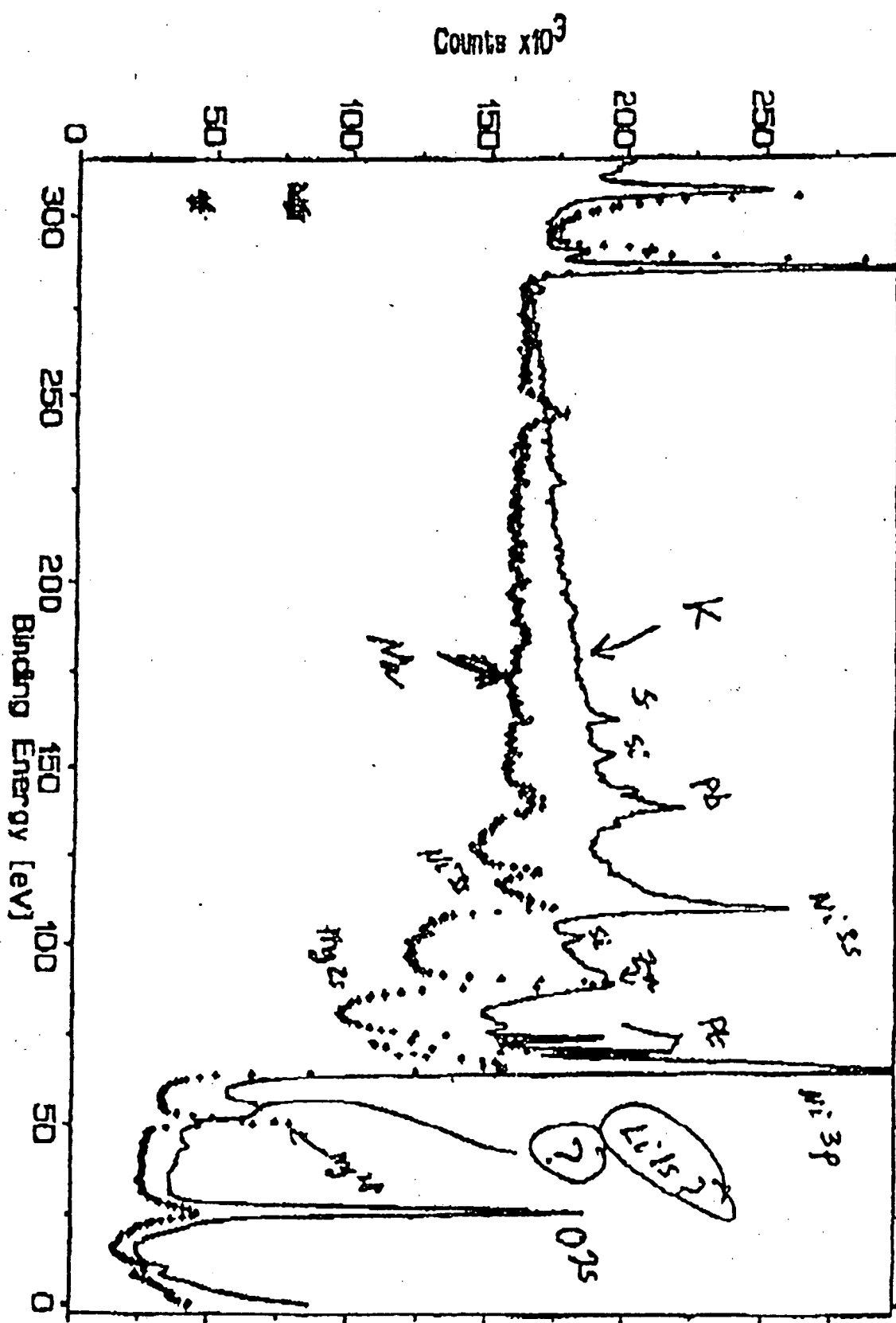
Note:

PROT LIB 01 PIR

TO

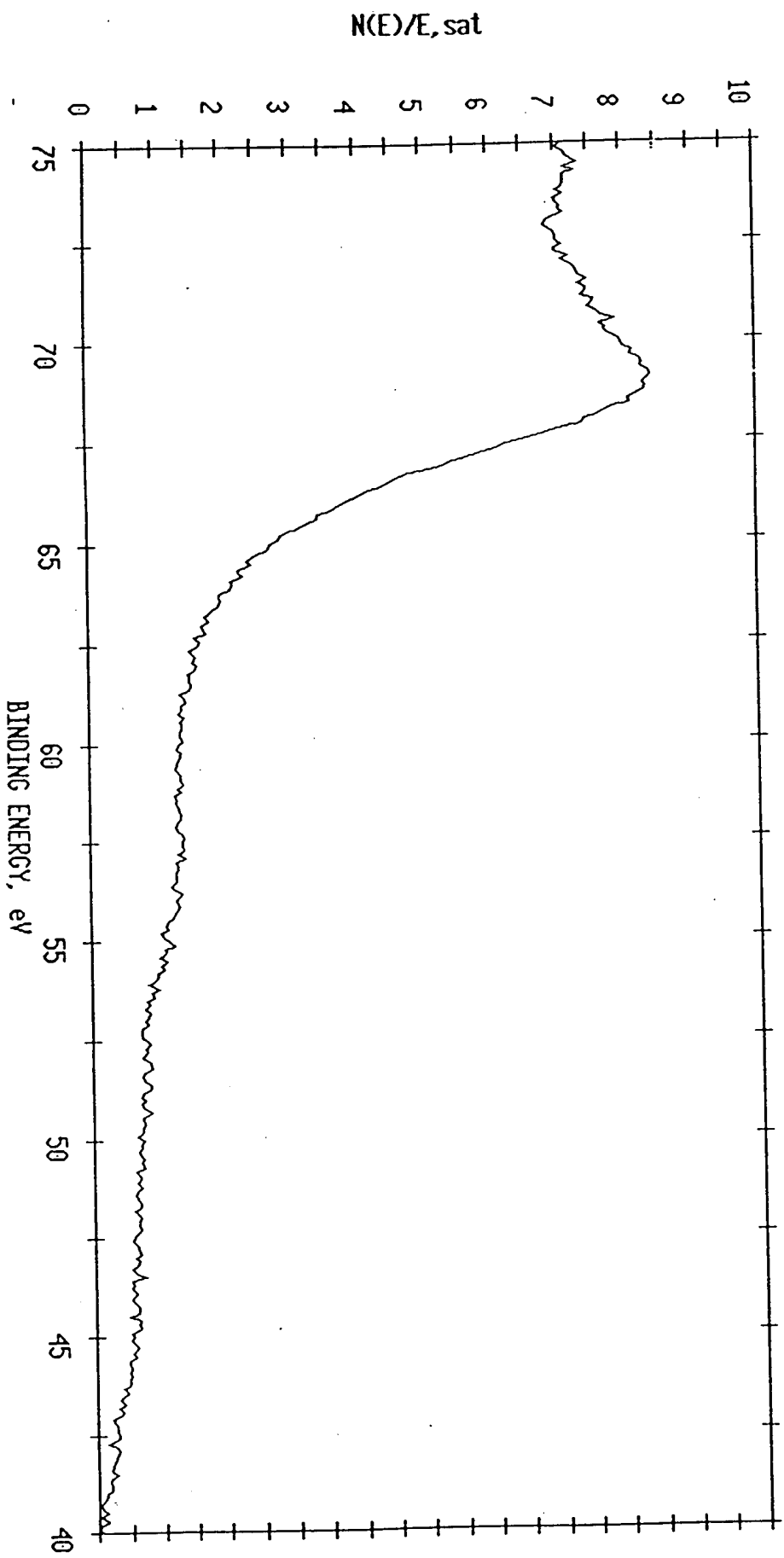
1L 106-28

1E137 8242 P.03/83

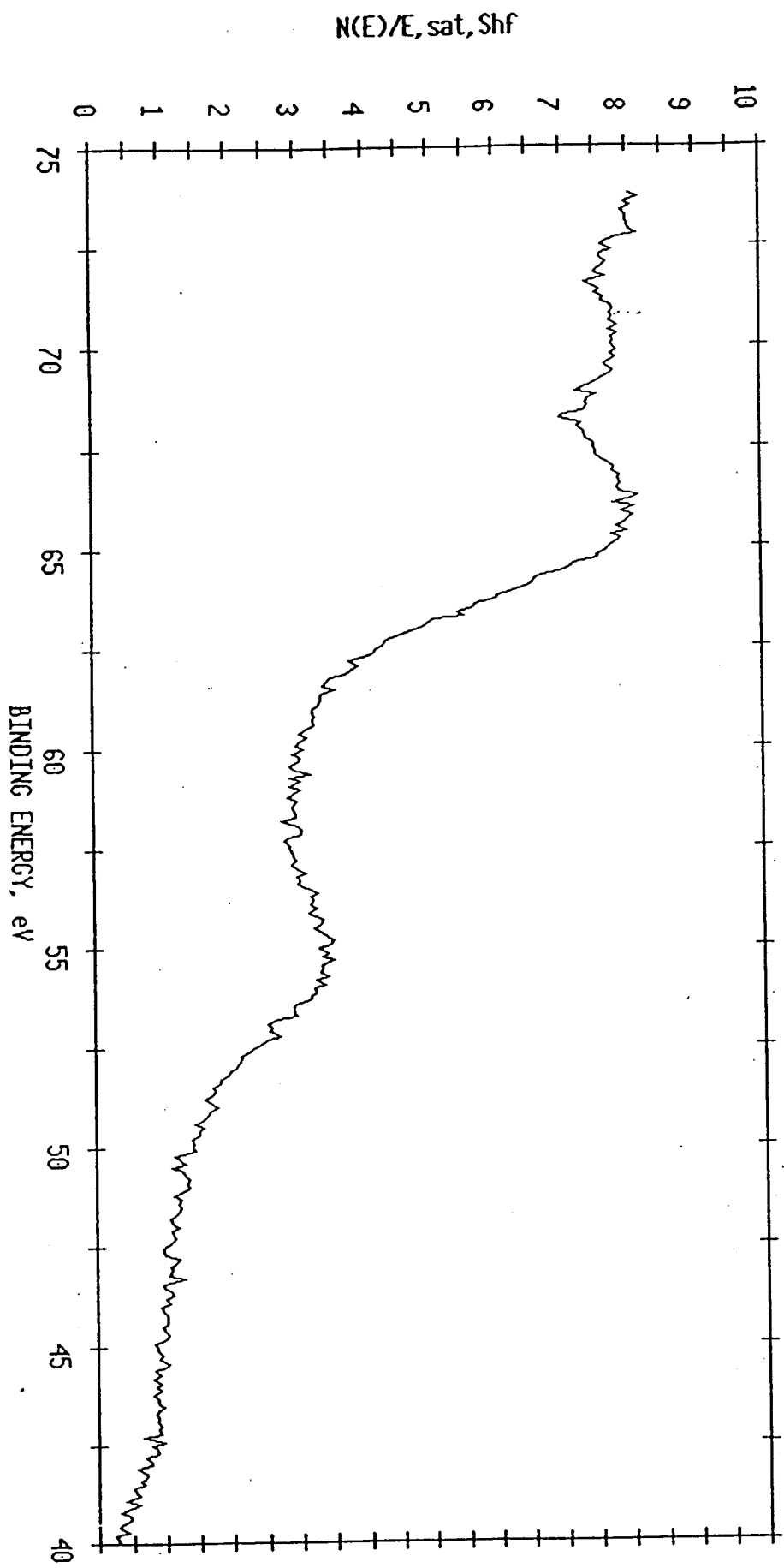


2 h - 1013

ESCA MULTIPLEX 11/18/93 EL= REC 2 ANGLE= 15 deg ACQ TIME=67.28 min  
FILE: Nitest20 Ni wire processed in lab. as received.  
SCALE FACTOR= 0.331 k c/s, OFFSET= 2.436 k c/s PASS ENERGY=143.050 eV Al 400  $\mu$



ESCA MULTIPLEX 11/24/93 EL= REG 2 ANGLE= 15 deg ACQ TIME=114.08 min  
FILE: Nitest50 Ni wire treated overnight at IRC.  
SCALE FACTOR= 0.116 k c/s, OFFSET= 1.036 k c/s PASS ENERGY=143.050 eV Al 400 W



a

Energy (eV)

54.700

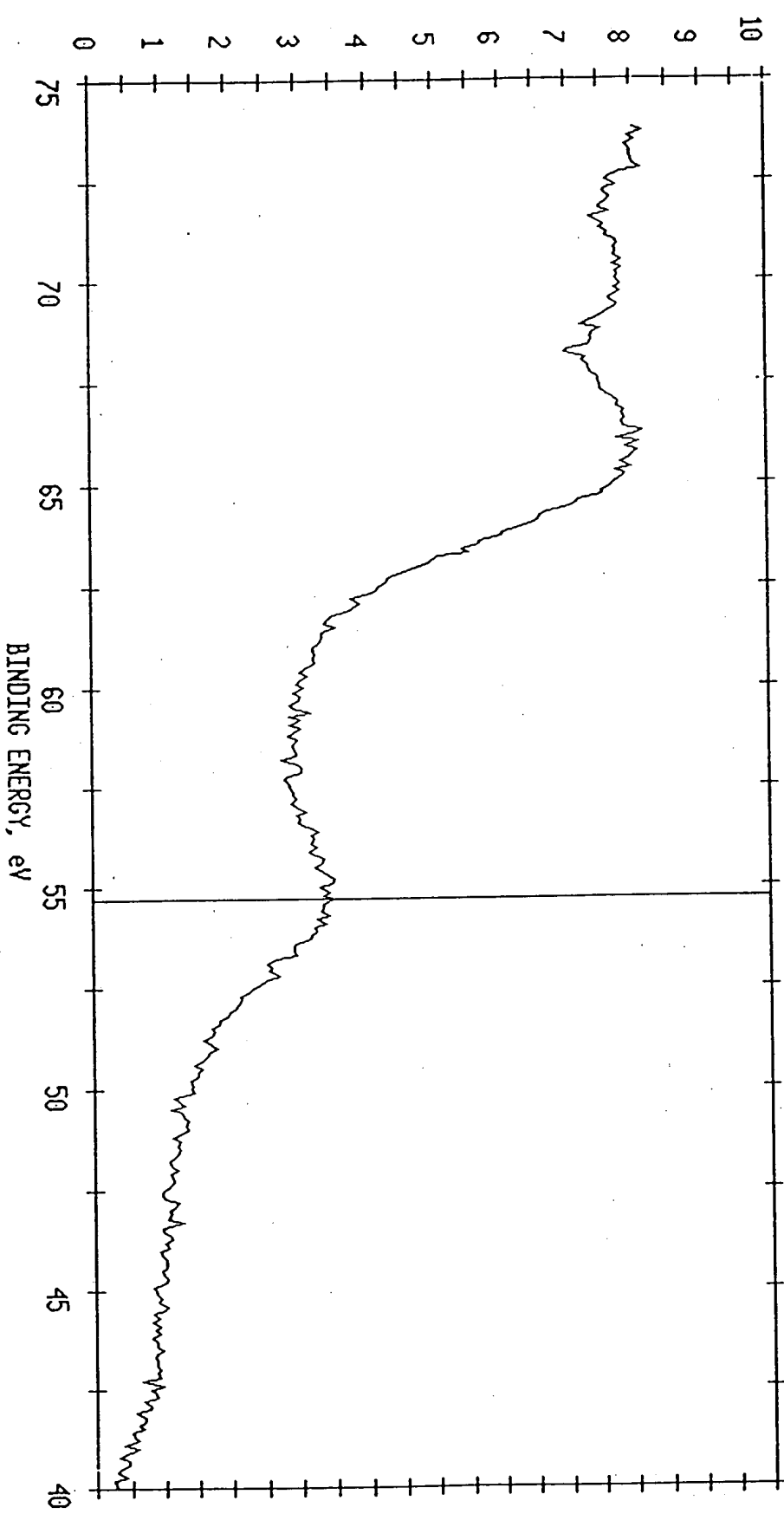
Cursor

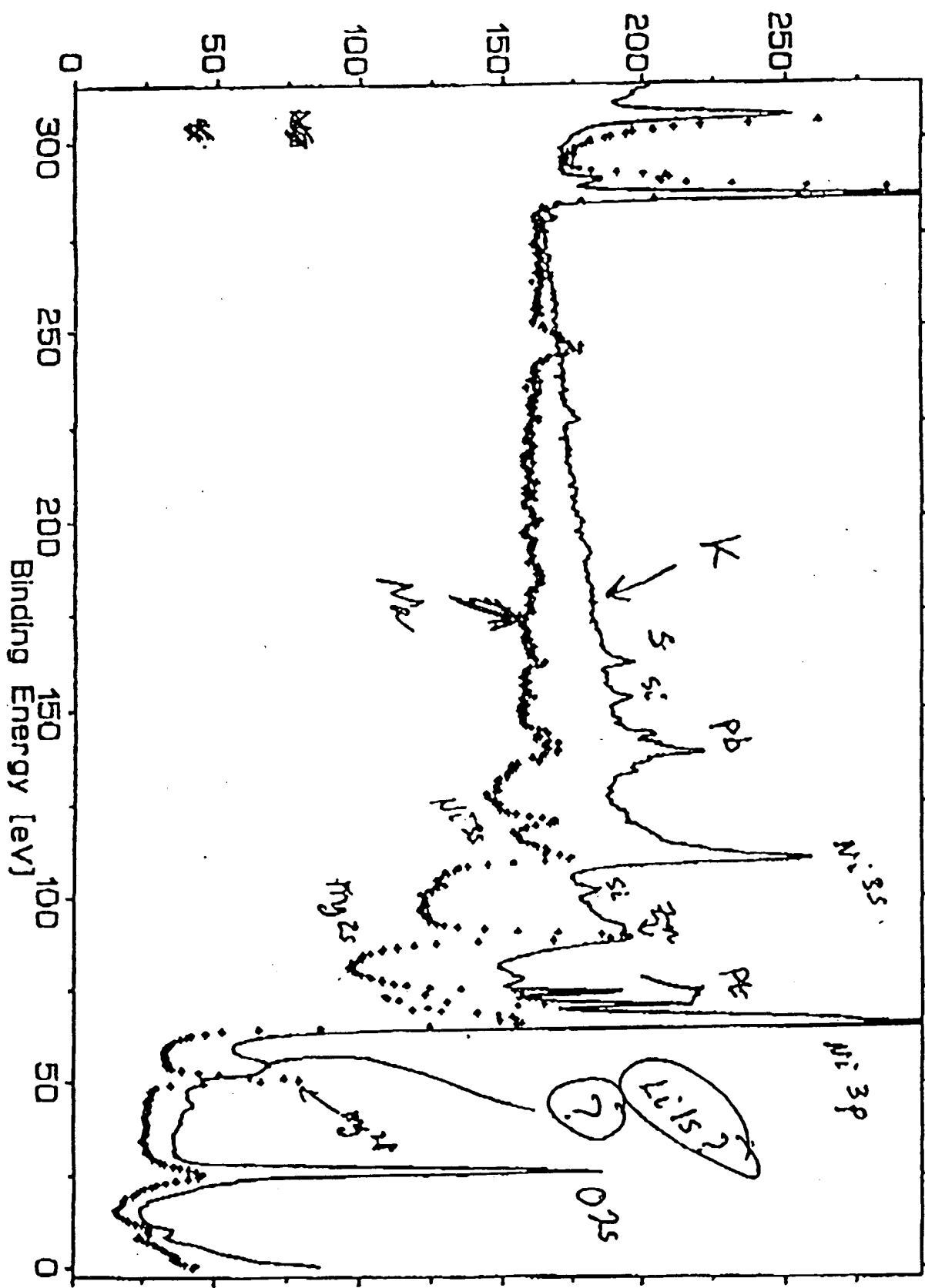
28173 Counts

Counts/Sec

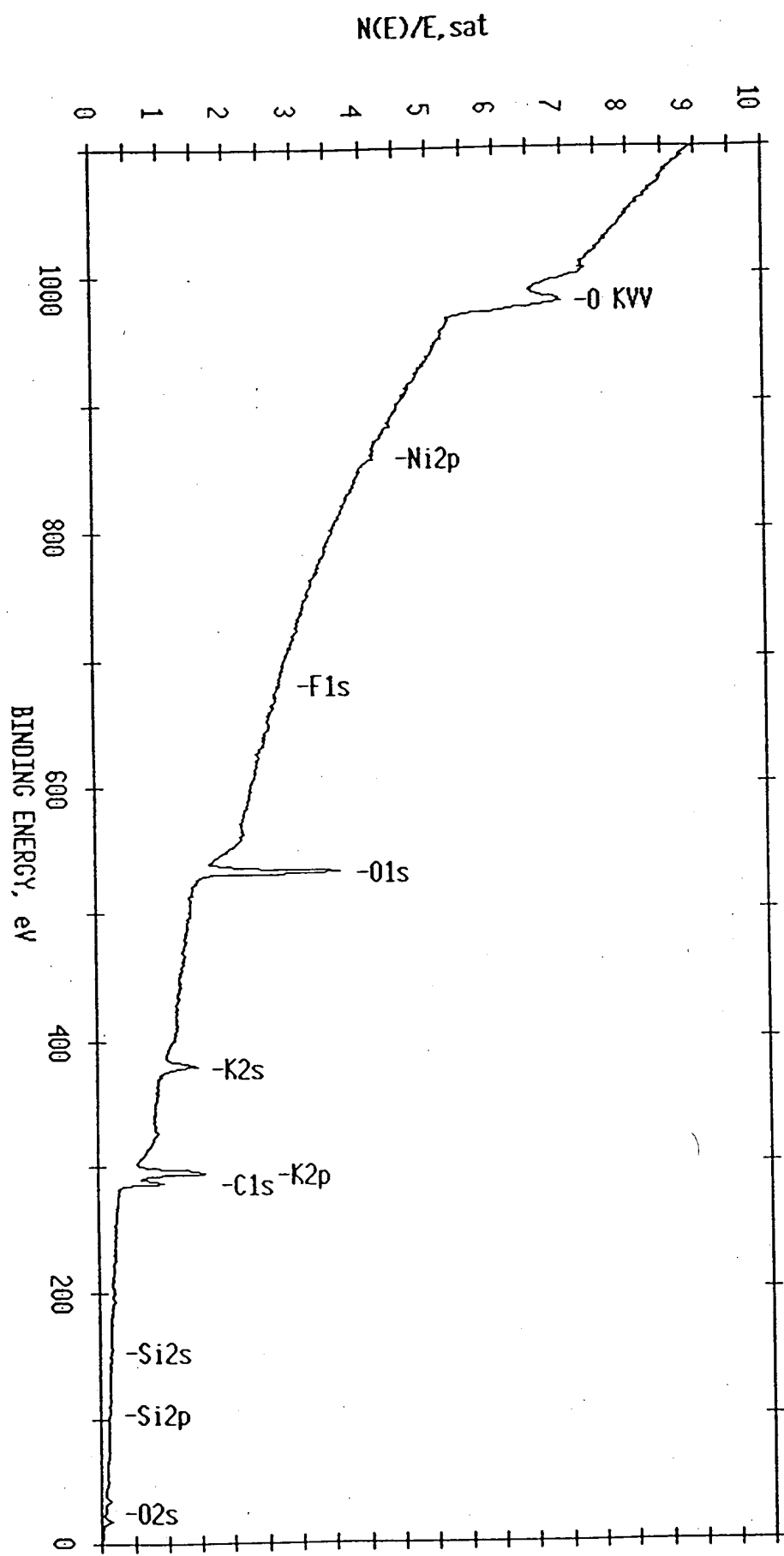
1445

N(E)/E, sat, Shf

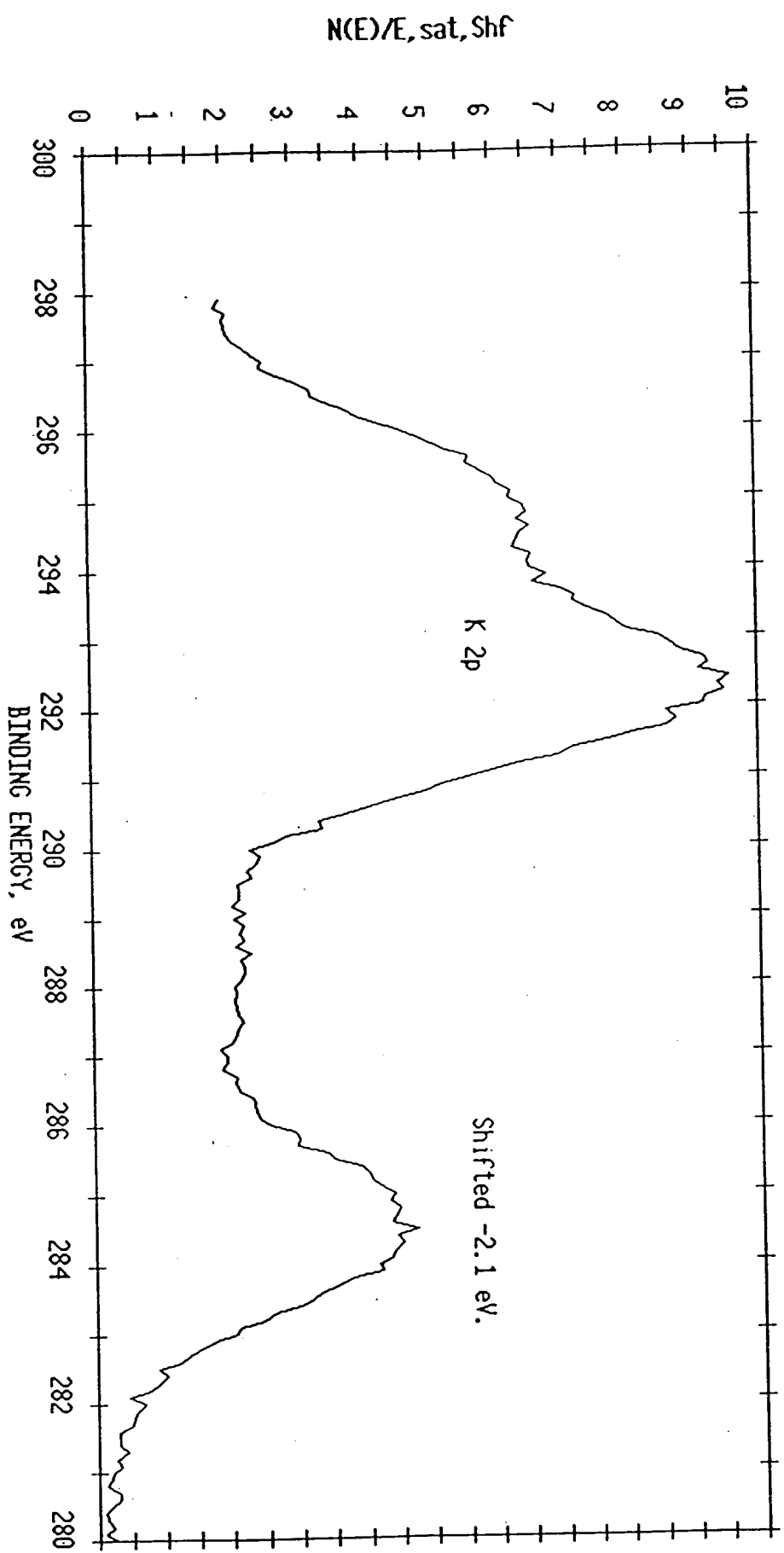


Counts  $\times 10^3$ 

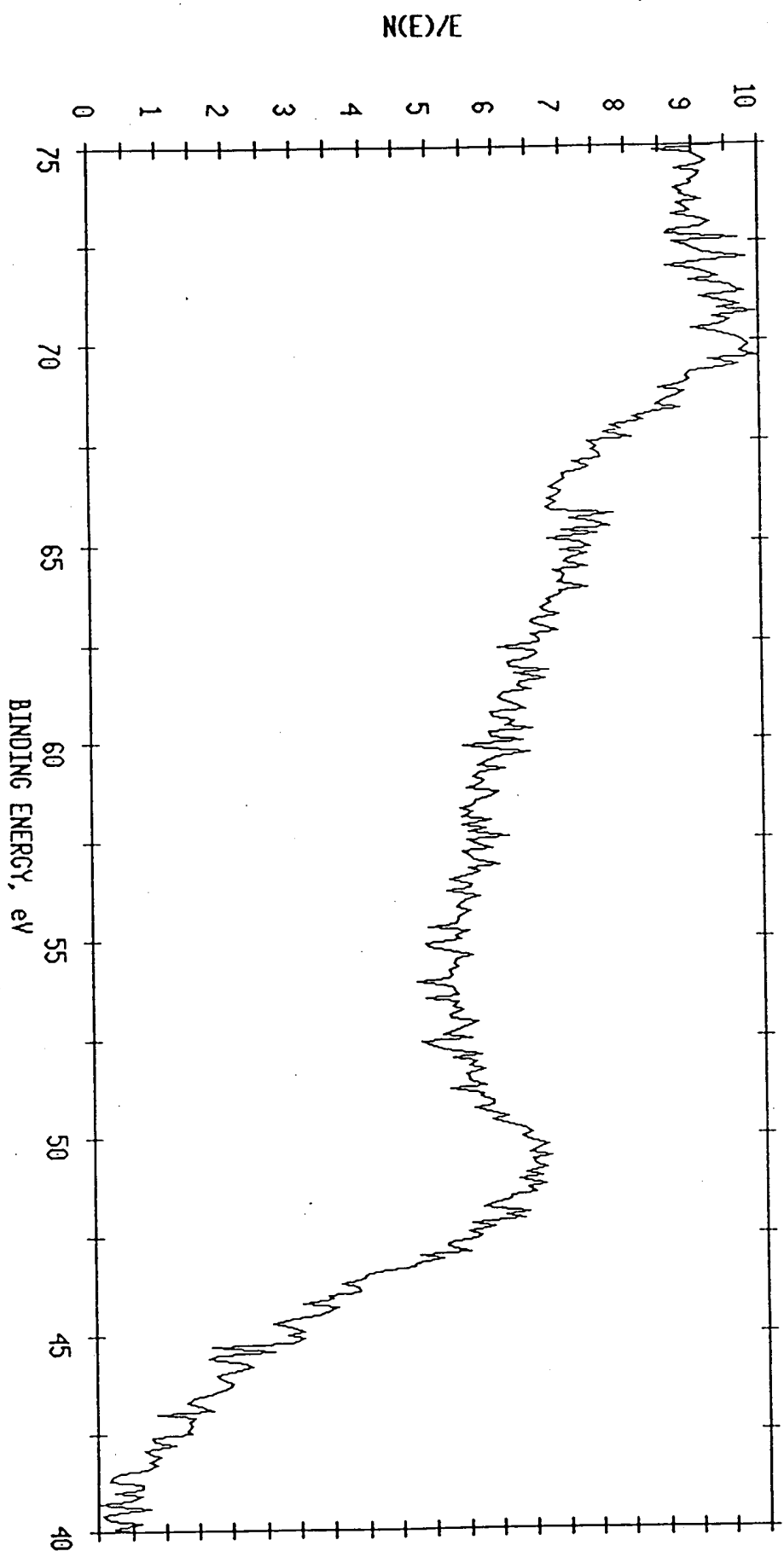
ESCA SURVEY 11/23/93 ANGLE= 15 deg ACQ TIME=29.36 min.  
FILE: Nitest40 Ni foil after treatment for 5 days.  
SCALE FACTOR= 9.221 k c/s, OFFSET= 0.532 k c/s PASS ENERGY=178.950 eV Al 400  $\mu$



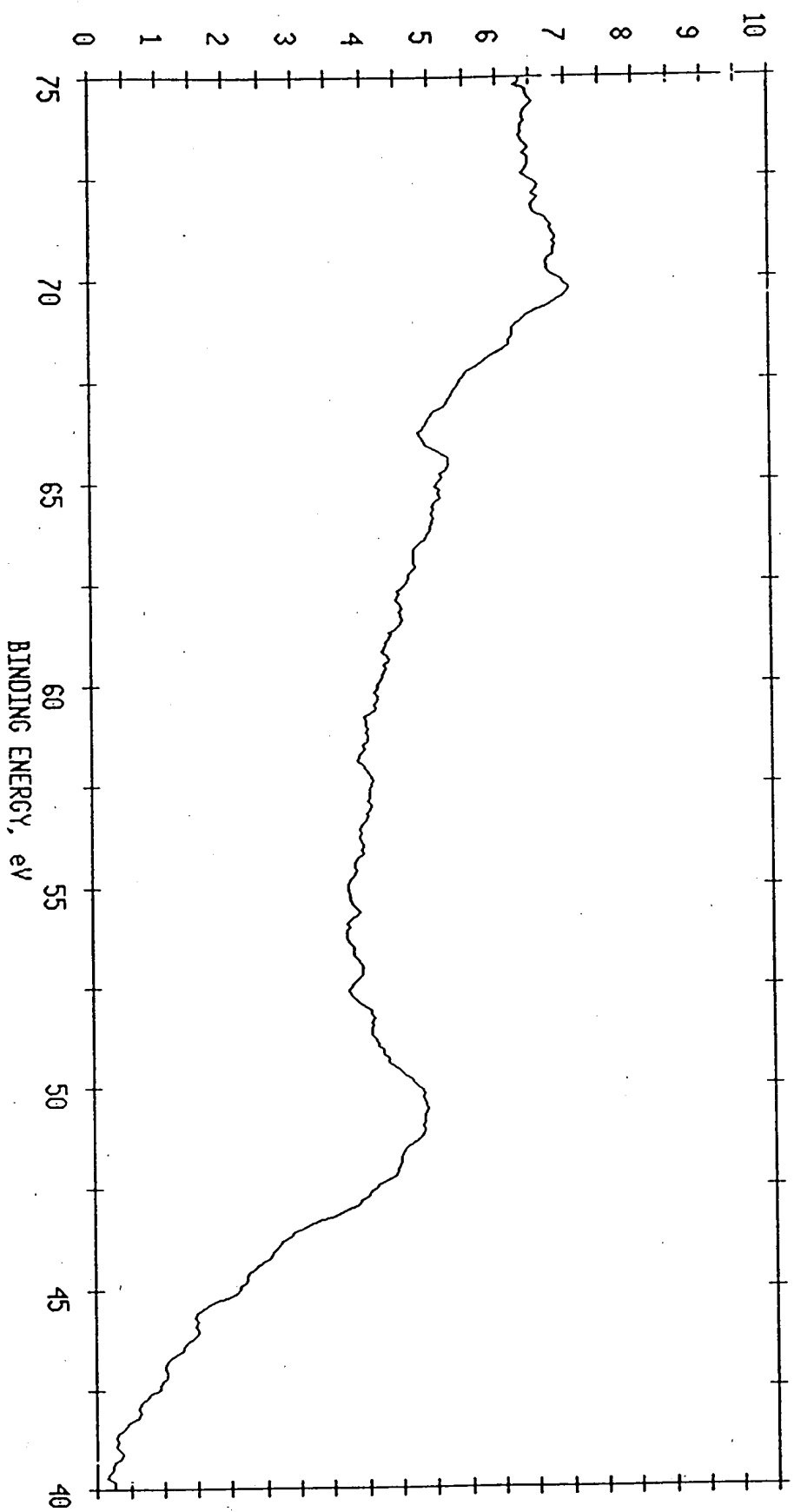
ESCA MULTIPLEX 11/23/93 EL=C1 REG 1 ANGLE= 15 deg ACQ TIME=2.51 min  
FILE: Nitest41 Ni foil after treatment for 5 days.  
SCALE FACTOR= 0.905 k c/s, OFFSET= 1.883 k c/s PASS ENERGY=143.050 eV Al 400 W



ESCA MULTIPLEX 11/23/93 EL= REG 2 ANGLE= 15 deg ACQ TIME=114.08 min  
FILE: Nitest41 Ni foil after treatment for 5 days.  
SCALE FACTOR= 0.029 k c/s, OFFSET= 0.855 k c/s PASS ENERGY=143.050 eV Al 400 W



N(E)/E<sub>sat</sub>,smol1



ESCA MULTIPLEX 11/23/93 EL= REG 2 ANGLE= 15 deg ACC TIME=114.08 min  
FILE: Nitest41 Ni foil after treatment for 5 days.  
SCALE FACTOR= 0.039 k c/s, OFFSET= 0.755 k c/s PASS ENERGY=143.050 eV Al 400  $\mu$

■ Energy (eV)

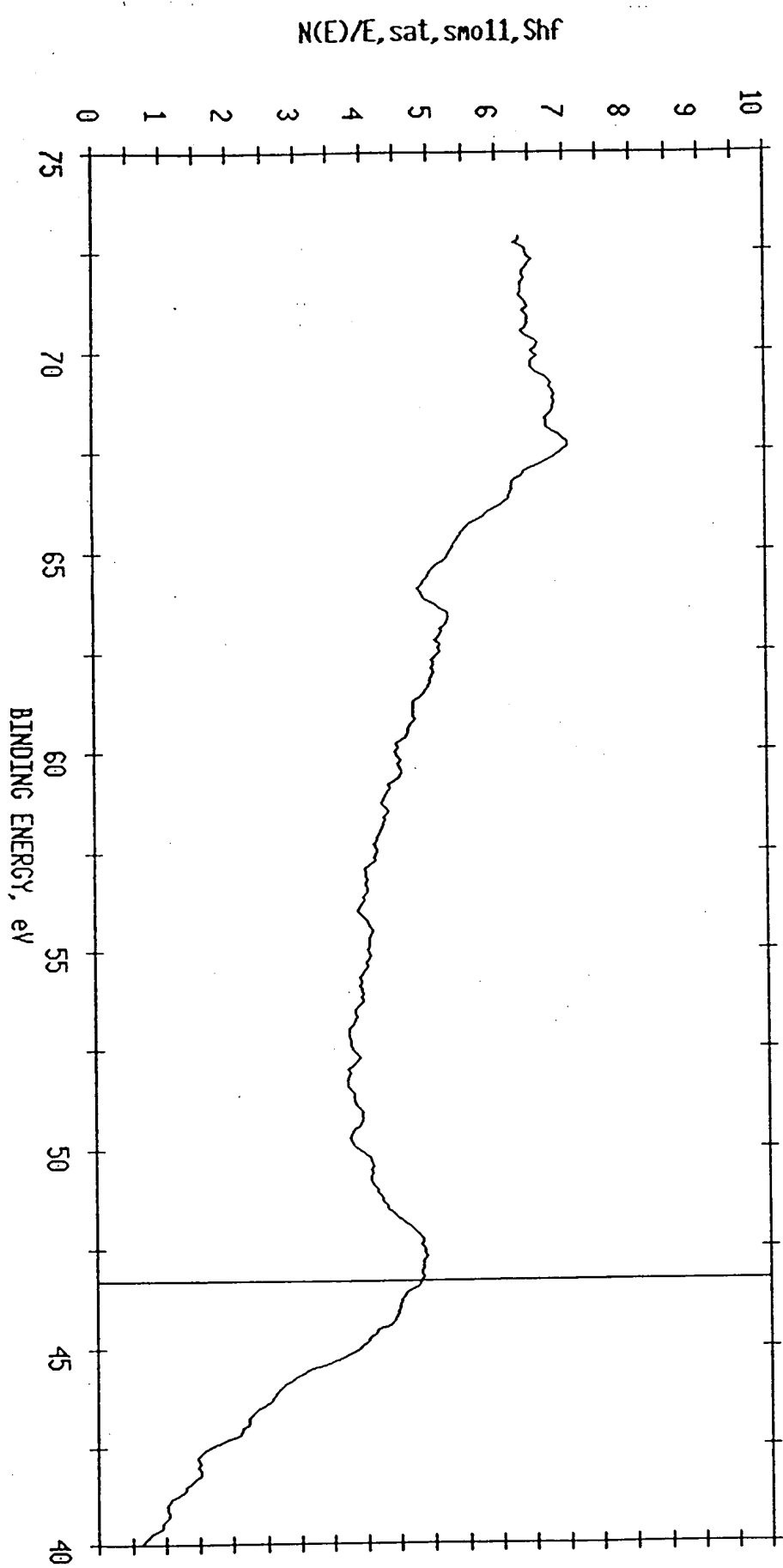
46.700

Counts

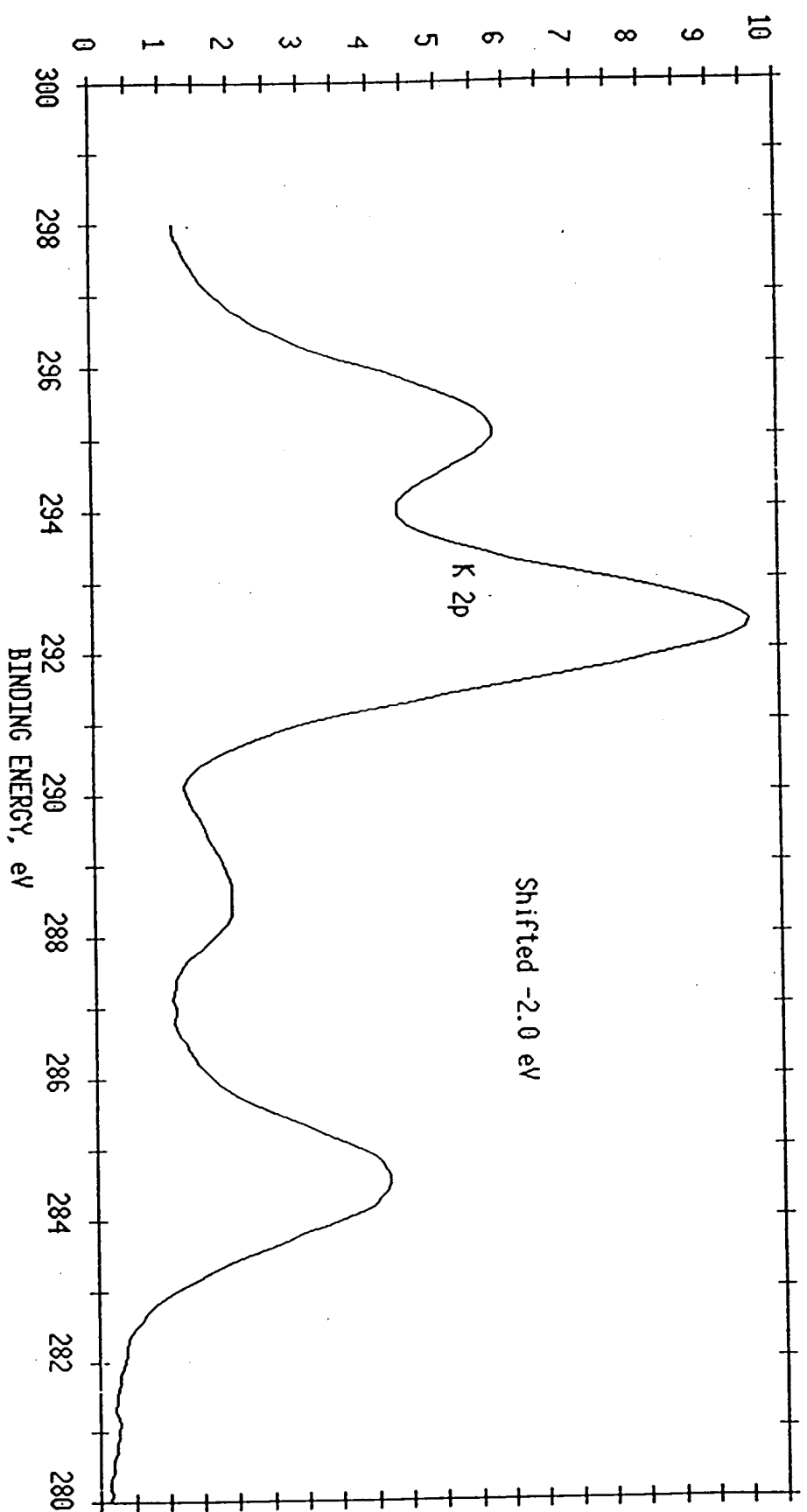
18374 Counts/Sec

942

CURSOR



N(E)/E, sat, small, Shf

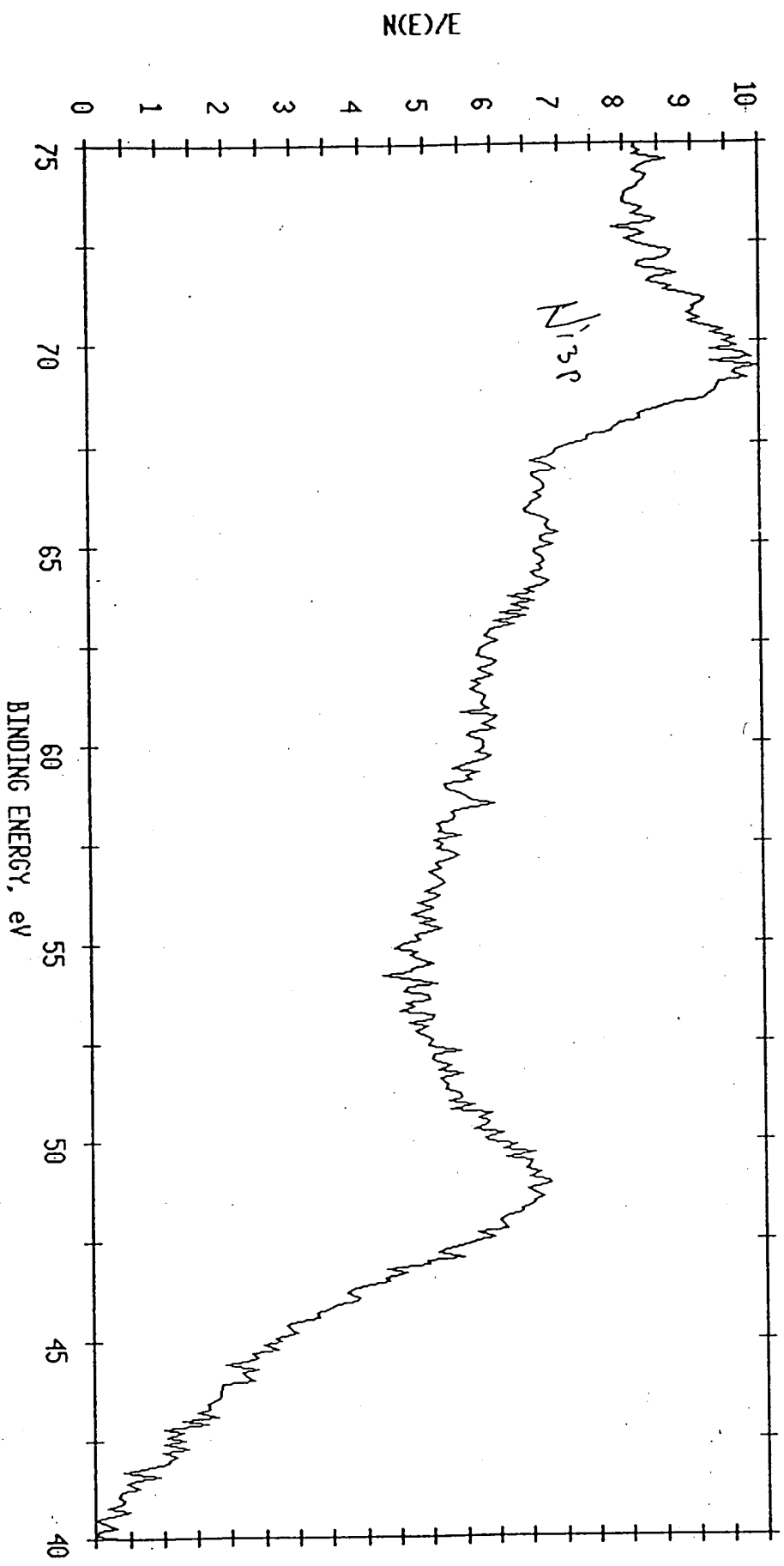


ESCA MULTIPLEX 11/23/93 EL=C1 REG 1 ANGLE= 15 deg ACQ TIME=4.19 min

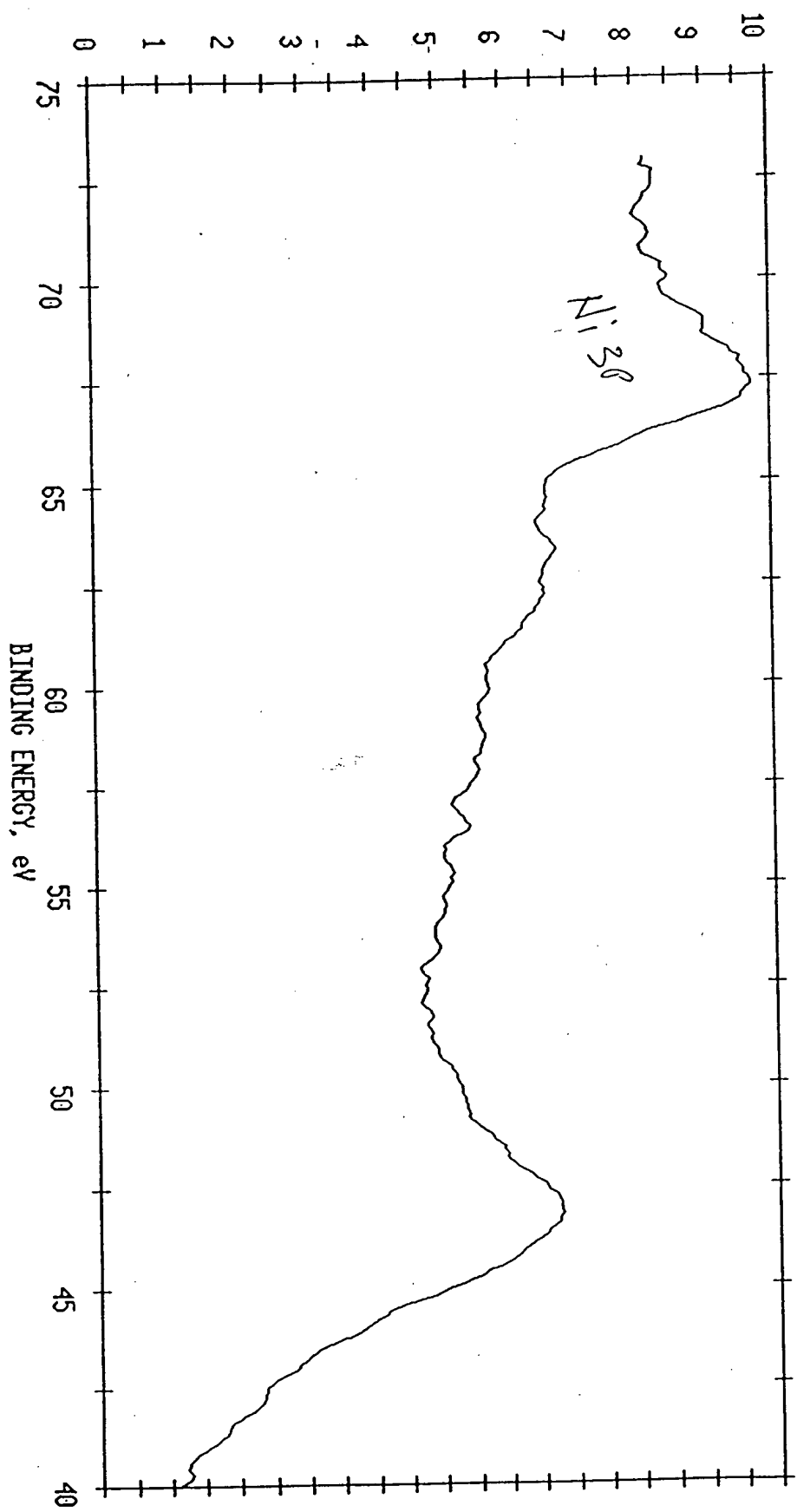
FILE: Nitest42 Ni foil after treatment for 5 days.

SCALE FACTOR= 0.378 K C/S. OFFSET= 0.689 K C/S PASS ENERGY= 71.550 eV AI 400 W

ESCA MULTIPLEX 11/23/93 EL= REG 2 ANGLE= 15 deg ACCQ TIME=609.86 min  
FILE: Nitest42 Ni foil after treatment for 5 days.  
SCALE FACTOR= 0.012 k c/s, OFFSET= 0.455 k c/s PASS ENERGY= 71.550 eV Al 400  $\mu$



N(E)/E, sat, sm011, Shf



ESCA MULTIPLEX 11/23/93 EL= REG 2 ANGLE= 15 deg ACQ TIME=609.86 min  
FILE: Nitest42 Ni foil after treatment for 5 days.  
SCALE FACTOR= 0.012 k c/s, OFFSET= 0.403 k c/s PASS ENERGY= 71.550 eV Al 400 W

3 Energy (eV)

46.800

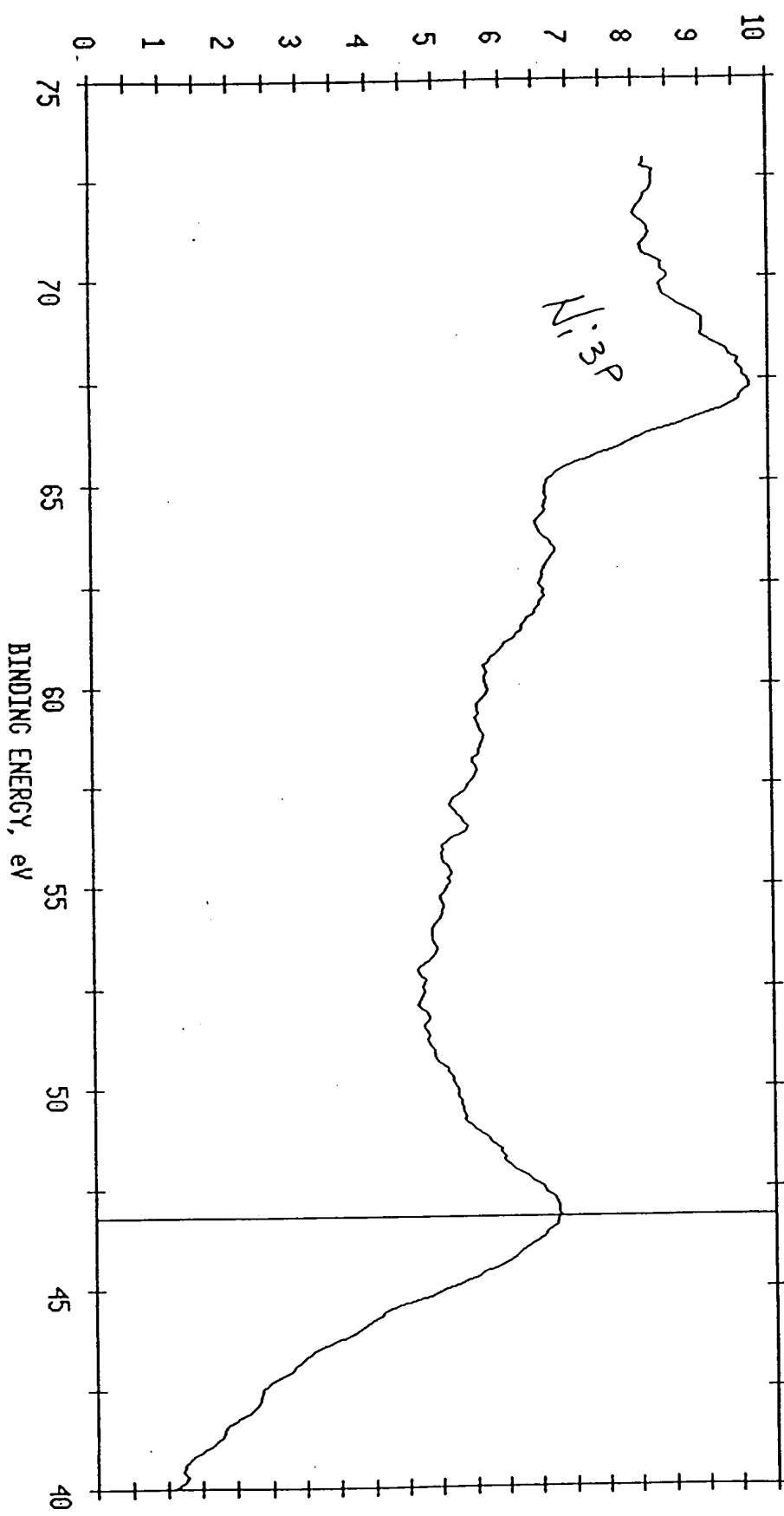
Cursor

Counts

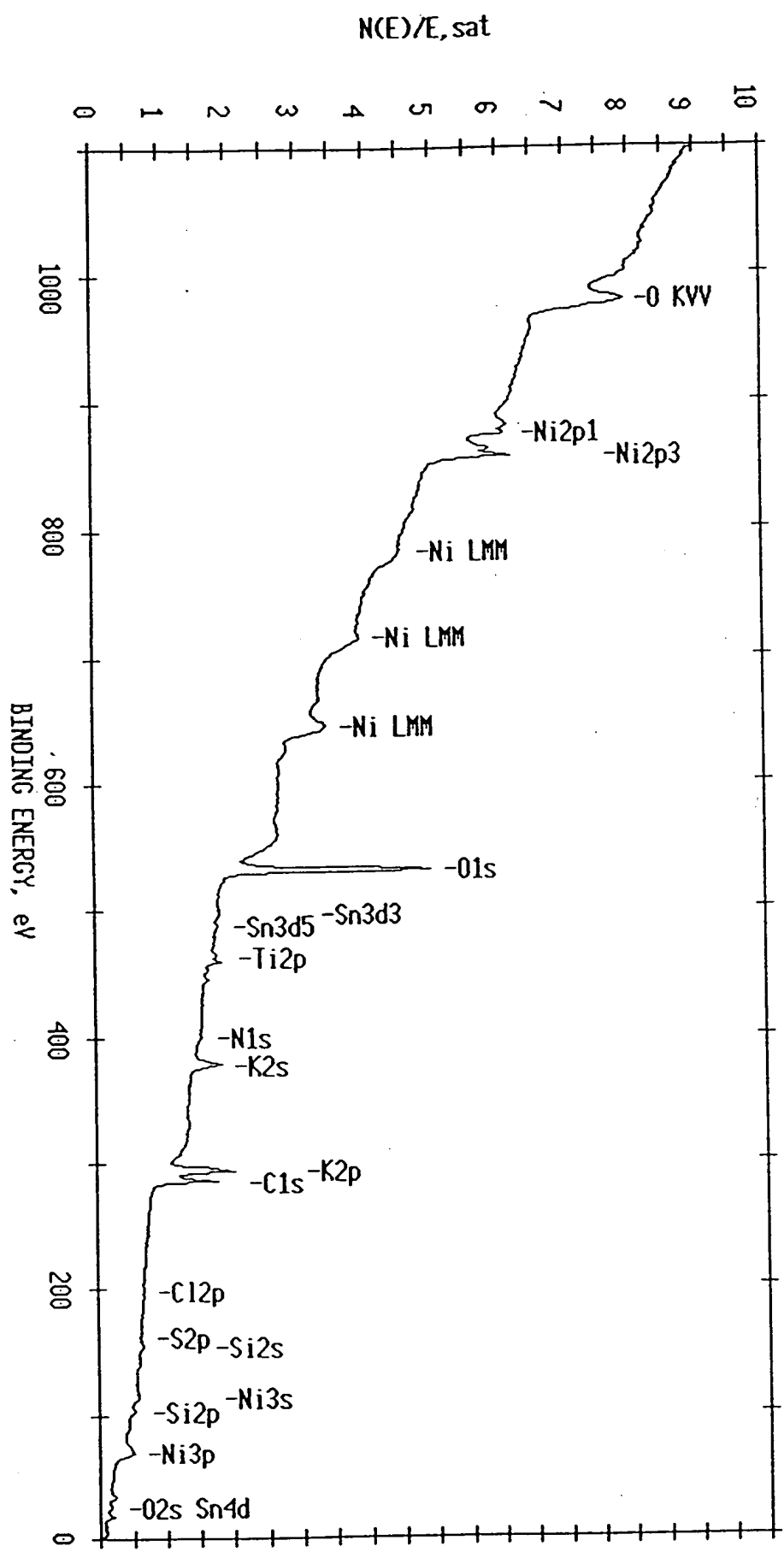
50692 Counts/Sec

486

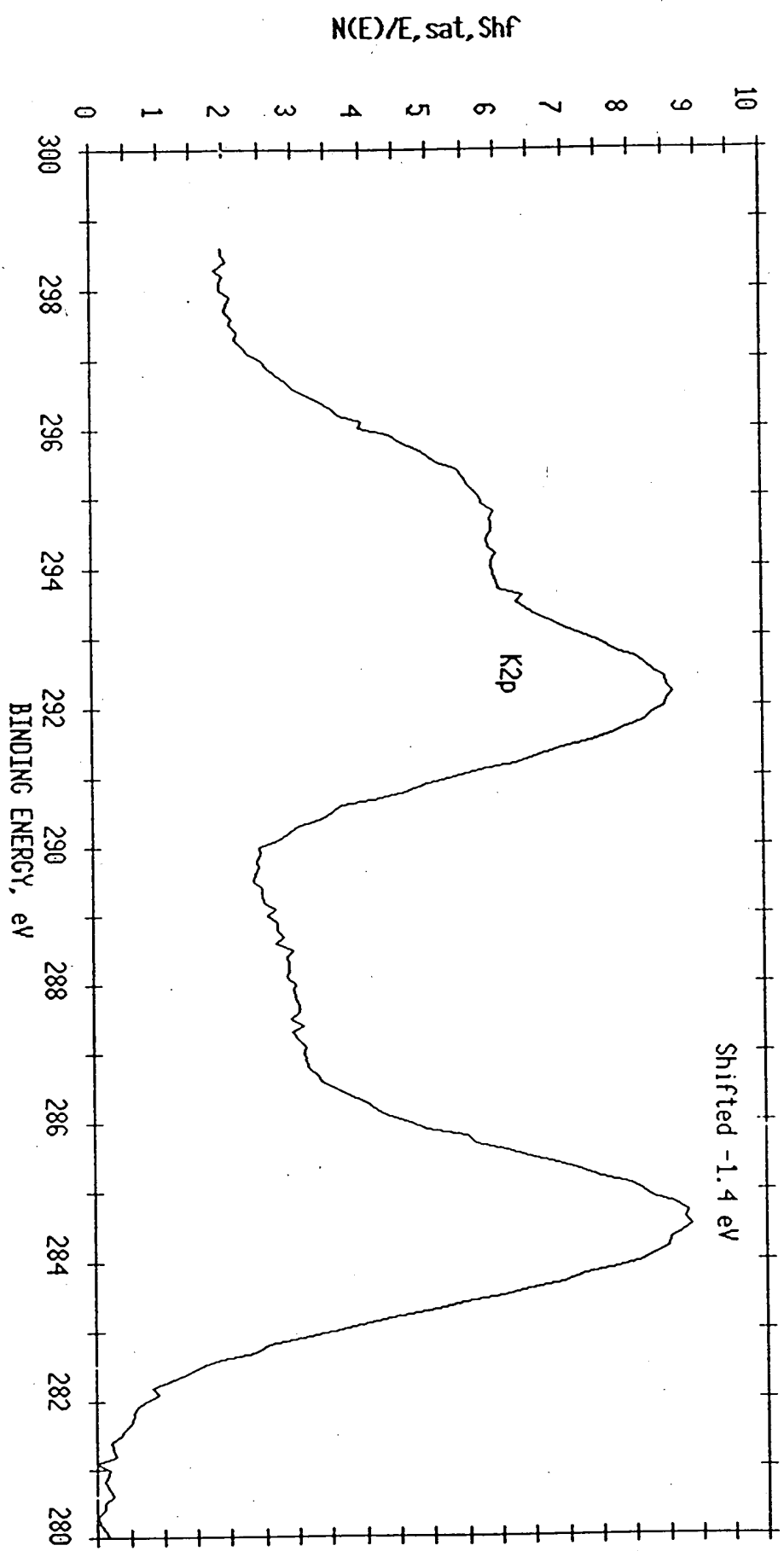
N(E)/E, sat, small, Shf



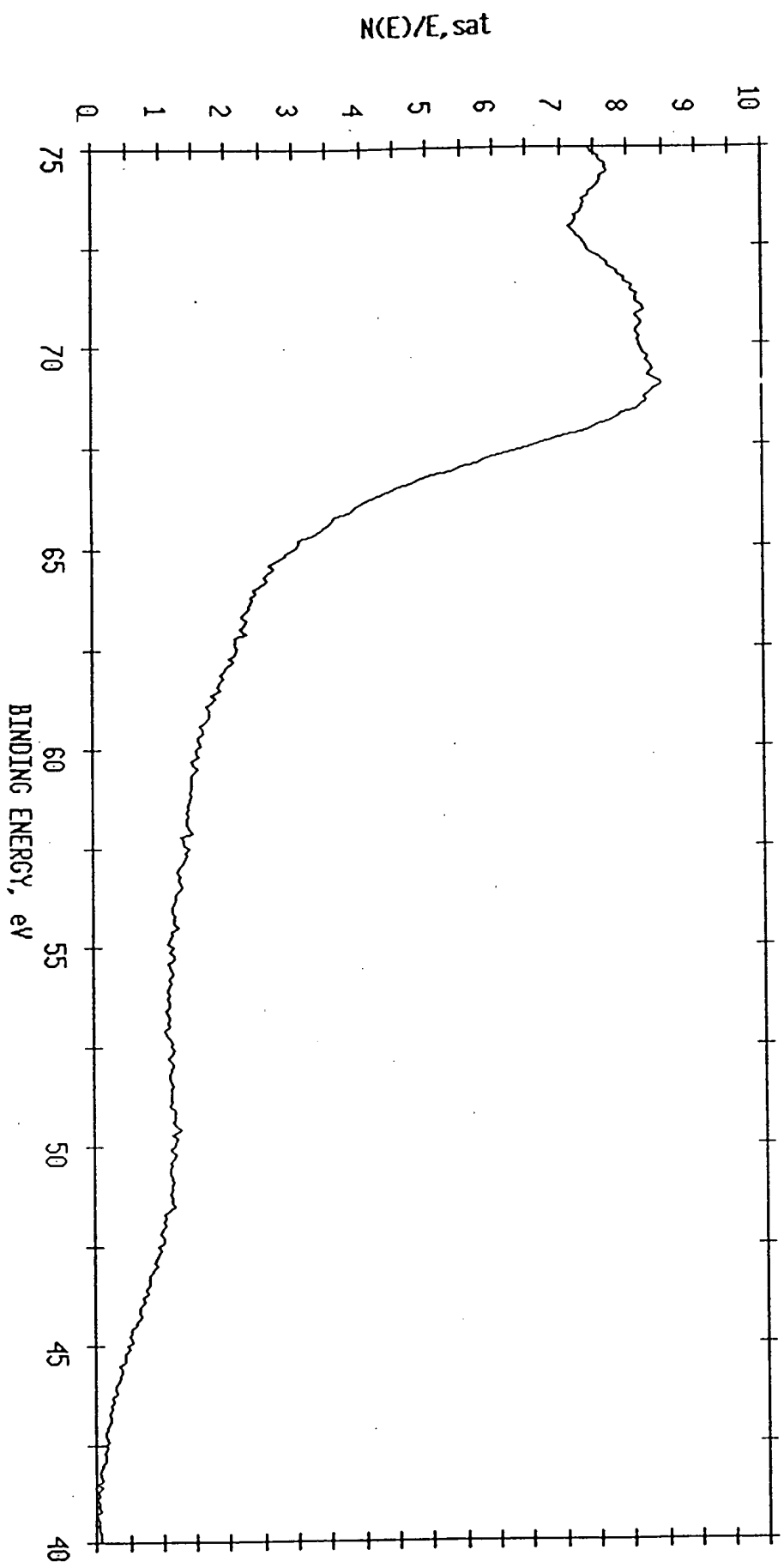
ESCA SURVEY 11/22/93 ANGLE= 15 deg ACC TIME=29.36 min  
FILE: Nitest31 Ni foil treated for 4 days (same foil as 24 hr treat.)  
SCALE FACTOR= 44.544 k c/s, OFFSET= 4.987 k c/s PASS ENERGY=178.950 eV Al 400 W



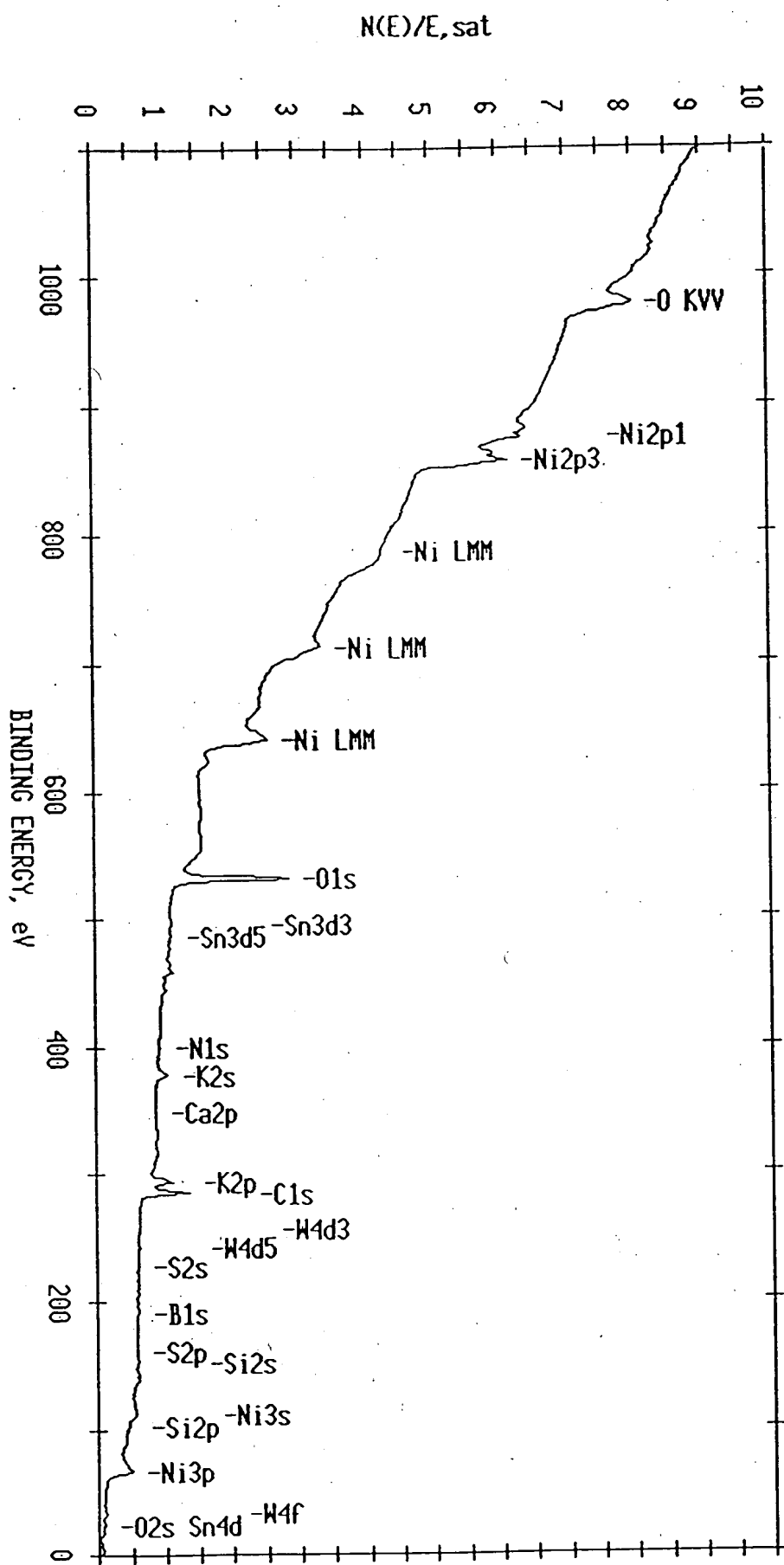
ESCA MULTIPLEX 11/22/93 EL=C1 REG 1 ANGLE= 15 deg ACQ TIME=1.67 min  
FILE: Nitest30 Ni foil treated for 4 days (same foil as 24 hr treat.)  
SCALE FACTOR= 4.250 k c/s, OFFSET= 25.454 k c/s PASS ENERGY=143.050 eV Al 400 W



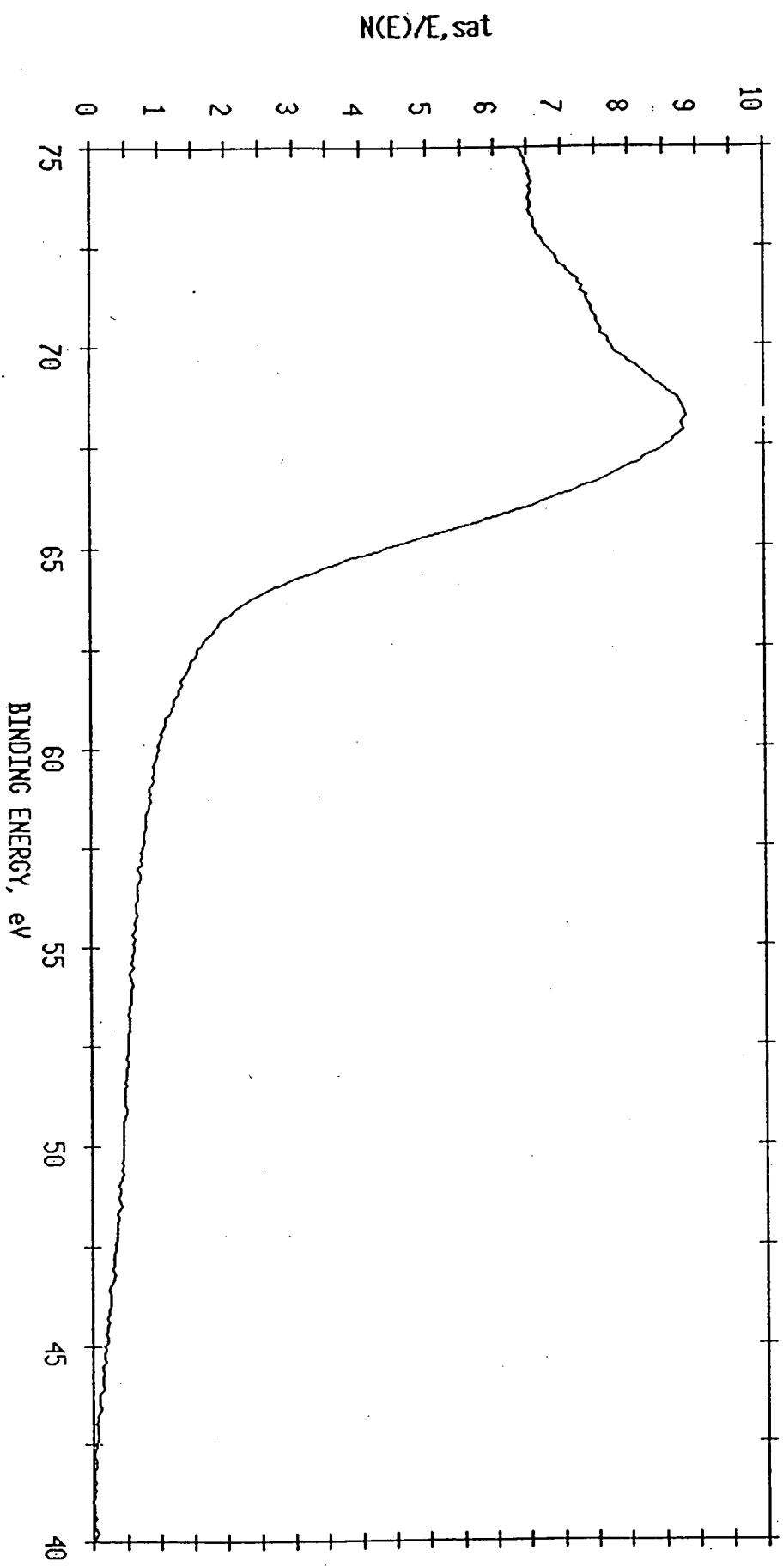
ESCA MULTIPLEX 11/22/93 EL= REG 2 ANGLE= 15 deg ACQ TIME=46.80 min  
FILE: Nitest30 Ni foil treated for 4 days (same foil as 24 hr treat.)  
SCALE FACTOR= 1.109 k c/s, OFFSET= 7.432 k c/s PASS ENERGY=143.050 eV Al 400  $\mu$



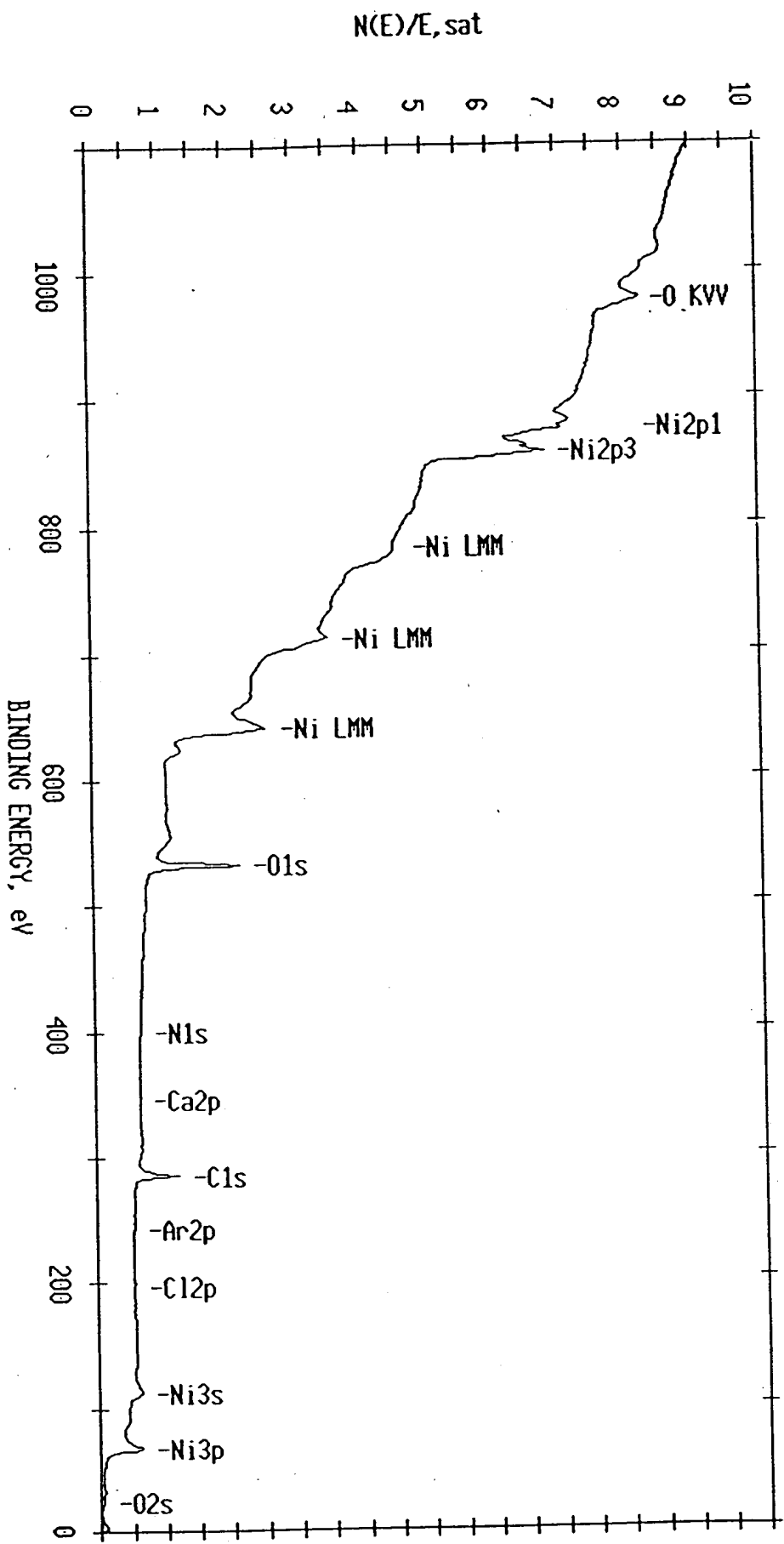
ESCA SURVEY 11/19/93 ANGLE= 15 deg ACC TIME=29.36 min  
FILE: Nitest26 Ni foil treated in lab for 24 hr. As received.  
SCALE FACTOR= 64.347 k c/s, OFFSET= 8.234 k c/s PASS ENERGY=178.950 eV Al 400  $\mu$



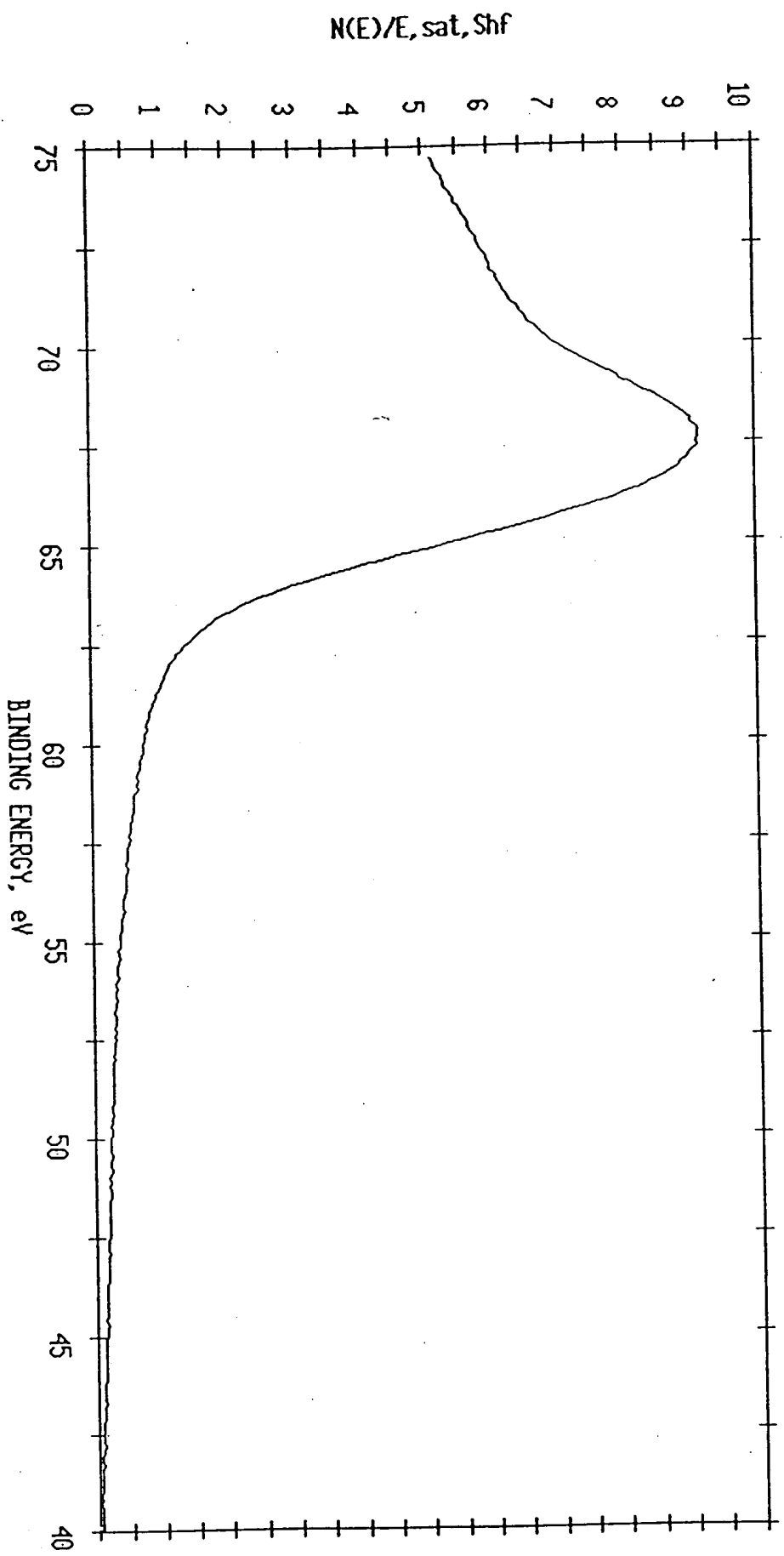
ESCA MULTIPLEX 11/19/93 EL= REG 2 ANGLE= 15 deg ACC TIME=84.83 min  
FILE: Nitest25 Ni foil treated in lab for 24 hr. As received.  
SCALE FACTOR= 1.920 k c/s, OFFSET= 8.515 k c/s PASS ENERGY=143.050 eV Al 400 W



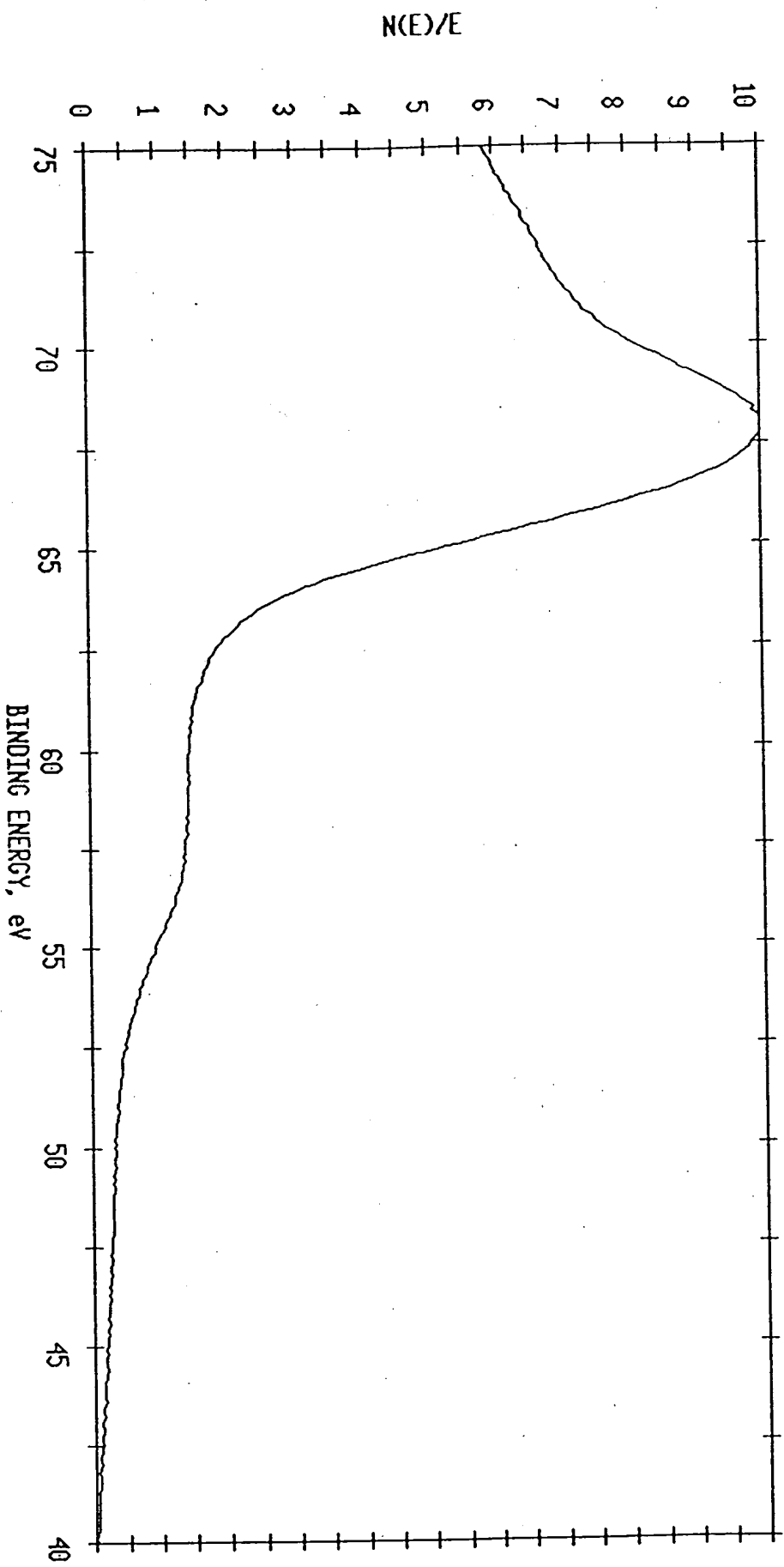
ESCA SURVEY 11/18/93 ANGLE= 15 deg ACQ TIME=29.36 min  
FILE: Nitest23 Ni foil untreated, as received.  
SCALE FACTOR= 80.815 k c/s, OFFSET= 11.386 k c/s PASS ENERGY=178.950 eV Al 400  $\mu$



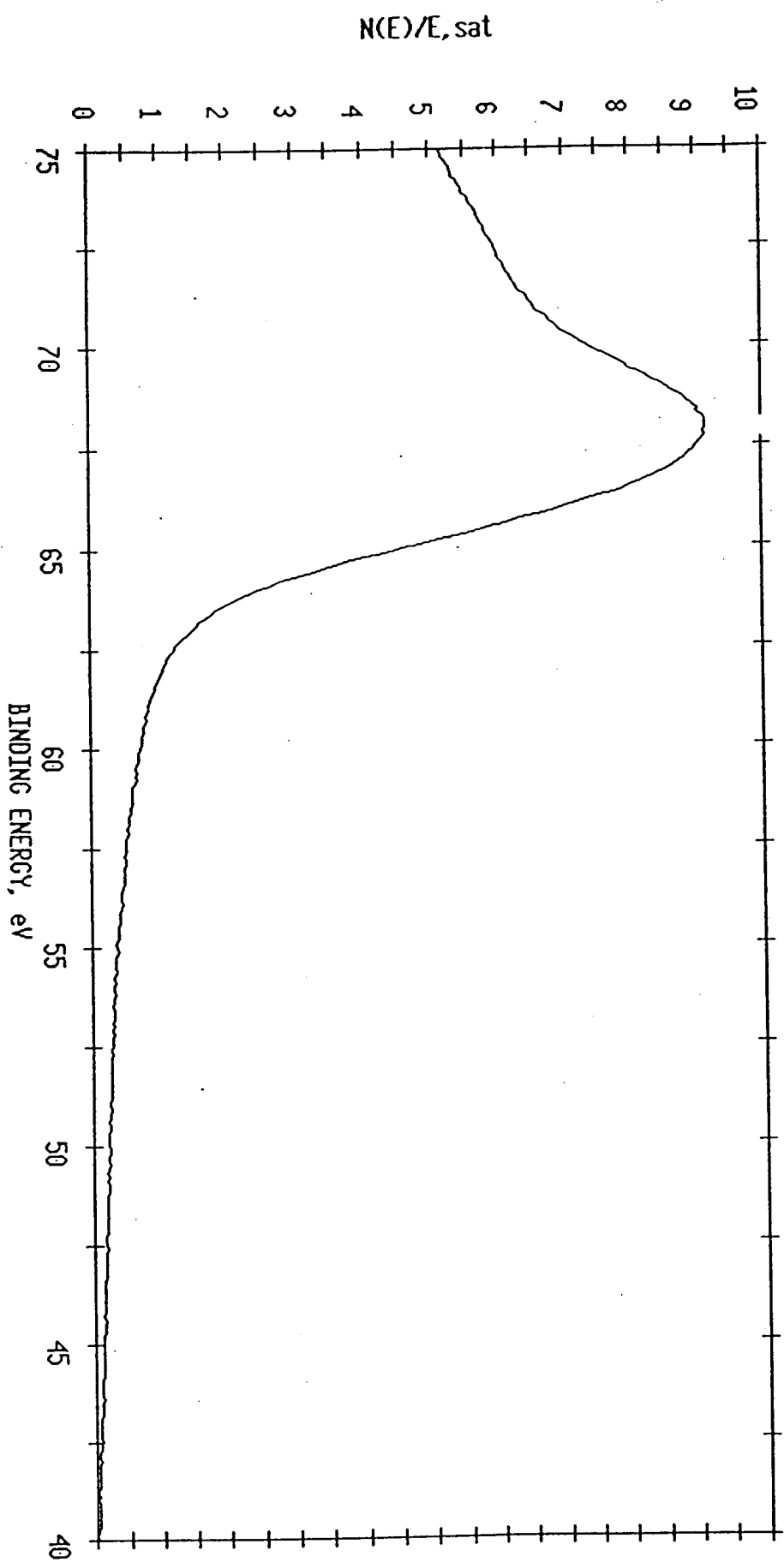
ESCA MULTIPLEX 11/18/93 EL= REG 2 ANGLE= 15 deg ACC TIME=76.05 min  
FILE: Nitest22 Ni foil untreated, as received.  
SCALE FACTOR= 3.401 k c/s, OFFSET= 9.545 k c/s PASS ENERGY=143.050 eV Al 400 W



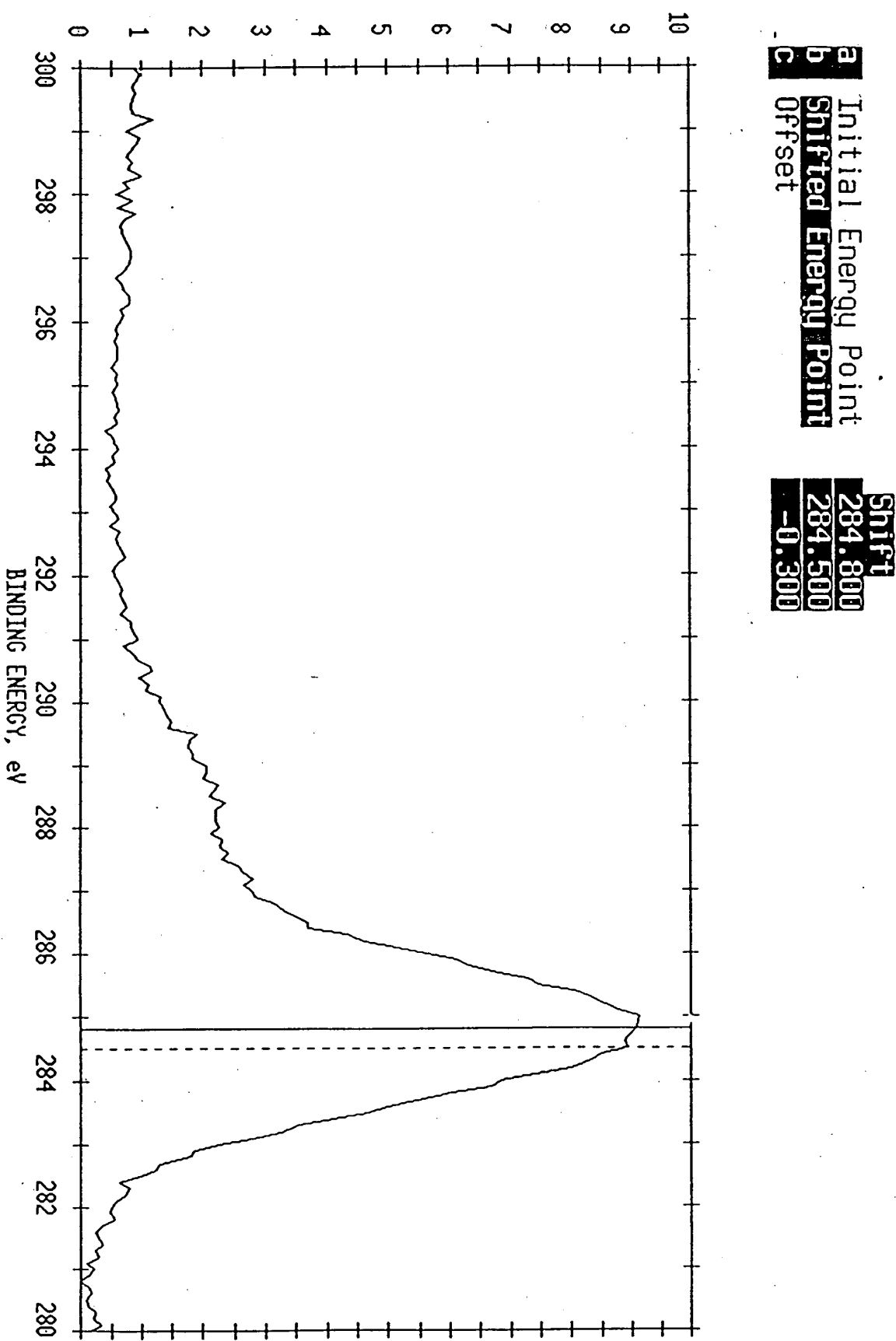
ESCA MULTIPLEX 11/18/93 EL= REG 2 ANGLE= 15 deg ACQ TIME=76.05 min  
FILE: Nitest22 Ni foil untreated. as received.  
SCALE FACTOR= 3.278 k c/s, OFFSET= 10.778 k c/s PASS ENERGY=143.050 eV Al 400 W



ESCA MULTIPLEX 11/18/93 EL= REG 2 ANGLE= 15 deg ACQ TIME=76.05 min  
FILE: Nitest22 Ni foil untreated as received.  
SCALE FACTOR= 3.401 k c/s, OFFSET= 9.545 k c/s PASS ENERGY=143.050 eV Al 400  $\mu$



$N(E)/E_{sat}$



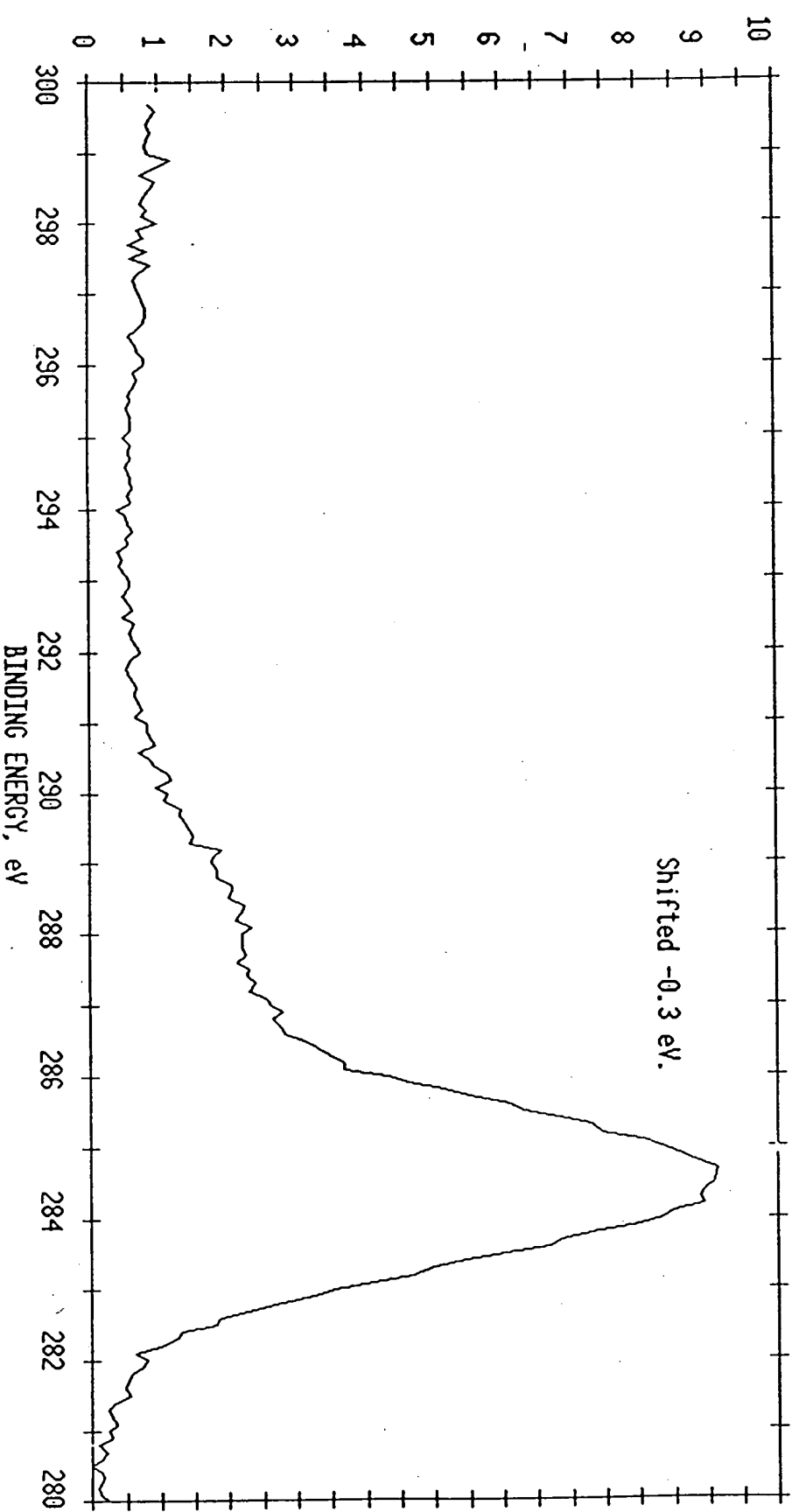
N(E)/E<sub>sat</sub>, Shf

ESCA MULTIPLEX 11/18/93 EL=C1 REG 1 ANGLE= 15 deg ACQ TIME=0.84 min

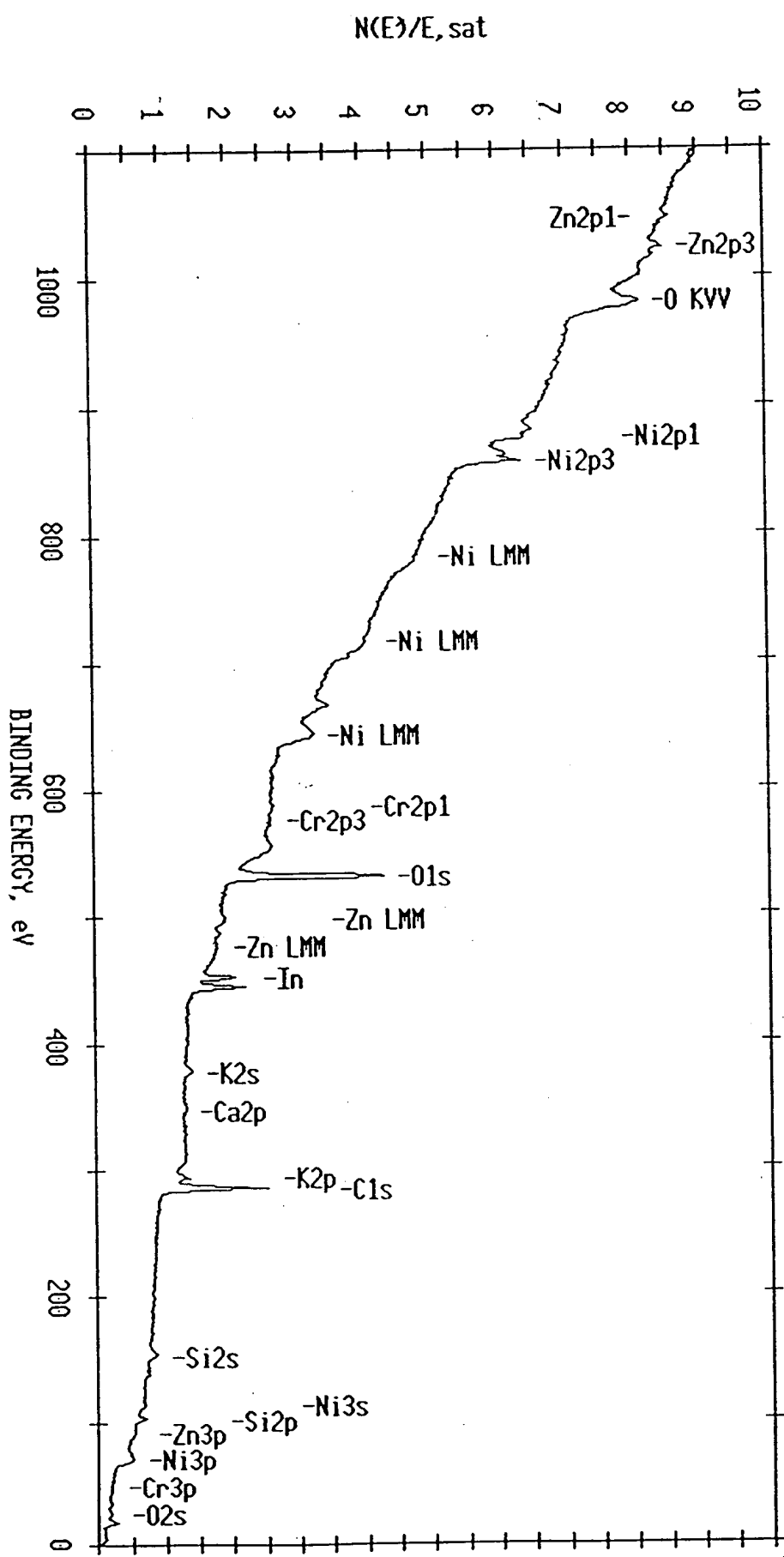
FILE: Nitest22 Ni foil untreated. as received.

SCALE FACTOR= 5.007 k c/s, OFFSET= 37.388 k c/s PASS ENERGY=143.050 eV Al 400 W

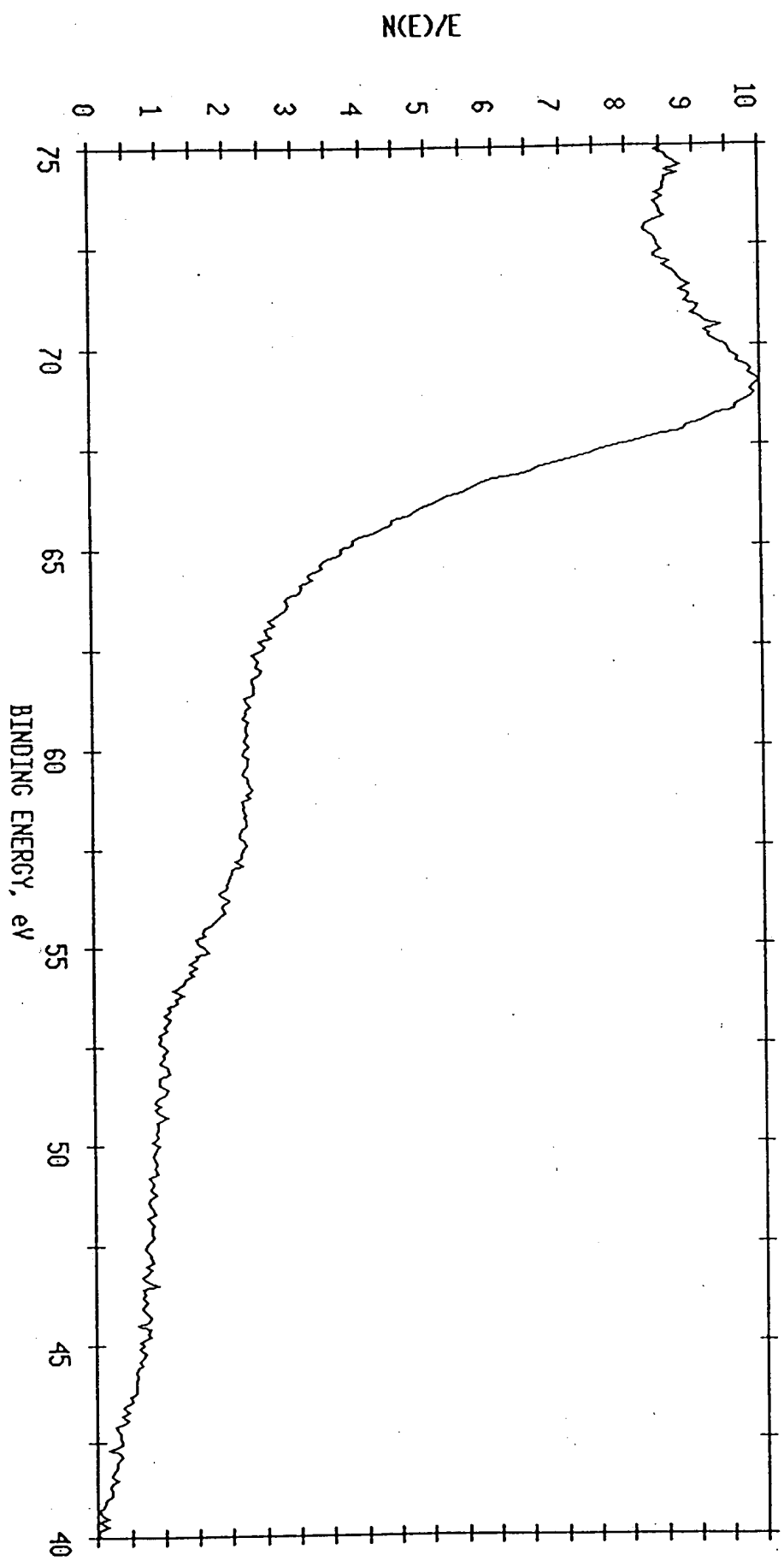
Shifted -0.3 eV.



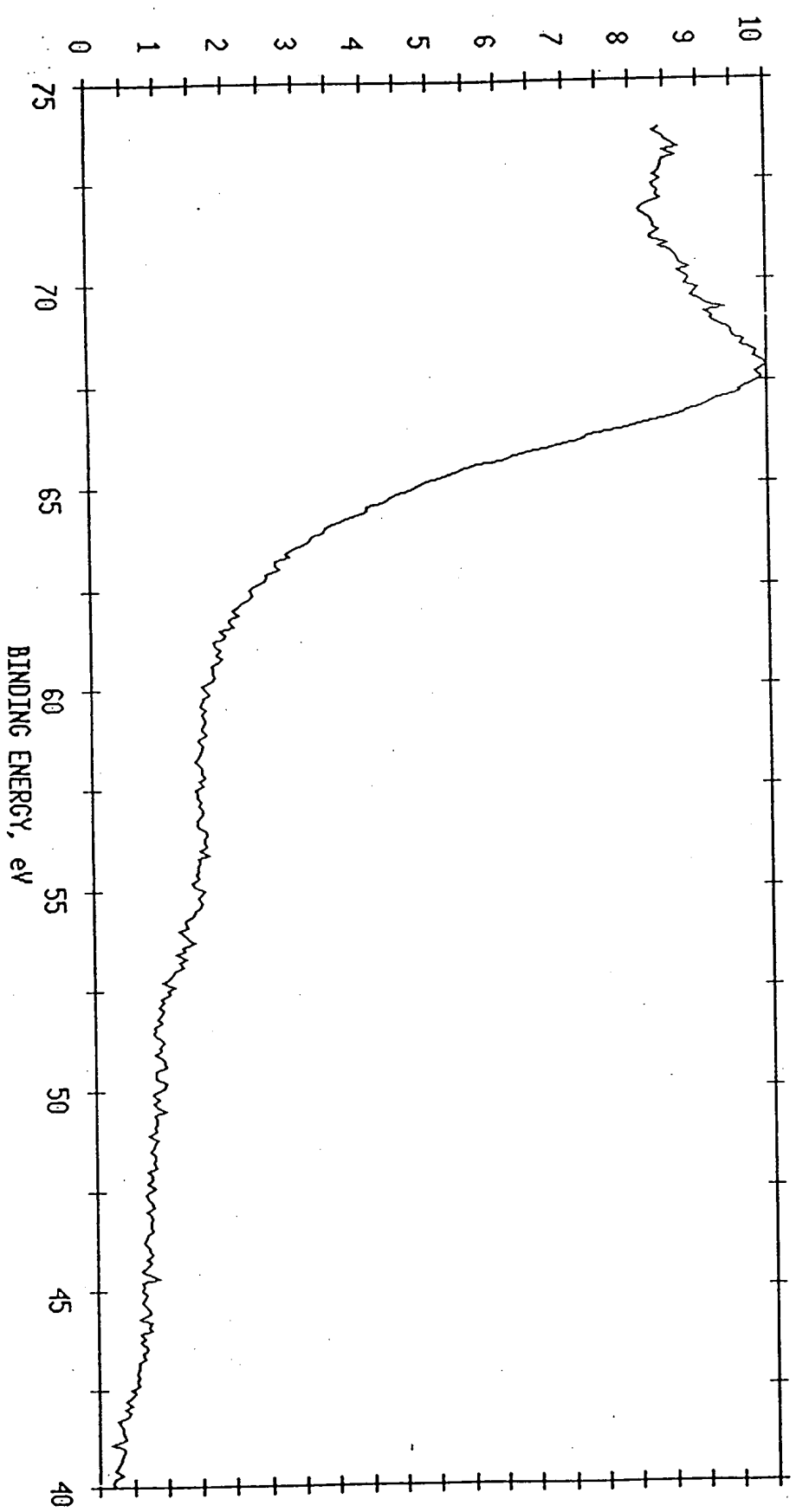
ESCA SURVEY 11/18/93 ANGLE= 15 deg ACQ TIME=29.36 min  
FILE: Nitest21 Ni wire processed in lab. as received  
SCALE FACTOR= 12.496 K c/s, OFFSET= 1.542 K c/s PASS ENERGY=178.950 eV Al 400  $\mu$



ESCA MULTIPLEX 11/18/93 EL= REG 2 ANGLE= 15 deg ACQ TIME=67.28 min  
FILE: Nitest20 Ni wire processed in lab. as received.  
SCALE FACTOR= 0.301 k c/s, OFFSET= 2.742 k c/s PASS ENERGY=143.050 eV AI 400  $\mu$



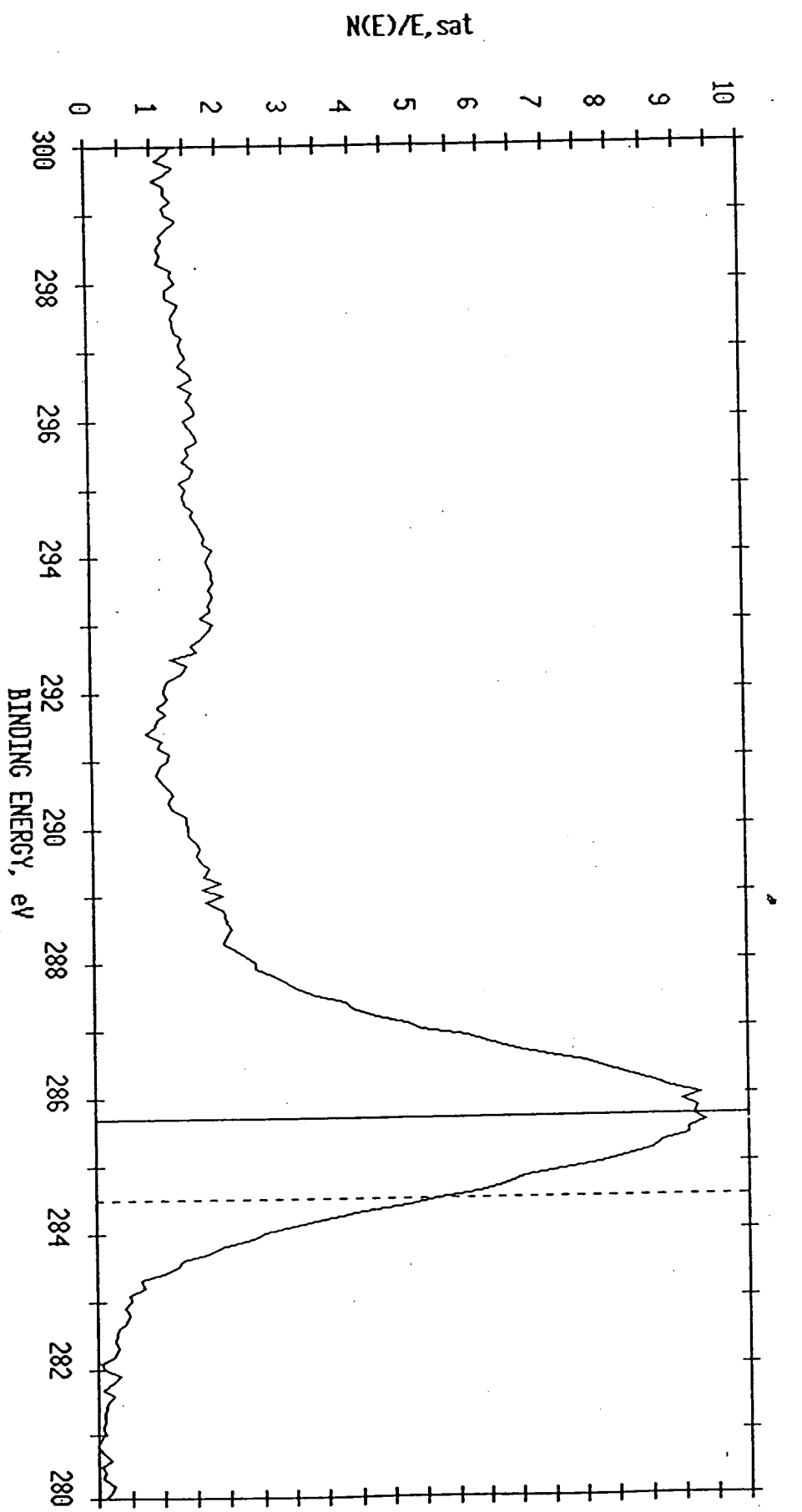
$N(E)/E_{sat}, Shf$



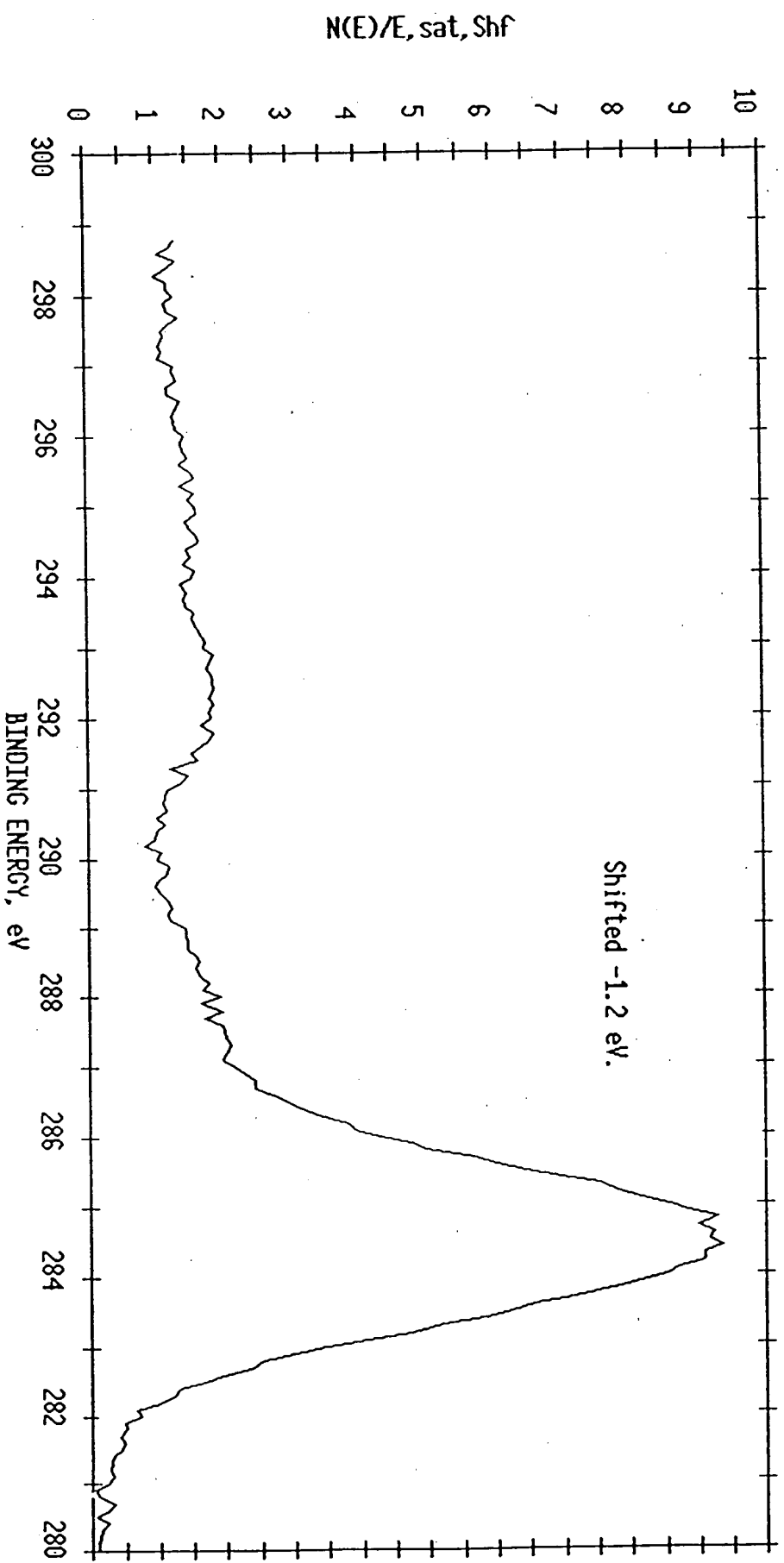
ESCA MULTIPLEX 11/18/93 EL= REG 2 ANGLE= 15 deg ACQ TIME=67.28 min  
FILE: Nitest20 Ni wire processed in lab. as received.  
SCALE FACTOR= 0.280 k c/s, OFFSET= 2.436 k c/s PASS ENERGY=143.050 eV Al 400  $\mu$

File N:\test\

a Initial Energy Point  
b Shifted Energy Point  
c Offset



ESCA MULTIPLEX 11/18/93 EL=C1 REG 1 ANGLE= 15 deg ACQ TIME=1.67 min  
FILE: Nitest20 Ni wire processed in lab. as received.  
SCALE FACTOR= 1.789 k c/s, OFFSET= 8.206 k c/s PASS ENERGY=143.050 eV Al 400  $\mu$



**E** Energy (eV)

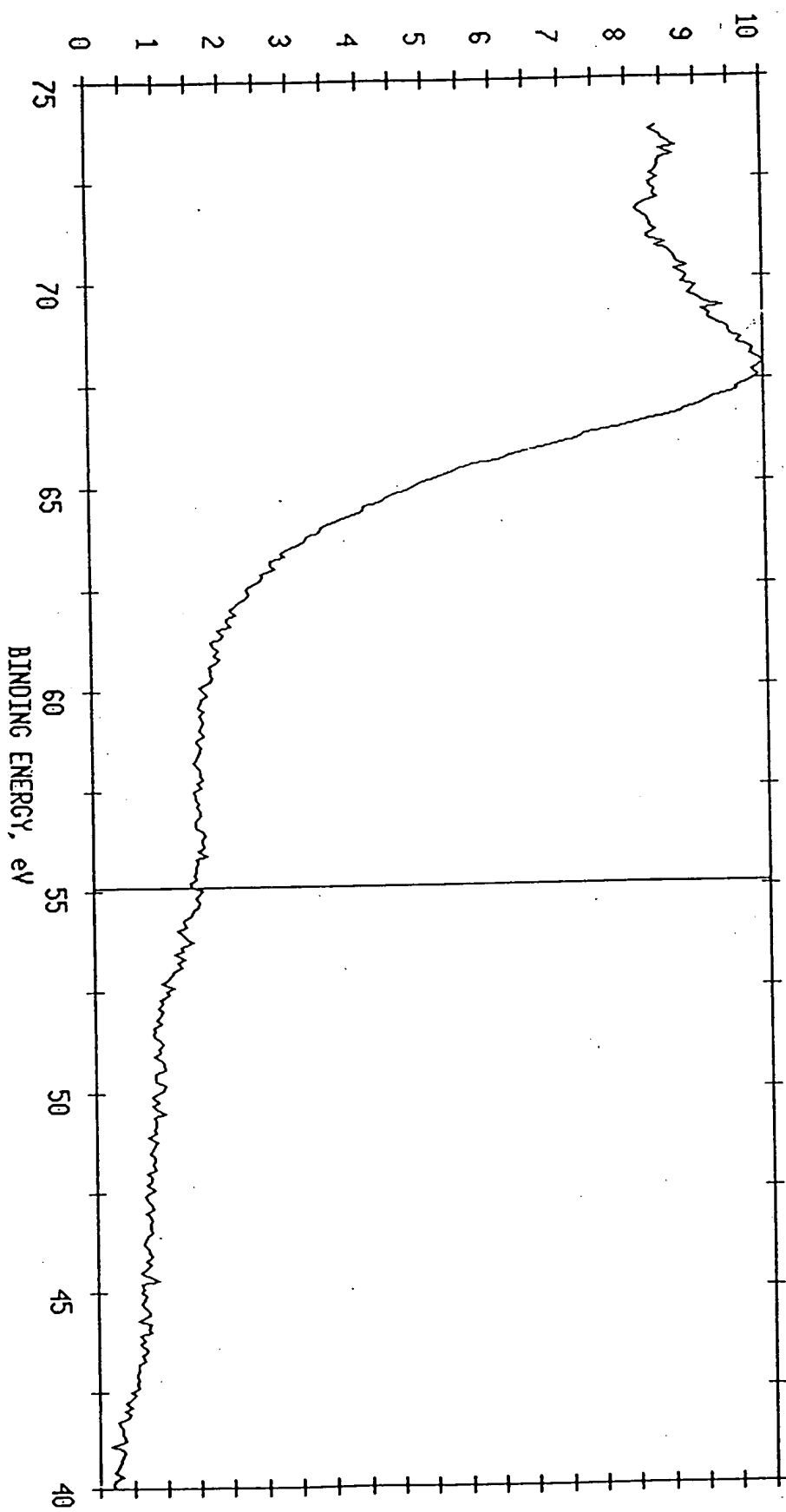
55.100

**Cursor**

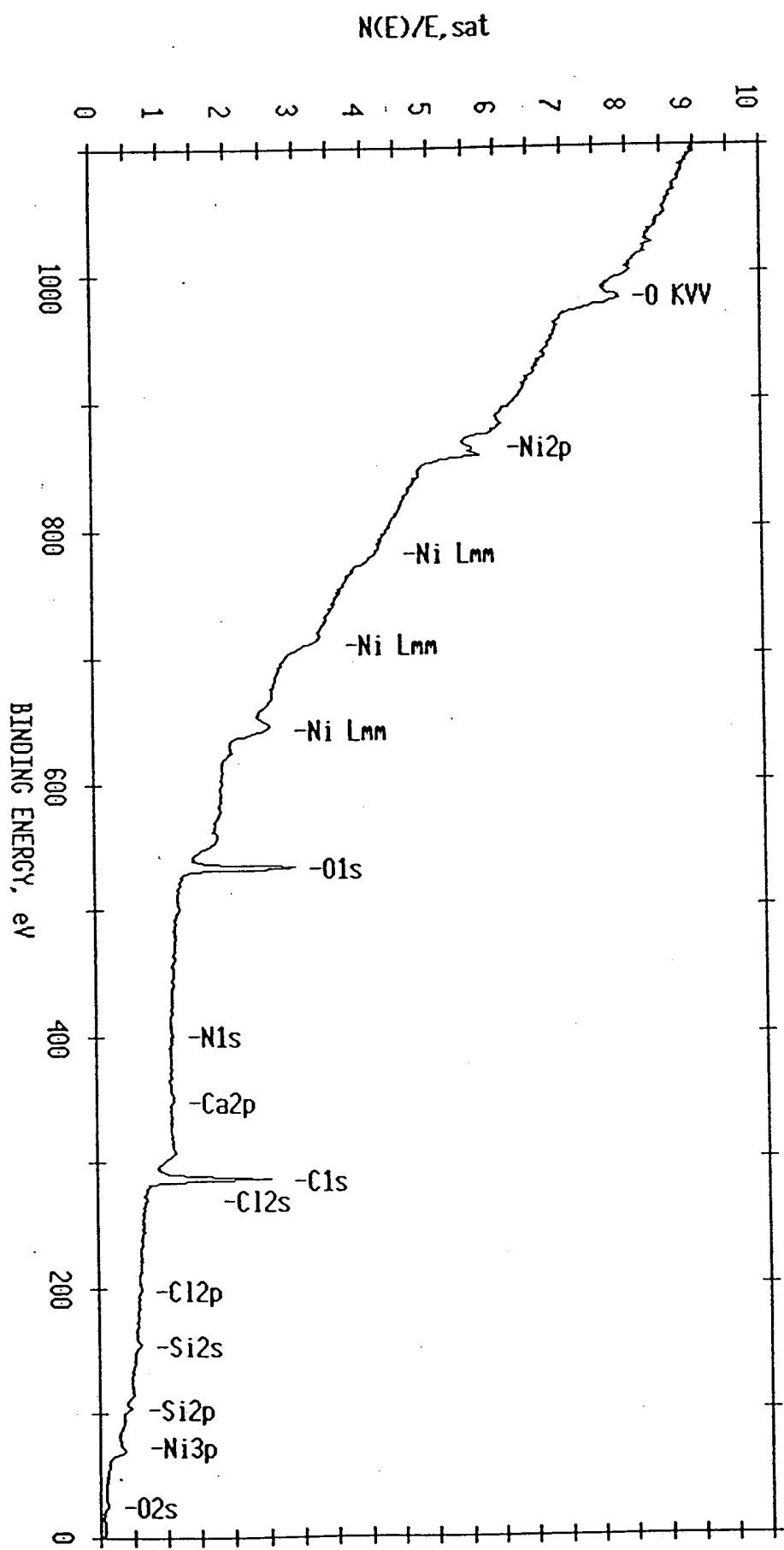
Counts 32758 Counts/Sec

2849

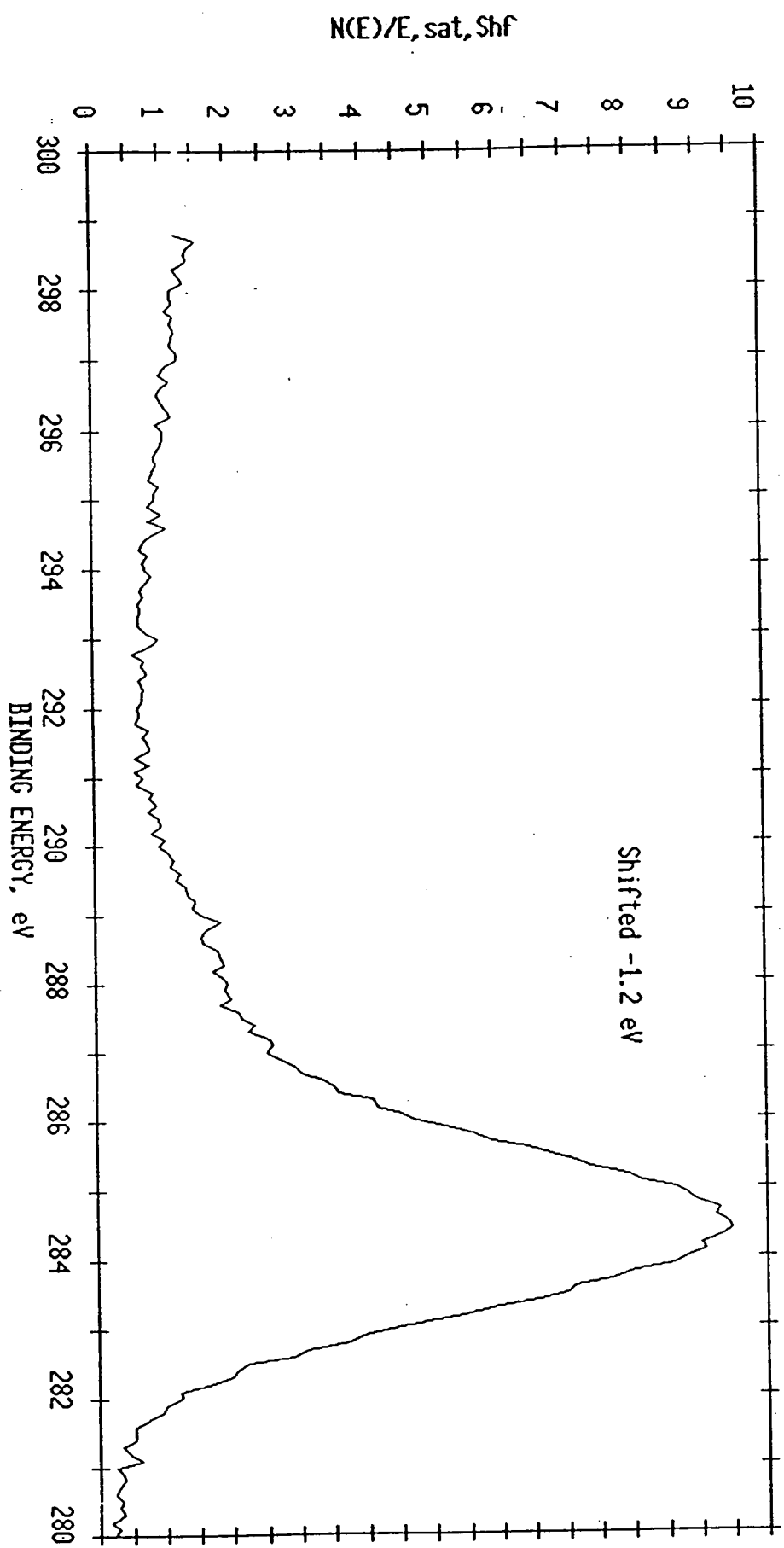
N(E)/E<sub>sat</sub>, Shf



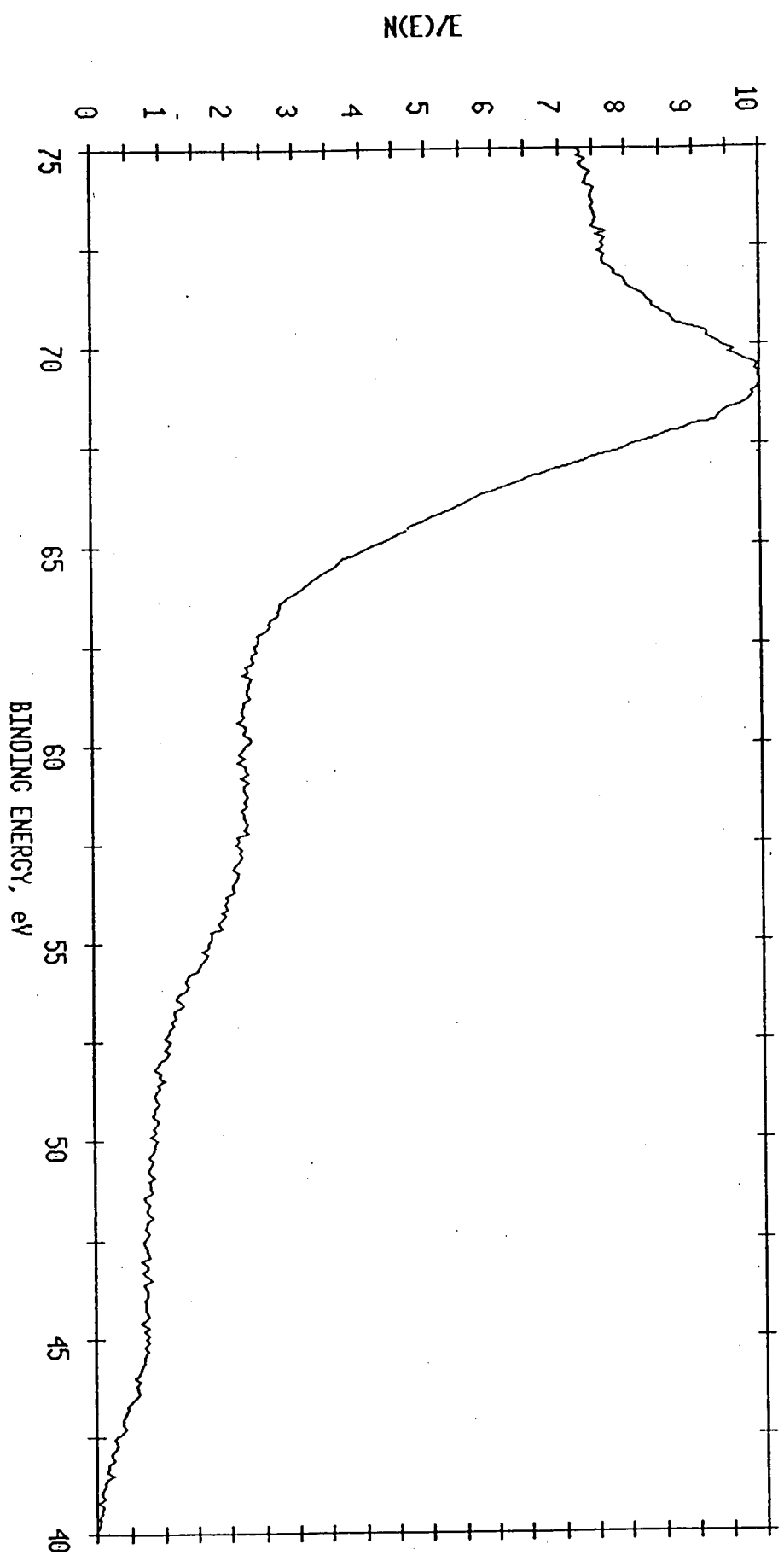
ESCA SURVEY 11/22/93 ANGLE= 15 deg ACQ TIME=29.36 min  
FILE: Nitest33 2nd Ni wire treated prior to IRC.  
SCALE FACTOR= 11.123 k c/s, OFFSET= 1.299 k c/s PASS ENERGY=178.950 eV Al 400  $\mu$



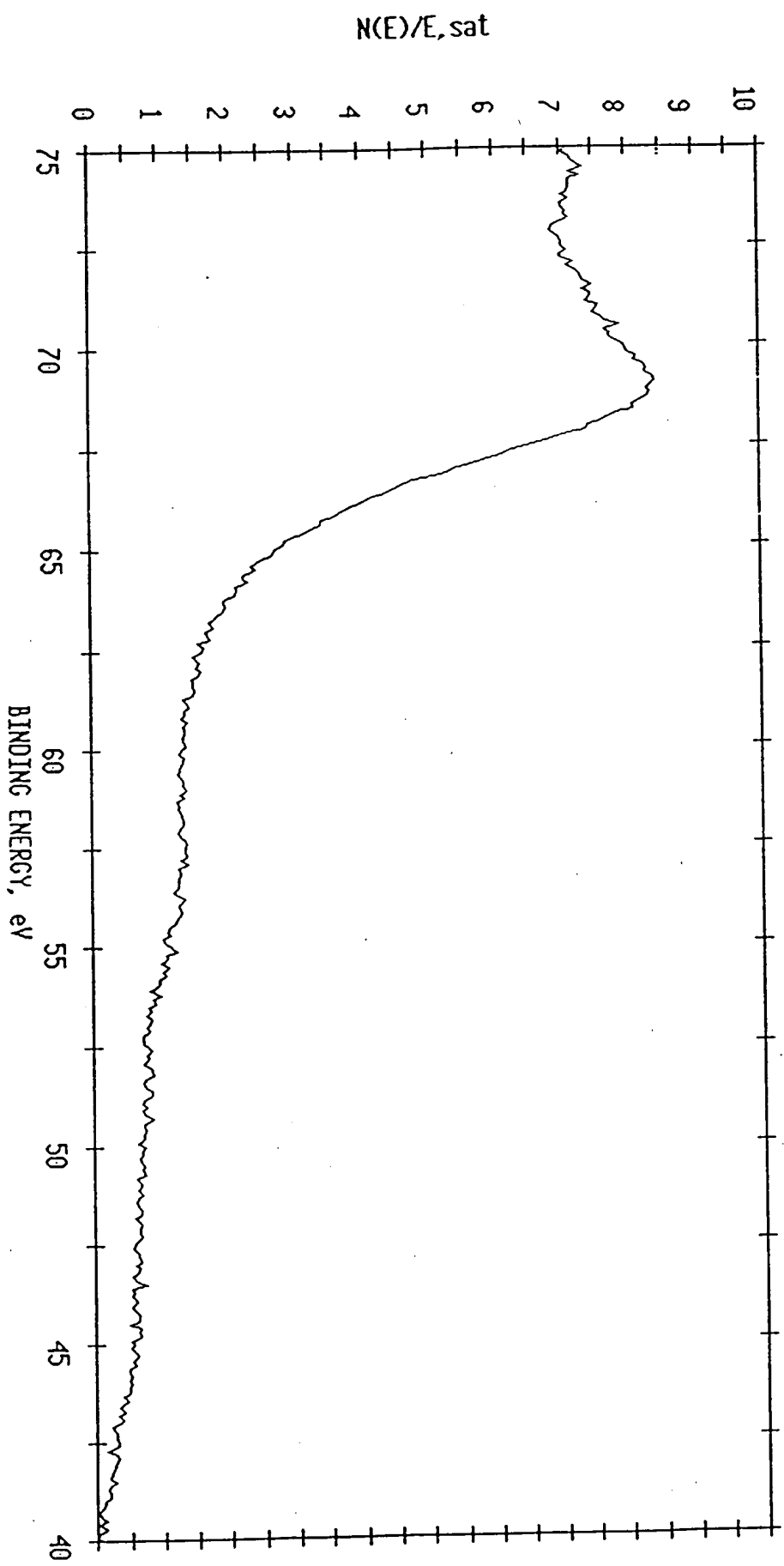
ESCA MULTIPLEX 11/22/93 EL=C1 REC 1 ANGLE= 15 deg ACQ TIME=1.67 min  
FILE: Nitest32 2nd Ni wire treated prior to IRC.  
SCALE FACTOR= 1.491 k c/s, OFFSET= 5.842 k c/s PASS ENERGY=143.050 eV Al 400 W



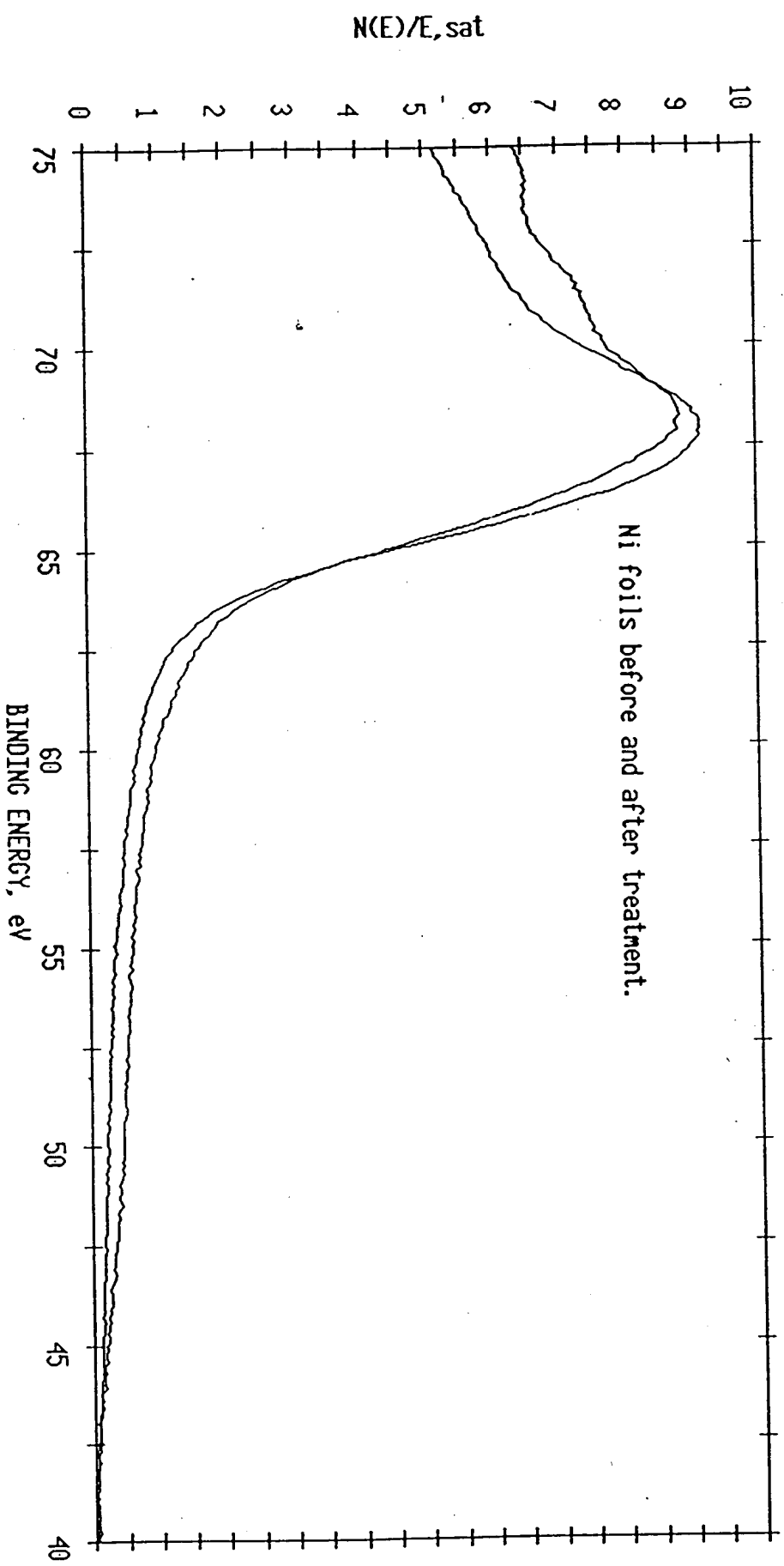
ESCA MULTIPLEX 11/22/93 EL= REG 2 ANGLE= 15 deg ACC TIME=96.53 min  
FILE: Nitest32 2nd Ni wire treated prior to IRC.  
SCALE FACTOR= 0.254 k c/s, OFFSET= 1.784 k c/s PASS ENERGY=143.050 eV Al 400 W



ESCA MULTIPLEX 11/18/93 EL= REG 2 ANGLE= 15 deg ACQ TIME=67.28 min  
FILE: Nitest20 Ni wire processed in lab. as received.  
SCALE FACTOR= 0.331 k c/s, OFFSET= 2.436 k c/s PASS ENERGY=143.050 eV Al 400  $\mu$

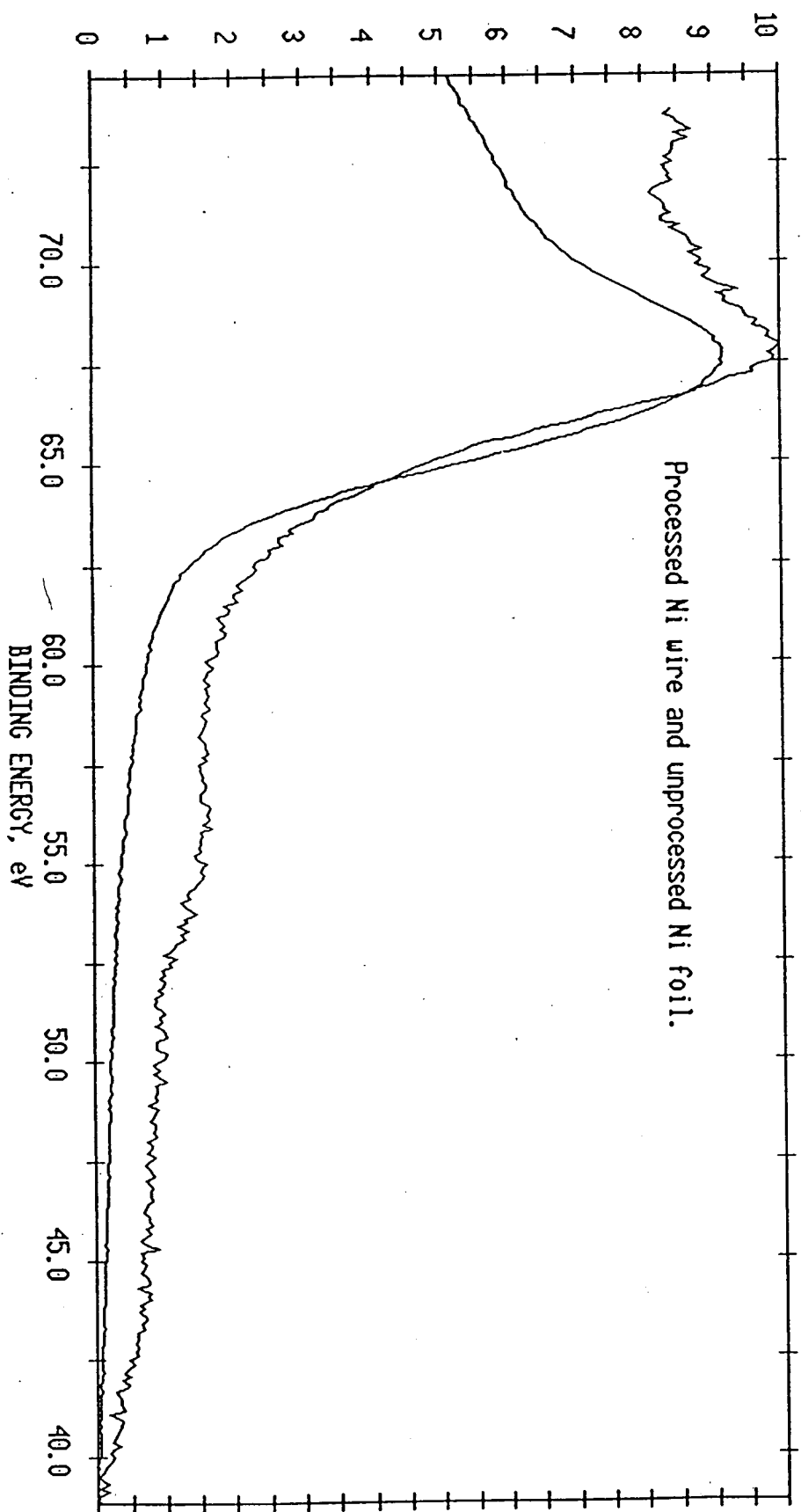


ESCA MULTIPLEX 11/19/93 EL= REG 2 ANGLE= 15 deg ACQ TIME=84.83 min  
FILE: Nitest25 Ni foil treated in lab for 24 hr. As received.  
SCALE FACTOR= 1.920 k c/s, OFFSET= 8.515 k c/s PASS ENERGY=143.050 eV Al 400  $\mu$



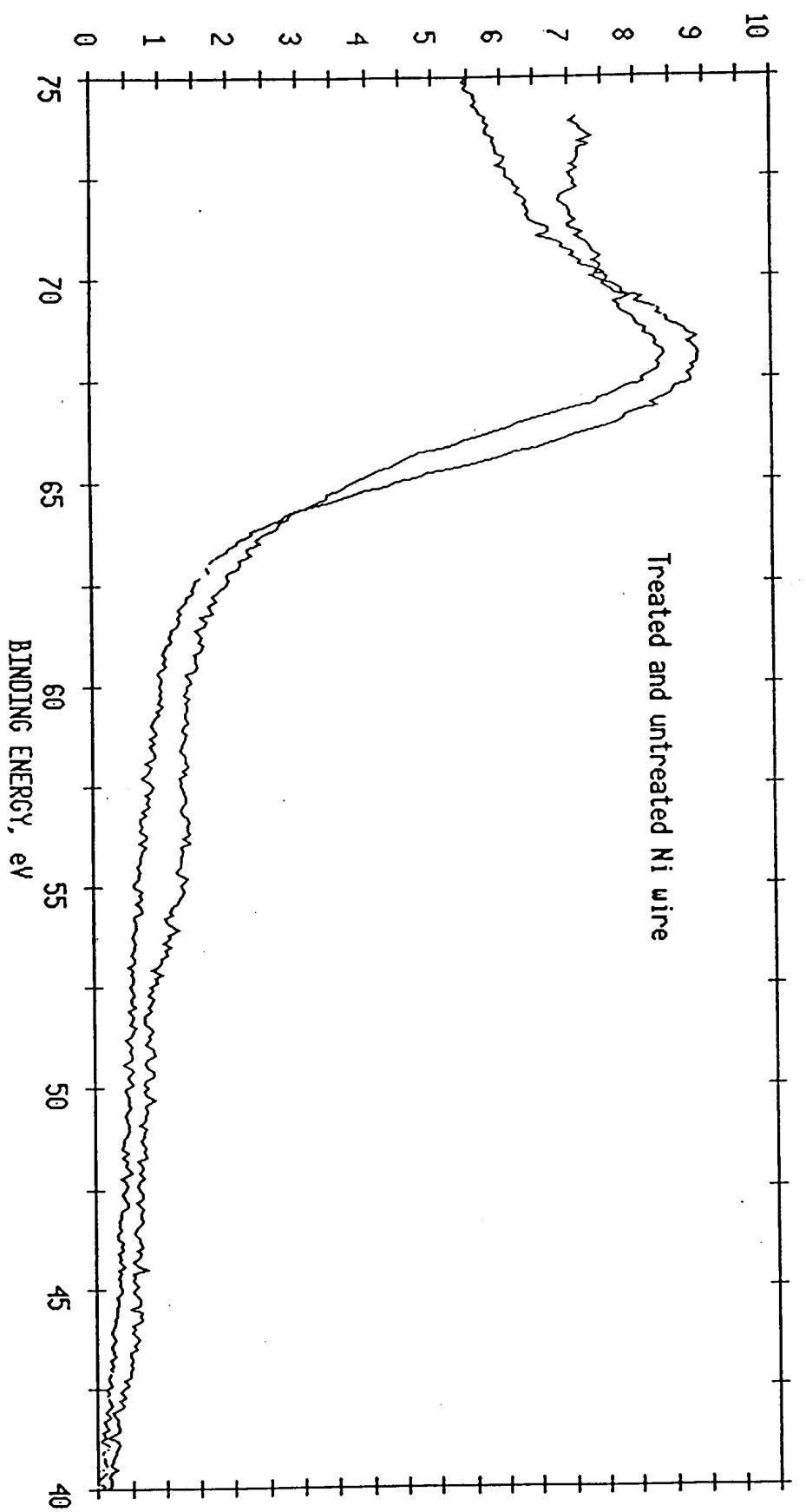
N(E)/E<sub>sat</sub>, Shf

ESCA MULTIPLEX 11/18/93 EL= REC 2 ANGLE= 15 deg ACQ TIME=76.05 min  
FILE: Nitest22 Ni foil untreated. as received.  
SCALE FACTOR= 3.401 k c/s, OFFSET= 9.545 k c/s PASS ENERGY=143.050 eV AI 400 M



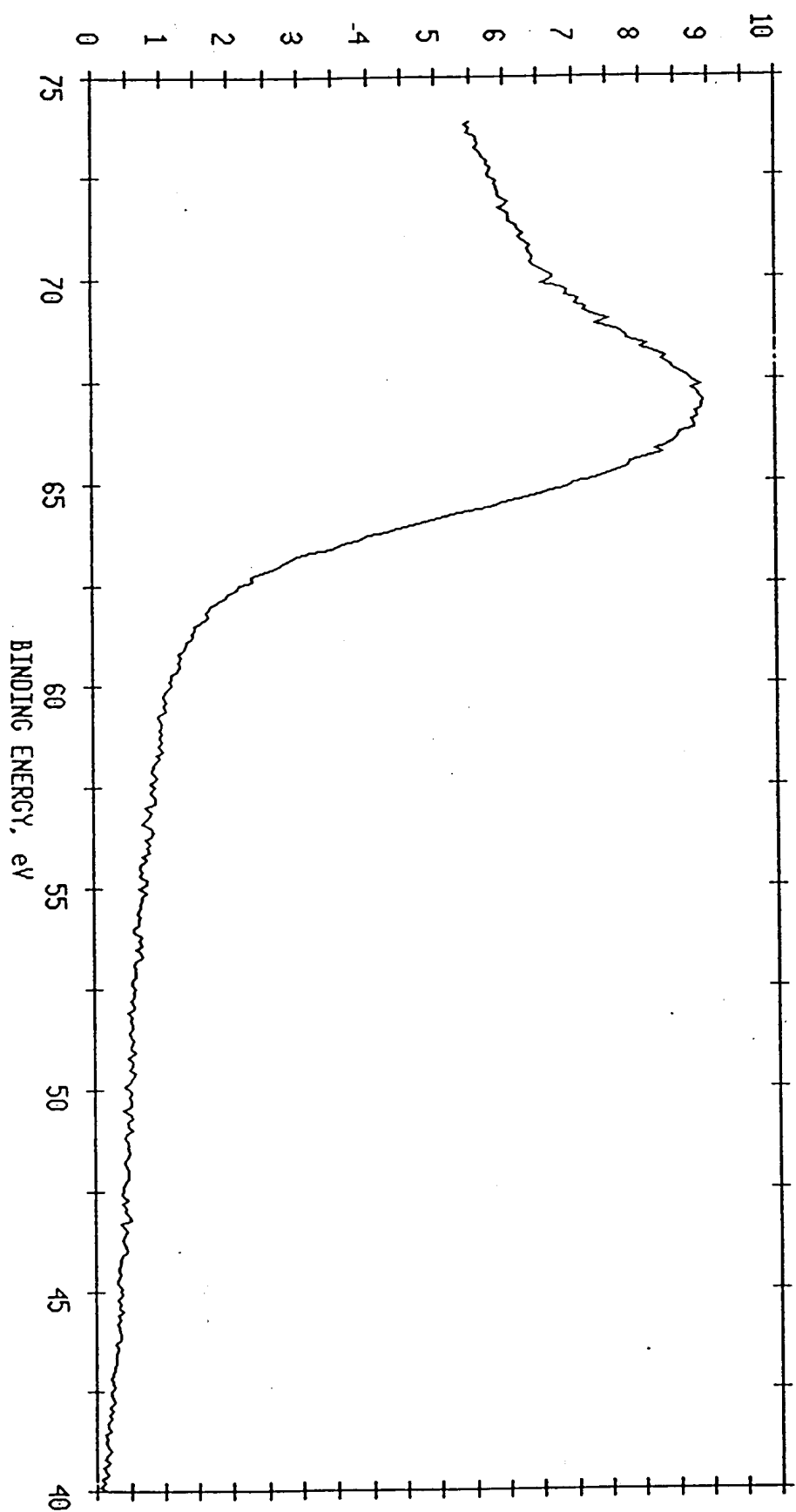
Processed Ni wire and unprocessed Ni foil.

N(E)/E<sub>sat</sub>, Shf



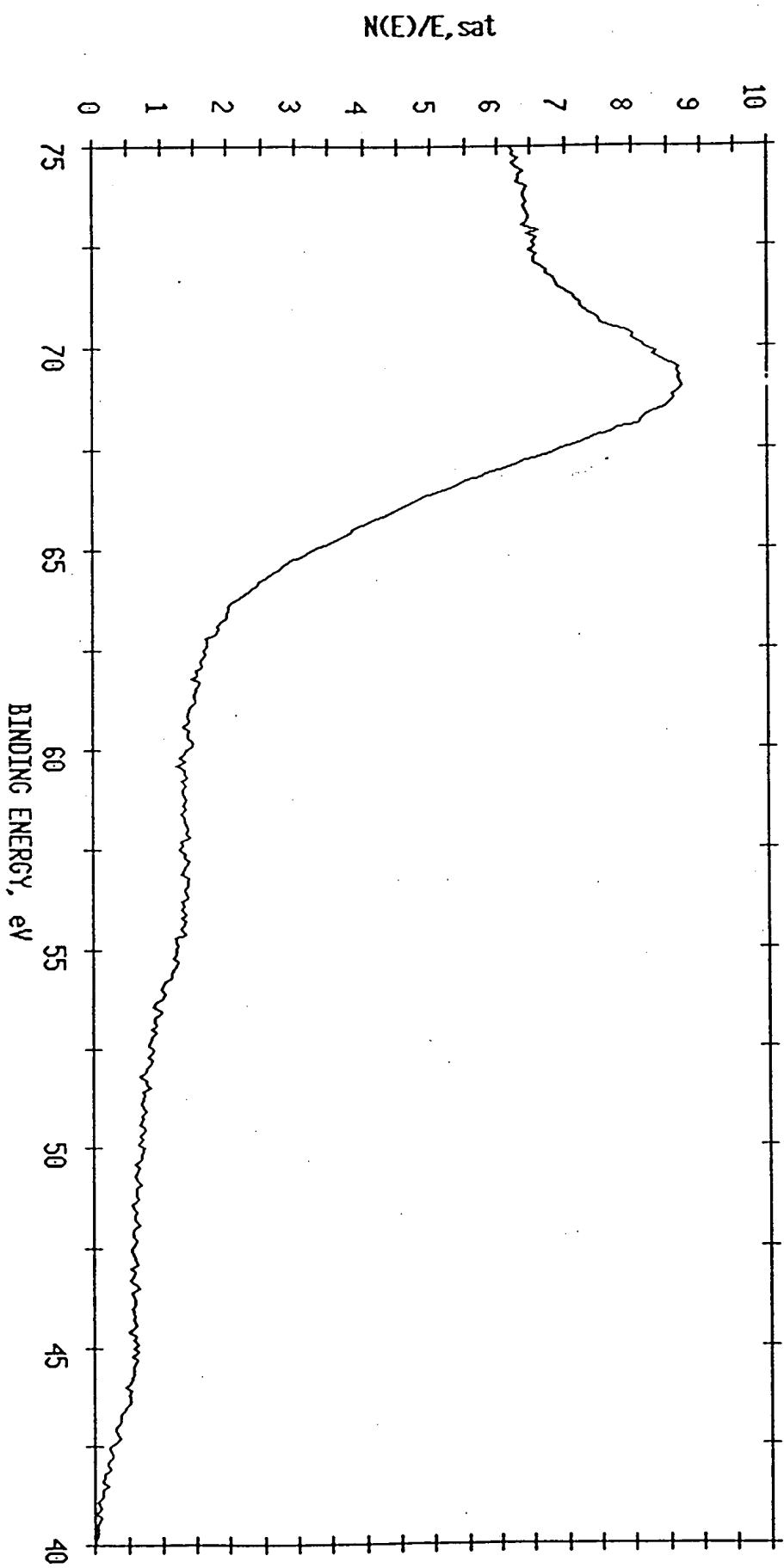
ESCA MULTIPLEX 11/18/93 EL= REG 2 ANGLE= 15 deg ACQ TIME=67.28 min  
FILE: Nitest20 Ni wire processed in lab. as received.  
SCALE FACTOR= 0.331 k c/s, OFFSET= 2.436 k c/s PASS ENERGY=143.050 eV Al 400  $\mu$

N(E)/E<sub>sat</sub>, Shf



ESCA MULTIPLEX 11/19/93 EL= REG 2 ANGLE= 15 deg ACQ TIME=61.43 min  
FILE: Nitest27 Ni wire untreated (base line) using Al X-Ray's.  
SCALE FACTOR= 0.326 k c/s, OFFSET= 1.491 k c/s PASS ENERGY=143.050 eV Al 400  $\mu$

ESCA MULTIPLEX 11/22/93 EL= REC 2 ANGLE= 15 deg ACQ TIME=96.53 min  
FILE: Nitest32 2nd Ni wire treated prior to IRC.  
SCALE FACTOR= 0.274 k c/s, OFFSET= 1.580 k c/s PASS ENERGY=143.050 eV Al 400  $\mu$



**LEHIGH X-RAY PHOTOELECTRON  
SPECTROSCOPY REPORT**

**CONFIDENTIAL**

During the past five months a series of XPS analyses have been carried out on 1) Ni electrodes that have been used for hydrolysis experiments, 2) various standards and 3) precursor electrode material. The results of these measurements are presented in this report.

### Experimental

The instrument conditions were similar, but not necessarily identical, for all the analyses. However, in all cases, a high quality spectrum was obtained over a minimum binding energy range of 80 to 0 eV. This completely covers the Ni 3p region and the region around 55 eV which is the approximate location of a n=1/2 to infinity transition of reduced energy state hydrogen. In many of the spectra, many other regions were also scanned. The specific regions depended upon the elements observed in a survey spectrum.

The first step in the analysis of electrodes from cells running at Lehigh consisted of removing the electrode from the cell while maintaining the electrode overvoltage during the removal. Immediately after disconnecting the electrode for the power supply, it was rinsed with distilled water and dried with an N<sub>2</sub> stream. A piece of suitable size was cut from the electrode, mounted on a sample stub and placed in the vacuum system. This procedure typically required 10 to 15 min. If the electrodes were from cells not running at Lehigh, the analyses were carried out on "as

"received" material without any additional surface preparation. Wire specimens were mounted such that the wire extended over the edge of the sample holder. This was done to eliminate any possible contributions to the spectrum from the sample holder material.

The preparation conditions and experimental conditions for the various samples are summarized below. The details of the cleaning, electrolyte preparation, etc. are recorded in Dr. Mills notebooks. These descriptions are intended to provide a quick identification only. Samples #1 to #9 were run using  $K_2CO_3$  electrolytes. Samples #10 to #14 were run with  $Na_2CO_3$  electrolytes.

Sample #1: Nickel foil was cleaned at Lehigh according to the standard procedure in place at the end of June, 1993. The  $K_2CO_3$  electrolyte was from the original batch used for earlier HPC experiments. A platinum counter electrode was used in this experiment. The cell was run for approximately 48 h from 6/24/93 to 6/26/93 prior to the analysis.

Sample #2: The preparation for this sample was nearly identical to that for sample #1. The major difference was the use of higher purity  $K_2CO_3$ . This cell ran for about 50 h from 6/30/93 to 7/2/93.

Sample #3: A freshly prepared electrode was placed in the solution used for sample #1, and the cell was operated for about 50 h from 6/30/93 to 7/2/93.

Sample #4: This is a re-analysis of sample #1 after sitting in a plastic bag for 26 days.

Sample #5: This is a re-analysis of sample #3 after sitting in a plastic bag for 26 days. A different portion of the electrode was analyzed.

Sample #6: Electrode material from a cell a HPC. The electrode was delivered on ice from HPC.

Sample #7: Nickel wire electrode with an extended running time at Lehigh of about 42 days.

Sample #8: Electrode material from a Ni-Ni cell that had been operating at Lehigh for 8 days.

Sample #9 Wire electrode removed on 10/1/93 from an HPC cell for which heat data is available. The sample was delivered under LN<sub>2</sub> by Bill Goode.

Sample #10 was taken from one of the two initial cells used for the first experiments at Lehigh.

Sample #11 was prepared using the same electrolyte and dewar that were used for sample #10. This cell was run for several weeks before the electrode was analyzed.

Sample #12 was obtained from a cell in which a small amount of ZnSO<sub>4</sub> had been added to the electrolyte.

Sample #13 was from a cell that had been running at HPC for an extended period of time. It was brought to Lehigh on ice and kept below freezing prior to being placed in the vacuum system.

Sample #14 was Ni wire taken from a control cell at HPC. It is the exact analog of Sample #9 except for the difference in electrolyte. Thermal data is available for this sample.

Specimens of pure elements and the passivation oxides of these elements that were analyzed to provide standards are not given sample numbers. The preparation conditions for these specimens are listed on the figures or given in the figure captions.

#### Results - K<sub>2</sub>CO<sub>3</sub> electrolyte samples and standard materials

A survey spectrum of sample #1 is shown in Fig 1. The primary elements are identified on the figure. Most of the unidentified peaks are secondary peaks or loss features associated with the primary elements. The detector was saturated in the high binding energy portion of the spectrum, which has the effect of flattening the peaks in this region and distorting their intensities relative to the peaks in the lower binding energy portion of the spectrum. Though this distortion tends to overemphasize the Sn component, it

still clear that Sn is a major component of the surface composition. It is the presence of Sn and/or other contaminant elements in many of the spectra that has obscured and complicated the interpretation of the data.

Figures 2 shows the low binding energy range for the specimen. The data were accumulated over many hours to yield this level of signal-to-noise without smoothing. The peaks which can be positively identified are labelled in the figure. The broad peak labelled X is the one of most interest because it falls near the predicted binding energy for a hydrino transition. It has a FWHM of about 5.1 eV, and it is centered at a binding energy of 54.6 eV. (It is important to note that binding energies in XPS are measured relative to the Fermi level, and not to the vacuum level.) However, it is necessary to eliminate all other possible explanations for this peak before it can be positively identified as resulting from a reduced energy state hydrogen atom. For example, the Pt  $5p_{3/2}$  falls at an energy of 51.4 eV, which is close to the predicted energy of 54.4 eV, and Pt can clearly be identified as a surface component from the Pt 4f peaks at 74.29 and 70.95 eV. From a spectrum of pure Pt, it was determined that the area ratio of the Pt  $5p_{3/2}$  peak to the total Pt 4f peak is 0.043, whereas, in the spectrum the area ratio of X to the Pt 4f peaks is 0.75. Thus, the area of X is about 17 times too large to attribute the peak to Pt. Other possible explanations that must be considered are fine structure or loss features associated with

either of the three major surface components, Ni (oxide), Sn (oxide), Zn (oxide) or small amounts of other elements which have their primary photoelectron peaks in the vicinity of 55 eV.

To examine these possibilities, several experiments were carried out. Figure 3 shows expanded scale spectra of Ni electrode foil material that has undergone a variety of treatments ranging from clean metal (scraped in vacuum) to room temperature oxidation in pure O<sub>2</sub> (oxidized at 30 kPa for 15 min at r.t.) to air passivation at room temperature (scraped in air immediately before insertion into the vacuum system). Examination of Figure 3 shows no evidence for any spectral features in the 65 to 45 eV energy range that can be associated with either Ni or its oxides for the experimental conditions that were explored. It seems unlikely that further oxidation or hydration of the oxide layer would result in the growth of any spectral features in this energy range.

The question of both Sn and Pt as the source of the peak is addressed by Figure 4. The Pt 5p<sub>3/2</sub> shown in the bottom curve is disproportionately large for the actual size of the Pt 4f peaks in the spectrum. The overemphasis is being used to show that the peak position does not match that of the known feature. The other two spectra are of clean Sn metal and a thick Sn oxide. Clean Sn metal has a bulk plasmon peak at about 53 eV. However, this peak is several times weaker than the plasmon at 38.7 eV. The 38.7 eV peak does not appear in the spectrum from Sample #1. Therefore, the

unknown peak cannot be ascribed to Sn metal. The thick Sn oxide shows no structure in the energy range from 65 to 30 eV. A comparison of the Sn peaks from sample #1 and the Sn oxide indicate that most of the Sn signal in the sample #1 spectrum is from oxidized Sn. Zinc also appears in the survey spectrum. Comparisons between Sample #1 and Zn metal and oxide are shown in Figs 5 and 6. The arguments for discounting a Zn contribution are the same as those used to eliminate Sn as the source of the feature.

With the exception of Li, there are no other common elements with a primary photoelectron peak at about 55 eV. Looking to other elements with secondary peaks at this position, the most probable candidate is the Fe 3p. The primary Fe peak, the 2p levels, are obscured by the very strong Ni Auger lines which overlap Fe 2p energy range. This possibility cannot be completely eliminated without further study, though spectral synthesis using spectra from clean Fe and clean Ni suggest that Fe concentrations of <5% relative to Ni should be discernible in the Fe 2p energy region.

Additional sets of data were obtained from Sample #1. One set of data were obtained after the specimen was heated to about 700 C. Another set of data were obtained after the electrode had been stored in air for 26 days. This was identified as Sample #4 in the experimental section. The comparisons are shown in Figure 7. Using the Mg 2p as a marker peak, it will be noted that the shape of the

feature changes upon heating and that the centroid shifts to a higher binding energy. The binding energy of the feature has also shifted to higher values in the spectrum of the stored specimen. The reasons for these changes are not obvious, especially for the heated specimen. Heating under UHV conditions tends to reduce oxides. Normally this results in peaks shifting to lower rather than higher binding energies. This is evident in Figure 8 which shows the Sn 4d spectrum of Sample #1 before and after heating. Also shown for comparison are spectra from a thick Sn oxide and Sn metal. Heating did not completely reduce the oxide, but the spectra show that it is more metallic than oxidized after the heating. The amount of Ni oxide was also reduced as a result of the heating. If the feature is an Fe 3p peak, the expected result would be a decrease in the binding energy upon heating rather than an increase.

In summary, the spectrum from Sample #1 yields a broad feature centered at about 55.4 eV. Most contaminant elements have been eliminated as the source of this feature, though the slight possibility remains that it is an Fe 3p peak or a very unusual contaminant. The feature undergoes slight changes in shape and shifts to slightly higher binding energies as a result of both heating and storage.

A survey spectrum from Sample #2, which was prepared using a higher purity  $K_2CO_3$ , is shown in Fig. 9. The amount of Sn is much lower

in this spectrum, though there are substantial amounts of Zn and Ti. An expanded spectrum of the lower binding energy range is shown in Figure 10. Many of the peaks are labelled. A further expansion and comparison is shown in Figure 11. It can be noted that the unknown feature is also present in this sample as well, though it is at a slightly higher binding energy.

A comparison of the lower binding energy region for Samples #2 and #3 is shown in Figure 12. There are two significant differences: 1) Sample #3 has a high concentration of Pt on the surface from the counter electrode and 2) there is no Ti and much less Zn on Sample #3. Both samples have very low Sn concentrations. Figure 13 shows a further expansion of the spectra together with a portion of a clean Pt spectrum. The feature at about 52 eV in the curve from Sample #3 is clearly the Pt  $5p_{3/2}$  photoelectron peak.

As indicated previously, Sample #4 is a reanalysis of Sample #1. The results from Sample #4 were discussed above to some extent. The only additional comment about Sample #4 is that the data show that the nickel oxide layer had thickened during the storage time.

Sample #5 was a reanalysis of sample #3. Spectra for Sample #5 are shown in Fig. 14. As expected, the spectra from both samples are very similar. The differences in composition can probably be attributed to sampling from different regions on the electrode. The feature at 52 eV can be attributed to the Pt concentration.

The low binding energy region of Sample #5 and a comparison with Sample #3 and Ni metal are shown in Fig. 14.

Sample #5 is very similar to sample #3 in that it used the initial electrolyte with a new electrode.

The spectrum in Fig. 15 is from Sample #6. It is a cathode that was run for an extended period of time at HPC and was delivered on ice. The surface is quite heavily covered with hydrocarbon. In addition, a number of other elements are observed on the surface including Ca, Nb, Si and Pt. As can be seen from Fig. 16, any information about the feature at 55 eV is hidden by the amount of Pt and other elements on the surface.

Figure 17 shows the survey spectrum of a wire cathode that was run for a very long time at Lehigh. In addition to the elements listed on the figure, there were also a small amounts of Ti and Mg on the surface. Figure 18 shows expanded views of the low binding energy region. The unknown feature is quite strong in the spectrum from Sample #7. Comparisons of the spectrum from Sample #7 and Sample #1 are also provided. It can be noted that the position is slightly different, but it is clearly the same feature.

The spectra from the Ni-Ni cell are shown in Figs. 19 and 20. In addition to the expected Ni and O, there are significant amounts of Te, In and Pb. The Te appears to mostly metallic. Both Pb and In

have oxide and metallic components. There is no strong evidence for a feature around 55 eV.

The final specimen of Ni in a  $K_2CO_3$  electrolyte was Sample #9 which came from a cell at HPC. The heat data available for this specimen. The survey spectrum in Fig. 21 shows that the only significant contaminant is In. There is also some K, which suggests that the rinsing may not have been complete. There is also a trace of Si. Figure 22 provides the expanded views of the lower binding energy regions. The center of the feature is closer to 57 eV than it is to 55 eV, but it is still very similar in shape to the features in the other spectra.

Of the seven different samples using the  $K_2CO_3$  electrolyte (Samples #1 and #4 were the same, as were Samples #3 and #5), four showed evidence of a feature at about the correct binding energy for a transition involving a fractional energy level hydrogen atom. These were Samples #1,, #2, #7, and #9.

#### Results - $Na_2CO_3$ electrolytes

The spectra for Sample #10 are shown in Figs. 23 and 24. The various elements detected on the surface are labelled on the figures. It was impossible to assess the possibility for a feature or lack thereof because of the very large amount of Mg that plated out during the electrolysis.

The results for Sample #11 are shown in Figs. 25 and 26. A large amount of Pt had plated out on the surface during this experiment, and the Pt 5p<sub>3/2</sub> peak interferes with any small features that might be at lower binding energy.

Sample #12 was from the experiment in which a small amount of Zn salt was added to the Na electrolyte. The spectra shown in Figs. 27 and 28 show a nearly complete coverage of the surface by Zn oxides or hydroxides. Pt and Mg are also visible on the surface. There was a small feature adjacent to the Mg 2p peak that could not be positively identified. However, a comparison with the feature obtained from Sample #7 shown in Fig. 28 shows that this peak is at a somewhat lower binding energy, and that its source is not the same as the feature in the spectrum from Sample #7.

No substantive information could be obtained from Sample #13 which came from an electrode run at HPC. This sample showed approximately the same characteristics as Sample #11, i.e., the surface was heavily covered with Pt. Spectra from this sample are shown in Figs. 29 and 30.

Sample #14 represented the best spectrum for a direct comparison between the electrode surfaces that are generated by the two types of electrolytes. The spectra shown in Figs. 31 & 32 indicate that the extraneous contamination is minor and does not obscure the interpretation of the data. There is only a very small trace of Mg

in the energy region of primary interest.

The comparison between electrodes which have been used in the two types of electrolyte solutions is explored further in the spectra shown in Figs. 32 & 33. The two samples represented by the spectra were prepared at HPC, and heat data is available for both. From a compositional and surface chemical standpoint, there are several similarities and differences between the samples. Both samples have small amounts of Si, Mg and S on the surface. The concentrations of these are not the same on both surfaces, but they are of the same order of magnitude. The Na sample has a small amount of lead on the surface; the K sample does not. The K sample has both K and In on the surface; the Na sample does not. Chemically, the Ni oxide layer on the K sample is thicker and more hydrated than on the Na sample. The most important difference is the fact that the K sample has the spectral feature at about 57 eV. There is no evidence of any structure in this region on the Na sample. The difference is most clearly illustrated in Fig. 34. I have been unable to associate the spectral feature at about 55 to 57 eV with any surface contaminant element, and the spectral comparison in Fig. 33 represents the best evidence to date for hydrino atoms.

#### Results - Cleaning treatments

The last figure, Fig. 35, illustrates the results of some cleaning

experiments that were carried out very early. The samples consisted of a piece of electrode material cleaned and treated with both peroxide and K electrolyte by Randy Mills at the time of starting the first experiment and other pieces of electrode material that were solvent cleaned only, cleaned with solvents and peroxide only, cleaned with solvents and immersed in electrolyte only, and cleaned with solvents and treated in the peroxide/electrolyte mixture. I carried out the latter experiments at Lehigh. The techniques used by HPC were duplicated to the best extent possible. Unfortunately, low binding energy region data were not obtained for some of the samples, but there are overall compositional results for all the specimens. The only elements present on the surface of the solvent cleaned and peroxide cleaned surfaces were Ni, O and C. After a 30 min immersion in K electrolyte only, a solvent cleaned sample showed that a small amount of Sn (<1 at.%) had deposited on the surface. Three pieces of electrode material were treated in the combined solution: one by Randy Mills and two by myself. The surface of the Mills' cleaned sample contained only Ni, O, and C. Both Zn and Sn were present on the two samples that I treated. Both of my specimens were treated in the same batch of peroxide/electrolyte solution, and the first of the two samples had far more of contaminant elements than the second. It may be that the solution "cleans up" as more sample area is treated, and that the amount of contaminant on the electrode surfaces will be a function of the history of the solutions.

The interesting aspect of the data shown in Fig. 35 is the feature at about 57 eV. It is present only on the two samples that I cleaned. However, the magnitude of the feature is about the same in both spectra even though there are clear differences in the amount of Zn and Sn on the surface as shown by the peaks at 10 eV and 28 eV. This is evidence that the feature is not related to Zn and Sn contamination. I was unable find any other elements on the surface that cause the feature.

In summary and conclusion, the following positive observation is offered:

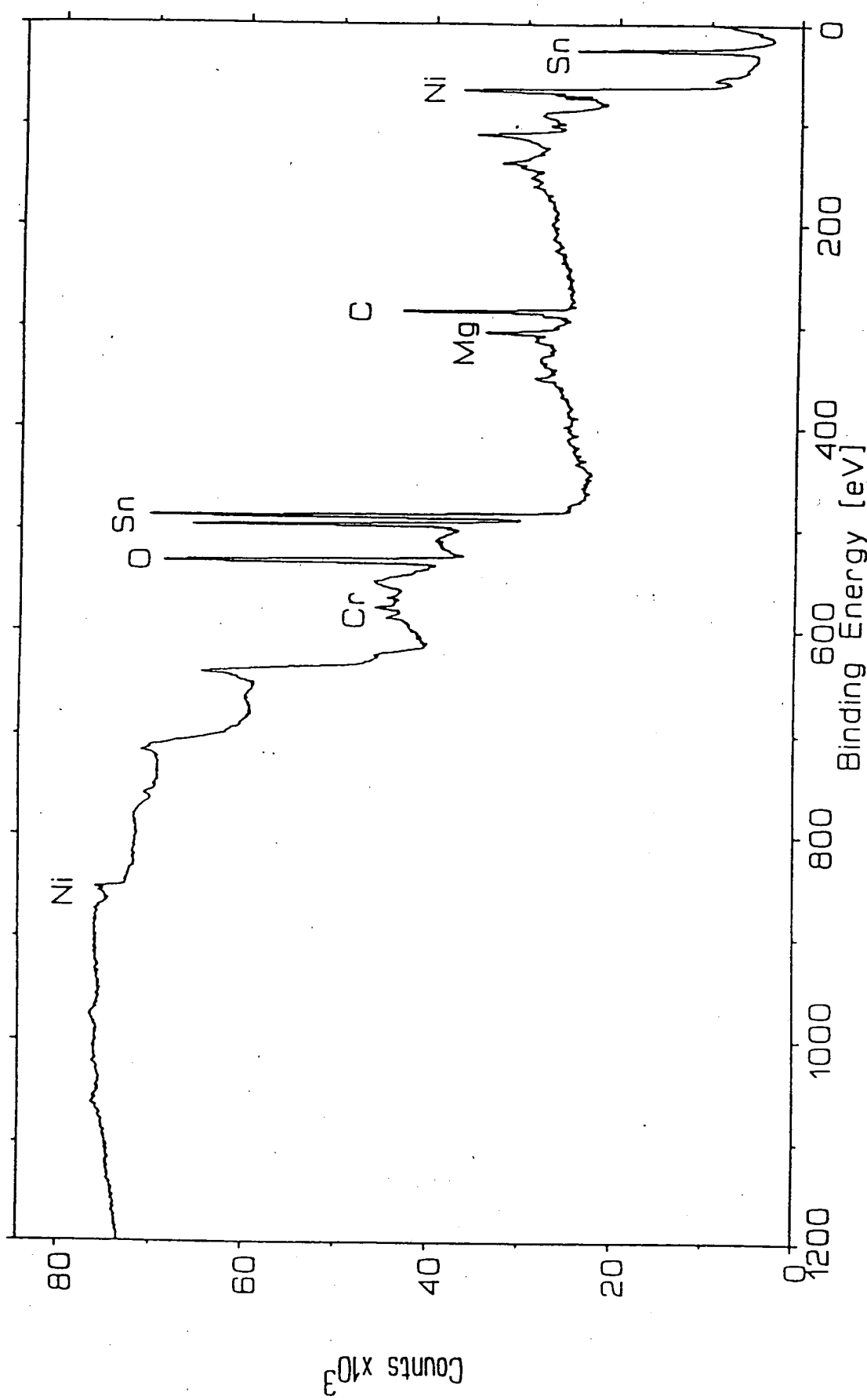
1. The persistent appearance of a spectral feature near the predicted binding energy for many of the electrodes used with a K electrolyte is an encouraging piece of evidence for the existence of reduced energy state hydrogen.

Other observations which do not discount the identification of the spectral feature as reduced energy state hydrogen, but which introduce uncertainty into the interpretation of the spectral feature are:

1. The spectral feature is only observed when there are contaminant elements of some type also present on the surface. However, it has not been possible to identify the feature as being directly related to any of the identified contaminants.

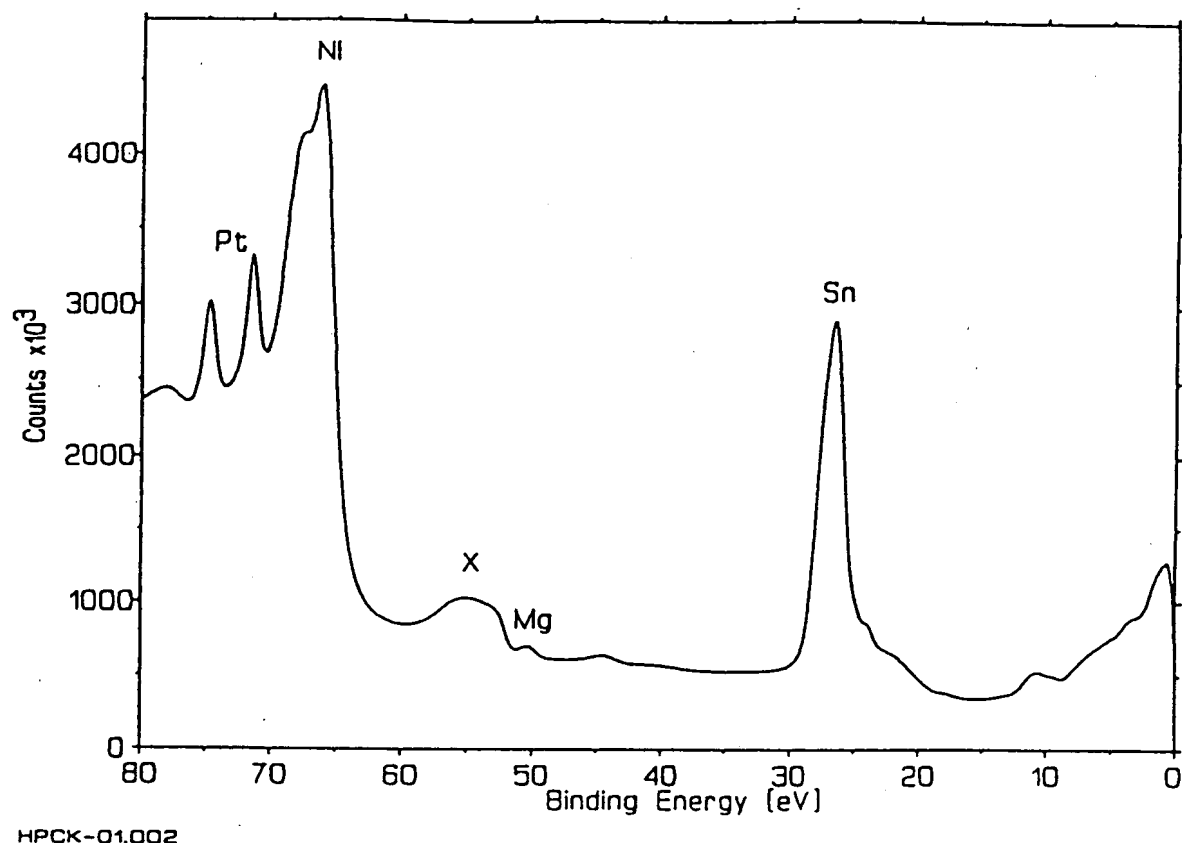
2. The feature persisted in Sample #1 even after being heated to >700°C. Normally, it is expected that hydrogen would diffuse out of the sample at these temperatures. In addition, the shape of the feature changed as result of heating.
3. Two of the hydrogen peroxide/potassium electrolyte treated foils exhibit the feature while another one does not. Coincidentally, the surfaces showing the feature have contaminant elements, whereas the surface not showing any contamination does not have a definable feature.
4. The position of the feature varied over about 2 ev if we examine all of the specimens. This would not be expected.

Figure 1

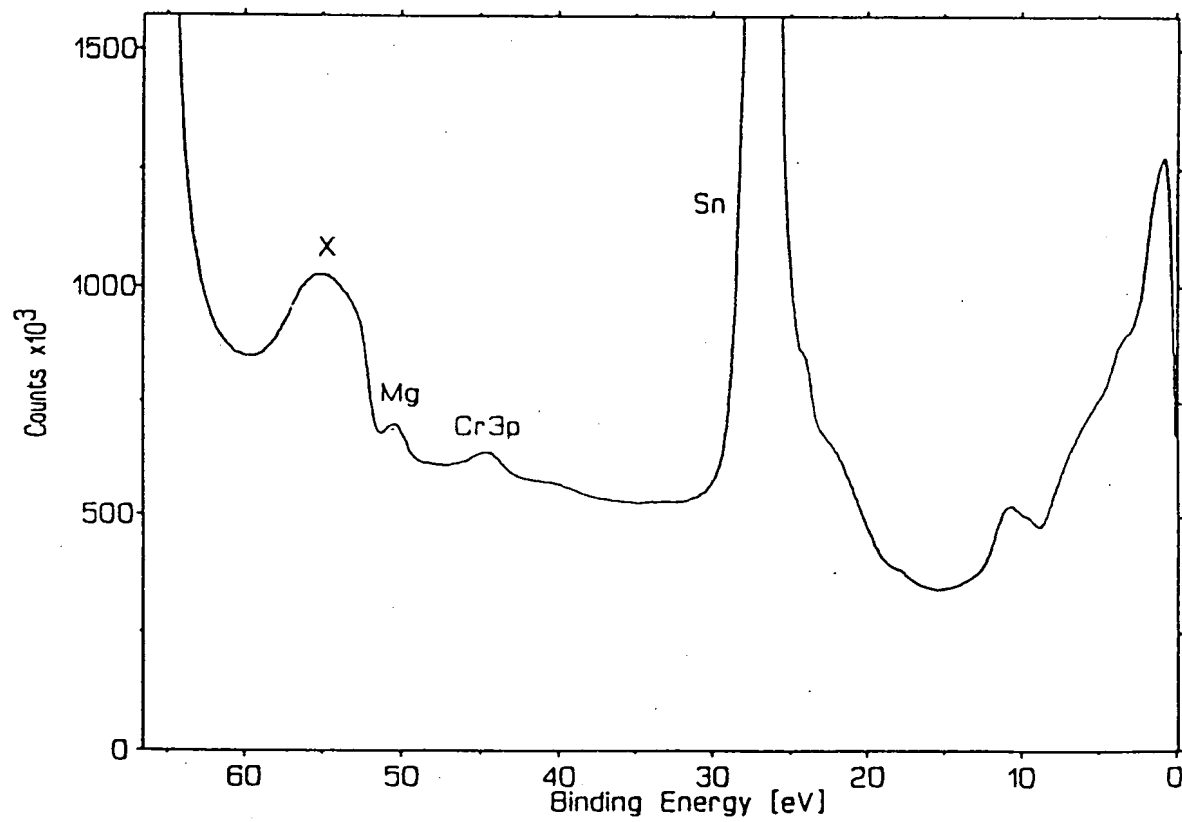


HPCCK-01.001

Figure 2



HPCK-01.002



HPCK-01.002

Figure 3

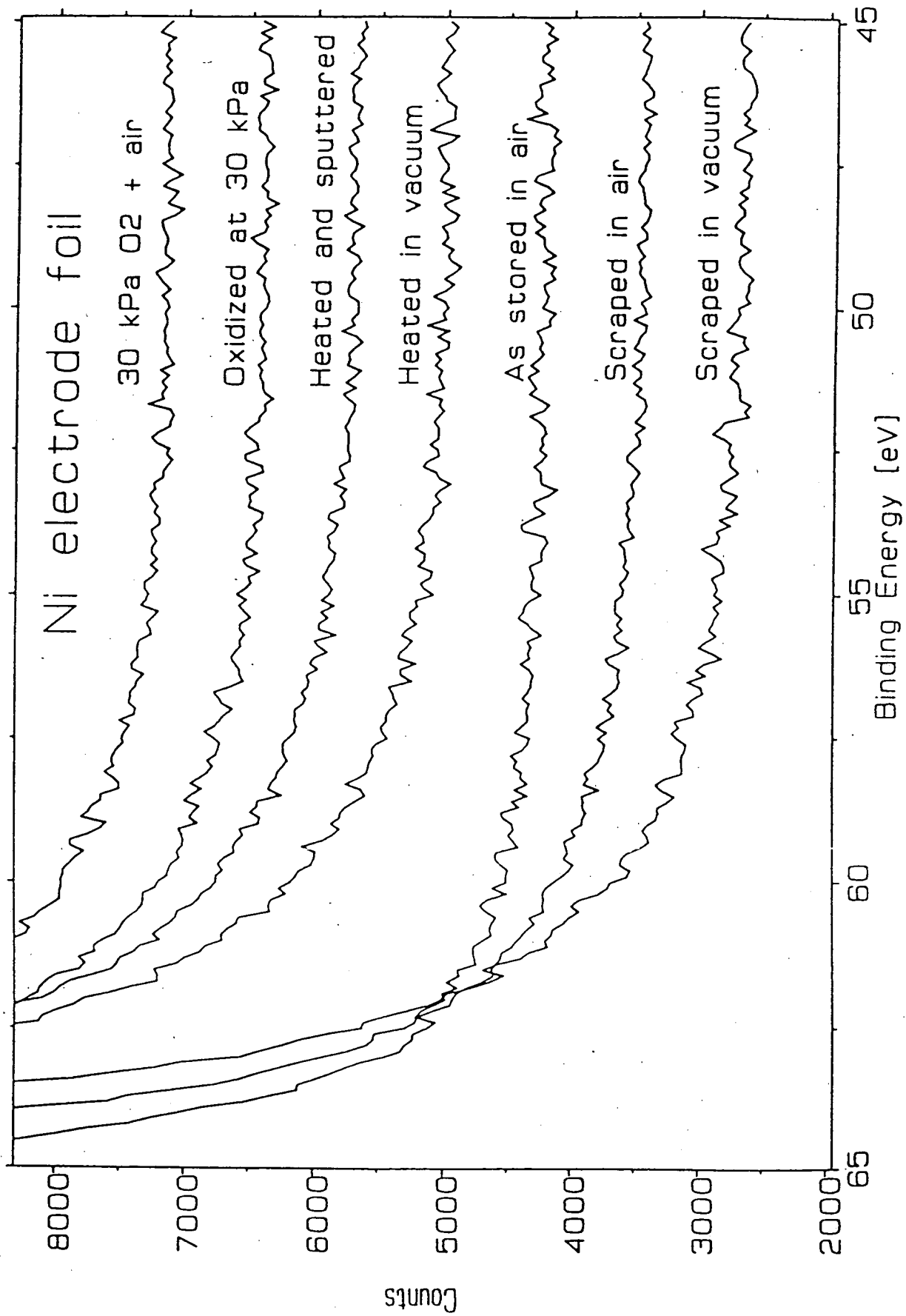


Figure 4

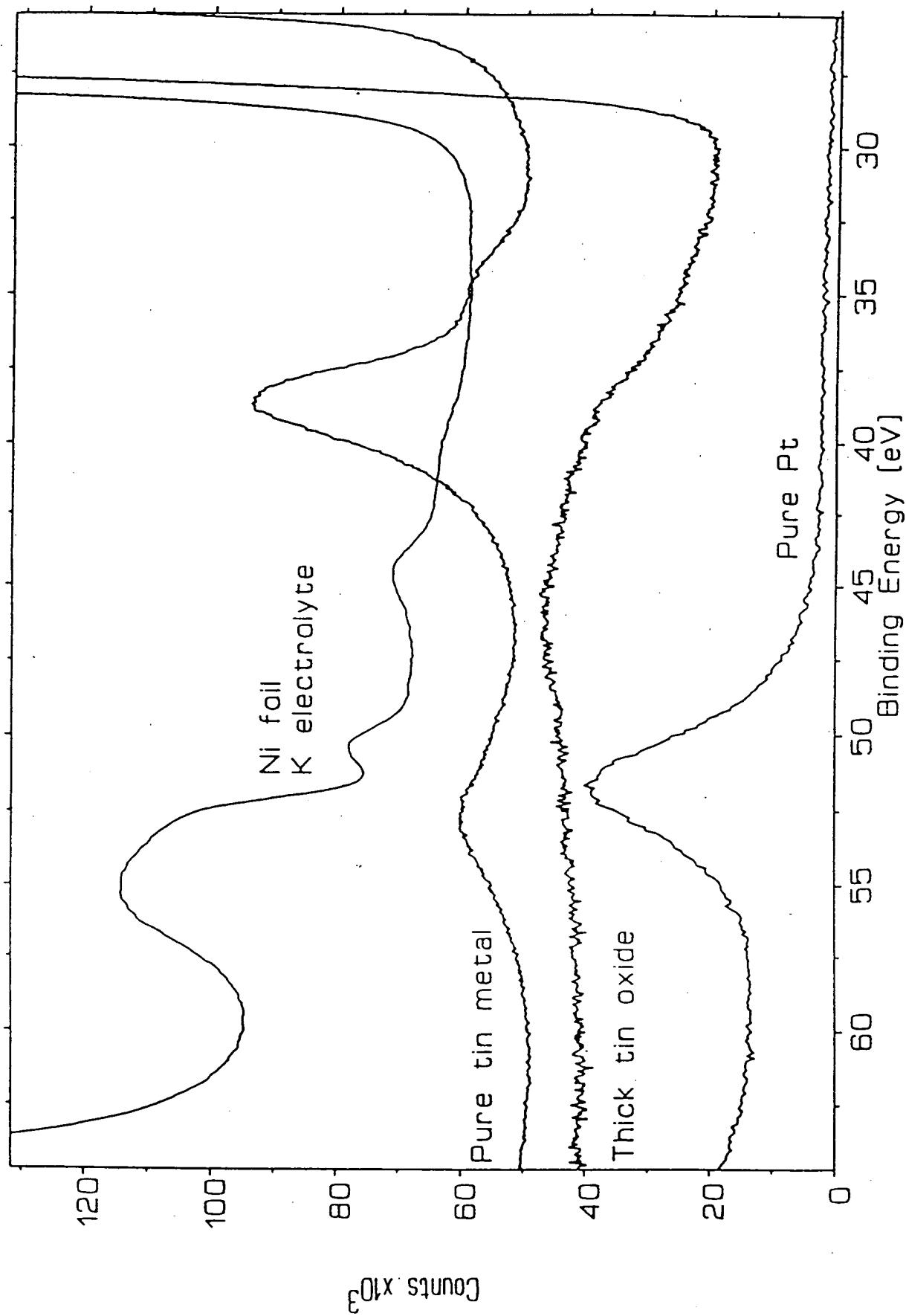
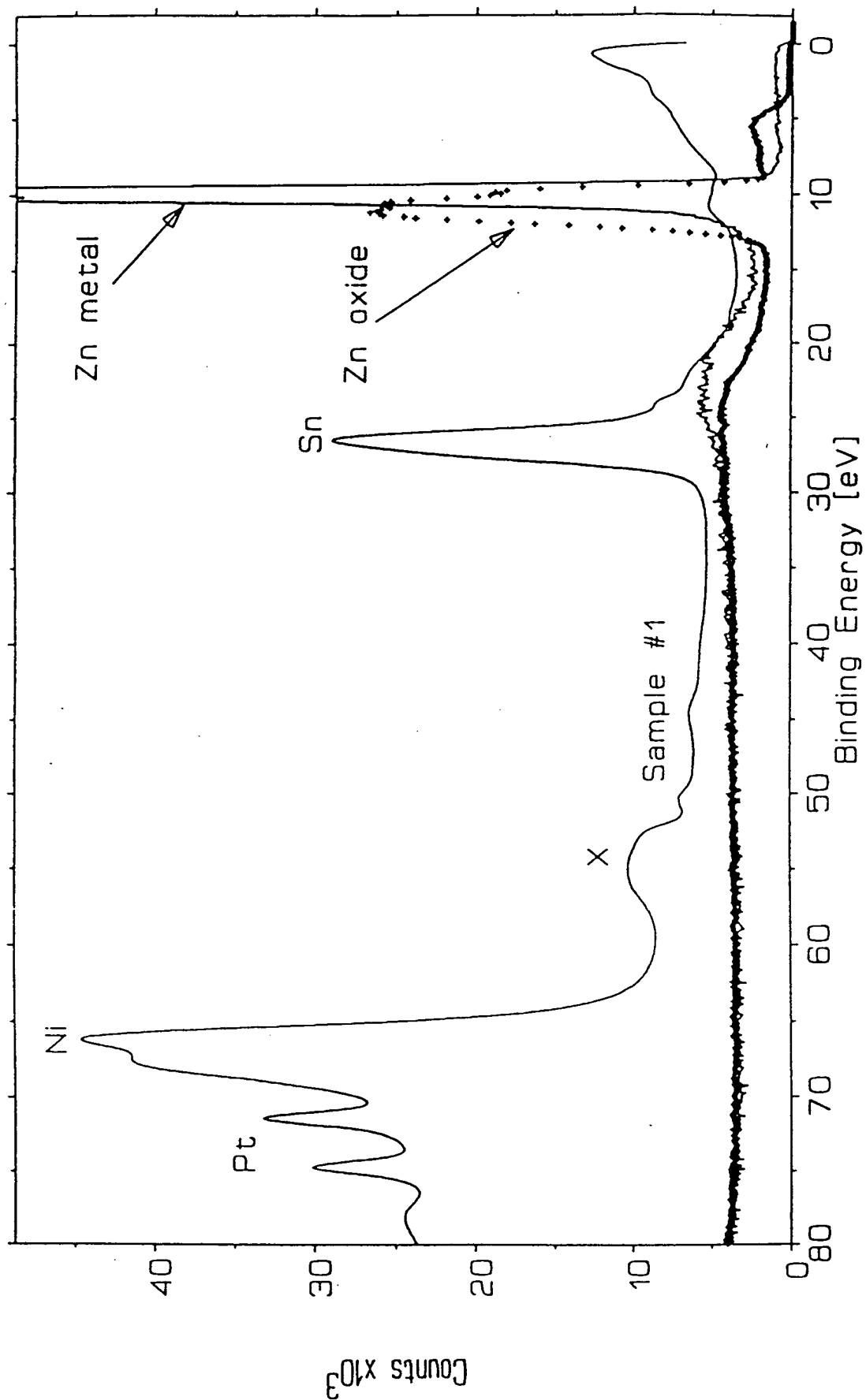
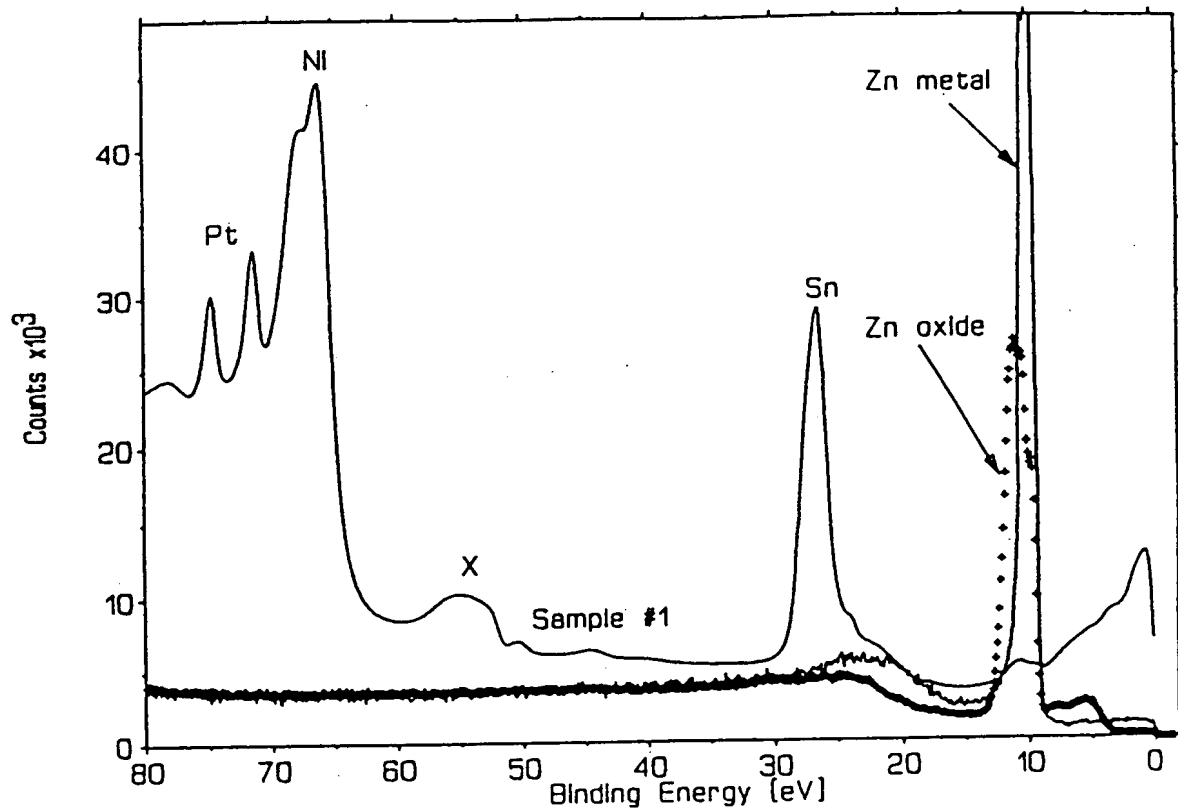


Figure 5

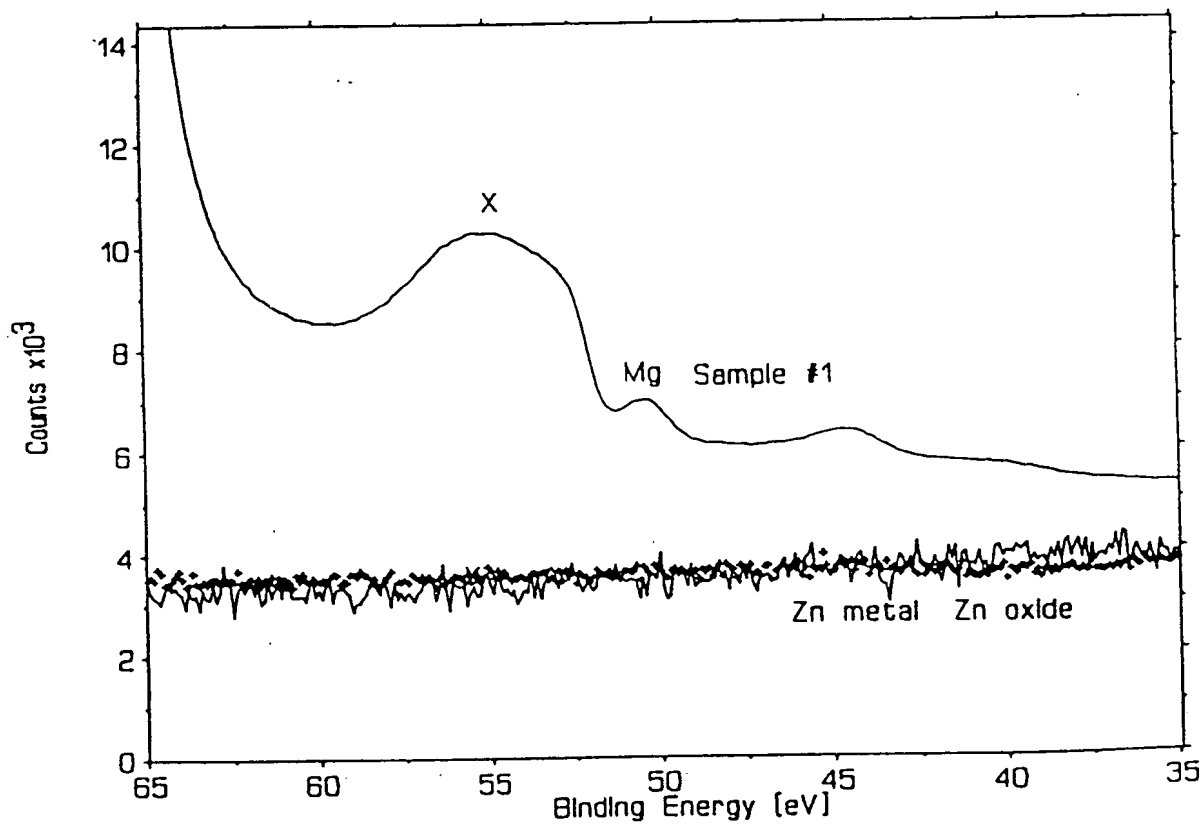


ZINC.007

Figure 6



ZINC.007



ZINC.007

Figure 7

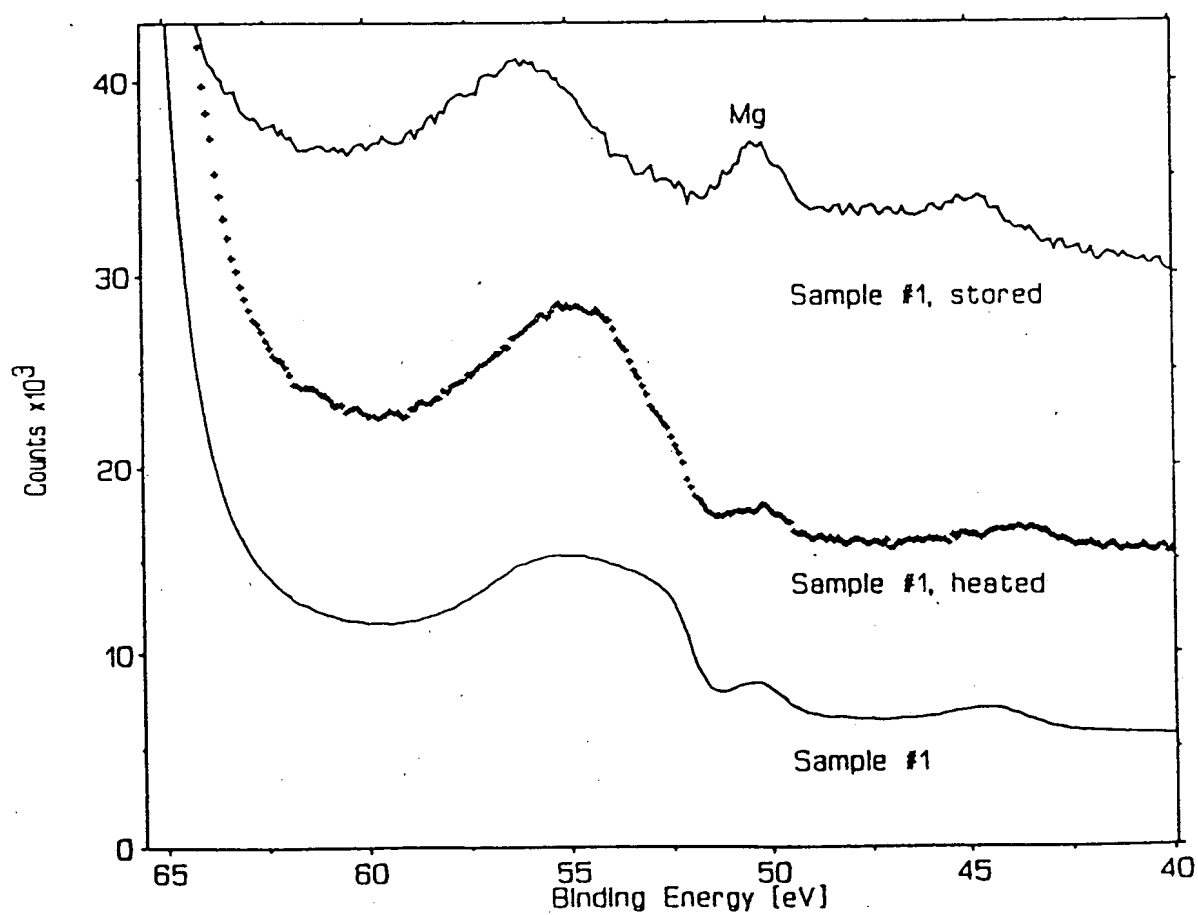
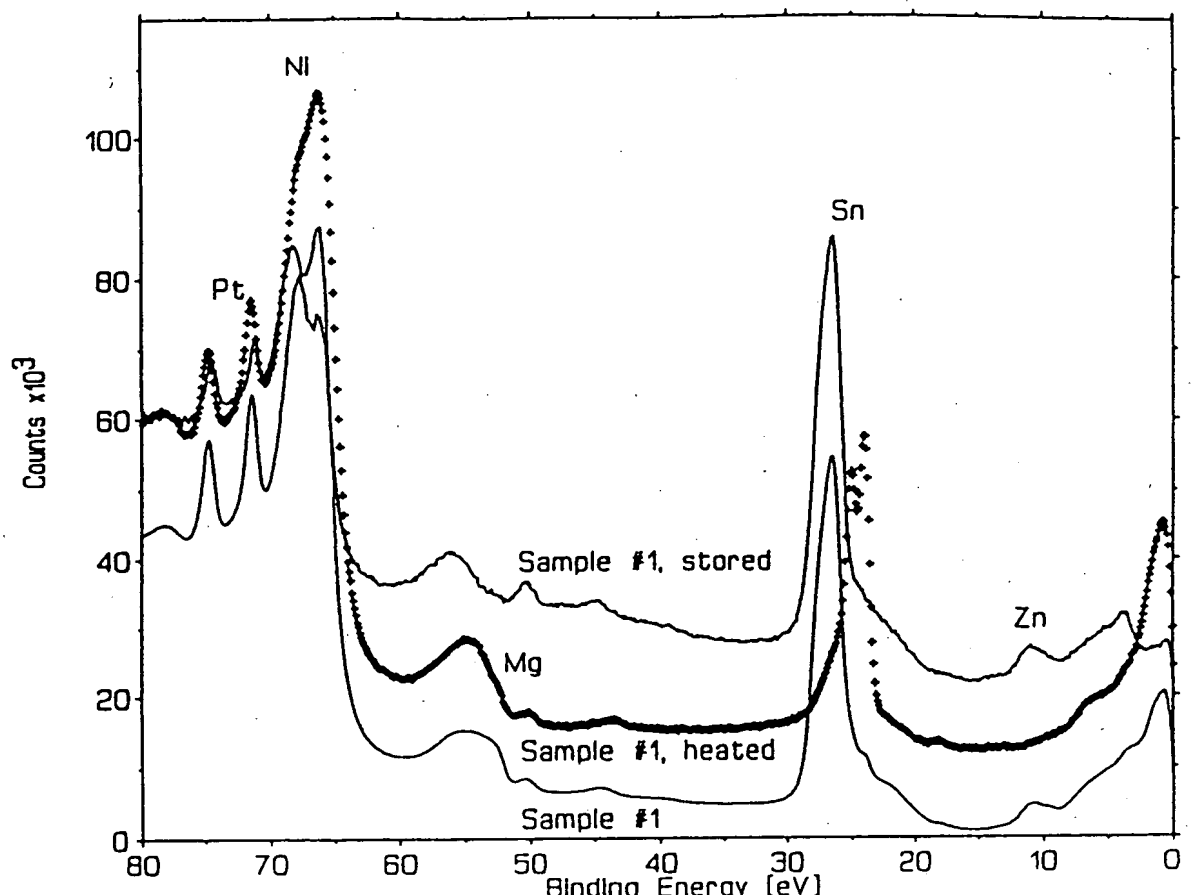


# Figure 8

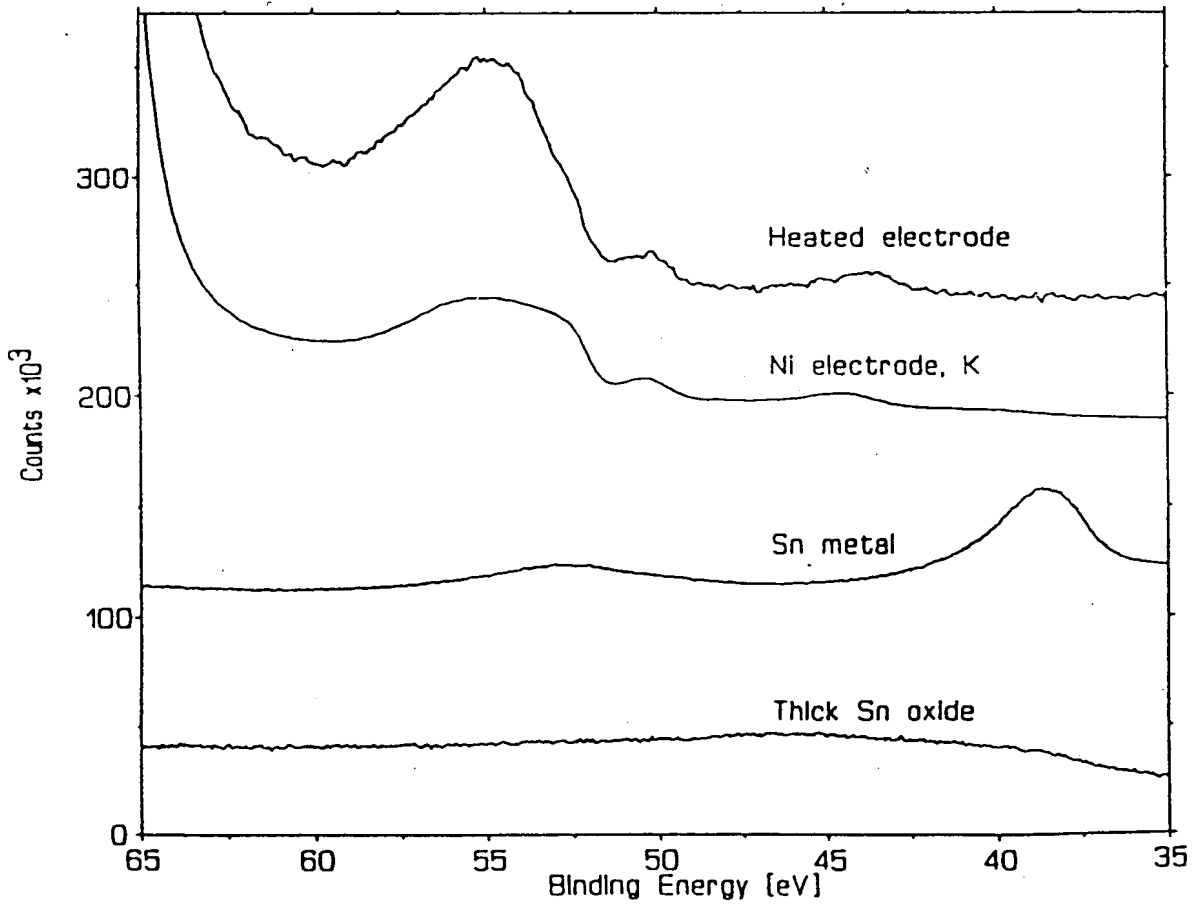
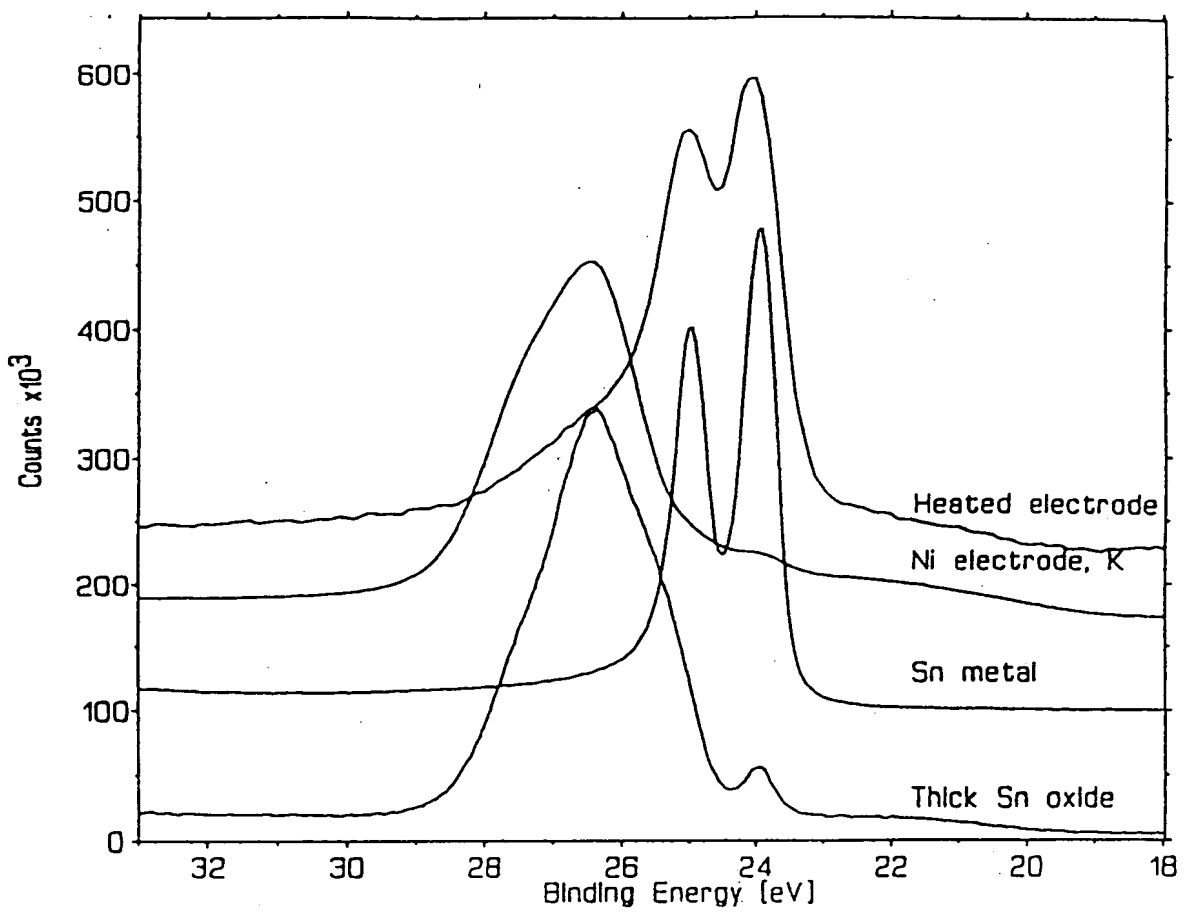
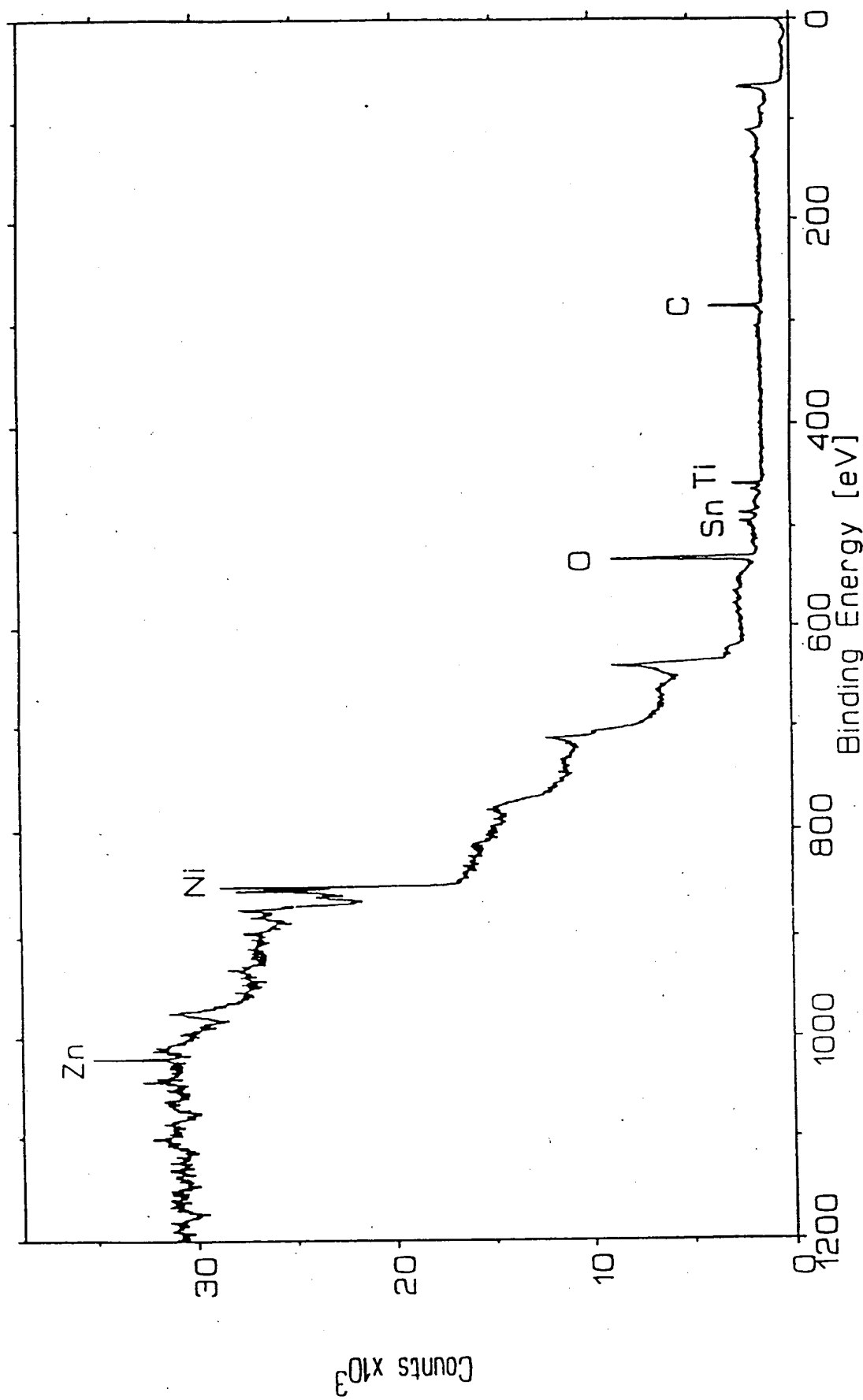


Figure 9



HPCK-02.001

Figure 10

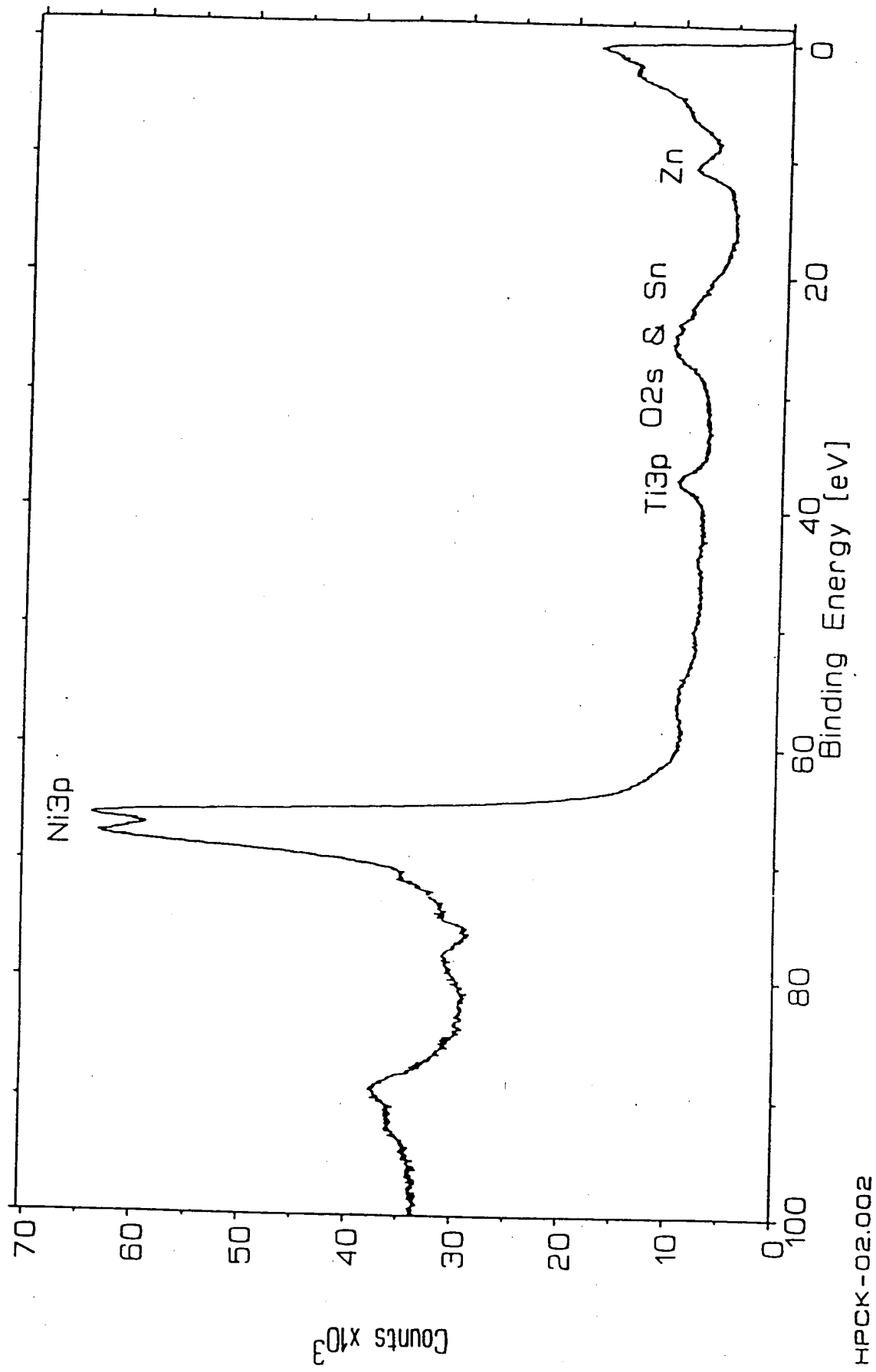


Figure 11

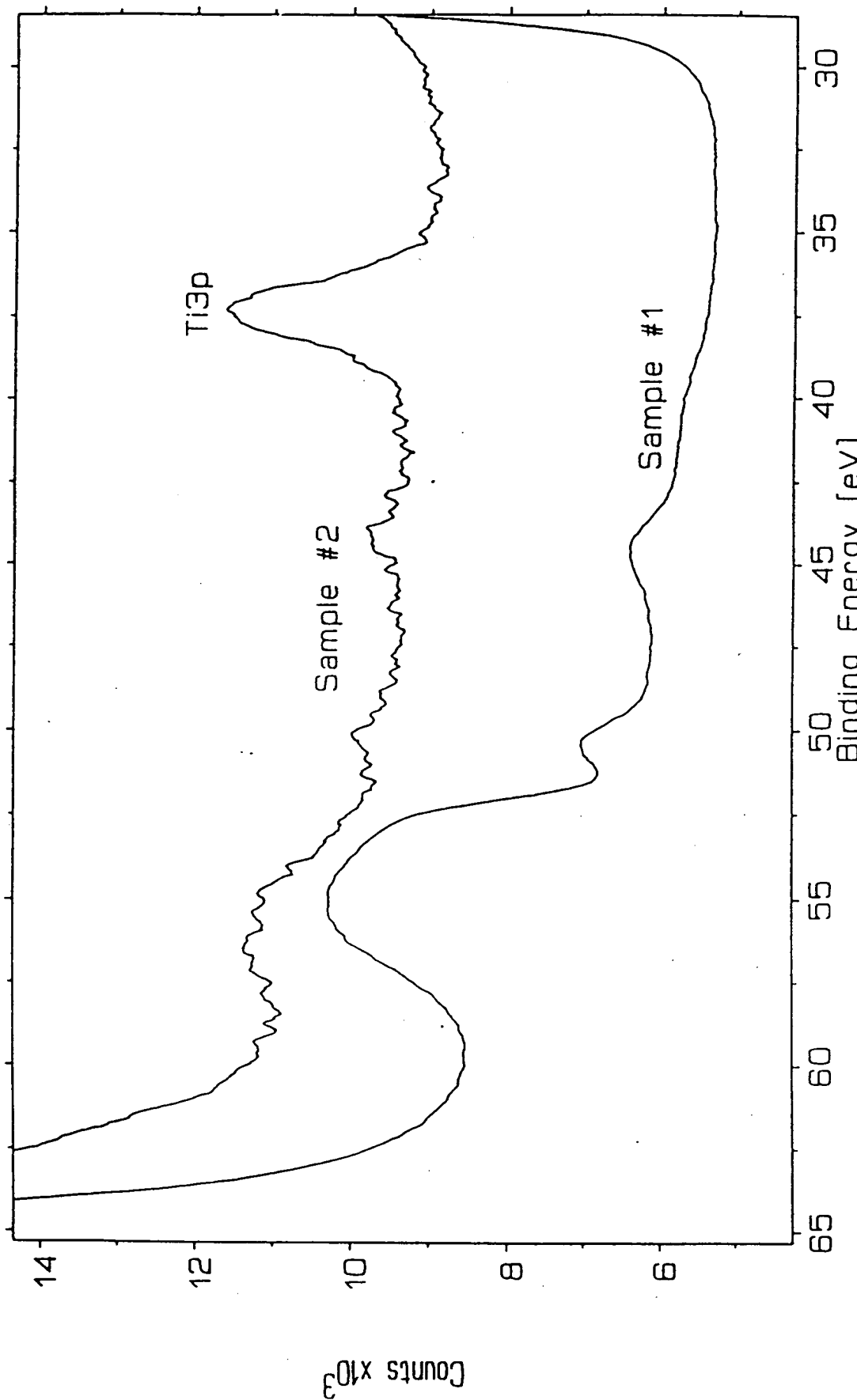


Figure 12

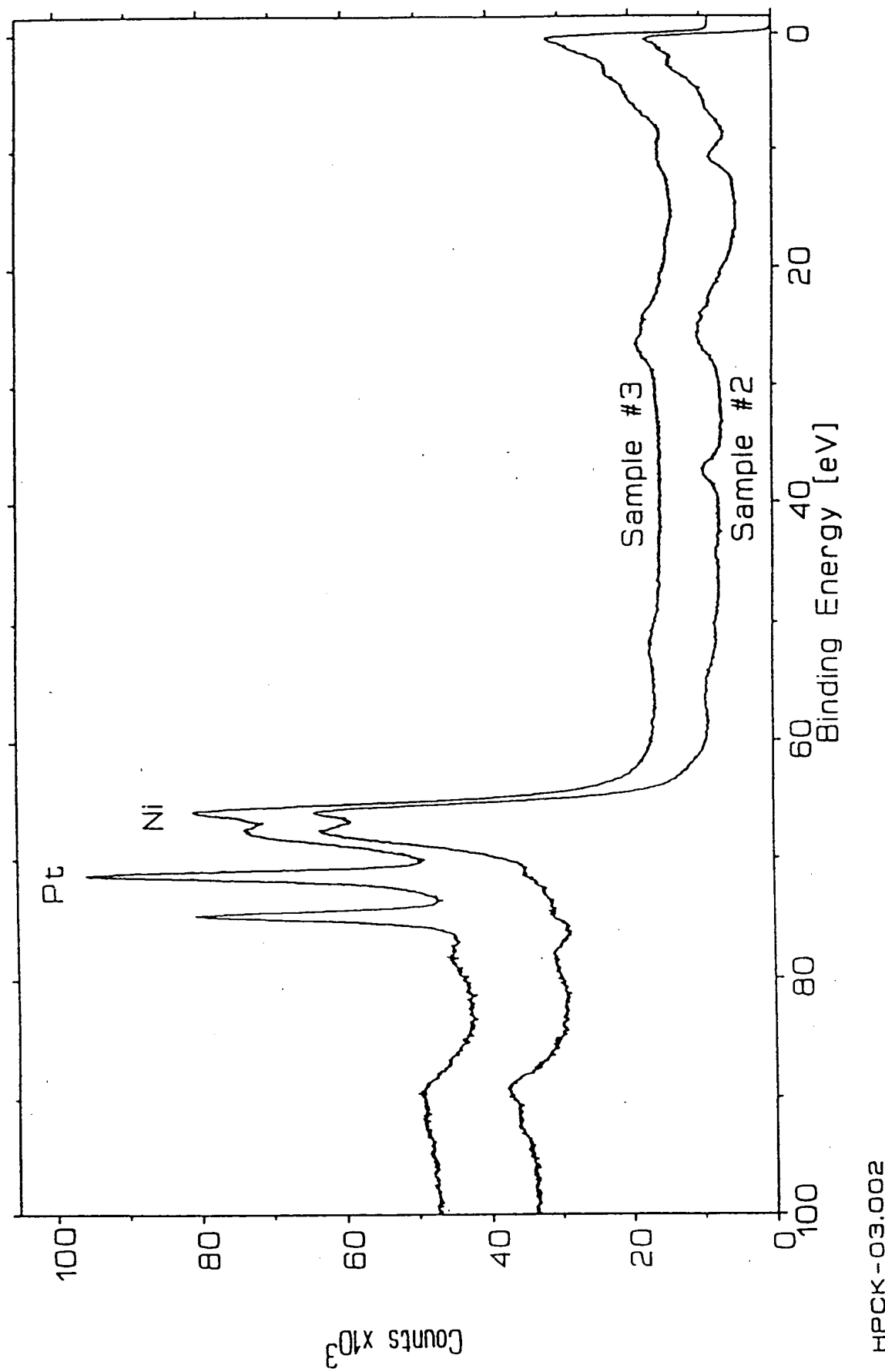


Figure 13

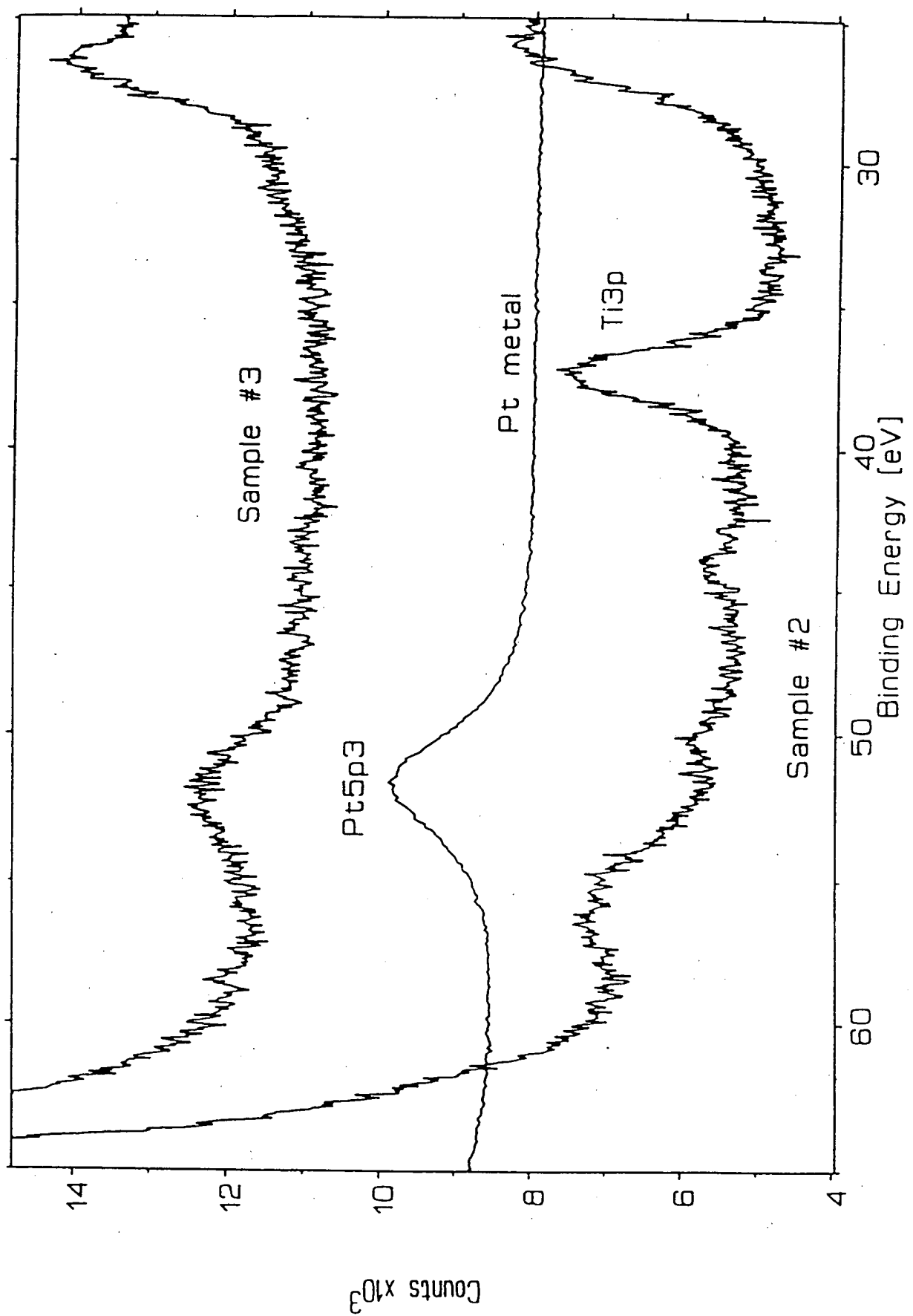
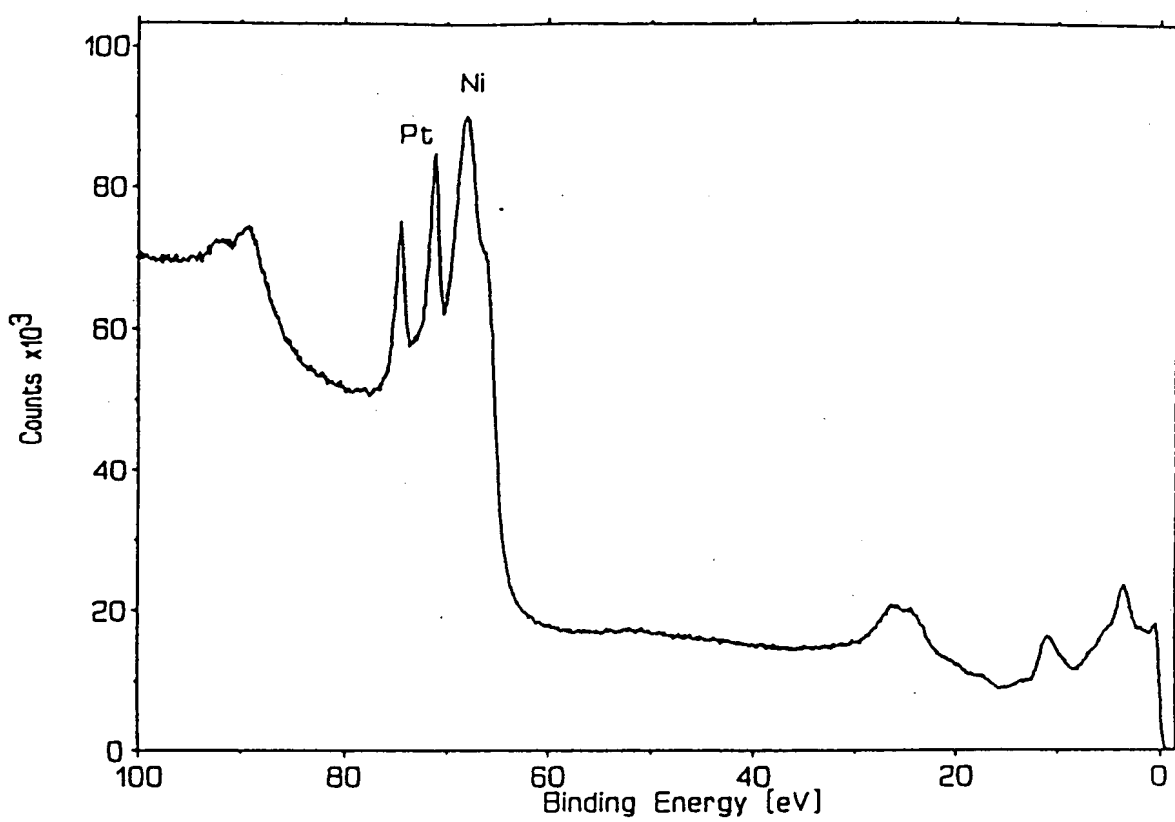
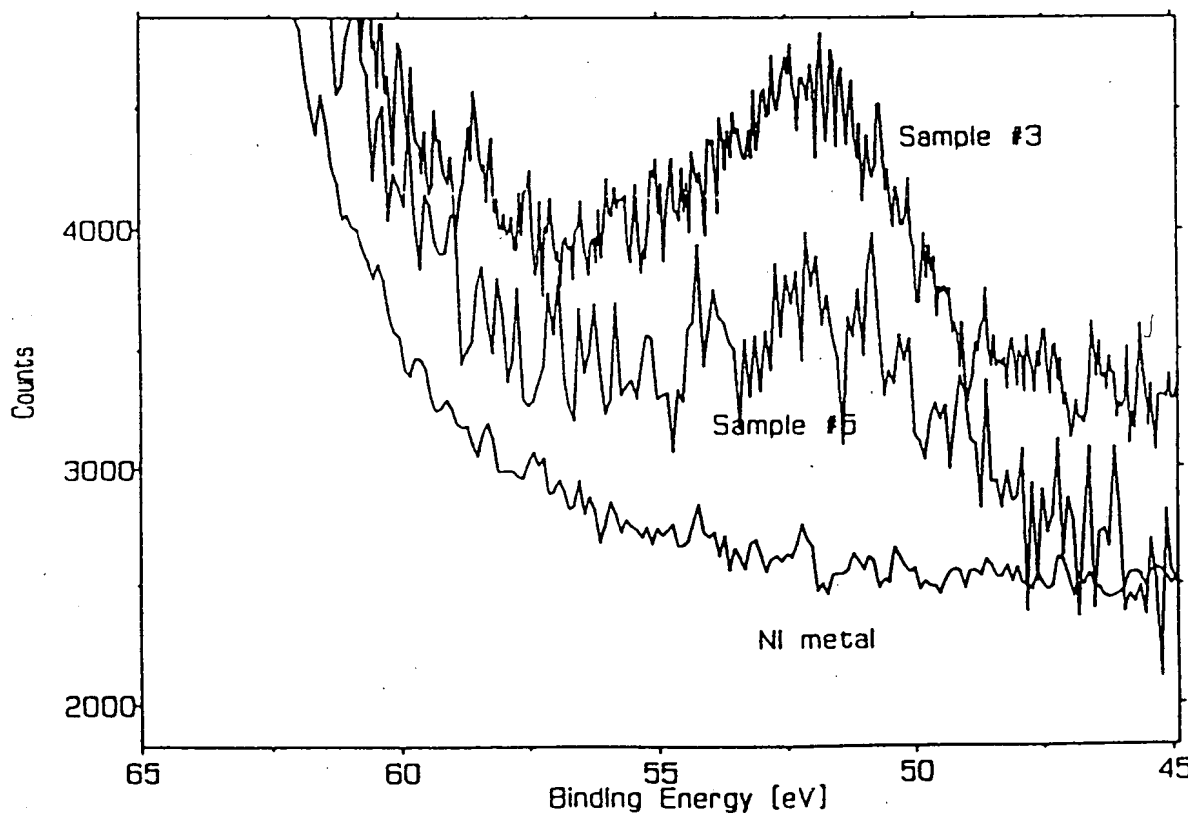


Figure 14

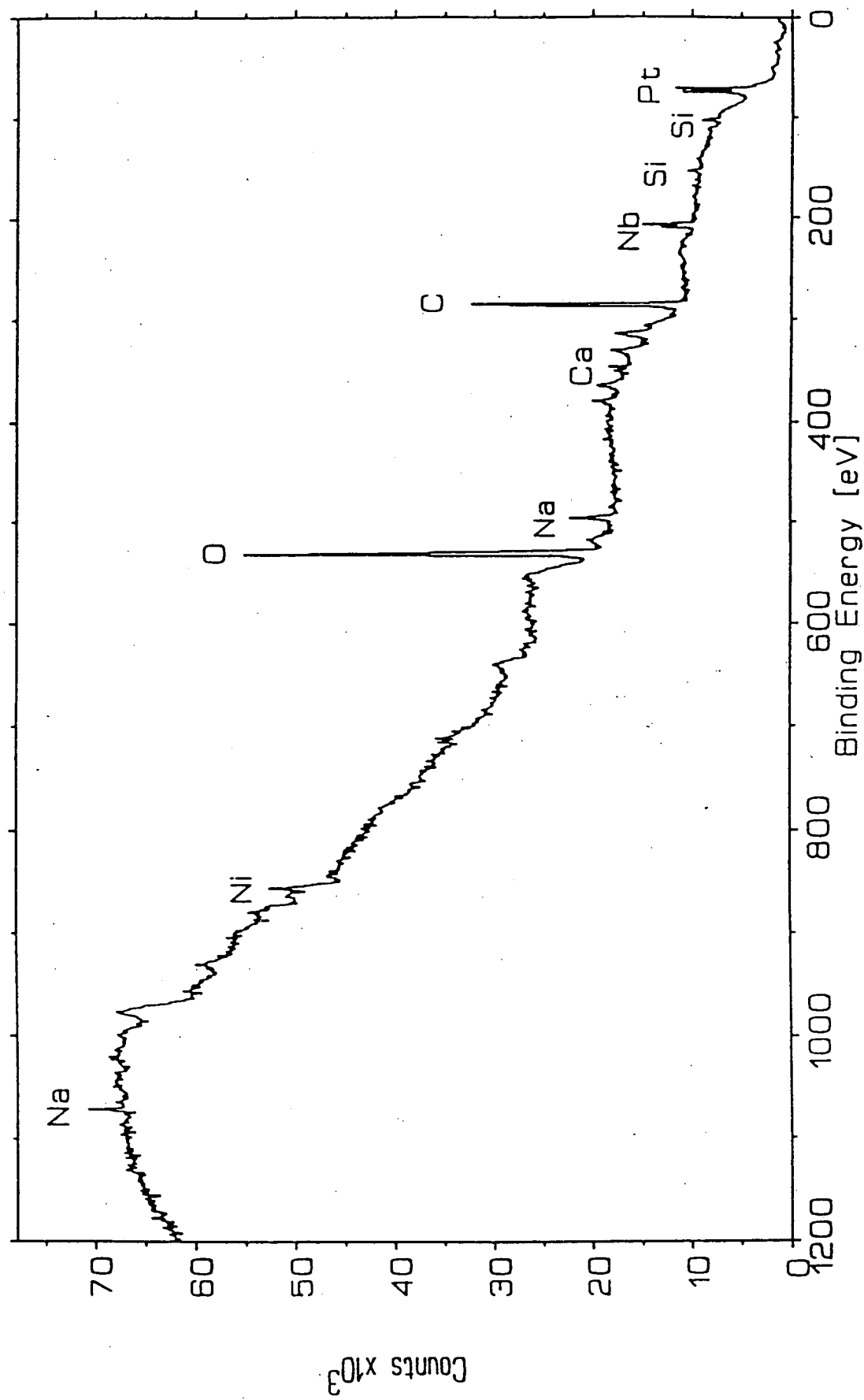


HPCK-05.001



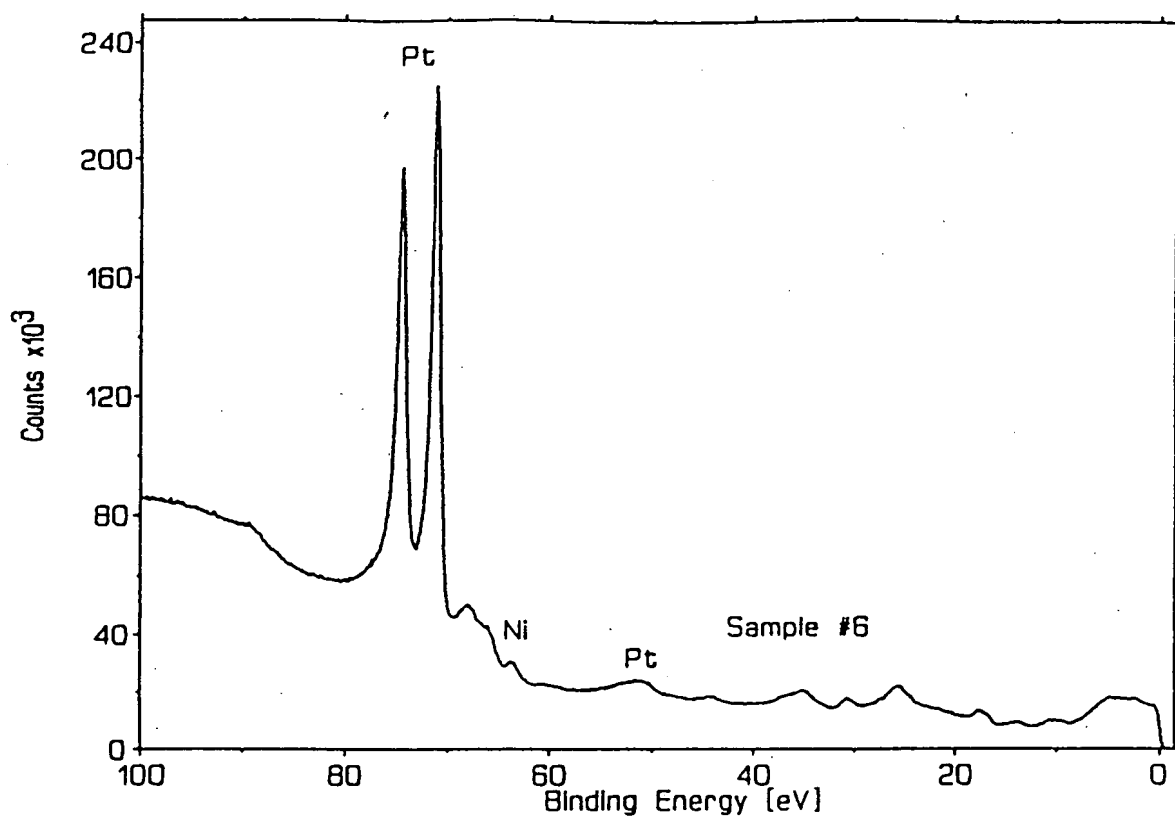
HPCK-05.001

Figure 15



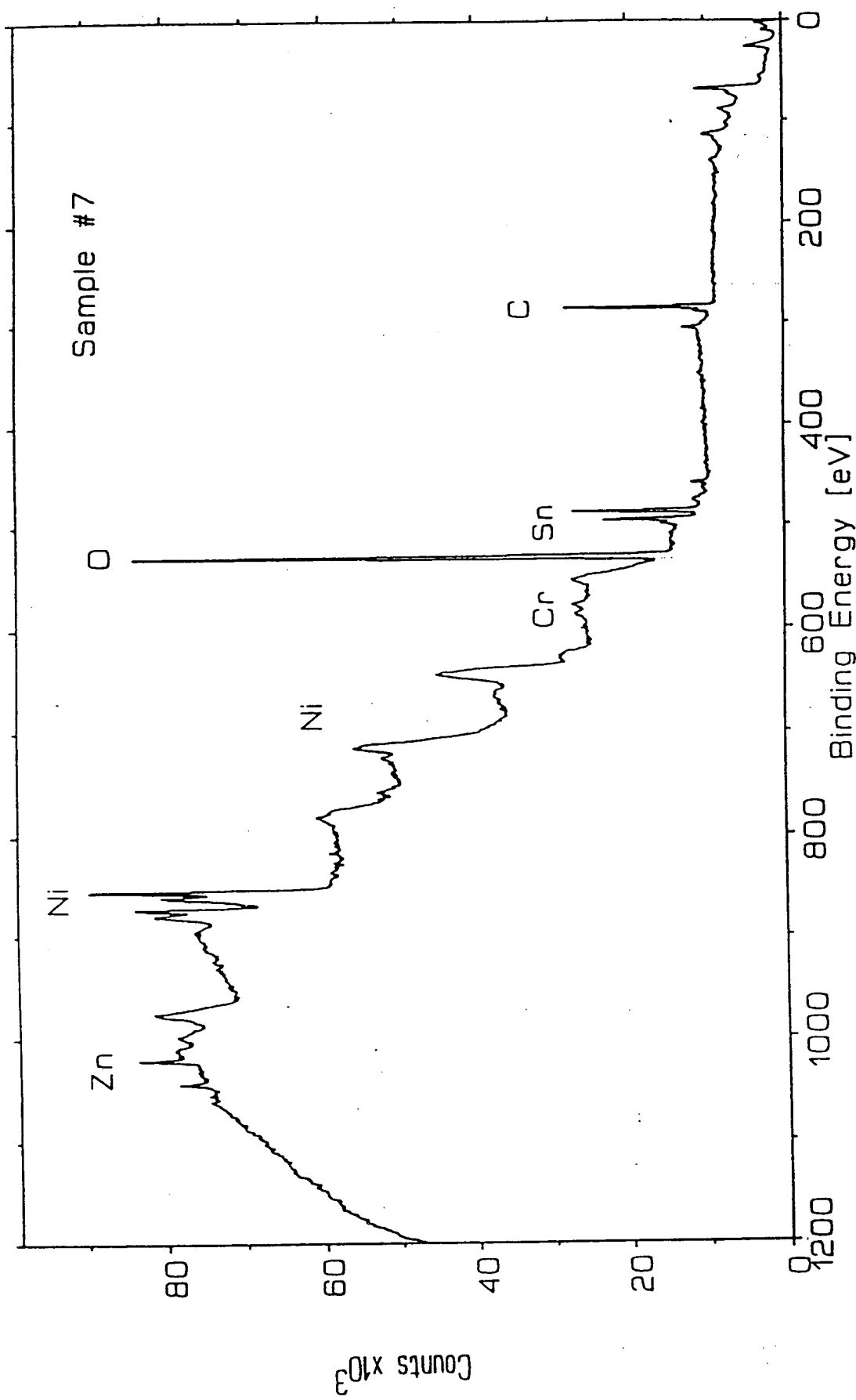
HPCK - 08.001

Figure 16

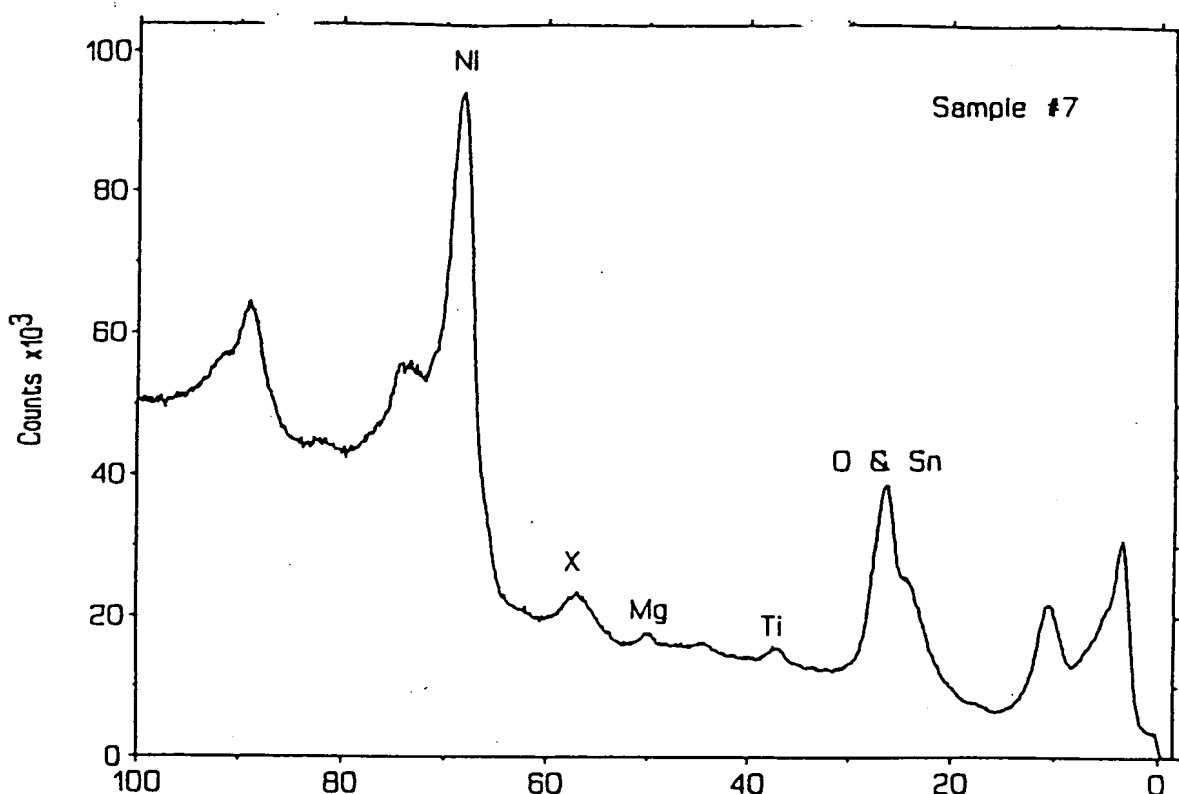


HPCK-08.001

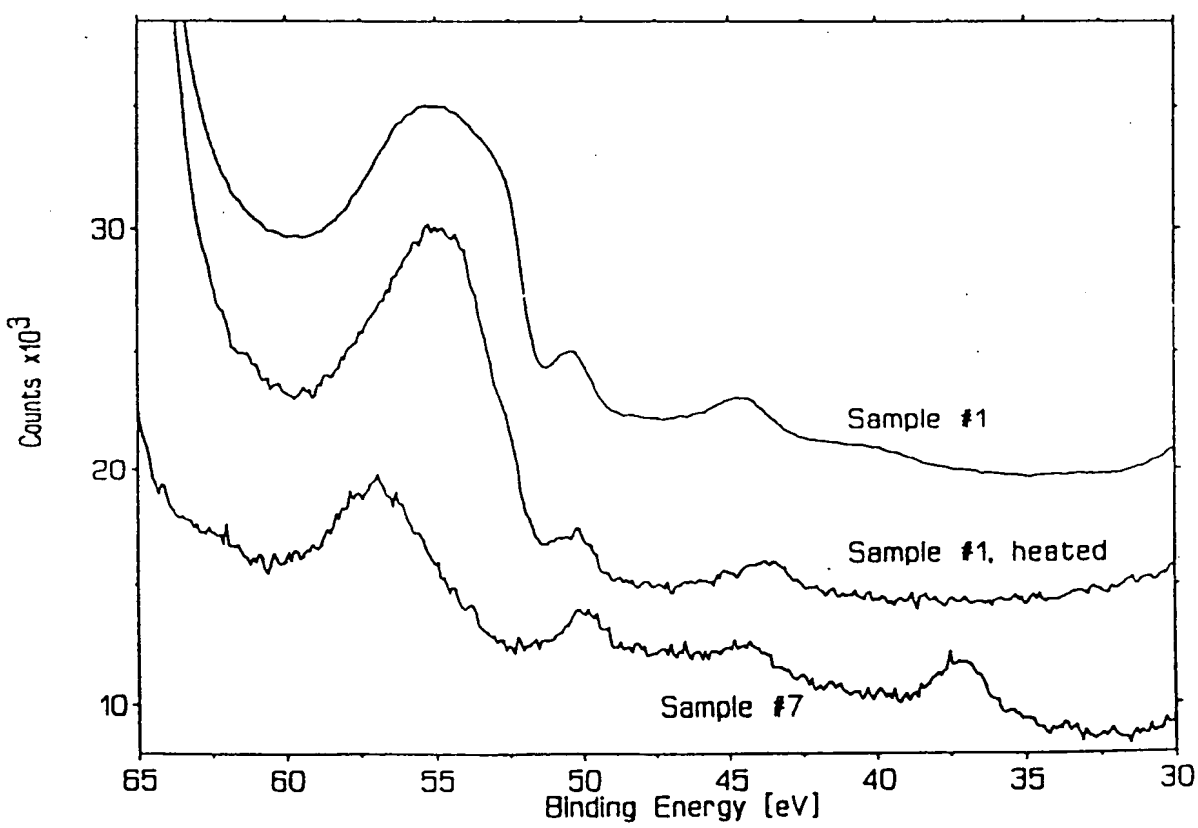
Figure 17



# Figure 18



HPCK-07.002



HPCK-07.002

Figure 19

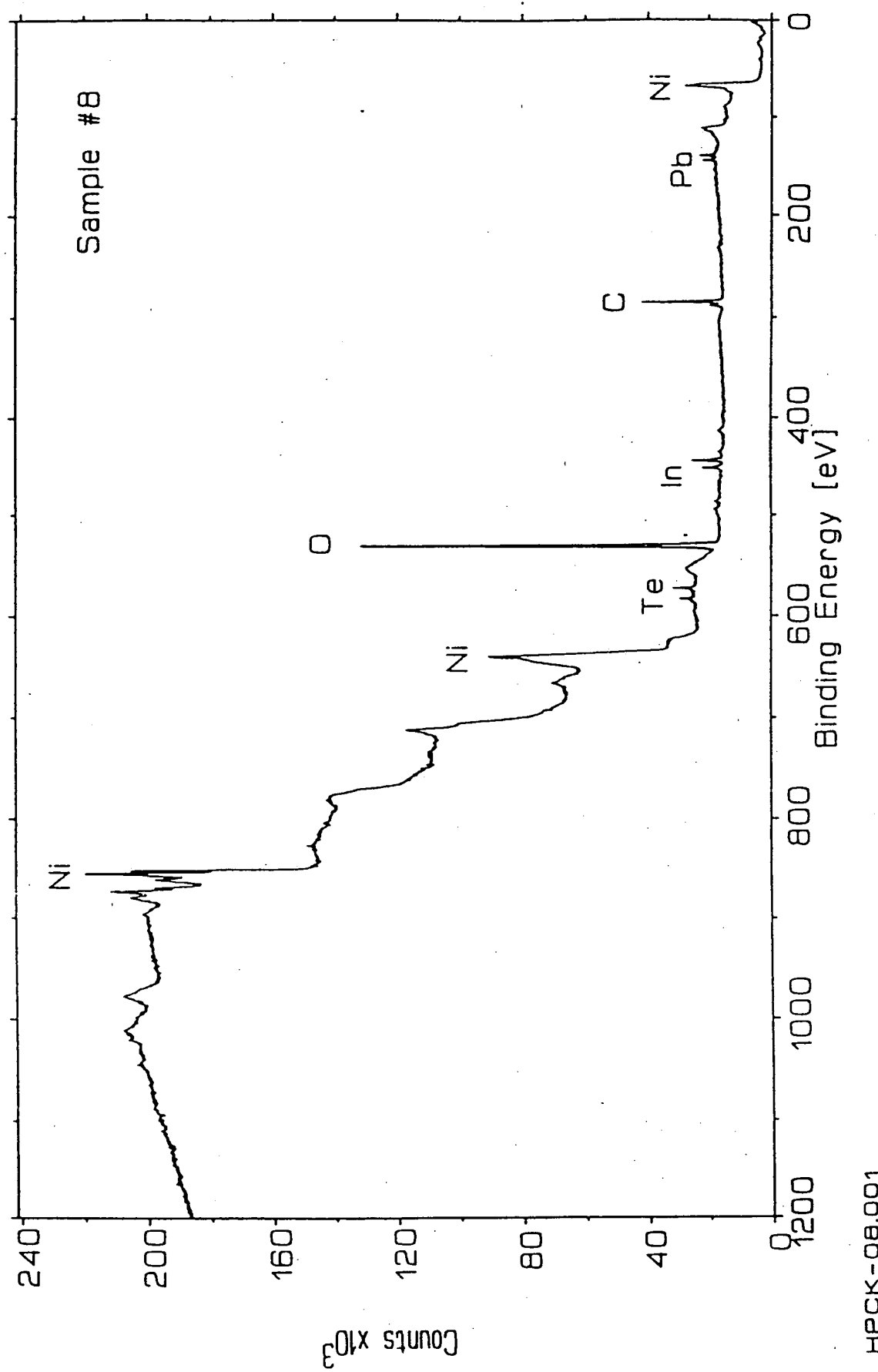
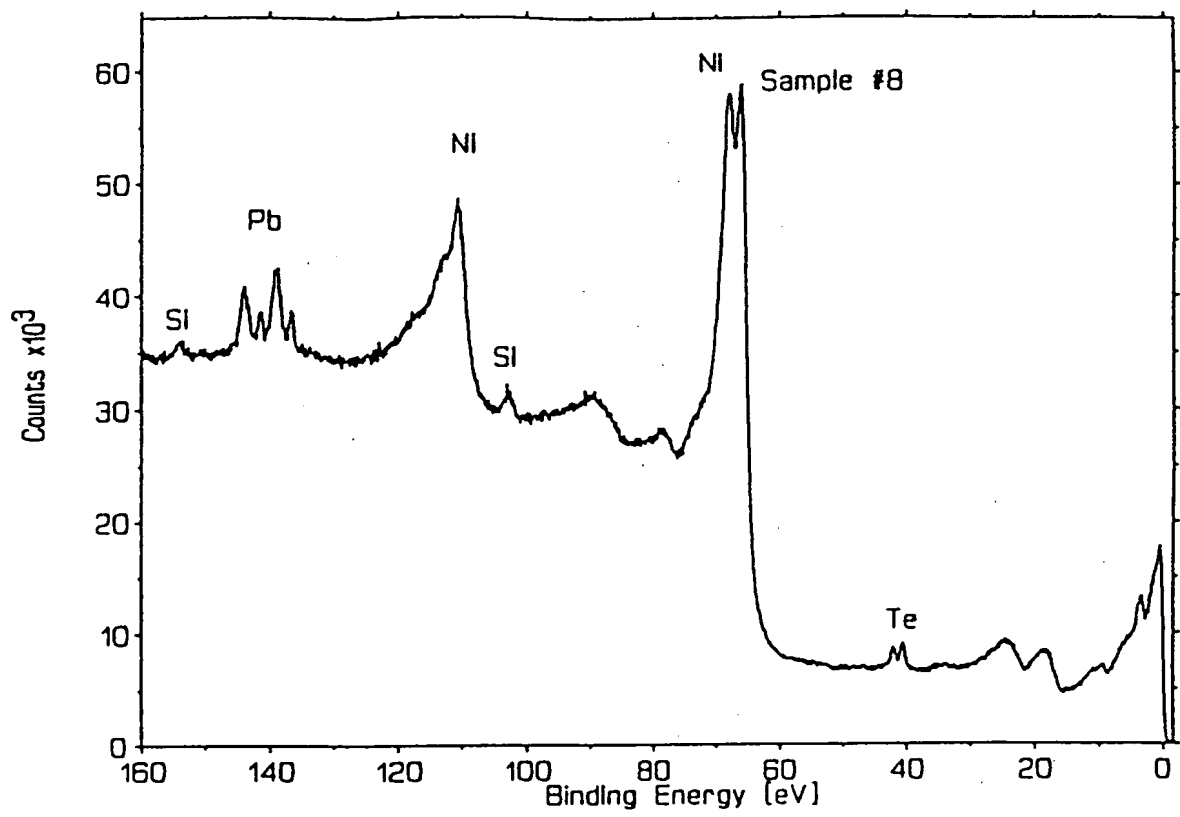
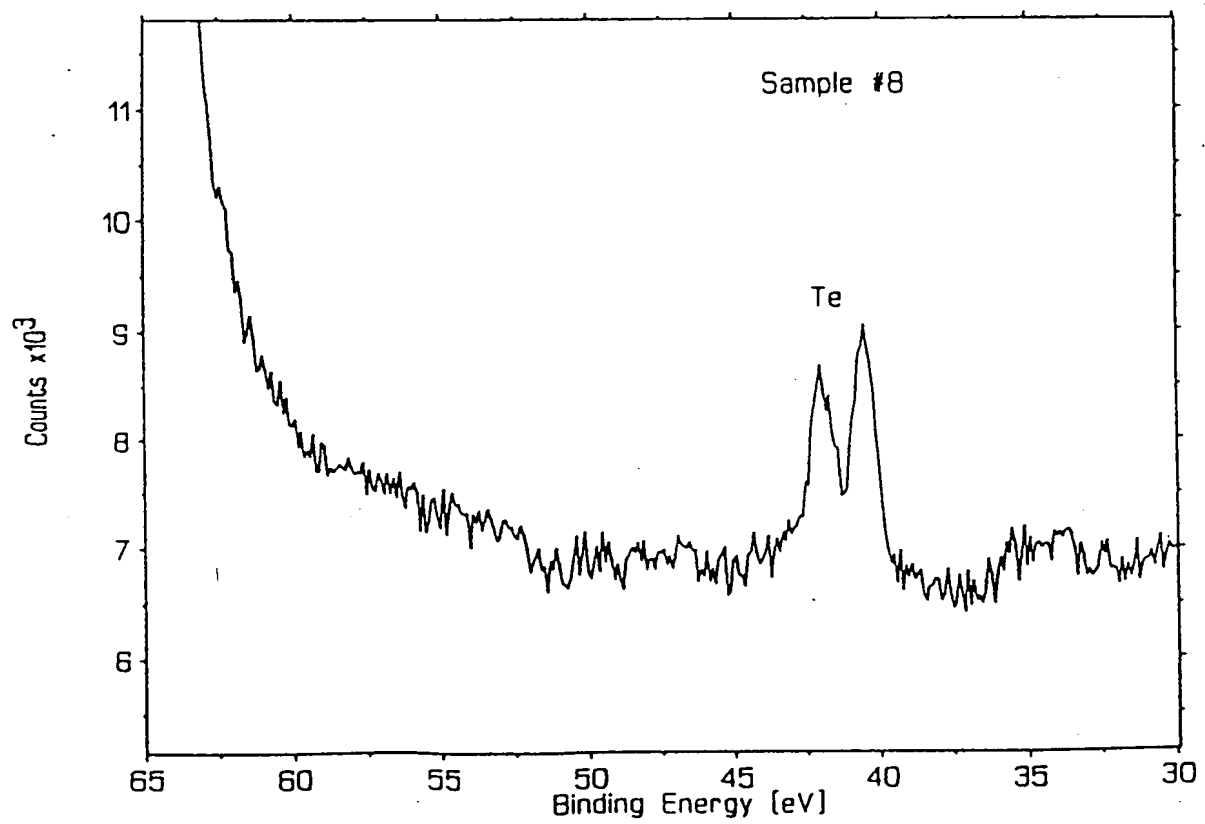


Figure 20



HPCK-08.003



HPCK-08.003

Figure 21

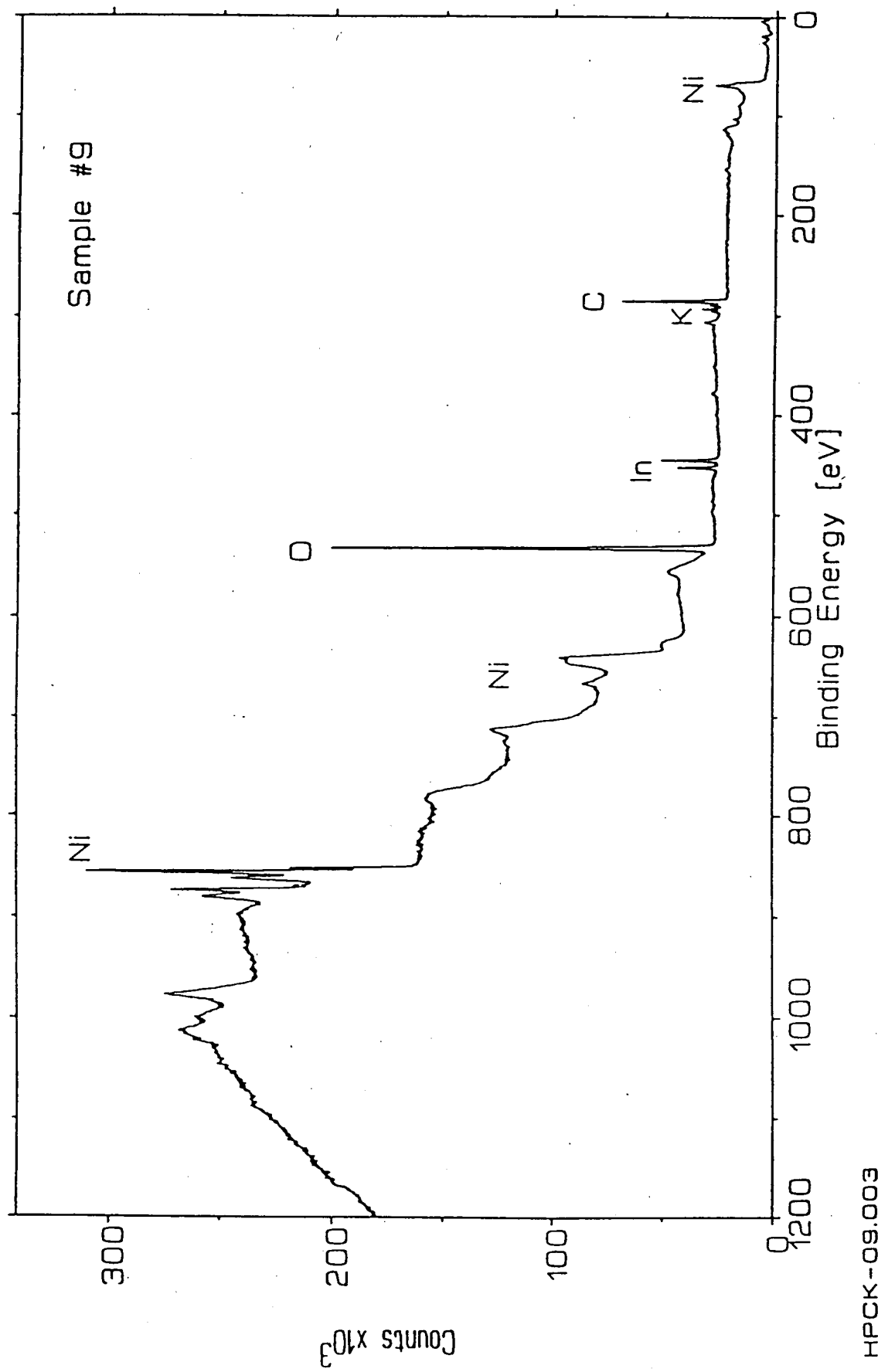
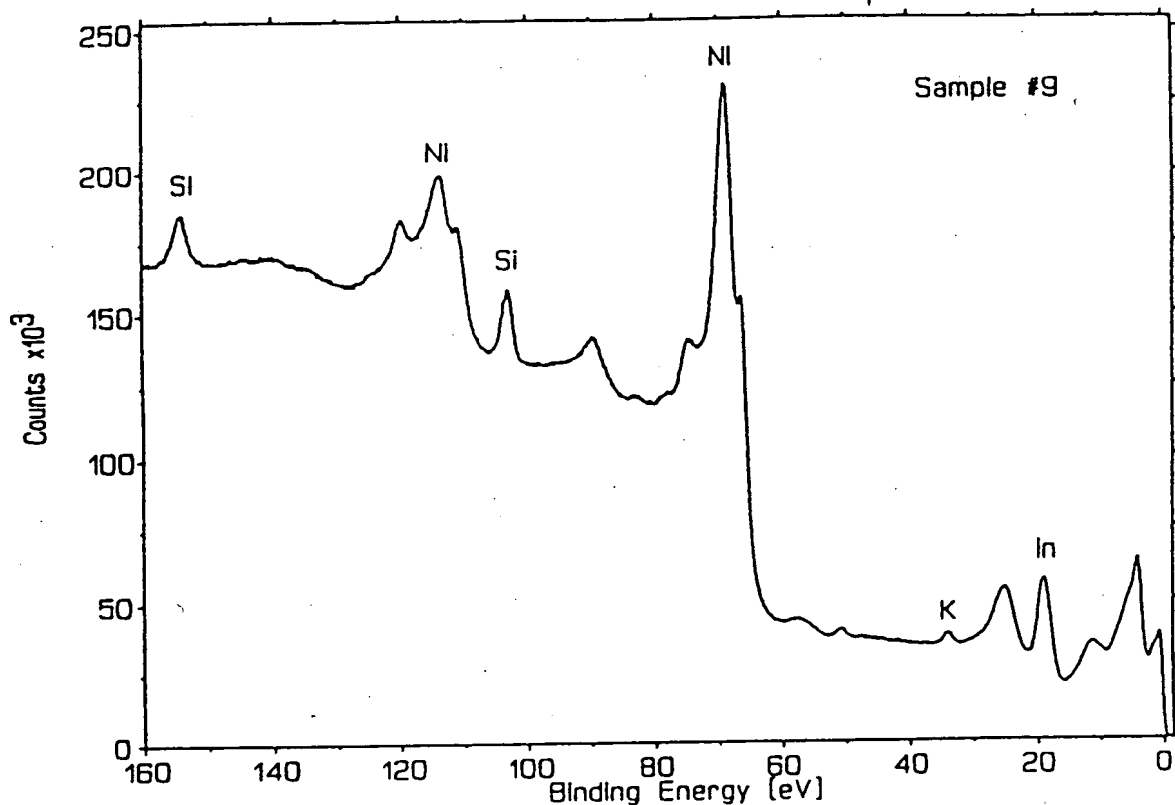
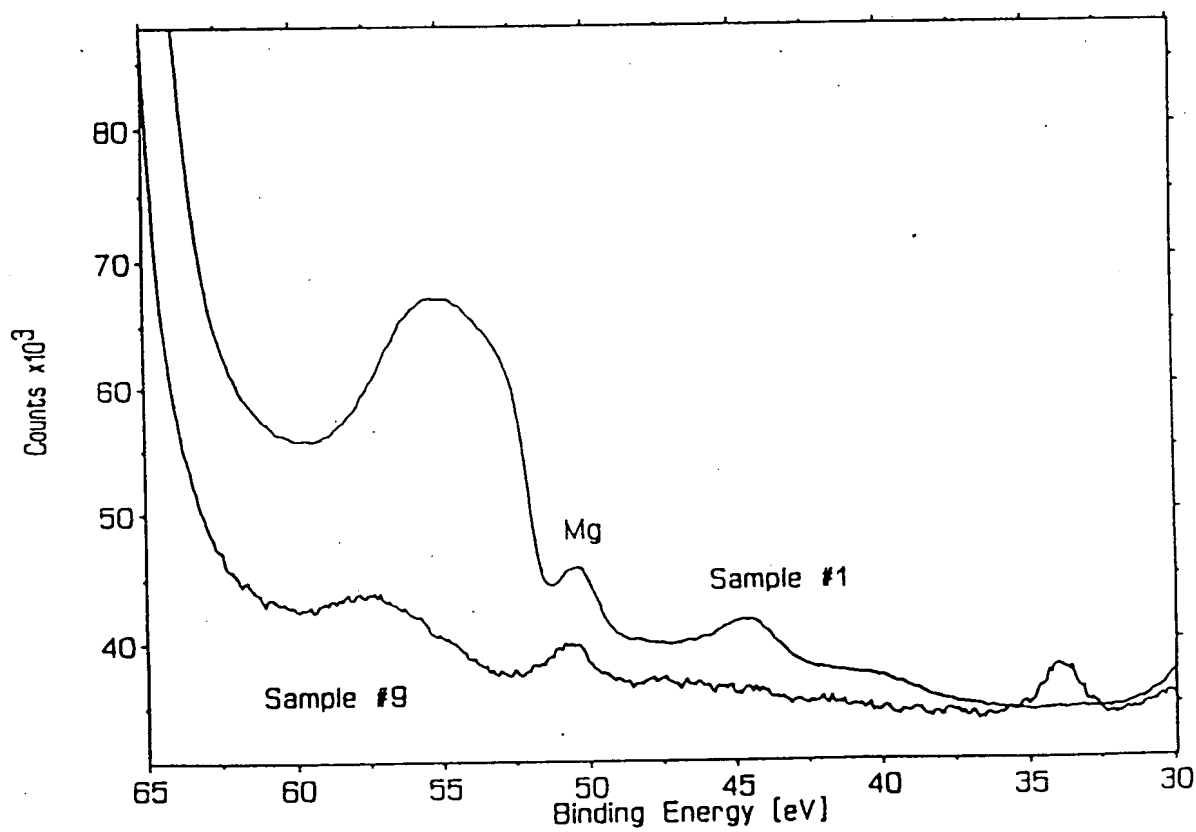


# Figure 22



HPCK-09.003



HPCK-09.003

Figure 23

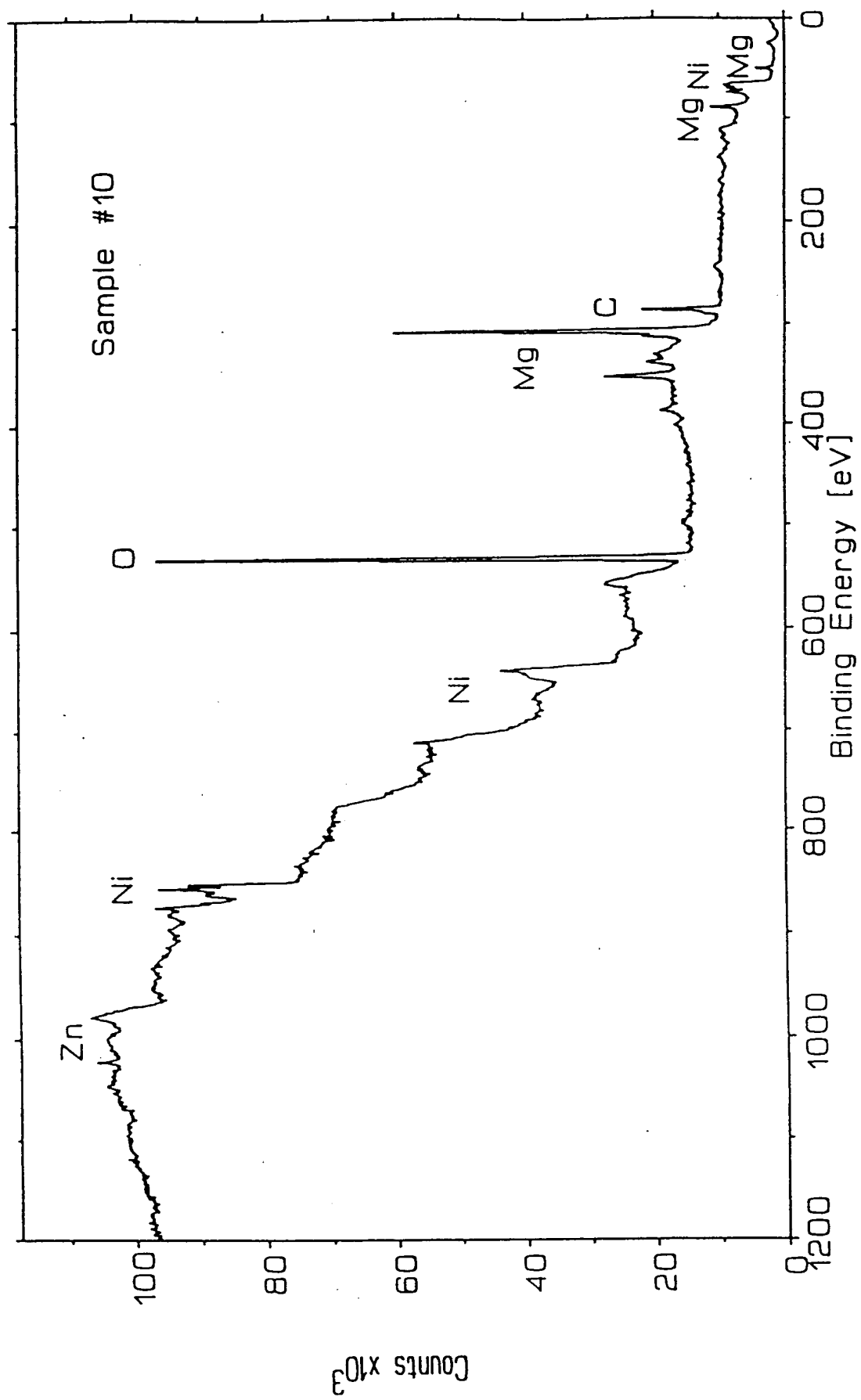
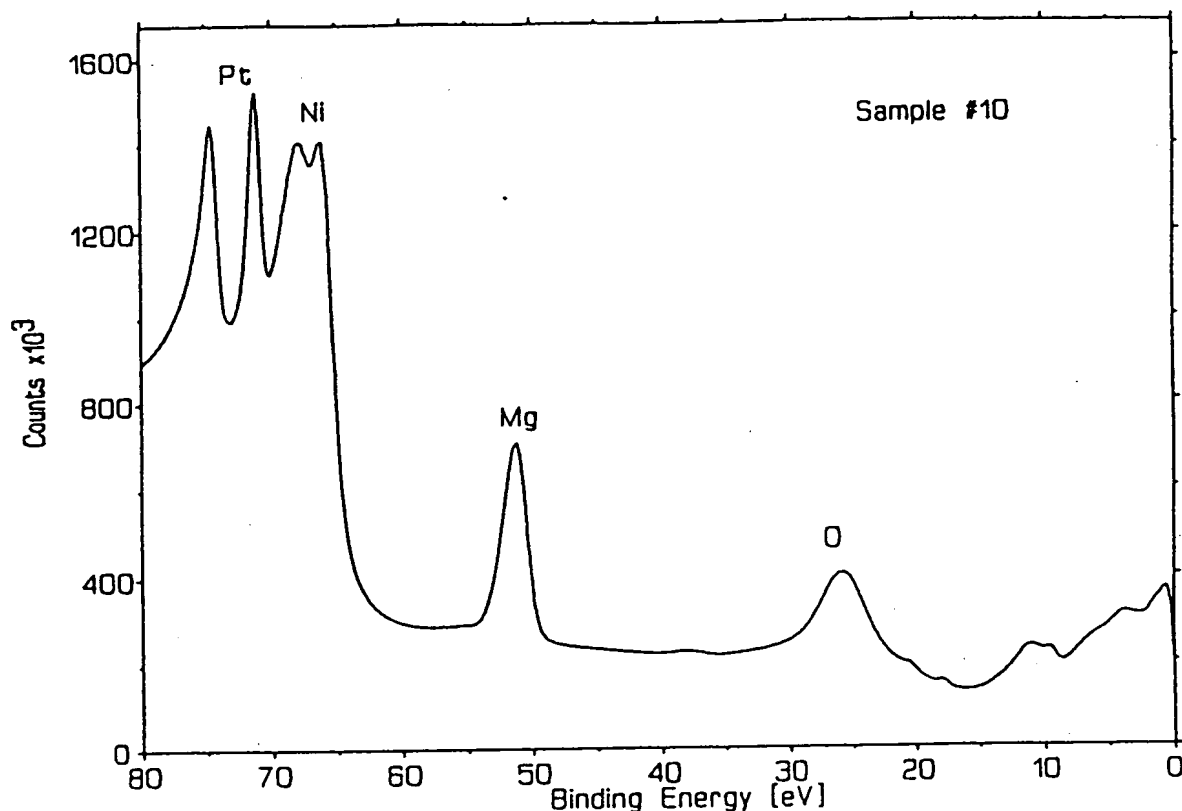
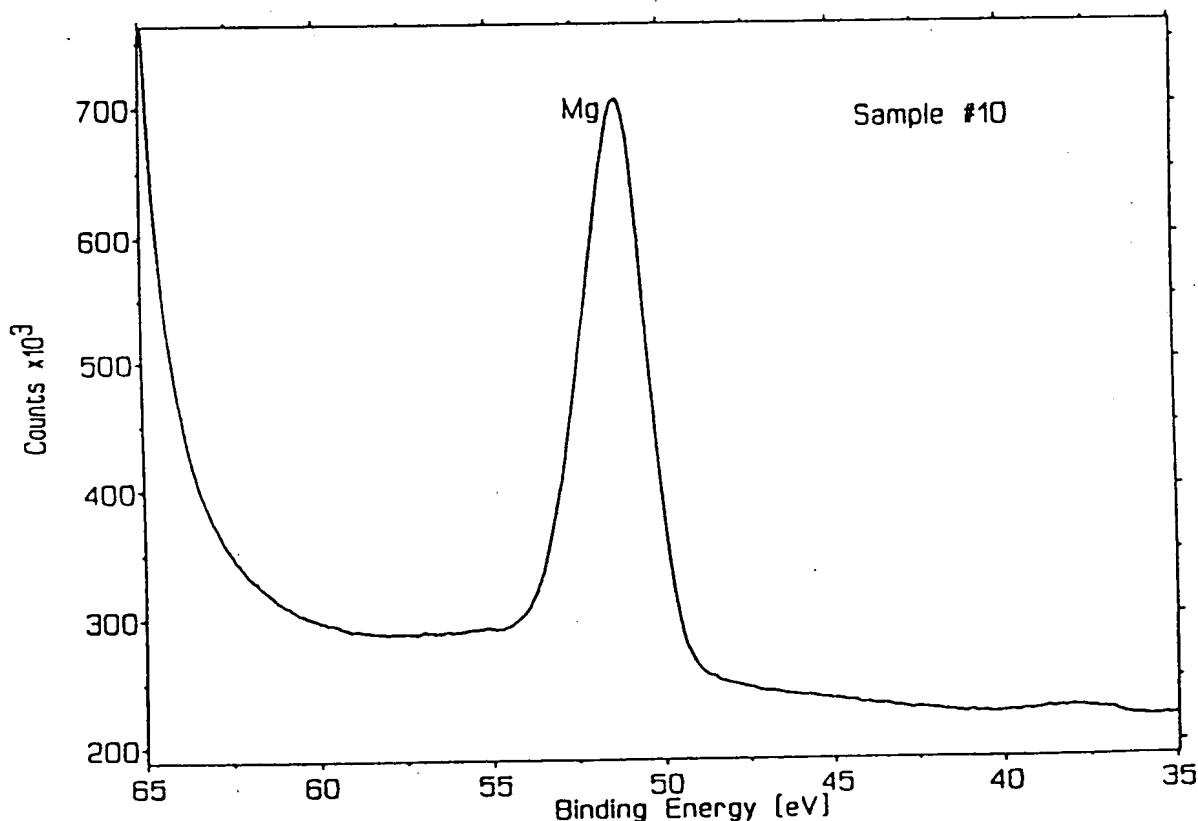


# Figure 24



HPCNA-01.002



HPCNA-01.002

Figure 25

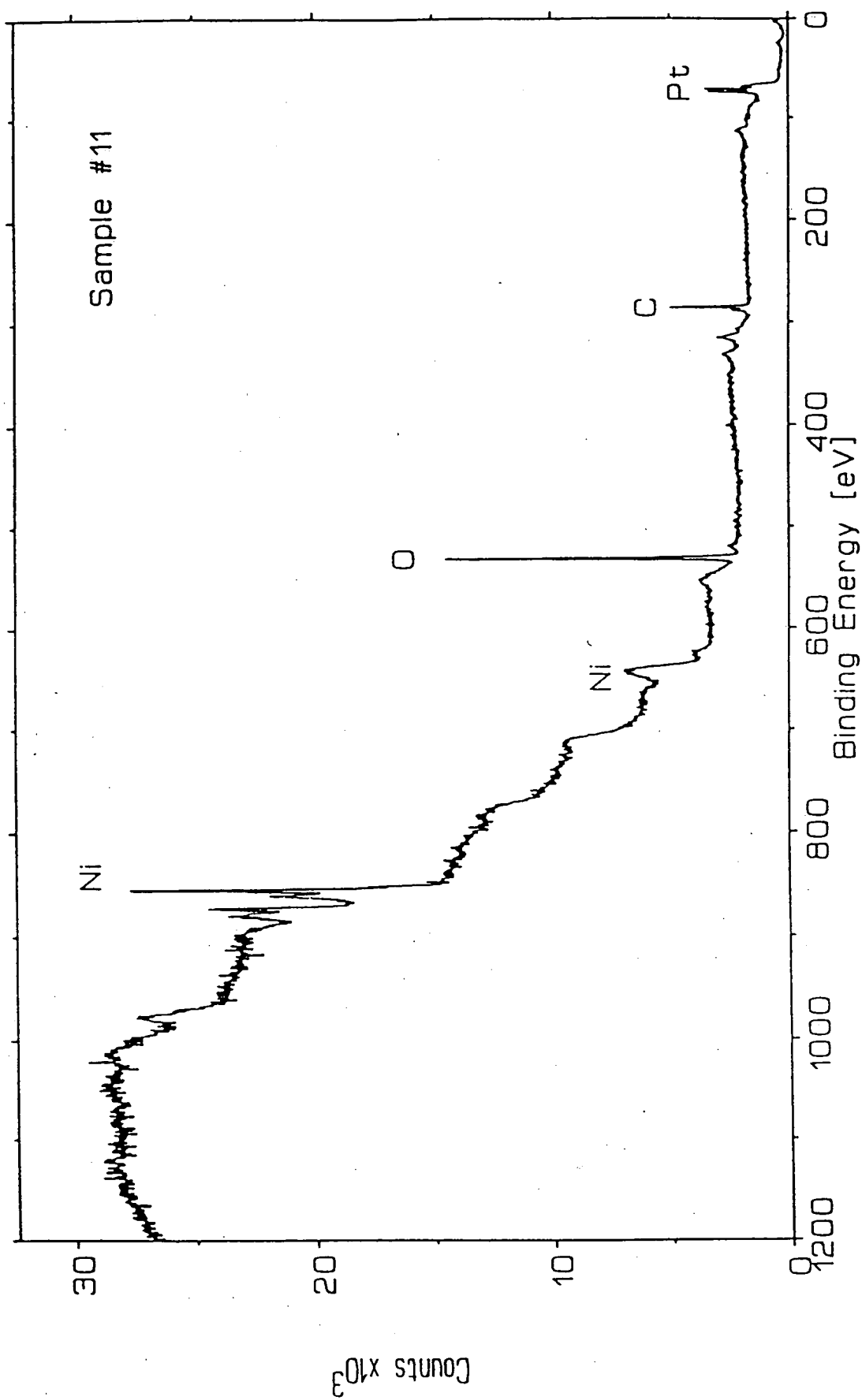


# Figure 26

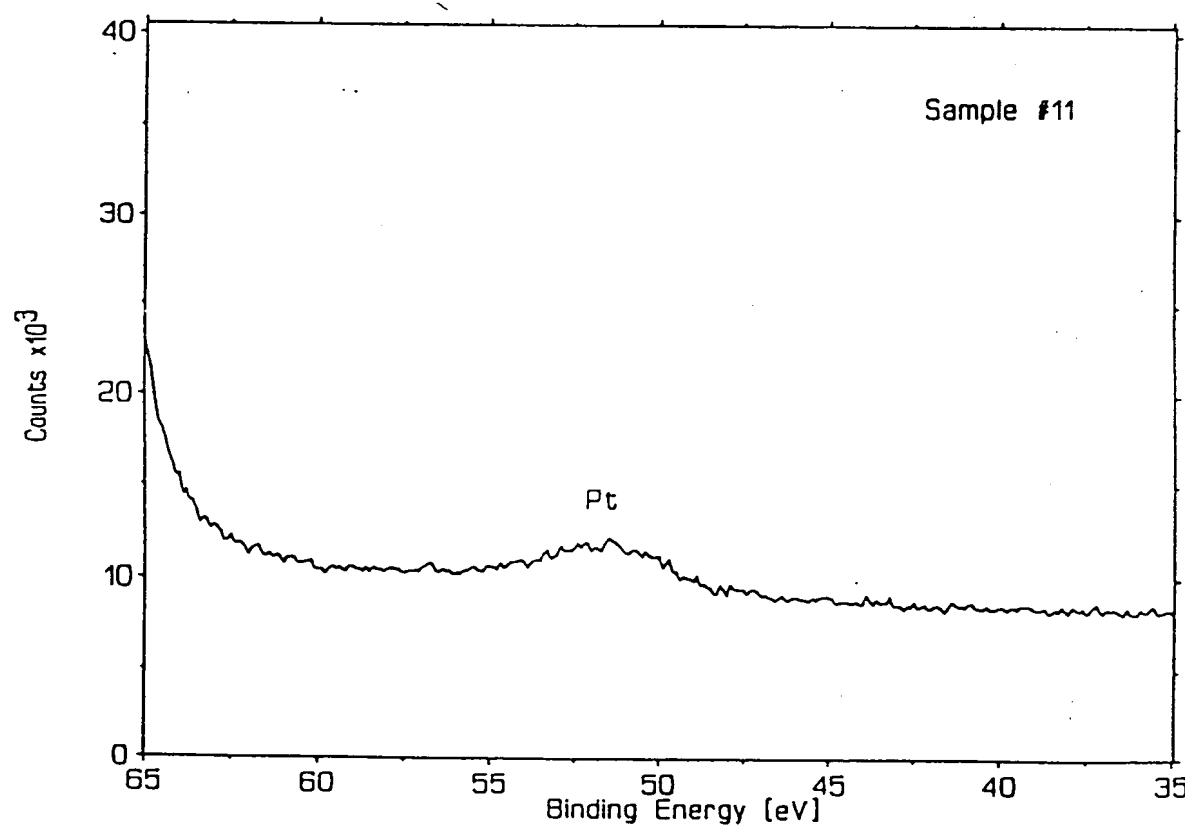
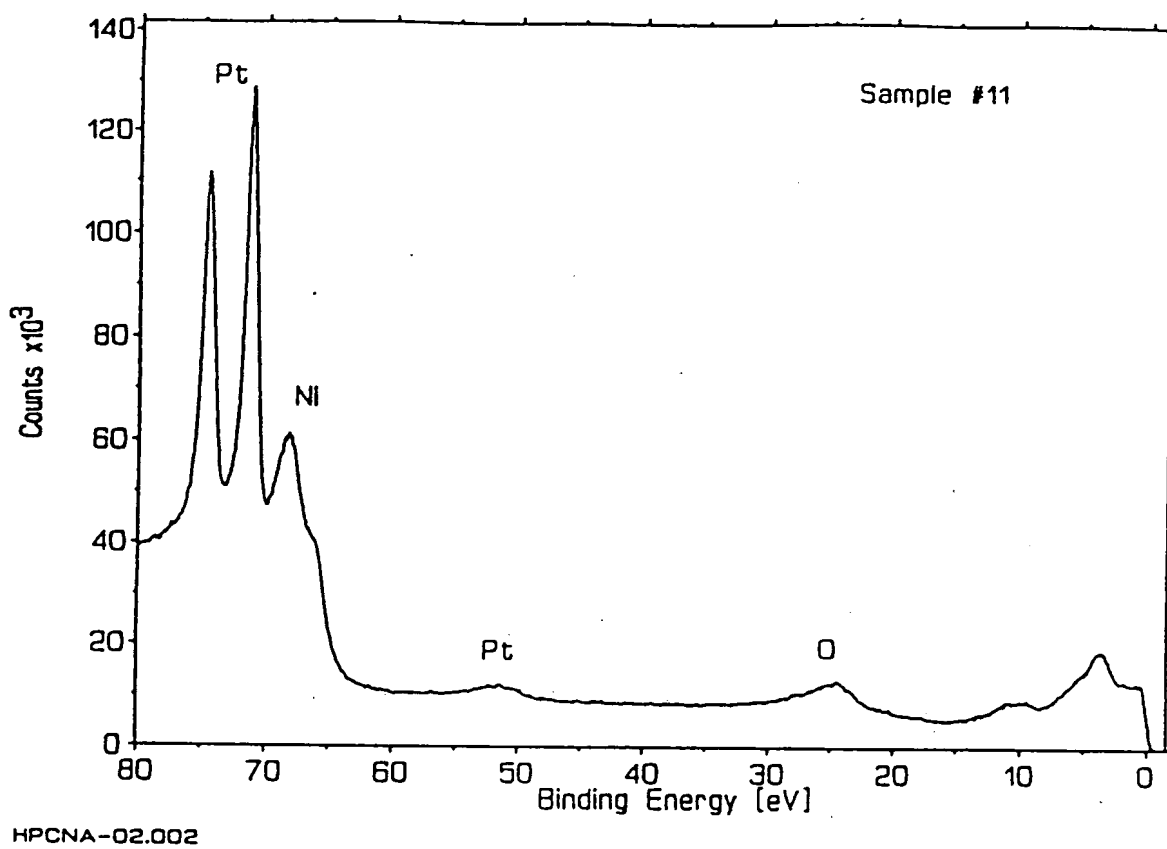


Figure 27

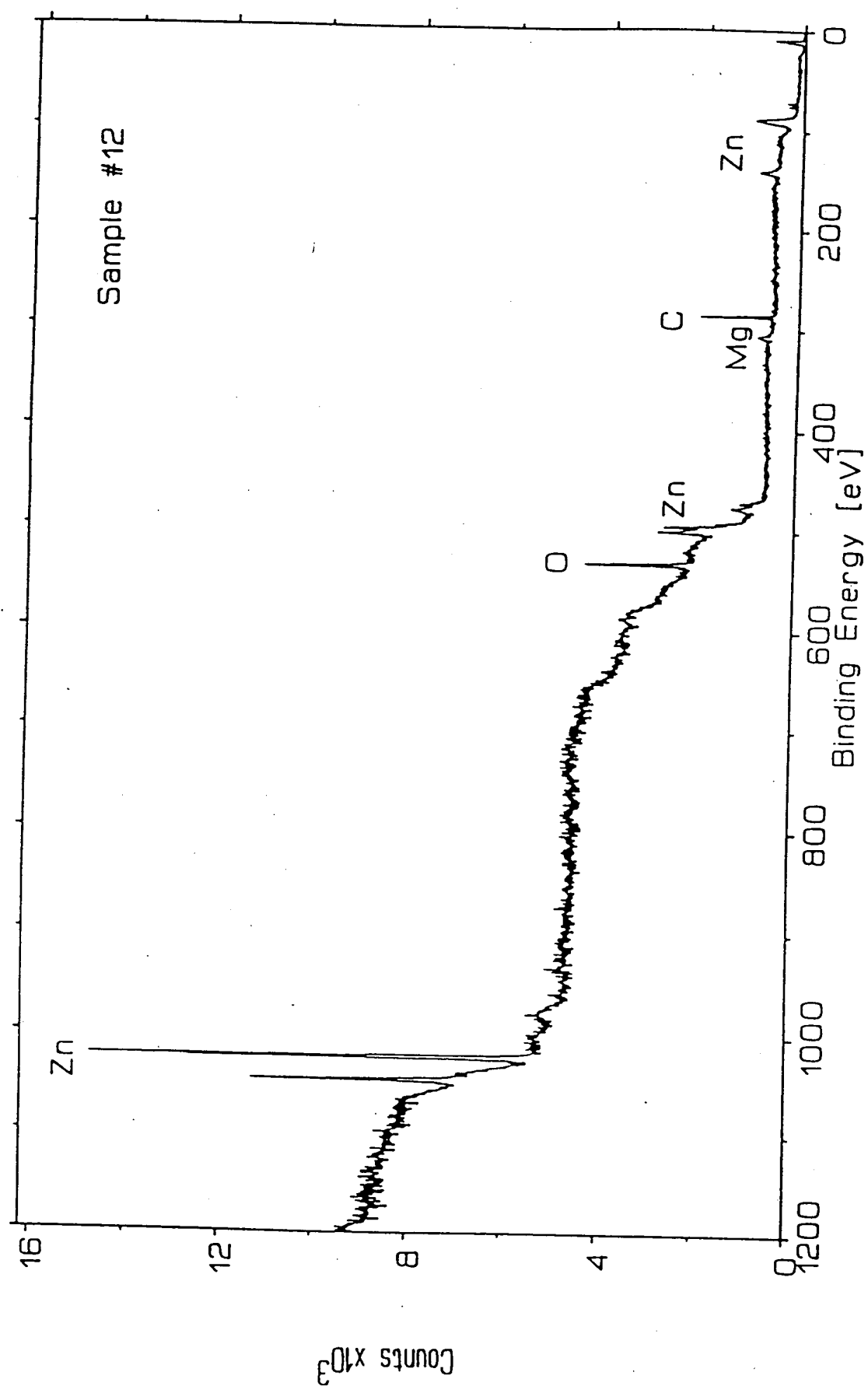


Figure 28

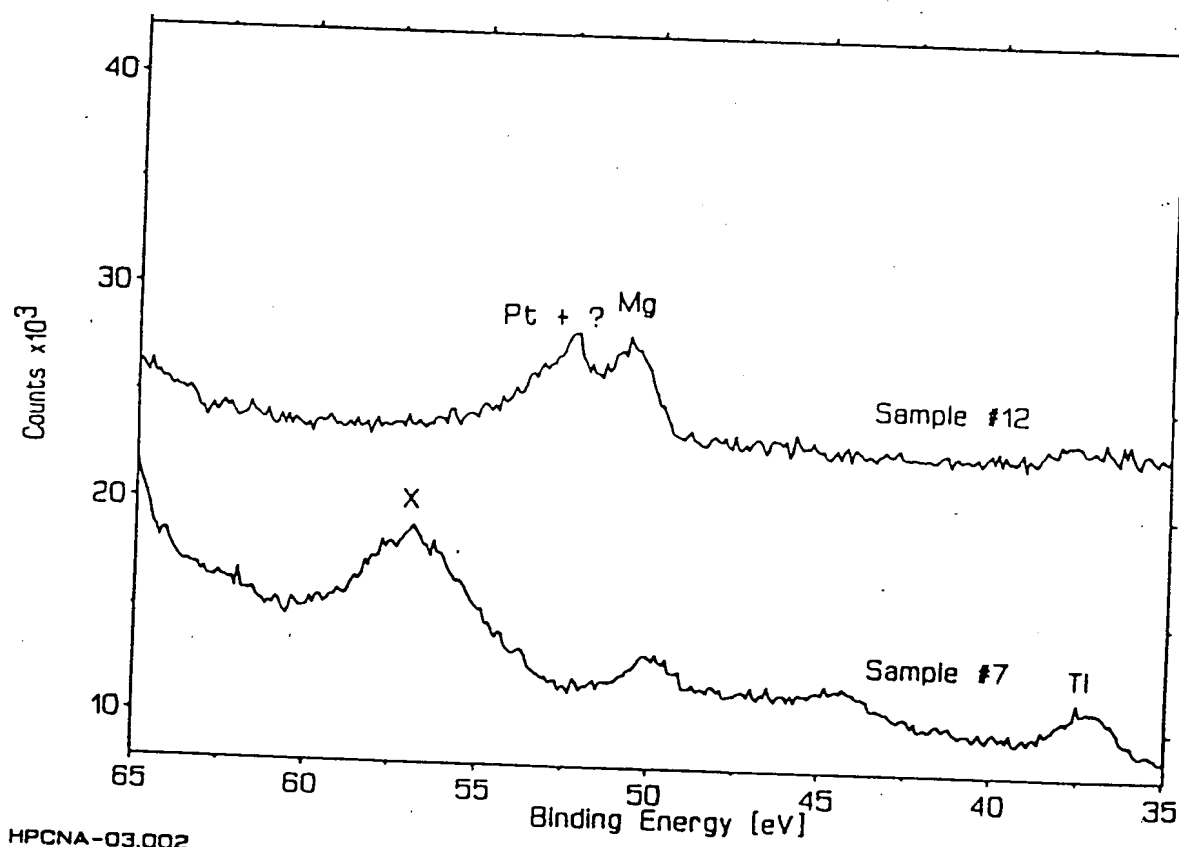
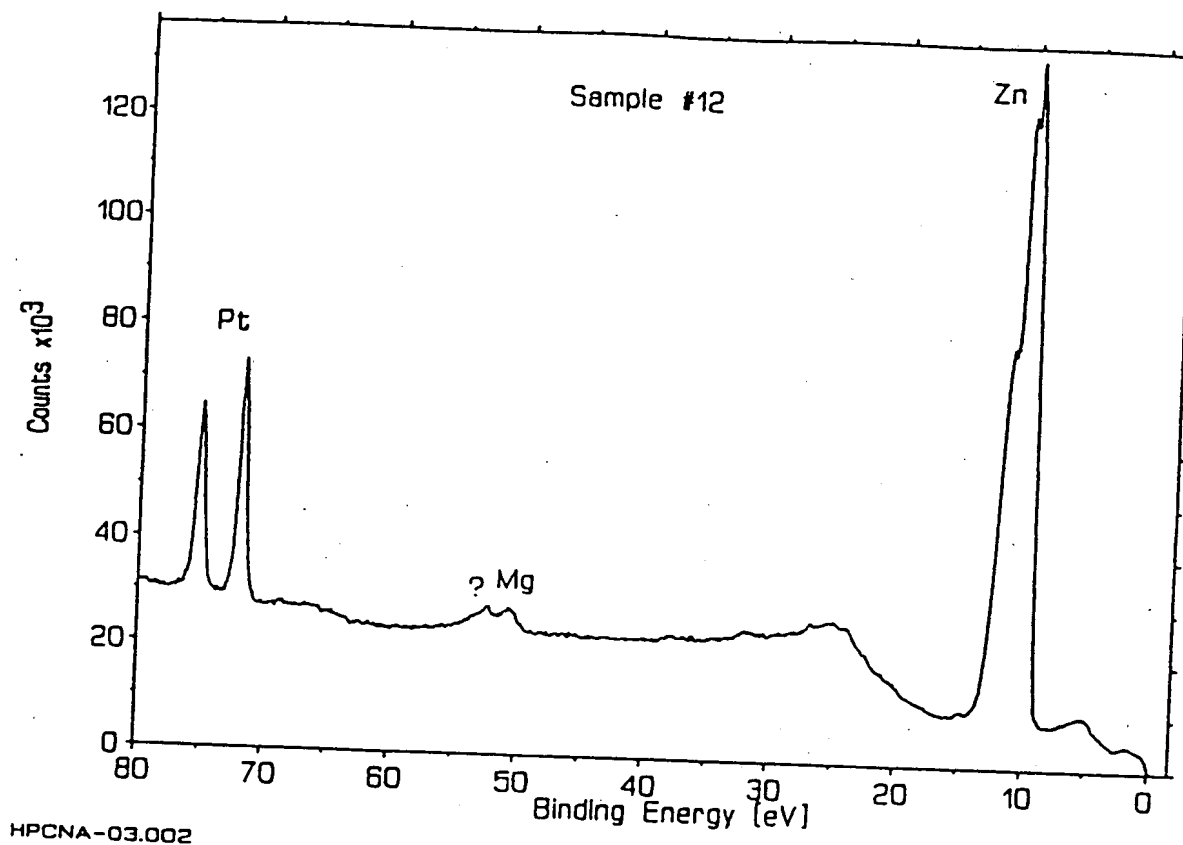


Figure 29

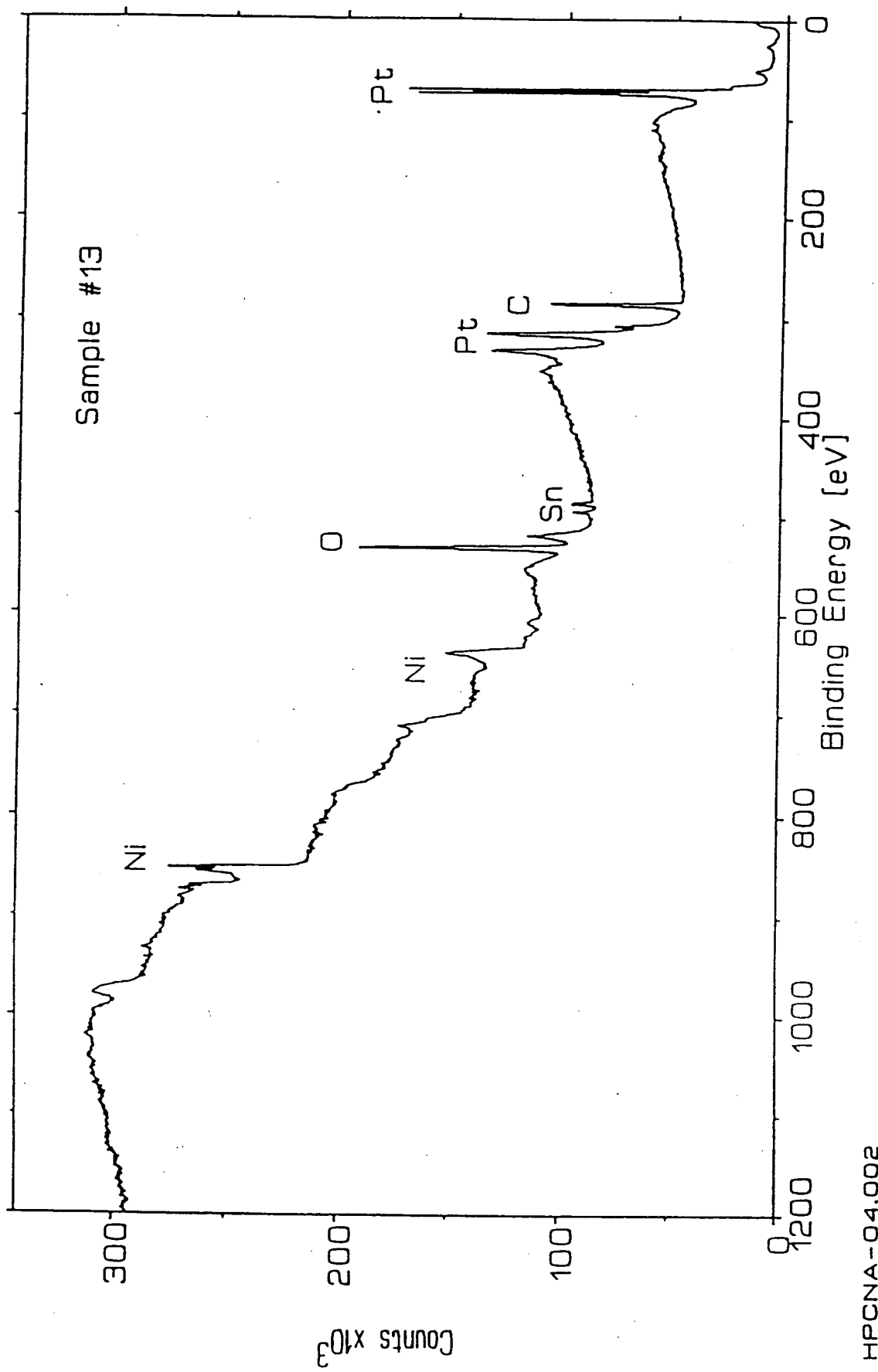


Figure 30

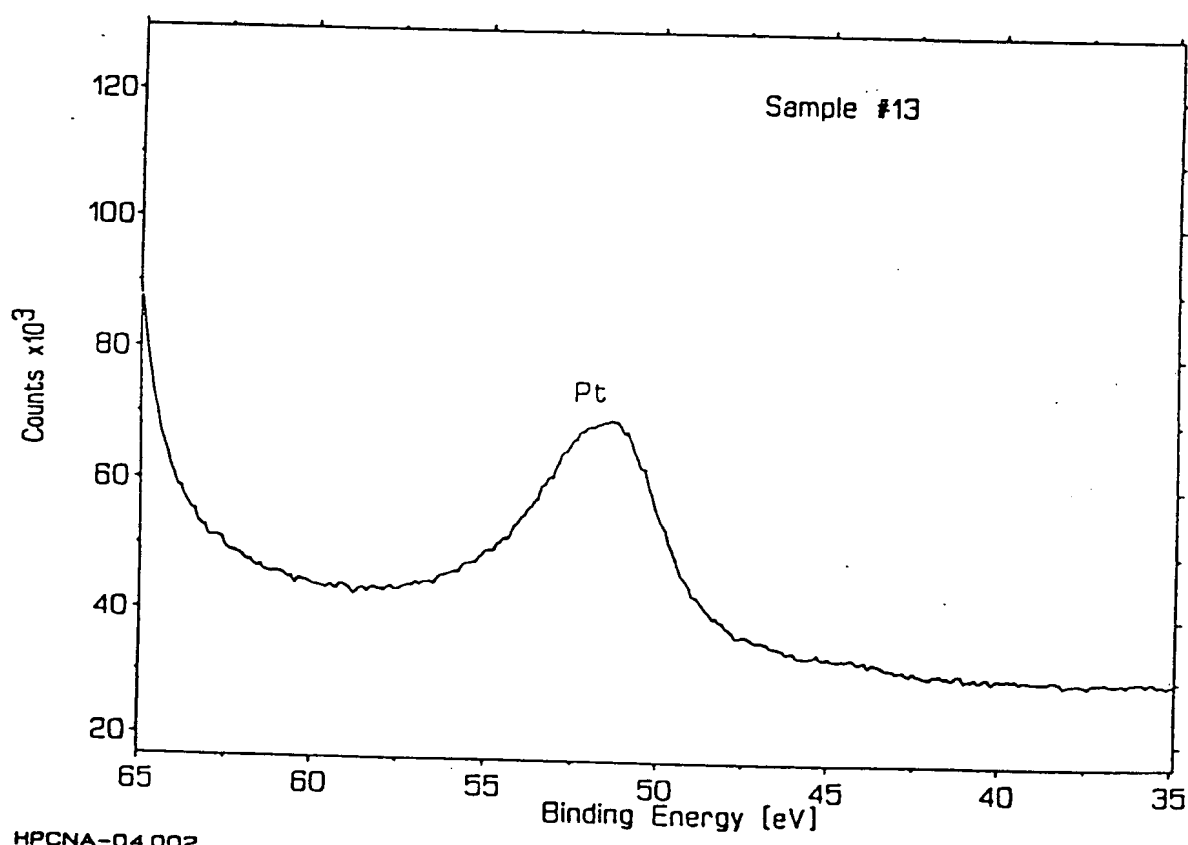
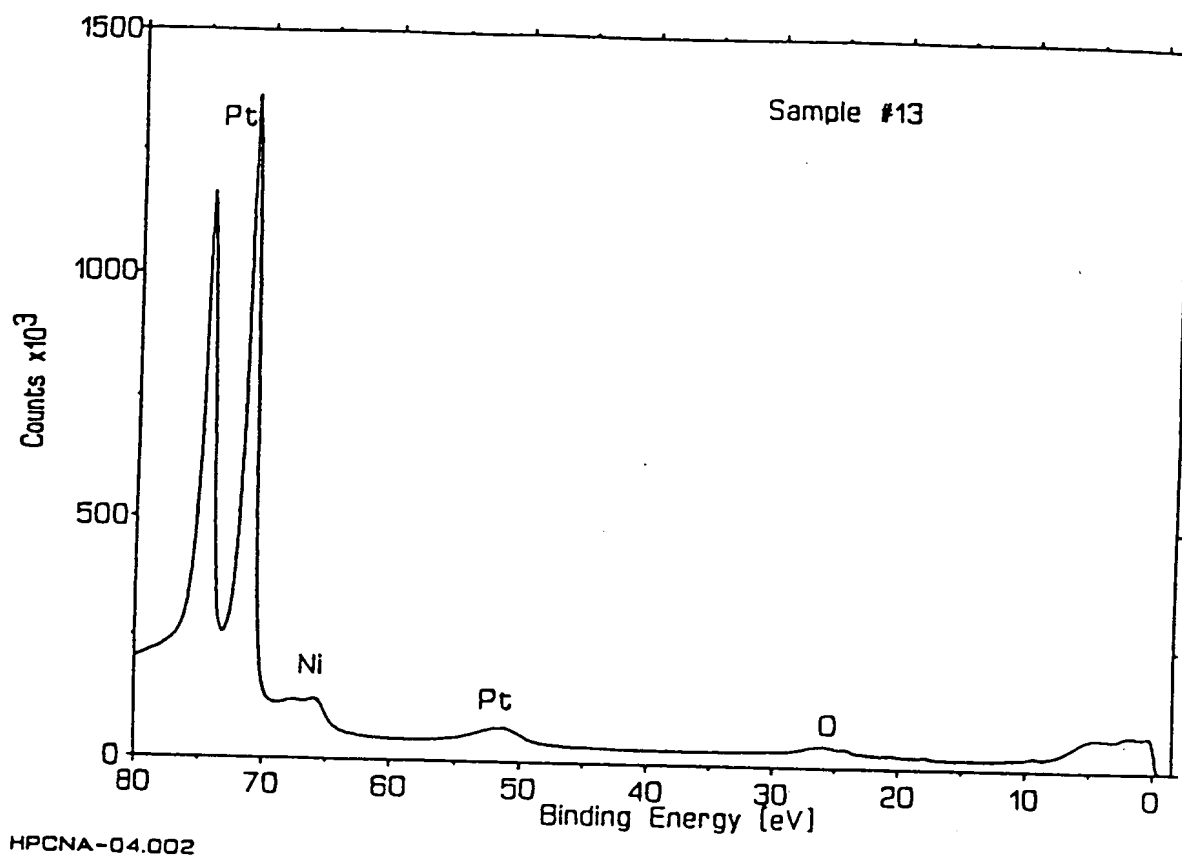
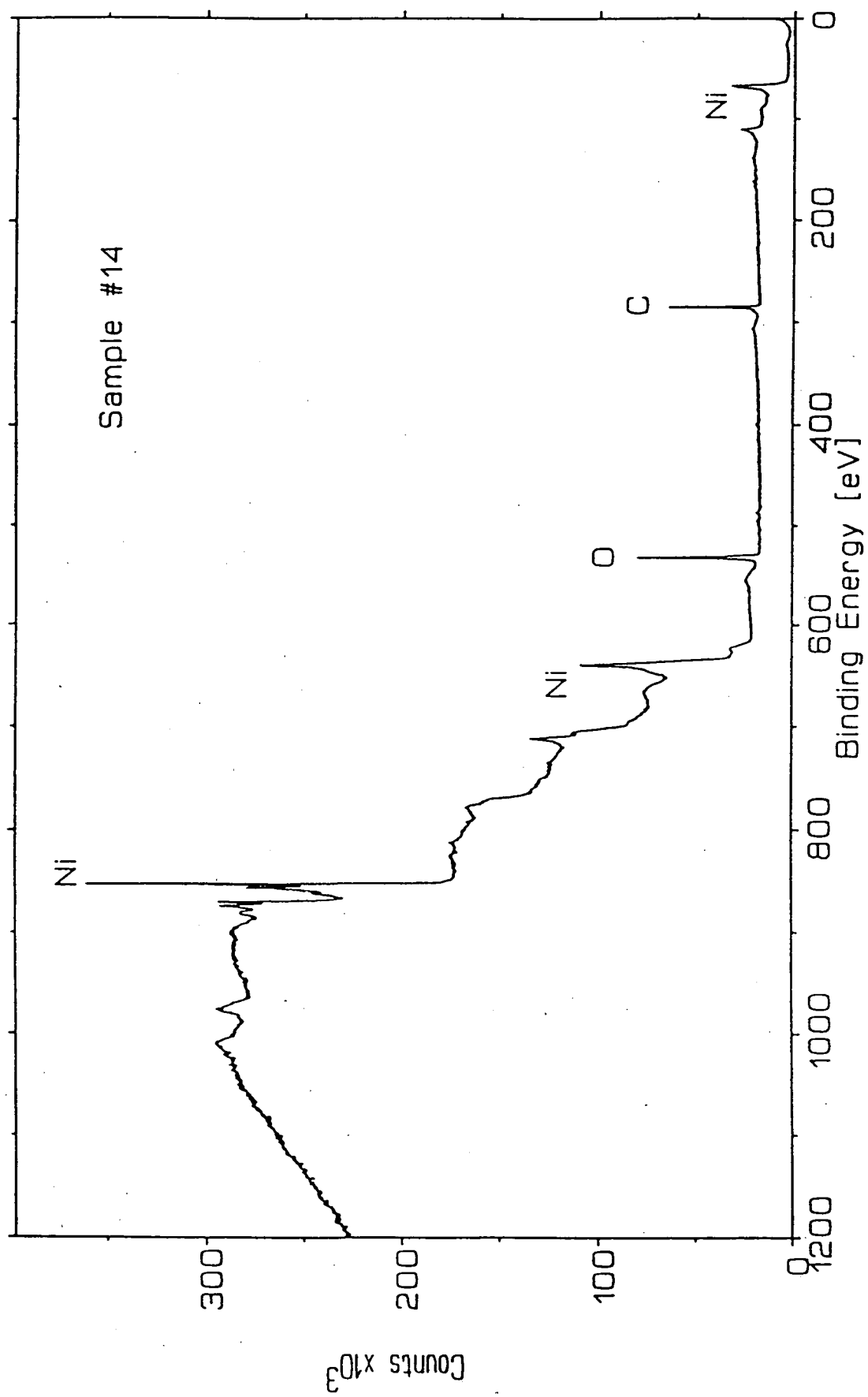


Figure 31



# Figure 32

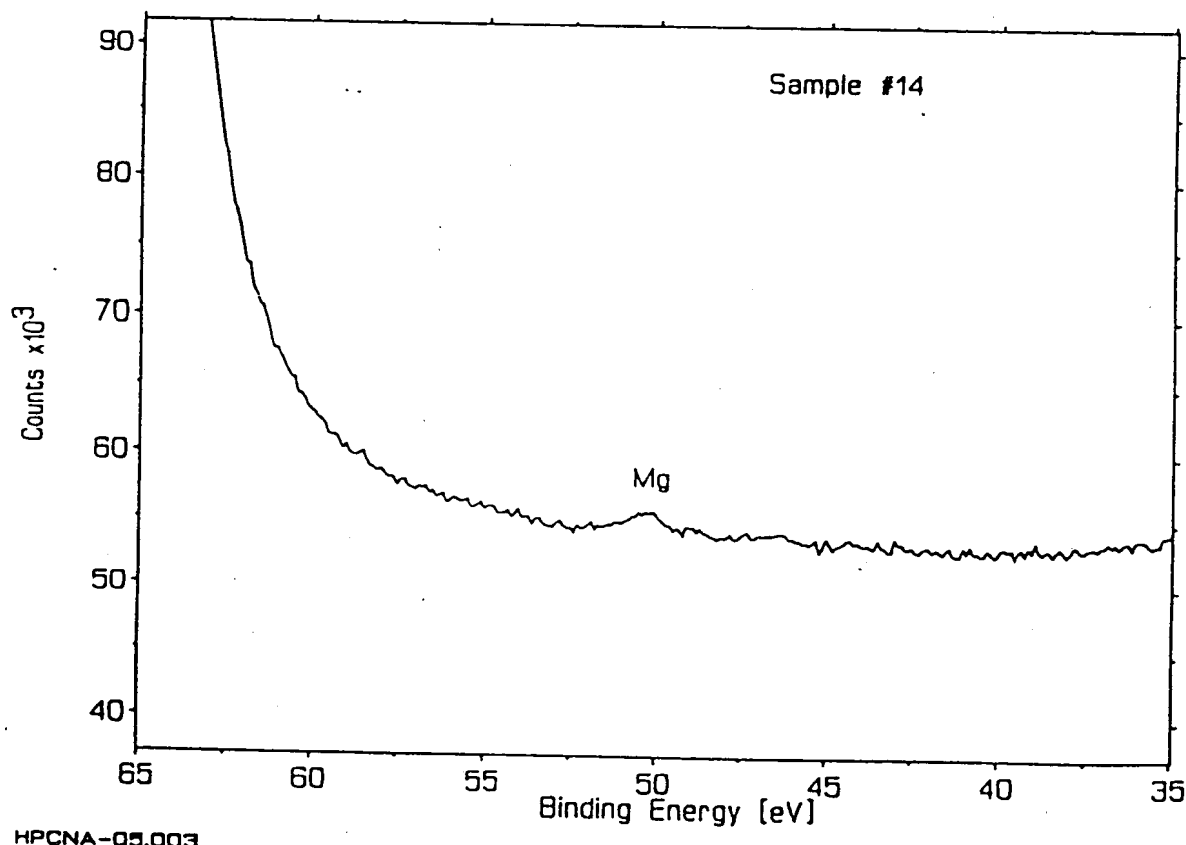
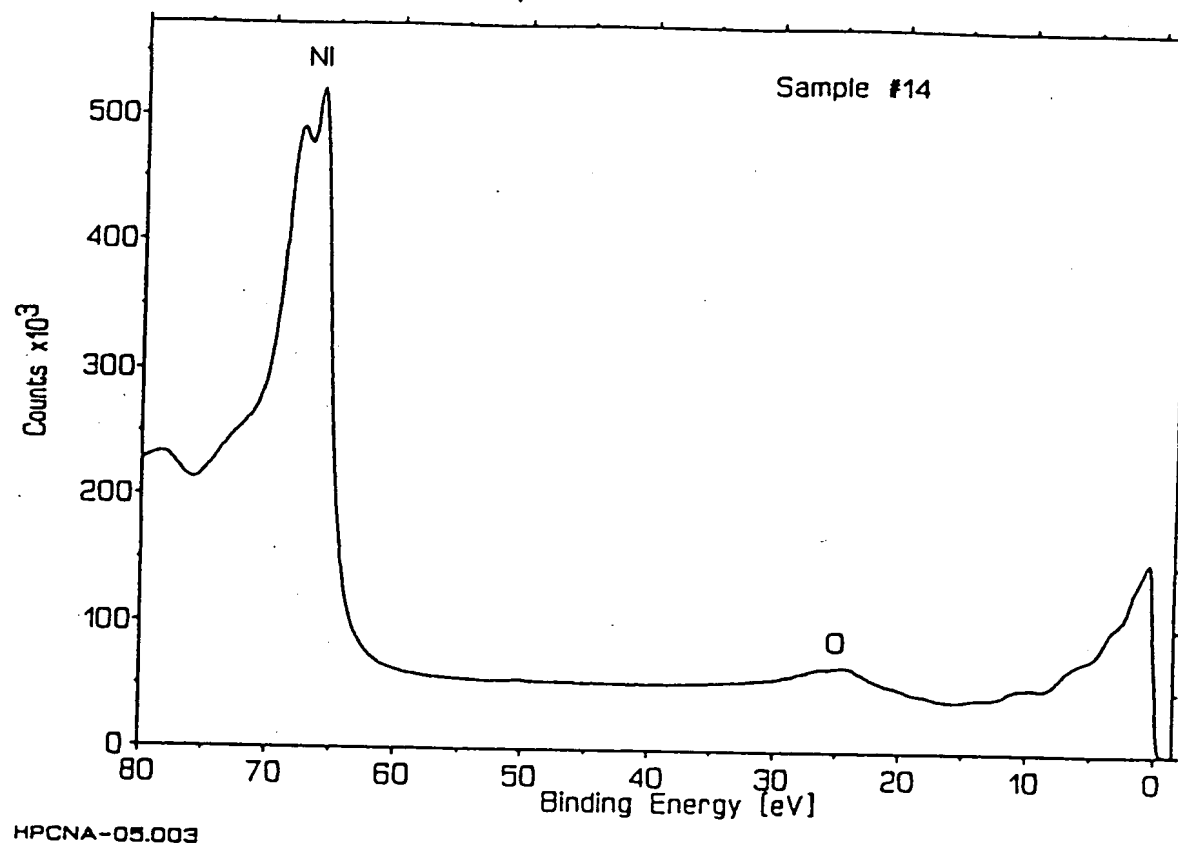


Figure 33

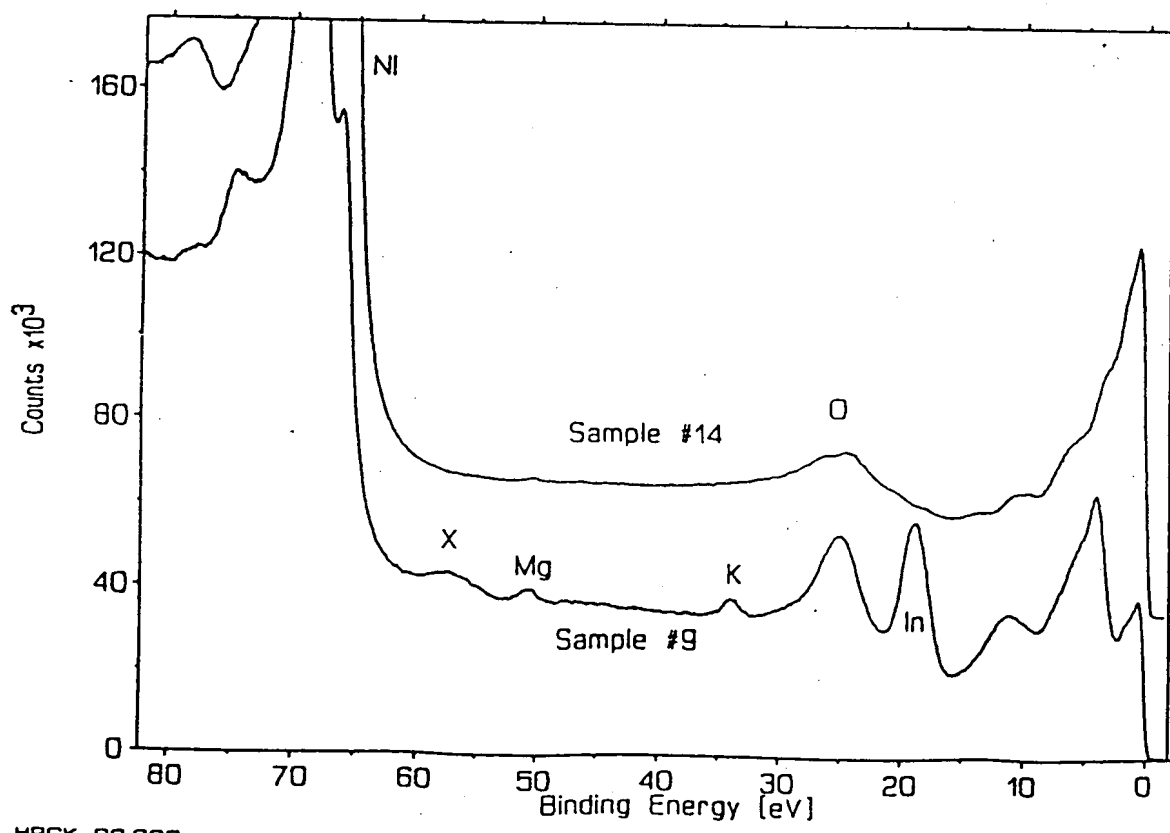
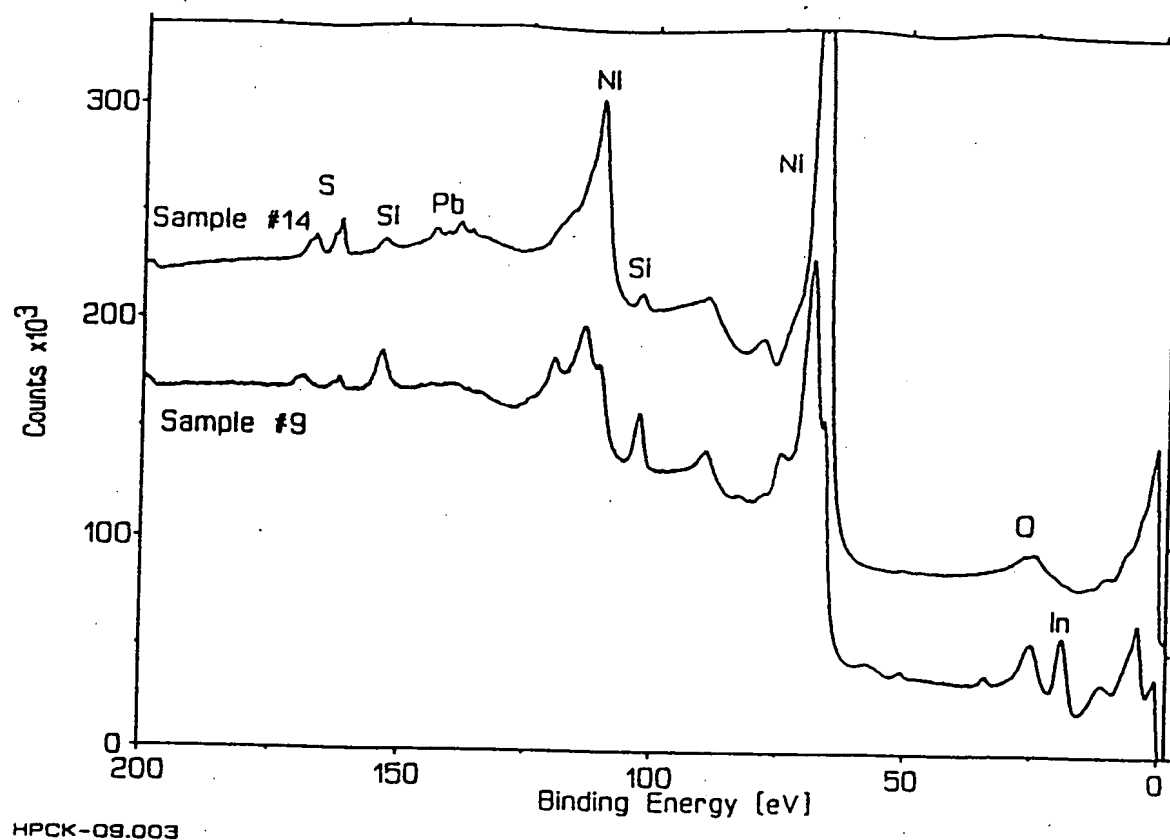


Figure 34

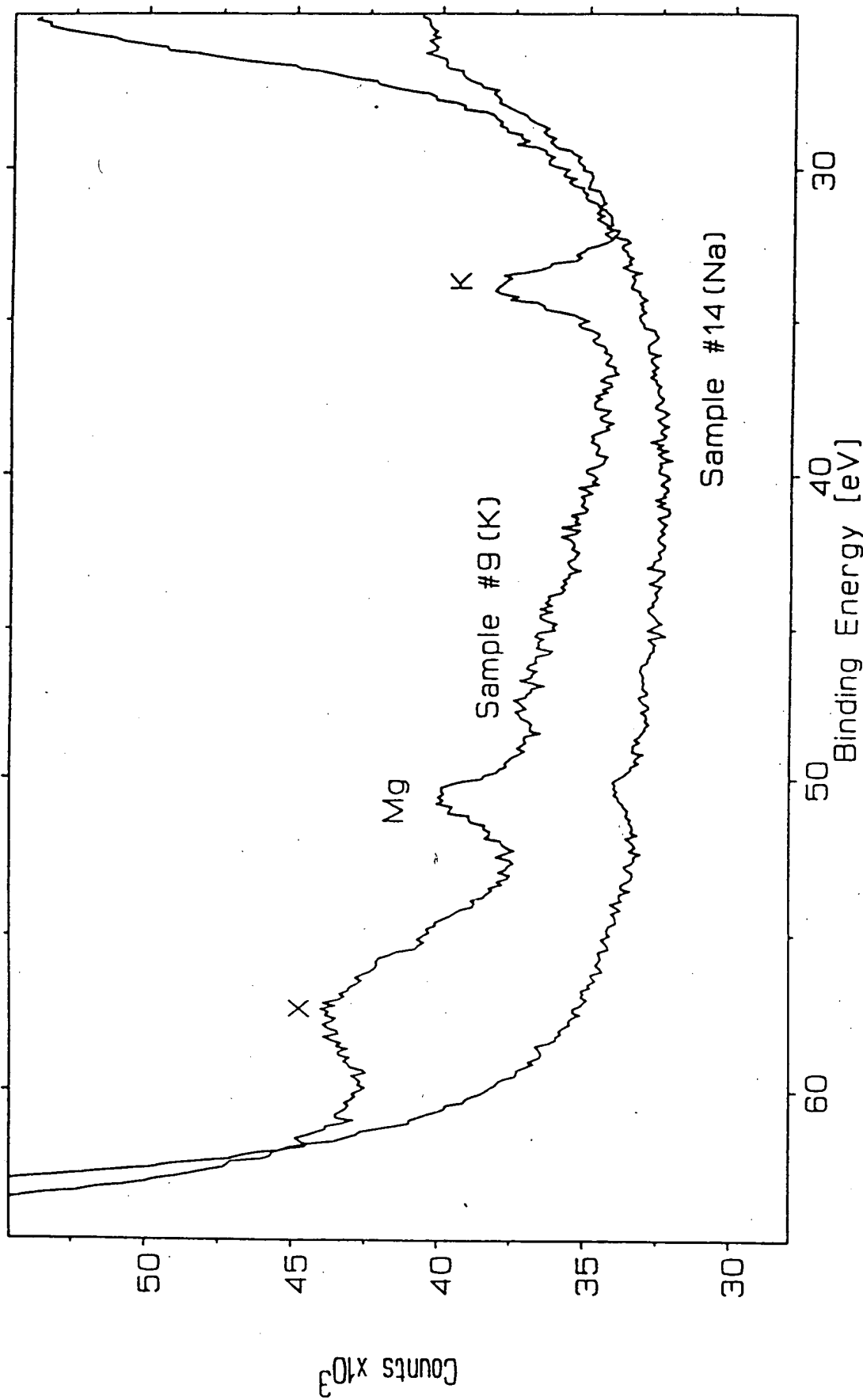
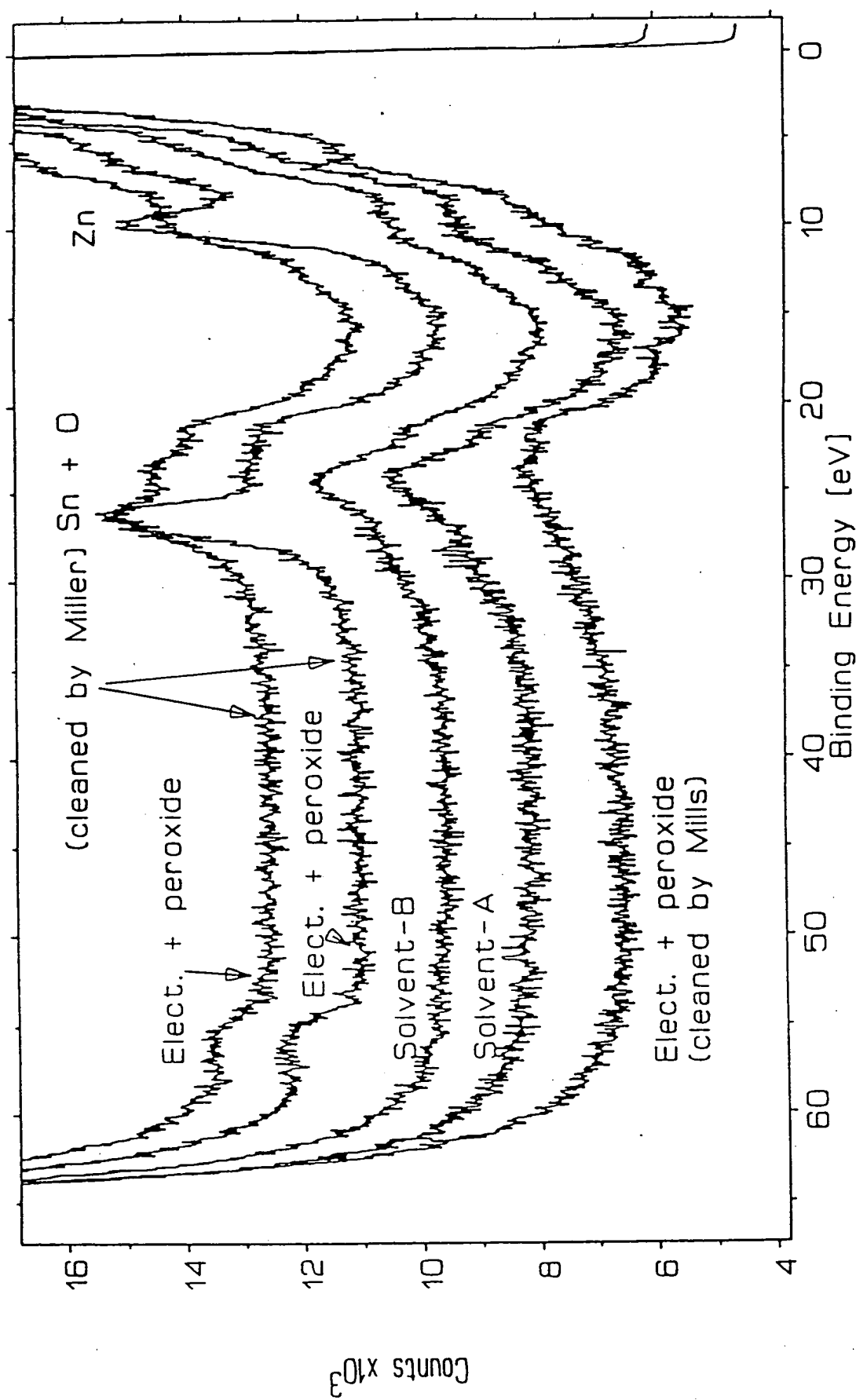


Figure 35



HPCREF.003

PATENT  
Attorney Docket No.: 9113-2-DI1

IN THE UNITED STATES PATENT AND TRADEMARK OFFICE

In re: Patent application of :  
Randell L. Mills : Group Art Unit:  
Serial No.: 08/467,911 : 2204  
Filed: June 6, 1995 : Examiner:  
For: ENERGY/MATTER CONVERSION : H.E. Behrend  
METHODS AND STRUCTURES :

EXHIBITS 20 THROUGH 31, VOLUME IV OF IV, SUPPORTING  
DECLARATION OF RANDELL L. MILLS, M.D.,  
UNDER 37 C.F.R. 1.32

CERTIFICATE OF MAILING  
UNDER 37 C.F.R. 1.8(a)

I hereby certify that this paper, along with any paper referred to as being attached or enclosed, is being deposited with the United States Postal Service on the date indicated below, with sufficient postage, as first class mail, in an envelope addressed to: Commissioner of Patents and Trademarks, Washington, D.C. 20231.

BY Randell L. Mills  
DATE: November 19, 1996

Testing Facility, Publication, or Reviewing Organization	Independent Test Facility	Report Date	Calorimetry Proof	Hydrino Proof	Dihidrino Proof	Mills Exhibit
HPC Recent Experimental Work	yes	Aug. '96	yes	--	--	1
HPC and Franklin and Marshall College Report for Atlantic Energy Corporation	yes*	Jul. '96	yes	yes	yes	2
Pennsylvania State University Report for HPC	yes	Jun. '96	yes	--	--	3
Pennsylvania State University Report for HPC	yes	Jan. '96	yes	--	--	4
NASA Lewis Research Center Technical Memorandum	yes	Feb. '96	yes	--	--	5
Mills et al., 28 Fusion Technology 1697	--	Nov. '95	yes	yes	yes	6
Jonathan Phillips 37 CFR 1.132 Declaration	yes	Jan. '95	yes	--	--	7
MIT Lincoln Laboratories Final Report (ACC Project)	yes	Apr. '95	yes	--	--	8
Mills et al., Analysis of MIT Lincoln Laboratories Data	--	Jan. '95	--	--	yes	9
Pennsylvania State University Report for HPC	yes	Sep. '94	yes	--	--	10
Thermacore's Final Report for Aero Propulsion and Power Directorate, Wright Laboratory, Air Force Material Command	yes	May '94	yes	yes	--	11
Westinghouse STC Report	yes	Feb. '94	yes	--	--	12
HPC Comments as to the Westinghouse STC Report	--	Feb. '94	yes	--	--	13
Thermacore Report, Hydrino Analysis by Lehigh University	yes	Mar. '94	yes	yes	--	14
Charles Evans & Associates XPS/ESCA Results	yes	Nov. '94	--	yes	--	15
Charles Evans & Associates TOF-SIMS Results	yes	Mar. '94	--	yes	--	16
Mills et al., 25 Fusion Technology 103	yes*	Jan. '94	yes	yes	yes	17
Idaho National Engineering Laboratory (INEL) XPS Report	yes	Nov. '93	--	yes	--	18

Testing Facility, Publication, or Reviewing Organization	Independent Test Facility	Report Date	Calorimetry Proof	Hydrino Proof	Dihidrino Proof	Mills Exhibit
Lehigh University XPS Report, Zettlemoyer Center for Surface Studies, Sinclair Laboratory	yes	Nov. '93	--	yes	--	19
Idaho National Engineering Laboratory (INEL) Excess Heat and XPS Report	yes	Jan. '93	yes	yes	--	20 18
Atomic Energy Of Canada Ltd., Chalk River Laboratories Study	yes	Nov. '93	yes	--	--	21
Moscow Power Engineering Institute, Appl. No. '845 Affidavit	yes	Feb. '93	yes	--	--	22
Testimony for Subcommittee on Energy of the Committee on Science, Space and Technology of U.S. Congress	--	May '93	yes	--	--	23
Shaubach and Gernert Affidavit Thermacore Testing Facility	yes	Aug. '92	yes	--	--	24
Noninski, 21 Fusion Technology 163, Franklin and Marshall College Laboratory	yes	Mar. '92	yes	--	--	25
Mills et al., 21 Fusion Technology 65	--	Aug. '91	yes	--	--	26
Brookheaven National Laboratory, Department of Applied Science Letter	yes	Oct. '91	yes	--	--	27
Discovery Documents from Arbitration No. 14 T 199 00196 H/J between HPC and AECL	--	Mar. '93	--	--	--	28
R.T.Bush, 22 Fusion Technology 301	--	Sep. '92	--	--	--	29
Jones et al., 99 J. Phys. Chem. 6973	--	Apr. '95	--	--	--	30
Notoya et al., Proc. of the Int'l Conf. on Cold Fusion, 421-426	--	Oct. '92	--	--	--	31
* - conducted by Thermacore and HPC						

PATENT  
Attorney Docket No.: 9113-2-DI1

IN THE UNITED STATES PATENT AND TRADEMARK OFFICE

In re: Patent application of :  
Randell L. Mills :  
Serial No.: 08/467,911 : Group Art Unit:  
Filed: June 6, 1995 : 2204  
For: ENERGY/MATTER CONVERSION : Examiner:  
METHODS AND STRUCTURES : H.E. Behrend

**EXHIBITS 20 THROUGH 31, VOLUME IV OF IV, SUPPORTING**  
**DECLARATION OF RANDELL L. MILLS, M.D.,**  
**UNDER 37 C.F.R. 1.32**

**CERTIFICATE OF MAILING**  
**UNDER 37 C.F.R. 1.8(a)**

I hereby certify that this paper, along with any paper referred to as being attached or enclosed, is being deposited with the United States Postal Service on the date indicated below, with sufficient postage, as first class mail, in an envelope addressed to: Commissioner of Patents and Trademarks, Washington, D.C. 20231.

BY Randell Mills  
DATE: 25 November 1996

## Experimental Verification by Idaho National Engineering Laboratory

### Methods

A search for excess heat during the electrolysis of aqueous potassium carbonate ( $K^+/K^+$  electrocatalytic couple) was investigated using cells supplied by HydroCatalysis Power Corporation and a cell fabricated by Idaho National Engineering Laboratory (INEL). To simplify the calibration of these cells, they were constructed to have primarily conductive and forced convective heat losses. Thus, a linear calibration curve was obtained. Differential calorimetry was used to determine the cell constant which was used to calculate the excess enthalpy. The cell constant was calculated during the experiment (on-the-fly-calibration) by turning an internal resistance heater off and on, and inferring the cell constant from the difference between the losses with and without the heater.

The general form of the energy balance equation for the cell in steady state is:

$$0 = P_{app1} + Q_{htr} + Q_{xs} - P_{gas} - Q_{loss} \quad (\text{III.1})$$

where  $P_{app1}$  is the electrolysis power;  $Q_{htr}$  is the power input to the heater;  $Q_{xs}$  is the excess heat power generated by the hydrogen "shrinkage" process;  $P_{gas}$  is the power removed as a result of evolution of  $H_2$  and  $O_2$  gases; and  $Q_{loss}$  is the thermal power loss from the cell. When an aqueous solution is electrolyzed to liberate hydrogen and oxygen gasses, the electrolysis power  $P_{app1}$  ( $=E_{app1}I$ ) can be partitioned into two terms:

$$P_{app1} = E_{app1}I = P_{cell} + P_{gas} \quad (\text{III.2})$$

An expression for  $P_{gas}$  ( $=E_{gas}I$ ) is readily obtained from the known enthalpy of formation of water from its elements:

$$E_{gas} = \frac{-\Delta H_{form}}{\alpha F} \quad (\text{III.3})$$

( $F$  is Faraday's constant), which yields  $E_{gas} = 1.48$  V for the reaction



The net faradaic efficiency of gas evolution is assumed to be unity; thus, Eq. (III.2) becomes

$$P_{cell} = (E_{app1} - 1.48V)I \quad (\text{III.5})$$

The cell was calibrated for heat losses by turning an internal resistance heater off and on while maintaining constant electrolysis and by inferring

the cell constant from the difference between the losses with and without the heater where heat losses were primarily conductive and forced convective losses. When the heater was off, the losses were given by

$$c(T_c - T_b) = P_{appl} + 0 + Q_{xs} - P_{gas} \quad (\text{III.6})$$

where  $c$  is the heat loss coefficient;  $T_b$  is ambient temperature and  $T_c$  is the cell temperature. When a new steady state is established with the heater on, the losses change to:

$$c(T_c' - T_b) = P'_{appl} + Q_{htr} + Q'_{xs} - P'_{gas} \quad (\text{III.7})$$

where a prime superscript indicates a changed value when the heater was on. When the following assumptions apply

$$Q_{xs} = Q'_{xs}; P_{appl} = P'_{appl}; P_{gas} = P'_{gas} \quad (\text{III.8})$$

the cell constant or heating coefficient  $a$ , the reciprocal of the heat loss coefficient( $c$ ), is given by the result

$$a = \frac{T_c' - T_c}{Q_{htr}} \quad (\text{III.9})$$

In all heater power calculations, the following equation was used

$$Q_{htr} = E_{htr} I_{htr} \quad (\text{III.10})$$

## LIGHT WATER CALORIMETRY EXPERIMENTS

### INEL EXPERIMENT I (DC Operation)

The present experiments were carried out by observing and comparing the temperature difference,  $\Delta T_1 = T(\text{electrolysis only}) - T(\text{blank})$  and  $\Delta T_2 = T(\text{electrolysis plus resistor heating}) - T(\text{blank})$  referred to unit input power.

The cell comprised a 10 gallon (33 in. x 15 in.) Nalgene tank (Model # 54100-0010). Two 4 inch long by 1/2 inch diameter terminal bolts were secured in the lid, and a cord for a heater was inserted through the lid.

The cathode comprised 1.) a 5 gallon polyethylene bucket which served as a perforated (mesh) support structure where 0.5 inch holes were drilled over all surfaces at 0.75 inch spacings of the hole centers and 2.) 5000 meters of 0.5 mm diameter clean, cold drawn nickel wire (NI 200 0.0197", HTN36NOAG1, Al Wire Tech, Inc.). The wire was wound uniformly around the outside of the mesh support as 150 sections of 33 meter length. The ends of each of the 150 sections were spun to form three cables of 50 sections per cable. The cables were pressed in a terminal connector which was bolted to the cathode terminal post. The connection was covered with epoxy to prevent corrosion.

The anode comprised an array of 15 platinized titanium anodes (15 - Engelhard Pt/Ti mesh 1.6" x 8" with one 3/4" by 7" stem attached to the 1.6" side plated with 100 U series 3000). A 3/4" wide tab was made at the end of the stem of each anode by bending it at a right angle to the anode. A 1/4" hole was drilled in the center of each tab. The tabs were bolted to a 12.25" diameter polyethylene disk (Rubbermaid Model #2666) equidistantly around the circumference. Thus, an array was fabricated having the 15 anodes suspended from the disk. The anodes were bolted with 1/4" polyethylene bolts. Sandwiched between each anode tab and the disk was a flattened nickel cylinder also bolted to the tab and the disk. The cylinder was made from a 7.5 cm by 9 cm long x 0.125 mm thick nickel foil. The cylinder traversed the disk and the other end of each was pressed about a 10 A /600 V copper wire. The connection was sealed with

Teflon tubing and epoxy. The wires were pressed into two terminal connectors and bolted to the anode terminal. The connection was covered with epoxy to prevent corrosion.

Before assembly, the anode array was cleaned in 3 M HCl for 5 minutes and rinsed with distilled water. The cathode was cleaned in 3% H<sub>2</sub>O<sub>2</sub>/ 0.57 M K<sub>2</sub>CO<sub>3</sub> and rinsed with distilled water. The anode was placed in the cathode support and the electrode assembly was placed in the tank containing electrolyte. The power supply was connected to the terminals with large cables.

The electrolyte solution comprised 28 liters of 0.57 M K<sub>2</sub>CO<sub>3</sub> (Alfa K<sub>2</sub>CO<sub>3</sub> 99%) in the case of the MC 3 cell or 28 liters of 0.57 M Na<sub>2</sub>CO<sub>3</sub> (Alfa Na<sub>2</sub>CO<sub>3</sub> 99%) in the case of the MC 2 cell.

The heater comprised a 57 ohm 1500 watt Incoloy coated cartridge heater which was suspended from the polyethylene disk of the anode array. It was powered by a regulated power supply. The voltage was measured with a digital meter, and the current was measured as a voltage across a precision resistor with a digital meter.

The stirrer comprised a 1 cm diameter by 43 cm long glass rod to which an 8 cm by 2.5 cm Teflon half moon paddle was fastened at one end. The rod passed through a bearing hole in the tank lid and through a bearing hole in the center of the anode array disk. The other end of the stirrer rod was connected to a variable speed stirring motor. The stirrer shaft was rotated at 4 Hz. With the stirrer connected, the stirrer motor drew 4.7 W. With the stirrer disconnected, the stirrer drew 4.4 W; thus, 0.3 W was the stirrer power.

Electrolysis was performed at 39.5 amps constant current with a constant current power supply. The cells were operated in the environmental chamber in the INEL Battery test Laboratory. The chamber maintained the average temperature of the cell surroundings within 1 °C. The bottom of the cell rested on a 1/2 inch thick sheet of Styrofoam.

The temperature was recorded with a series of Teflon-coated Type E thermocouples inserted in several places. The ambient temperature reference was a closed one-liter container of water

with a thermocouple nominally in the center of the water volume.

Data from thermocouples, voltages, and currents were logged by one of the Battery Lab's computer based data systems and recorded at 5 minute intervals. The delta temperature ( $\Delta T = T(\text{electrolysis only}) - T(\text{blank})$ ) and electrolysis power were plotted. The heating coefficient was determined "on the fly" by the addition of heater power. The delta temperature  $\Delta T_2 = T(\text{electrolysis + heater}) - T(\text{blank})$ ) and the electrolysis power and heater power were plotted.

Mass spectroscopy of the gasses evolving from the MC 3 ( $K_2CO_3$ ) cell was performed using a VG Instruments model SXP-50 high-precision mass spectrometer with 0.01-amu mass resolution and 6 decade sensitivity.

A 100 ml sample of the 0.57 M  $K_2CO_3$  electrolyte of the MC 3 ( $K_2CO_3$ ) cell was removed after 20 days of cell operation, and a chemical analysis was performed on the electrolyte using an Inductively Coupled Plasma-Atomic Emission Spectrometer.

## RESULTS

### Light Water Calorimetry

The results of the electrolysis for INEL cell runs MC 2 and MC 3 at 39.5 A constant current appear in Figure 1 (hand plot of data by INEL scientists). As shown in Figure 1, the MC 3 ( $K_2CO_3$ ) cell intercepts the Total Input Power axis at 35 W; whereas, the MC 2 ( $Na_2CO_3$ ) cell intercepts the Total Input Power axis at 59 W. The input power to electrolysis gases given by Eqs. (III.2-III.5) is  $(39.5)(1.48) = 58.5$  W. The production of excess enthalpy of 25 W is observed with the MC 3 ( $K_2CO_3$ ) cell, and energy balance is observed with the MC 2 ( $Na_2CO_3$ ) cell.

Mass spectroscopic analysis of the gasses evolved by the MC 3 ( $K_2CO_3$ ) cell showed that a significant fraction of the sample was air with standard constituents. When the spectrum associated with air was removed, the residue showed a majority of diatomic hydrogen and oxygen gases in approximately the 2:1 proportion expected from the electrolysis and residual water vapor. There were no hydrocarbons, no metallic constituents or other anomalies except that a slightly higher than expected hydrogen to oxygen ratio was observed. No

tritium or deuterium measurements above normal background were observed.

Chemical analysis of an electrolyte sample from the MC 3 ( $K_2CO_3$ ) cell after 20 days of operation found the following components at levels above the background levels in the water used to fill and replenish the cell: 1.7 ppm silicon, 1.1 ppm sulfur, and 46.5 ppm sodium in addition to the  $K_2CO_3$  salt. Small quantities of silicon are known impurities in the nickel wire and may have also come from the glassware used in various processes. Sulfur is a common impurity in the salt, and it may have come from the resin beds used for water deionization. Sodium is a probable salt impurity, and it may also have come from hand contact with the system. The potassium was measured at 43,000  $\mu g/ml$  corresponding to a salt molarity of 0.55 M (within measurement error of the initial 0.57 molarity determined by weighing the salt and measuring the water for the initial charge). The electrolyte retained its molarity. The cell potential characteristics were essentially unchanged over the duration of operation. There were no nickel or other metallic compounds present in the electrolyte. A visual inspection of the cell showed that all of the structural components were intact. The cell comprised about 155 moles of nickel in the cathode, about 6.5 moles of titanium in the anodes, and about 13.7 moles of  $K_2CO_3$ . The only material consumed in the cell was nano-pure deionized water.

### INEL EXPERIMENT II (Pulsed Power Operation)

The MC 3 ( $K_2CO_3$ ) cell was wrapped in a one-inch layer of urethane foam insulation about the cylindrical surface. The top was not insulated. The bottom of the cell rested on a 1/2 inch thick sheet of Styrofoam.

The cell was operated in a pulsed power mode. A current of 10 amperes was passed through the cell for 0.2 seconds followed by 0.8 seconds of zero current for the current cycle. The cell voltage was about 2.4 volts, for an average input power of 4.8 W. The electrolysis power average (Eq. (III.5)) was 1.84 W, and the stirrer power was measured to be 0.3 W. Thus, the total average net input power was 2.14 W. The cell was operated at various resistance heater settings, and the temperature

difference between the cell and the ambient as well as the heater power were measured.

## RESULTS

### Light Water Calorimetry

The results of the excess power as a function of cell temperature with the MC 3 cell operating in the pulsed power mode at 1 Hz with a cell voltage of 2.4 volts, a peak current of 10 amperes, and a duty cycle of 20 % appears in Figure 2.

Figure 2 shows that the excess power is temperature dependent for pulsed power operation, and the maximum excess power shown in Figure 2 is 18 W for an input electrolysis joule heating power of 2.14 W. Thus, the ratio of excess power to input electrolysis joule heating power is 850 %.

### INEL EXPERIMENT III (Forced Convection Calorimetry Of INEL Cell)

INEL scientists constructed an electrolytic cell comprising a nickel cathode, a platinized titanium anode, and a 0.57 M K<sub>2</sub>CO<sub>3</sub> electrolyte. The cell design appears in Appendix 1. The cell was operated in the environmental chamber in the INEL Battery test Laboratory at constant current, and the heat was removed by forced air convection in two cases. In the first case, the air was circulated by the environmental chamber circulatory system alone. In the second case, an additional forced air fan was directed onto the cell.

The cell was equipped with a water condensor, and the water addition to the cell due to electrolysis losses was measured.

## RESULTS

### Light Water Calorimetry

The data of the forced convection heat loss calorimetry experiments during the electrolysis of a 0.57 M K<sub>2</sub>CO<sub>3</sub> electrolyte with the cell appears in Table 1 and Figure 3. The comparison of the calculated and measure water balance of the INEL cell appears in Table 2 and Figure 4.

The intercept of the Net Input Power (calculated using Eq. (III.5)) axis of Figure 3 for both cases of forced convection is 13 W. Thus, 13 W of excess power was produced by the INEL cell. This excess power can not be attributed to recombination of the hydrogen and oxygen as indicated by the

equivalence of the calculated and measured water balance as shown in Figure 4.

Figure 1.

THERMAL CONDUCTANCE CALIBRATION (11/25)

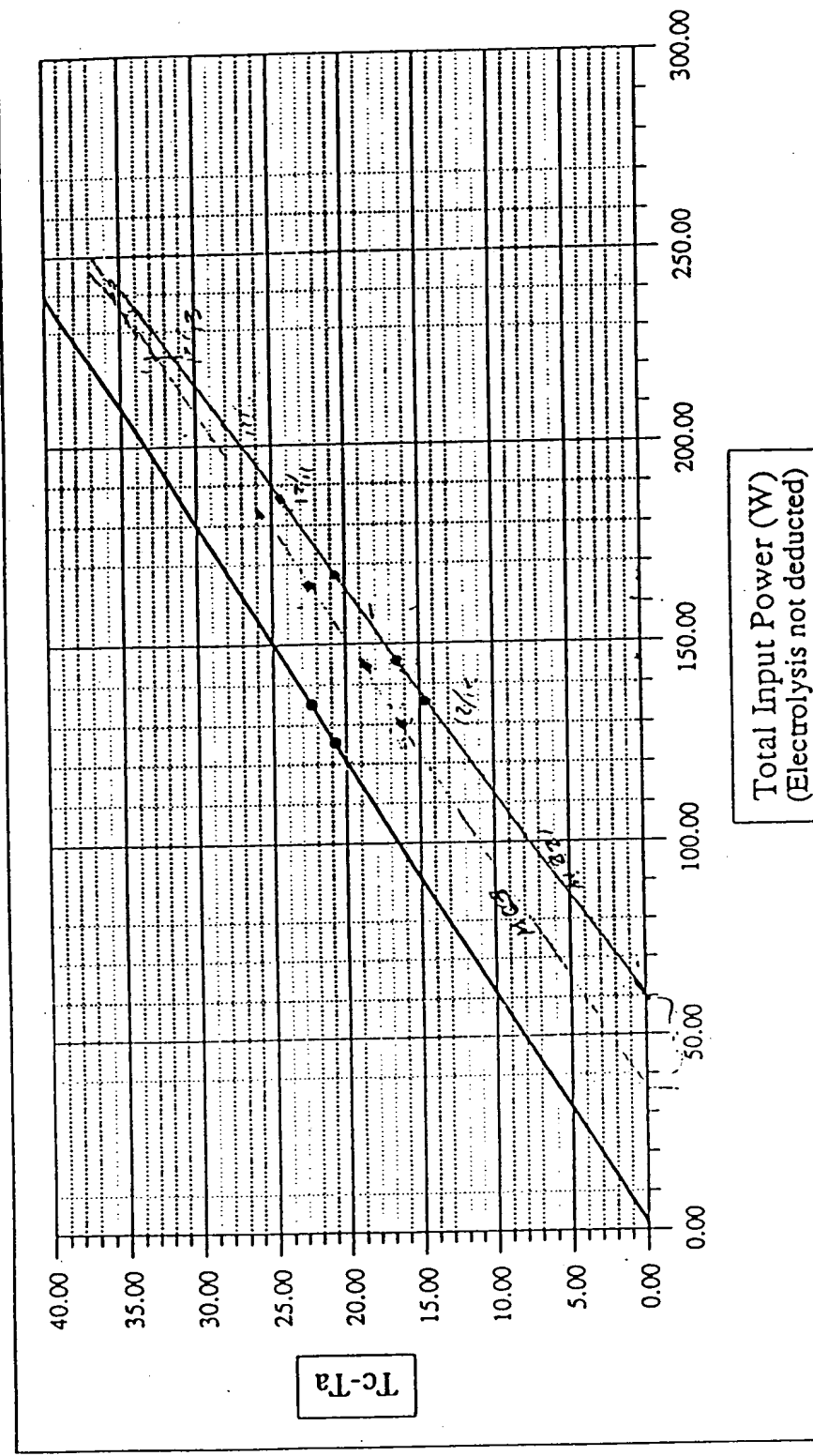


Figure 2.

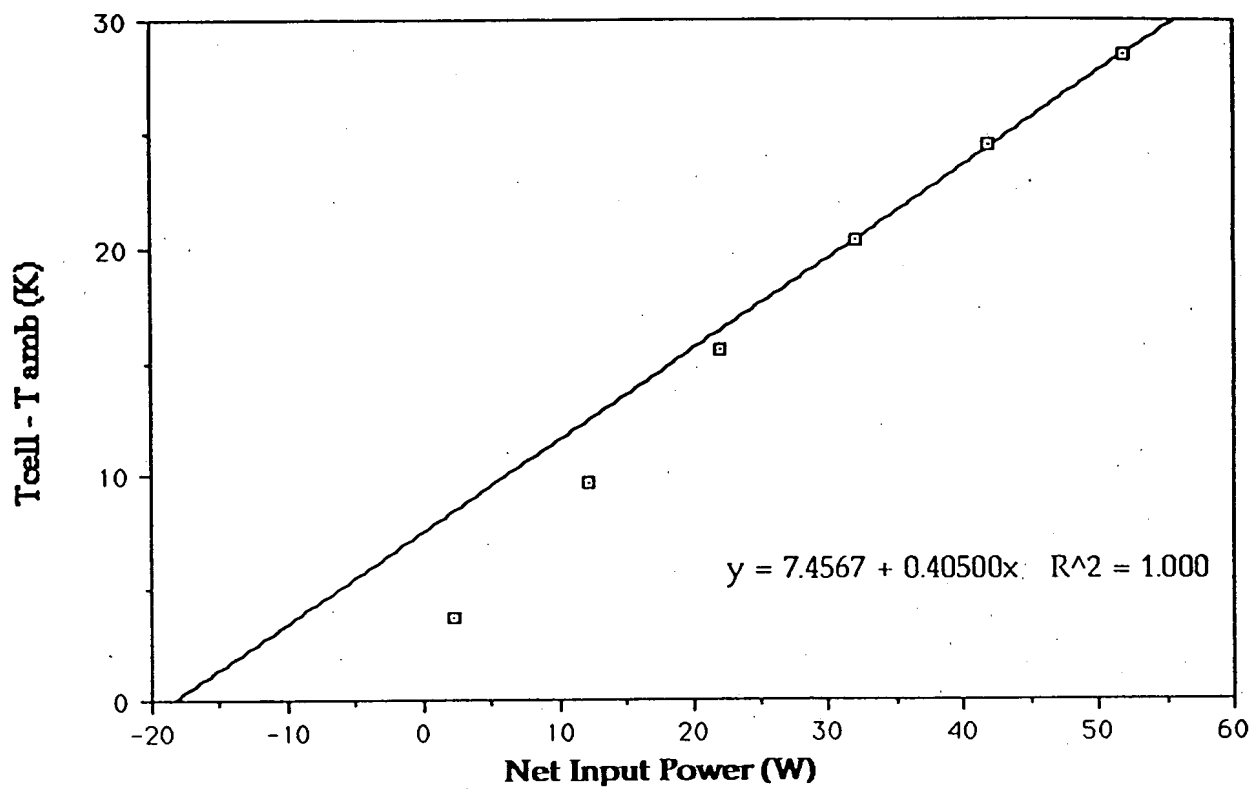
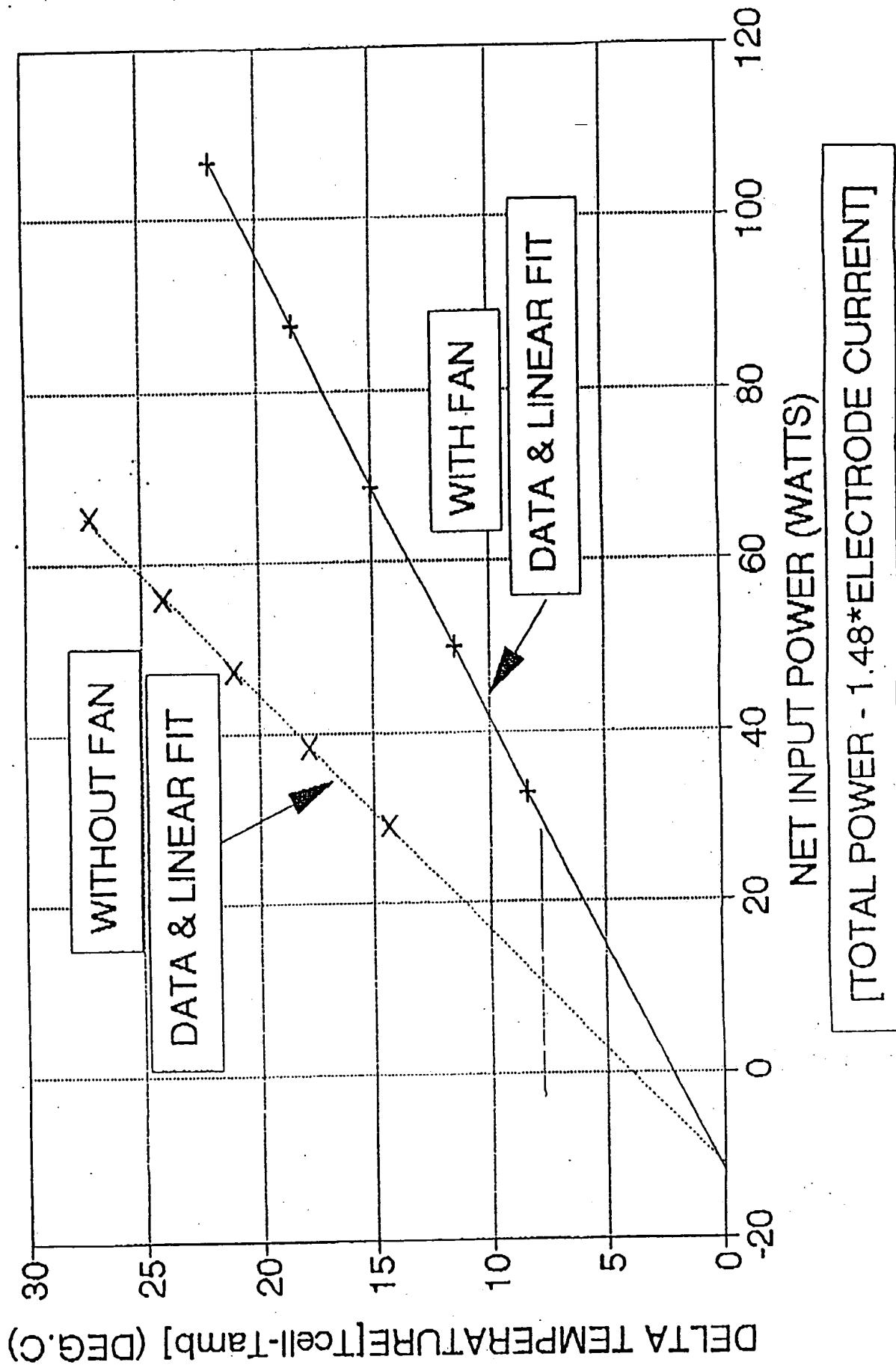


Figure 3.

IC1

T99 THRU T103 & T105 THRU T109



# IC1 WATER ADDITION

1/9/93 THRU 1/29/93

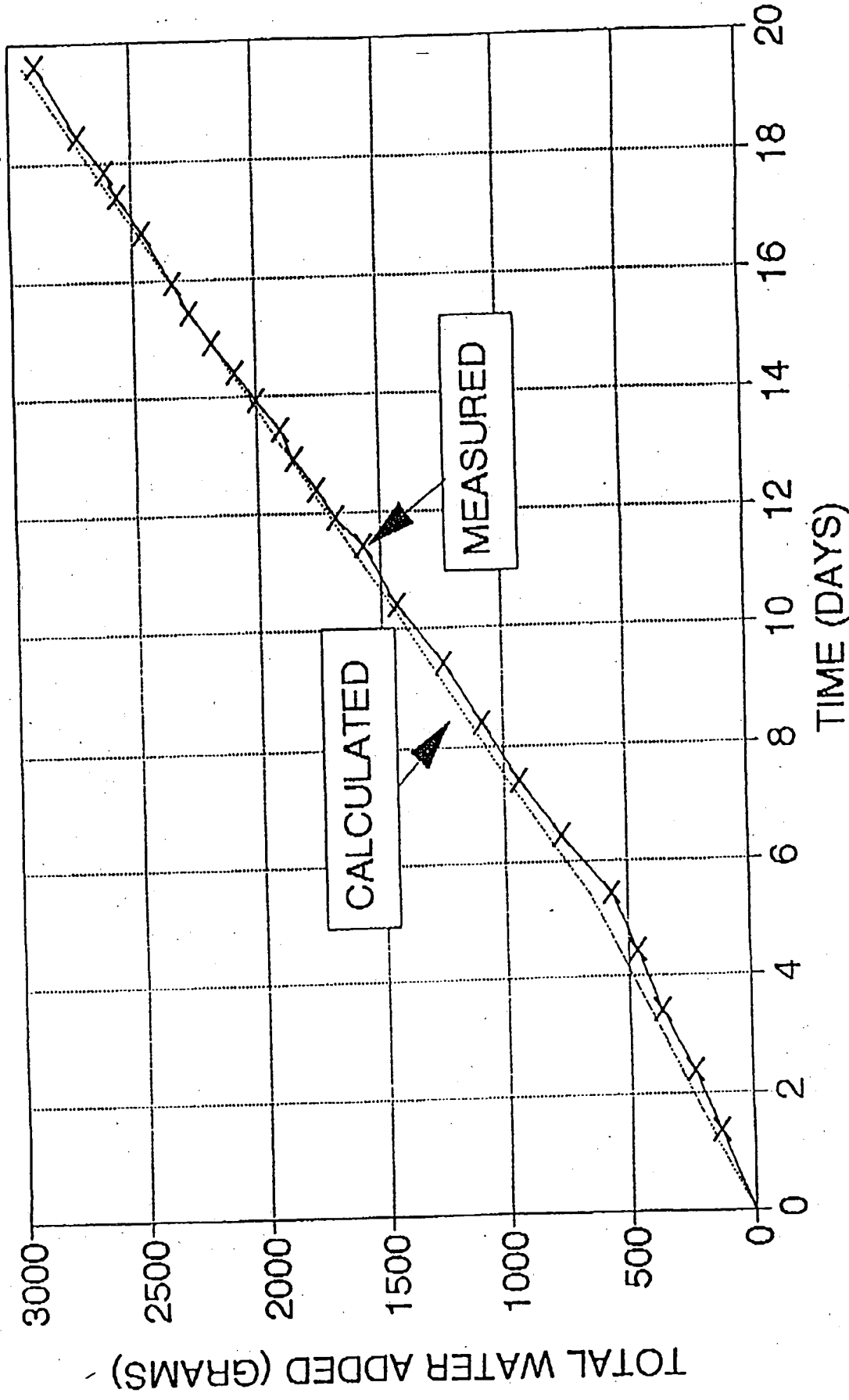


Table 1.

## FILE IC1

TEST NO.	TOTAL POWER	DELTA TEMP	LF DT	DELTA TEMP	LF DT	PWR·A*1.48
T99	94.8	27.2	27.36265			65.2962
T100	85.2	24.05	23.93155			55.6962
T101	76.8	21.05	20.92933			47.2962
T102	67.8	17.75	17.71267			38.2962
T103	58.57	14.3	14.4138			29.0662
	18.24		-0.00042			-11.2638
T105	136.07			21.95	21.94573	106.5662
T106	117.05			18.42	18.42674	87.5462
T107	98.25			14.95	14.94844	68.7462
T108	79.45			11.47	11.47015	49.9462
T109	62.58			8.35	8.348937	33.0762
	17.45			-0.00082		-12.0538

Table 2.

ICI WATER ADDITION; FILE ICIWATER

DATE	TIME			QPRO	QPRO	DATE+TIME	ELECTRO	WATER	WATER	WATER	TOTAL	ADDED/CALC
	DATE	HOURS	MINUTES	SECONDS	TIME	DAYs	AMPS	GRAMs	TOTAL	CALO	CALO	
01/09/93	81	30	0	0.005633	33978.9	-0.00416667	16	0	0	0	0	0
01/11/93	7	15	0	0.302063	33980.3	1.402083333	15	131	131	169.9935	169.9935	0.77061781
01/12/93	7	10	0	0.298611	33981.3	2.398611111	16	108	238	120.4645	290.468	0.82283844
01/13/93	7	20	0	0.311606	33982.31	3.411805556	14.94	131	370	121.9693	412.4473	0.89705426
01/14/93	7	66	0	0.330556	33983.33	4.430568866	14.94	89	468	122.8582	535.1066	0.85777747
01/15/93	7	60	0	0.326389	33984.33	5.426366869	14.93	102	581	118.8186	654.9243	0.8566875
01/16/93	8	28	0	0.351349	33985.35	6.461388889	18.83	205	788	184.6302	819.5648	0.93465404
01/17/93	6	19	0	0.346528	33986.36	7.446527778	19.93	168	934	169.8341	979.3887	0.9536861
01/18/93	7	42	0	0.320833	33987.32	8.420833333	19.94	160	1084	158.6065	1135.055	0.98426301
01/19/93	7	32	0	0.313888	33988.31	9.413888889	19.93	164	1836	159.4995	1293.468	0.96864903
01/20/93	7	25	0	0.309028	33989.31	10.40902778	19.84	194	1492	159.9143	1456.369	0.98394292
01/21/93	7	42	0	0.320833	33990.32	11.420833333	19.93	133	1686	182.511	1617.86	0.96731620
01/21/93	10	28	0	0.811111	33990.81	11.911111111	19.93	110.5	1875.9	78.7469	1696.626	0.98754029
01/22/93	7	32	0	0.313888	33991.31	12.413888889	19.93	83	1708.6	80.76359	1777.378	0.98837791
01/22/93	10	37	0	0.817361	33991.82	12.817361111	19.93	92	1850.6	80.86513	1850.249	0.99583923
01/23/93	7	32	0	0.313888	33992.31	13.413888889	19.94	48	1888.5	79.78976	1938.034	0.97856862
01/23/93	10	19	0	0.804681	33992.6	13.904681111	18.93	102	1998.8	78.85744	2018.882	0.99088111
01/24/93	7	28	0	0.311111	33993.31	14.411111111	19.93	84	2082.5	81.31128	2098.203	0.99281593
01/24/93	10	20	0	0.805556	33993.81	14.905555566	19.93	83	2175.8	79.41613	2177.818	0.99902727
01/26/93	7	38	0	0.318055	33994.32	15.418065566	19.93	94	2269.6	82.31512	2259.033	1.00423318
01/25/93	20	-1	0	0.834026	33994.83	15.93402778	19.93	86	2334.5	82.87281	2342.806	0.99645461
01/26/93	10	31	0	0.888184	33995.89	16.78818444	19.93	122	2450.5	137.1919	2479.998	0.99052488
01/27/93	7	45	0	0.322917	33996.32	17.42291667	19.93	98	2552.5	101.9458	2581.844	0.98858624
01/27/93	10	35	0	0.732639	33996.73	17.83263889	19.94	56	2608.6	85.8408	2847.784	0.98518331
01/28/93	7	47	0	0.324306	33997.32	18.42430556	19.93	107	2715.6	85.03047	2742.815	0.99004191
01/29/93	12	50	0	0.634722	33998.53	19.63472222	19.94	171	2886.5	194.5069	2937.523	0.98289741

## Appendix I.

DATE: December 16, 1992  
 TO: Richard Deaton MS 4139, Ext. 6-2016, FAX 6-2681  
 FROM: R. L. Drexler M8 3123, Ext. 6-1789  
 SUBJECT: INEL CELL CATHODE ESTIMATE

Attached are the following sketches and revised sketches:

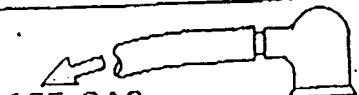
Cathode Assembly for INEL CELL	12/16/92
Narrow Cathode Strap for INEL CELL	12/16/92
Cathode C-1 INEL CELL	12/2/92
Mandrel - Cathode Winding	12/8/92
Electrode Bus Ring INEL CELL	12/15/92

Would you please give us a firm estimate for fabrication of two "identical" cathode assemblies per the 12/16/92 sketch, and two Electrode Bus Rings per the 12/15/92 sketch.

The cathode windings could be made on a mandrel per the sketch 12/8/92 or similar suitable arrangement.

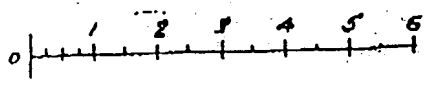
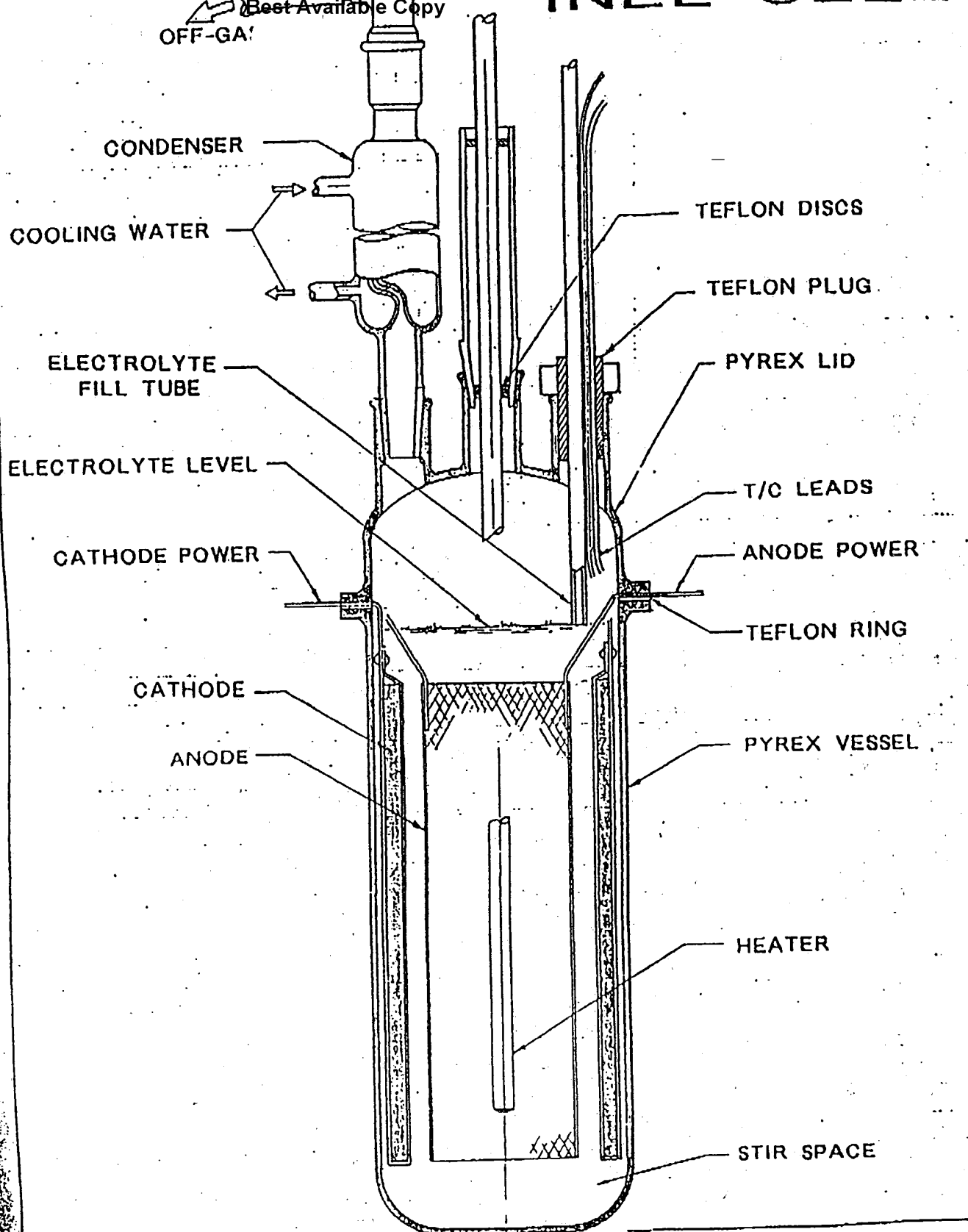
These cathodes and bus rings are similar to those previously fabricated except:

1. The straps are 0.5 in. wide rather than 1.0 in. wide. These narrower straps would be flat rather than arched to fit the winding curvature.
2. There are no secondary straps as were added to the windings of the first cathode assembly.
3. Windings would be less dense than the first winding. A much steeper pitch is probably necessary to achieve the more open wind.
4. Weight of the NI-200 wire of each winding should be very close to 3.33 pounds, and both windings should have the same weight as closely as possible.
5. Slots in the Teflon Buss Ring for the cathode straps would be 0.50 wide rather than the 1.0 width of the first ring.



Best Available Copy  
OFF-GA

# INEL CELL



CATHODE ASSEMBLY

FOR  
INEL CELL

CATHODE STRAP

CATHODE WINDINGS

Best Available Copy

R2D  
11-25-92  
12-15-92

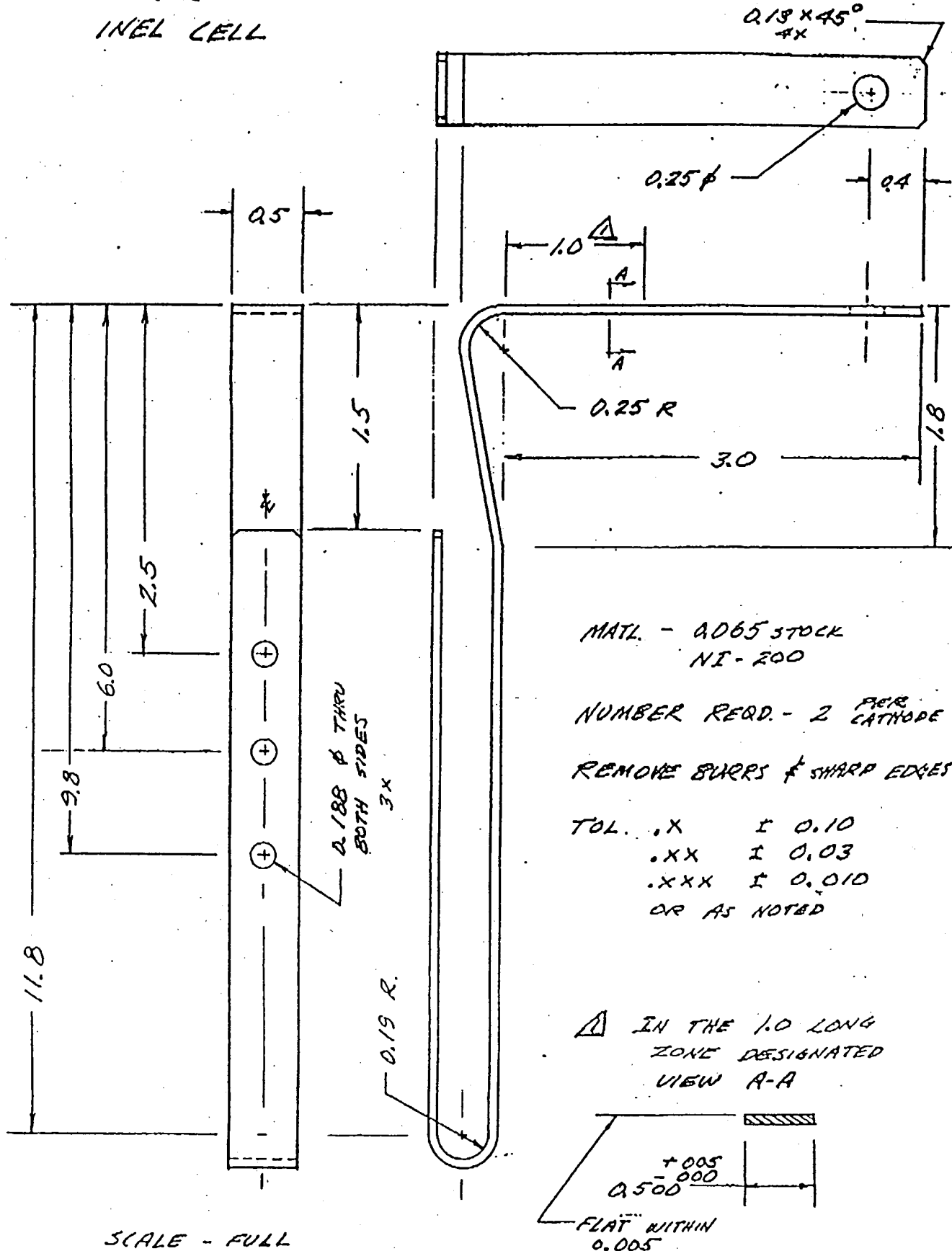
RIVET 6X - MAKE FROM  
0.187" Ø NI-200 ROD.  
INSTALL FOR TIGHT CLAMONIC  
LOAD BETWEEN STRAPS AND  
WINDING.

△ ALIGN BOTH STRAPS  
IN PLANE AT 30°  
WITH WINDING

NARROW CATHODE STRAP

KTA  
12-15-92

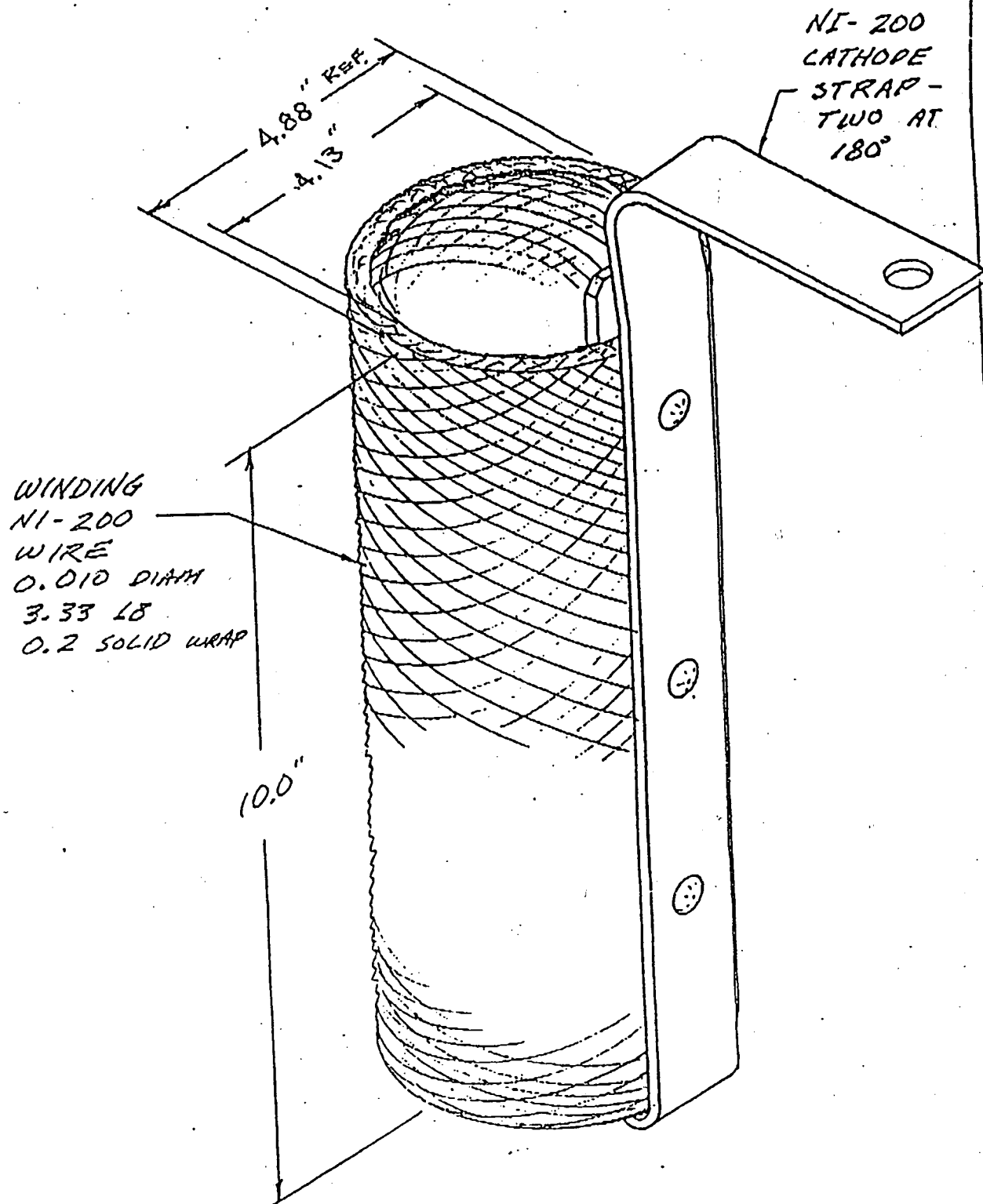
FOR  
INEL CELL



10-15-92  
10-21-92  
12-2-92

# CATHOLE C-1

## INEL CELL



NUMBER REOD. — ONE PER CELL

AECL Research

**CALORIMETRY FOR A Ni/K<sub>2</sub>CO<sub>3</sub> CELL**

by

M.T. Craw-Ivanco, R.P. Tremblay, H.A. Boniface and J. Hilborn

Chemical Engineering Branch  
Chalk River Laboratories  
Chalk River, ON  
K0J 1J0

1994 June

AECL Research

**CALORIMETRY FOR A Ni/K<sub>2</sub>CO<sub>3</sub> CELL**

by

M.T. Craw-Ivanco, R.P. Tremblay, H.A. Boniface and J. Hilborn

**SUMMARY**

Experiments were conducted to assess the possibility of excess heat production in light-water electrolytic cells. The program comprised six basic experiments in which the magnitude of heat production was monitored calorimetrically over a period of several days. The first three experiments were conducted with a relatively high power (about 10 W). In the first two experiments, there was an indication that some significant recombination of the electrolysis gases was occurring; therefore, an experiment was conducted in which a hydrogen/oxygen recombiner catalyst was introduced to the electrolysis cell. No conclusive evidence of excess power generation was observed. These experiments were performed at power levels in excess of those recommended by Randell Mills, of Hydrocatalysis Power Corporation (HPC). The electrode assembly was modified by Randell Mills, and on the direction of HPC a second series of experiments was conducted at lower power (~1 W), this time with ambiguous results because of measurement difficulties. In the higher power experiments (#1, #2 and #3), no net excess or deficit energy was observed greater than experimental error. According to Mills, this result was consistent with operation at currents and voltages substantially higher than 1 mA·cm<sup>-2</sup> and 2.5 V. The lower power experiments were done within the recommended current density and voltage, and according to Mills the expected excess heat would be about 0.25 W. Various methods of analysis were applied to the results of experiments #4, #5 and #6. Some of these analyses indicated possible excess heat at approximately this level. A model was developed to help elucidate the heat transfer characteristics of the system and hence give some insight to the energy balance data for low-power experiments.

Chemical Engineering Branch  
Chalk River Laboratories  
Chalk River, ON  
K0J 1J0

1994 June

## 1. INTRODUCTION

Since the original claims of excess heat production in electrolytic cells by Pons and Fleishman, a considerable body of work has emerged, both experimental and theoretical. Fairly comprehensive reviews of the literature have been given recently.<sup>[1,2]</sup> While the original "excess heat generation" experiments concentrated on heavy-water solutions and noble metal cathodes, more recently several studies to investigate excess heat production with a K<sub>2</sub>CO<sub>3</sub>/light-water electrolyte in an electrolytic cell with a nickel cathode and platinum anode have been reported.<sup>[3-6]</sup>

The inventor of this work is Randell Mills, of Hydrocatalysis Power Corporation (HPC), who has reported excess power generation of 50 to 100% of the input electrical power with constant current and as high as 10 to 15 times input power with pulsed current.<sup>[6]</sup> Our work aimed to repeat the experiments of Randell Mills, to determine whether excess heat generation was observable in our experimental system. The experimental program was therefore conducted in close collaboration with personnel from HPC.

## 2. EXPERIMENTAL

### 2.1 Materials and Supplies

Potassium carbonate was purchased from the Aldrich Chemical Company and certified to be 99.99% pure. Nickel wire was obtained from Alfa Chemicals and all gases used came from Linde. Distilled 18 MΩ·cm deionized water was used for making up the electrolyte solution. To ensure no contamination of the electrode system all glassware was washed in HCl, rinsed copiously with distilled water and dried overnight in a vacuum oven at 200°C. In the first experiment, the cathode and anode were dipped in concentrated HCl for one hour, and then rinsed thoroughly with distilled de-ionized water. In subsequent experiments, the anode was treated as in experiment 1, but the cathode material was immersed in a 0.57 M K<sub>2</sub>CO<sub>3</sub>/3%H<sub>2</sub>O<sub>2</sub> solution for thirty minutes, and then rinsed with distilled de-ionized water.<sup>[7]</sup> Once the cell had been cleaned all manipulations were carried out using nylon gloves. At no time were the electrodes immersed in electrolyte solution without current flowing. In experiment #3, AECL wetprüofed catalyst # QA87-204 was inserted into the top of the electrolysis cell, to ensure complete recombination of all of the electrolysis gases.

### 2.2 Cell Design

To reproduce the conditions of Mills' experiments, a new cell was designed and constructed, as shown in Figure 1. The cell volume was approximately 1200 mL. The electrode support was constructed from polypropylene. The central cathode comprised 100 m of 0.5 mm nickel wire. Around the outer section of the electrode support, six 4-mm diameter glass rods were positioned (~1 cm from the central cathode) to support the 1.5-mm diameter platinum wire anode. The ratio of cathode to anode surface area was approximately 20:1. For the first experiment the electrode wires were connected directly to the power supply; for subsequent experiments the anode and cathode wires were clipped at the point of exit from the electrolyte solution and replaced by #16 American Wire Gauge (AWG) copper wire, to minimize resistive losses. The cell was stirred with a magnetically coupled glass stirring-rod assembly fitted with a Teflon paddle. Electrolysis gases were passed from the cell via the vent tube and a molecular sieve drier to a Tylan thermal mass flow transducer, to determine the quantity of gas being released from the cell. The mass flow transducer was calibrated using a stoichiometric (2:1) H<sub>2</sub>/O<sub>2</sub> gas mixture against a soap bubble meter. Gases emitted from the electrolysis cell were sampled and analyzed by gas chromatography. The ratio of hydrogen to oxygen in the effluent from the cell was found to be 2.14:1.00.

## 1. INTRODUCTION

Since the original claims of excess heat production in electrolytic cells by Pons and Fleishman, a considerable body of work has emerged, both experimental and theoretical. Fairly comprehensive reviews of the literature have been given recently.<sup>[1,2]</sup> While the original "excess heat generation" experiments concentrated on heavy-water solutions and noble metal cathodes, more recently several studies to investigate excess heat production with a K<sub>2</sub>CO<sub>3</sub>/light-water electrolyte in an electrolytic cell with a nickel cathode and platinum anode have been reported.<sup>[3-6]</sup>

The inventor of this work is Randell Mills, of Hydrocatalysis Power Corporation (HPC), who has reported excess power generation of 50 to 100% of the input electrical power with constant current and as high as 10 to 15 times input power with pulsed current.<sup>[6]</sup> Our work aimed to repeat the experiments of Randell Mills, to determine whether excess heat generation was observable in our experimental system. The experimental program was therefore conducted in close collaboration with personnel from HPC.

## 2. EXPERIMENTAL

### 2.1 Materials and Supplies

Potassium carbonate was purchased from the Aldrich Chemical Company and certified to be 99.99% pure. Nickel wire was obtained from Alfa Chemicals and all gases used came from Linde. Distilled 18 MΩ-cm deionized water was used for making up the electrolyte solution. To ensure no contamination of the electrode system all glassware was washed in HCl, rinsed copiously with distilled water and dried overnight in a vacuum oven at 200°C. In the first experiment, the cathode and anode were dipped in concentrated HCl for one hour, and then rinsed thoroughly with distilled de-ionized water. In subsequent experiments, the anode was treated as in experiment 1, but the cathode material was immersed in a 0.57 M K<sub>2</sub>CO<sub>3</sub>/3%H<sub>2</sub>O<sub>2</sub> solution for thirty minutes, and then rinsed with distilled de-ionized water.<sup>[7]</sup> Once the cell had been cleaned all manipulations were carried out using nylon gloves. At no time were the electrodes immersed in electrolyte solution without current flowing. In experiment #3, AECL wetproofed catalyst # QA87-204 was inserted into the top of the electrolysis cell, to ensure complete recombination of all of the electrolysis gases.

### 2.2 Cell Design

To reproduce the conditions of Mills' experiments, a new cell was designed and constructed, as shown in Figure 1. The cell volume was approximately 1200 mL. The electrode support was constructed from polypropylene. The central cathode comprised 100 m of 0.5 mm nickel wire. Around the outer section of the electrode support, six 4-mm diameter glass rods were positioned (~1 cm from the central cathode) to support the 1.5-mm diameter platinum wire anode. The ratio of cathode to anode surface area was approximately 20:1. For the first experiment the electrode wires were connected directly to the power supply; for subsequent experiments the anode and cathode wires were clipped at the point of exit from the electrolyte solution and replaced by #16 American Wire Gauge (AWG) copper wire, to minimize resistive losses. The cell was stirred with a magnetically coupled glass stirring-rod assembly fitted with a Teflon paddle. Electrolysis gases were passed from the cell via the vent tube and a molecular sieve drier to a Tylan thermal mass flow transducer, to determine the quantity of gas being released from the cell. The mass flow transducer was calibrated using a stoichiometric (2:1) H<sub>2</sub>/O<sub>2</sub> gas mixture against a soap bubble meter. Gases emitted from the electrolysis cell were sampled and analyzed by gas chromatography. The ratio of hydrogen to oxygen in the effluent from the cell was found to be 2.14:1.00.

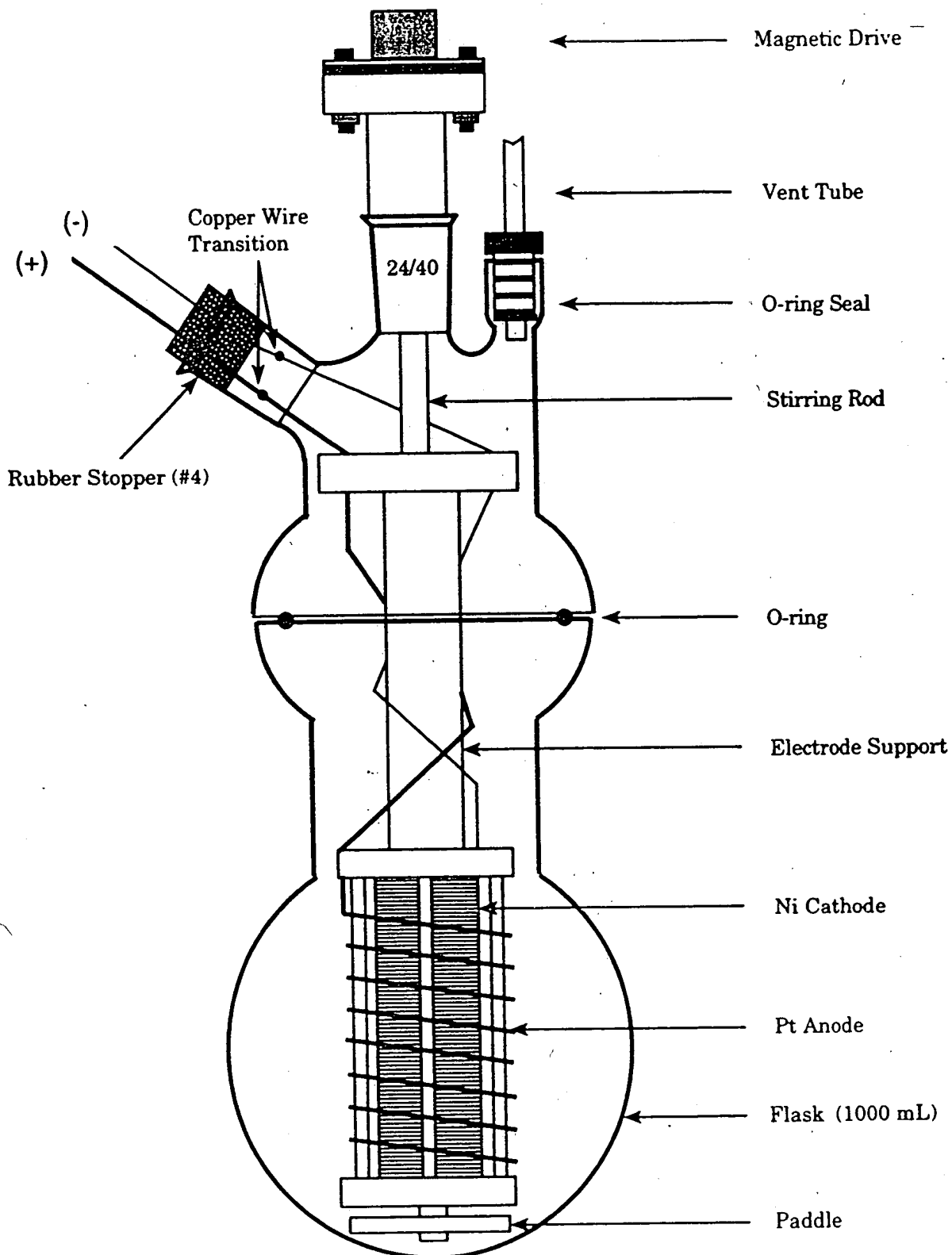


Figure 1 - Electrolysis Cell

### 2.3 Temperature Control

A temperature-controlled enclosure was employed for these experiments, to ensure that fluctuations in the ambient temperature would not adversely affect the experimental results. The entire experimental system is shown in Figure 2, and a schematic illustrating the system water flow is shown in Figure 3. The ambient temperature in the enclosure was controlled by heat lamps, a cooling coil and a fan to circulate the air in the enclosure (minimum  $2.5 \text{ m}^3 \cdot \text{h}^{-1}$ ).

### 2.4 Operating Conditions

The electrolysis cell was immersed in water inside the stainless-steel dewar and surrounded by a coil of copper tubing. Water was circulated through this coil to absorb heat from the cell when electrolysis was occurring. The experiment was designed in such a way that, for a given current, the theoretical heat generation was calculated and the inlet temperature of the water flowing through the copper coil adjusted such that the outlet temperature from the cooling coil would be approximately equivalent to the dewar temperature and the ambient temperature of the enclosure.

The ambient temperature and the dewar temperature were chosen as 35 to 37°C. The inlet temperature of water to the cooling coil was approximately 22 to 24°C, and the outlet temperature was approximately equal to the dewar temperature. The water circulating in the cooling coil was stored in a 25 L reservoir tank and passed through a constant temperature water bath (to obtain a temperature of 22 to 24°C) via insulated lines and a heat exchanger (to further ensure the appropriate inlet temperature) to the cooling coil in the dewar. The flow rate of water was controlled and monitored by an HPLC pump; as a check on the flow rate, the water was also passed to a weighing tank, which, when full, emptied into a drain tank equipped with a level controller and recycle loop to re-fill the water reservoir. In this way, the experiment could be run continuously with minimum operator intervention.

System temperatures, exit gas flow rate, water flow rate, voltage and current were all monitored and stored using a Data Translation DT2805 computer data acquisition system linked to a PC. A computer program was written for data acquisition and signals were recorded.

### 2.5 Instrumental Uncertainties and Estimation of Experimental Errors

Components of the experimental system were calibrated and where possible the experimental uncertainty associated with each of the following measurements was established or, where necessary, calculated:

- i. - Voltage, current and hence input power.
- ii. - Temperature measurements.
- iii. - Flow rate of water to cooling coil.
- iv. - Power from recombination of gases.
- v. - Resistive losses in lead wires.
- vi. - Effect of ambient temperature on dewar temperature.

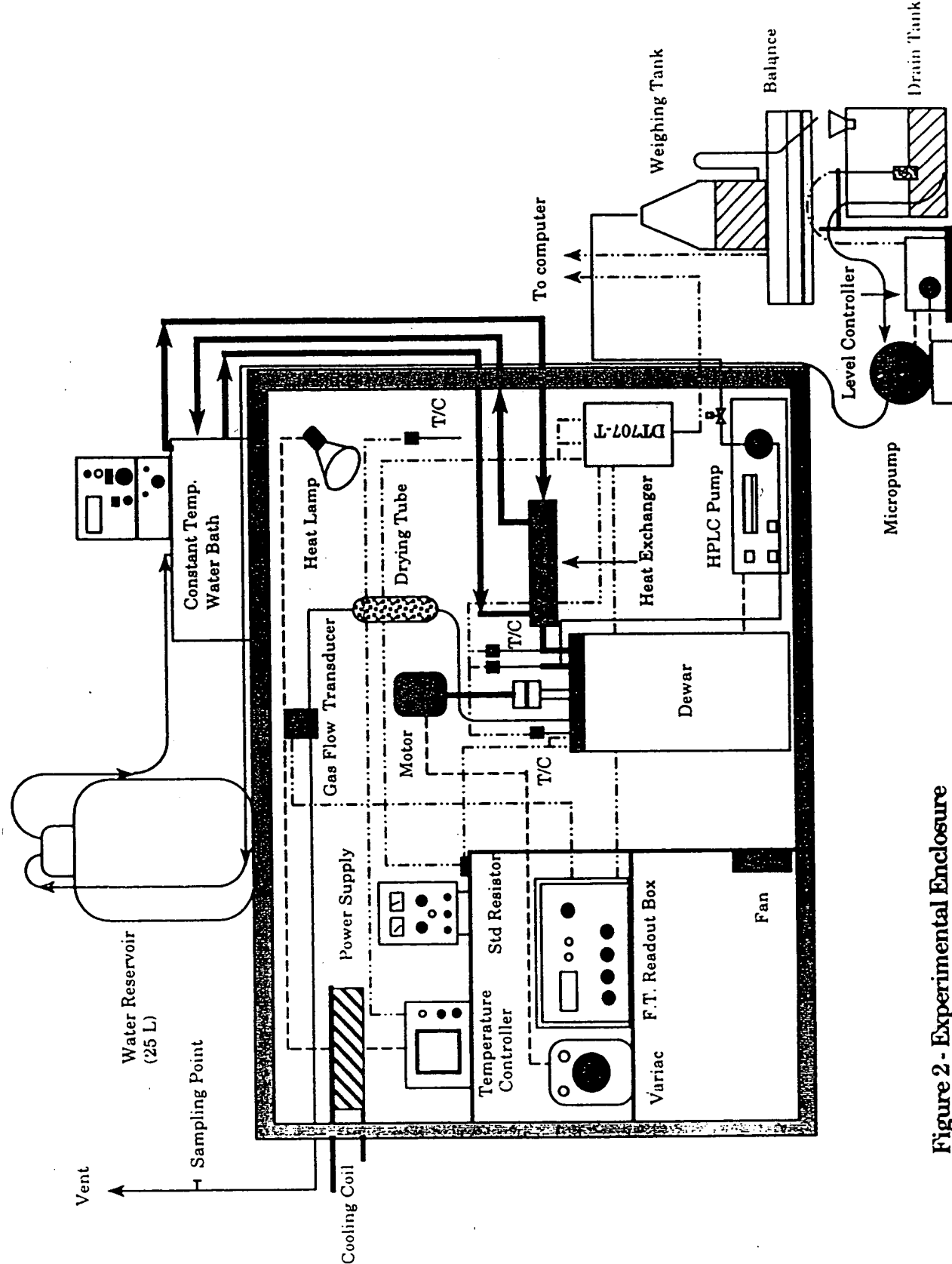


Figure 2 . Experimental Enclosure

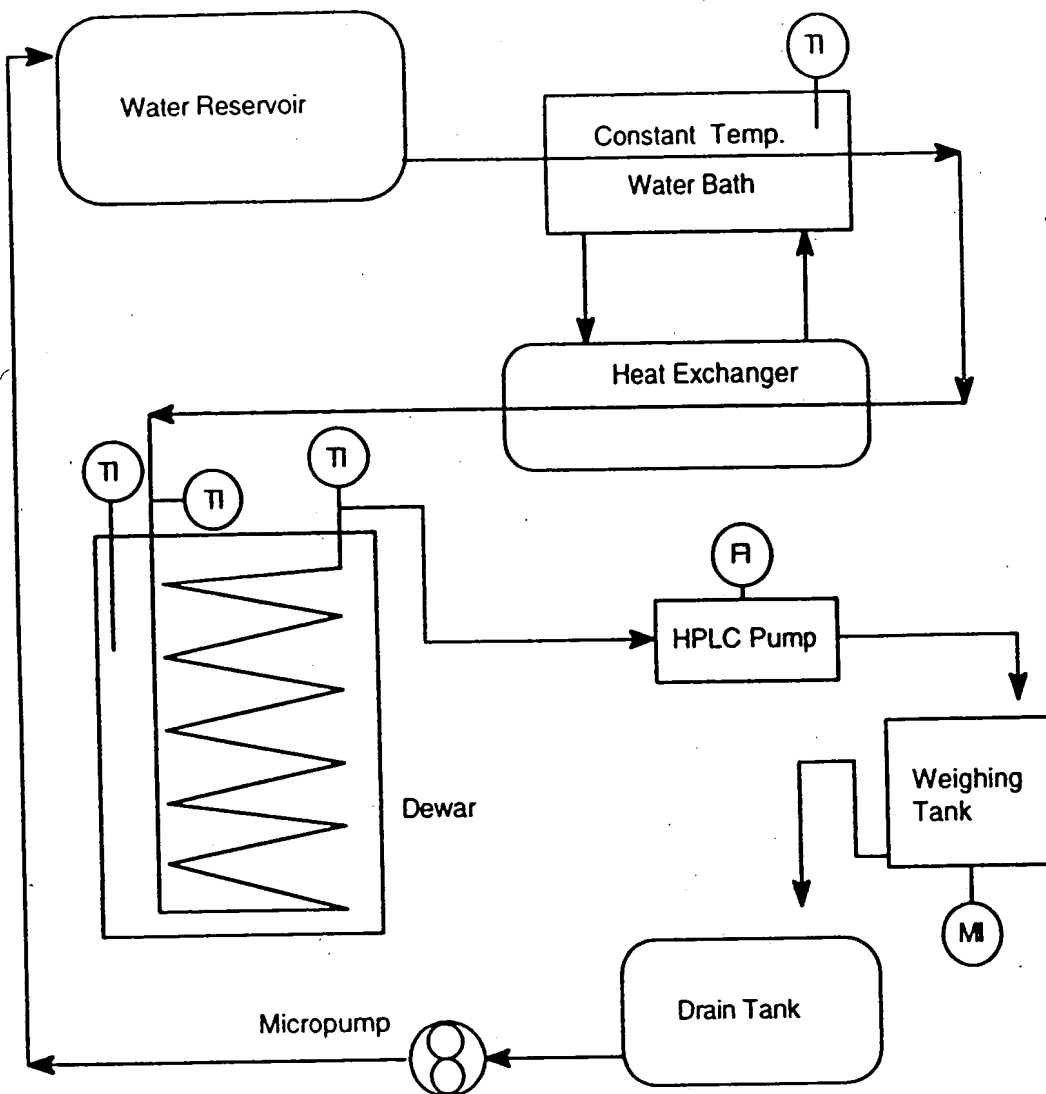


Figure 3 - Water Flow Diagram

### i. Voltage and Current Measurements

The voltage and current were recorded with the computer data acquisition system. The DT2805 board A/D subsystem has an accuracy of  $\pm 0.1\%$  FSR and a precision of  $\pm 1$  LSB (0.025%). The computer readout was compared with a 4.5 digit Fluke 8060A electronic multimeter. All readings were in agreement to four significant figures. The voltage was measured across supply wires near the entry to the cell, as shown in Figure 4. The current was obtained by measuring the voltage drop across a 10 W,  $100 \pm 1$  m $\Omega$  resistor. The exact resistor value was obtained using the voltage drop measured by the computer and the current flowing through the resistor as measured by a Fluke 8060A and a Fluke 77 multimeter. The resistor value was found to be  $103.8 \pm 2.3$  m $\Omega$  over the operating range. The input power was calculated from:

$$\text{Power} = \text{Voltage} \times \text{Current}$$

The error associated with the calculation of the input power is estimated to be approximately  $\pm 2.2\%$ .

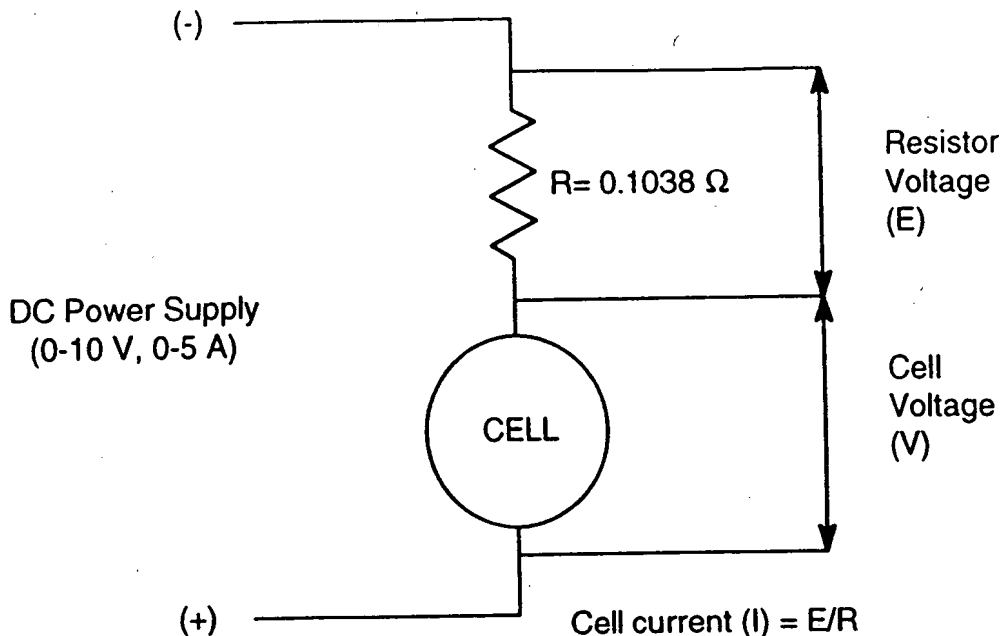


Figure 4 - Cell Electrical Measurements

## ii. Temperature Measurements

A Data Translation DT707-T screw terminal panel was used to make all the connections to the Data Translation DT2805 data acquisition board. The DT707-T is equipped with a thermocouple cold-junction compensation circuit (CJC). The CJC circuit provides a means by which to determine the temperature of the DT707-T board. The computer program was written to permit compensation for errors by the cold-junction thermocouple formed at the DT707-T. The CJC was calibrated following the procedure described in the user manual.

Since the board was located inside the test enclosure, the temperature of the board was used as a measure of the ambient temperature in the enclosure. The water inlet, outlet, and dewar temperature were measured using copper-constantan thermocouples (Type T, Limits of error  $\pm 1^\circ\text{C}$ ). The temperature difference between the water inlet and outlet was used in the calculation to determine the power output of the cell. Small variations in the temperature measured by two independent thermocouples can occur. To eliminate this type of potential repeatability error, the two thermocouples used to measure the water inlet and outlet temperature were matched so that both thermocouples indicated the same temperature when immersed in an ice bath or in boiling water to within  $0.1^\circ\text{C}$ .

The thermocouples were calibrated and the error associated with  $\Delta T$  measurements at the input and output of the cell were found to be within  $\pm 0.35\%$ .

## iii. Flow Rate of Cooling Water

The flow rate of cooling water was controlled with the HPLC pump. The water was passed through the cooling coil and then to a reservoir situated on top of a balance. The mass of water in the reservoir was monitored (using the computer), and after approximately 100 minutes the average flow rate was calculated and compared with the flow rate reading recorded with the pump. The pump value for cooling-water flow rate was determined to be accurate to  $\pm 0.3\%$ . The output power from the cell was calculated using the mass reading from the balance. If the balance reading fell below 98% of the pump reading, then the pump average flow was used to calculate the output power.

The power derived from the electrolytic cell ( $P_{cool}$ ) was calculated according to the following equation:

$$P_{\text{cool}} = Q C_p \Delta T$$

where:

- $C_p$  is the heat capacity of liquid water and taken as  $4.184 \text{ J}\cdot\text{g}^{-1}\cdot\text{K}^{-1}$ ,
- $\Delta T$  is the difference in temperature between the inlet and outlet of the cooling coil, and
- $Q$  is the flow rate of water to the cooling coil in  $\text{g}\cdot\text{s}^{-1}$  (as determined from the balance).

The limit of accuracy attainable for power out measurements is estimated to be within 2%.

#### iv. Power from Recombination of Electrolytic Gases

Recombination of hydrogen and oxygen produced on electrolysis is possible, and therefore all gases being released from the cell must be measured and accounted for. The power associated with recombination may be calculated from:

$$P_{\text{rec}} = \Delta H_{300 \text{ K}} (Q_{\text{calc}} - Q_{\text{meas}}) \times \frac{2}{3} \times \frac{1}{22.4}$$

where:

- $P_{\text{rec}}$  = the power added to the system from recombination of hydrogen and oxygen,
- $\Delta H_{300 \text{ K}} = -285.771 \text{ kJ}\cdot\text{mol}^{-1}$ ,<sup>[8]</sup> enthalpy of formation of  $\text{H}_2\text{O}(\text{g})$  from  $\text{H}_2$  and  $\text{O}_2$  in their standard states at 298 K and 101.325 kPa,
- $Q_{\text{calc}}$  = gas flow rate ( $\text{L}\cdot\text{s}^{-1}$ ) from the cell assuming no recombination,
- $Q_{\text{meas}}$  = actual exit dry gas flow rate ( $\text{L}\cdot\text{s}^{-1}$ ) as measured experimentally,  
2/3 accounts for stoichiometric ratio of hydrogen and oxygen, and  
22.4 L is the volume occupied by one mole of a gas at STP.

The instrumental error on the mass flow transducer used for gas flow measurements is estimated to be  $\pm 1\%$ .

#### v. Estimation of Resistive Losses in Lead Wires to the Cell

Resistive losses in the lead wires to the cell were calculated based on the following data:

Platinum wire #16 AWG has a resistive loss of  $0.000764 \Omega\cdot\text{cm}^{-1}$  at  $18^\circ\text{C}$ .<sup>[9]</sup> The length of wire from the cell to the power supply was approximately 31 cm; therefore, total resistance was approximately  $0.024 \Omega$ . For nickel wire, #16 AWG, the resistance is given as  $0.00381 \Omega\cdot\text{cm}^{-1}$ .<sup>[9]</sup> The length of nickel wire used was ~39 cm; therefore, the total resistance in the nickel wire is estimated to be  $0.15 \Omega$ . Power associated with these two resistances may be calculated from:

$$P_{\text{res}} = I^2 R$$

Which, for experiment #1, was:

$$\begin{aligned} P_{\text{res}} &= I^2(R_{\text{Pt}} + R_{\text{Ni}}) \\ &= (2.822 \text{ A})^2 \times (0.024 \Omega + 0.15 \Omega) \\ &= 1.38 \text{ W} \end{aligned}$$

To minimize these losses, the platinum and nickel lead wires were replaced with #16 AWG copper wire. The resistance of this wire is documented as  $0.000132 \Omega \cdot \text{cm}^{-1}$ .<sup>[9]</sup> Using 39 cm of copper wire for each electrode with a current of 2.822 A, the total resistive losses drop to 0.082 W. Therefore, copper was substituted for the nickel and platinum lead wires after the first experiment. In experiments #4, #5, #6, and in the calibration runs Cal1W1 and Cal1W2, the current never exceeded 1 A; therefore, the resistive losses in the copper lead wire were always less than  $5.15 \times 10^{-3} \text{ W}$ .

#### vi. Estimation of Fluid Frictional Power in a Pipe

The power loss due to the friction of the cooling water flowing in the cooling tube ( $P_f$ ) may be estimated, assuming the flow is laminar. Using the Hagen-Poiseuille equation for frictional head loss ( $\Delta p$ ) in a circular tube:

$$\Delta p = \frac{128 \mu L Q}{\pi D^4}$$

Assuming a 10 m long tube (L) with a 2 mm inside diameter (D) and about  $10 \text{ g} \cdot \text{min}^{-1}$  pure water flowing inside (Q), the head loss is:

$$\begin{aligned} \Delta p &= \frac{128 \times 10^{-3} \frac{\text{kg}}{\text{m} \cdot \text{s}} \times 10 \text{ m} \times \frac{10^{-6} \text{ m}^3}{60 \text{ s}}}{\pi \times (0.002 \text{ m})^4} \\ &= 424 \text{ Pa} \end{aligned}$$

and the power is:

$$\begin{aligned} P_f &= Q \Delta p \\ &= \frac{10^{-5} \text{ m}^3}{60 \text{ s}} \times 424 \text{ Pa} \\ &= 7.1 \times 10^{-5} \text{ W} \end{aligned}$$

Thus, for this situation, the frictional power is negligible.

#### vii. Estimation of Stirring Power Loss

Power added to the system by stirring may be estimated from the following correlations for the dimensionless power number ( $N_p$ ):<sup>[10]</sup>

$$\begin{aligned} N_p &= \frac{80}{R_e} \text{ at low Reynolds number} \\ &= 6 \text{ at high Reynolds number} \end{aligned}$$

where:

$$N_p = \frac{P_{st}}{\rho N^3 D^5}$$

$$Re = \frac{D^2 N \rho}{\mu}$$

In this case, the impeller was 40 mm diameter ( $D$ ) and rotating at 2 rev·s<sup>-1</sup> ( $N$ ) in electrolyte ( $\rho = 1000 \text{ kg} \cdot \text{m}^{-3}$ ,  $\mu = 10^{-3} \text{ kg} \cdot \text{m}^{-1} \cdot \text{s}^{-1}$ ). Thus the power added by stirring was between:

$$\begin{aligned} P_{st} &= \frac{80 \mu}{D^2 N \rho} \rho N^3 D^5 \\ &= 80 \mu N^2 D^3 \\ &= 80 \times 10^{-3} \frac{\text{kg}}{\text{m} \cdot \text{s}} \times (2 \text{ s}^{-1})^2 \times (0.04 \text{ m})^3 \\ &= 2 \times 10^{-5} \text{ W} \end{aligned}$$

and:

$$\begin{aligned} P_{st} &= 6 \rho N^3 D^5 \\ &= 6 \times 10^3 \frac{\text{kg}}{\text{m}^3} \times (2 \text{ s}^{-1})^3 \times (0.04 \text{ m})^5 \\ &= 5 \times 10^{-3} \text{ W} \end{aligned}$$

Therefore, in the worst-case scenario the power added to the cell from stirring is about 5 mW.

## 2.6 Estimation of Total Power In and Total Power Out of Cell

The total power delivered to the cell has several potential sources and may be calculated from:

$$P_{tot,in} = P_{e,in} + P_{rec} + P_{fr} + P_{st}$$

where:

- $P_{e,in}$  is power from voltage and current delivered to the cell,
- $P_{rec}$  is power from recombination of electrolysis gases,
- $P_{fr}$  is power from the frictional pressure drop in the cooling coil, and
- $P_{st}$  is power produced from the stirrer.

The total electrical power provided to the cells is simply:

$$P_{e,in} = IV$$

and the power used for the electrolysis reaction is:

$$P_{elec} = IV_0$$

where:

- $V$  = the total cell voltage,
- $V_0$  = the hydrogen/oxygen thermoneutral cell voltage (1.48 V), and
- $I$  = the cell current in A.

$P_{rec}$ ,  $P_{fr}$  and  $P_{st}$  are calculated as shown in Section 2.5.

The total output power from the cell can also be estimated:

$$P_{\text{tot,out}} = P_{\text{cool}} + P_{\text{elec}} + P_{\text{res}} + P_{\text{cond}}$$

where:

- $P_{\text{cool}}$  is the portion of input power used to heat up the cooling water,
- $P_{\text{elec}}$  is the portion of input power used in electrolysis of water,
- $P_{\text{res}}$  is the resistive losses in the lead wires, and
- $P_{\text{cond}}$  is the portion of power used to evaporate the water that is carried out (as vapor) with the evolved gases.

In a similar fashion the total input energy and output energy can be defined as:

$$E_{\text{tot,in}} = E_{e,\text{in}} + E_{\text{rec}} + E_{\text{fr}} + E_{\text{st}}$$

and,

$$E_{\text{tot,out}} = E_{\text{cool}} + E_{\text{elec}} + E_{\text{res}} + E_{\text{cond}}$$

or:

$$E_{\text{tot,in}} = \int_{t_1}^{t_2} P_{e,\text{in}} dt + \int_{t_1}^{t_2} P_{\text{rec}} dt + \int_{t_1}^{t_2} P_{\text{fr}} dt + \int_{t_1}^{t_2} P_{\text{st}} dt$$

and,

$$E_{\text{tot,out}} = \int_{t_1}^{t_2} P_{\text{cool}} dt + \int_{t_1}^{t_2} P_{\text{elec}} dt + \int_{t_1}^{t_2} P_{\text{res}} dt + \int_{t_1}^{t_2} P_{\text{cond}} dt$$

## 2.7 System Calibration

The cell was calibrated using a  $1 \Omega$  resistor as an immersion heater. This resistor was installed on the electrode assembly and the cell filled with de-ionized distilled water. The resistor was connected to the power supply using 1 m of #16 AWG copper lead wires. The ambient temperature was set at  $37^\circ\text{C}$  and the inlet power set to the desired value. After all the temperatures and process conditions were stabilized, the water flow rate and inlet temperature were adjusted such that the power output matched the power input.

Once the power input and output were matched, the data acquisition system was reset and the system was monitored over an extended period of time, to determine whether there was any drift, offset or fluctuation in the input or output power of the system. The mean input and output power for 7 W and 15 W calibration studies, along with standard deviations of these measurements, are shown in Table 1.

Temperature measurements were recorded during the resistance heater power calibration studies, to determine whether small fluctuations in the ambient temperature had any effect on the dewar temperature or the recorded outlet temperature. There was no significant effect of variations in the ambient temperature on the dewar temperature, providing the fluctuations in the ambient temperature were kept to a minimum. Mean temperatures with standard deviation data are listed in Table 1. Similar experimental data are also listed in Table 1 for the pump calibration and the mass-flow transducer calibration.

Table 1 - Statistical Analysis of Calibration Data

Quantity	Mean	Standard Deviation	% Error
Input Power (7 W)	7.35	0.0123	0.17
Output Power (7 W)	7.49	0.1673	2.22
Input Power (15 W)	14.56	0.0391	0.26
Output Power (15 W)	14.76	0.2603	1.78
Pump Flow ( $0.12 \text{ g}\cdot\text{s}^{-1}$ )	0.12	0.0004	0.28
Pump Flow ( $0.24 \text{ g}\cdot\text{s}^{-1}$ )	0.24	0.0007	0.29
Vent Gas Flow Rate ( $\text{mL}\cdot\text{min}^{-1}$ )	26.53	0.14	0.52

### 3. RESULTS

#### Experiments #1, #2 and #3

In all of these experiments, 1200 mL of 0.57 M  $\text{K}_2\text{CO}_3$  solution was placed in the electrolysis cell. The cell current was set at 0.25 A before the electrode assembly was immersed in the electrolyte, in accordance with the directions from Mills' Laboratory.<sup>[7]</sup> After inserting the electrode and sealing the cell, the current was increased to 2.822 A, to give a current density of  $1.8 \text{ mA}\cdot\text{cm}^{-2}$ . The system was operated until the dewar temperature and outlet temperature from the copper coil surrounding the cell were stabilized.

The voltage corresponding to this cell current was 4.93 V, which resulted in an input power of 13.86 W being delivered to the cell. Of this 13.86 W, it is expected that 4.177 W would be used for electrolyzing water (assuming electrolysis voltage equals 1.48 V). The remainder of the power would be used to increase the temperature of the water circulating around the electrolysis cell in the copper coil. The basic energy balance data for experiments #1, 2 and 3 were computed as shown in Table 2.

The surface area of the cathode was about  $1500 \text{ cm}^2$ . The current density recommended by Mills was less than  $1 \text{ mA}\cdot\text{cm}^{-2}$ , thus the recommended current was about 1.4 A. The actual current was approximately twice this value. Furthermore, Mills recommended that the cell voltage not exceed 2.5 V. Using the cell resistance calculated from the voltage and current of experiment #1, the recommended input parameters were a cell current of 1.4 A, a cell voltage of 2.1 V and an input power of 2.94 W.

Table 2 - Data from Experiments #1, #2 and #3

Expt. #	Electrical Energy In (W·h)	Thermal Energy Out (W·h)	Total Electrolysis Energy (W·h)	Measured Gas Released (L)	Theoretical Gas Production (L)
1	723.6	517.1	212.6	67.59	89.80
2	1154.5	685.3	481	184.25	203.15
3	1196.7	1203.97	-	-	-

The total input energy to the cell may be calculated as follows for experiment #1:

$$\begin{aligned} E_{\text{tot,in}} &= E_{e,\text{in}} + E_{\text{rec}} + E_{\text{fr}} + E_{\text{st}} \\ &= 723.6 \text{ W}\cdot\text{h} + 52.4 \text{ W}\cdot\text{h} + 0 \text{ W}\cdot\text{h} + 0.26 \text{ W}\cdot\text{h} \\ &= 776.3 \text{ W}\cdot\text{h} \end{aligned}$$

$$\begin{aligned} E_{\text{tot,out}} &= E_{\text{cool}} + E_{\text{elec}} + E_{\text{res}} + E_{\text{cond}} \\ &= 517.1 \text{ W}\cdot\text{h} + 212.6 \text{ W}\cdot\text{h} + 70.25 \text{ W}\cdot\text{h} + 2.91 \text{ W}\cdot\text{h} \\ &= 802.7 \text{ W}\cdot\text{h} \end{aligned}$$

The first experiment was designed to identify potential operating problems. Recombination appeared to play a significant role in the overall energy balance; therefore, it was concluded that the absolute quantity of gas evolved from the system should be monitored very closely, and that particular attention should be paid to all potential leaks. Another possible source of error was resistive losses in the lead wires.

The quantity of water evaporated from the cell and adsorbed in the trap for experiment #1 was calculated by weighing the molecular sieve trap before and after the experiment. The mass of liquid adsorbed on the molecular sieve was recorded as 4.3 grams or 0.24 moles of water (which corresponds to a saturation temperature of about 40°C in the gas leaving the cell). The enthalpy of vaporization is approximately 44 kJ·mol<sup>-1</sup>.

From the integrated data there would appear to be an overall energy gain of 26.4 W·h in experiment #1, which would translate to approximately 0.5 W of power, or 3% of the input power. It is believed that, under the conditions of the experiment, this figure is within experimental error.

According to the experiments of Mills *et al.*, excess power to the extent of 1 mW·cm<sup>-2</sup> of cathode surface would be expected, which in this experiment would translate to 1.5 W of power or an energy of 76.4 W·h.

In experiment #2, the reaction system was modified slightly, to minimize all potential power losses, ensure that there were no gas leaks and ensure that the measurement of gas evolution was indeed accurate. Further advice was sought from Randell Mills, of HPC, concerning operating conditions.

Prior to beginning the second experiment, a new cathode was rolled as described in Experiment 1. The cathode was then soaked in K<sub>2</sub>CO<sub>3</sub>/3% H<sub>2</sub>O<sub>2</sub> as described in section 2. The platinum wire was soaked in HCl, rinsed in distilled deionized water and installed in the electrode assembly. A 0.57 M solution (1200 mL) of K<sub>2</sub>CO<sub>3</sub> was placed in the electrolysis cell, the current turned on at 0.25 A and the electrode assembly immersed in the electrolyte. Since the nickel and platinum lead wires were replaced with copper, the overall cell resistance was reduced; therefore, for a current of 2.822 A the voltage required dropped to approximately 3.5 V. Hence, the input power to the cell was in the region of 9.87 W.

The surface area of the cathode was about 1500 cm<sup>2</sup>. The current density recommended by Mills was less than 1 mA·cm<sup>-2</sup>, thus the recommended current was about 1.4 A. The actual current was approximately twice this value. Furthermore, Mills recommended that the cell voltage not exceed 2.5 V. Using the cell resistance calculated from the voltage and current of experiment #1, the recommended input parameters were a cell current of 1.4 A, a cell voltage of 1.83 V and an input power of 2.57 W.

Approximately 9% of the expected electrolysis gas was missing, implying that this portion of gas had recombined. The energy associated with this recombination is calculated as 44.5 W·h. In addition, a small fraction of water vapor was carried from the cell in the effluent gas stream and adsorbed in the molecular sieve trap. The quantity of water adsorbed in the trap was calculated by weighing the molecular sieve trap before and after the experiment. The mass of liquid adsorbed on the molecular sieve was recorded as 11.7 grams or 0.65 moles of water (which corresponds to a saturation temperature of about 40°C in the gas leaving the cell - as in experiment #1). The energy lost from the system as a result of evaporation was calculated as 28.6 kJ or 7.9 W·h.

Summing up all the appropriate input terms for experiment #2:

$$\begin{aligned} E_{\text{tot,in}} &= E_{e,\text{in}} + E_{\text{rec}} + E_{\text{fr}} + E_{\text{st}} \\ &= 1154.5 \text{ W}\cdot\text{h} + 44.5 \text{ W}\cdot\text{h} + 0 \text{ W}\cdot\text{h} + 0.578 \text{ W}\cdot\text{h} \\ &= 1199.7 \text{ W}\cdot\text{h} \end{aligned}$$

Similarly, the total power released from the cell, neglecting heat loss, can be obtained:

$$\begin{aligned} E_{\text{tot,out}} &= E_{\text{cool}} + E_{\text{elec}} + E_{\text{res}} + E_{\text{cond}} \\ &= 685.3 \text{ W}\cdot\text{h} + 481 \text{ W}\cdot\text{h} + 9.4 \text{ W}\cdot\text{h} + 7.9 \text{ W}\cdot\text{h} \\ &= 1183.6 \text{ W}\cdot\text{h} \end{aligned}$$

The energy difference is therefore 16 W·h (or 0.14 W), or 1.4%. This energy is, however, apparently lost from the system, and we suspect that this "loss" reflects the operating constraints of the system.

One of the areas of concern in this type of experiment is accounting for energy added to the system from recombination of the electrolysis gases. One way to eliminate any uncertainty concerning recombination would be to recombine all of the electrolysis gas in a closed reactor. In order to do this another experiment was conducted identical to Experiment #2, but with a recombiner catalyst housed in the top portion of the electrolysis cell. The electrolysis cell was run under a slight excess of oxygen ( $2 \text{ mL} \cdot \text{min}^{-1}$ ) to eliminate potential explosion hazards.

The difference in input and output energy can be computed as before:

$$\begin{aligned} E_{\text{tot,in}} &= E_{e,\text{in}} + E_{\text{rec}} + E_{\text{fr}} + E_{\text{st}} \\ &= 1196.7 \text{ W}\cdot\text{h} + 0 \text{ W}\cdot\text{h} + 0 \text{ W}\cdot\text{h} + 0.561 \text{ W}\cdot\text{h} \\ &= 1197.3 \text{ W}\cdot\text{h} \end{aligned}$$

Similarly, the total energy released from the cell can be obtained:

$$\begin{aligned} E_{\text{tot,out}} &= E_{\text{cool}} + E_{\text{elec}} + E_{\text{res}} + E_{\text{cond}} \\ &= 1203.97 \text{ W}\cdot\text{h} + 0 \text{ W}\cdot\text{h} + 9.44 \text{ W}\cdot\text{h} + 0 \text{ W}\cdot\text{h} \\ &= 1213.4 \text{ W}\cdot\text{h} \end{aligned}$$

Net energy production during the recombination experiment was therefore 16.1 W·h, which translates to 0.13 W or 1.3% of input power. This quantity of energy falls within the experimental error expected for this experiment. There would therefore not appear to be any real evidence for excess heat production in the large-scale cell as constructed and operated in this laboratory.

On further consultation with Randell Mills, it was agreed that the cell assembly would be sent to HPC, where a new anode and cathode would be fitted, the cell returned to AECL and a fourth experiment conducted. HPC provided analysis of AECL's departures from their protocol concerning operating conditions necessary for the observation of excess heat in a light-water electrolytic cell:

1. The cathode should not be electrolyzed above 2.5 V nor 1 amp current.
2. Rigorous cleaning steps as described in Section 2 should be conducted.
3. Back pressure in the cell must be avoided at all costs: at a partial pressure of 0.1 atm hydron molecules, the catalytic reaction reaches equilibrium. Further tests with open cells demonstrated the higher the back pressure on an open cell, the less excess heat was observed for that cell.

These points were noted and the experimental system modified accordingly.

#### Experiments #4, #5 and #6

The electrodes were assembled at HPC using the AECL electrode holder. The cathode was constructed from three 30.76 m lengths of 0.38 mm nickel (Alfa Chemicals); the 1.5 mm diameter platinum wire anode was that of experiments #1, #2 and #3. The surface area of the cathode was  $1101.4 \text{ cm}^2$ . To ensure that the conditions of the experiment were adhered to, the cell voltage was set at 2.4 V. With this voltage the current never exceed 1 A. Assuming no excess power generation, the actual power expected was in the region of 1 W. In order to detect this relatively small amount of power, the cooling water flow rate was reduced significantly, to ensure that the temperature change of the cooling water was high enough to be recorded accurately.

According to HPC, this electrode system was expected to produce a maximum of  $1 \text{ mW} \cdot \text{cm}^{-2}$  of the cathode which carried a current of approximately  $1 \text{ mA} \cdot \text{cm}^{-2}$ . The cathode surface area was  $1100 \text{ cm}^2$  and it was estimated that approximately half was exposed to the electrolyte. Thus, the predicted excess power was approximately 0.25 W which, with this experimental arrangement, would amount to 25% excess power.

Experiment #4 was an open cell, whereas in experiments #5 and #6, the cell used for experiment #4 was fitted with the same recombiner catalyst used in experiment #3. These two experiments were

then run in the same way as experiment #3, except that in experiment #6 the water cooling was turned off and the run was quite short.

### Calibration Runs

At the end of experiment #6, the power was turned off, but the experiment was allowed to continue in order to study the transfer of heat between the dewar and the surroundings. Following this, two low-power calibration tests were performed with a  $1\ \Omega$  resistor arranged in the same way as the previous calibrations. In addition, a number of different heat transfer tests were done on the dewar. (These calibration runs were clearly desirable for an experimental setup that was designed for power measurements in the 10 W range, but was now being used for experiments in the 1 W range.)

The following tables (Table 3a, 3b and 3c) lists the experimental sequence of events for the last two experiments and the two calibration runs. The data in Tables 3b and 3c were obtained by averaging 10 readings starting at the times indicated.

Table 3a - Procedure for Experiments #5 and #6 and Calibrations #1 and #2

Experiment number	Date started	Duration (h)	Experiment duration (min)	Procedure description
5a	July 26	42	2520	Power and cooling on
5b	July 28	31	4380	
6a	July 29	48	2880	Water cooling off
6b	July 31	24	4320	Power and cooling off
6c	August 1	23	5700	Oxygen flow off, mercury thermometer installed
Cal 1W1	August 4	40	2400	Cooling and power on
Cal 1W2a	August 6	29	1740	Power on, cooling off
Cal 1W2b	August 7	41	4200	Power and cooling off

Table 3b - Test results for Experiments #5 and #6

Experiment #	5a		5b		6a		6b		6c	
Date	7/26	7/28	7/28	7/29	7/29	7/31	7/31	8/1	8/1	8/2
Time	1405	0805	0805	1447	1605	1603	1608	1606	1606	1525
Voltage (V)	2.29	2.34	2.34	2.34	2.34	2.34	0	0	0	0
Current (A)	0.706	0.376	0.376	0.329	0.329	0.329	0	0	0	0
Power (W)	1.62	0.88	0.88	0.77	0.77	0.77	0	0	0	0
T <sub>dewar</sub> (°C)	35.54	36.53	36.53	36.68	36.78	37.29	37.29	36.86	36.86	36.92
ΔT <sub>dewar</sub> (°C)		0.99		0.15		0.51		-0.43		0.06
T <sub>ambient</sub> (°C)	35.76	35.77	35.77	35.78	35.37	35.12	35.13	35.27	35.27	35.17
T <sub>controller</sub> (°C)	36.0	36.0	36.0	36.0	36.0	36.0	36.0	36.0	36.0	36.0
T <sub>mercury</sub> (°C)								36.9	36.9	36.9
E <sub>e,in</sub> (W·h)	0.14	50.56	0	23.69	0.06	37.06	0	0	0	0
E <sub>cool</sub> (W·h)	0.13	54.28	0	23.34	0	0	-0	0	0	0
E <sub>cool</sub> -E <sub>e,in</sub> (W·h)		3.73		-0.35		-37.0		0		0

Table 3b - Test results for Calibrations #1 and #2

Experiment #	Cal 1W1		Cal 1W2a		Cal 1W2b	
Date	8/4	8/6	8/6	8/7	8/7	8/9
Time	1601	0800	0903	1403	1459	0759
Voltage (V)	0.996	0.996	0.998	0.991	0	0
Current (A)	0.988	0.988	0.988	0.988	0	0
Power (W)	0.98	0.98	0.99	0.98	0	0
T <sub>dewar</sub> (°C)	35.07	35.46	35.65	37.09	37.08	36.84
ΔT <sub>dewar</sub> (°C)		0.39		1.44		-0.24
T <sub>ambient</sub> (°C)	35.23	35.20	35.18	34.87	34.88	35.01
T <sub>controller</sub> (°C)	36.0	36.0	36.0	36.0	36.0	36.0
T <sub>mercury</sub> (°C)	36.9	36.9	36.9	36.7	36.7	36.9
E <sub>e,in</sub> (W·h)	0.1	39.44	0.08	29.39	0	0
E <sub>cool</sub> (W·h)	0.1	40.88	0	0	0	0
E <sub>cool</sub> -E <sub>e,in</sub> (W·h)		1.44		-29.4		0

During experiment #5a the cell resistance was increasing, so that the input current decreased from 0.71 A to 0.38 A (power went from 1.62 W to 0.88 W). The power was constant through most of experiment #5b and all through experiment #6a. At the beginning of experiment #6c a mercury thermometer was placed in the enclosure on top of the dewar in order to check the enclosure ambient temperature. From this time until the end of the calibrations the temperature indicated by this thermometer was 36.8±0.1°C.

Following the method used for experiments #1 to #3, the results for experiments #4 to #6 are given in Table 4.

Table 4 - Data from Experiments #4, #5 and #6

Expt. #	Electrical Energy In E <sub>e,in</sub> (W·h)	Thermal Energy Out E <sub>cool</sub> (W·h)	Electrolysis Energy E <sub>elec</sub> (W·h)	Measured Gas Released (L)	Theoretical Gas Production (L)	Calculated Recombination Energy E <sub>rec</sub> (W·h)
4	142.7	65.4	87.1	21.8	36.8	35.3
5	74.0	77.4	47.2	-	-	47.2
6	36.7	0	23.2	-	-	23.2

(Note that in experiment #6 no heat was possible because the heat exchanger had been turned off. The cell temperature increased 0.51°C)

After studying the results of the last two experiments and the calibration runs, two new terms in the overall energy balance were introduced. The first term (E<sub>loss</sub>) allowed for the energy that would leak through the dewar walls and lid due to the small difference between the temperature inside and outside the dewar. The second term (E<sub>cap</sub>) was to account for the storage of heat in the dewar contents (heat transfer fluid and the complete cell), given the difference in temperature in the dewar between the start and end of a run. The terms can be defined:

$$P_{loss} = U(T_{dewar} - T_{ambient})$$

$$E_{cap} = C_p \cdot \text{dewar}(T_{end} - T_{start})$$

where:

$U$	= overall heat transfer coefficient of the dewar ( $\text{W}\cdot\text{K}^{-1}$ )
$C_{p,\text{dewar}}$	= specific heat of the dewar contents ( $\text{W}\cdot\text{h}\cdot\text{K}^{-1}$ )

The total energy output is thus given by:

$$E_{\text{tot,out}} = E_{\text{cool}} + E_{\text{elec}} + E_{\text{loss}} + E_{\text{cap}}$$

The value of  $C_{p,\text{dewar}}$  was estimated to be at least  $17.4 \text{ W}\cdot\text{h}\cdot\text{K}^{-1}$ , based on the fact that the dewar had a volume of about 15 L, which, if filled only with water, would give this heat capacity. Given the different materials in the cell and the inner walls of the dewar, a best estimate of the heat capacity of the dewar contents was put at about  $20 \text{ W}\cdot\text{h}\cdot\text{K}^{-1}$ . The heat transfer coefficient was estimated from literature data for typical vacuum insulated containers to be between  $0.05$  and  $0.1 \text{ W}\cdot\text{K}^{-1}$ , although this was expected to be on the low side, because the lid was not tightly sealed.

A number of calibration runs were done to try to determine the values of these two parameters. A number of cooling curves were obtained and from these, coupled with all the other evidence, it was clear that the estimate of the dewar heat capacity was reasonable. However, the heat transfer coefficient was obviously incorrect.

During the calibrations, a check was made of the precision and accuracy of the thermocouples. These were found to be very good, giving temperatures within about  $\pm 0.1 \text{ K}$ . However, the ambient temperature was determined at the board used for the thermocouple junctions, and during the calibrations this was found to be low by anything up to  $2 \text{ K}$ . The temperature reading of the enclosure controller was found to be approximately  $0.8 \text{ K}$  below the actual ambient temperature measured by a calibrated mercury-in-glass thermometer placed close to the lid of the dewar, and this value did not vary by more than  $0.2 \text{ K}$  over the course of the calibration runs (about five days).

A preliminary analysis of the results for experiment #5a was made with the aid of the results of calibration Cal 1W1, since the two runs had approximately the same duration. During this calibration run, the dewar temperature rose by  $0.39 \text{ K}$ . Given that there was no electrolysis and the output energy must be equal to the input energy, an energy balance for this situation is thus:

$$\begin{aligned} E_{\text{loss}} &= E_{\text{e,in}} - E_{\text{cool}} - E_{\text{cap}} \\ &= 39.44 - 40.88 - 20 \times 0.39 \text{ W}\cdot\text{h} \\ &= -9.24 \text{ W}\cdot\text{h} \end{aligned}$$

Given that in experiment #5a the measured dewar temperature was always above the dewar temperature in calibration Cal 1W1, the value  $-9.24 \text{ W}\cdot\text{h}$  represents a conservative estimate of the energy loss for experiment #5a as long as the ambient temperature was the same for both runs. In this case the energy balance can be calculated:

$$\begin{aligned} E_{\text{tot,out}} &= E_{\text{cool}} + E_{\text{elec}} + E_{\text{loss}} + E_{\text{cap}} \\ &= 54.15 + 0.0 - 9.24 + 20 \times 0.99 \text{ W}\cdot\text{h} \end{aligned}$$

$$\begin{aligned} E_{\text{tot,in}} &= E_{\text{e,in}} + E_{\text{rec}} \\ &= 50.56 + 0.0 \text{ W}\cdot\text{h} \end{aligned}$$

$$\begin{aligned} E_{\text{ex}} &= E_{\text{tot,out}} - E_{\text{tot,in}} \\ &= 54.15 - 9.24 + 20 \times 0.99 - 50.56 \text{ W}\cdot\text{h} \\ &= 14.15 \text{ W}\cdot\text{h} \end{aligned}$$

This excess heat of about  $14 \text{ W}\cdot\text{h}$  is equivalent to 28% of the input energy.

Mathematical Modeling

The above method of analysis includes the assumptions that the ambient temperature and the heat transfer coefficient remained the same through the series of experiments and calibrations. Useful information may be gained by studying the temperature of the system as the power input and cooling were changed. A more powerful means of analyzing the data was to model the system using all the major energy terms (neglecting frictional energy, stirring energy, evaporative enthalpy and lead-wire resistance) as a function of time. The model thus estimated the temperature of the dewar contents as a function of time with the fitted parameters  $U$ ,  $C_{p,\text{dewar}}$ ,  $T_{\text{start}}$  and  $\Delta T_{a,e}$  or  $T_{a,e}$ . The fitting was done using a least-squares method comparing the measured dewar temperature with the calculated dewar temperature. The following assumptions were made:

- $U$  is independent of temperature
- $C_{p,\text{dewar}}$  is  $20 \text{ W}\cdot\text{h}\cdot\text{K}^{-1}$ , and

either:

- The ambient temperature recorded at the junction board ( $T_{\text{ambient}}$ ) was in error by the constant amount  $\Delta T_{a,e}$ . The effective ambient temperature ( $T_{a,e}$ ) is thus  $T_{\text{ambient}} + \Delta T_{a,e}$ ,

or:

- The ambient temperature was constant and equal to  $T_{a,e}$ .

The two models represent some conjectures as to what was most strongly influencing the heat loss from the dewar. The constant ambient temperature model goes on the assumption that the enclosure temperature controller was doing its job. The constant error in ambient temperature model assumes that the ambient temperature measurement was still following the enclosure temperature, but was being influenced by some heat source such as the nearby enclosure wall or radiant heat from the enclosure heaters.

Put in its differential form, the model is:

$$T_{\text{dewar},2} = T_{\text{dewar},1} + \frac{\int_{t_1}^{t_2} P_{c,in} dt + \int_{t_1}^{t_2} P_{rec} dt + \int_{t_1}^{t_2} -P_{cool} dt + \int_{t_1}^{t_2} -P_{elec} dt + \int_{t_1}^{t_2} -U(T_{\text{dewar}} - T_{a,e}) dt}{C_{p,\text{dewar}}}$$

Since the model was integrated numerically, it was first converted to the following difference form:

$$T_{\text{dewar},1+\Delta t} = T_{\text{dewar},1} + \frac{P_{c,in} \Delta t + P_{rec} \Delta t - P_{cool} \Delta t - P_{elec} \Delta t - U(T_{\text{dewar}} - T_{a,e}) \Delta t}{C_{p,\text{dewar}}}$$

and the integration was done using rectangular integration, because the time intervals were so short relative to the rate of change of the measured variables.

The advantage of this model becomes clear after looking at the form of the last equation and noting that the only term that depends on temperature is the heat transfer term ( $E_{loss}$ ). The significance of this is that the heat transfer term is the only one which will produce a curve in the dewar temperature/time function. Thus, in all the runs (both experiments and calibrations) where there is significant curvature in the dewar temperature, the heat transfer coefficient  $U$  can be estimated from the shape of the curve independently of other effects. This, of course, presumes that the excess heat predicted by Mills is not a significant function of temperature (over, at most, 3 K). Note also, however, that the actual estimate of  $U$  is somewhat influenced by the estimate of the ambient temperature.

The model can be judged first on how well the modeled dewar temperature matched the measured dewar temperature over the course of a run, and then (most importantly) on whether the parameters

were consistent from run to run and consistent with the estimates. Table 5 summarizes the results of the modeling of the calibration runs (including an earlier, higher-power run) and reports the fitted values of heat transfer coefficient and effective ambient temperature or error in ambient temperature. The term called Standard Error is the square root of the sum of the squares of the differences between the modeled dewar temperature and the measured dewar temperature divided by the number of time intervals in the run. The term  $E_{net}$  is defined in the same way as  $E_{ex}$  ( $= E_{tot,out} - E_{tot,in}$ ).

Table 5a - Model Fitting Results for Constant Error in Ambient Temperature

Run	Time (h)	Energy in (W·h)	$\Delta T_{a,e}$ (K)	U (W·K <sup>-1</sup> )	$E_{loss}$ (W·h)	Standard Error (K)	$E_{net}$ (W·h)
Cal 1W1	40.4	39.8	0.28	1.60	-9.35	0.060	-0.43
Cal 1W2	71.5	28.9	1.80	1.65	4.82	0.071	-1.30
Cal 15W	26.2	382.0	0.55	1.46	7.29	0.068	-1.54

Table 5b - Model Fitting Results for Constant Ambient Temperature

Run	Time (h)	Energy in (W·h)	$T_{a,e}$ (°C)	U (W·K <sup>-1</sup> )	$E_{loss}$ (W·h)	Standard Error (K)	$E_{net}$ (W·h)
Cal 1W1	40.4	39.8	35.49	1.82	-9.75	0.060	-0.84
Cal 1W2	71.5	28.9	36.72	1.37	7.73	0.095	1.61
Cal 15W	26.2	382.0	38.08	1.51	-25.92	0.140	-8.78

The figures given in the Appendix (Figures A1 to A6) present the results of the modeling for the calibration runs, showing the match between measured and calculated dewar temperature. From the standard errors in Tables 5a and 5b and from Figures A1 to A6, it is clear that the constant error in ambient temperature model is much more consistent with the experimental results. This model was therefore selected to perform the analysis of the experiments. Another reasonable assumption is that the heat transfer coefficient is constant. While some reservations might be held about the possible variation in U because of the way the top of the dewar may be placed from run to run, with such high values of U as are given in Tables 5a and 5b, it is expected that the dewar must have lost its vacuum and therefore the dewar walls must be the main area of heat loss compared with the 50 mm thick polystyrene top. The best value to assume for U would appear to be 1.46 W·K<sup>-1</sup> since this was calculated for the higher power run where errors are expected to be less.

A slightly troubling result of the modeling is the low ambient temperature during calibration run Cal 1W1. If we believe the temperature shown by the mercury thermometer represents the true effective ambient temperature, then  $T_{a,e}$  is low by at least 1.2°C. If, conversely, the ambient temperature is fixed at 36.7°C, then the best fit for the heat transfer coefficient is found to be 0.15 W·K<sup>-1</sup> and the standard error is 0.075 K. For comparison, Figure A2a shows the result of this set of parameters. Clearly, the fit is poor and the value of the heat transfer coefficient is too low to be credible.

In order to look at the experiments, two approaches could be taken. The first is to repeat the modeling following the method used for the calibration runs and look at the parameters which are fitted to see if they are reasonable. The second approach might be to modify the model slightly to allow for another parameter, namely  $E_{ex}$  with the simple assumption that  $P_{ex}$  would be constant over an experiment. The modification would be simply:

$$T_{dewar,2} = T_{dewar,1} + \frac{\int_{t_1}^{t_2} P_{e,in} dt + \int_{t_1}^{t_2} P_{rec} dt + \int_{t_1}^{t_2} -P_{cool} dt + \int_{t_1}^{t_2} -P_{elec} dt + \int_{t_1}^{t_2} -U(T_{dewar} - T_{a,e}) dt + \int_{t_1}^{t_2} P_{ex} dt}{C_{p,dewar}}$$

and thus:

$$T_{\text{dewar},t+\Delta t} = T_{\text{dewar},t} + \frac{P_{\text{c,in}} \Delta t + P_{\text{rec}} \Delta t - P_{\text{cool}} \Delta t - P_{\text{elec}} \Delta t - U(T_{\text{dewar}} - T_{\text{a,e}}) \Delta t + P_{\text{ex}} \Delta t}{C_{p,\text{dewar}}}$$

Using the first approach, we can assume that the ambient temperature error is constant over the entire experiment, i.e. it is not necessary to divide the experiments into #5a and #5b, or #6a, #6b and #6c. Table 6a presents the results of this model.

**Table 6a - Model without  $P_{\text{ex}}$**

Run	Time (h)	Energy in (W·h)	$\Delta T_{\text{a,e}}$ (K)	U (W·K <sup>-1</sup> )	E <sub>loss</sub> (W·h)	Standard Error (K)	E <sub>net</sub> (W·h)
Expt #4	93.6	142.7	1.21	1.46	0.9	0.086	0.2
Expt #5	73.0	74.0	0.91	1.46	-28.0	0.064	-0.8
Expt #6	93.4	36.7	1.70	1.46	38.7	0.089	3.5

Table 6b gives the results of the model with  $P_{\text{ex}}$  included.

**Table 6b - Models with  $P_{\text{ex}}$**

Run	Time (h)	Energy in (W·h)	$\Delta T_{\text{a,e}}$ (K)	U (W·K <sup>-1</sup> )	E <sub>loss</sub> (W·h)	Standard Error (K)	E <sub>ex</sub> (W·h)	E <sub>net</sub> (W·h)
Expt #4	93.6	142.7	1.07	1.46	20.0	0.086	19.2	0.2
Expt #5	73.0	74.0	0.82	1.46	-18.1	0.064	9.9	-0.8
Expt #6	93.4	36.7	1.65	1.46	44.8	0.078	6.0	3.5

In this model the excess energy term was found to be between 10% and 15% of the input energy. Figures are included in the Appendix showing the measured and predicted dewar temperature for all the above cases (Figures A7 to A12). There is clearly a better fit for experiment #6 when the excess heat term is included.

Table 7 summarizes the results of the energy balances, showing that E<sub>net</sub> is within ±5% of the input electrical energy, except for run #6. The difficulty however, lies in deciding whether the model parameters are reasonable and whether there is any way to choose between the two models.

**Table 7 - Overall Energy Balance Terms**

Run	-E <sub>e,in</sub> (W·h)	-E <sub>rec</sub> (W·h)	E <sub>cool</sub> (W·h)	E <sub>elec</sub> (W·h)	E <sub>loss</sub> (W·h)	E <sub>cap</sub> (W·h)	E <sub>ex</sub> (W·h)	E <sub>net</sub> (W·h)
Expt #4	-142.7	-35.3	65.4	87.1	0.9	24.9	-	-0.4
Expt #5	-74.0	-47.2	77.4	47.2	-28.0	23.8	-	-0.7
Expt #6	-36.7	-23.2	0	23.2	38.7	1.4	-	3.2
Expt #4	-142.7	-35.3	65.4	87.1	20.0	24.9	19.2	-0.4
Expt #5	-74.0	-47.2	77.4	47.2	-18.1	23.8	9.9	-0.7
Expt #6	-36.7	-23.2	0	23.2	44.8	1.4	6.0	3.2

#### 4. DISCUSSION

In the higher power experiments (#1, #2 and #3), no net excess or deficit energy was observed greater than experimental error. According to Mills, this result was consistent with operation at currents and voltages substantially higher than  $1 \text{ mA} \cdot \text{cm}^{-2}$  and 2.5 V. The lower power experiments were done within the recommended current density and voltage, and according to Mills the expected excess heat would be about 0.25 W. Various methods of analysis were applied to the results of experiments #4, #5 and #6. Some of these analyses indicated possible excess heat at approximately this level.

In experiments #4, #5 and #6, an effort was made to model the results in a consistent manner to account for the observations. The parameters that were used in the models were chosen because they were either unknown or appeared to be measured incorrectly. However, they were not expected to vary widely or completely randomly. In all models the ambient temperature correction was not very consistent. This variation may well be related to the total heat load on the system enclosure temperature control system. The effective ambient temperature was not consistent either (and the corresponding model was consequently not used to analyze the experiments), even though the temperature controller for the enclosure was absolutely steady (apparently), as was the thermometer that was placed in the enclosure during experiment #6c (at least within 0.2 K).

It seemed reasonable to assume a constant value of U from the results of the higher power calibration and use this for all analyses. However, this would only be valid if the heat transfer is just through the dewar walls. If significant heat transfer occurs through the lid, the value of U would change each time the lid was removed and replaced.

It is instructive and revealing to consider the sensitivity of the results to the different parameters used in the modeling. The most critical is the ambient temperature estimate. If we take an average heat transfer coefficient of say  $1.5 \text{ W} \cdot \text{K}^{-1}$  and an average experiment duration of 60 hours, then a 0.1 K error in the ambient temperature corresponds to an error of 9 W·h in the heat loss term, which is approximately equal to the magnitude of the expected excess heat. It is unlikely that any of our temperature measurement were within this level of accuracy and it was unfortunate that the dewar had such poor insulating properties.

In fact the above calculation for the sensitivity of the heat loss to the ambient temperature also applies to the temperature inside the dewar. It is very likely that in the unstirred dewar, there would have been significant temperature gradients, especially top-to-bottom. It would be reasonable to assume that such temperature gradients in the dewar during calibration runs would be quite different from the gradients during closed cell operation with the recombiner. More than half the heat in experiments #5 and #6 was released to the dewar contents in the top of the cell where the recombiner was placed. In other cases, calibrations or open cell operation, all or most of the heat is released through the electrolyte in the lower part of the cell. There is no obvious way to deduce the magnitude of the temperature gradients from the results presented here.

Both the temperature inside the dewar and the ambient temperature were point measurements. Total heat loss from the dewar depends on the heat lost from all parts of the dewar surface and therefore is affected by any temperature profiles either inside or outside. Point measurements can, at best, only be an indication of the average temperature. The modeling is an attempt, with only limited success, at finding an *effective* ambient temperature which is consistent with the measured temperature-time function in the dewar. Stirring the dewar contents, circulating the ambient air and using non-radiant heat in the enclosure would have significantly improved the representativeness of the point temperature measurements.

In experiment #4 an open cell was used and the off gases vented through a mass-flow transducer. With the low-voltage experiments the off-gases were typically evolved at a rate of  $3 \text{ mL} \cdot \text{min}^{-1}$  (compared to a flow rate of  $26 \text{ mL} \cdot \text{min}^{-1}$  in the higher voltage experiments). At low flow rates, the absolute accuracy of the mass-flow transducer used was a source of some concern, but from the data we have there would appear to be a higher recombination rate in experiment #4 than in experiments #1 and #2. This fits with the expected mechanism for recombination, which is the reaction between each of the gases with nascent gas bubbles at the opposite electrode — especially at the anode, which was made of the highly catalytically active material, platinum. Recombination is strongly promoted by stirring the electrolyte, as was done in these experiments. If, however, it is assumed that none of

the electrolysis gases recombine, the energy balance for this experiment (see Table 7) seems to indicate that up to 54.5 W·h of excess heat was produced ( $35.3 \text{ W}\cdot\text{h} + 19.2 \text{ W}\cdot\text{h}$ ). This figure corresponds to 38% of the electrical input energy and agrees with the amount predicted by Mills.

A major part of this work was the development of a model to simulate the heat transfer characteristics of the calorimeter. The model, which includes the thermal capacity of the dewar contents and the heat exchange through the dewar walls and top, was reasonably successful in closing the energy balance except for experiment #6. Assuming a constant ambient temperature of  $36.70^\circ\text{C}$ , the results of experiment #6 would indicate about 14 Wh of excess heat produced. This figure corresponds to 38% of the electrical input energy. This result agrees with the amount predicted by Mills.

Experiments #4, #5 and #6 stretched the capabilities of the experimental system to the limit. Any further work in this area would require more sensitive and accurate temperature-measuring devices, and a considerably more efficient dewar.

##### 5. REFERENCES

1. P.L. Hagelstein, Summary of the Third International Conference on Cold Fusion, Presented at MIT, 1993 January 16.
2. E. Storms, *Fusion Technology*, **20**, 433 (1991).
3. R.T. Bush, *Fusion Technology*, **22**, 301 (1992).
4. R. Notoya and M. Enyo, Proc. ICCF3, Dec (1992).
5. R. Mills and S.P. Kneizys, *Fusion Technology*, **20**, 65 (1991).
6. R. L. Mills, W.R. Good and J.J. Farrell in *Unification of Spacetime, the Forces, Matter and Energy*, 1992, Science Press, Pa.
7. W.A. Good, Personal Communication 1993, June 8.
8. JANAF Thermochemical Tables, Third Edition, **14**, (1), 1274 (1985)
9. Handbook of Physics and Chemistry, 71 st Edition, CRC Press, 15-30 (1991)
10. R.H. Perry and D.W. Green, *Perry's Chemical Engineers' Handbook*, 6th edition, McGraw-Hill, 1984.

## Appendix

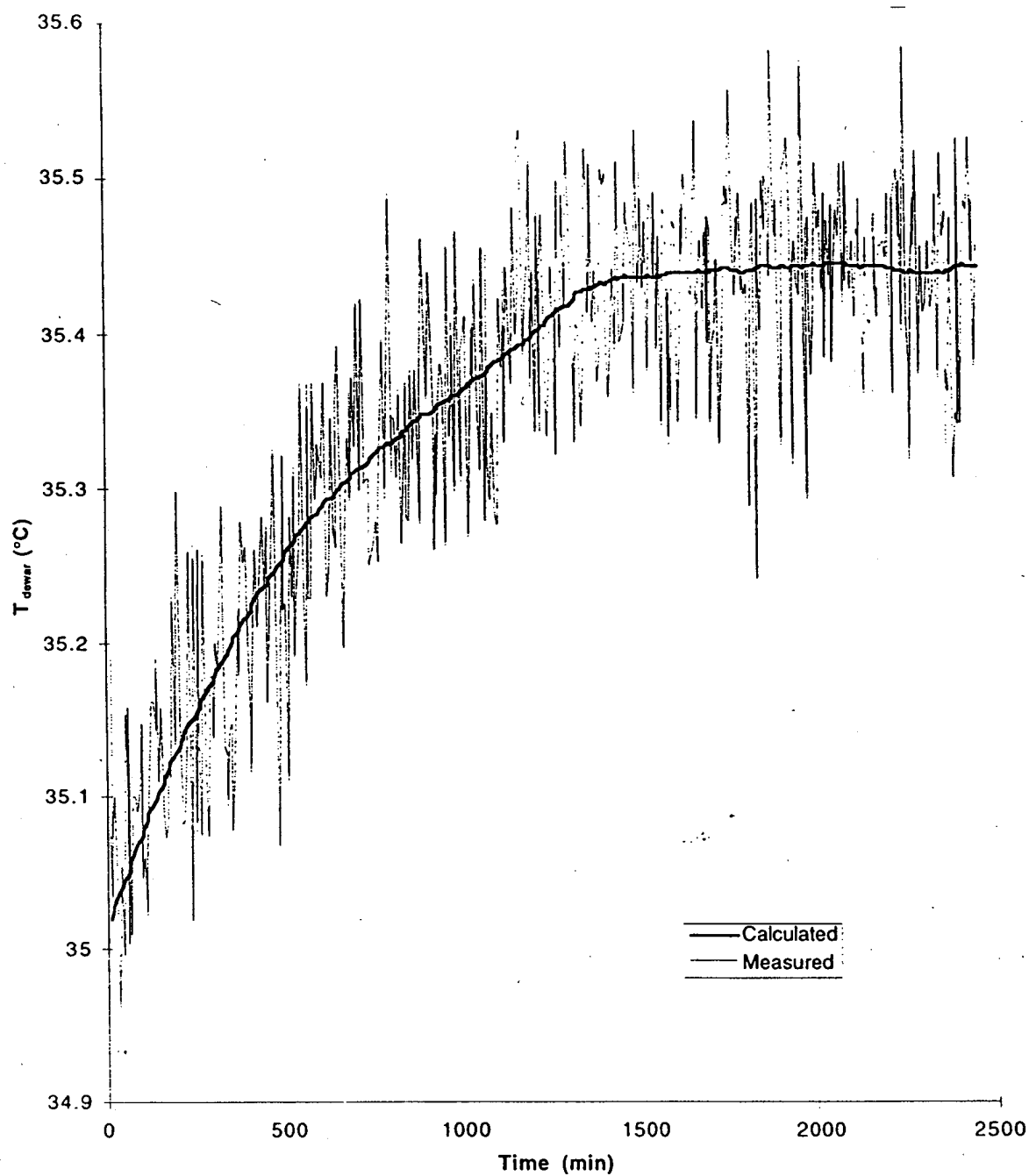


Figure A1 - Dewar Temperature Modelling in Calibration CallW1  
using Constant Error in Ambient Temperature

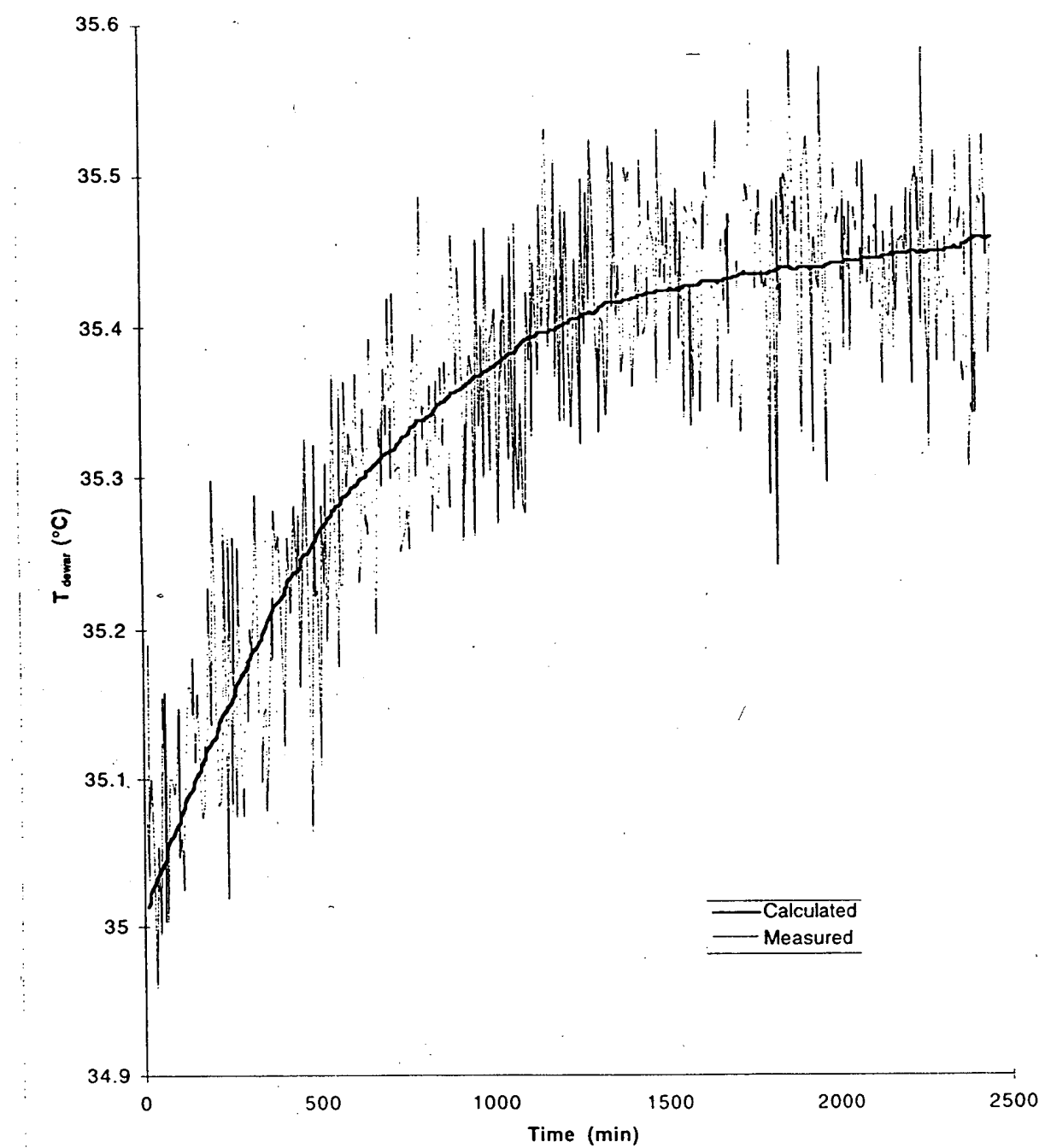


Figure A2 - Dewar Temperature Modelling in Calibration Cal1W1  
using Constant Ambient Temperature

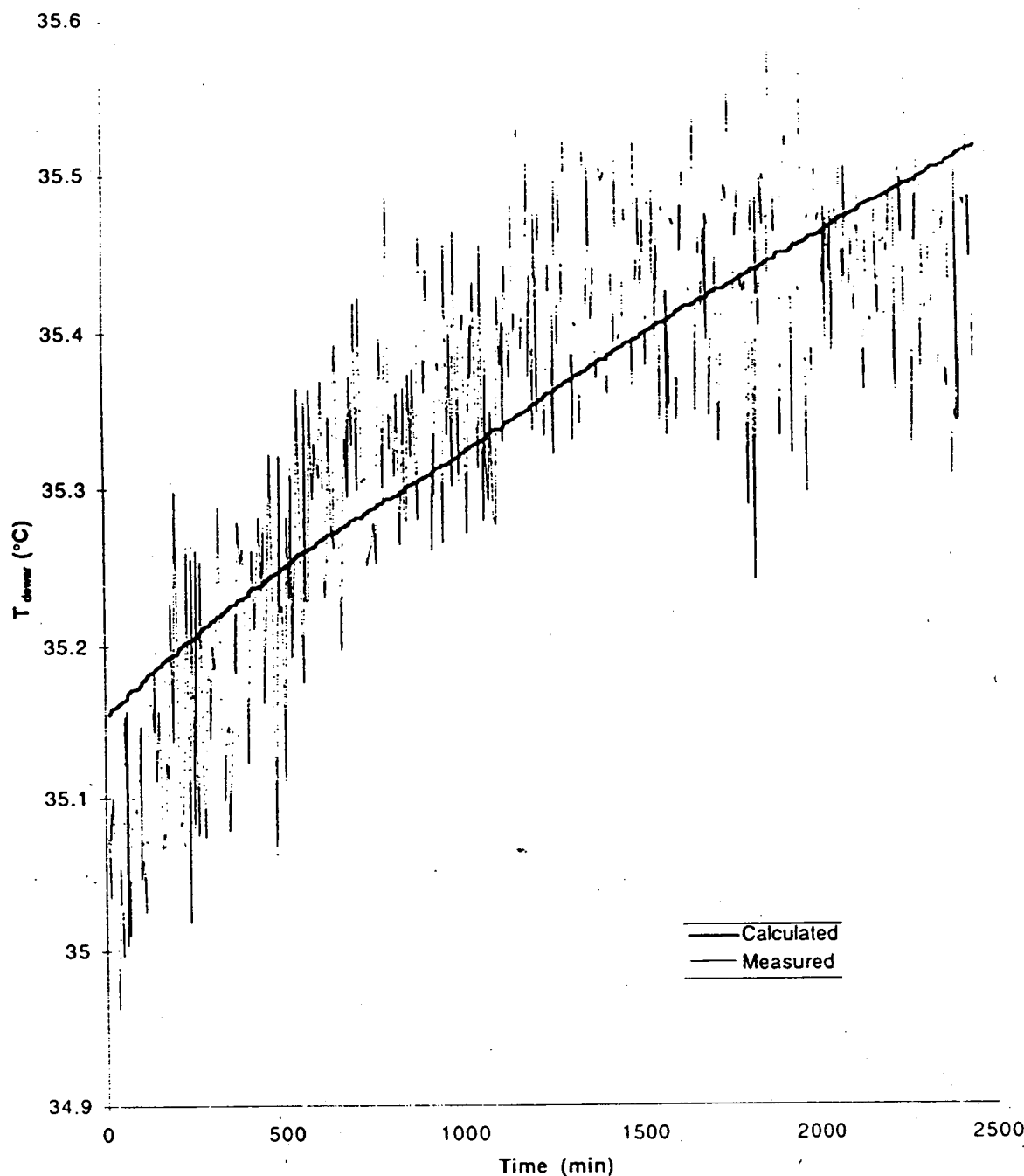


Figure A2a - Dewar Temperature Modelling in Calibration Cal1W1  
using Ambient Temperature set to 36.7°C

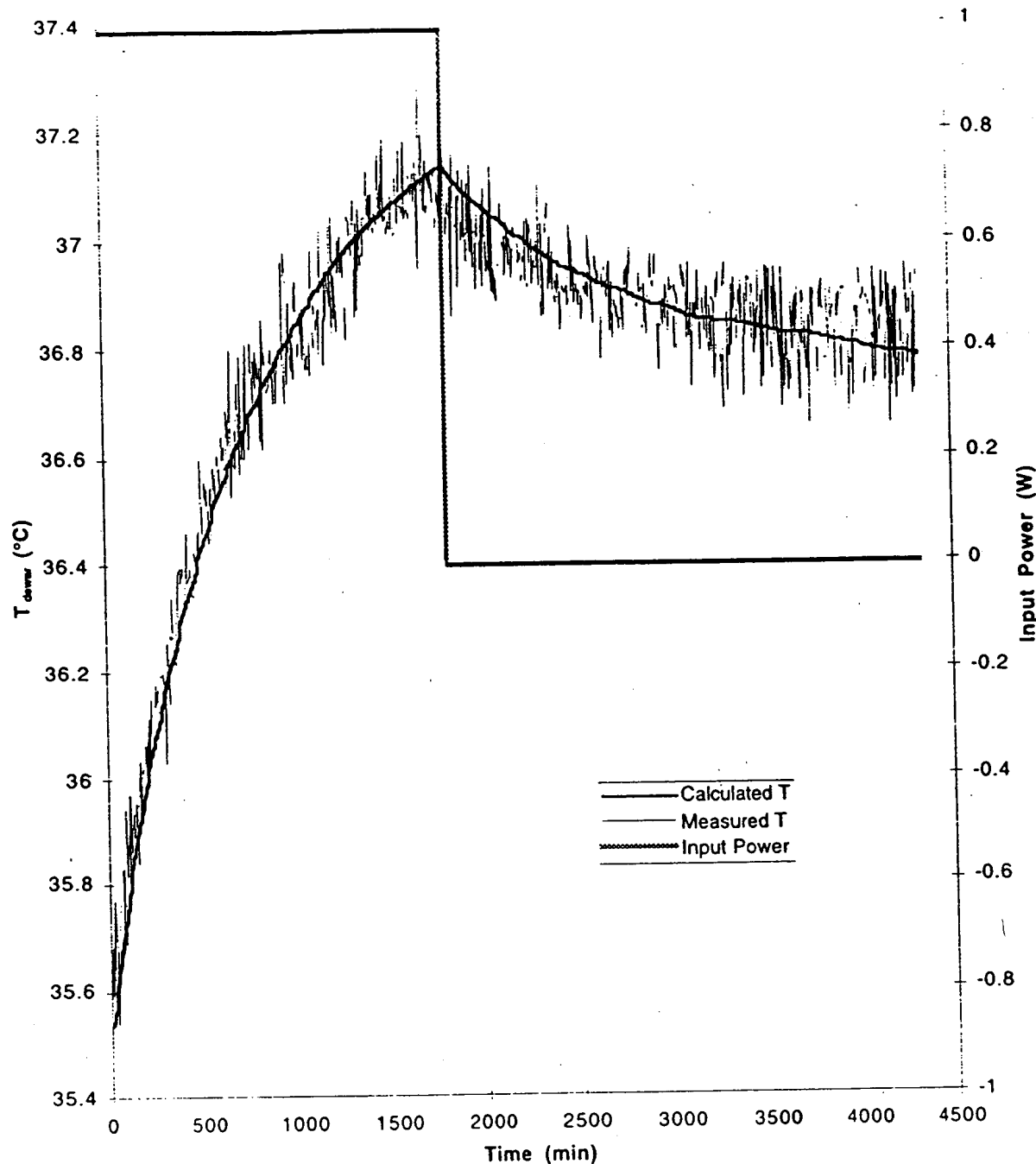


Figure A3 - Dewar Temperature Modelling in Calibration Cal1W2  
using Constant Error in Ambient Temperature

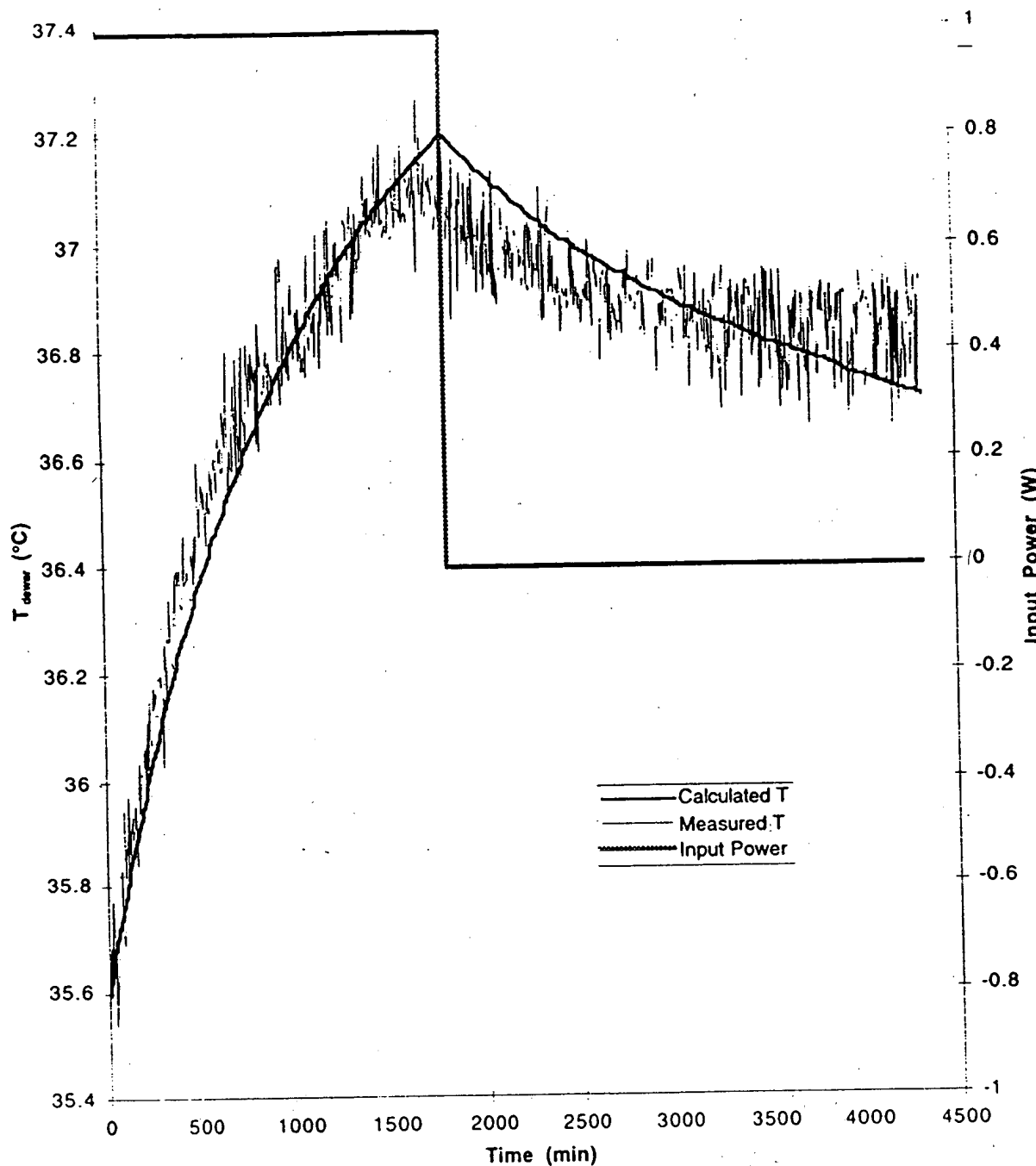


Figure A4 - Dewar Temperature Modelling in Calibration CallW2  
using Constant Ambient Temperature

38

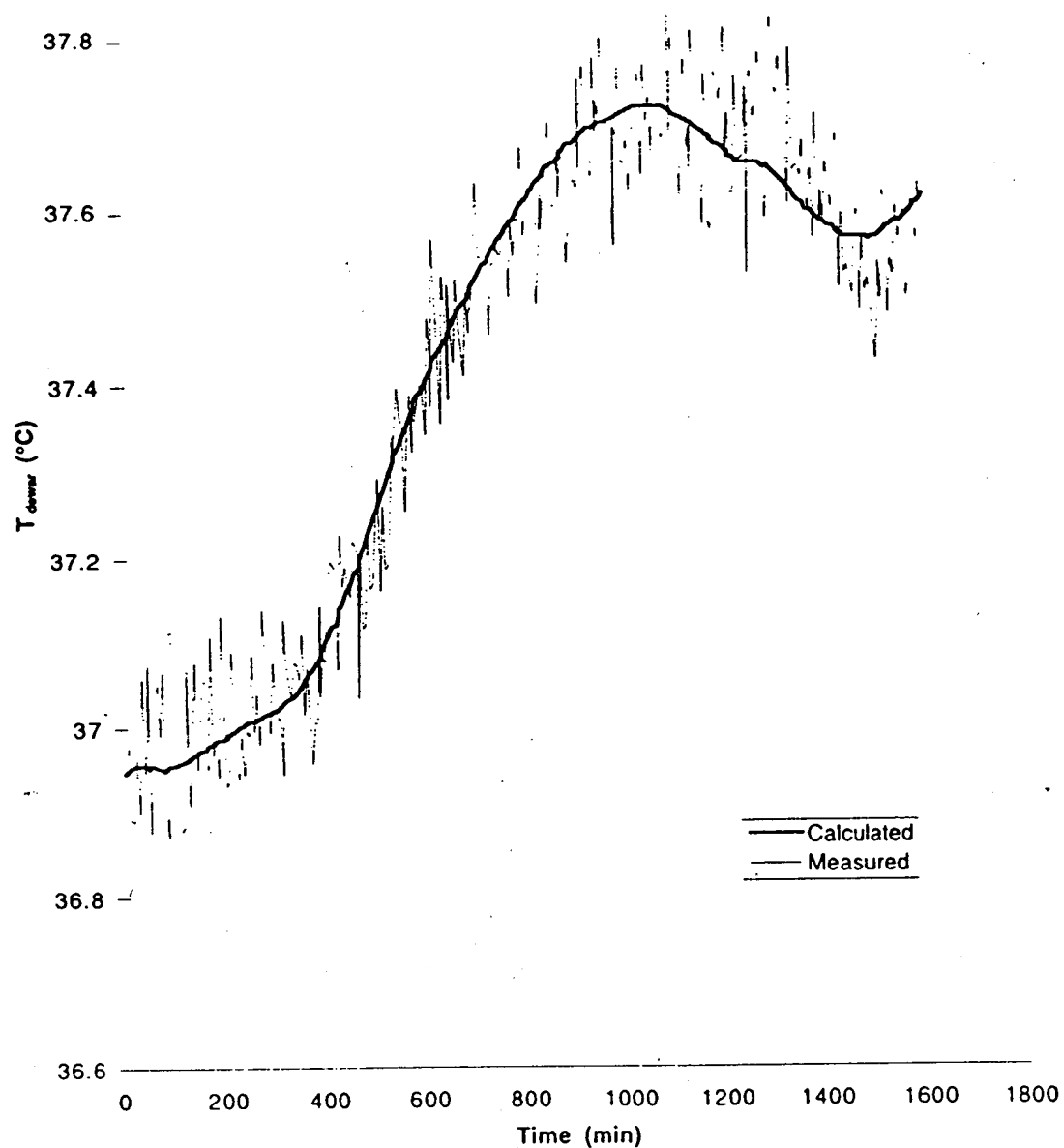


Figure A5 - Dewar Temperature Modelling in Calibration Cal15W  
using Constant Error in Ambient Temperature

38

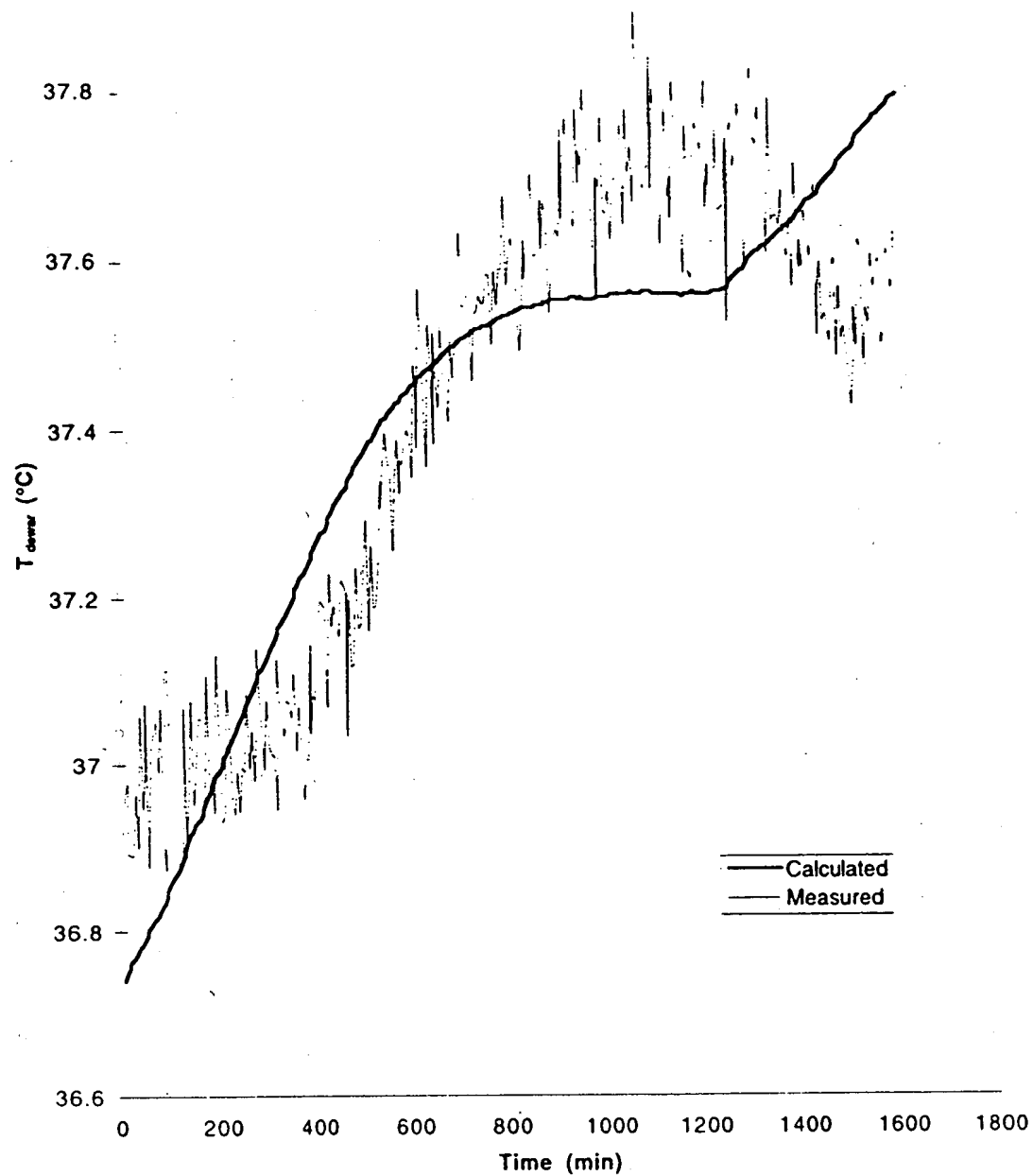


Figure A6 - Dewar Temperature Modelling in Calibration Cal15W  
using Constant Ambient Temperature

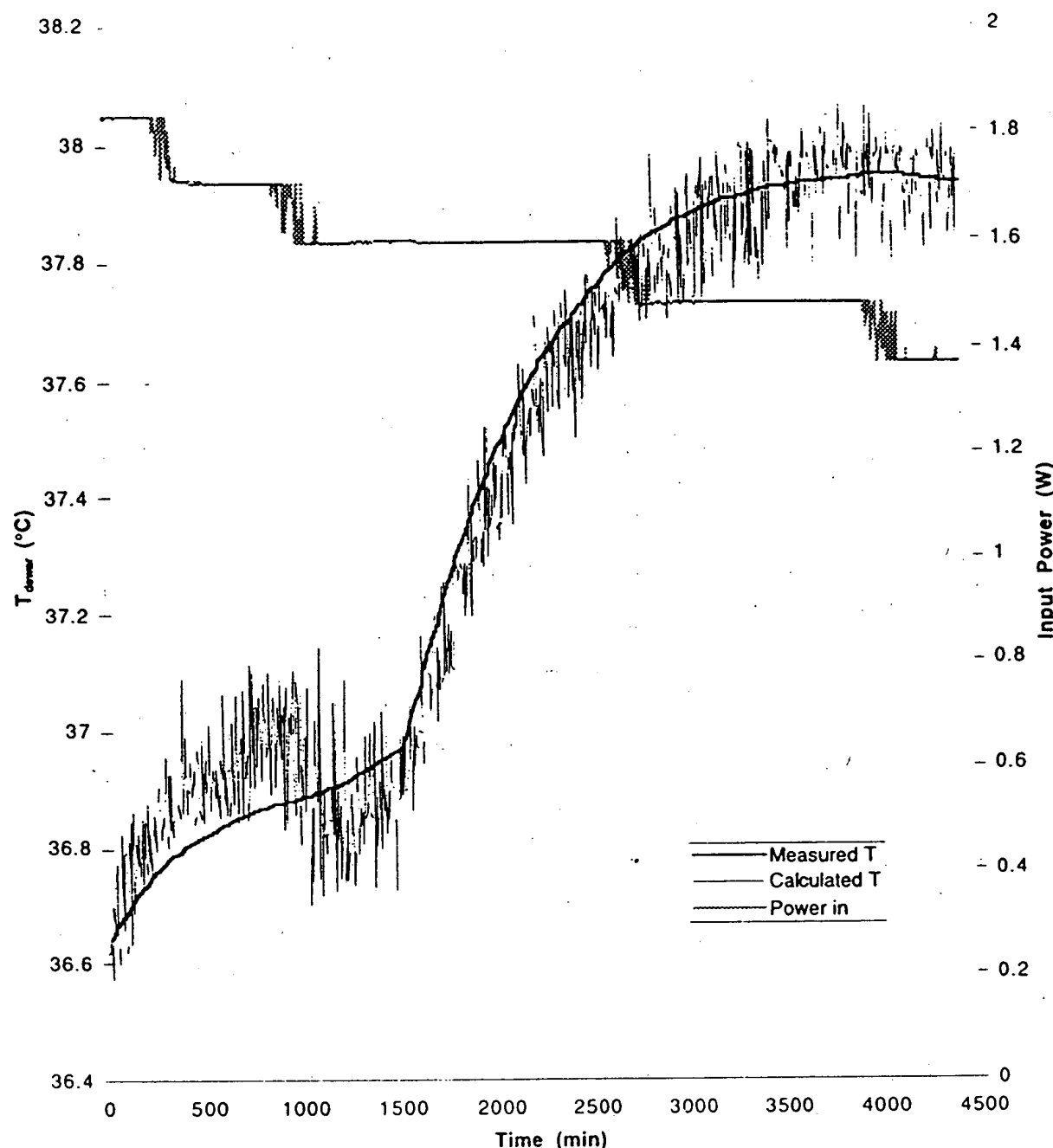


Figure A7 - Dewar Temperature Modelling in Experiment #4  
using Constant Error in Ambient Temperature and  $P_{ex}=0$

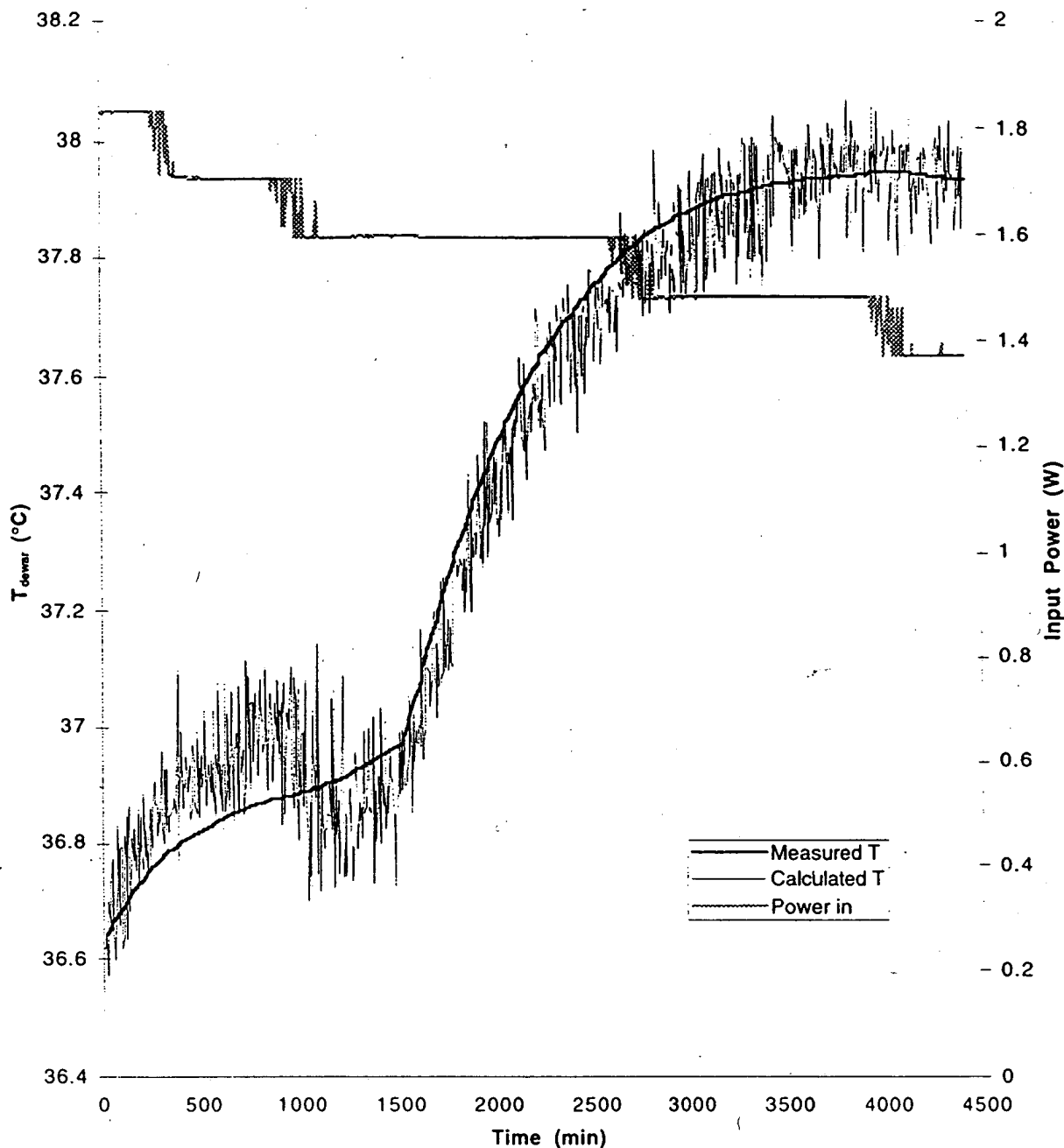


Figure A8 - Dewar Temperature Modelling in Experiment #4  
using Constant Error in Ambient Temperature and  $P_{ex} \neq 0$

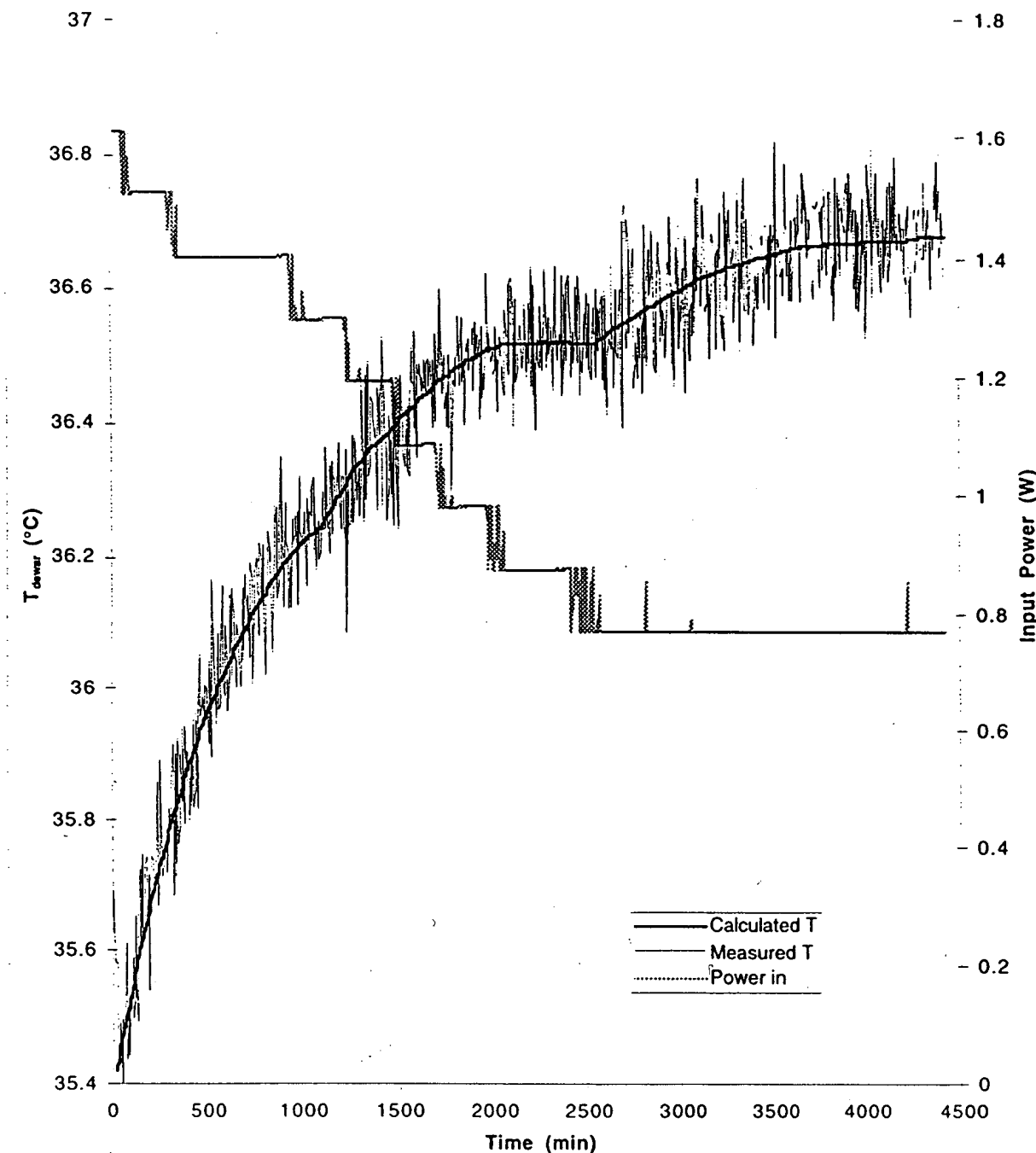


Figure A9 - Dewar Temperature Modelling in Experiment #5  
using Constant Error in Ambient Temperature and  $P_{ex}=0$

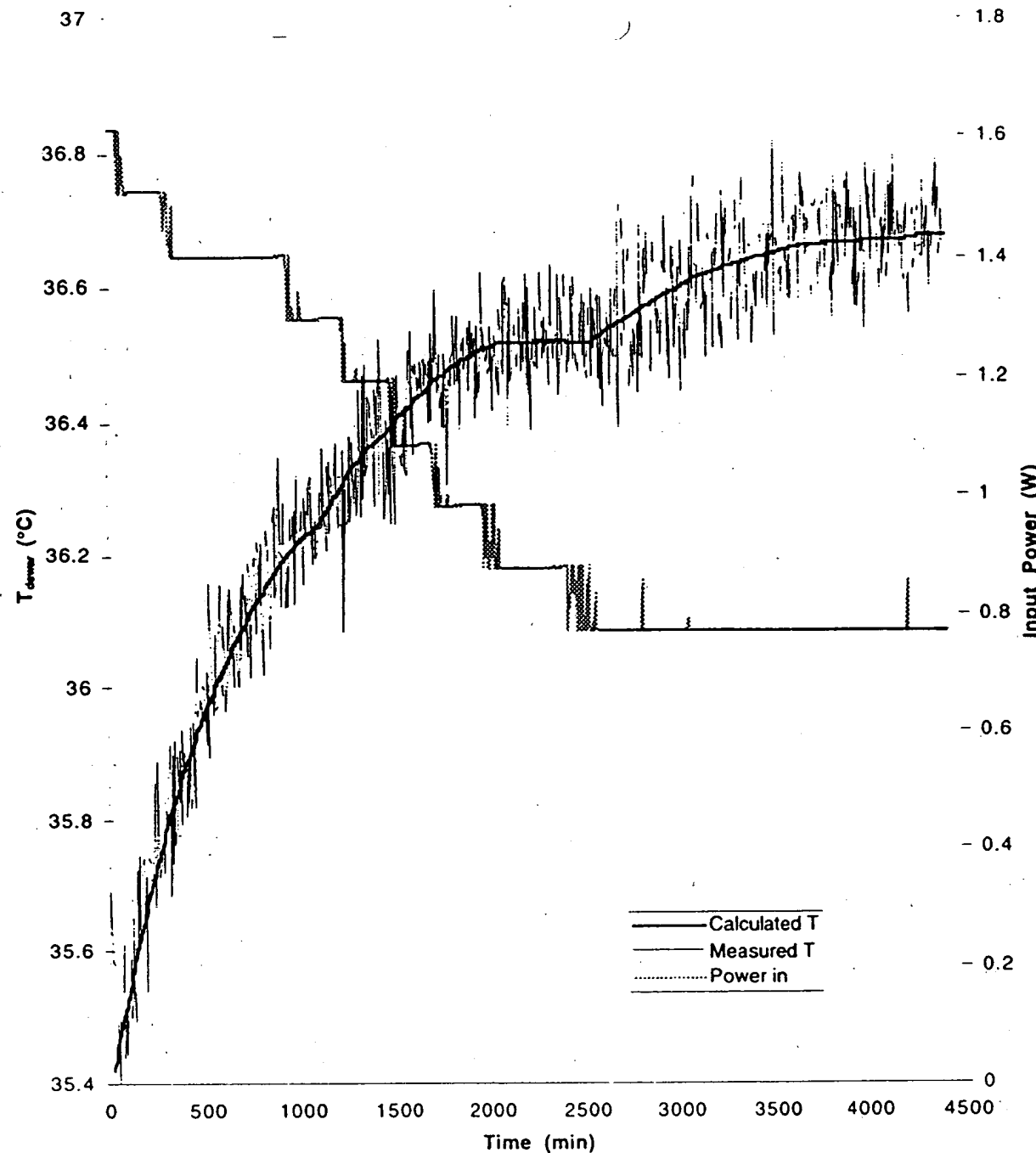


Figure A10 - Dewar Temperature Modelling in Experiment #5  
using Constant Error in Ambient Temperature and  $P_{ex} \neq 0$

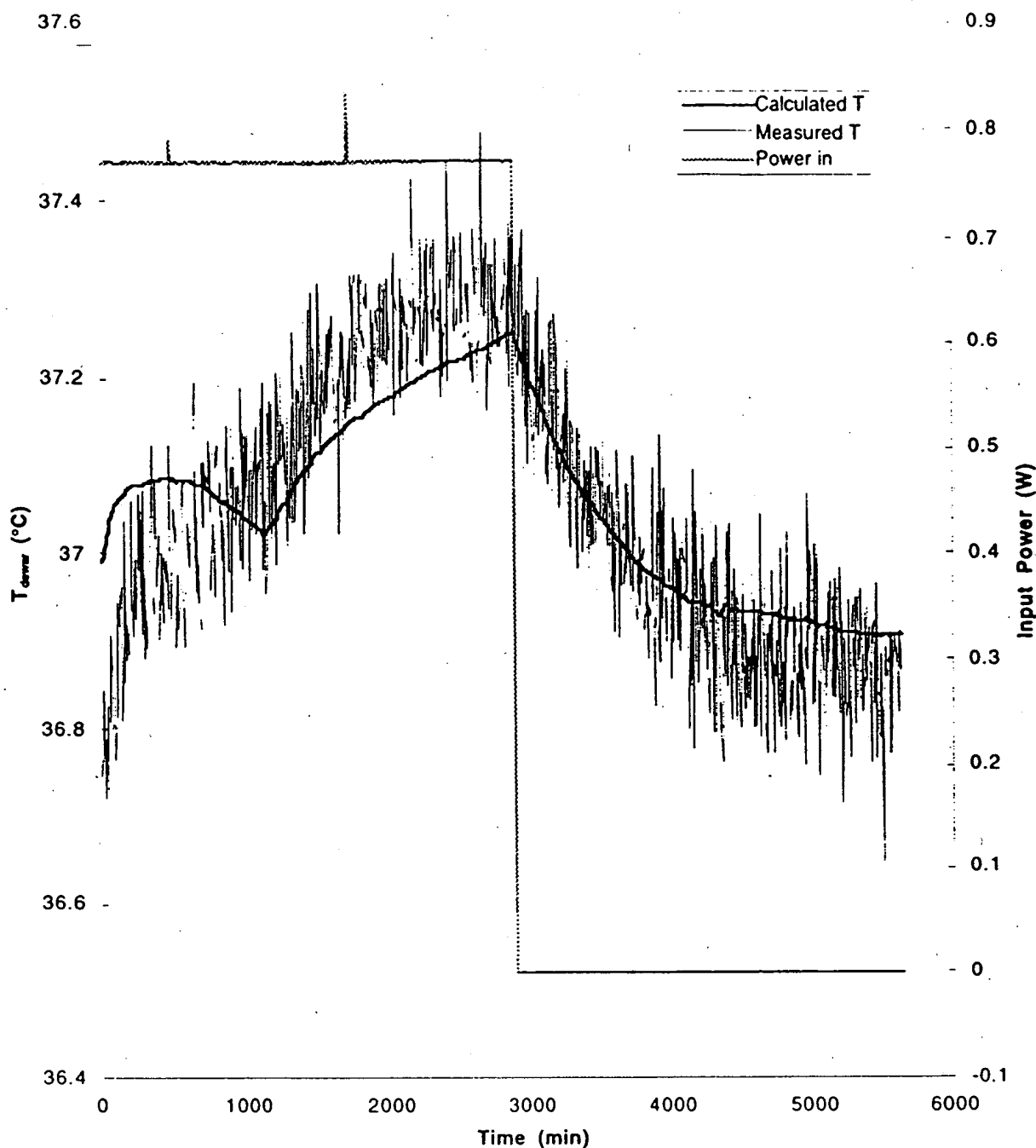


Figure A11 - Dewar Temperature Modelling in Experiment #6  
using Constant Error in Ambient Temperature and  $P_{ex}=0$

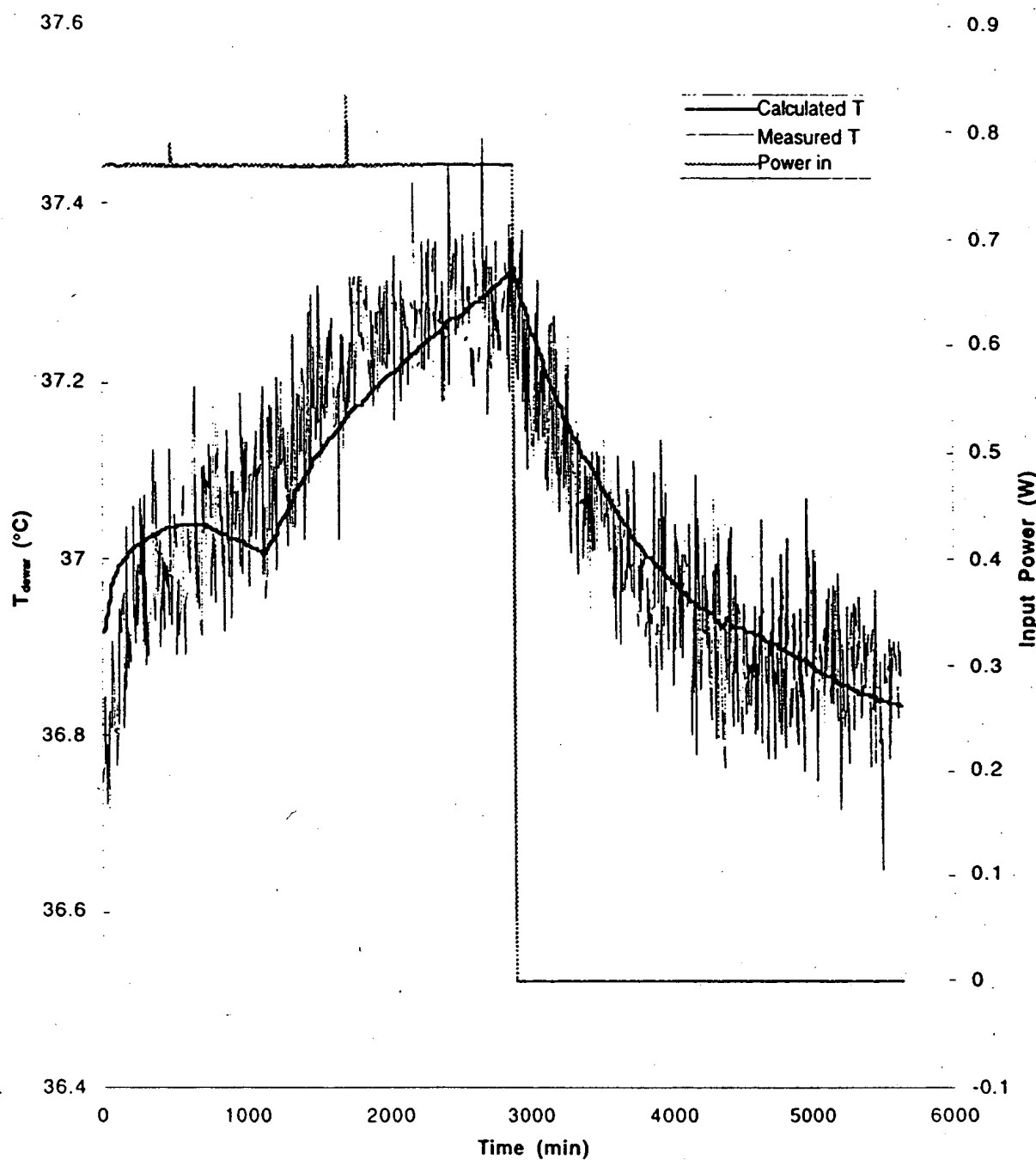


Figure A12 - Dewar Temperature Modelling in Experiment #6  
using Constant Error in Ambient Temperature and  $P_{ex} \neq 0$

In re Application of

MILLS

Appl. No. 07/825, 845

Filed:

For: ENERGY/MATTER CONVERSION  
METHODS AND STRUCTURES

---

The Hon. Commissioner of Patents  
and Trademarks  
Washington, DC 20231

Sir:

Sergei B.Nesterov, residing at 4-12 Remizova st. Moscow,  
Russia, 113186 declares and states that:

1.I received a Bachelor of Science degree in cryophysics  
engineering (physics and technology of low temperatures) , Moscow  
Power Engineering Institute ( MPEI), 1980.

2.In 1980-81 I worked as an engineer at Cryogenics Department  
MPEI, participating in development of elements of the thermal  
management of space crafts a) heat pipes; b) thermal radiator.

3. PhD degree in nuclear fusion products pumping, MPEI, 1985.  
Since 1989 I am an associate professor at MPEI Cryogenics  
Department.

4. In 1982-83 I participated in developing of systems of fusion  
reaction products pumping and regeneration.

5. I am currently the Head of MPEI Cryogenics Center and the senior manager responsible for creating a model of pumping block of nuclear fusion products for ITER project (International Thermonuclear Engineering Reactor).

My current work includes also development of technology for protective coverings, creation of highly effective systems for purification of sewage.

6. I am the author and co-author of numerous technical reports and papers, of which selected publications are shown in the attachment.

Alexei P.Kryukov, residing at 11/2-63  
Sadovaya-Chernogryazskaya st., Moscow, Russia 103064 declares and states that:

1. I received a Bachelor of Science degree in industrial heat power from MPEI in 1972.

2. I received a PhD degree in heat transfer, MPEI, 1977.

Postdoctorial - DSc(Eng) - MPEI, 1990 , Molecular Physics.

3. I am currently a Professor in Cryogenics Department, MPEI, and also a senior scientist in fundamental research of transport processes on the interphasic gas-condensate.

4. In 1976-79 together with Professor Labuntsov (MPEI) we developed an approximate method of strong evaporation and

condensation analysis. Based on the principles of the molecular kinetic theory, simple formulae were suggested for engineering practice. These formulae are valid at subsonic vapour velocities. A comparison of the calculation results with the experimental data of Niknejad and Rose ( see: Niknejad J. and Rose J.W. in Proc.Royal Soc.London.1981 Vol.378.P.305-327; Kosasie A.K. and Rose in Proc. 7-th ASME National Heat Transfer Conference San-Diego, USA, 1992 ) on strong condensation of mercury showed a good agreement. In 1986 Pong L. and Moses G.A. generalized method used by Dr. Labuntsov and me to the problem of strong condensation in the presence of a noncondensable gas (see: Pong L. and Moses G.A. in Phys.Fluids. 1986.Vol.29.No.6P.1796- 1804).

In 1987 an accurate analysis of heat-mass transfer on vapour-liquid interphase at the reflection of sound wave on this surface was made by me and Dr.Labuntsov. It was shown that for liquid metal and superfluid helium the sound reflection coefficient was very small. As a result a large part of sound energy incoming to interphase was converted into heat on this surface.

In 1983-1991 I studied the processes of evaporation and condensation on the base of the Boltzmann equation solutions. Some theoretical results for supersonic condensation were confirmed by my own experimental data at cryogenic temperatures. ¶

5. My previous work includes research and development of cryovacuum means for helium and hydrogen isotopes pumping. I also studied processes of heat transfer in superfluid helium. As a co-author of Steve Van Sciver (USA) I theoretically received a value of the recovery heat flux from boiling in superfluid helium

6. I am the author and co-author of numerous scientific papers and technical reports, of which selected publications are shown in the attachment.

Sergei B.Nesterov and Alexei P.Kryukov together declare and state that:

1. We have reviewed and understand the concept covered by the subject U.S. application No.07/825,845 of Dr.Randell L.Mills and we are personally familiar with the methods and apparatus disclosed therein.
2. We ( hereinafter MPEI ) have conducted independent experiments on nominally identical apparatus to that made by Dr. Randell Mills ( hereinafter HPC ) to check HPC's method and results, since July of 1992.
3. MPEI's experiments show 0.75 watts of heat output with only 0.3 watts of heat input. Excess energy on the order of 0.45 watts has been produced reliably and continuously over the last three months. Scintillation counter measurements show no signs of radiation external to the cell.

#### DESCRIPTION OF THE MPEI CELL

The MPEI experimental cells were assembled comprising a 1000 ml silvered vacuum jacketed dewar with a 10 cm opening. The cathode was a 7.5 cm wide by 5 cm long by 0.125 mm thick nickel foil (Aldrich 99.9 %, cold roll, clean Ni ) spiral of 9 mm diameter

by tightly rolling the nickel foil about a 9 mm rod. The rod was removed. The leads were inserted into glass tubes to insure that no recombination of the evolving gases occurred. The anode was a platinized titanium ( Engelhard Pt/Ti mesh 2 by 2 inches ) covered with 100  $\mu$  platinum series 3000 ). The cathode and anode cables were connected to terminals bolted to the cell lid. The lid was made of resin glass. A foam plastic disk was set under the lid to lessen heat losses. The disk was 1 cm thick covered by film foil. See Figure 1.

Before assembly, the anode array was cleaned in 3 M HCl for 5 minutes and rinsed with distilled water. The cathode was rinsed with distilled water.

The electrolyte solution comprised 1 liter of 0.57 M K<sub>2</sub>CO<sub>3</sub> (Alfa K<sub>2</sub>CO<sub>3</sub> 98% ).

The heater comprised a 6.6 ohm Nichrome wire. It was inserted into the glass jacket and suspended with Teflon covered leads.

It was powered by an Invar constant power (  $\pm 0.1\%$  ) supply (Model B-5-49). The heater resistance was measured by means of calibration resistor. The current (  $\pm 0.1\%$  ) was recorded with amperemeter M 903. The electrolysis current (  $\pm 0.1\%$  ) was measured by amperemeter M 903.

The temperature (  $\pm 0.1^{\circ}\text{C}$  ) was recorded with a microcomputer thermometer (MPEI). To provide temperature control copper-constantan thermocouples were used.

The temperature (  $\Delta T = T$  (electrolysis only) -  $T$  (ambient) ) and the electrolysis power were recorded regularly. The heating coefficient was determined "on the fly" by the addition of heater power at 72 hour increments where 24 hours were allowed for steady state to be achieved. The temperature  $\Delta T_2 = T$  (electrolysis + heater) -  $T$  (ambient) was recorded as well as the electrolysis power. The ambient temperature was measured from a

blank cell that comprised a closed 1 liter silvered vacuum jacketed dewar containing 1 liter of H<sub>2</sub>O placed near the electrolysis cell.

The electrolyte solution was stirred by a 0.7 cm open prolate spheroid magnetic stirring bar which was spun by a mixing motor made in Czechoslovakia.

Figure 2 shows the electrolysis cell on test.

## RESULTS

A heat balance of the cell is shown in Figure 3; some of MFEI results are shown in Table 1. From Table 1 it is clear that by growth of electrolyte temperature due to the increase of load of the additional heater electrolysis current grows at constant voltage of 3 V. Calculation method for 0.45 watts of excess power is represented graphically in Figure 4.

The theory that led to the discovery of this electrolytic process was developed by Dr. Randell Mills, HPC, Lancaster, Pennsylvania. This theory is covered by a patent application entitled "Energy/Matter Conversion Methods and Structure", and is described in the Fusion Technology article "Excess Heat Production by the Electrolysis of an Aqueous Potassium Carbonate Electrolyte and the Implications for Cold Fusion" by Dr. Mills and S. Kneizys, the article entitled "A Unified Theory Derived from First Principles" (submitted to the Physical Review for publication by Dr. Mills and W. Good), the article entitled "Two Electron Atoms and Elastic Electron Scattering by Helium" (submitted to Physical Review for publication by Dr. Mills) and the books entitled "The Grand Unified Theory", by Dr. Mills and Dr. J. Farrell, "Unification of spacetime, the forces, matter and energy" by R. Mills.

Under the Mil' theory the predominant source of heat is believed to be an electrocatalytically induced reaction whereby hydrogen atoms undergo transitions to quantized energy levels of lower energy than the conventional "ground state". These lower energy states correspond to fractional quantum numbers. The hydrogen electronic transition requires the presence of an energy hole of approximately 27.2 eV provided by electrocatalytic reactant(s) (such as  $\text{Pd}^{2+}/\text{Li}^+$ ,  $\text{Ti}^{2+}$ , or  $\text{K}^+/\text{K}^+$ ), and results in "shrunken atoms" analogous to muonic atoms. Calorimetry of continuous electrolysis of aqueous potassium carbonate ( $\text{K}^+/\text{K}^+$  electrocatalytic couple) at a nickel cathode was performed in the calorimetry cells. Total power out exceeded total input power by a factor of 2.5 as described, above.

MPEI tests results are summarized as follows:

1. Evaluation of the electrolyte after three months operation shows no significant change in its density and molar concentration.
2. The cell was disassembled and inspected after over one month of operation at 0.1 amper. This inspection showed no visible signs of a reaction between the electrodes and electrolyte. The cell was re-assembled and is operating as before, producing excess heat for three months.
3. Measurements of neutrons were not considered necessary since light water is used in place of deuterium. A scintillation counter was placed next to the cell. No radiation levels above background were detected indicating that nuclear reactions are not involved.
4. Water makeup rates match the Faraday usage plus evaporation.

We declare further that all statements made herein of our own knowledge are true and that all statements made on information and belief are believed to be true; and further that these statements

and the like [ ] made are punishable by fine or imprisonment, or both, under Section 1001 or Title 18 of the United States Code and that such willful false statements may jeopardize validity of the application or any patent issuing thereon.

**Figure 1. CELL ASSEMBLY**

---

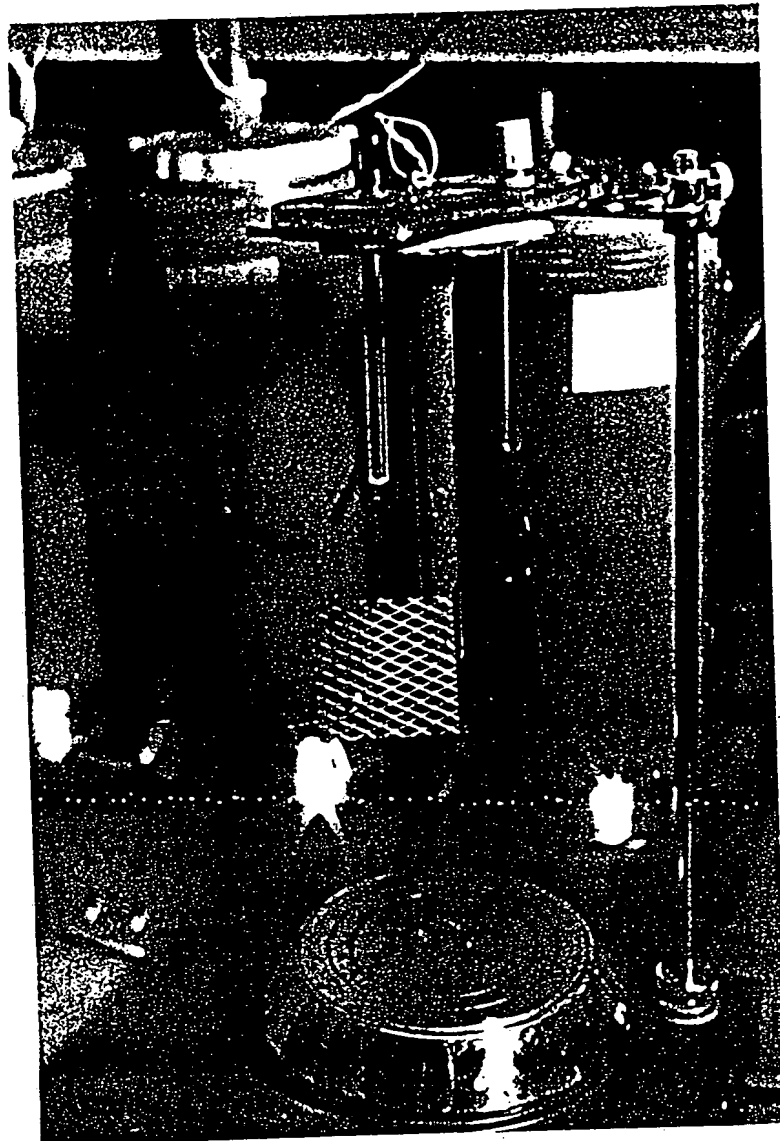


Figure 2. ELECTROLYTIC CELLS ON TEST

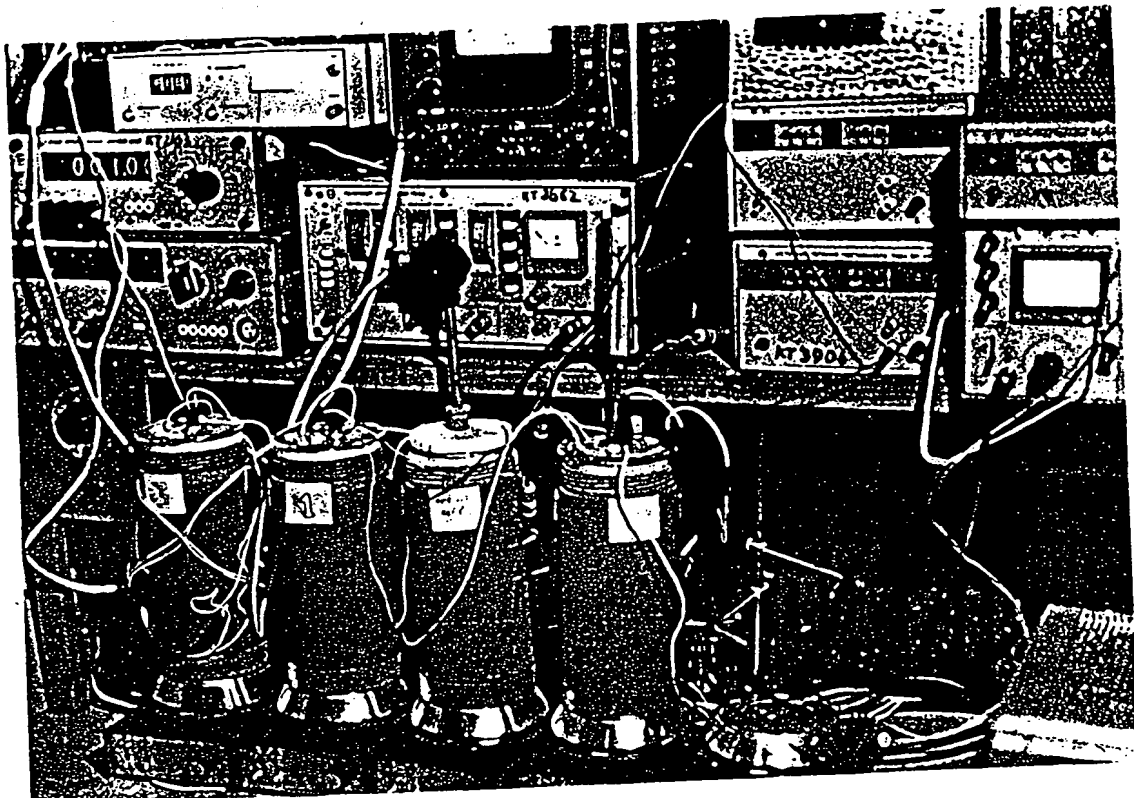
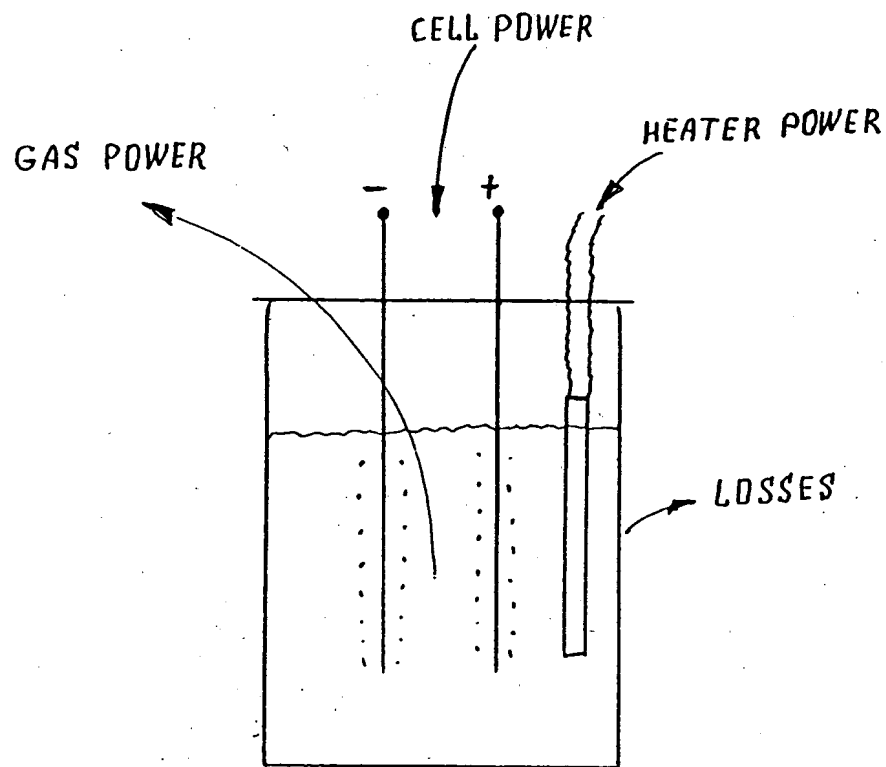


Figure 3. CELL HEAT BALANCE



$$\text{cell power} = VI$$

$$\text{gas power} = 1.48 I$$

$$\text{ohmic power} = (V - 1.48) I$$

$$\text{heater power} = V_H I_H$$

Losses - measured incrementally

Figure 4. METHOD FOR CALCULATING  
EXCESS POWER

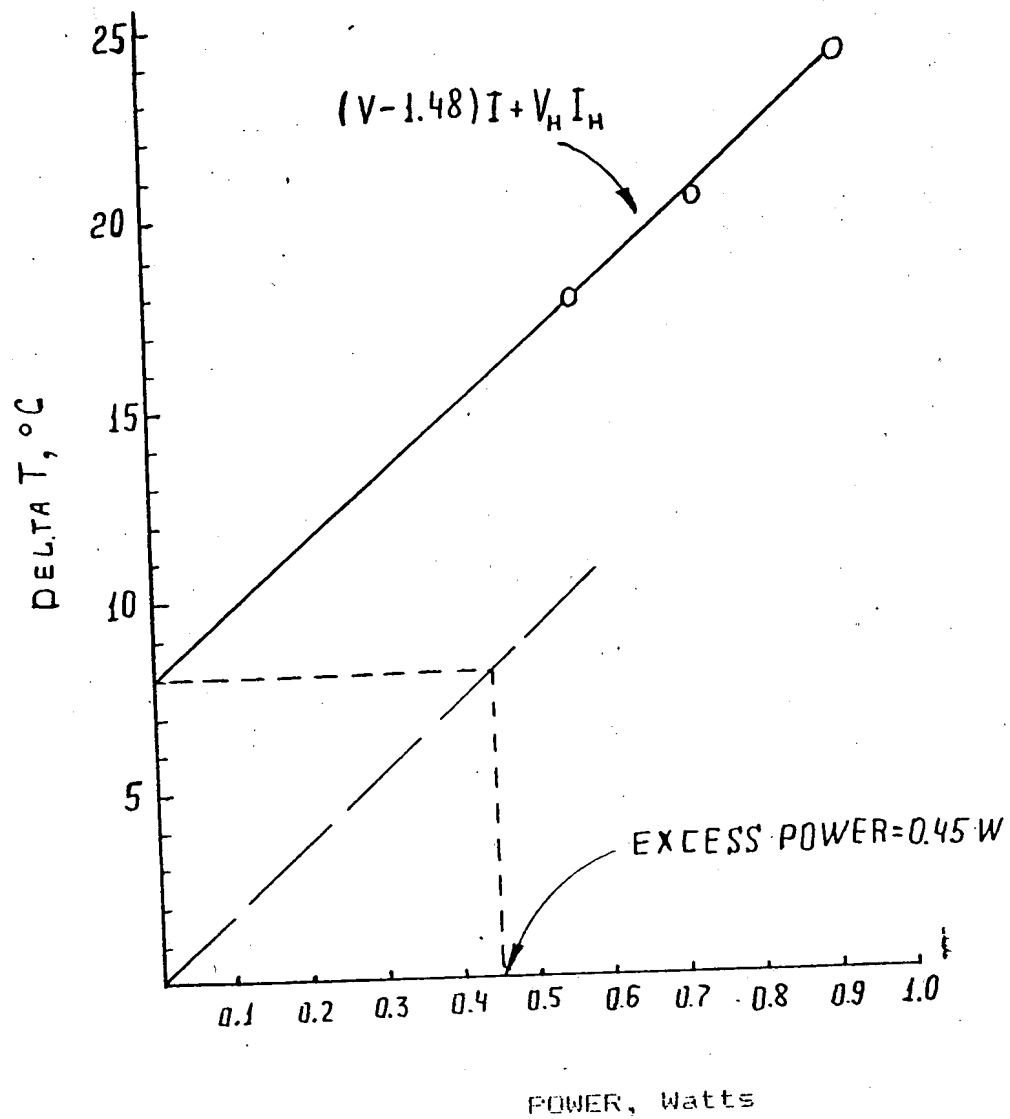


TABLE 1. Summary of MPEI Test Results

Input Conditions			Output Conditions				Output Input
V (Volts)	A (Amps)	Total Input Power=VI (Watts)	Total Output Power (Watts)	Subcomponents (Watts)			
				Gas 1.48I	Excess	Ohmic Heating = (V-1.48)I	
3.00	0.100	0.300	0.750	0.148	0.450	0.152	2.50
3.00	0.107	0.321	0.771	0.158	0.450	0.163	2.40
3.00	0.121	0.363	0.813	0.179	0.450	0.184	2.24

ATTACHMENT

Sergei B.Nesterov

Head of MPEI Cryogenics Center

Kryukov A.P. and Nesterov S.B. Investigation of helium cryosorption on layers of condensed argon. Book: Proceed. of III All-Union Conf. on Engineering Problems of Fusion Reactors: M.:TSNII-atominform, 4, 1984.

Kryukov A.P., Nesterov S.B.. Sidorov E.V. Helium cryosorption by layers of condensed gases. VANT, series Thermonuclear Fusion, 1, 1986.

Koresheva E.R, Kryukov A.P., Nesterov S.B., Nikitenko A.I. Dependence of sorptional properties of argon and nitrogen cryolayers on formation conditions. Soviet Physics - Lebedev Institute Reports. Allerton Press, Inc., N.Y.10011. Vol.1. 1987.

Nesterov S.B. Untersuchungen zum Prozess der Kryosorption von  $^4\text{He}$ . 17 Symposium Tieftemperatur-Physik und Tieftemperatur-Technik, Dresden, 1988.

Gurevich L.S., Nesterov S.B., Kryukov A.P. and Bichkov A.I. Helium cryosorption at temperature lower than 4.2 K.. Plasma devices and Operations, 1, 1991.

Nesterov S.B., Kryukov A.P. Helium and hydrogen pumping by layers of condensed gases. Vacuum Science and Physics, 1, 1992.

book: Gurevich L.S., Kryukov A.P., Nesterov S.B. and Saksaganski G.L. Cryosorptional devices of vacuum pumping. Moscow, 1991.

Kryukov A.P.  
Professor of MPEI Cryogenics Department

Labuntsov D.A., Kryukov A.P. Analysis of intensive evaporation and condensation. Int.J. Heat Mass Transfer, 22, 1979.

Kryukov A.P., Van Scriver S.W. Calculation of the recovery heat flux from film boiling in superfluid helium. Cryogenics, 9, 1981.

Kryukov A.P., Mlynsky A.V., Voronin A.V., Shishkova I.N., Cheremissine F.G. Creation of cryovacuum systems on the base of simulation in rarefied gases. Proc. 4-th Int. Conf. on Computational Methods and Experimental Measurements, Computers and Experiments in Mechanics, Capri, Italy, 1989.

Kryukov A.P., Kolesnikov N.V. Some ways of film condensation intensification. Proc. 2-nd Int.Symp. on Condensers and Condensation, Univ. of Bath, U.K., 1990.

Kryukov A.P.. Strong subsonic and supersonic condensation on a plane surface. Proc. 17-th Int. Symp. on Rarefied Gas Dynamics, ed. by A.E. Beylich (VCH, Weinheim), 1991.

Kryukov A.P. One-dimensional steady condensation at vapour velocities comparable with sound velocity. Izv. AN USSR. Mech.Fluid and Gas, 3, 1985.

Labuntsov D.A., Kryukov A.P. Reflection of sound from free surface of liquid. Teplosif. Vys.Temp., 25, 1987.

Kryukov A.P. The influence of condensation coefficient on the vapour flow at condensation with sub- and supersonic velocities. Izv. AN USSR, Mech. Fluid and Gas, 2, 1988.

Kryukov A.P., Mlynsky A.V. Investigation of nitrogen condensation process in molecular-viscous regime. ZPMTF /English Translation: J.Appl.Mech. and Techn. Phys./4, 1988.

Kryukov A.P., Dubovitsky Y.A., Mlynsky A.V. Experimental determination of sticking coefficients of helium ion desublimate gases at low temperatures. Poverhnost, 10, 1989.

Aristov V.V., Kryukov A.P., Cheremissine F.G., Shishkova I.N. The Boltzmann equation solving for the plane jet flows with condensation on a cryopanel. Zh.Vych. i Mat. Fiz., vol.31, No.7 1991.

textbook: Labuntsov D.A., Yagov V.V., Kryukov A.P. Fundamentals of Two-Phase Systems Mechanics. Moscow Powe Engineering Institute, 1988.

By: S. Nesterov

Sergei B.Nesterov

Date: 2/26/93

By: A. Kryukov

Alexei P.Kryukov

Date: 2/26/93

USA EMBASSY, MOSCOW

On this, the 26th day of February, 1993, before me a notary public, the undersigned officer, personally appeared Sergei B.Nesterov and Alexei P.Kryukov, known to me (or satisfactorily proven) to be the persons whose names are subscribed to the within instrument, and acknowledged that they executed the same for the purposes therein contained.

In witness whereof, I hereunto set my hand and official seal.



Notary Public

**THOMAS J. HUSHEK**  
Vice Consul of the United  
States of America

Russian Federation .....  
Moscow Oblast .....  
City of Moscow .....  
Embassy of the United States of America  
Consular Section .....

## **HydroCatalysis Power Technology**

Statement of  
**Dr. Randell L. Mills**  
HydroCatalysis Power Corporation  
Greenfield Corporate Center  
1860 Charter Lane  
Lancaster, PA 17601  
Before the  
Subcommittee on Energy  
of the  
Committee on Science, Space, and Technology  
U. S. House of Representatives  
May 5, 1993

## **Abstract**

HydroCatalysis Power Corporation (HPC) has an extensive theoretical and experimental research program of producing energy from light-water electrolytic cells. HPC and Thermacore Inc, Lancaster, PA are cooperating in developing a commercial product. (Thermacore is a well respected defense contractor and its expertise is in the field of heat transfer). Presently, all of the demonstration cells of HPC and Thermacore produce excess power immediately and continuously. Cells producing 50 watts of excess power and greater have been in operation for more than one year. Some cells can produce 10 times more heat power than the total electrical power input to the cell. A steam-producing prototype cell has been successfully tested. The source of excess energy is **not** from fusion or other nuclear reactions. Energy is released in a catalytic process whereby the electron of the hydrogen atom is induced to undergo a transition to a lower electronic energy level than the "ground state" as defined by the usual model of the atom. The lower energy states of hydrogen have been identified in nature. HPC and Thermacore are conducting other experiments to demonstrate that this lower-energy form of hydrogen is the "ash" of heat producing cells. A summary of the technology follows:

## **HydroCatalysis Technology**

HydroCatalysis technology is an almost unlimited source of energy released from the hydrogen in ordinary water. An electric current is passed through water to generate hydrogen atoms. Ions present in the reaction vessel induce the electrons to go to energy levels lower than the "ground state", and heat energy is released. Many of the theoretical and practical aspects have been solved. The theory is published in a book entitled "Unification of Spacetime, the Forces, Matter, and Energy" (Randell L. Mills, Science Press, 1992). The book gives equations, derived from first principles, which unify the partial theories of chemistry and physics (See Appendix I).

Ten experimental parameters of the energy cells have been studied that increase the power output. A power output 10 times the ohmic power input has been obtained. The details of these experiments were published in the August 1991 issue of Fusion Technology (Mills, R., Kneizys, S., "Excess Heat Production by the Electrolysis of an Aqueous Potassium Carbonate Electrolyte and the Implications for Cold Fusion", Fusion Technology, 210, (1991), pp. 65-81). The work has been replicated by scientists who are specialists in the field. The experiment has been scaled-up by a factor of one thousand, and the scaled-up heat cell results have been independently confirmed by Thermacore Inc. Patents covering the

compositions of matter, structures, and methods of the HydroCatalysis process have been filed by HPC worldwide with a priority date of April 21, 1989. HPC and Thermacore are presently fabricating a steam-producing demonstration cell.

If heavy water is used in place of normal water, fusion of deuterium atoms can occur and can produce small amounts of tritium and other nuclear particles as reported by many research groups reporting "cold fusion". However, the small number of nuclear particles emitted can only account for a billionth of the heat released, and the fundamental nature of the phenomenon is physical/chemical, and not nuclear. A complete description of this process can be found in the works cited above.

### **Applications**

The technology can generate enormous amounts of heat using ordinary water. The implications of this development are extremely significant. The heat from this process can be used to meet the United States' demand for energy cleanly and cheaply. Over time, it appears to be possible to phase out all coal-fired and oil-fired electric power plants. This would end global warming and abate air and water pollution. Moreover, it may be possible to phase out nuclear power plants.

One of the conversion products of this process, hydrogen, is an excellent fuel, which could be used to run cars, buses, and trains cleanly. When hydrogen is used as a fuel, the combustion product is water. The HydroCatalysis process is the basis of an ecologically sound energy system that starts with water and ends with water. In light of the fact that the Earth's surface is largely water, HPC now possesses a clean energy source that will last as long as the sun itself.

### **Controversy**

There are presently two major objections to HydroCatalysis energy technology:

1.) What is the ash?

The majority of evidence indicates that even if nuclear product signals are real and different from background signals then the heat reported is orders of magnitude larger than that corresponding to these low levels of nuclear products. Therefore, the skeptics argue that the heat measurements are erroneous. In actuality, the heat measurements are accurate, and the source of the heat is not from a nuclear reaction. It is due do a heat releasing reaction whereby a lower chemical energy form of hydrogen is formed.

2.) Theoretical: According to quantum mechanics, hydrogen can only have energies given by the following Rydberg formula

$$E_{\text{photon}} = \frac{e^2}{4\pi\epsilon_0 a_0} \left[ \frac{1}{n_1^2} - \frac{1}{n_2^2} \right] = \hbar\nu \quad (1)$$

where  $n_1$  and  $n_2$  are integers. Mills' theory predicts that in addition to the energy states of hydrogen given by Eq. (1) with  $n_1$  and  $n_2$  being integers, new lower energy states are possible given by Eq. (1) with  $n_1$  and  $n_2$  being fractions. See Figure 1. The lower energy states of hydrogen have been assigned experimentally. The Mills theory predicts exactly the spectral observations of the extreme ultraviolet background emission from interstellar matter (given by Eq. (1) with  $n_1$  and  $n_2$  being fractions), which characterizes dark matter, and HPC is conducting further verification of data that demonstrates that the lower-energy form of hydrogen is the "ash" of heat producing cells.

## Plan

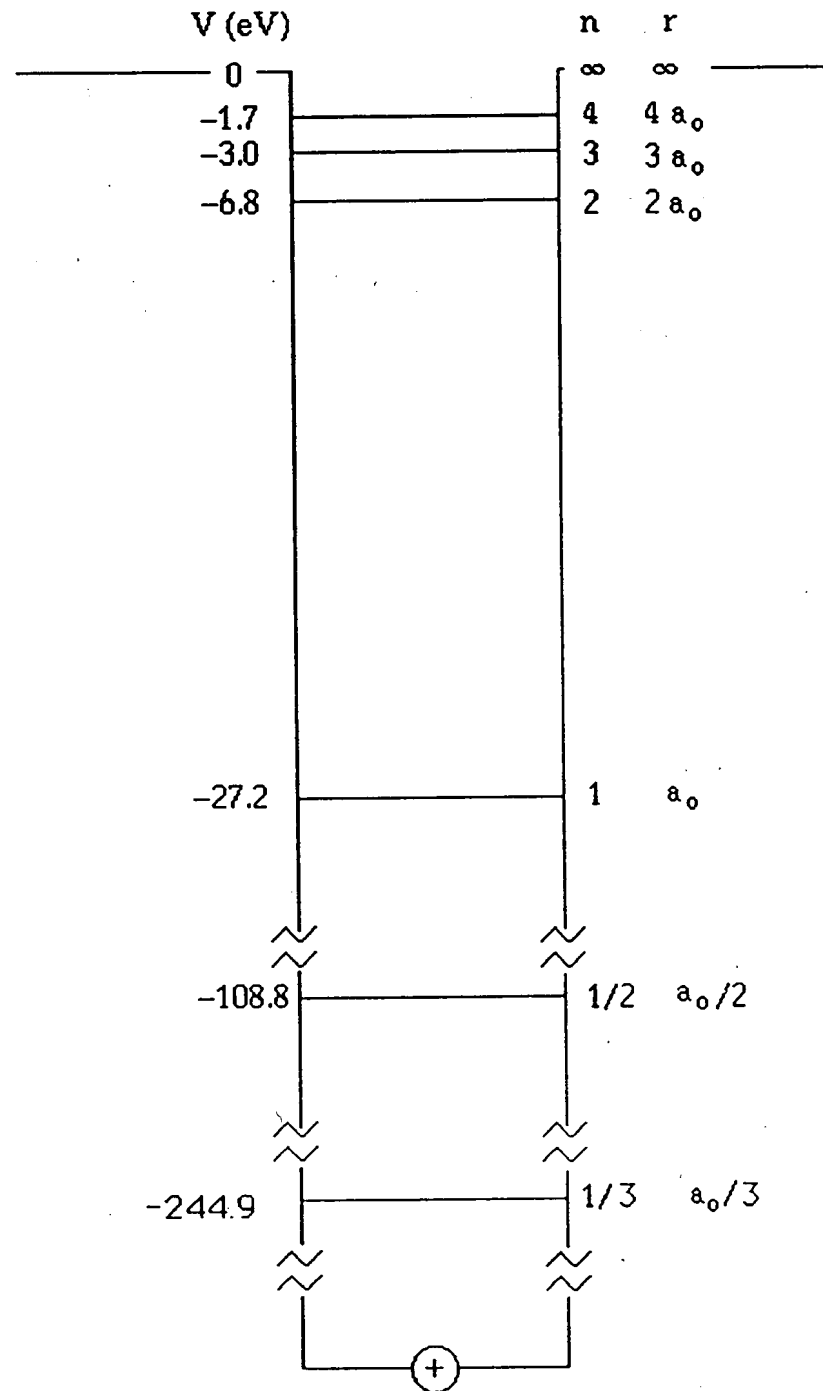
HPC's technology is revolutionary. In order to warrant a large scale research and development program from industry and government, it is apparent that four critical goals must be achieved. HPC has elected to prove all aspects of the technology. These goals are as follows:

- 1.) A Complete Theory
- 2.) Demonstrate that Lower-Energy Hydrogen is Ubiquitous in Nature
- 3.) Identification of the Lower-Energy Hydrogen in the Lab as Produced by Excess Heat Producing HPC Cell
- 4.) Develop an Incontrovertible Power Demonstration Device

### Success to date:

- 1.) Theory Published and Book Will Soon Be Available Throughout the World Through a Reputable Publishing Company
- 2.) Theory Reviewed by Academia with Their Support
- 3.) Assignment of Dark Matter Spectrum Submitted for Publication Which Demonstrates that Lower-Energy Hydrogen is Ubiquitous in Nature
- 4.) Paper Submitted on Catalytic Couples- Other Researchers Results Explained
- 5.) Thermacore Awarded Contract by a Federal Government Agency to Develop HydroCatalysis Power Equipment
- 6.) EPRI Contract Awarded to Canadian National Lab
- 7.) Technological Advances by HPC and Thermacore
- 8.) Large Scale Steam Producing Incontrovertible Demonstration Device- Reduction of the Technology to Practice Presently Being Scaled Up from a Prototype Device
- 9.) Independent Replication by Other Labs
- 10.) Identification of the Lower-Energy Hydrogen in the Lab - Identification of the "Ash"

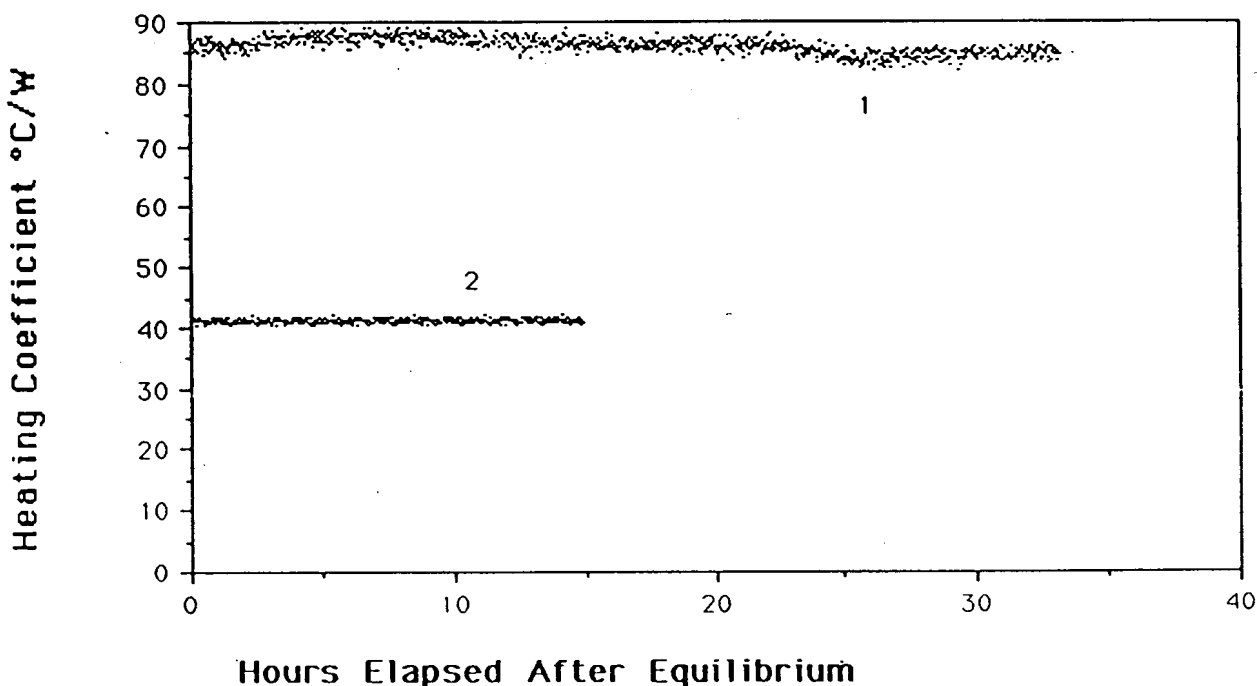
Figure 1. The Potential Energy Well of a Hydrogen Atom.



## Calorimetry

Mills' theory predicts that the exothermic catalytic reaction whereby the electrons of hydrogen atoms are stimulated to relax to a lower energy level corresponding to fractional quantum states by providing an energy hole resonant with this transition will occur during the electrolysis of  $K_2CO_3$  light-water solutions but will not occur during the electrolysis of  $Na_2CO_3$  light-water solutions. The results of the electrolysis with a nickel cathode at 83 mA constant current and heater run of  $K_2CO_3$  appear in Figure 2. The heating coefficient of the electrolysis run was 87  $^{\circ}C/W$ ; whereas, the heating coefficient of the heater run (calibration) was 41  $^{\circ}C/W$ . The higher the heating coefficient, the more heat released in the process.

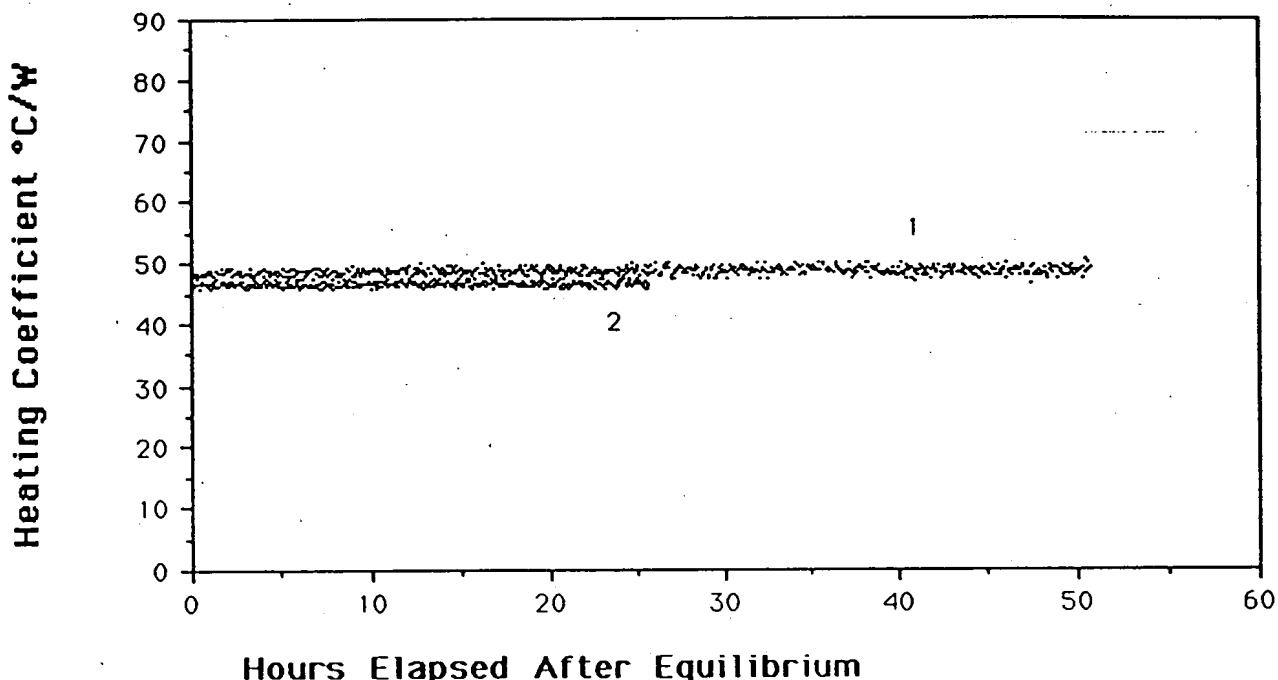
Figure 2. Plot of the heating coefficients versus time. 1 - electrolysis with a nickel cathode at 0.083 A in  $K_2CO_3$ , 2 - resistor working in  $K_2CO_3$ .



The results of the electrolysis at 81 mA constant current and heater run of  $Na_2CO_3$  appear in Figure 3. The heating coefficient of the electrolysis run was 47  $^{\circ}C/W$ ; whereas, the heating coefficient

of the heater run (calibration) was 46 °C/W. The production of excess heat is not observed.

Figure 3. Plot of the heating coefficients versus time. 1 - electrolysis at 0.081 A in  $\text{Na}_2\text{CO}_3$ , 2 - resistor working in  $\text{Na}_2\text{CO}_3$ .



Almost all electrolysis experiments will be similar to the case of  $\text{Na}_2\text{CO}_3$ , above. Only a few combinations of electrolytes/electrodes such as the  $\text{K}_2\text{CO}_3$  case above, will yield excess heat.

## **Appendix I**

**TITLE:** Unification of Spacetime, the Forces, Matter, and Energy

**LENGTH:** 220 pages

**SUBJECT AREA:** Physics/Chemistry

**AUTHOR:** Dr. Randell L. Mills  
President, HydroCatalysis Power Corporation  
HydroCatalysis Power Corporation  
Greenfield Corporate Center  
1860 Charter Lane  
Suite 208  
Lancaster, PA 17601  
(717)-291-6673

**SHORT ABSTRACT:** The fundamental laws of Nature are derived and are shown to be applicable on all scales. Electricity and magnetism (Maxwell's equations), gravity (curvature of space-time by matter; Einstein's General Relativity), transformations among space-time inertial frames (Einstein's Special Relativity), and Newtonian mechanics, and the strong and weak forces are unified. Creation of matter from energy equations are derived and these equations give the masses of the fundamental particles. A broad spectrum of major physical observables are calculated from derived equations that contain fundamental constants only. There is excellent agreement between the calculated values and experimentally determined values.

**SUMMARY:** To overcome the shortcomings of quantum mechanics, physical laws which are exact on all scales were sought. Rather than engendering the electron with a wave nature as suggested by the Davisson-Germer experiment and fabricating a set of associated postulates and mathematical rules for wave operators, a new theory was derived from first principles. The novel theory unifies Maxwell's Equations, Newton's Laws, and Einstein's General and Special Relativity. Theoretical predictions conform with experimental observations. The closed form calculations of a broad spectrum of fundamental phenomena contain fundamental constants only. Equations of the one electron atom are derived which give four quantum numbers, the Rydberg constant, the ionization energies, the results of the Stern-Gerlach experiment, the electron g factor, the spin angular momentum energies, the excited states, the results of

the Davisson-Germer experiment, the parameters of pair production, and the hyperfine structure interval of positronium. Ionization energies of two and three electron atoms are given as well as the bond energies, vibrational energies, and bond distances of molecular hydrogen and the molecular hydrogen ion. From the closed form solution of the helium atom, the predicted electron scattering intensity is derived. The closed form scattering equation matches the experimental data; whereas, calculations based on the Born model of the atom "utterly fail" at small scattering angles. The implications for the invalidity of the Schrödinger and Born model of the atom and the dependent Heisenberg Uncertainty Principle are discussed. The atomic equations of gravitation are derived from which the gravitational constant and the masses of the leptons and the neutron and proton are derived. The magnetic moments of the nucleons are derived. The beta decay energy of the neutron and the binding energy of deuterium are calculated. Also, the theory predicts exactly the spectral observations of the extreme ultraviolet background emission from interstellar matter, which characterizes dark matter; it provides a resolution of the solar neutrino paradox, and it provides a basis to produce heat in electrolytic cells which represents an endless supply of cheap, clean energy.

Sir:

Robert M. Shaubach, residing at 1104 Brunnerville, Rd.,  
Lititz, Pennsylvania declares and states that:

1. I received a Bachelor of Science degree in electrical engineering from Union College, Schenectady, New York, 1967, and attended graduate nuclear engineering courses at Catholic University, Maryland.
2. I am currently a Manager, Development Operations, at Thermacore, Inc., located at 780 Eden Road, Lancaster, PA 17601. I have been with Thermacore since 1981.
3. As Manager of the Development Operation, I am responsible for Thermacore's contract and in-house developments in the heat transfer field. I am responsible for seeing that Thermacore maintains technical excellence in development programs while meeting budget and schedule constraints.

4. I have been instrumental in furthering the understanding of the performance of sintered wick structures both self-pumped and mechanically augmented. This includes modeling two phase flow in wicks and helping to develop vapor resistant arteries. This new understanding has led to several patents as well as setting the World's record in heat pipe heat flux levels of over 100 kW/cm<sup>2</sup>.

5. My professional career has been devoted primarily to the energy field. This includes structural and thermal analysis and experimental work covering laser mirror coolers, heat pipes, sintered wick structures, two phase flow and heat transfer, thermally driven pumps, absorption coolers, air/air heat exchangers and resolution of technical problems with Naval and commercial ship propulsion and auxiliary systems as well as nuclear and fossil generating plants and industrial processes. My experience covers project engineering and management through corporate responsibility for research, development and engineering.

6. My previous work includes the development of heat pipes for cooling hypersonic aircraft wing and cowl leading edges, heat pipes for fuel cell coolers, and articulated heat pipe/heat pipe joint for the Air Force, and the development of double effect absorption heat pump heat exchangers for a commercial customer.

7. I have made significant contributions to the development of a unique gas fired pump for a solar augmented gas fired hot water system and an air/air heat exchanger for the commercial market.

8. I have designed the laser mirror heat pipe cooler for the Air Force and performed the thermal/optical distortion analyses for the silicon heat pipe laser mirror cooler on Contract No. F33615-82C-5127.

9. I am the author or co-author of numerous technical reports and papers, of which selected publications are shown in the attachment.

Nelson J. Gernert residing at 6016 Schoolhouse Road, Elizabethtown, PA declares and states that:

1. I received a B.S. in mechanical engineering from Pennsylvania State University in 1983.

2. I am currently a Development Engineer/Group Leader at Thermacore, Inc., located at 780 Eden Road, Lancaster, PA 17601. I have been with Thermacore since 1983.

3. At Thermacore, I have worked on research and development contracts directly related to heat transfer technology.

4. I am currently the principal investigator on the Thermacore Research and Development effort evaluating the performance of Dr. Randell Mills' Electrolytic Power Cell.

5. I have been the principle investigator on numerous contracts and as a result I have extensive experience in conducting contract R&D. A brief summary of these contracts is provided in the attachment.

6. I am the author or co-author of numerous technical reports, papers, of which selected publications are shown in the attachment.

Robert M. Shaubach, and Nelson J. Gernert together declare and state that:

1. We have reviewed and understand the concept covered by the subject U.S. application No. 07/825,845 of Dr. Randell L. Mills and we are personally familiar with the methods and apparatus disclosed therein.

2. We (hereinafter Thermacore) have conducted independent experiments on nominally identical apparatus to that made by Dr. Randell Mills (Hereinafter HPC) to check HPC's method and results, since March of 1992.

3. Thermacore's experiments and test results have corroborated HPC's results, showing 78 watts of heat output with only 28 watts of heat input. Excess energy on the order of 50 watts has been produced reliably and continuously over the last several months. Thermacore's spectral metallurgical evaluations show that neither the electrolyte nor the electrodes are being consumed. Scintillation counter measurements show no signs of radiation external to the cell.

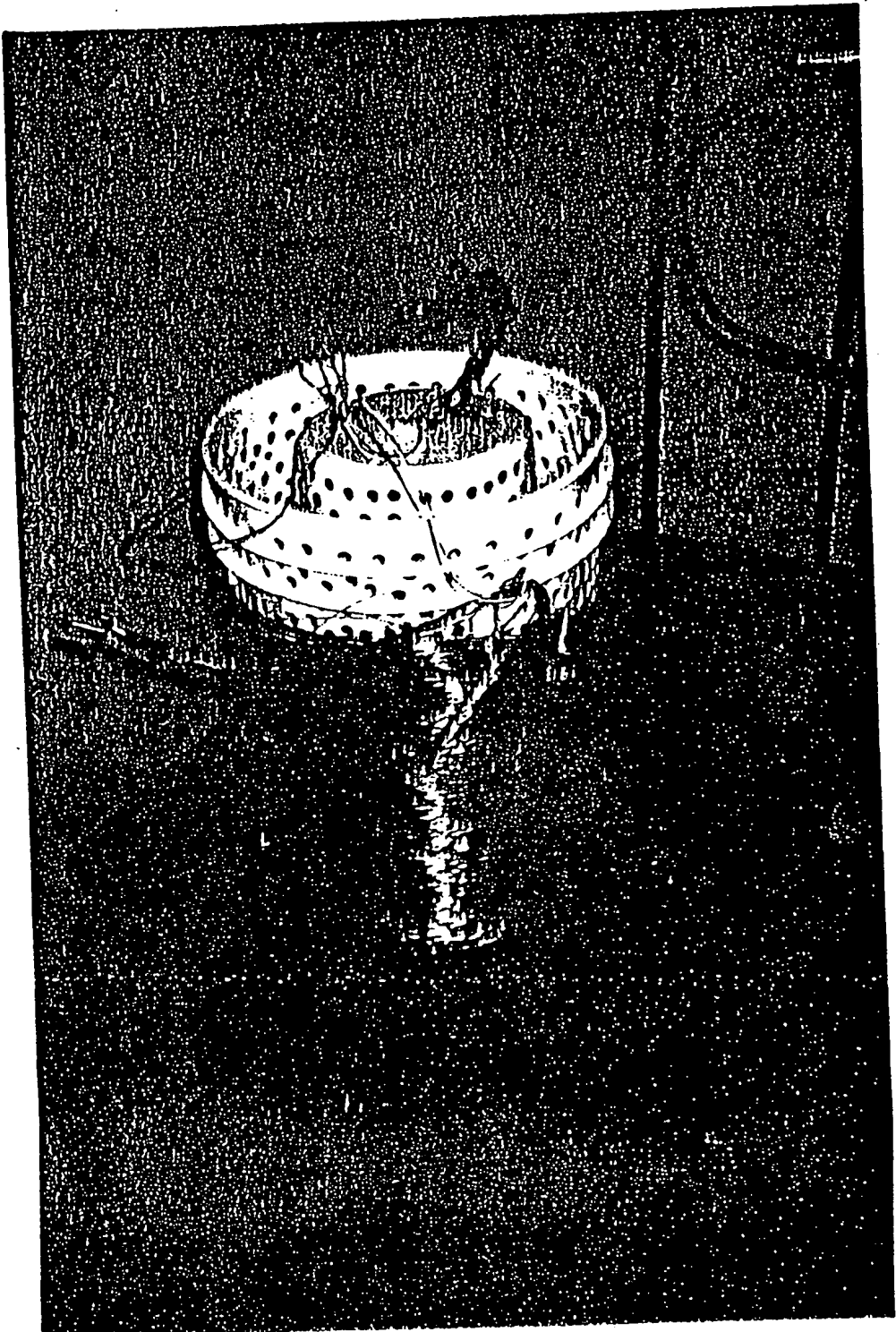
#### Description of the Thermacore Cell

The Thermacore cell is comprised of a 38 liter (33 cm diameter x 53 cm high) Nalgene tank (Model #54100-0010). Two 4 inch long by  $\frac{1}{2}$  inch diameter terminal bolts were secured in the lid, and a cord for a heater was inserted through the lid.

The cathode is comprised of 1) a 19 liter polyethylene bucket which served as a perforated (mesh) support structure where 1.3 cm holes were drilled over all surfaces at 1.9 cm spacings of the hole centers and 2) 5000 meters of 0.5 mm diameter nickel wire (NI 200 0.0197", HTN36NOAG1, AI Wire Tech, Inc.). The wire was wound around the outside of the mesh support at about 150 sections of 33 meter length. The ends of each of the 150 sections were twisted to form three cables of 50 sections per cable. The cables were pressed in a terminal connector which was bolted to the cathode terminal post. The connection was covered with epoxy to prevent corrosion. See Figure 1. A center cathode was also made from 5000 meters of the 0.5 mm diameter nickel wire. The wire was wound in a toroidal shape with three cables pressed into a terminal connector which was bolted to the cathode terminal post and epoxy coated. The cathode was inserted into an ellipsoidal shaped perforated polyethylene container.

The anode is an array of 15 commercially available, chemically inert platinized titanium anodes (10 - Engelhard Pt/Ti mesh 4 cm x 20 cm with one 1.9 cm by 17.7 cm stem attached to the 4 cm side plated with 100  $\mu$  Pt series 3000). A 1.4 cm wide tab was made at the end of the stem of each anode by bending it at a right angle to the anode. A 0.64 cm hole was drilled in the center of each tab. The tabs were bolted to a 31 cm diameter polyethylene disk (Rubbermaid Model #2666) equidistantly around the circumference. Thus, an array was fabricated having the 15 anodes suspended from the disk. The anodes were bolted with 0.64 cm polyethylene bolts. Sandwiched between each anode tab and the disk was a flattened nickel cylinder also bolted to the tab and the disk. The cylinder

Figure 1. NICKEL WIRE CATHODE



was made from a 7.5 cm x 9 cm long x 0.125 mm thick nickel foil. The cylinder traversed the disk, and the other end of each was pressed about a 10 AWG/600 V copper wire. The connection was sealed with shrink tubing and epoxy. The wires were pressed into three terminal connectors and bolted to the anode terminal. The connection was covered with epoxy to prevent corrosion. See Figure 2 for the anode and Figure 3 for the assembly.

Before assembly, the anode array was cleaned in 3 M HCL for 5 minutes and rinsed with distilled water. The cathode was rinsed with distilled water. The anode was placed in the cathode support and the electrode assembly was placed in the tank containing electrolyte. The power supply was connected to the terminals with automotive battery cables.

The electrolyte solution comprised 36 liters of 0.57 M  $K_2CO_3$ , (Alfa  $K_2CO_3$  99%).

The heater comprised a 69 ohm 1000 watt cartridge heater which was suspended from the polyethylene disk of the anode array. It was powered by an Invar constant power ( $\pm 0.1\%$ ) supply (Model #TP 36-18). The voltage ( $\pm 0.1\%$ ) and current ( $\pm 0.1\%$ ) were recorded with a Fluke 8600A multimeter.

Electrolysis was performed at 16, 25 and 50 amperes direct current with a constant current ( $\pm 0.2\%$ ) power supply (Kepco Model #ATE 6-50M). A 75 amp condition was achieved using two Kepco Model #ATE 6-50M power supplies in parallel. They were also programmed to provide a square wave at a peak of 101.5 amps when driven by a frequency generator set at a 7% duty cycle at 2 Hz.

Figure 2.  
P' TINUM COATED TITANIUM NODES

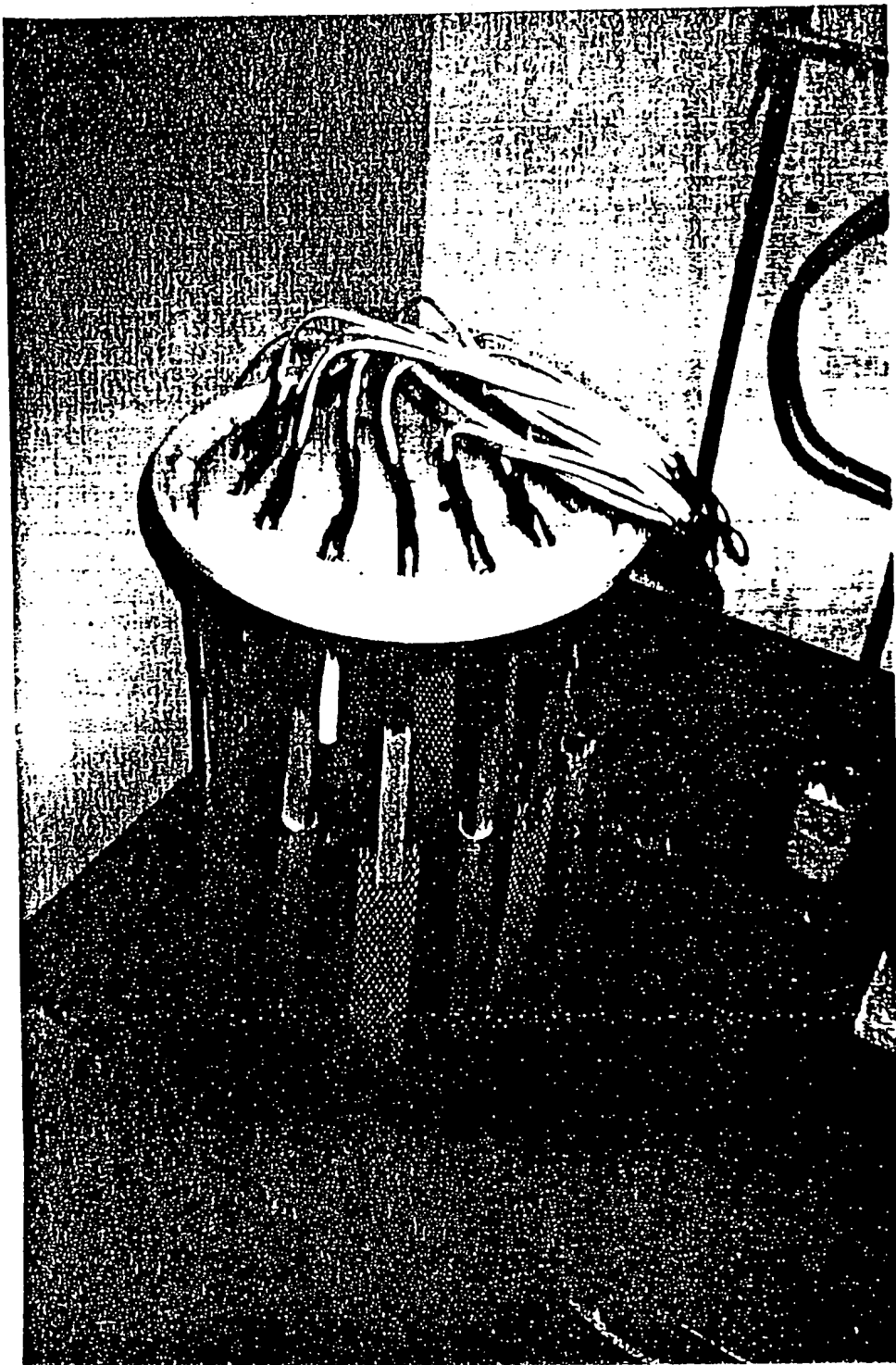
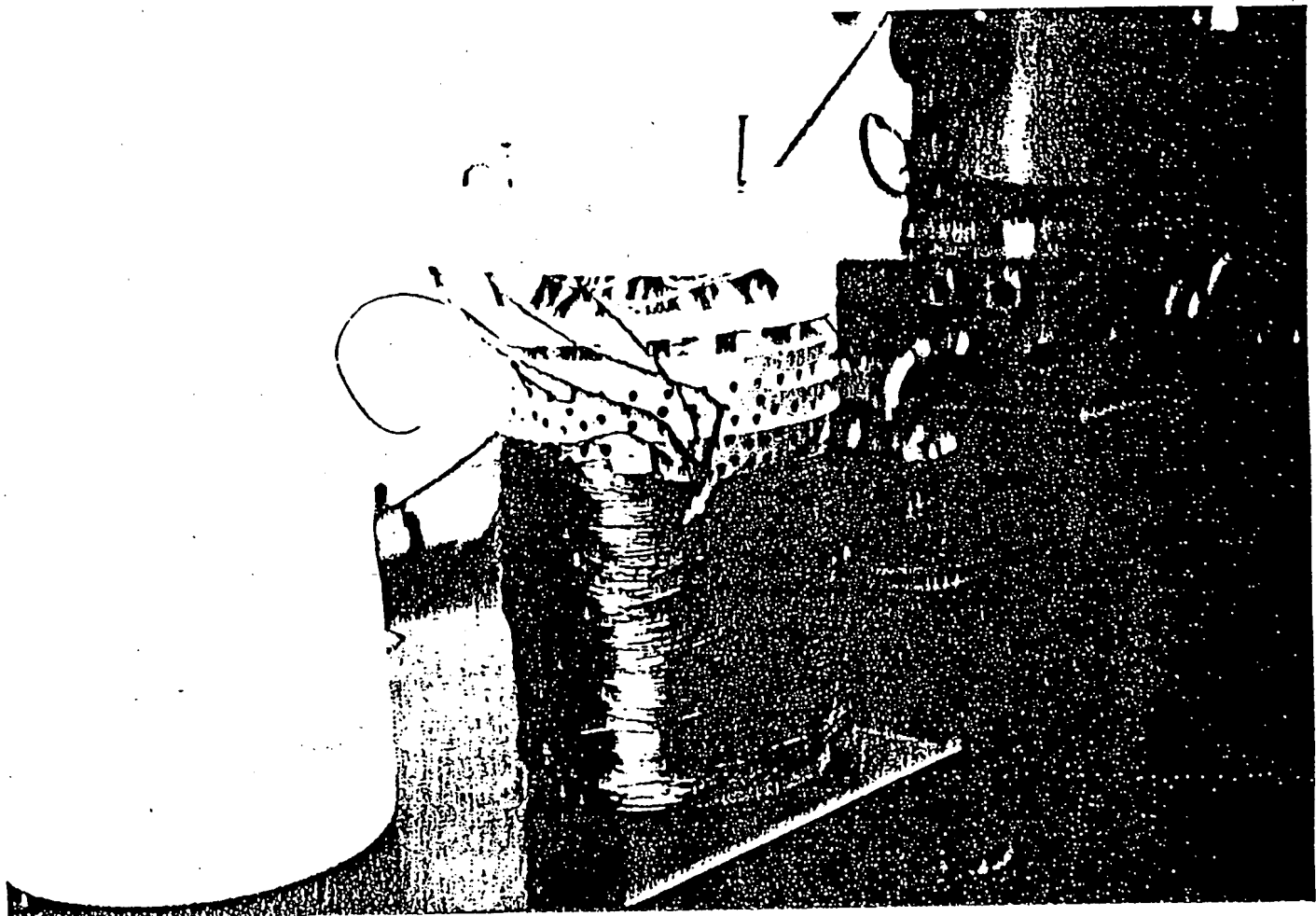


Figure 3. Cell Assembly



The voltage ( $\pm 0.1\%$ ) was recorded with a Fluke 8600A multimeter. The current ( $\pm 0.5\%$ ) was read from an Ohio Semitronics Current Transducer Model CTA101.

The temperature ( $\pm 0.1^\circ\text{C}$ ) was recorded with a microcomputer thermometer (Omega HH21) which was inserted through a 0.64 cm hole in the tank lid and anode array disk.

The temperature ( $\Delta T = T$  (electrolysis only) -  $T$ (ambient)) and the electrolysis power were recorded regularly. The heating coefficient was determined "on the fly" by the addition of 20 watts of heater power at 72 hour increments where 24 hours was allowed for steady state to be achieved. The temperature  $\Delta T_g = T$  (electrolysis + heater) -  $T$ (ambient) was recorded as well as the electrolysis power. The ambient temperature was measured from a blank cell that was comprised of a closed 10 gallon Nalgene tank (Model 541000-0010) containing 40 liters of  $\text{H}_2\text{O}$  placed 0.5 meters from the electrolysis cell. Figure 4 shows the electrolysis cell on test.

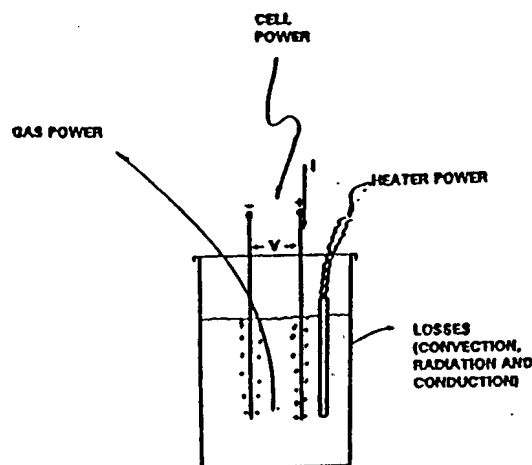
### Results

Both HPC and Thermacore obtained similar results on separate nominally identical cells using separate instrumentation. A heat balance is shown in Figure 5; some of the Thermacore results are shown in Table 1.

Figure 4.  
ELECTROLYTIC CELL ON TEST



FIGURE 5. CELL HEAT BALANCE



$$\begin{aligned}
 \text{CELL POWER} &= VI \\
 \text{GAS POWER} &= 1.48I \\
 \text{OHMIC POWER} &= (V-1.48)I \\
 \text{HEATER POWER} &= v_{th}I \\
 \text{LOSSES} &= \text{MEASURED INCREMENTALLY}
 \end{aligned}$$

TABLE 1. Summary of Thermacore Test Results

Input Conditions			Output Conditions				<u>Output</u> <u>Input</u>
V (Volts)	I (Amps)	Total Input Power = VI (Watts)	Total Output Power (Watts)	Subcomponents (Watts)			
				Gas 1.48I	Excess ± 20%	Ohmic Heating = (V-1.48)I	
2.96	25.1	74.3	124	37.1	50	36.9	1.7
3.25	49.9	162	212	73.8	50	88.2	1.3
3.42	75.0	257	307	111	50	146	1.2
3.98	101.5*	28.3	78.3	10.5	50	17.8	2.8

\* Pulsed with a square wave at a 7% duty cycle @ 2.0 Hz

The method for calculating the 50 watts of excess power is represented graphically in Figure 6 for the 50 amperes direct current (ADC) case. The electrolyte temperature rise above ambient is plotted versus heat added to the electrolyte. A straight line is projected through the data to the ordinate. The intercept and slope of this line is used to estimate the 50 watts of excess power as shown in Figure 6.

Figure 7 shows the data for 16, 25 and 75 amps direct current superimposed on the curve for 50 amps. Notice that the excess energy of about 50 watts is independent of the cell current between 25 and 75 amps. The excess energy begins to drop off at current levels below 25 amps. Figure 8 also includes temperature versus

FIGURE 6.: METHOD FOR CALCULATING EXCESS POWER

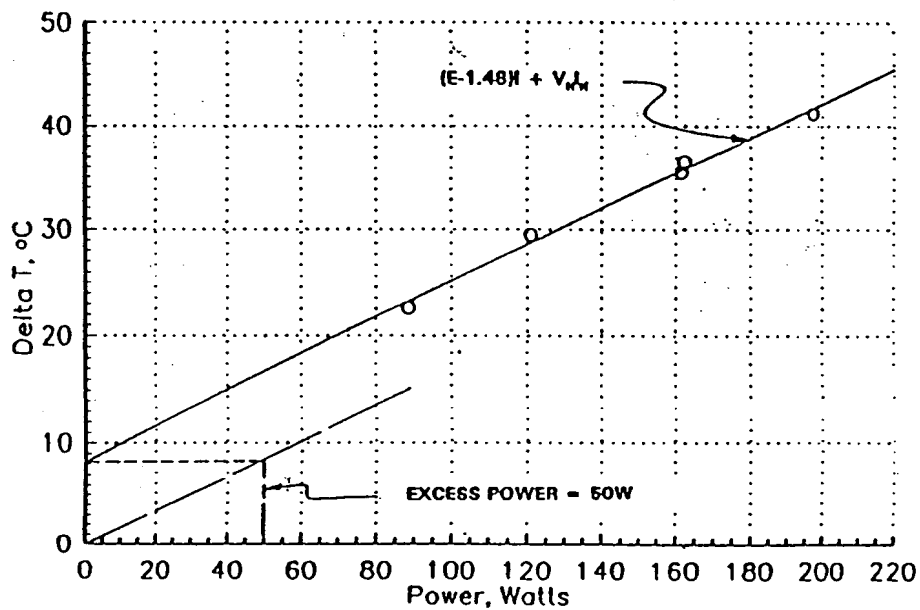


FIGURE 7. ELECTROLYTIC CELL COMPARED TO BLANK

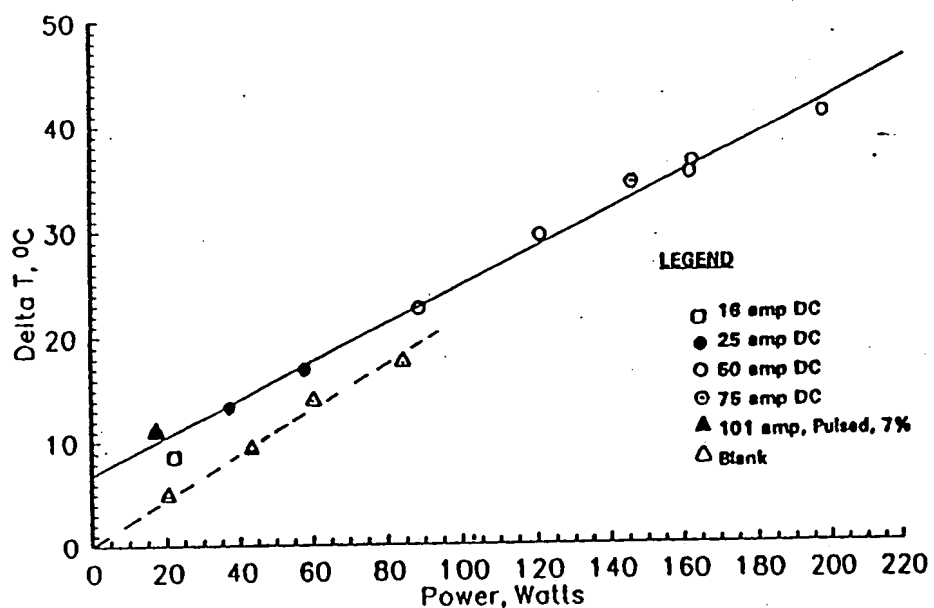
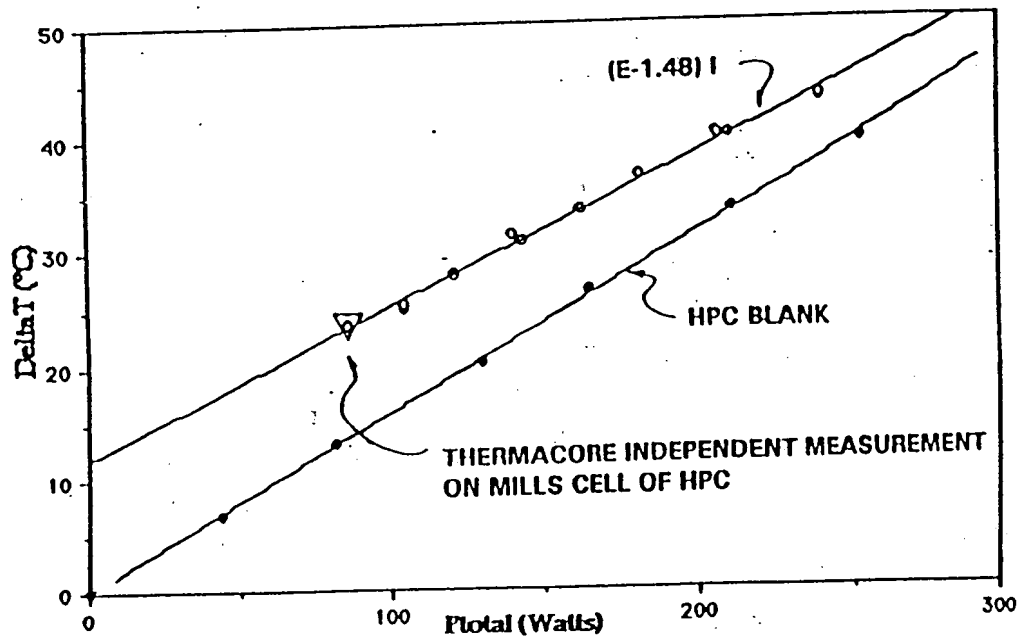


FIGURE 8. HPC DATA FOR 50 AMPERES DC



power data for an  $I^2R$  heated blank of the same geometry as the cell. These data project through zero which is consistent with the mathematical modeling of the heat balance.

The theory that led to the discovery of this electrolytic process was developed by Dr. Randell Mills, HPC, Lancaster, Pennsylvania, as described below:

Dr. Randell Mills has developed a theory for the electrochemical process discussed herein. This theory is covered by a patent application entitled "Energy/Matter Conversion Methods and Structure", and is described in the Fusion Technology article entitled, "Excess Heat Production by the Electrolysis of an Aqueous Potassium Carbonate Electrolyte and the Implications for Cold Fusion" by Dr. Mills and S. Kneizys, the article entitled "A Unified Theory Derived from First Principles" submitted to the Physical Review for publication by Dr. Mills and W. Good, the article entitled "Two Electron Atoms and Elastic Electron Scattering by Helium", submitted to Physical Review for publication by Dr. Mills and the book entitled, The Grand Unified Theory, by Dr. Mills and Dr. T. Farrell.

In technical terms, under the Mills theory the predominant source of heat is believed to be an electrocatalytically induced reaction whereby hydrogen atoms undergo transitions to quantized energy levels of lower energy than the conventional "ground state". These lower energy states correspond to fractional quantum numbers. The hydrogen electronic transition requires the presence of an energy hole of approximately 27.2eV provided by electrocatalytic reactant(s) (such as  $PD^{2+}/Li^+$ ,  $Ti^{2+}$ , or  $K^+/K^+$ ), and results in

"shrunken atoms" analogous to muonic atoms. Calorimetry of pulsed current and continuous electrolysis of aqueous potassium carbonate ( $K^+/K^+$  electrocatalytic couple) at a nickel cathode was performed in the calorimetry cells. Total power out exceeded total input power by a factor of 2.8 as described, above.

Thermacore tests and results are summarized as follows:

1. Metallurgical samples of the nickel cathode in service for 720 hours were subjected to spectral analyses and were photomicrographed. Results show no unusual changes or reactions between the nickel and electrolyte. The wire appears to remain unchanged after one month of operation.
2. Evaluation of the electrolyte after one month operation shows no significant change in its density and molar concentration. Spectral analyses of the electrolyte show no significant concentrations of the nickel, titanium or platinum from the electrodes, thus, a reaction between the electrolyte and electrodes is probably not occurring.
3. Evaluation of gas samples from the cell show hydrogen, oxygen and trace amounts of nitrogen. No significant quantities of CO, or  $CO_2$  were found, confirming that the  $K_2CO_3$  electrolyte is not degrading.

4. The cell was disassembled and inspected after over one month of operation at 50 amperes. This inspection showed no visible signs of a reaction between the electrodes and electrolyte. The cell was re-assembled and is operating as before, producing about 50 watts of excess energy, 24 hours a day.
5. Measurements of neutrons were not considered necessary since light water is used in place of deuterium. A scintillation counter was placed next to the cell. No radiation levels above background were detected indicating that nuclear reactions are not involved.
6. Water makeup rates match the Faraday usage plus evaporation. Evaporation was quantified by condensing moisture from the gas effluent, collecting the water condensate, and measuring the condensate rate.
7. Thermacore has taken independent measurements on the original HPC cell using Thermacore equipment. These measurements help confirm the accuracy of HPC data as shown in Figure 8.
8. Results show that heat for a given cell, input power can be reduced while maintaining a constant output power. For example, by pulsing the electrical input at fractional duty cycles the 2 Hz, 100 ampere rectangular wave with a 7 percent duty cycle provides an output/input power ratio of 2.8. This ratio is a factor of 2.5 better than the ratio obtained using straight 75 ampere DC power (See Table 1).

9. As stated in the text above, cell excess power remains almost constant and does not appear to increase significantly at current levels above 25 amperes, DC. The reason for this is not well understood. The HPC theory is that the formation of "shrunken" hydrogen will only occur with the  $H_1$  atom and not the  $H_2$  molecule. The  $H_1$  atom must contact two potassium ions that provide the proper energy hole. This contact may be required to occur on the surface of the nickel electrode; perhaps from  $H_1$  coming out of solution from NiH formed at the surface of the nickel. The rate of  $H_2$  formation relative to the rate of the energy releasing hydrogen atom transition reaction could limit the excess power where excess hydrogen formed at current levels above 25 amperes is lost in the form of  $H_2$ .

By: Robert M. Shaubach

Robert M. Shaubach

Date: 8-24-92

By: Nelson J. Gernert

Nelson J. Gernert

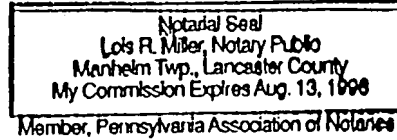
Date: 8/24/92

COMMONWEALTH OF PENNSYLVANIA)  
                                ) SS:  
COUNTY OF LANCASTER         )

On this, the 24th day of August, 1992, before me a notary public, the undersigned officer, personally appeared Robert M. Shaubach and Nelson J. Gernert, known to me (or satisfactorily proven) to be the persons whose names are subscribed to the within instrument, and acknowledged that they executed the same for the purposes therein contained.

In witness whereof, I hereunto set my hand and official seal.

Lori R. Miller  
Notary Public



ATTACHMENT

Robert M. Shaubach  
Manager, Development Operations, Thermacore, Inc.

Selected Publications

"Articulated Heat Pipe Design, Fabrication, and Test Report:, Contract F33615-81-C-3413, Prepared by Air Force Flight Dynamics Laboratory, Wright Patterson Air Force Base, Ohio, January 1983.

"Evaluation of Submarine Auxiliary System Closed Cycled Vaporization Cooling", Contract N00167-83-M-1504, Prepared for David Taylor Naval Ship Research and Development Center, Annapolis, Maryland, June 1982.

"Articulated Heat Pipe Concepts and Developments", D.M. Ernst and R. M. Shaubach, SAB Technical Paper 831102, Thirteenth Intersociety Conference on Environmental Systems, July 1983.

"Heat Transport Across Structural Boundaries", Robert M. Shaubach, AIAA-84-0977, AIA 20th Thermophysics Conference, Williamsburg, Virginia, June 1985.

"Boiling and Two-Phase Flow in the Capillary Porous Structure of Heat Pipe", B.S. Singh and R.M. Shaubach, June 1987.

"Advanced Heat Pipe Technology for Space Heat Transport and Rejection Technologies", G.Y. Eastman, D.M. Ernst, R.M. Shaubach and J. E. Toth, Space Power, Vol. 9, No. 1, 1990.

"Boiling in the Heat Pipe Evaporator Wick Structures", R.M. Shaubach, P.M. Dussinger and J.E. Bogart, International Heat Transfer Conference, Minsk, USSR, May 1990.

NELSON J. GERNERT  
Thermacore, Inc.  
Position: Development Engineer/Group Leader  
Clearance: DOD Secret

Summary of Contracts

- NAS9-18674 - 1992 Phase I SBIR - This is a recent effort to demonstrate the feasibility of a thin membrane heat pipe radiator for heat rejection on the lunar surface.
- NAS8-39345 - 1992 Phase I SBIR - Under this contract, Mr. Gernert is developing a new type of furnace to enhance crystal growth in a gravity free environment.
- NAS8-38901 - 1991 Phase I SBIR - Under this contract, Mr. Gernert demonstrated the feasibility of the Moving Gradient Heat Pipe Furnace. The proposed follow-on Phase II effort has been awarded and contract release is pending.
- NAS8-38437 - 1990 Phase I SBIR - Mr. Gernert demonstrated the feasibility of using lightweight composite materials in the construction of heat pipes for space applications. His success lead him to the following Phase II effort.
- NAS8-38965 - 1991 Phase II SBIR - This Phase II is for the development of a 15 meter long composite material radiator heat pipe for space. This Phase II began in June 1991.
- Under a 1988 Phase I and subsequent Phase II contracts to the Navy, Mr. Gernert developed a Flexible Heat Pipe Cold Plate to cool electronics mounted on an actuator being developed for the Navy F/A-18 aircraft.
- NAS8-37261 - 1986 Phase II SBIR - Under this contract, Mr. Gernert developed two 15 meter long aluminum/ammonia radiator heat pipes for heat rejection in space.
- NAS9-17305 - 1985 Phase II SBIR - In this program, Mr. Gernert developed a 16 meter long deployable radiator heat pipe for heat rejection in space. This heat pipe had two flexible joints which enabled it to be folded into thirds to form a compact deployable radiator.

Selected Publications

"High Performance Flexible Heat Pipes," R.M. Shaubach and N.J. Gernert, 20th AIAA Thermophysics Conference, Williamsburg, Virginia, June 19-21, 1983.

"Analysis and Performance Evaluation of Heat Pipes With Multiple Heat Sources," N.J. Gernert, 4th AIAA Thermophysics and Heat Transfer Conference, Boston, Massachusetts, June 2-4, 1986.

"Flexible Heat Pipe Cold Plates for Aircraft Thermal Control" NJ. Gernert, D.B. Sarraf, M. Steinburg. SAE Aerotech Conference, Long Beach, CA, September 24-27, 1991.

"A Thermal Analysis of an F/A-18 Wing Section for Actuator Thermal Control", N.J. Gernert, D.B. Sarraf. 1992 SAE Aerospace Atlantic Conference, Paper No. 921034, Dayton, Ohio, April 7-10, 1992.

"Sodium Heat Pipe with Sintered Wick and Artery Effects of Non-Condensable-Gas on Performance" R.M. Shaubach, N.J. Gernert, Space Nuclear Power Conference, Albuquerque, New Mexico, January 1992.

# EXCESS HEAT DURING THE ELECTROLYSIS OF A LIGHT WATER SOLUTION OF $K_2CO_3$ WITH A NICKEL CATHODE

COLD FUSION

## TECHNICAL NOTE

KEYWORDS: excess energy, electrolysis of  $H_2O$ , nickel cathode

V. C. NONINSKI\* Laboratory for Electrochemistry of Renewed Electrode-Solution Interface (LEPGER), P.O. Box 9, Sofia 1504, Bulgaria

Received July 5, 1991

Accepted for Publication August 19, 1991

*Experimental results of differential heat loss calorimetry measurements during the electrolysis of light water solutions of  $K_2CO_3$  and  $Na_2CO_3$  with a nickel cathode are presented. A significant increase in temperature with every watt input, compared with the calibration experiment, is observed during the electrolysis of  $K_2CO_3$ . This effect is not observed when  $Na_2CO_3$  is electrolyzed. No trivial explanation (in terms of chemical reactions, change in heat transfer properties, etc.) of this effect has been found so far. If the nontriviality of the observed overcoming of the energy break-even barrier is further confirmed, this phenomenon may find application as an important new energy source.*

## EXPERIMENTAL DETAILS

The experiments were carried out by observing and comparing the temperature difference,  $\Delta T_1 = T_{\text{electrolysis only}} - T_{\text{blank}}$  and  $\Delta T_2 = T_{\text{resistor heating only}} - T_{\text{blank}}$  referred to unit input power, between two identical 200-ml silver-coated vacuum-jacketed dewars. A calorimeter dewar having the same configuration and containing the same amount of electrolyte, same type of electrodes (nickel cathode and platinum anode), resistor heater, and thermistor (thermometer) and stirred at the same speed was used as a blank; neither electrolysis nor heating by the resistor was carried out in this dewar. Experiments were also carried out by using as a blank a dewar used in a previous experiment and vice versa. This exchange was done to ensure that the effect was not due to any difference in the thermal properties of the two specific dewars used. Each dewar had a 3-cm opening, and a 2-cm-thick tapered rubber stopper was placed 1 cm into the dewar. The experimental apparatus for the differential calorimetry used in these studies is shown in Fig. 1. Unlike the studies in Ref. 4, the resistor and the electrolytic circuit were not run simultaneously in this study; the effects of heating by the resistor and by the electrolysis circuit were studied in separate runs.

As is usual in electrochemistry, measures were taken to avoid impurities in the system, especially organic substances. While it is unclear at this point what the relationship is, if any, between the contamination effect on the hydrogen overpotential and that on the eventual excess heat, one should recall the known problems with the reproducibility of the hydrogen overpotential, which can be overcome only by ensuring the lowest possible level of impurities. Certain procedures should be applied to reproduce the excess heat effect. For instance, before starting the experiment, mechanically scour the platinum anode with steel wool, soak overnight in concentrated  $HNO_3$ , and then rinse with distilled water. Remove the nickel cathode from its container with rubber gloves, and cut and bend it in such a way such that no organic substances are transferred to the nickel surface. Preferably, dip the nickel cathode into the working solution under an electrolysis current, and avoid leaving the nickel cathode in the working solution in the absence of an electrolysis current. Clean the electrolysis dewar, and free it of organic contaminants.

After assembling the experimental setup, the nickel cathode was subjected to anodizing by a constant electrolysis current of 0.083 A for 1 h. Then, the direction of the electrolysis

## INTRODUCTION

The studies in this paper follow the general lines of the work of Fleischmann and Pons,<sup>1</sup> although electrolysis of  $D_2O$  is usually considered when excess energy is claimed. Observation of excess energy production during the electrolysis of  $H_2O$  was first mentioned by Pons and later rejected.<sup>1</sup> Pons et al., however, explicitly state the possibility of obtaining excess energy during electrolysis of ordinary water (using nickel as a cathode, among other proposed metals) in Ref. 2. Unexplained excess heat in light water is also claimed in a paper by Bush et al.<sup>3</sup> Mills and Kneizys<sup>4</sup> claim to have obtained excess energy above the amount spent during the electrolysis of a  $K_2CO_3$  ordinary water solution with a nickel cathode. The excess energy effect, according to these authors, is not observed when  $Na_2CO_3$  is electrolyzed. Furthermore, unusual effects during the electrolysis of light water have also been reported by Matsumoto.<sup>5</sup>

This paper compares the heating coefficients for a nickel/platinum (Ni/Pt) circuit with those for a resistor heater in vacuum-jacketed dewar electrolytic cells containing  $K_2CO_3$  or  $Na_2CO_3$ . Note that the excess energy effect from an electrochemical system containing  $K^+$  ( $Li^+$  is usually used in these studies) in  $D_2O$  is reported in Ref. 6.

\*Visiting scholar at Franklin and Marshall College, Chemistry Department, Lancaster, Pennsylvania.

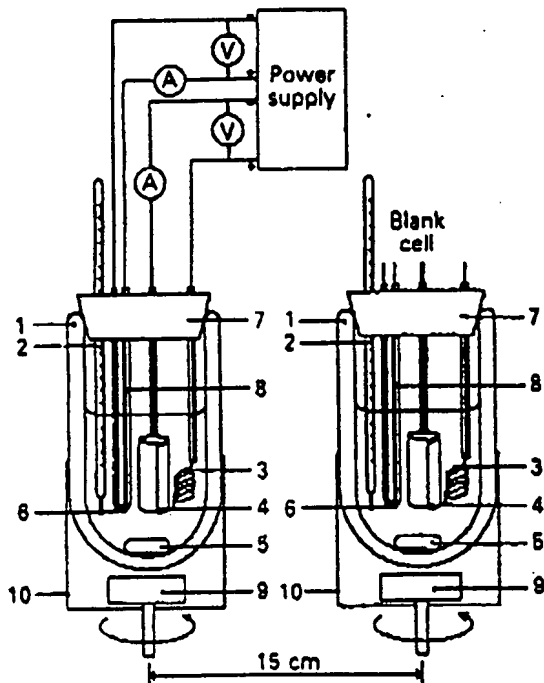


Fig. 1. Experimental setup: (1) vacuum-jacketed dewar, (2) thermometer, (3) platinum anode, (4) nickel cathode, (5) magnetic stirring bar, (6) resistor heater, (7) rubber stopper, (8) Teflon tubing, (9) magnetic stirrer, and (10) aluminum cylinder.

current was reversed (platinum anode and nickel cathode), and the electrolysis was carried out for 14 to 16 h.

The electrolysis heating power was calculated as  $P_{el} = (E_{el} - 1.48)I_{el}$ , where  $E_{el}$  is the applied electrolysis voltage,  $I_{el}$  is the electrolysis current (the term "electrolysis power" is used here for convenience, denoting only the power contributing to the joule heating effect during the electrolysis), and 1.48 V is the isoenthalpic voltage, which at the temperatures studied practically coincides with the thermoneutral voltage. The resistor heater power was calculated as  $P_h = I_R E_R$ , where  $I_R$  denotes the resistor current and  $E_R$  denotes the resistor voltage.

The cathode was a 7.5-cm-long  $\times$  4-cm-wide  $\times$  0.0125-cm-thick nickel foil (Aldrich 99.9+%) spiralled into a cylindrical form. The anode was a 0.1-cm-diam  $\times$  10-cm-long platinum wire (Johnson-Matthey). The spiral anode and the cylindrical cathode were parallel to each other. The leads were inserted into Teflon tubes to prevent any recombination of the evolving gases. The electrolyte solution in both dewars was 153 ml of 0.57 M  $K_2CO_3$  or 0.57 M  $Na_2CO_3$  in  $H_2O$ . The distilled water was from the common distiller of the Chemistry Department of Franklin and Marshall College. The power was delivered by a Zenith SP-2718 power supply (alternating current component <0.1%). The resistance heater was a 100- $\Omega$ , 1% precision, metal oxide resistor in a 2-mm-o.d. Teflon tube. The electrolyte solution in both dewars was stirred simultaneously (synchronized for the two dewars) by two identical spheroidal ellipse magnetic bars rotated by two magnetic stirrers at  $\sim$ 300 rpm. Electrolysis voltage and current were measured by two Keithley 169 multimeters, and the resistor voltage and current were measured by Extech 380198 and

Micronota 22-185 A multimeters with 0.01-V and 0.001-A accuracy, respectively. The use of vacuum-jacketed dewars, rather than air-jacketed dewars or simple flasks, made the measurements more sensitive (higher heating coefficient). In a vacuum-jacketed dewar unit, input power leads to a greater steady-state temperature, thus enabling differences in steady-state temperatures (for the same configuration) to be more pronounced. The temperatures in this study were monitored continuously using the capability of the standard calorimeters (Parr P-318) to record the temperature continuously (with  $0.01^\circ C$  accuracy) on their strip-chart recorder (Fisher Record-all Series 5000).

## RESULTS AND DISCUSSION

The results of the study are shown in Figs. 2 through 5. Figure 4 is based on the data presented in Figs. 2 and 3. Figure 2 shows the absolute change in the measured temperatures of the dewars at different conditions, while Fig. 3 shows the input powers in each case. It can be seen from Fig. 3 that while the input power with the resistors working was constant as expected, the input electrolysis power was not, and there is a time lag between the application of power and the temperature response. We compensated for this by selecting appropriate power values when calculating the heating coefficients plotted in Fig. 4 (more precisely, the term "heating coefficient" refers only to the steady-state values of the quantities in Fig. 4; the last parts of the curves in Fig. 4 can be considered to represent steady state). The heating coefficients plotted in Fig. 4 were calculated using the average power plotted in Fig. 3. Note that other reasonable ways of referring the observed  $\Delta T$  to the applied power are possible; however, even the most conservative approach gives the same qualitative effect as that seen in Fig. 4. Studies currently in progress, using a data acquisition system, show sustained steady-state production of excess heat for many days. Results from these studies are presented elsewhere.

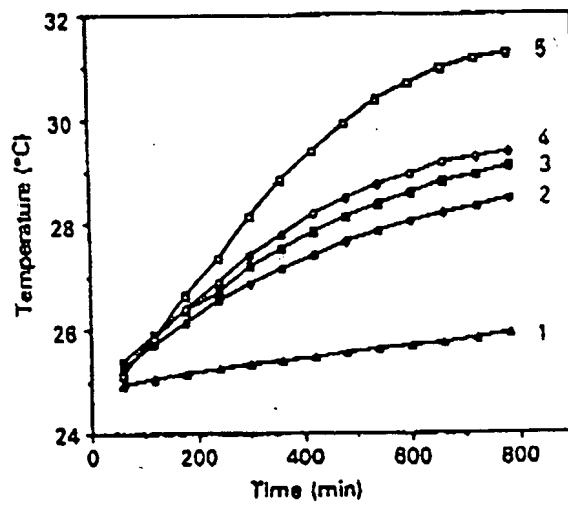


Fig. 2. Time history of temperatures: (1) blank cell (this curve is used as the blank for computing the heating coefficients of Fig. 4); (2)  $K_2CO_3$  calibration cell (with only resistor heater working); (3)  $Na_2CO_3$  calibration cell; (4)  $K_2CO_3$  electrolysis cell (with only electrolysis working); and (5)  $Na_2CO_3$  electrolysis cell.

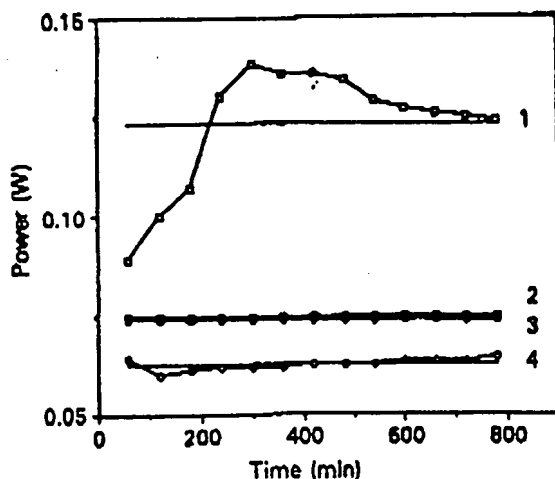


Fig. 3. Time history of the applied power: heating power with (1) electrolysis in the  $\text{Na}_2\text{CO}_3$  cell, (2) the resistor in the  $\text{Na}_2\text{CO}_3$  cell, (3) the resistor in the  $\text{K}_2\text{CO}_3$  cell, and (4) electrolysis of the  $\text{K}_2\text{CO}_3$  cell. The thermoneutral voltage is 1.48 V. For the calculations presented in this paper, mean values of the electrolysis powers in the  $\text{Na}_2\text{CO}_3$  and  $\text{K}_2\text{CO}_3$  cells are used, shown as solid lines in curves 1 and 4.

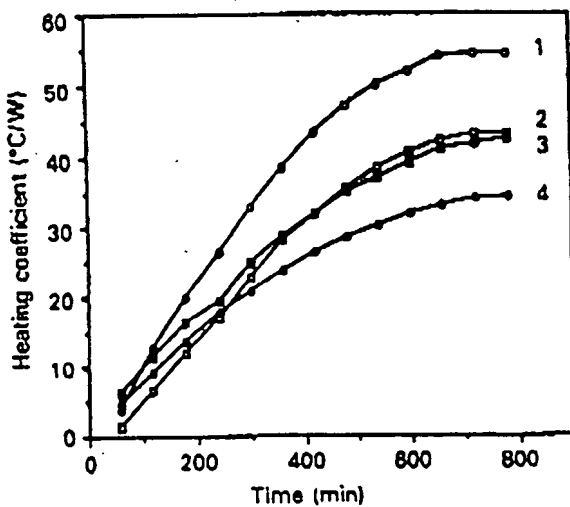


Fig. 4. Plot of the heating coefficients over time: (1) electrolysis at 0.083 A in  $\text{K}_2\text{CO}_3$ , (2) resistor working in  $\text{Na}_2\text{CO}_3$ , (3) electrolysis at 0.083 A in  $\text{Na}_2\text{CO}_3$ , and (4) resistor working in  $\text{K}_2\text{CO}_3$ .

The heating coefficient of the  $\text{Na}_2\text{CO}_3$  cell is plotted in Fig. 4. The heating coefficient for the resistor heater only and that for the electrolysis circuit only are essentially identical. This is to be expected for a given dewar and a given electrolyte when steady state is reached: The  $\Delta T$  corresponding to a unit heating power has a strictly defined value, determined by the properties of the materials through which heat is being lost. The properties of the cell are unaltered during operation. Specifically, the volume of electrolyte remains practically constant: -0.2% of the solution volume is being electrolyzed during the 12-h operation of the Ni/Pt cell.

In contrast, the calorimeter containing  $\text{K}_2\text{CO}_3$  showed very different behavior. The heating coefficient of the  $\text{K}_2\text{CO}_3$  cell is plotted over time in Fig. 4. The heating coefficient-time curve of the working electrolysis cell is clearly above the curve of the dewar in which only a resistor is working. The value of the heating coefficient with the Ni/Pt circuit working is  $-50^\circ\text{C}/\text{W}$ , while the heating coefficient with only the resistor working is  $-30^\circ\text{C}/\text{W}$ . Therefore, the output power obtained through the Ni/Pt circuit is  $\sim 160\%$  of the input power. The time-integrated power (i.e., energy) input into the system during the course of the experiment in Fig. 4 is  $\sim 4800 \text{ J}$  compared with the output power of  $\sim 8000 \text{ J}$ . Thus, Fig. 4 shows a significant difference in the thermal behavior of two identical systems that differ only in the positive ions of the salt.

A trivial explanation for this behavior of the  $\text{K}_2\text{CO}_3$  cell is not straightforward. In fact, the electrolysis should be expected to lead to a decrease in the heating coefficients compared with those of the cells in which only the resistor is working "... consistent with additional heat losses caused by gas evolution ..." which is currently observed only in the  $\text{Na}_2\text{CO}_3$  cell.

The erroneous attribution of the effect to temperature gradients was eliminated by testing for minute spatial variations of the temperature over time. Three thermistors were positioned  $\sim 2.5 \text{ cm}$  apart at the bottom, middle, and upper part of the electrolyte. The results, shown in Fig. 5, clearly demonstrate that no difference is observed (within the limit of detection,  $0.01^\circ\text{C}$ ).

Note that the electrolysis is always started with a newly manufactured cathode from the batch of 99.9%+ purity nickel. The use of new nickel excludes any possibility that the effect is due to the decomposition of species formed before the beginning of the electrolysis. The reaction of hydride formation is exothermic with a standard enthalpy of formation<sup>6</sup> of  $-8.79 \pm 0.59 \text{ kJ} \cdot \text{mol}^{-1} \text{ H}_2$ . However, if all of the hydrogen evolved during the run became hydride, an energy contribution would result that is more than one order of magnitude less than the excess heat that is observed according to Fig. 4. This can easily be calculated based on the amount of hydrogen evolved over  $\sim 12$  to  $14 \text{ h}$  at a rate of  $0.083 \text{ A}$ . Although the overall amount of energy produced in the experiment is relatively low, it is clear that the observed effect is outside the error limit of the experiment, which is of the order of  $\pm 1^\circ\text{C}/\text{W}$ , calculated from the accuracies of the measured parameters at the respective ranges.

It is not known what trivial chemical reaction might be triggered by the applied electrolysis that would be capable of producing the observed amount of excess heat. Some exotic farfetched possibilities for explaining the difference in electrochemical behavior between  $\text{K}_2\text{CO}_3$  and  $\text{Na}_2\text{CO}_3$  can be postulated. One such example is the formation of formic acid, e.g., by the reaction  $\text{HCO}_3^- + 2\text{H}_2\text{O} \rightarrow \text{HCOOH} + 3\text{OH}^-$ , or methane if  $\text{KHCO}_3$  is present in the electrolyte. However, even if such possibilities are invoked, it should not be forgotten that energy is also being spent for these electrochemical reactions, which will again result in an isoenthalpic (or thermoneutral) voltage. In most cases, the value of this thermoneutral voltage may exceed 1.48 V, which will cause cooling rather than heating of the solution. This is indicative of even higher excess energy values. A reaction that readily comes to mind is oxygen reduction. It is well known, however, that nickel is a poor catalyst of oxygen reduction, and the current density of this reaction is negligibly small compared with the current density applied here ( $\sim 1 \text{ mA/cm}^2$ ).

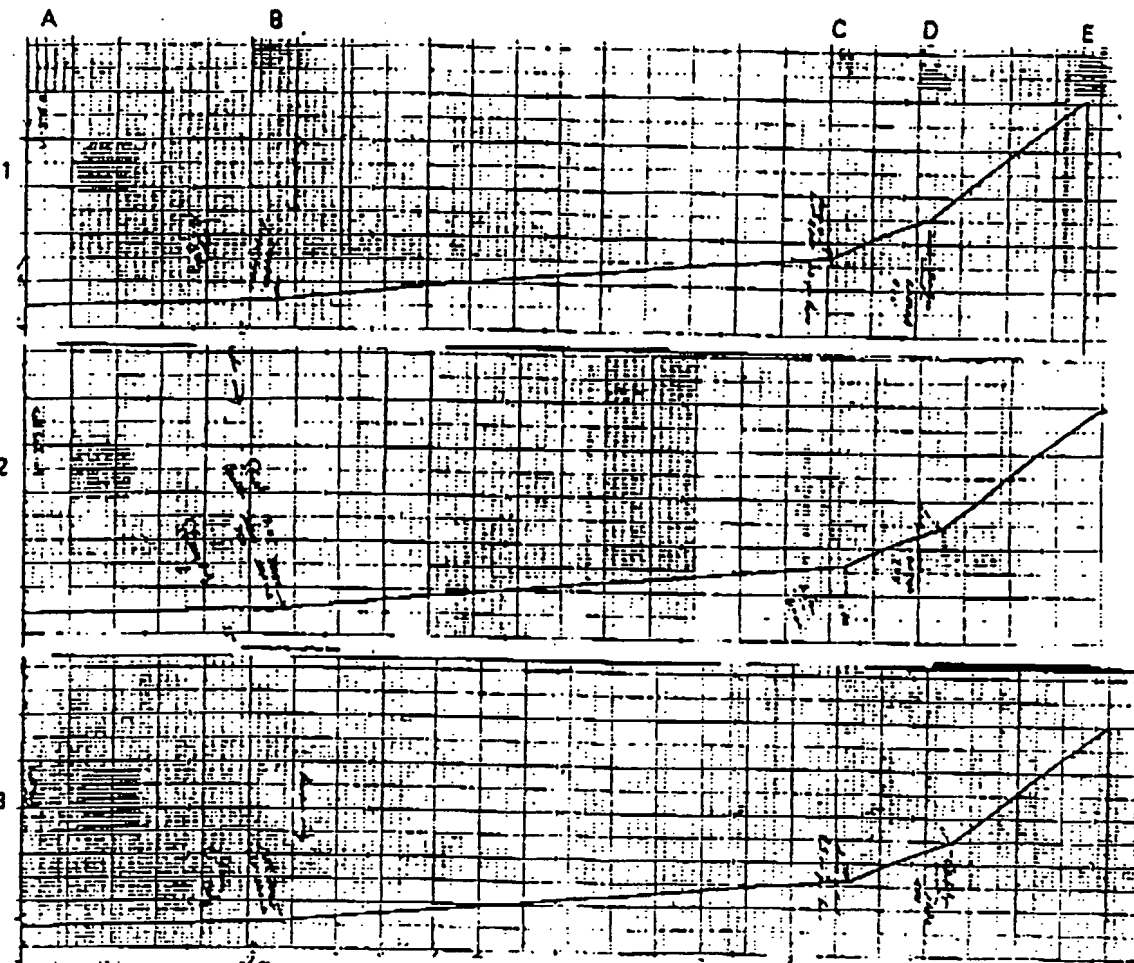


Fig. 5. Temperature changes at three points within the solution: (1) at the top, (2) in the middle, and (3) at the bottom. The setup used for this study is similar to that presented in Fig. 1, but in the working cell there are three thermistors instead of one. Section A-B: x axis scale = 30 division/h, y axis scale = 0.2°C/division, stirring only; section B-C: x axis scale = 30 division/h, y axis scale = 0.2°C/division, resistor only; section C-D: x axis scale = 5 division/h, y axis scale = 0.2°C/division, resistor only; and section D-E: x axis scale = 5 division/h, y axis scale = 0.2°C/division, electrolysis only.

These possibilities were rejected after study of the correspondence of the Faraday efficiency of the evolved H<sub>2</sub> and O<sub>2</sub> gases. This was done in a separate experiment by collecting the evolved gases and comparing the measured volume of the gases with the volume corresponding to the quantity of electricity that had passed through the cell over a given time. Note also that the absence of appreciable H<sub>2</sub>(D<sub>2</sub>) + O<sub>2</sub> recombination has been noted by a number of investigators, even in systems that contain metals (e.g., palladium) that are known to be good catalysts of that reaction (e.g., Refs. 9 through 14). Other preliminary studies (mass spectroscopy, pH measurements, titration) before and after the experiment showed no unexpected species or pH change. These studies should be continued further.

The problem of recombination is a crucial one in this study (note again that the excess heat here is calculated after subtracting 1.48 V), however, and it deserves special attention in any further experiments. On the other hand, as we have noted,<sup>6</sup> the problem of recombination (and the other related calorimetric problems) preferably should not be solved by studying the effect in a closed cell with a recombiner. The recombiner adds new unknowns since the kinetics

of the recombination of H<sub>2</sub> and O<sub>2</sub> to H<sub>2</sub>O should be well understood through studies such as those in Ref. 15. On the other hand, since the claimed excess energy itself is a newly found, unstudied phenomenon, no additional conditions should be imposed because their eventual effect on the reproducibility of the excess energy is unknown. For instance, it is not clear whether the ability of the recombiner to recombine not only the H<sub>2</sub> and O<sub>2</sub> evolving through electrolysis but also all other quantities of H<sub>2</sub> and O<sub>2</sub> existing in the gas and the liquid phase, thus creating concentration gradients, will be a hindering factor for the appearance of excess energy.

An explanation for the increase in the heating coefficient for a Ni/Pt circuit might be that an additional source of energy of unknown nature is acting from within that adds to the energy input to the cell from without. If this nontrivial possibility is confirmed, this effect will be of great importance as an alternative energy source. Further calorimetric sophistication is necessary to further confirm the reality of the observed effect and to obtain a quantitative assessment of its magnitude. For instance, to avoid errors of a subjective nature, a data acquisition and processing system is necessary. The measurements should be carried out at constant input

Noninski

## EXCESS HEAT WITH LIGHT WATER SOLUTION

power and for longer periods of time so that curves like curve 1 of Fig. 2 reach a clear and sustained steady state. Maintaining a constant ambient temperature is also a requirement in these studies. Such studies are now in progress. To fully avoid concerns connected with the peculiarities of heat transfer during bubble evolution, it is necessary, together with heat loss calorimetry measurements (including Seebeck), that this effect be observed in an adiabatic-type calorimeter (bomb calorimeter) similar to the one used in Ref. 6. Note, however, that despite the opinions of some researchers, if careful studies are carried out, calorimetric techniques are not only capable but are the only ones that can decisively prove (or disprove) the reality of the effect in question. There is also no reason to expect that time spans of tens of hours will be insufficient to definitely rule out (or conclusively confirm) a trivial explanation of the observed effect if the studies are conducted carefully. It seems, however, that the reality of the effect can qualitatively be established with the described procedure. It seems also that the reported effect is reproducible and can easily be demonstrated.

It is the author's understanding that speculations (invoking reactions of nuclear or any other origin) as to why overcoming the energy break-even barrier might come about should be carried out only after firmly establishing the reality of the claimed effect through experiments. This circumstance is not new for science. One may recall the experimental findings of Davison and Germer, Einstein, Wien, Compton, and others, which were unexplainable at the level of knowledge at their time. These experimental findings virtually caused the birth of 20th century physics, especially quantum mechanics. Even one of the most recent scientific discoveries—high-temperature superconductivity—whose reality is undeniable, still remains unexplained, which does not make this experimentally found effect less important.

Since the problem of the reality (nontriviality) of the excess energy reported here is of primary concern, we leave open the questions for the theoretical explanation of the phenomenon.

## CONCLUSIONS

The experimental results presented here show that there is more evidence than usually considered for the eventual production of excess energy during the electrolysis of water. Therefore, further efforts seem to be justified for verifying the claim of Fleischmann and Pons for overcoming the energy break-even barrier through electrolysis.

Contrary to the opinion expressed in Refs. 16 and 17, it does not seem plausible that light water should be used as a "control" when excess energy is being sought during the electrolysis of heavy water.

## ACKNOWLEDGMENTS

The author wishes to thank J. J. Farrell, Franklin and Marshall College, for his kind invitation to use his laboratory for these studies. Thanks are also due to James McBreen, Brookhaven National Laboratory; David Worledge, Electric Power Research Institute; and M. H. Miles, Naval Weapons Center, for useful discussions. The author would like to thank also W. R. Good for technical help.

The author also wishes to thank the two referees for their careful reading of the manuscript and for their useful remarks.

## REFERENCES

1. M. FLEISCHMANN and S. PONS, "Electrochemically Induced Nuclear Fusion of Deuterium," *J. Electroanal. Chem.*, 262, 301 (1989); see also Errata, *J. Electroanal. Chem.*, 263, 187 (1989).
2. S. PONS, M. FLEISCHMANN, C. WALLING, and J. SIMONS, "Method and Apparatus for Power Generation," International Application Published Under Patent Cooperation Treaty (PCT/US90/01328; International Publication Number WO 90/10935) (Mar. 13, 1989).
3. B. F. BUSH, J. J. LAGOWSKI, M. H. MILES, and G. S. OSTROM, "Helium Production During the Electrolysis of D<sub>2</sub>O in Cold Fusion Experiments," *J. Electroanal. Chem.*, 304, 271 (1991).
4. R. L. MILLS and S. P. KNEIZYS, "Excess Heat Production by the Electrolysis of an Aqueous Potassium Carbonate Electrolyte and the Implications for Cold Fusion," *Fusion Technol.*, 20, 65 (1991).
5. T. MATSUMOTO, "Cold Fusion Observed with Ordinary Water," *Fusion Technol.*, 17, 490 (1990).
6. V. C. NONINSKI and C. I. NONINSKI, "Determination of the Excess Energy Obtained During the Electrolysis of Heavy Water," *Fusion Technol.*, 19, 364 (1991).
7. G. M. MISKELLY, M. J. HEBEN, A. KUMAR, R. M. PENNER, M. J. SAILOR, and N. S. LEWIS, "Analysis of the Published Calorimetric Evidence for Electrochemical Fusion of Deuterium in Palladium," *Science*, 246, 793 (1989).
8. G. ALEFELD and J. VOLKL, Eds., *Hydrogen in Metals II*, p. 173, Springer-Verlag (1967).
9. V. J. CUNNANE, R. A. SCANNELL, and D. J. SCHIFFRIN, "H<sub>2</sub> + O<sub>2</sub> Recombination in Non-Isothermal, Non-Adiabatic Electrochemical Calorimetry of Water Electrolysis in an Undivided Cell," *J. Electroanal. Chem.*, 269, 163 (1989).
10. R. C. KAINTHALA et al., "Sporadic Observation of the Fleischmann-Pons Heat Effect," *Electrochim. Acta*, 34, 1315 (1989).
11. D. E. WILLIAMS et al., "Upper Bounds on 'Cold Fusion' in Electrolysis Cells," *Nature*, 342, 375 (1989).
12. T. R. JOW, E. PLICHTA, C. WALKER, S. SLANE, and S. GILMAN, "Calorimetric Studies of Deuterated Pd Electrodes," *J. Electrochem. Soc.*, 137, 2473 (1990).
13. D. ALBAGLI et al., "Measurement and Analysis of Neutron and Gamma-Ray Emission Rates, Other Fusion Products, and Power in Electrochemical Cells Having Pd Cathodes," *J. Fusion Energy*, 9, 133 (1990).
14. J. DIVISEK, L. FURST, and J. BALEJ, "Energy Balance of D<sub>2</sub>O Electrolysis with a Palladium Cathode. Part II. Experimental Results," *J. Electroanal. Chem.*, 278, 99 (1990).
15. M. J. JONCICH and N. J. HACKERMAN, "The Reaction of Hydrogen and Oxygen on Submerged Platinum Electrode Catalysts. I. Effect of Stirring, Temperature and Electric Polarization," *J. Phys. Chem.*, 57, 674 (1953).
16. H. FURST, cited after "Hopes for Nuclear Fusion Continue to Turn Cool," *Nature*, 338, 691 (1989).
17. J. MADDOX, "What to Say About Cold Fusion," *Nature*, 338, 701 (1989).

# EXCESS HEAT PRODUCTION BY THE ELECTROLYSIS OF AN AQUEOUS POTASSIUM CARBONATE ELECTROLYTE AND THE IMPLICATIONS FOR COLD FUSION

COLD FUSION

TECHNICAL NOTE

KEYWORDS: cold fusion, calorimetry, electrolysis

RANDELL L. MILLS Mills Technologies, The Griest Building  
Suite 700 I, 8 North Queen Street, Lancaster, Pennsylvania 17603

STEVEN P. KNEIZYS Ursinus College, Academic Computing  
Collegeville, Pennsylvania 19426

Received February 20, 1991

Accepted for Publication April 1, 1991

According to a novel atomic model, the predominant source of heat of the phenomenon called cold fusion is the electrocatalytically induced reaction whereby hydrogen atoms undergo transitions to quantized energy levels of lower energy than the conventional ground state. These lower energy states correspond to fractional quantum numbers. The hydrogen electronic transition requires the presence of an energy hole of  $-27.21\text{ eV}$  provided by electrocatalytic reactants (such as  $\text{Pd}^{2+}/\text{Li}^+$ ,  $\text{Ti}^{4+}$ , or  $\text{K}^+/\text{K}^+$ ) and results in "shrunken atoms" analogous to muonic atoms. In the case of deuterium, fusion reactions of shrunken atoms predominantly yielding tritium are possible. Calorimetry of pulsed current and continuous electrolysis of aqueous potassium carbonate ( $\text{K}^+/\text{K}^+$  electrocatalytic couple) at a nickel cathode is performed in single-cell dewar calorimetry cells. Excess power out exceeded input power by a factor of  $>37$ .

ics, and the strong and weak forces are unified. Their theory is a quantum theory in which the four quantum numbers of the electron of the one-electron atom arise naturally without gamma factors and provide an explanation for the seemingly contradictory and inconsistent observations of cold fusion. A summary of the development of the theory pertinent to cold fusion follows.

## II. THE ONE-ELECTRON ATOM

One-electron atoms include the hydrogen atom,  $\text{He(I)}$ ,  $\text{Li(II)}$ ,  $\text{Be(III)}$ , and so on. In each case, the nucleus contains  $Z$  protons and the atom has a net positive charge of  $(Z - 1)e$ . All forces are central. The mass-energy and angular momentum of the electron are constant; this requires that the equation of motion of the electron be temporally and spatially harmonic. Thus, Laplace's equation applies and

$$\left(\nabla^2 + \frac{1}{v^2 \delta t^2}\right)V = 0. \quad (1)$$

### II.A. The Boundary Condition

The condition for radiation by a moving charge is derived from Maxwell's equations. To radiate, the space-time Fourier transform of the charge density function must possess components that are synchronous with waves traveling at the speed of light.<sup>2</sup> Alternatively, for nonradiative states, the charge density function must not possess space-time Fourier components that are synchronous with waves traveling at the speed of light.

### II.B. The Radial Function

Mills and Farrell<sup>1</sup> do not solve for the radial function from Laplace's equation. Rather, they treat this as a boundary value problem and assume a delta function for the radial function:

$$f(r) = \delta(r - r_a). \quad (2)$$

## I. INTRODUCTION

As a result of the *de facto* assumptions of quantum mechanics and the incomplete or erroneous models that often follow, the prediction and development of useful or functional systems and structures requiring an accurate understanding of atomic structure and energy transfer have been limited. The Schrödinger equation, for example, does not explain the phenomenon referred to as "cold" nuclear fusion: large anomalous heat release and trace tritium production of certain heavy water electrolytic cells having a palladium cathode and a lithium electrolyte. Thus, advances in this field are largely limited to laboratory discoveries that have limited or suboptimal utility. To remedy the shortcomings and inconsistencies of quantum mechanics, Mills and Farrell<sup>1</sup> developed a novel theory for which the fundamental laws of nature are shown to be applicable on all scales. Maxwell's equations, Einstein's general and special relativity, Newtonian mechan-

where  $r_n$  is an allowed radius. [Note that the boundary condition for solution of the radial function of the hydrogen atom with the Schrödinger equation is  $\Psi \rightarrow 0$  as  $r \rightarrow 0$ . Here, however, the boundary condition is embodied in Eq. (2).] Thus, this trial function implies that the allowed states are two-dimensional spherical shells (zero thickness) of charge density (and mass density) at specific radii  $r_n$ . These shells are referred to as electron orbit spheres. When the form of the charge density function is known, the boundary condition (for nonradiation) can be applied to determine specific conditions for  $r_n$ . Here, the results of Mills and Farrell<sup>1</sup> are given:

$$2\pi(nr_1) = 2\pi r_n = n\lambda_1 = \lambda_n . \quad (3)$$

where

$$n = 1, 2, 3, 4, \dots$$

$$n = \frac{1}{2}, \frac{3}{2}, \frac{5}{2}, \dots$$

$\lambda_1$  = allowed wavelength for  $n = 1$

$r_1$  = allowed radius for  $n = 1$ .

There are several noteworthy features of Eq. (3):

1. Values of  $n$  other than the traditional 1, 2, 3, ..., are allowed.

2. The potential energy is a constant (at a given  $n$ ) because the electron is at a fixed distance  $r_n$  from the nucleus:

$$V_n = \frac{-Ze^2}{4\pi\epsilon_0 r_n} , \quad (4)$$

where  $\epsilon_0$  is the permittivity of free space.

3. The kinetic energy and velocity squared are constant because the atom does not radiate at  $r_n$  and the potential energy is constant:

$$T_n = \frac{1}{2}m_e v_n^2 . \quad (5)$$

4. The linear momentum must be constant:

$$p_n = \pm m_e v_n . \quad (6)$$

5. The wavelength must be constant. Using the de Broglie relationship,

$$\lambda_n = \frac{\hbar}{p_n} = \frac{\hbar}{m_e v_n} . \quad (7)$$

### III.C. The Angular Function

The radial function for the electron indicates that the electron is two-dimensional. Therefore, the angular mass density function  $A(\theta, \phi, t)$  of the electron must be a solution of the Laplace equation in two dimensions (plus time):

$$\left( \nabla^2 + \frac{1}{v^2} \frac{\delta^2}{\delta t^2} \right) A(\theta, \phi, t) = 0 \quad (8)$$

or

$$\left[ \frac{1}{r^2 \sin\theta} \frac{\delta}{\delta\theta} \left( \sin\theta \frac{\delta}{\delta\theta} \right)_{\text{re}} + \frac{1}{r^2 \sin^2\theta} \left( \frac{\delta^2}{\delta\phi^2} \right)_{\text{re}} + \frac{1}{v^2} \frac{\delta^2}{\delta t^2} \right] \times A(\theta, \phi, t) = 0 . \quad (9)$$

where  $v$  is the linear velocity of the electron.

Conservation of momentum and energy allows the angular functions and time functions to be separated:

$$A(\theta, \phi, t) = Y(\theta, \phi)K(t) . \quad (10)$$

Charge is conserved as well, and the charge of an electron can be superimposed on its mass. That is, the angular mass density function  $A(\theta, \phi, t)$  is also the angular charge density function.

The electron orbit sphere experiences a constant potential energy because it is fixed at  $r = r_n$ . To avoid being pulled into the nucleus, the orbit sphere must rotate. It is the rotation of the orbit sphere that causes angular momentum. The rotational energy of a rotating body is

$$E_{\text{rotational}} = \frac{1}{2}I\omega^2 , \quad (11)$$

where

$I$  = moment of inertia

$\omega$  = angular velocity.

The angular velocity must be constant (at a given  $n$ ) because  $r$  is constant, and the energy and angular momentum are constant. The allowed angular velocities are related to the allowed frequencies by

$$\omega_n = 2\pi\nu_n . \quad (12)$$

The allowed frequencies are related to the allowed velocities by

$$v_n = \nu_n \lambda_n . \quad (13)$$

The allowed velocities and angular frequencies are related to  $r_n$  by

$$v_n = r_n \omega_n , \quad (14)$$

$$\omega_n = \frac{\hbar}{m_e r_n^2} , \quad (15)$$

and

$$v_n = \frac{\hbar}{m_e r_n} . \quad (16)$$

The magnitude of the angular momentum  $|L|$  must be constant. The constant is  $\hbar$ :

$$|L_n| = m_e v_n r_n = m_e \frac{\hbar}{m_e r_n} r_n = \hbar . \quad (17)$$

Thus, Eq. (9) becomes

$$-\frac{\hbar^2}{2I} \left[ \frac{1}{\sin\theta} \frac{\delta}{\delta\theta} \left( \sin\theta \frac{\delta}{\delta\theta} \right)_{\text{re}} + \frac{1}{\sin^2\theta} \left( \frac{\delta^2}{\delta\phi^2} \right)_{\text{re}} \right] \times A(\theta, \phi, t) = EA(\theta, \phi, t) . \quad (18)$$

The space-time angular function  $A(\theta, \phi, t)$  is separated into an angular function and a time function,  $Y(\theta, \phi)K(t)$ . The time-harmonic function  $K(t) = \exp(i\omega_n t)$  is a solution. [Here, again, the boundary condition (for nonradiation) determines the specific conditions for  $\omega_n$ .] When the time-harmonic function is eliminated,

$$-\frac{\hbar^2}{2I} \left[ \frac{1}{\sin\theta} \frac{\delta}{\delta\theta} \left( \sin\theta \frac{\delta}{\delta\theta} \right)_{\text{re}} + \frac{1}{\sin^2\theta} \left( \frac{\delta^2}{\delta\phi^2} \right)_{\text{re}} \right] \times Y(\theta, \phi) = EY(\theta, \phi) . \quad (19)$$

Equation (19) is the equation for the rigid rotor. The angular function can be separated into a function of  $\theta$  and a function of  $\phi$ , and the solutions are well known.<sup>3</sup> The energies are given by

$$E_{\text{rotational}} = \frac{\hbar^2 l(l+1)}{2I} , \quad l = 0, 1, 2, 3, \dots \quad (20)$$

The angular functions are the spherical harmonics  $Y_l^m(\phi, \theta)$ . The spherical harmonic  $Y_1(\phi, \theta) = 1, s = \frac{1}{2}$ , is also a solution. The spherical harmonics can be positive or negative (depending on  $\theta$ ): the most negative value is  $-1$ . But the mass of the electron cannot be negative, and the charge cannot be positive. Thus, to ensure that the function is always positive or zero, the form of the angular solution must be

$$Y_S(\phi, \theta) + Y_l^m(\phi, \theta), \quad (21)$$

where  $Y_S(\phi, \theta)$  is called the angular spin function and  $Y_l^m(\phi, \theta)$  is called the angular orbital function. The function  $Y_l^m(\phi, \theta)$  can be thought of as a modulation function. Thus, the angular momentum can be thought of as arising from a spin component and an orbital component that have corresponding energies. One result of this model for  $l = 0$  [uniform charge (mass) density] is that some of the angular momentum (kinetic energy) is not counted in the spin angular momentum (rotational energy). That is, for any spin axis, there is an infinite number of great circles with planes passing through that axis with angles other than 90 deg. All points on any one of these great circles are moving, but not all of that motion is part of the spin angular momentum (rotational energy); only that motion perpendicular to the spin axis is part of the spin angular momentum (rotational energy). Thus, the spin angular momentum (rotational energy) is always less than the total angular momentum (kinetic energy). The following relationships must hold:

$$E_{\text{rotational}} = \frac{1}{2} I \omega^2 \leq \frac{1}{2} m v^2, \quad (22)$$

$$I \omega \leq \hbar, \quad (23)$$

and

$$I \leq m r^2. \quad (24)$$

Furthermore, it is known from the Stern-Gerlach experiment that a beam of silver atoms splits into two components when passed through an inhomogeneous magnetic field. The measured spin angular momentum is  $\sqrt{\frac{1}{4}}\hbar$ , and the angular momentum in the direction of the applied field is  $\pm\hbar/2$ . Given a uniform density of points traveling on great circles with a total angular momentum of  $\hbar$ , it can be shown<sup>1</sup> that the projection of the total angular momentum onto the spin axis is  $\sqrt{\frac{1}{4}}\hbar$ . The Stern-Gerlach experiment implies a magnetic moment of one Bohr magneton and an associated angular momentum quantum number of  $\frac{1}{2}$ . Historically, this quantum number is called the spin quantum number  $m_s$ , and that designation is maintained.

## II.Q. The Magnetic Field from the Spinning Orbit Sphere

The orbit sphere is a spinning shell of negative charge. For  $l = 0$ , the orbit sphere gives rise to a magnetic moment of one Bohr magneton.<sup>3</sup>

$$\beta = \frac{e\hbar}{2m_e} = 9.274 \times 10^{-24} \text{ J/T}, \quad (25)$$

and a magnetic field,<sup>1</sup>

$$H = \begin{cases} \frac{e\hbar}{m_e r_n^3} (i_r \cos \theta - i_\theta \sin \theta), & \text{for } r < r_n \\ \frac{e\hbar}{2m_e r^3} (i_r 2 \cos \theta - i_\theta \sin \theta), & \text{for } r > r_n \end{cases} \quad (26) \quad (27)$$

Note that the magnetic field is a constant for  $r < r_n$ .

It can be shown<sup>1</sup> that the energy stored in the magnetic field of the electron orbit sphere is

$$E_{\text{mag}} = \frac{\pi \mu_0 e^2 \hbar^2}{m_e r_n^3}. \quad (28)$$

## II.E. Determination of $r_n$

The one-electron orbit sphere is a spherical shell of negative charge (total charge =  $-e$ ) of zero thickness at a distance  $r_n$  from the nucleus (charge =  $+Ze$ ). For the ground state ( $n = 1$ ), the centrifugal force of the electron is given by

$$f_{\text{centrifugal}} = \frac{m_e v_1^2}{r_1}. \quad (29)$$

The centripetal force is the Coulombic force  $f_{\text{Coul}}$  between the electron and the nucleus:

$$f_{\text{Coul}} = \frac{Z_{\text{eff}} e^2}{4\pi\epsilon_0 r_1^2}, \quad (30)$$

where  $\epsilon_0$  is the permittivity of free space. Thus,

$$\frac{m_e v_1^2}{r_1} = \frac{Z e^2}{4\pi\epsilon_0 r_1^2}. \quad (31)$$

Using Eq. (16),

$$r_1 = \frac{4\pi\epsilon_0 \hbar^2}{Z e^2 m_e}. \quad (32)$$

The Bohr radius is substituted into Eq. (32):

$$a_0 = \frac{4\pi\epsilon_0 \hbar^2}{e^2 m_e} \quad (33)$$

and

$$r_1 = \frac{a_0}{Z}. \quad (34)$$

## II.F. Energy Calculations

The potential energy  $V$  can be calculated from the force between the electron and the nucleus [Eq. (30)] and the radius  $r_1$ :

$$V = \frac{-Ze^2}{4\pi\epsilon_0 r_1} = \frac{-Z^2 e^2}{4\pi\epsilon_0 a_0} = -Z^2 \times 4.3675 \times 10^{-18} \text{ J} \\ = -Z^2 \times 27.2 \text{ eV}. \quad (35)$$

Because this is a central force problem, the kinetic energy  $T$  is  $-\frac{1}{2}V$ :

$$T = \frac{Z^2 e^2}{8\pi\epsilon_0 a_0} = Z^2 \times 13.159 \text{ eV}. \quad (36)$$

The same result can be obtained from  $T = \frac{1}{2}m_e v_1^2$  and Eq. (16).

Alternatively, the kinetic energy, which is equal to the stored electric energy  $E_{\text{ele}}$ , can be calculated from<sup>4</sup>

$$T = E_{\text{ele}} = -\frac{1}{2} \epsilon_0 \int_{-\infty}^{r_1} \epsilon^2 dv, \quad (37)$$

where

$$\epsilon = \frac{Ze}{4\pi\epsilon_0 r^3}.$$

Thus, as the orbit sphere shrinks from  $\infty$  to  $r_1$ ,

$$E_{ele} = -\frac{1}{2} \epsilon_0 \int_0^{2\pi} \int_0^{\pi} \int_{-\infty}^{r_1} \epsilon^2 r^2 \sin\theta dr d\theta d\phi \quad (38)$$

$$= -\frac{Z^2 e^2}{8\pi\epsilon_0} \int_{\infty}^{r_1} \frac{1}{r^2} dr \quad (39)$$

$$= \frac{Z^2 e^2}{8\pi\epsilon_0 a_0} = Z^2 \times 2.1837 \times 10^{-18} \text{ J} \quad (40)$$

### III. EXCITED STATES OF THE ONE-ELECTRON ATOM

It is well known that resonator cavities can trap electromagnetic radiation of discrete resonant frequencies. The orbit sphere is a resonator cavity and can trap photons of discrete frequencies. Thus, photon absorption occurs as an excitation of a resonator mode.

An electron in the ground state ( $n = 1$ ) is in force balance:

$$\frac{m_e v_1^2}{r_1} = \frac{Ze^2}{4\pi\epsilon_0 r_1^2}. \quad (41)$$

When an electron in the ground state absorbs a photon of sufficient energy to take it to a new nonradiative state ( $n = 2, 3, 4, \dots$ ), force balance must be maintained. This is possible only if  $Z_{eff} = Z/n$ ; therefore,

$$\frac{m_e v_n^2}{r_n} = \frac{Z_{eff} e^2}{4\pi\epsilon_0 r_n^2}. \quad (42)$$

The reduction of the charge from  $Ze$  to  $Ze/n$  is caused by trapping a photon in the orbit sphere cavity—a spherical cavity. The photon's electric field creates standing waves in the cavity with an effective charge of  $(-1 + 1/n)Ze$  (at  $r_n$ ). The total charge experienced by the electron is the sum of the proton and photon charge components. The equation for these trapped photons can be solved as a boundary value problem of Laplace's equation.

For the hydrogen atom, the boundary conditions are that the radial electric field of the photon at  $r_n$  is

$$\epsilon \hat{i}_{r,\text{photon}} = \left( -1 + \frac{1}{n} \right) \frac{e}{4\pi\epsilon_0 (r_n)^2}. \quad n = 2, 3, 4, \dots \quad (43)$$

The general form of the solution to Laplace's equation in spherical coordinates is

$$\Phi(r, \theta, \phi) = \sum_{l=0}^{\infty} \sum_{m=-l}^l [A_{l,m} r^l + B_{l,m} r^{-(l+1)}] \times [Y_{l,m}(\theta, \phi) + Y_s(\theta, \phi)]. \quad (44)$$

All  $A_{l,m}$  are zero because the electric field given by the potential must be inversely proportional to the radius to obtain force balance. The electric field is the gradient of the potential:

$$\epsilon = -\nabla \Phi \quad (45)$$

and

$$\epsilon \hat{i}_r = -\frac{\delta \Phi}{\delta r} \hat{i}_r. \quad (46)$$

Thus,

$$\epsilon \hat{i}_r = \sum_{l=0}^{\infty} \sum_{m=-l}^l B_{l,m} (l+1) r^{-(l+2)} [Y_l^m(\phi, \theta) + Y_s^m(\phi, \theta)]. \quad (47)$$

Given that  $\epsilon(\text{proton}) = +e/4\pi\epsilon_0 r_n^2$  and that the electric fields of the proton and photon must superimpose to yield a field equivalent to a central point charge of  $+Ze/n$ , the photon electric field for each mode is determined as follows. The angular part of the charge density function of the orbit sphere at force balance must be in phase with the electric field of the orbit sphere because the relationship between the total electric field equation and the photon charge density function is given by Maxwell's equation in two dimensions:

$$\mathbf{n} \cdot (\epsilon_1 - \epsilon_2) = \frac{\sigma}{\epsilon_0}, \quad (48)$$

where

$\mathbf{n}$  = normal unit vector ( $\hat{i}_r$ )

$\epsilon_1 = 0$  = electric field outside of the orbit sphere

$\epsilon_2$  = total electric field at  $r_n = na_0$

$\sigma$  = surface charge density.

Thus,

$$\begin{aligned} \epsilon \hat{i}_{r,\text{photon}}|_{r_n=na_0} &= \frac{e^2}{4\pi\epsilon_0 (na_0)^2} \left( -1 + \frac{1}{n} \operatorname{Re} \{ i[Y_l^m(\phi, \theta) + Y_s^m(\phi, \theta)] \} \right) \\ &= \sum_{l=0}^{\infty} \sum_{m=-l}^l -B_{l,m} (l+1) (na_0)^{-(l+2)} \end{aligned} \quad (49)$$

$$\times \operatorname{Re} \{ i[Y_l^m(\phi, \theta) + Y_s^m(\phi, \theta)] \}. \quad (50)$$

for

$n = 2, 3, 4, \dots$

$l = 1, 2, \dots, n-1$

$m = -l, -l+1, \dots, 0, \dots, +l$ ,

and

$$\begin{aligned} \epsilon \hat{i}_{r,\text{photon},n,l,m}|_{r_n=na_0} &= \frac{e^2}{4\pi\epsilon_0 (na_0)^2} \left( -1 + \frac{1}{n} \operatorname{Re} \{ i[Y_l^m(\phi, \theta) + Y_s^m(\phi, \theta)] \} \right) \\ &= \sum_{l=0}^{\infty} \sum_{m=-l}^l B_{l,m} \end{aligned} \quad (51)$$

Therefore,

$$\sum_{l=0}^{\infty} \sum_{m=-l}^l B_{l,m} = \frac{e(na_0)^l}{4\pi\epsilon_0 (l+1)} \left( -1 + \frac{1}{n} \right) \quad (52)$$

and

$$\begin{aligned} \epsilon \hat{i}_{r,\text{photon},n,l,m} &= \frac{e(na_0)^l}{4\pi\epsilon_0} \frac{1}{r^{(l+2)}} \\ &\times \left( -1 + \frac{1}{n} \operatorname{Re} \{ i[Y_l^m(\phi, \theta) + Y_s^m(\phi, \theta)] \} \right). \end{aligned} \quad (53)$$

where

$\epsilon_{r\text{total}}$  = sum of the photon and proton electric fields:

$$\begin{aligned}\epsilon_{r\text{total}} &= \frac{e}{4\pi\epsilon_0 r^2} + \frac{e(na_0)^l}{4\pi\epsilon_0} \frac{1}{r^{l+2}} \\ &\times \left( -1 + \frac{1}{n} \operatorname{Re} \{ i[Y_l^m(\phi, \theta) + Y_s^m(\phi, \theta)] \} \right).\end{aligned}\quad (54)$$

For  $r = na_0$ , the magnitude of the total radial electric field is

$$\epsilon_{r\text{total}} = \left[ \frac{e}{4\pi\epsilon_0(na_0)^2} + \frac{e}{4\pi\epsilon_0(na_0)^2} \right] \left( -1 + \frac{1}{n} \right) \quad (55)$$

and

$$\epsilon_{r\text{total}} = \frac{1}{n} \frac{e}{4\pi\epsilon_0(na_0)^2}. \quad (56)$$

For quantum numbers  $n$ ,  $l$ , and  $m$ , the potential functions are solutions to Laplace's equation. All boundary conditions are met for the corresponding electric fields. Thus, Eq. (54) is the solution of the excited modes of the resonator cavity (orbit sphere). And, the quantum numbers of the electron are  $n$ ,  $l$ ,  $m(m_i)$ , and  $m_s$ , as described in Sec. II.

The energy of the photon that excites a mode in a stationary spherical resonator cavity from radius  $a_0$  to radius  $na_0$  is

$$E_{\text{photon}} = \frac{e^2}{4\pi\epsilon_0 a_0} \left( 1 - \frac{1}{n^2} \right) = h\nu = \hbar\omega. \quad (57)$$

After multiplying Eq. (57) by

$$\frac{a_0}{a_0} = \frac{4\pi\epsilon_0\hbar^2}{e^2 m_e a_0},$$

where  $a_0$  is given by Eq. (33),  $\omega_{\text{photon}}$  is

$$\omega_{\text{photon}} = \frac{\hbar}{m_e a_0^2} \left( 1 - \frac{1}{n^2} \right). \quad (58)$$

In the case of an electron orbit sphere, the resonator possesses kinetic energy before and after the excitation. The kinetic energy is always one-half of the potential energy. As a result, the energy and angular frequency to excite an electron orbit sphere is only one-half of the values in Eqs. (57) and (58).

The angular velocity of an electron orbit sphere of radius  $na_0$  is

$$\omega_n = \frac{\hbar}{m_e(na_0)^2}. \quad (59)$$

The change in angular velocity of the orbit sphere for an excitation from  $n = 1$  to  $n = n$  is

$$\Delta\omega = \frac{\hbar}{m_e(a_0)^2} - \frac{\hbar}{m_e(na_0)^2} = \frac{\hbar}{m_e(a_0)^2} \left( 1 - \frac{1}{n^2} \right). \quad (60)$$

The kinetic energy change of the transition is

$$\frac{1}{2} m_e (\Delta\omega)^2 = \frac{1}{2} \frac{e^2}{4\pi\epsilon_0 a_0} \left( 1 - \frac{1}{n^2} \right) = \frac{1}{2} \hbar\omega. \quad (61)$$

The change in angular velocity of the electron orbit sphere [Eq. (60)] is identical to the angular velocity of the photon necessary for the excitation  $\omega_{\text{photon}}$  [Eq. (58)]. The energy of the photon to excite the equivalent transition in an electron

orbit sphere is one-half of the excitation energy of the stationary cavity because the change in kinetic energy of the electron orbit sphere supplies one-half of the necessary energy. The photon can carry zero or  $\pm\hbar$  units of angular momentum [Eq. (17)]. Thus, during excitation, the spin, orbital, or total angular momentum of the orbit sphere can change by zero or  $\pm\hbar$ . The electron transition rules arise from conservation of angular momentum. The radius of an orbit sphere increases with the absorption of electromagnetic energy. On ionization, the orbit sphere radius goes to infinity, and the electron is a plane wave (consistent with double-slit experiments) with a de Broglie wavelength of  $\lambda = \hbar/p$ .

#### IV. PAIR PRODUCTION

Matter and energy are interconvertible and are, in essence, different states of the same entity. The state, matter or energy, is determined by the laws of nature and the properties of space-time. A photon propagates according to Maxwell's equations at the speed of light in space-time with intrinsic impedance  $\eta$ . Matter as a fundamental particle is created in space-time from a photon. Matter obeys the laws of special relativity, the relationship of motion to space-time, and space-time is curved by matter according to the laws of general relativity. Relationships must exist between these laws and the implicit fundamental constants. The conversion of energy into matter requires a transition state in which the identification of the entity as matter or energy is impossible. From the properties of the entity, as matter or energy, and from the physical laws and the properties of space-time, the transition state hereafter called a virtual orbit sphere is derived.

For example, a photon of energy 1.02 MeV becomes a positron and an electron in the presence of charge. This phenomenon, called pair production, involves the conservation of mass/energy, charge, and angular momentum. Pair production occurs as an event in space-time where all boundary conditions are met according to the physical laws: Maxwell's equations, Newton's laws, and Einstein's special and general relativity, where matter and energy are indistinguishable by any physical property. Matter exists as orbit spheres; thus, the conversion of energy to matter must involve the orbit sphere equations derived earlier. It must also depend on the equations of electromagnetic radiation and the properties of space-time because matter is created from electromagnetic radiation as an event in space-time.

Matter and light obey the wave equation relationship:

$$v = \lambda \frac{\omega}{2\pi}. \quad (62)$$

The boundary condition for nonradiation by a virtual orbit sphere is

$$2\pi(r_n^*) = 2\pi(nr_1^*) = n\lambda_1^* = \lambda_n^*, \quad (63)$$

where

$$n = 1, 2, 3, 4, \dots$$

or

$$n = \frac{1}{2}, \frac{3}{2}, \frac{5}{2}, \dots$$

and where  $r^*$  and  $\lambda^*$  are the allowed radii and wavelengths for the virtual matter in question.

The relationship between the potential energy of an

electron orbit sphere and the angular velocity of the orbit sphere is

$$V = \hbar\omega^* = \frac{1}{n} \frac{e^2}{4\pi\epsilon_0 n a_0} . \quad (64)$$

It can be demonstrated that the velocity of the electron orbit sphere satisfies the relationship for the velocity of a wave by substitution of Eqs. (3) and (15) into Eq. (62), which gives Eq. (16). Similarly, the relationship among the velocity of light in free space  $c$ , frequency  $\omega$ , and wavelength  $\lambda$  is

$$c = \lambda \frac{\omega}{2\pi} , \quad (65)$$

and the energy of a photon of frequency  $\omega$  is

$$E = \hbar\omega . \quad (66)$$

Recall from Sec. III that a photon of discrete frequency  $\omega$  can be trapped in the orbit sphere of an electron that serves as a resonator cavity of radius  $r_n$  where the resonance excitation energy of the cavity is given by Eq. (64).

The angular velocities of the orbit sphere and trapped photon are the same, and the ratio of their linear velocities is

$$\frac{v_n}{c_{\text{photon}}} = \frac{\lambda_n \frac{\omega_n}{2\pi}}{\lambda_{\text{photon}} \frac{\omega_{\text{photon}}}{2\pi}} = \frac{\lambda_n}{\lambda_{\text{photon}}} , \quad (67)$$

where the subscripts  $n$  refer to orbit sphere quantities.

Consider a virtual electron orbit sphere, which is defined as the transition state between light and matter where light and matter are indistinguishable. For this case, the velocity of the electron virtual orbit sphere is the speed of light in the inertial reference frame of the photon that formed the virtual orbit sphere. Substituting  $c$  for  $v_n$  in Eq. (62),  $\lambda_n$  given by Eq. (3) [where  $r_1$  is given by Eqs. (32) and (33)] for  $\lambda$ , and of  $\omega_n$  given by Eq. (15) for  $\omega$  results in

$$c = 2\pi n a_0 \frac{\hbar}{m_e (n a_0)^2} . \quad (68)$$

Maxwell's equations provide that

$$c = \left( \frac{1}{\epsilon_0 \mu_0} \right)^{1/2} . \quad (69)$$

The result of substituting Eqs. (33) and (69) into Eq. (68) is

$$\frac{1}{n} = \frac{\hbar}{m_e c a_0} = \frac{\hbar (\epsilon_0 \mu_0)^{1/2}}{m_e} \frac{e^2 m_e}{4\pi\epsilon_0 \hbar^2} = \frac{1}{4\pi} \left( \frac{\mu_0}{\epsilon_0} \right)^{1/2} \frac{e^2}{\hbar} = \alpha^{-1} . \quad (70)$$

In fact,  $\alpha$  is the fine-structure constant (a dimensionless constant for pair production).<sup>3</sup> The experimental value is  $\frac{1}{137.03604}$ . However, by the boundary condition for nonradiation [Eqs. (3) and (63)]  $1/n$  must be 1 divided by an integer. That integer is exactly 137.

The permeability  $\mu_0$  of free space is defined as  $4\pi \times 10^{-7} \text{ N/A}^{-2}$ . The experimental permittivity  $\epsilon_0$  of free space is extremely close to  $1/36\pi \times 10^{-9} \text{ F/m}$ , and the experimental value of  $e^2/h$  is extremely close to  $\frac{1}{4110}$ .

To match the boundary condition [Eq. (3)],  $h/e^2 = 4110 = (30)(137)$  exactly, and  $\epsilon_0 = 1/36\pi \times 10^{-9} \text{ F/m}$  exactly.

In a similar fashion, the intrinsic impedance of free space can be calculated as

$$\eta = \left( \frac{\mu_0}{\epsilon_0} \right)^{1/2} = \left( \frac{4\pi \times 10^{-7}}{\frac{1}{36\pi} \times 10^{-9}} \right)^{1/2} = 120\pi \Omega , \quad (71)$$

and the speed of light is determined to be exactly

$$c = \frac{1}{(\mu_0 \epsilon_0)^{1/2}} = 3 \times 10^8 \text{ m/s} . \quad (72)$$

The result that  $c$  is exactly  $3 \times 10^8 \text{ m/s}$  may appear counter-intuitive given the arbitrary nature of the definitions of metres and seconds. However, mks units are not arbitrary. They are defined according to mutually dependent relationships between the constants and the electric and magnetic force laws. The units take on significance by the definition of  $\mu_0$  in terms of Newtons per square ampere. It can be demonstrated<sup>1</sup> that this definition fixes the exact value of the constants and gives rise to an exact definition of the second, metre, and kilogram.

The radius of the virtual electron orbit sphere is  $a_0/137$ , and the potential energy  $V$  is given by Eq. (64), where  $n$  is  $\frac{1}{137}$ :

$$V = -\frac{(137)^2 e^2}{4\pi\epsilon_0 a_0} . \quad (73)$$

Substituting

$$a_0 = \frac{4\pi\epsilon_0 \hbar^2}{m_e e^2} ,$$

$$\frac{\hbar}{e^2} = (30)(137) ,$$

$$\eta = \left( \frac{\mu_0}{\epsilon_0} \right)^{1/2} = 120\pi ,$$

and

$$c = \left( \frac{1}{\epsilon_0 \mu_0} \right)^{1/2}$$

into Eq. (73) results in

$$V = m_e c^2 . \quad (74)$$

Furthermore, the result of the multiplication of both sides of Eq. (15) by  $\hbar$ ,  $r_n = n a_0$ , and substituting

$$n = \frac{1}{137} ,$$

$$a_0 = \frac{4\pi\epsilon_0 \hbar^2}{m_e e^2} ,$$

$$\frac{\hbar}{e^2} = (30)(137) ,$$

$$\eta = \left( \frac{\mu_0}{\epsilon_0} \right)^{1/2} = 120\pi ,$$

and

$$c = \left( \frac{1}{\epsilon_0 \mu_0} \right)^{1/2}$$

yields

$$\hbar\omega_{1/137} = m_e c^2 . \quad (75)$$

The relativistic factor.

$$\gamma = \frac{1}{\left[1 - \left(\frac{v}{c}\right)^2\right]^{1/2}}$$

for an orbit sphere at radius  $r^*/137$  ( $a_0/137$  for the electron) is  $2\pi$ . The energy stored in the magnetic field of the electron orbit sphere is

$$E_{mag} = \frac{\pi \mu_0 e^2 h^2}{(m_e)^2 r_n^3} . \quad (76)$$

As a result of substituting  $a_0/137$  for  $r_n$ , 137 for  $Z_{eff}$  (recall that  $r_n = a_0/Z_{eff}$ ), the relativistic mass  $2\pi m_e$  for  $m_e$ ,

$$a_0 = \frac{4\pi\epsilon_0 h^2}{m_e e^2} ,$$

$$\frac{h}{e^2} = (30)(137) ,$$

$$\eta = \left(\frac{\mu_0}{\epsilon_0}\right)^{1/2} = 120\pi .$$

and

$$c = \left(\frac{1}{\epsilon_0 \mu_0}\right)^{1/2}$$

is

$$E_{mag} = m_e c^2 . \quad (77)$$

Thus, the energy stored in the magnetic field of the virtual electron orbit sphere equals the electrical potential energy of the virtual orbit sphere. The magnetic field is a relativistic effect of the electrical field; thus, equivalence of the potential and magnetic energies when  $v = c$  is given by special relativity where these energies are calculated using Maxwell's equations. The energy stored in the electric and magnetic fields of a photon are equivalent. The corresponding equivalent energies of the virtual orbit sphere are the electrical potential energy and the energy stored in the magnetic field of the orbit sphere.

Space-time is an electrical  $LC$  circuit with an intrinsic impedance of exactly

$$\eta = \left(\frac{\mu_0}{\epsilon_0}\right)^{1/2} = \left(\frac{\frac{4\pi \times 10^{-7}}{1}}{36\pi \times 10^{-9}}\right)^{1/2} = 120\pi . \quad (78)$$

The circumference of the virtual electron orbit sphere is  $2\pi a_0/137$ . The relativistic factor for the radius of  $a_0/137$  is  $2\pi$ ; thus, due to relativistic length contraction, the total capacitance of free space of the virtual orbit sphere of radius  $a_0/137$  is

$$C = \frac{2\pi \frac{a_0}{137} \epsilon_0}{2\pi} = \epsilon_0 \frac{a_0}{137} . \quad (79)$$

where  $\epsilon_0$  is the capacitance of space-time per unit length (farad per metre). Similarly, the inductance is

$$L = \frac{2\pi \frac{a_0}{137} \mu_0}{2\pi} = \mu_0 \frac{a_0}{137} . \quad (80)$$

where  $\mu_0$  is the inductance per unit length (henry per metre).

Thus, the resonance frequency of a virtual electron orbit sphere is

$$\omega^* = \frac{1}{(LC)^{1/2}} = \frac{1}{\left(\epsilon_0 \frac{a_0}{137} \mu_0 \frac{a_0}{137}\right)^{1/2}} . \quad (81)$$

Using

$$a_0 = \frac{4\pi\epsilon_0 h^2}{m_e e^2} ,$$

$$\frac{h}{e^2} = (30)(137) ,$$

$$\eta = \left(\frac{\mu_0}{\epsilon_0}\right)^{1/2} = 120\pi ,$$

and

$$c = \left(\frac{1}{\epsilon_0 \mu_0}\right)^{1/2} ,$$

then

$$\omega^* = \frac{m_e c^2}{h} . \quad (82)$$

Thus, the  $LC$  resonance frequency of free space for a virtual electron orbit sphere equals the angular frequency of the photon that forms the virtual orbit sphere.

The impedance of any  $LC$  circuit goes to infinity when it is excited at the resonance frequency. Thus, the electron virtual orbit sphere is an  $LC$  circuit excited at the corresponding resonance frequency of free space. The impedance of free space becomes infinite, and electromagnetic radiation cannot propagate. At this event, the frequency, wavelength, velocity, and energy of the virtual orbit sphere are equal to that of the photon. The mass/energy of the electron virtual orbit sphere is exactly the rest mass at infinity. Thus, a real orbit sphere electron is formed at infinity (with zero velocity) from the electron virtual orbit sphere in the presence of a central electric field of

$$\epsilon = \frac{+e}{4\pi\epsilon_0 r^2} , \quad (83)$$

where all of the electron virtual orbit sphere equations developed herein apply to this central field.

Actually, due to conservation of charge, a positron and an electron are formed of two photons of energy equal to the rest mass/energy of the electron. (Photons superimpose; thus, pair production occurs with a single photon of energy equal to twice the rest mass of an electron.)

For pair production, angular momentum is conserved. All photons carry  $\hbar$  angular momentum, and the angular momentum of all matter as orbit spheres is  $\hbar$  [see Eq. (17)]. The radius of particle creation is  $r_i^*/137$ . This radius is equal to the Compton wavelength bar  $\lambda_c$ , where  $\lambda_c = \hbar/mc$ . It arises naturally from the boundary condition of no radiation [Eqs. (3) and (63)], (where  $n = \frac{1}{137}$ ), the de Broglie relationship [Eq. (7)], and the fact that the velocity of the virtual orbit sphere equals  $c$ :

$$r_i^*/137 = \frac{\hbar}{mc} = \lambda_c . \quad (84)$$

The correct prediction of electron and positron creation (pair production) having a dimensionless cross section of  $\frac{1}{137}$  establishes the validity of electron states corresponding to fractional quantum numbers. In Sec. V, it is demonstrated that

the transition to fractional quantum states and the resulting "shrunken" atoms account for the phenomenon called cold fusion.

## V. HECTOR AND COULOMBIC ANNIHILATION FUSION (COLD FUSION)

For the hydrogen atom, the radius of the ground-state orbit sphere is  $a_0$ . This orbit sphere contains no photonic waves, and the centripetal force and the Coulombic force balance. Thus,

$$\frac{m_e v_i^2}{a_0} = \frac{e^2}{4\pi\epsilon_0 a_0^2}. \quad (85)$$

It is shown in Sec. III that the electron orbit sphere is a resonator cavity that can trap electromagnetic radiation of discrete frequencies. The photon potential functions are solutions of Laplace's equation. The photons decrease the nuclear charge to  $1/n$  and increase the radius of the orbit sphere to  $na_0$ . The new configuration is also in force balance:

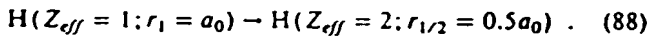
$$\frac{m_e v_n^2}{na_0} = \frac{e^2/n}{4\pi\epsilon_0 (na_0)^2}. \quad (86)$$

Mills and Farrell<sup>1</sup> propose, however, that the orbit sphere resonator can trap photons that increase the nuclear charge and decrease the radius of the orbit sphere. This occurs, for example, when the orbit sphere couples to another resonator cavity that can absorb energy—this is the absorption of an energy hole. The absorption of an energy hole destroys the balance between the centrifugal force and the increased central Coulombic force. As a result, the electron is pulled toward the nucleus. If another allowed state that obeys the boundary conditions is not available, the electron plunges into the nucleus.

Now, recall that, for the  $\text{He}^+$  ion ( $Z = 2$ , a one-electron atom), an allowed state exists at  $0.5a_0$ . It can be shown that if a ground-state hydrogen atom emits a photon of  $\sim 27$  eV, two photons are created—one is ejected and one remains in the orbit sphere. The photonic wave in the orbit sphere creates an effective charge at the orbit sphere such that the electron experiences an effective charge of  $+2e$  and establishes a new centripetal/Coulombic equilibrium at  $r_{1/2} = 0.5a_0$ . That is, the orbit sphere shrinks from  $r_1 = a_0$  to  $r_{1/2} = a_0/2$ :

$$\begin{aligned} V &= -\frac{Z_{eff} e^2}{4\pi\epsilon_0 r_{1/2}} = -\frac{2 \times 2e^2}{4\pi\epsilon_0 a_0} \\ &= -4 \times 27.178 \text{ eV} = -108.70 \text{ eV}. \end{aligned} \quad (87)$$

The kinetic energy of the shrunken orbit sphere is  $-\frac{1}{2}V$  or  $T = 54.35$  eV. The ground-state hydrogen atom has a net energy of  $-13.59$  eV, and the final hydrogen atom has a net energy of  $-54.42$  eV (the same as  $\text{He}^+$ ), and  $\Delta E = -40.83$  eV for the reaction



That is,  $-27$  eV is lost with the absorption of the energy hole, and  $-14$  eV is given off after absorption of the energy hole.

It is shown later that the resonance energy hole of a hy-

drogen atom that excites resonator modes of radial dimensions  $a_0/(m + 1)$  is

$$m \times 27.2 \text{ eV}, \quad (89)$$

where

$$m = 1, 2, 3, 4, \dots$$

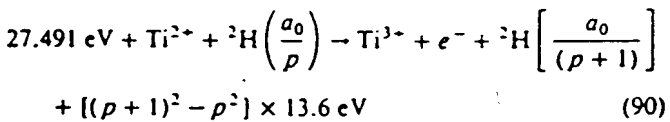
After resonant absorption of the hole, the radius  $a_0$  of the orbit sphere shrinks to  $a_0/(m + 1)$ , and after  $p$  cycles of resonant shrinkage, the radius is  $a_0/(mp + 1)$ .

In other words, the radial ground-state field can be considered as the superimposition of Fourier components. The removal of negative Fourier components of energy  $m \times 27.2$  eV, where  $m$  is an integer, gives rise to a larger positive electric field inside the spherical shell, which is a time-harmonic solution of Laplace's equations in spherical coordinates. In this case, the radius at which force balance and nonradiation are achieved is  $a_0/(m + 1)$ , where  $m$  is an integer. In decaying to this radius from the ground state, a total energy of  $[(m + 1)^2 - 1^2] \times 13.6$  eV is released. The process is hereafter referred to as hydrogen emission by catalytic thermal electronic relaxation (HECTOR).

The electric field of a hydrogen atom, or a deuterium atom, is zero for  $r > r_n$ , where  $r_n$  is the radius of the orbit sphere of the electron. Thus, as the orbit sphere shrinks, approaching nuclei experience a smaller Coulombic barrier, and the internuclear distance (between two deuterium atoms, for example) shrinks as well. As the internuclear separation decreases, fusion is more probable. In muon-catalyzed fusion, for example, the internuclear separation is reduced by  $\sim 200$  (the muon-to-electron mass ratio), and the fusion rate increases by  $\sim 80$  orders of magnitude. In a catalytic system that produces energy holes of 27.21 eV, deuterium atoms can be repeatedly shrunk, and the internuclear separation can be much smaller than the muon reduction. These smaller internuclear distances yield much higher fusion rates. Mills and Farrell<sup>1</sup> call this fusion process Coulombic annihilation fusion (CAF).

It is important to note that the products of CAF are tritium,  ${}^3\text{H}$ , and protons,  ${}^1\text{H}$ . In hot fusion, deuterium nuclei collide randomly and produce  $\sim 50\%$   ${}^3\text{H}$  plus  ${}^1\text{H}$  and  $\sim 50\%$   ${}^3\text{He}$  plus a neutron. In CAF, however, the nuclei are moving slowly and will collide in the most favored Coulombic arrangement—with the two protons as far from each other as possible. Thus, for CAF, significantly more  ${}^3\text{H}$  will be produced than  ${}^3\text{He}$ .

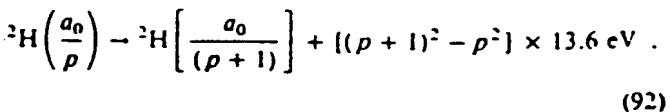
Titanium(II) is one of the catalysts that can cause resonant shrinkage because the third ionization energy is 27.49 eV [ $m = 1$  in Eq. (89)]. Thus, the shrinkage cascade for the  $p$ 'th cycle is



and

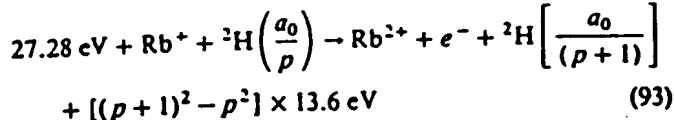


The overall reaction is

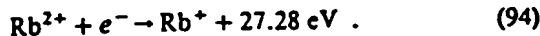


Note that the energy given off as the atom shrinks is much greater than the energy lost to the energy hole, and the energy released is large compared to conventional chemical reactions.

Rubidium(I) is also a potential catalyst. The second ionization energy is 27.28 eV:

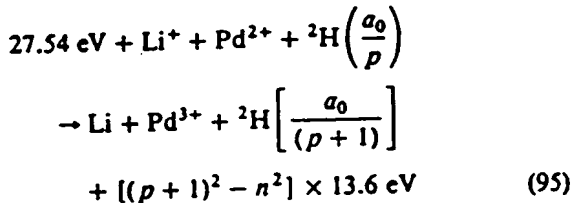


and

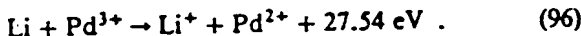


The overall reaction is the same as Eq. (92).

Less efficient catalytic systems hinge on the coupling of three resonator cavities. For example, the third ionization energy of palladium is 32.93 eV. This energy hole is obviously too high for resonant absorption. However, Li(I) releases 5.392 eV when it is reduced to Li. The combination of Pd(II) to Pd(III) and Li(I) to Li, then, has a net energy change of 27.54 eV:

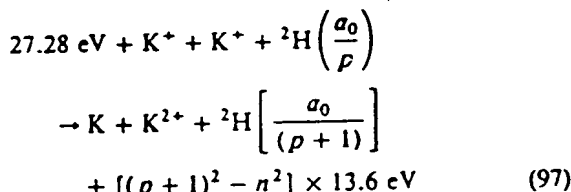


and

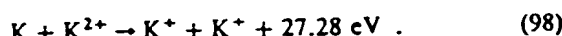


The overall reaction is the same as Eq. (92).

An efficient catalytic system that hinges on the coupling of three resonator cavities involves potassium. For example, the second ionization energy of potassium is 31.63 eV. This energy hole is obviously too high for resonant absorption. However, K(I) releases 4.34 eV when it is reduced to K. The combination of K(I) to K(II) and K(I) to K, then, has a net energy change of 27.28 eV.



and



The overall reaction is the same as Eq. (92).

In general, absorption of an energy hole causes the orbit sphere to undergo a transition from one stable nonradiative radius to another stable nonradiative radius. The Coulombic force is attractive; thus, the orbit sphere shrinks when the effective nuclear charge increases. The orbit sphere has an initial radius  $r_n$ , initial effective nuclear charge  $Z_{eff}$ , and initial velocity  $v_n$  given by the condition for nonradiation:

$$2\pi(nr_1) = n\lambda_1, \quad n = 1, 2, 3, 4, \dots. \quad (99)$$

and

$$v_n = \frac{\hbar}{m_e n a_0}. \quad (100)$$

At force balance,

$$\frac{\hbar^2}{m_e(r_n)^3} = \frac{Z_{eff}e^2}{4\pi\epsilon_0(r_n)^2}. \quad (101)$$

Shrinkage occurs because the effective nuclear charge increases by an integer  $m$  when Eqs. (99), (100), and (101) are satisfied by the introduction of an energy sink of a coupled resonator, such as an electron orbit sphere resonator cavity comprising an electrochemical couple. The coupled resonator provides energy holes and affects the shrinkage transition from the initial radius  $a_0/(mp+1)$  and a nuclear charge of  $(mp+1)$  to the second radius  $[a_0/(m(p+1)+1)]$  and a nuclear charge of  $m(p+1)+1$ . Energy conservation and the boundary condition that trapped photons must be a solution to Laplace's equation determine that the energy hole to cause a shrinkage is given by Eq. (89). As a result of coupling, the deuterium atom emits a photon of  $m \times 27.21$  eV, and this photon is absorbed by the coupled resonator. Stated another way, the deuterium atom absorbs an energy hole of  $m \times 27.21$  eV. The energy hole absorption causes a second photon to be trapped in the deuterium atom electron orbit sphere. Recall from Sec. III that electromagnetic radiation of discrete energy can be trapped in a resonator cavity. As shown previously, the photonic equation must be a solution of Laplace's equation in spherical coordinates. The photon field comprises an electric field that provides force balance and a nonradiative orbit sphere. The solution to this boundary value problem of the radial photon electric field is given by

$$\epsilon \hat{E}_{r,\text{photon},l,m} = \frac{e}{4\pi\epsilon_0} \frac{(na_0)''}{r^{l+2}} \{-1 + n[Y_l''(\phi, \theta) + Y_s''']\}. \quad (102)$$

It is apparent from this equation that, for  $l=0$  and given an initial radius of  $[a_0/(mp+1)]$  and a final radius of  $[a_0/(m(p+1)+1)]$ , the nuclear charge is increased by  $m$  with the absorption of an energy hole of  $m \times 27.2$  eV. The potential energy decreases by this energy; thus, energy is conserved. However, the force balance equation is not initially satisfied as the effective nuclear charge increases by  $m$ . Further energy is emitted as force balance is achieved at the final radius. By replacing the initial radius with the final radius and by increasing the charge by  $m$  in Eq. (101),

$$\begin{aligned} & [m(p+1)+1]^3 \frac{\hbar^2}{m_e a_0^3} \\ & = [m(p+1)+1]^2 \frac{[(m(p+1)+1)e]e}{4\pi\epsilon_0 a_0^2}. \end{aligned} \quad (103)$$

force balance is achieved and the orbit sphere is nonradiative.

The energy balance for  $m=1$  is as follows. An initial energy of 27.21 eV is emitted as the energy hole absorption event. This increases the effective nuclear charge by one and decreases the potential by 27.21 eV. More energy is emitted until the total energy released is  $[(p+1)^2 - p^2] \times 13.6$  eV.

In general, the resonance energy to cause shrinkage of the radius from  $a_0$  to  $a_0/(m+1)$  is  $m \times 27.21$  eV, where  $m = 1, 2, 3, 4$ . The resonant absorption of this energy hole causes the effective nuclear charge to increase by  $m$ . And, the energy released in going from infinity to  $a_0/(m+1)$  is  $(m+1) \times (m+1) \times 13.6$  eV or  $(m+1)^2 \times 13.6$  eV.

Energy holes add. The corresponding effective charges resulting from the absorption of energy holes also add. Thus, any combination of energy holes that sums to  $m \times 27.21$  eV,

where  $m$  is the same as the  $m$  for the final radius ( $a_0/m + 1$ ) leads to shrinkage to the same final radius of the orbit sphere.

## VI. METHODS

A search for excess heat during the electrolysis of aqueous potassium carbonate ( $K^+/K^+$  electrocatalytic couple) was investigated using single-cell, silvered, vacuum-jacketed dewars. To simplify the calibration of these cells, they were constructed to have primarily conductive heat losses. Thus, a linear calibration curve was obtained. Three methods of differential calorimetry were used to determine the cell constant, which was used to calculate the excess enthalpy:

1. The cell constant was calculated during the experiment (on-the-fly-calibration) by turning an internal resistance heater off and on and inferring the cell constant from the difference between the losses with and without the heater.

2. The cell constant was determined with no electrolysis processes occurring by turning an internal-resistance heater off and on for a well-stirred dewar cell and inferring the cell constant from the difference between the losses with and without the heater. This method overestimates the cell constant because there is no gas flow (which adds to the heat losses).

3. In the third method, rather than keeping the ambient temperature constant while raising the cell temperature with heater power input, the ambient temperature was lowered and heater power was applied to maintain a constant cell temperature. This method caused the least perturbation to temperature-dependent electrochemical processes.

The general form of the energy balance equation for the cell in steady state is

$$0 = P_{app} + Q_{hir} + Q_{ex} - P_{gas} - Q_{loss} \quad (104)$$

where

$P_{app}$  = electrolysis power

$Q_{hir}$  = power input to the heater

$Q_{ex}$  = excess heat power generated by an unknown process

$P_{gas}$  = power removed as a result of evolution of  $H_2$  and  $O_2$  gases

$Q_{loss}$  = thermal power loss from the cell.

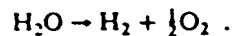
When an aqueous solution is electrolyzed to liberate hydrogen and oxygen gases, the electrolysis power  $P_{app}$  ( $= E_{app} I$ ) can be partitioned into two terms:

$$P_{app} = E_{app} I = P_{cell} + P_{gas} \quad (105)$$

An expression for  $P_{gas}$  ( $= E_{gas} I$ ) is readily obtained from the known enthalpy of formation of water from its elements:

$$E_{gas} = \frac{-\Delta H_{form}}{\alpha F} \quad ,$$

where  $F$  is Faraday's constant, which yields  $E_{gas} = 1.48 \text{ V}$  for the reaction



The net Faradaic efficiency of gas evolution is assumed to be unity; thus, Eq. (105) becomes

$$P_{cell} = (E_{app} - 1.48V)I \quad (106)$$

The cell was calibrated for heat losses by turning an internal resistance heater off and on while maintaining constant electrolysis and by inferring the cell conductive constant from the difference between the losses with and without the heater, where heat losses were primarily conductive losses through the top of the dewar. When the heater was off, the losses were given by

$$c(T_c - T_b) = P_{app} + 0 + Q_{ex} - P_{gas} \quad (107)$$

where

$c$  = conductive heat loss coefficient

$T_b$  = ambient temperature

$T_c$  = cell temperature.

When a new steady state is established with the heater on, the losses change to

$$c(T'_c - T_b) = P'_{app} + Q'_{hir} + Q'_{ex} - P'_{gas} \quad (108)$$

where a superscript prime indicates a changed value when the heater was on. When the following assumptions apply,

$$Q_{ex} = Q'_{ex} \quad .$$

$$P_{app} = P'_{app} \quad .$$

and

$$P_{gas} = P'_{gas} \quad .$$

the cell constant  $a$ , the reciprocal of the conductive loss coefficient  $c$ , is given by

$$a = \frac{T'_c - T_c}{Q_{hir}} \quad . \quad (109)$$

Also, the slope of the plot of  $\Delta T = T_c - T_b$  versus  $P_T = Q_{hir} + P_{cell}$  is the cell constant:

$$a = \frac{\Delta T' - \Delta T}{\Delta P_T} \quad . \quad (110)$$

## VII. EXPERIMENTAL

An electrolytic cell was assembled comprising a 500-ml, silvered, vacuum-jacketed dewar with a 5-cm opening covered with a 0.75-in.-thick tapered rubber stopper (vessel A) fitting 0.25 in. into the dewar mouth or a 200-ml, silvered, vacuum-jacketed dewar with a 3-cm-diam opening covered with Parafilm (vessel B).

The cathode was a 7.5-cm-wide  $\times$  5-cm-long  $\times$  0.125-mm-thick nickel foil (Aldrich 99.9+%) spiral with a 9-mm diameter and 2-mm pitch with a nickel lead strip (cathode A) or a 5-cm-long  $\times$  0.75-cm-diam graphite rod with a 0.127-mm platinum lead (cathode B). The nickel cathode was prepared by tightly rolling the nickel foil about a 9-mm rod. The rod was removed, and the spiral was formed by partially unrolling the foil.

The anode was a 10-cm  $\times$  1-mm-diam spiraled platinum wire (Johnson-Matthey) with a 0.127-mm platinum lead wire (anode A) or a 2.5-cm-diam  $\times$  7.5-cm-high platinum basket with a 1-mm-diam platinum lead wire (anode B). When anode A was utilized, the cathode/anode separation distance was 1 cm. When anode B was used, the cathode/anode separation distance was 1.2 cm.

The electrolyte solution was 100 ml of 0.57 M aqueous  $K_2CO_3$  (Aldrich  $K_2CO_3 \cdot \frac{1}{2} H_2O$  99+%) (solution A) or

100 ml of 0.57 M aqueous  $\text{Na}_2\text{CO}_3$  (Aldrich  $\text{Na}_2\text{CO}_3$ , American Chemical Society primary standard 99.95+%) (solution B).

The resistance heater used during calibration and operation comprised a 100 or 10.5  $\Omega$ , 1% precision metal oxide resistor in a 2-mm-o.d. Teflon tubing powered by a variable direct current (dc) voltage power source ( $\pm 0.5\%$ ).

A constant dc current ( $\pm 0.1\%$ ) was provided by the circuit shown in Fig. 1 (mode C). A constant dc voltage power supply ( $\pm 0.5\%$ ) was used directly in the continuous current mode (mode B). A power controller with the circuit shown in Fig. 2 was used to provide intermittent current (mode A). The current voltage parameters were an intermittent square-wave with an offset voltage of  $\sim 2.2$  V, a peak voltage of  $\sim 2.75$  V, with a peak current of  $\sim 175$  mA, an  $\sim 35\%$  duty cycle, and a fre-

quency of  $\sim 500$  Hz. The voltage and current waveforms are shown in Figs. 3 and 4, respectively.

In stirring mode A, the electrolyte solution was stirred with a 7-mm  $\times$  2-cm spheroidal ellipse magnetic stirring bar that was spun by a 6-cm-long open magnet mounted on an open shaft revolving at 750 rpm under the dewar. The shaft was that of an open mixing motor (Flexa-Mix model 76, Fisher). The temperature correction for the Joule heating of stirring was determined from an identical experimental apparatus that was only stirred.

In stirring mode B, the electrolyte solution was stirred by a 2-cm-wide  $\times$  1-cm-high glass paddle connected to a 40-cm-long  $\times$  5-mm-o.d. glass rod that entered the dewar vertically through a 6-mm-i.d. vacuum greased glass tube implanted through the rubber stopper covering the dewar. The rod was rotated at 380 rpm by a mixing motor (Lightnin model L, Mixing Equipment Company) controlled by a variable auto-transformer (Powerstat model 116B). The temperature correction for the Joule heating of stirring was determined by stirring the electrolyte and measuring its temperature relative to the temperature of an unstirred matched cell before initiating an experiment. Otherwise, the experiments were stirred by gas sparging from the gases produced during electrolysis.

Nickel cathodes were initially operated in reverse polarity with a continuous or time-averaged current of 80 mA for 30 min to break in a new cathode. This operation conditions the electrode and makes the electrolysis more surface uniform. Following any change in heater power, an intentional ambient temperature change, or commencement of electrolysis, time was allowed for the cell temperature to establish a

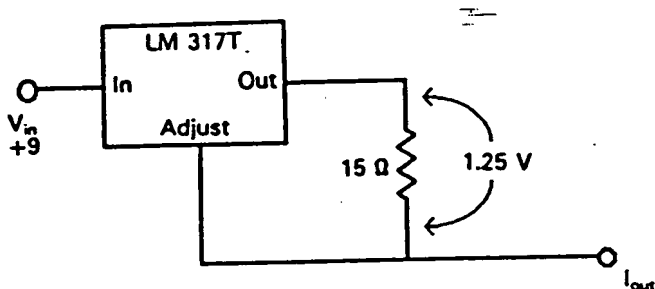


Fig. 1. Schematic of the circuit used to provide constant dc current.

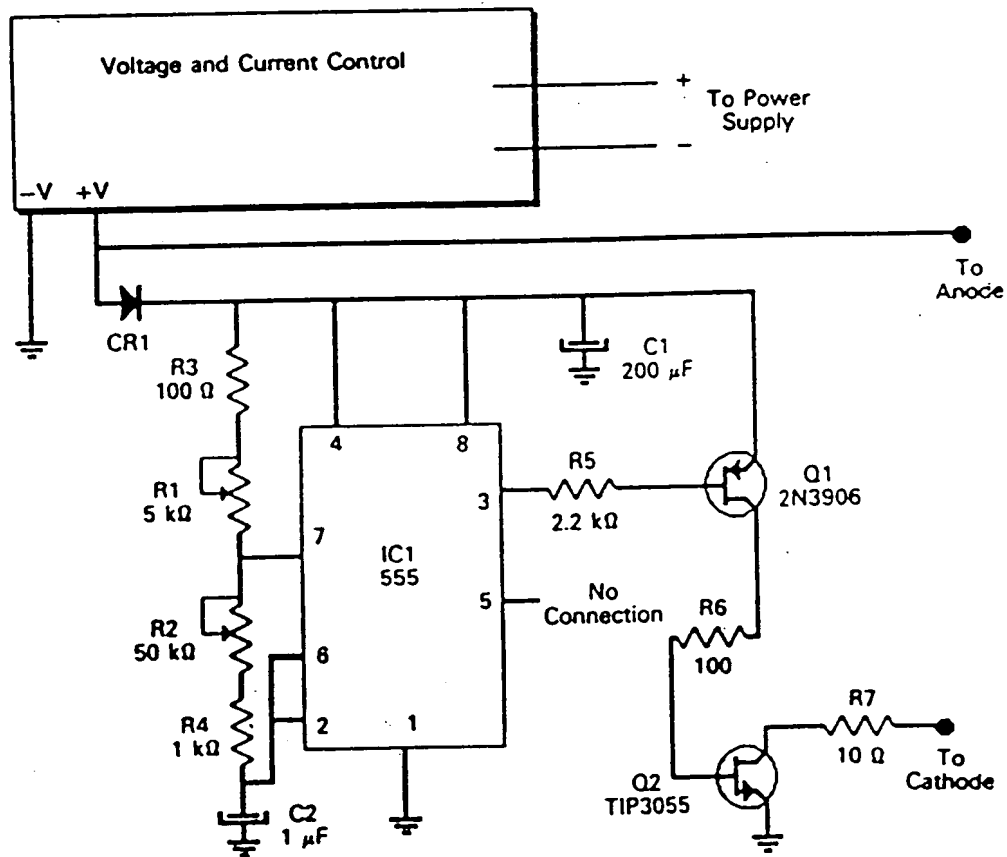


Fig. 2. Schematic of the circuit used to provide intermittent (on/off) dc voltage.

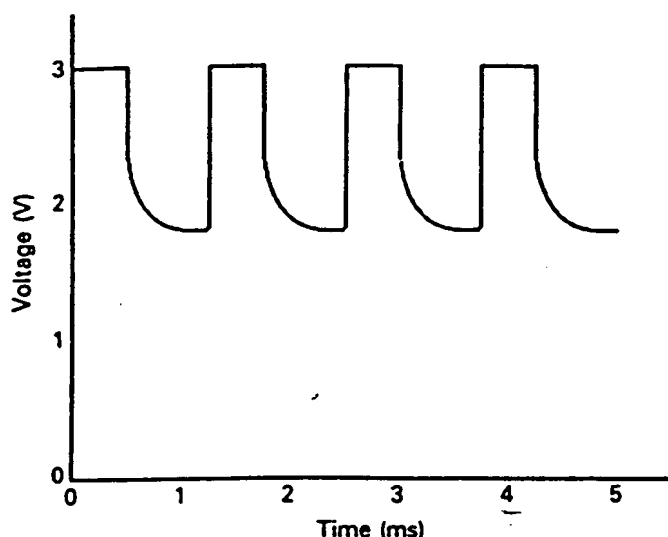


Fig. 3. Voltage versus time oscilloscope trace of the circuit of Fig. 2.

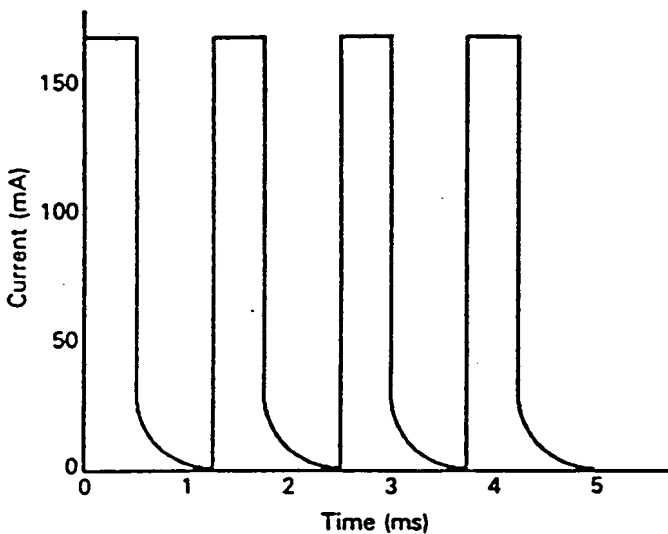


Fig. 4. The current versus time oscilloscope trace of the circuit of Fig. 2.

new steady state before data were recorded. The time for the temperature to stabilize following the commencement of electrolysis was typically 12 h. The time for the temperature to stabilize following an increase of heater power of  $\sim 0.3$  W was  $\sim 4$  h for cells with no electrolysis and for electrolytic cells operating for  $>12$  h. The dewar was agitated prior to a temperature reading to ensure thorough thermal mixing.

The outside of the vessel was maintained at ambient air temperature, which was monitored, and the difference between cell and a matched nonoperative cell was determined with a thermometer ( $\pm 0.1^\circ\text{C}$ ). Ambient temperature fluctuations per 24 h were typically  $<0.5^\circ\text{C}$ . (The matched nonoperative cell was structurally and chemically identical, but the electrolysis current was zero and the heater power was zero. In the case of stirring mode A, the matched nonoperative cell was stirred identically.)

For another method, rather than keeping the ambient temperature constant while raising the cell temperature with

heater power input, the ambient temperature was lowered by adjusting the thermostatic control of the room temperature, and heater power was applied to maintain an approximately constant cell temperature. The room temperature and heater power were adjusted until the excess heat before and after the change in ambient temperature were equal. The ambient temperature reached a steady-state temperature ( $\pm 0.1^\circ\text{C}$ ) in 8 h, and the cell reached a steady-state temperature ( $\pm 0.1^\circ\text{C}$ ) 4 h later. The temperature difference between the cell and a matched nonoperative cell was determined with a thermometer ( $\pm 0.1^\circ\text{C}$ ).

For circuit A, peak voltage measurements were made with an oscilloscope (BK model 2120), and the time-averaged current was determined from a multimeter voltage measurement ( $\pm 0.2\%$ ) across a calibrated resistor ( $1 \Omega$ ) in series with the lead to the cathode. The waveform of the pulsed cell was a square wave. Since there was current only during the peak voltage interval of the cycle,  $P_{app}$  [Eq. (105)] is given by the product of the peak voltage and the peak current and the duty cycle, which is the product of the peak voltage and the time-averaged current. In circuit B, voltage across the cell was measured with the multimeter, and the current was determined from the multimeter voltage measurement across a calibrated resistor ( $1 \Omega$ ) in series with the lead to the cathode. For this mode,  $P_{app}$  [Eq. (105)] is given by the product of the constant voltage and the constant current.

## VIII. RESULTS

A summary of the results of the excess enthalpy released during the electrolysis of potassium carbonate ( $\text{K}^+/\text{K}^+$  electrocatalytic couple) as well as the results for the control (sodium carbonate, for which no electrocatalytic reaction of  $\sim 27.21$  eV is possible) are given in Table I, which also lists the experiment number. Experiments designated with a number followed by an "A" had heat added to the experiment designated by the same number.

Figures 5 through 9 show the difference between experimental cell temperature and the temperature of a matched

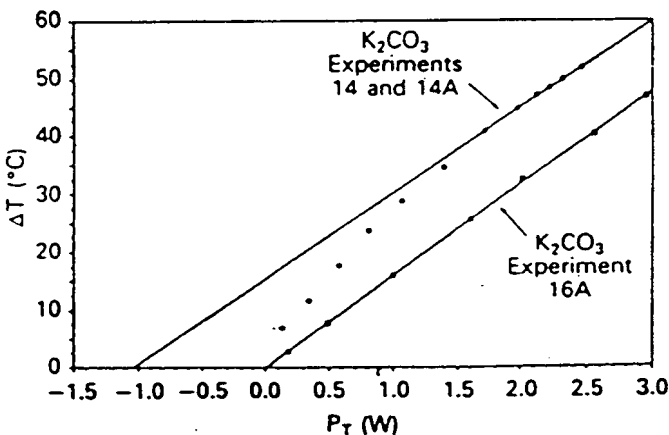


Fig. 5. Plots of the differences between cell temperature and the temperature of a matched nonoperative cell ( $\Delta T$ ) as a function of total power  $P_T$  for (a)  $\text{K}_2\text{CO}_3$ , experiments 14 and 14A in which the electrolysis current was maintained at  $-85$  mA and (b)  $\text{K}_2\text{CO}_3$ , experiment 16A in which electrolysis current was zero. Increasing temperatures were recorded as the calibration resistor was stepped in power. The curves are fit to the solid symbols.

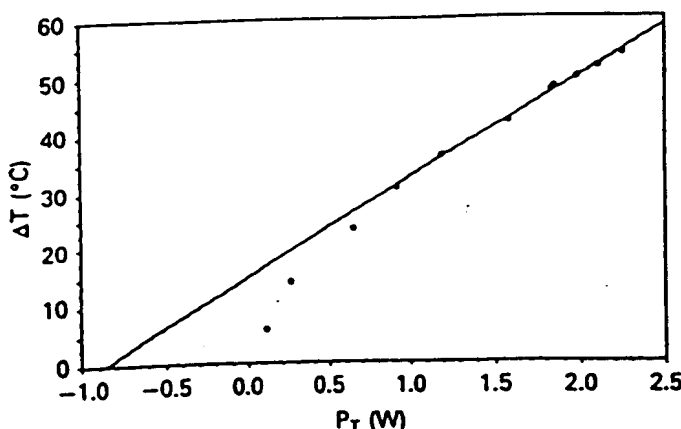


Fig. 6. Plot of the difference between cell temperature and the temperature of a matched nonoperative cell ( $\Delta T$ ) as a function of total power  $P_T$  for  $K_2CO_3$ , experiments 15 and 15A, in which the electrolysis current was maintained at 82 mA. Increasing temperatures were recorded as the calibration resistor was stepped in power. The curve was fit to the solid circles.

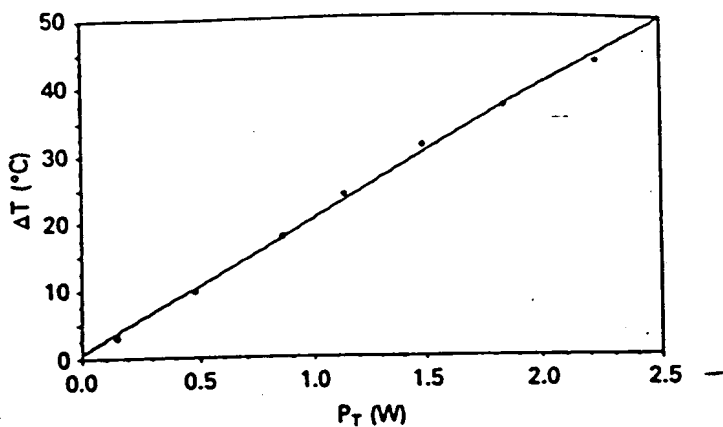


Fig. 8. Plot of the difference between cell temperature and the temperature of a matched nonoperative cell ( $\Delta T$ ) as a function of total power  $P_T$  for  $Na_2CO_3$ , experiments 18 and 18A. The electrolysis current was maintained at 79.7 mA. Increasing temperatures were recorded as the calibration resistor was stepped in power.

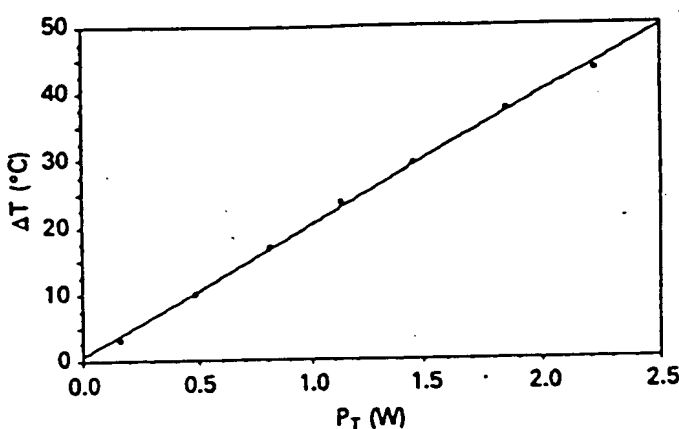


Fig. 7. Plot of the difference between cell temperature and the temperature of a matched nonoperative cell ( $\Delta T$ ) as a function of total power  $P_T$  for  $K_2CO_3$ , experiment 17A. The electrolysis current was zero. Increasing temperatures were recorded as the calibration resistor was stepped in power.

nonoperative cell ( $\Delta T$ ) as a function of total power  $P_T$  for different electrolysis currents. The value of  $P_T$  is

$$P_T = P_{cell} + Q_{heat},$$

where  $P_{cell}$  is calculated using Eq. (106). Increasing temperatures were recorded as the calibration resistor was stepped in power.

In  $K_2CO_3$ , experiment 16A, there was no hydrogen to react, and this experiment is a control of differential calorimetry for  $K_2CO_3$ , experiments 14 and 14A. The plot for  $K_2CO_3$ , experiment 16A (see Fig. 5) is linear with an  $x$  intercept and a  $y$  intercept of zero, which indicates no excess heat. However, the plot for  $K_2CO_3$ , experiments 14 and 14A ( $K^+/K^+$  electrocatalytic couple) (see Fig. 5) is highly nonlinear in the 25 to 50°C temperature range and approximately linear thereafter. Interpolation of the linear data to the  $y$  intercept indicates an excess temperature of  $-15^{\circ}$ C. Interpolation of the linear data to the  $x$  intercept indicates an excess power of  $-10$  times the input power.

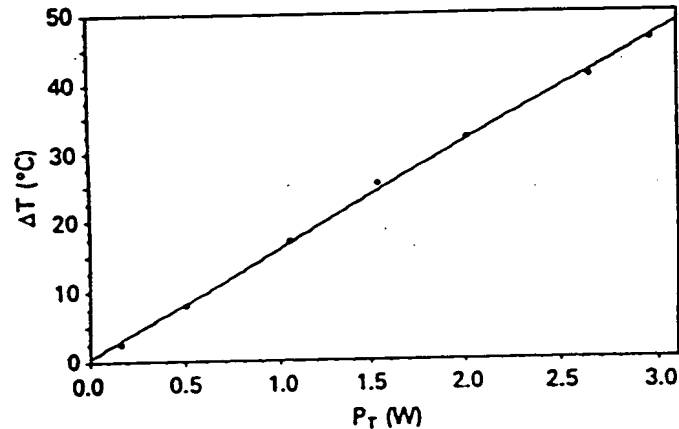


Fig. 9. Plot of the difference between cell temperature and the temperature of a matched nonoperative cell ( $\Delta T$ ) as a function of total power  $P_T$  for  $Na_2CO_3$ , experiments 19 and 19A. The electrolysis current was maintained at 79.7 mA. Increasing temperatures were recorded as the calibration resistor was stepped in power.

The plot of  $\Delta T$  versus  $P_T$  for  $Na_2CO_3$ , experiments 18 and 18A and 19 and 19A are shown in Figs. 8 and 9, respectively. No electrocatalytic reaction of  $-27.21$  eV is possible for sodium; thus, these experiments represent controls that are essentially chemically identical but lack an electrocatalytic couple to induce the electrons of hydrogen atoms to relax to a quantized potential energy level below that of the ground state by providing a redox energy-energy hole (27.28 eV) resonant with this transition. These plots are linear with an  $x$  intercept and a  $y$  intercept of zero, which indicates no excess heat. However, the plots for  $K_2CO_3$ , experiments 14, 14A, 15, and 15A ( $K^+/K^+$  electrocatalytic couple), shown in Figs. 5 and 6, respectively, are highly nonlinear in the 25 to 50°C range.

TABLE  
Percentage Excess Enthalpy Where the Cell Constant

Experiment	Solution	Cathode	Anode	Vessel	Stirring Mode	Mode	Duty Cycle (%)	Frequency (Hz)
K <sub>2</sub> CO <sub>3</sub>								
1	A	A	A	A		A	40	500
1A	A	A	A	A		A	40	500
1AA	A	A	A	A		A	40	500
2	A	AA	A	A		A	35	500
2A	A	A	A	A		A	35	500
3	A	B	A	A		A	40	500
3A	A	B	A	A		A	35	500
4	A	A	A	A		A	35	500
4A	A	A	A	A		A	35	500
5	A	A	A	A		A	35	500
5A	A	A	A	A		A	35	500
6	A	A	A	A		A	35	500
6A	A	A	A	A		A	35	500
7	A	A	A	A		A	35	500
7A	A	A	A	A		A	35	500
8	A	A	A	A		B		
8A	A	A	A	A		B		
9	A	A	A	A		A	35	500
9A	A	A	A	A		A	35	500
10	A	A	A	A		A	35	500
10A	A	A	A	A		A	35	500
11A	A	A	A	A		A	35	500
12A	A	A	A	A		B		
13	A	A	A	A		A	35	500
13A	A	A	A	A		A	35	500
14	A	A	A	A		B		
14A	A	A	A	A		B		
15	A	A	A	B		C		
15A	A	A	A	B		C		
16A	A	A	A	B				
17A	A	A	A	B				
Na <sub>2</sub> CO <sub>3</sub>								
18	B	A	A	A	A	C		
19	B	A	A	A	A	C		

\*See Sec. VII for an explanation of the experimental configurations.

<sup>a</sup>Q<sub>hir</sub> = heater watts added to raise the temperature of the cell during operation.

<sup>b</sup>ΔT = T<sub>c</sub> - T<sub>b</sub>.

<sup>c</sup>ΔT<sub>hir</sub> = aQ<sub>hir</sub> = temperature change in the cell due to the heater.

<sup>d</sup>ΔΔT = ΔT - ΔT<sub>hir</sub>.

<sup>e</sup>ΔT<sub>cell</sub> = aP<sub>cell</sub>.

temperature range and approximately linear thereafter. Interpolation of the linear data to the y intercept indicates an excess temperature of ~15°C. Interpolation of the linear data to the x intercept indicates an excess power of ~10 times the input power. For each experiment, the upper limit of the cell parameter *a* was determined from the slope at ~55°C.

Linear plots of ΔT versus P<sub>T</sub> for heater alone (no electrolysis) K<sub>2</sub>CO<sub>3</sub> control experiments 16A (Fig. 5) and 17A (Fig. 7), which go through zero at the origin, validate the original assumptions that the losses were conductive. The upper

limit of the cell parameter *a* was determined from the slope. The cell parameter was slightly lower for electrolytic cells compared to matched nonelectrolytic cells, as shown in Fig. 5. This is attributed to the additional heat loss due to gas flow in the electrolytic cells.

The results of the determination of the cell constant, Q<sub>ir</sub>, and Q'<sub>ir</sub> at an operating temperature of ~32°C appear in Table II. For calibration runs (K<sub>2</sub>CO<sub>3</sub> experiments 20A1, 20A2, 20A3, and 20A4), the ambient temperature was ~2 to 5°C lower than in the reference cell (K<sub>2</sub>CO<sub>3</sub> experiment 20).

I

Was Determined by On-the-Fly-Calibration\*

Offset Voltage (V)	Peak Voltage (V)	Peak Current (mA)	Cell Constant (°C/W)	$Q_{hr}^a$ (W)	$\Delta T^b$ (°C)	$\Delta T_{hr}^c$ (°C)	$\Delta \Delta T^d$ (°C)	$\Delta T_{ref}^e$ (°C)	Excess Heat <sup>f</sup> (%)
2.73	3.43	180	14.8	0	8.9			2.08	328
2.36	2.96	112	15	1.044	29	15.67	13.33	1	1234
2.32	3.22	212	14.8	2.196	47.2	32.9	14.3	2.17	557
2.19	2.79	231	14.8	0	4.2			1.56	169
2.55	3.15	217	14.8	2.196	45	32.9	12.1	1.88	544
2.93	3.63	163	14.8	0	6.2			2.42	156
2.795	3.295	231	14.8	2.196	49.5	32.94	16.56	2.17	662
2.185	2.685	254	14.8	0	4.5			1.58	183
2.02	2.42	245	14.8	2.21	46.5	33.17	13.33	1.19	1016
2.12	2.72	225	14.8	0	4.8			1.45	231
2.01	2.51	248	14.8	2.22	43	33.3	9.7	1.32	634
2.425	3.125	205	14.5	0	5.4			1.71	215
2.47	2.97	208	14.5	2.22	44.5	33.3	11.2	1.57	612
2.17	2.77	246	15.7	0	4.3			1.74	147
2.04	2.54	228	15.7	0.911	25	14.3	10.7	1.33	705
	2.42	75	16.9	0	4.2			1.19	252
	2.28	80	16.9	0.99	28.1	16.73	11.37	1.08	953
2.1	2.4	131	14.8	0	3.1			0.626	395
2	2.1	114	14.8	0.778	25.7	11.51	14.19	0.367	3766
2.1	2.4	117	14.6	0	2.8			0.551	408
2	2.25	117	14.6	1.96	41.2	28.65	12.5	0.461	2621
2.5	2.8	114	18	0.76	22.6	13.68	8.91	0.95	838
	2.31	80	15.6	0.771	23.7	12	11.7	1.036	1027
2	2.55	243	15.25	0	4.4			1.39	217
2.1	2.6	217	15.25	1.537	38.9	23.4	15.5	1.3	1094
	3.08	85	14.8	0	6.9			2.01	243
	2.9	89	14.8	1.59	40.9	23.5	17.4	1.87	830
	2.748	82	17.5	0	5.7			1.82	213
	2.247	82	17.5	2.028	51.5	35.5	16.01	1.01	1355
			15.9						
			15.5						
	3.48	79.7	19.7	0	3.2			3.14	1.9
	3.37	79.7	19.6	0	3			2.95	1.6

$$\text{Excess heat} = \begin{cases} \frac{\Delta T - \Delta T_{cell}}{\Delta T_{cell}} \times 100, & \text{when heater was off} \\ \frac{\Delta \Delta T - \Delta T_{cell}}{\Delta T_{cell}} \times 100, & \text{when heater was on.} \end{cases}$$

and heater power was added to make the temperature of each calibration cell approximately equal to the cell temperature of the reference cell. The cell constant was determined by subtracting Eq. (107) with the parameters of the reference run from Eq. (108) with the parameters of each calibration run, and Eq. (106) was used to determine  $P_{cell}$  for each equation. It was assumed that the losses were conductive and that  $Q_{\alpha} = Q'_{\alpha}$ . The assumption that the losses  $Q_{loss}$  were conductive for these silvered dewars is supported by the data of Figs. 8 and 9. The assumption that  $Q_{\alpha} = Q'_{\alpha}$  was verified by

calculating these parameters from the cell constant determined.

#### IX. DISCUSSION

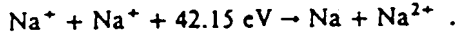
The data clearly indicate that excess heat was generated. Once the technique was perfected, each experiment using potassium carbonate produced excess heat. Some experiments were permitted to operate for weeks, and the excess heat remained relatively constant. What is the source of this excess

TABLE  
Determination of the Cell Constant by Lowering the Ambient Temperature

Experiment	Solution	Cathode	Anode	Vessel	Stirring Mode	Mode	Voltage (V)	
K <sub>2</sub> CO <sub>3</sub> 20	A	A	A	A	B	B	2.38	
20A1	A	A	A	A	B	B	3.08	
20A2	A	A	A	A	B	B	3.11	
20A3	A	A	A	A	B	B	3.11	
20A4	A	A	A	A	B	B	3.2	

enthalpy? Electrochemical reactions that consume the electrolyte can be ruled out because any proposed electrochemical reactant would be completely consumed over the duration of these experiments. Nickel forms a hydride during cathodic electrolysis, but this process is endothermic.<sup>6</sup> The weight of the nickel cathode was unchanged by use in a heat-producing cell to within 0.00001 g (the cathode was rinsed after 36 h of operation, then dried and degassed in vacuum before the final weight was determined). The only remaining candidates are heat-releasing reactions involving the electrolytically generated hydrogen or oxygen atoms or molecules. Because the excess enthalpy exceeds that which can be accounted for due to complete recombination, new processes must be sought.

The results are consistent with the release of heat energy from hydrogen atoms where the K<sup>+</sup>/K<sup>+</sup> electrocatalytic couple induces the electrons of hydrogen atoms to relax to a quantized potential energy level below that of the ground state by providing a redox energy-energy hole (27.28 eV) resonant with this transition. The balanced reaction is given by Eqs. (92), (97), and (98). Excess heat was also measured when K<sub>2</sub>CO<sub>3</sub> was replaced by Rb<sub>2</sub>CO<sub>3</sub>. The Rb<sup>+</sup> ion (energy hole from the second ionization is 27.28 eV) alone is electrocatalytic according to the reaction given by Eqs. (92), (93), and (94). No excess heat was observed when K<sub>2</sub>CO<sub>3</sub> was replaced by Na<sub>2</sub>CO<sub>3</sub> as demonstrated with Na<sub>2</sub>CO<sub>3</sub> experiments 18 and 18A and 19 and 19A, shown in Figs. 8 and 9, respectively. For sodium or sodium ions, no electrocatalytic reaction of -27.21 eV is possible. For example, 42.15 eV of energy is absorbed by the reverse of the reaction given in Eq. (98), where Na<sup>+</sup> replaces K<sup>+</sup>:



It has not been overlooked that other researchers have reported anomalous heat,<sup>7</sup> tritium,<sup>7,8</sup> and neutron production<sup>7</sup> during electrolysis of heavy water using a lithium salt electrolyte and a palladium cathode. The excess enthalpy is reported to be substantially larger than can be accounted for by nuclear reactions that produce tritium or neutrons.<sup>7</sup> In these cases, the couple is Pd<sup>2+</sup>/Li<sup>+</sup> (27.54 eV). The balanced reaction is given by Eqs. (92), (95), and (96). The excess heat arises from the HECTER process, and the trace nuclear reactions are due to CAF as described in Sec. V. The HECTER process produces much greater quantities of heat energy than typical chemical reactions.

Neutron<sup>9,10</sup> and tritium<sup>10</sup> emissions from heavy water electrolytic cells using a titanium cathode and deuterium gas cells with titanium shavings have been reported. The tritium-to-neutron ratio is reported to be 10<sup>8</sup> (Ref. 10) as opposed to the 1:1 branching ratio of <sup>3</sup>H to <sup>3</sup>He observed for hot fu-

sion. This result is anticipated for CAF. In the case of titanium, Ti<sup>2+</sup> (27.49 eV) is electrocatalytic according to the reaction given by Eqs. (90), (91), and (92).

The data indicate that the shrinkage reaction is temperature dependent. This is clearly demonstrated by the nonlinear curves in Figs. 5 and 6 and by comparing the heated experiments (Table I) and the experiment of the same number for which heater power was zero. Most chemical reactions double their rates for each 10°C rise in temperature. Increasing temperature increases the collision rate between the hydrogen atoms and the electrocatalytic couple, which increases the shrinkage reaction rate. With large temperature excursions from room temperature, the kinetic energy distribution of the reactants can be sufficiently altered to cause the energy effecting the hydrogen shrinkage transition and the electrocatalytic redox reaction to conform to a greater or lesser extent. The rate is proportional to the extent of conformation or resonance of these energies.

The source of reactant hydrogen atoms is aqueous electrolytic production on the surface of the nickel cathode. Electrolysis and the associated ohmic losses consume (i.e., require) input power. The losses obviously rise with a rise in current. However, increased current increases the concentration of reactant hydrogen atoms. A trade-off exists between total excess power and percentage excess power. It was found that increasing the current with a concomitant increase in the concentration of reactant hydrogen atoms increases the total excess power but decreases the percentage excess power. During continuous electrolysis, much of the reactant hydrogen is lost as evolved gas. It was anticipated that more efficient production of reactant hydrogen could be provided by an electrolysis circuit that periodically generates reactant hydrogen atoms and allows them to react in the absence of further power dissipation. Comparing the experiments of Table I with pulsed peak current of ~115 mA with those with continuous ~80-mA current electrolysis, it can be appreciated that the efficiency of heat generation is correlated with the efficiency of hydrogen atom generation. For example, the input power of K<sub>2</sub>CO<sub>3</sub> experiment 9A, which was pulsed, is one-third that of K<sub>2</sub>CO<sub>3</sub> experiment 8A, which was operated with continuous current. The ratio of the percentage excess power of K<sub>2</sub>CO<sub>3</sub> experiment 9A to K<sub>2</sub>CO<sub>3</sub> experiment 8A is 3. An intermittent current (i.e., on-off) electrolysis circuit increases the percentage of excess heat by providing an optimal concentration of hydrogen atoms (reactants) while minimizing ohmic and electrolysis power losses. The frequency, duty cycle, peak voltage, step waveform, peak current, and offset voltage were adjusted to achieve the optimal shrinkage reaction rate and concomitant power while minimizing ohmic and

## While Maintaining Constant Cell Temperature by Addition of Heat

Current (mA)	$P_{cell}$ (W)	$Q_{hir}$ (W)	$P_T$ (W)	$\Delta T$ (°C)	Cell Constant	$Q_{rs}$ (W)	$Q'_{rs}$ (W)
79	0.0711	0	0.0711	3.2			
90	0.144	0.3249	0.4689	9.6	16.09	0.128	0.128
85	0.1386	0.1681	0.3067	7	16.13	0.127	0.127
81	0.132	0.2621	0.3942	8.4	16.095	0.128	0.128
100	0.172	0.2621	0.4341	9	15.98	0.129	0.129

electrolysis power losses. When the  $K^+/K^+$  electrocatalytic couple was used with carbonate as the counterion, nickel as the cathode, and platinum as the anode, an intermittent square-wave with an offset voltage of  $\sim 2.2$  V, a peak voltage of  $\sim 2.75$  V, a peak current of  $\sim 120$  mA, an  $\sim 35\%$  duty cycle, and a frequency of  $\sim 500$  Hz optimized the percentage excess power.

Although only the results for carbonate are reported, a strong dependence of the excess enthalpy on the structure and charge of the counterion was found. For carbonate, the transition state to the fractional quantized state of the hydrogen atom likely involves a neutral complex of carbonate with two juxtaposed potassium ions. The counterion of the electrocatalytic couple of the electrolytic solution can affect the shrinkage reaction rate by altering the energy of the transition state. For example, the transition state complex of the  $K^+/K^+$  electrocatalytic couple with the hydrogen atom has a +2 charge and involves a three-body collision, which is unfavorable. A -2 charged oxyanion can bind the two potassium ions; thus, it provides a neutral transition-state complex of lower energy, whose formation depends on a binary collision, which is greatly favored. The rate depends on the separation distance of the potassium ions as part of the complex with the oxyanion. The greater the separation distance, the less favorable is the transfer of an electron between them. A close juxtaposition of the potassium ions increases the rate.

Further work to enhance the power, to search for chemical species with shrunken hydrogen atoms, and to search for products of predicted subsequent nuclear processes (CAF) following the shrinkage reaction are in progress. Preliminary data indicate that the electrolysis of a heavy water potassium carbonate electrolyte at a nickel cathode produces significant

quantities of tritium, but the amount is much less than can account for the heat observed.

## REFERENCES

1. R. L. MILLS and J. J. FARRELL, *The Grand Unified Theory*, Science Press (1989).
2. H. A. HAUS, "On the Radiation from Point Charges," *Am. J. Phys.*, 54, 1126 (1986).
3. D. A. MCQUARRIE, *Quantum Chemistry*, University Science Books, Mill Valley, California (1983).
4. E. M. PURCELL, *Electricity and Magnetism*, McGraw-Hill Book Company, New York (1965).
5. S. I. S. HUGHES, *Elementary Particles*, Cambridge University Press (1972).
6. G. ALEFELD and J. VOLKL, Eds., *Hydrogen in Metals II*, p. 176, Springer Verlag (1967).
7. M. FLEISCHMANN, S. PONS, W. ANDERSON, L. J. LI, and M. HAWKINGS, "Calorimetry of the Palladium-Deuterium-Heavy Water System," *J. Electroanal. Chem.*, 287, 293 (1990).
8. E. STORMS and C. TALCOTT, in *Proc. Workshop on Cold Fusion Phenomena*, Santa Fe, New Mexico, May 23-25, 1989.
9. S. JONES et al., "Observation of Cold Nuclear Fusion in Condensed Matter," *Nature*, 338, 737 (1989).
10. P. IYENGAR et al., "Bhabha Atomic Research Centre Studies on Cold Fusion," *Fusion Technol.*, 18, 32 (1990).

EEPE  
EEPE

BROOKHAVEN NATIONAL LABORATORY

ASSOCIATED UNIVERSITIES, INC.

Department of Applied Science  
Bldg. 480

Upton, Long Island, New York 11973

(516) 282-7685  
FAX 666-  
FAX (516) 282-4071

October 16, 1991

Dr. Walter Polansky  
U.S. Department of Energy  
Washington D.C.

Dear Dr. Polansky:

As you are aware, Dr. Nonnisski recently spent a week at BNL as a guest of Dr. McBreen and myself. The purpose of the visit was to demonstrate a thermo-electrochemical effect originally described by Dr. Randy Mills of Lancaster, Pennsylvania. As per your request, this is a short review of what I observed. I am not making any inference as to the impressions, observations, or conclusions drawn by Dr. McBreen.

The experiment can be briefly described as follows. A well insulated dewar was filled with a ~0.7M solution of potassium carbonate and distilled water. A nickel cathode and platinum anode were immersed in the solution along with a resistor and thermistor. The dewar was covered and became, in essence, a heat flow calorimeter. A known amount of power was applied to the resistor and the temperature of the dewar was increased until equilibrium was reached, typically 24 hours. The temperature rise in the dewar,  $\Delta T$ , was divided by the power dissipated in the resistor yielding a slope with units of "O/Watt". The resistor power was terminated and the dewar was allowed to cool down. A voltage was next applied across the platinum anode and the nickel cathode. The solution was electrolyzed with hydrogen being liberated at the cathode and oxygen at the anode. The temperature of the dewar again increased and reached equilibrium after ~24 hours. The temperature of the dewar increased because some of the applied electrolysis power was dissipated in the cell. The temperature rise of the dewar,  $\Delta T$ , is divided by the electrolysis power dissipated in the dewar yielding a slope with units of "C/Watt", as was done for the resistor. To correct for the evolution of gasses in the dewar the thermoneutral voltage, 1.48 Volts, was subtracted from the applied voltage, V. The electrolysis power dissipated in the dewar was obtained by multiplying the corrected voltage,  $V - 1.48V$ , by the electrolysis current.

The claim is as follows. The temperature rise in the dewar is greater in the case of electrolysis as compared to using a resistor, even though the dissipated power is equal in both cases. According to Dr. Mills' theory, this apparent "excess power" is due to the fact that the electron in a hydrogen atom can "decay" to stable subinteger quantum levels.

Dr. Nonnisski demonstrated this thermal effect at BNL. Before proceeding further a few comments are in order. I did not check the calibration of his equipment nor did I observe his experimental technique in great detail. The time was not available to me. There were no obvious errors and as the effect has been claimed by Dr. Mills and Dr. Nonnisski for some

Dr. Walter Polansky  
October 16, 1991  
Page Two.

time, I feel it is probably correct. What was typically observed is as follows. For a dissipated power through the resistor of 0.1 Watt a dewar temperature rise of  $3^{\circ}\text{C}$  was measured. The slope, as previously defined, was therefore  $30^{\circ}\text{C}/\text{Watt}$ . If the electrolysis power dissipated in the dewar was say 0.3 Watts, a temperature rise of  $3^{\circ}\text{C}$  was observed giving a slope of  $60^{\circ}\text{C}/\text{Watt}$ . The question is, why does the power dissipated in the dewar, when applied electrolytically, give a larger temperature rise as compared to a resistor? One possibility is that the evolving gasses are recombining in the dewar. Dr. Nonraski checked this by measuring the Faraday efficiency of the electrolysis in a separate experiment. There appeared to be little gaseous recombination. I must emphasize that the quantity of gasses evolving from the dewar were not measured. Gaseous recombination in the dewar was not, therefore, unequivocally ruled out. Another possibility is that there is a chemical reaction occurring. For example can potassium carbonate be catalytically decomposed into say potassium hydroxide? Finally, the process of electrolysis infuses the solution with fine bubbles. These bubbles would be expected to change the thermal characteristics of the calorimeter. I discussed this with Dr. Nonraski and he produced some experimental results from the literature indicating that the bubbles should have decreased the measured value of the slope and not increase it (as compared to a resistor).

In summary, there appears to be an unusual thermal effect (at very low power levels) which occurs during the electrolysis of potassium carbonate solutions. The presence of "excess power" has not, however, been demonstrated much less "proved". A number of basic experiments need to be performed to eliminate some of the possibilities previously outlined. Finally, there are probably many other possible explanations for explaining this thermal anomaly and these would, of course, also need to be investigated.

Sincerely,

  
Harold Williamson  
Materials Science Division

HW/mal

## LOCAL ENERGY SYSTEMS

1993 January 25

## AECL Research

Chalk River Laboratories  
 Chalk River Ontario  
 Canada K0J 1J0  
 Tel (613) 584-3311  
 Fax (613) 584-4024  
 Telex 053-34555

## EACL Recherche

Laboratoires de Chalk River  
 Chalk River (Ontario)  
 Canada K0J 1J0  
 Tel (613) 584-3311  
 Fax (613) 584-4024  
 Télex 053-34555

Dr. R.T. Bush  
 California State Polytechnic University  
 POMONA, California  
 USA  
 91768

Dear Dr. Bush:

Two separate investigations of Mills' light water cell will be carried out in Canada, one at the Electrochemical Science and Technology Centre at the University of Ottawa, and the other at the Chalk River Laboratories. Both experimental programs will be starting in February.

I note from your recent paper (Fusion Technology 22, Sept. 1992) that: "It may be possible to ascribe the fact that we were able to observe excess heat for a sodium cell, whereas Mills and Kneizys did not detect any, to the difference in cathode. Mills and Kneizys employed nickel plate, whereas we employed a different alloy of nickel". Has there been any progress in resolving the question of cathode material?

We shall certainly be searching for calcium in the electrolyte, and in particular the rare isotope calcium 42. If you can suggest any new experiments that would be helpful, I would welcome your input. My fax number is (613) 584-2227.

Yours sincerely,

Dr. John Hilborn

JH/yws  
 Attachments

# A LIGHT WATER EXCESS HEAT REACTION SUGGESTS THAT "COLD FUSION" MAY BE "ALKALI-HYDROGEN FUSION"

COLD FUSION

## TECHNICAL NOTE

KEYWORDS: cold fusion, alkali-hydrogen fusion, nuclear transmutation

ROBERT T. BUSH *California State Polytechnic University  
Physics Department, Pomona, California 91768*

Received July 12, 1991

Accepted for Publication December 2, 1991

Mills and Kneizys presented data in support of a light water "excess heat" reaction obtained with an electrolytic cell highly reminiscent of the Fleischmann-Pons "cold fusion" cell. The claim of Mills and Kneizys that their excess heat reaction can be explained on the basis of a novel chemistry, which supposedly also explains cold fusion, is rejected in favor of their reaction being, instead, a light water cold fusion reaction. If it is the first known light water cold fusion reaction to exhibit excess heat, it may serve as a prototype to expand our understanding of cold fusion. From this new hypothetical vantage point, a number of potential nuclear reactions are deduced, including those common to past cold fusion studies.

This broader pattern of nuclear reactions is typically seen to involve a fusion of the nuclides of the alkali atoms with the simplest of the alkali-type nuclides, namely, protons, deuterons, and tritons. Thus, the term "alkali-hydrogen fusion" seems appropriate for this new type of reaction with three subclasses: alkali-hydrogen fusion, alkali-deuterium fusion, and alkali-tritium fusion. A significant part of the difference between alkali-hydrogen fusion and thermonuclear fusion is hypothesized to involve an effect that is essentially the opposite of the well-known Mössbauer effect. Transfer of energy to the lattice is shown to be consistent with the uncertainty principle and special relativity. The implications of alkali-hydrogen fusion for theoretical models for cold fusion are

considered. Boson properties are suggested to be unimportant for alkali-hydrogen fusion, which apparently rules out the prospect that a Bose-Einstein condensation could be involved in cold fusion.

A new three-dimensional transmission resonance model (TRM) is sketched that avoids Jändel's criticism of the one-dimensional TRM. When the new TRM is coupled with the alkali-hydrogen fusion hypothesis for cold fusion, it suggests a solution for the surface, or near-surface, excess heat effect for cold fusion in the form of a reaction between  $^6\text{Li}$  and a deuteron to produce  $^4\text{He}$ , or between two deuterons to produce predominantly  $^4\text{He}$ . A lattice effect essentially opposite to an "unklapp" process suggests that energy should be given to the lattice in the reaction.

Finally, preliminary experimental evidence in support of the hypothesis of a light water nuclear reaction and alkali-hydrogen fusion is reported. Excess heat has been detected with light water-based electrolytes for the separate cases of  $\text{K}_2\text{CO}_3$ ,  $\text{Na}_2\text{CO}_3$ ,  $\text{Rb}_2\text{CO}_3$ , and  $\text{RbOH}$ . Preliminary evidence for a correlation between the amount of elemental strontium produced in the case of  $\text{Rb}_2\text{CO}_3$  as the electrolyte, or of elemental calcium produced in the case of  $\text{K}_2\text{CO}_3$  as the electrolyte, and the total excess heats produced in the respective cells has been mixed. Evidence is presented that appears to strongly implicate the transmission resonance phenomenon of the new TRM.

## INTRODUCTION

An electrolytic light water reaction recently reported by Mills and Kneizys<sup>1</sup> was experimentally demonstrated to exhibit an "excess heat effect" according to which the output energy exceeds the input energy to a significant extent. The reaction involves the electrolysis of potassium carbonate in light water, employing a nickel foil cathode and a spiraled platinum wire anode. The reported energy gains for the reaction [i.e., (total heat output - total energy input)/(total energy input)] range from ~1.5 to an impressive 3.8. The maximum ratio of peak excess power out to the input power is claimed to have been >37. Thus, considering mankind's

need for inexpensive, safe, and nonpolluting energy, the interest in their reaction transcends that of pure science. Their experiment has been independently verified by Noninski,<sup>2</sup> a highly regarded calorimetrist, so their reaction and excess heat effect should be taken seriously. However, efforts conducted by Ontario Hydro to reproduce the Mills and Kneizys results have been unsuccessful.<sup>3</sup>

Bush and Eagleton, of California State Polytechnic University (Cal Poly), have conducted successful electrolytic experiments employing a nickel cathode, a platinum anode, and a light water-based 0.57 M potassium carbonate electrolytic solution. With this setup, which is very similar to that of Mills and Kneizys, we have achieved excess power with current

Draft, June 1973

**Recombination during the Electrolysis of  
Light Water in 0.6 M K<sub>2</sub>CO<sub>3</sub>,**

**Can It Account for the Reports of Excess Heat?**

Jonathan E. JONES, Lee D. HANSEN, Steven E. JONES,  
David S. SHELTON, James M. THORNE and Lawrence B. REES

Departments of Physics and Chemistry  
Brigham Young University  
Provo, UT 84602

Funded by: EPRI

No references

## Introduction

Reports of excess heat during electrolysis of ~~in~~ light water with  $K_2CO_3$  electrolyte and a nickel cathode and platinum anode, bring with them the tantalizing possibility of a cheap, environmentally favorable energy source. Claims of excess heat range from 1 to 3 times the input power to an extraordinary >37 time the input power. However, explaining and understanding the source of the excess heat is crucial for further development of such an energy source.

The conceivably endless supply of energy available from fusion has led to the proposal of "new" fusion theories -- fusion of hydrogen and potassium<sup>1</sup> and the fusion of ordinary hydrogen atoms,<sup>2</sup> according to the "Nattoh" model. A new "novel atomic model" has also been proposed to explain the excess heat in these electrolytic cells.<sup>3</sup>

This paper will look at three different sources of measurable heat.

1. The heat input into the cell
2. The heat from evaporation of water
3. The heat from recombination of evolved gasses

Using several cells, the different heat sources were isolated and measured and/or calculated. This method has led researchers at BYU to the conclusion that the excess heat observed in the electrolysis of  $K_2CO_3$  in a light water solution with a nickel cathode and platinum anode can be attributed to the recombination of the evolved gasses.

## Theory

During electrolysis the solution around the cathode becomes saturated with hydrogen while the solution around the anode becomes saturated with oxygen. Oxygen thus migrates to the cathode and hydrogen migrates to the anode. If either hydrogen or oxygen contact the surface of a catalytic electrode where the other gas is being evolved, recombination (reaction (1)) will take place.



The surfaces of both platinum and nickel are excellent catalyst for recombination. In fact the exchange current densities( $i_{eq}$ ) are highest for Ni, Pt, and Pd when compared to other metals in their period.  $i_{eq}$  is a measure of the reversibility of the electrolysis reaction or the rate of the exchange reaction in the equilibrium state and is a function of the electrode material, the solution composition, the operating temperature, and other factors<sup>4</sup>. It is not a measure of the rate of recombination as defined by equation (1), but higher exchange current densities correspond to more catalytic surfaces.

Recombination lowers the cell voltage and increases the heat output by the cell. The cell voltage is lower because 2 electrons will be liberated in the recombination process, creating a voltage that opposes the applied voltage. The remaining energy left over from the formation of water is released as heat energy.

Several precautions mention by those claiming "fusion" or "novel chemistry that can damage the reaction are:

1. Contamination such as organic material on the electrodes
2. Leaving the electrode in the electrolyte without current
3. Obstructions between the electrodes that increase the path of the ions or evolved gas

These precautions will all greatly diminish recombination of hydrogen and oxygen in any electrolytic cell.

Excess heat can be calculated from many different reference points. All excess heat mention in this paper will be calculated from the by equation (2). This equation assumes no recombination; thus if recombination is occurring the reports of excess heat are erroneous. All mention of excess heat from BYU's results is erroneous in this way.

$$\% \text{Excess} = \frac{q_{\text{meas}} - q_{\text{cell}}}{q_{\text{cell}}} (100) \% \quad (2)$$

$q_{\text{meas}}$  is the measured heat rate output in the calorimeter.  $q_{\text{cell}}$  is calculated by equation (3).

$$q_{\text{cell}} = I(V_{\text{cell}} - V_{\text{gas}}) \quad (3)$$

...where  $I$  is the cell current,  $V_{\text{cell}}$  is the total voltage across the cell, and  $V_{\text{gas}}$  is the electrolysis voltage given by equation (4).

$$V_{\text{gas}} = \frac{\Delta H_{\text{form}}}{F} = 1.48 \text{ W/A} \quad (4)$$

The heat of recombination can be obtained from equation (5).

$$q_{\text{rec}} = I \left( \frac{\Delta H_{\text{form}}}{F} \right) * f_{\text{gas}} \quad (5)$$

...where  $f_{\text{rec}}$  is the fraction of evolved gas that is recombined,  $f_{\text{rec}}$  is dependent on the cathode material, geometry of the electrodes, and any stirring devices that help to transfer oxygen to the cathode or hydrogen to the anode.

Assuming that 50% of the gas recombines in a typical cell ( $I = 1 \text{ mA}$ ,  $V_{\text{cell}} = 1.8 \text{ V}$ ), equation (2) shows that the cell would yield approximately 2.3 times the input power. This is about 100% more excess heat than that observed at BYU. However, 2.3 times the input power is consistent with results reported by Bush<sup>1</sup>, Matsumoto<sup>2</sup>, Mills and Kneisys<sup>3</sup>, Srinivasan<sup>4</sup>, and Noninski<sup>5</sup>.

Reports of 300+% excess heat can be attributed to recombination, because most of the cells employ a different configuration than BYU (see BYU's configuration in figure 1). One of the most common configurations is a Pt anode spiraled around a Ni cathode. Compared to BYU's configuration, the spiral configuration reduces the resistance of the cell, because the electrodes are closer together; thus, the chance of recombination is increased, because the evolved gases have a much greater probability of reaching the opposite electrode. The reduced cell voltage and increased recombination both increase the excess heat as calculated by equation (6).

Because of the manner in which excess heat is defined by equation (8),<sup>6</sup> heat due to recombination will increase the calculated percent of excess heat. If recombination occurs,  $V_{\text{cell}}$  will decrease, causing  $q_{\text{cell}}$  to decrease. Therefore, the numerator of equation (2) will increase as the denominator decreases. Thus, the percentage of excess heat will be increased substantially.

This theory has been tested at BYU and has held in several different variations of the Ni/Pt light water electrolysis cell.

#### Experiment 1

At the request of E.P.R.I., we set out to test the claims of excess heat in Ni/Pt light water cells. Our first cell is shown in figure 1.

The cell was powered by a constant voltage D.C. power supply. The cell was connected in series with a 10 kΩ trimpot which was used to adjust the current in the cell. The leads, #32 copper wire, were kept small to minimize heat loss through the leads.

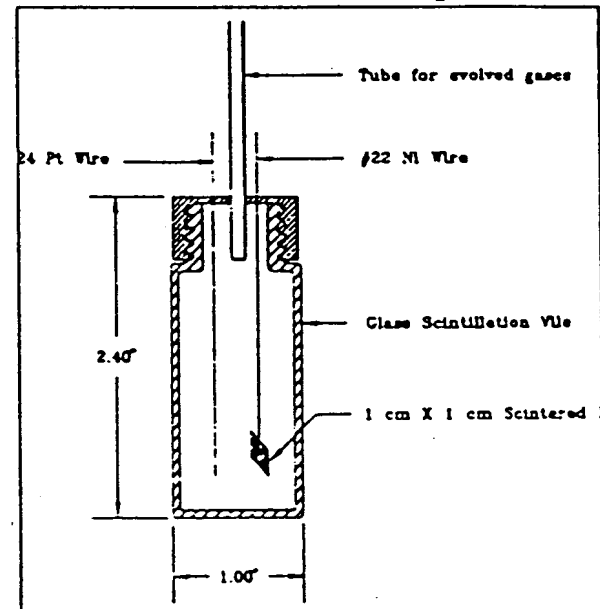


Figure 1 The cell used in experiments 1 and 2.

A Hart Scientific isothermal calorimeter was used to make the heat measurements.

The results of the first run are shown in figure 2.

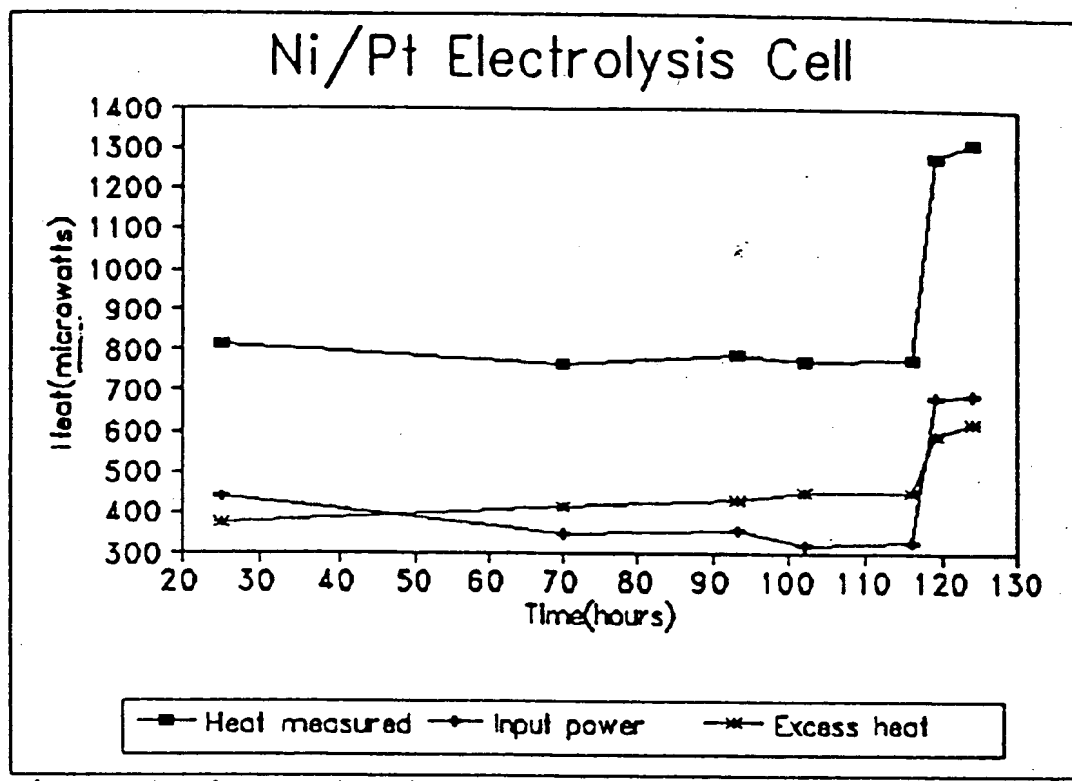


Figure 2 shows the input power, measured output of the calorimeter and the calculated excess heat.

Once the calorimeter had stabilized, between 90% and 130% excess heat was observed.

The current of the cell was approximately 1 mA. After 115 hours the current in the cell was raised from 1 mA to 1.6 mA. The voltage across the cell remained between 1.8 V and 1.95 V.

The input power was calculated using equation (3), including the heat of evaporation due to evolved gases.

The calorimeter was calibrated electrically with the heaters in each calorimeter cell.

Figure 2 shows excess of up to 130% of the input power. Although others had claimed the excess heat was not due to recombination, until the evolved gases could be accounted for this was not assumed.

## Experiment 2

Since the rate of evolved gases can be calculated by equation (7), we decided to measure the gas evolution from the cell. This proved to be much more difficult than we had first suspected.

$$G_{\text{evol}} = \frac{I_{\text{cell}}}{96,500 \text{ coul/equi}} * 0.75 \text{ mol/equi} * 30.5 \text{ l/mol} \quad (6)$$

...where  $I_{\text{cell}}$  is the cell current.

For a cell operating at 1 mA, 0.853 ml/hr will evolve. We tried to measure this flow rate using a soap bubble in a graduated 1 ml pipette. At approximately 1 ml/hr the gas either diffused through the soap bubble or was lost through other leaks in the system. A mercury barometer was also considered; however, mercury has a catalytic surface and the gases might have recombined on the surface of the mercury causing an inaccurate measurement.

Although we did not succeed in measuring the gas evolution rate we observed the excess heat remains approximately constant once the electrolyte became saturated with hydrogen and oxygen. Figure 3 shows results with the cell in figure 1 at different power inputs.

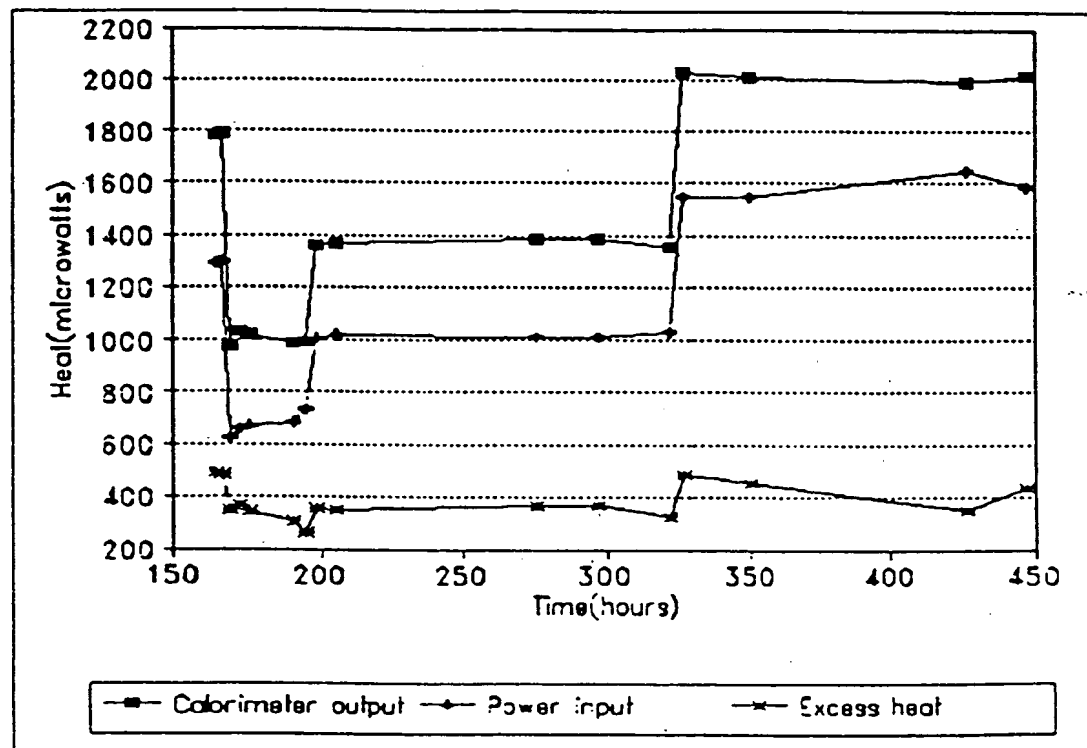


Figure 3 shows the Ni/Pt electrolysis cell running at 0.5 mA, 1 mA, and 1.6 mA. The input power calorimeter output, and excess heat are graphed versus time.

### Experiment 3

When we could not accurately measure the gas evolution rate, methods of suppressing recombination were discussed. The following techniques will quell recombination.

1. Inserting an ion transport membrane between the electrodes
2. Bubbling nitrogen through the electrolyte to purge the O<sub>2</sub> and H<sub>2</sub>,
3. Placing a barrier between the two electrode that would inhibit the migration of gas between electrodes

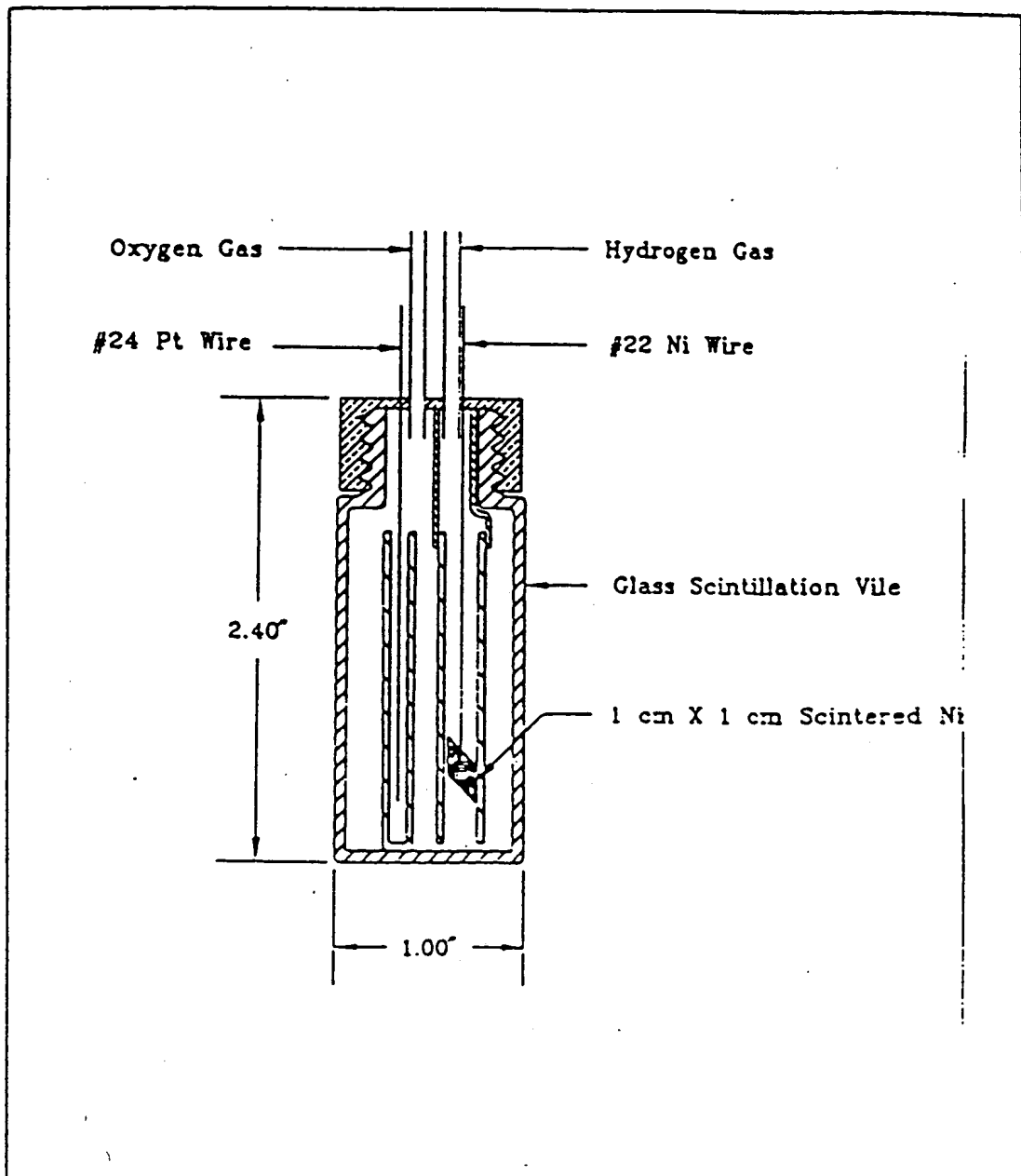


Figure 4 The cell used in experiment 3.

We decided to use glass tubes as a barrier to inhibit the migration between the electrodes, as shown in figure 4. A glass tube, closed at the bottom, surrounded the Pt anode with the top submerged in the electrolyte. A second tube, open at the bottom, enclosed the nickel cathode. The nickel tube was vented through a separate tube so the gases could not recombine before leaving the calorimeter.

Figure 5 shows the resulting heat measurements with the tubes on, then with the tubes off, and again with the tubes on as shown in figure 4.

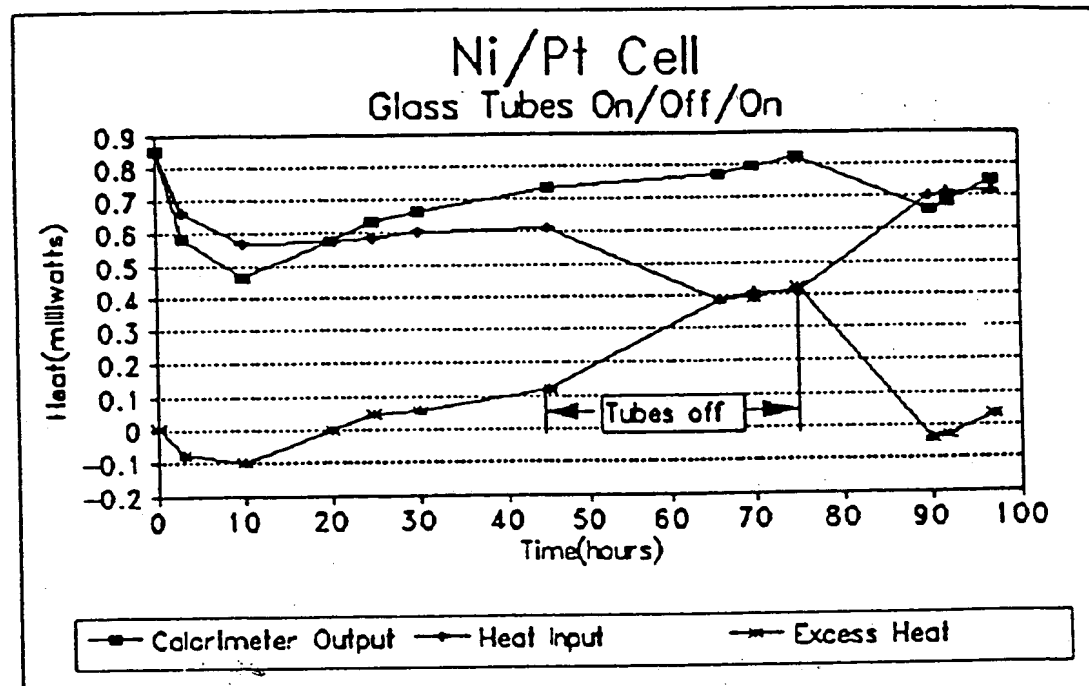


Figure 5 shows the calorimeter output, the input power, and the excess heat as a function of time. The period for when the tubes were off is marked.

The ion path increased for this configuration, thus increasing the cell voltage. This accounts for the increased input power while the tubes were on. When the tubes were taken off the input power decreased, but the heat measured by the calorimeter increased.

The increase in measured heat along with the decrease in input power gave up to 114% excess heat while the tubes were off. While the tubes were on the percent excess heat was, within the error of the experiment, zero. This demonstrated a direct correlation between the ability for gases to migrate to recombining surfaces and the observed excess heat.

#### Experiment 4

Experiment 4 was set up to verify that recombination was taking place on the sintered nickel cathode and to determine what percent of the evolved gases could recombine.

A fine gas frit was placed in the bottom of the cell as shown in figure 6. The parameters for the anode, cathode and electrolyte

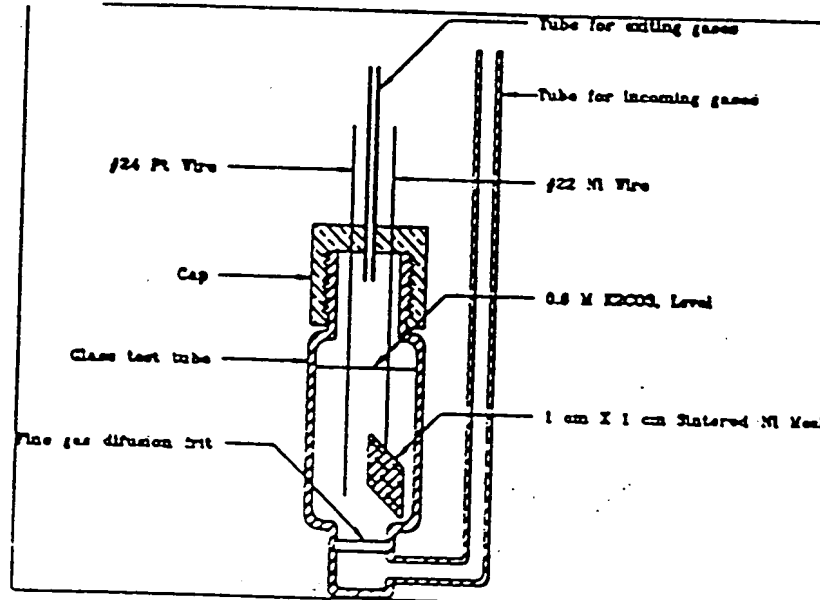


Figure 6 The cell used in experiment 4.

were the same as experiments 1, 2, and 3. Nitrogen was pumped through the cell to purge it of evolved gases, thus eliminating

recombination. Oxygen was pumped through the cell saturating the electrolyte with oxygen, thus if recombination occurred it would be at the nickel cathode(hydrogen electrode).

A baseline was established by measuring the calorimeter output at different flow rates with no electrolysis. The baseline was also calculated for each flow rate. The baseline was the same for nitrogen and oxygen at the same flow rate. The calculated and measured baseline were the same.

The results of experiment 3 are shown in figures 7.

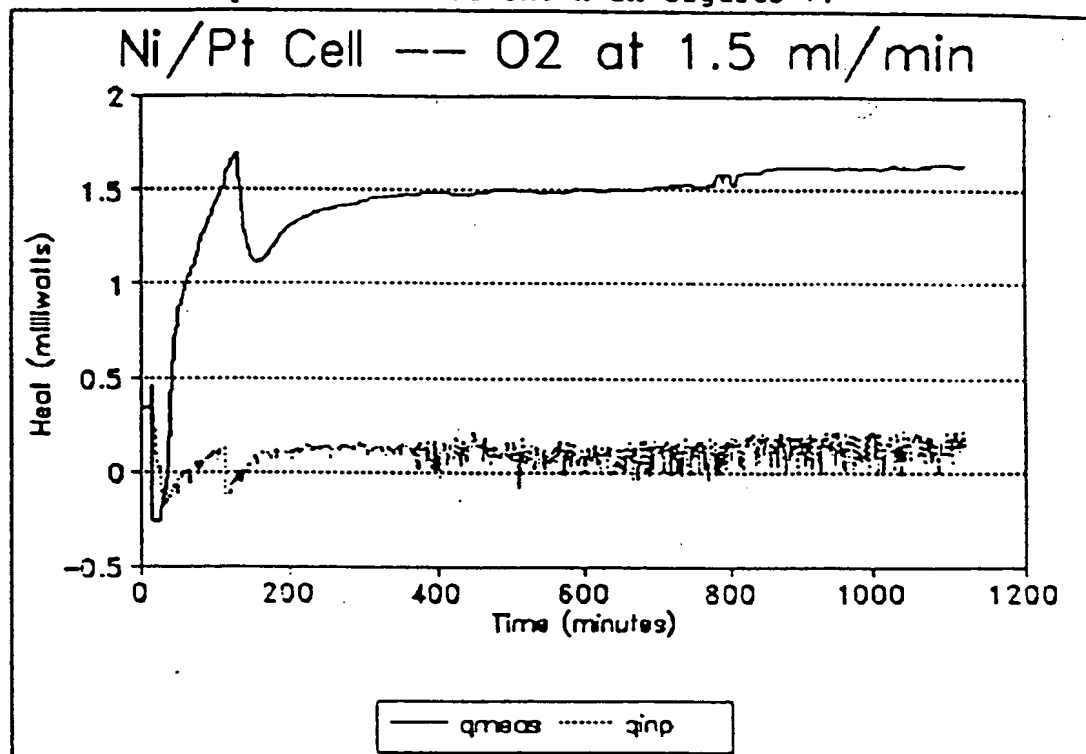


Figure 7 The results of the cell running with oxygen flowing.

When the nitrogen was flowing through the cell, the first 60 minutes of figure 7 show the power input into the cell (calculated assuming no recombination) equal to the calorimeter output. The cell ran at this level for 40 hours(not shown in figure 7) before the oxygen was turned on. The nitrogen purged the cell of the evolved gases; so no recombination occurred and no excess heat was observed.

With the oxygen flowing, the cell behaved differently. First, the cell voltage dropped below 1.48 volts. If no recombination is assumed then the calculated input power will be negative which is very difficult to explain. However, if recombination is occurring then it will operate as a fuel cell. In the operation of a fuel-cell hydrogen is burned creating both heat energy and electrical energy. Fuel cells have been studied extensively and are used in many space application.

In the nickel light water cell the nickel cathode will store hydrogen, forming a nickel hydride. In the presence of oxygen and a driving voltage the hydrogen and oxygen will recombine, i.e. reaction (1), releasing the heat of formation of water and two electrons. The liberated electrons decrease the cell voltage -- below 1.48 if enough hydrogen is stored -- causing a decrease in the input power. The heat of recombination increases in calorimeter output, thus the percent excess heat (equation (2)) becomes very large.

For example Mills reports excess heat of 1 to 16 times the input power. This appears to be extraordinary until one looks at the data. For experiments #3, 4, 17, and 18 reported in "Unification of Spacetime the Forces, Matter, and Energy" by Randell L. Mills the difference ( $V_{cell} - 1.48$ ) is less than 0.2 volts making  $q_{cell}$  puny. It is interesting that these are the experiments that give him the most excess heat. Note, it is realized that recombination cannot account for all of the excess heat reported by Mills (some runs report excess heat greater than IV). However, their results may be greatly inflated by assuming no recombination, because they are running with a pulsed power supply and assuming a square wave pulse, which may not be the case if recombination is occurring.

Figure 7 shows the variation in  $q_{inp}$ , the input power given by equation (3), resulting from recombination in the cell. The nickel stores hydrogen for a while then the hydrogen recombines lowering the cell voltage and adding heat to the cell. This causes the cell voltage to cycle, thus the variation in  $q_{inp}$ . The calorimeter output does not show the variation because it's equilibration time is too long.

Using equation (2) to calculate the percent excess heat could give an infinite %excess heat if the right point were chosen. Being practical, the average cell voltage is approximately 1.6 volts and the cell current is 1.08 mA, thus  $q_{inp} = 1.08(1.6 - 1.48) = 0.13 \text{ mW}$ . The calorimeter output on an average was 23 mV plus the 170 mV baseline for the gas flow. Taking  $(23 \text{ mV} + 170 \text{ mV}) * 7.88 \mu\text{W/mV}$  gives  $q_{out} = 1.52 \text{ mW}$ , where  $7.88 \mu\text{W/mV}$  is the calorimeter constant. Therefore the percent excess heat is  $(1.52 - 0.13) / 0.13 = 10.7$  or 1000-% excess heat. This can be done for each point on the graph in figure 7, but it doesn't make any sense for the points where  $q_{inp} = 0$  or is negative. The point, equation (2) is only valid when there is no recombination.

The total power input into the cell is given by  $I_{cell} * V_{cell}$ . For the average cell voltage and current this yields 1.73 mW, which is greater than the calorimeter output. Equation (5) gives us the fraction of gas that must recombine to account for the excess heat. For  $q_{out}$  and the cell current given in the proceeding paragraph 77% of the gas must recombine. This is very reasonable because oxygen is being bubbled past a catalytic nickel hydride. Nickel is used in fuel cells as a recombiner. In fact to within the error of the experiment 100% of the gas is recombining at 800 minute mark on in figure 7.

### Experiment 5

To be reassured the excess heat was not nuclear in origin, x-rays were looked for in two nickel light water cells. A portion of the cell was cut out and replaced with a thin piece of plastic. The nickel was placed against the edge of the plastic and the cell was placed very near the window to the x-ray detector, to assure that the 7.5 keV K-alpha nickel x-ray would not be attenuated and could be detected.

After 75 hours, no Ni K- $\alpha$  or Ni K- $\beta$  x-rays were detected coming from the first cell.

The second cell was looked at for more than a week with no Ni K- $\alpha$  or Ni K- $\beta$  x-ray emmisions detected. Figure 8 shows the x-ray background for this run with no significant Ni x-rays.

The absence of x-rays argues strongly against nuclear reactions as the origin of the excess heat.

### Conclusion

Recombination can account for the excess heat reported in all of the nickel light water cells except those that exceed the total input power ( $I^*V$ ). Even when the measured output exceeds  $I^*V$ , subtle errors in the measurement of the input power or the calorimeter output could allow recombination to account for the excess heat. Figure 7 shows the effect recombination has on the cell voltage. If measurements are not taken regularly, then the calculated input power may be highly underestimated. This will be of particular concern in experiments which use pulsed power, like that of R. Millis. The bottom line is, until the cell set up guarantees that there will be no recombination or care is taken to assure accurate measurements when recombination is occurring, reports of excess heat in light water nickel cells must be questioned.

RUN 20733  
SAMPLE NI-CELL

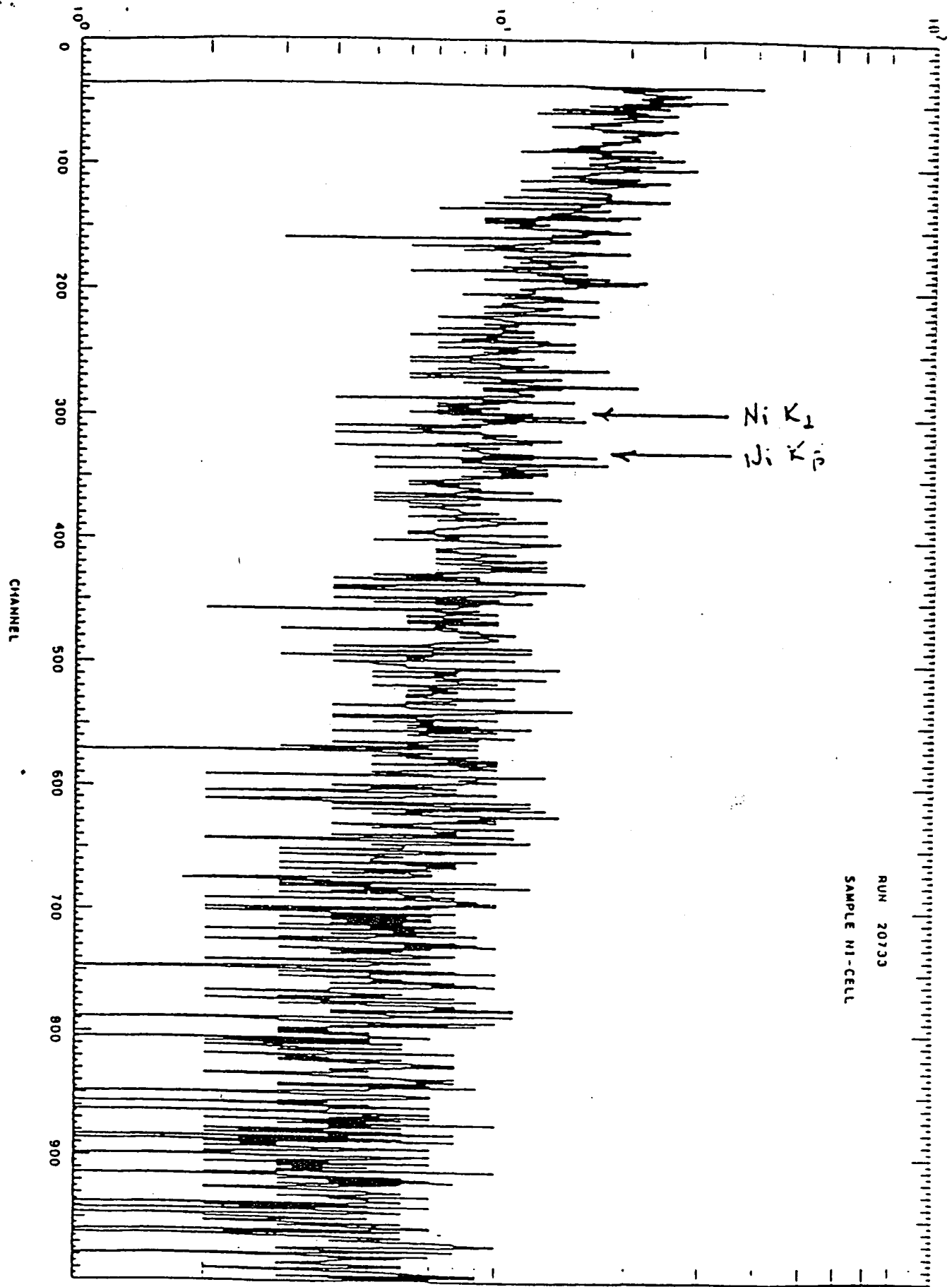


Figure 8

California State Polytechnic University, Pomona  
College of Science  
3801 West Temple Avenue  
Pomona, California 91768  
Telephone: (909) 869-3431  
FAX: (909) 869-4396



Page 1 of 3 Pages

Date: 2/27/97

To:	Dr Jim Hilborn	From:	Dr Robert T. Bush
FAX:	613-584-4010	Department:	Physics
Address:	Chalk River	Phone:	X4018
Subject:	Suggested Mutual Project		

Comments:

Jim,

I appreciate your considerity this.

Very Best Regards,

AECL 001220

FAX

4/22/93

To: Dr. Jim Hilborn, Atomic Energy of Canada  
Chalk River, Ontario, Canada (fax: 613-584-4010)

From: Dr. Robert T. Bush, Physics Department, California State Polytechnic University, Pomona, Ca 91768, U.S.A. (fax: 909-869-4396)

Dear Jim:

The electrolyte samples that we are interested in having Chalk River analyze are from two light water electrolytic cells (cells 63 and 64) run in series and made as identical as possible, except that the electrolyte of 63 employed nanopure water (deuterium deuterioxide is about one out of every 5,000 molecules), whereas that of cell 64 employed de-deuterated water (deuterium deuterioxide is about one out of every 500,000 molecules). Otherwise, both electrolytes were 0.57 M potassium carbonate. Five samples of electrolyte were taken from each cell over the approximately 68 day period of cell operation [Charging began 2/4/93. Cell 64 was stopped on 4/14/93, and 63 is still operating as of today (4/22/93)]. The post-run samples we would send you have evidenced calcium levels between about 1ppm and 1.5 ppm on the basis of flame AA tests, and these are consistent with the amounts of excess heat measured calorimetrically assuming potassium to be the nuclear parent. However, we will dilute these post-run samples with nanopure water to one-third their present concentration in order to save out essentially identical samples for additional work if this is okay with you:

Six Proposed Samples for Analysis (ppm's are for elemental calcium)

(1) Virgin electrolyte (nanopure water, 0.57 M rubidium carbonate):

(0.10 ppm)

(2) Nanopure water sample: (0.00 ppm)  
Cell 63:

(3) Post-run sample 63-a: (2/25/93), (1.55 + 0.08)ppm

(4) Post-run sample 63-e: (4/8/93), (1.02 + 0.05)ppm

AECL 001221

Cell 64:

(5) Post-run sample 64-1: (2/25/93), (1.49 + 0.08)ppm

(6) Post-run sample 64-6: (4/8/93), (0.93 + 0.06)ppm

It would be possible also to send a sample of the virgin cathode material (nickel fibrex) and post-run cathode material from both cells 63 and 64. However, initially, the primary interest would be to see if there is a relative isotope abundance shift of calcium 42 relative to 43 in the electrolyte. The relative abundances of these two isotopes could also be looked at relative to calcium 44, assuming that one can show that Ti-44 (47 year half-life) is not an interferent, as seems reasonable. (However, the electrolyte should be checked by flame AA for titanium to assure this. There may, of course, be molecular interferences.) As you know a significant shift would be an undeniable signature of a nuclear reaction.

We appreciate your willingness to consider this mutual project that could hasten an understanding of the light water excess heat effect.

Sincerely yours,

Dr. Robert T. Bush

PS: Our latest cells are made of teflon (earlier pyrex cells were coated with teflon) so that this could not be a source of calcium. (The anode is platinum wire.) The virgin nickel mesh cathode material is contaminated with calcium, but all of our studies indicate that the cathodic current drives the  $\text{Ca}^{++}$  ions from the electrolyte and into the nickel mesh. This effect, accompanied possibly by the transmutation of the calcium itself accounts for the fact that an equilibrium level (concentration) of calcium of about 1 ppm of calcium was reached in this experiment in both cells.

PPS: Please accept my apologies for getting this to you later than we had discussed.

AECL 001222

## LOCAL ENERGY SYSTEMS

## FAX TRANSMITTAL SHEET

DATE: 1993 April 28

ATTENTION: Dr. Robert Bush

COMPANY: California State Polytechnic University

FAX NUMBER: 909-869-4396

FROM: Dr. John Hilborn

## PAGES TO FOLLOW:

## COMMENTS:

Thanks for your Fax message describing your six electrolyte samples.

The good news - Our laboratory would be able to determine the isotopic abundances in your samples with adequate precision.

The bad news - It would be necessary to do some wet chemistry prior to mass spectrometry, in order to eliminate potassium. The set-up cost would be high, resulting in a total cost of \$6000 to \$8000 for the six samples.

Options - Find some money.  
 Find a less costly laboratory.  
 Wait for 1 or 2 months, and hopefully we could include your samples with ours at no extra cost. Right now we have to watch our budget.

---

Fax Number: (613)584-4010      or      (613)584-2227

If there are problems with transmission, please call (613)584-3311 Ext. 6016 or 4959

---

**MILBANK, TWEED, HADLEY & MCCLOY**

**1 CHASE MANHATTAN PLAZA**

**LOS ANGELES**  
213-892-4000  
FAX: 213-629-5063

**NEW YORK, N.Y. 10005-1413**

**TOKYO**  
813-3504-1050  
FAX: 813-3595-2790

**WASHINGTON, D.C.**  
202-835-7500  
FAX: 202-835-7586

**212-530-5000**  
FAX: 212-530-5219

**HONG KONG**  
852-2971-4888  
FAX: 852-2840-0792

**LONDON**  
44-171-448-3000  
FAX: 44-171-448-3029

**MOSCOW**  
7-501-258-5015  
FAX: 7-501-258-5014

**SINGAPORE**  
65-534-1700  
FAX: 65-534-2733

**JAKARTA**  
CORRESPONDENT OFFICE  
6221-252-1272  
FAX: 6221-252-2750

**December 26, 1995**

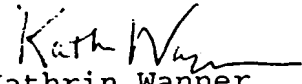
Michael O'Hayer, Esq.  
Duane, Morris & Heckscher  
735 Chesterbrook Boulevard  
Chesterbrook Corporate Center  
Wayne, PA 19087

**Re: 14 T 199 00196 95 H/J**  
**HydroCatalysis Power Corporation**  
**and Atomic Energy of Canada, Limited**

Dear Mr. O'Hayer:

Enclosed please find additional documents (Bates stamped AECL 001518 through AECL 001532) being produced in response to claimant's request for the production of documents.

Sincerely yours,

  
Kathrin Wanner

KW:pml  
Enclosure  
VIA FEDERAL EXPRESS

CC: Russell E. Brooks

3/2/93

Call to Tom Passell

9-1-415-855-2000

Tom HAS IT ON HIS LIST

- He is concerned after some very recent work performed by SRI to prove that it didn't work in light water. was possibly motivated by desire to stay in a D<sub>2</sub>O based system.
- He needs some re-assurance that we are not working with the pre-conceived idea that it won't work - I assured him this was not the case. (Maybe AECL's D<sub>2</sub>O possible benefit is a nagging concern)
- I assured him that we had Mills blessing and were planning to succeed and add. I suggested a conference call to give him assurances.

Lot of people can show this  
Pre-convinced that they can show  
Make it not work SRI.

← Calibration →

Swung to <sup>from</sup> Heavy Water  
light Water

Reassure - the

10<sup>9</sup> 30

Huf 3214

# AECL EACL

## AECL Research

Chalk River Laboratories  
Chalk River Ontario  
Canada K0J 1J0  
Tel (613) 584-3311  
Fax (613) 584-4024  
Telex 053-34555

## EACL Recherche

Laboratoires de Chalk River  
Chalk River (Ontario)  
Canada K0J 1J0  
Tél (613) 584-3311  
Fax (613) 584-4024  
Telex 053-34555

### FAX TRANSMITTAL SHEET

**DATE:** 1993 March 31

**ATTENTION:** John Preston

**COMPANY:** MIT Technology Licensing Office

**FAX NUMBER:** (617)258-6790

**FROM:** John Hilborn

**PAGES TO FOLLOW:** nil

**COMMENTS:** Brian Ahern suggested that I discuss with you our mutual interest in verifying and explaining reports of excess heat production from electrolytic cells.

A Mills-type cell incorporating a nickel cathode and potassium and sodium carbonate electrolytes, will be constructed and tested at our Chalk River laboratory under contract to EPRI. If you believe that a meeting would be useful, I would like to visit your laboratory on Friday this week or early next week. I have visited R.L. Mills twice in Lancaster, PA, and could find no obvious errors in his observations of approximately 50 Watts of excess heat production from his potassium carbonate cells. I have also visited R.M. Shaubach at Thermacore Inc. Please FAX reply to (613)584-4010.

---

Fax Number: (613)584-4010 or (613)584-4024

If there are problems with transmission, please call (613)584-3311 Ext. 4943 or 4959

---

AECL 001521

# A LIGHT WATER EXCESS HEAT REACTION SUGGESTS THAT "COLD FUSION" MAY BE "ALKALI-HYDROGEN FUSION"

ROBERT T. BUSH *California State Polytechnic University  
Physics Department, Pomona, California 91768*

Ran '91

COLD FUSION

## TECHNICAL NOTE

KEYWORDS: *cold fusion, alkali-hydrogen fusion, nuclear transmutation*

Received July 12, 1991  
Accepted for Publication December 2, 1991

Mills and Kneizys presented data in support of a light water "excess heat" reaction obtained with an electrolytic cell highly reminiscent of the Fleischmann-Pons "cold fusion" cell. The claim of Mills and Kneizys that their excess heat reaction can be explained on the basis of a novel chemistry, which supposedly also explains cold fusion, is rejected in favor of their reaction being, instead, a light water cold fusion reaction. If it is the first known light water cold fusion reaction to exhibit excess heat, it may serve as a prototype to expand our understanding of cold fusion. From this new hypothetical vantage point, a number of potential nuclear reactions are deduced, including those common to past cold fusion studies.

This broader pattern of nuclear reactions is typically seen to involve a fusion of the nuclides of the alkali atoms with the simplest of the alkali-type nuclides, namely, protons, deuterons, and tritons. Thus, the term "alkali-hydrogen fusion" seems appropriate for this new type of reaction with three subclasses: alkali-hydrogen fusion, alkali-deuterium fusion, and alkali-tritium fusion. A significant part of the difference between alkali-hydrogen fusion and thermonuclear fusion is hypothesized to involve an effect that is essentially the opposite of the well-known Mössbauer effect. Transfer of energy to the lattice is shown to be consistent with the uncertainty principle and special relativity. The implications of alkali-hydrogen fusion for theoretical models for cold fusion are

considered. Boson properties are suggested to be unimportant for alkali-hydrogen fusion, which apparently rules out the prospect that a Bose-Einstein condensation could be involved in cold fusion.

A new three-dimensional transmission resonance model (TRM) is sketched that avoids Jändel's criticism of the one-dimensional TRM. When the new TRM is coupled with the alkali-hydrogen fusion hypothesis for cold fusion, it suggests a solution for the surface, or near-surface, excess heat effect for cold fusion in the form of a reaction between  $^6\text{Li}$  and a deuteron to produce  $^4\text{He}$ , or between two deuterons to produce predominantly  $^4\text{He}$ . A lattice effect essentially opposite to an "umklapp" process suggests that energy should be given to the lattice in the reaction.

Finally, preliminary experimental evidence in support of the hypothesis of a light water nuclear reaction and alkali-hydrogen fusion is reported. Excess heat has been detected with light water-based electrolytes for the separate cases of  $\text{K}_2\text{CO}_3$ ,  $\text{Na}_2\text{CO}_3$ ,  $\text{Rb}_2\text{CO}_3$ , and  $\text{RbOH}$ . Preliminary evidence for a correlation between the amount of elemental strontium produced in the case of  $\text{Rb}_2\text{CO}_3$  as the electrolyte, or of elemental calcium produced in the case of  $\text{K}_2\text{CO}_3$  as the electrolyte, and the total excess heats produced in the respective cells has been mixed. Evidence is presented that appears to strongly implicate the transmission resonance phenomenon of the new TRM.

## I. INTRODUCTION

An electrolytic light water reaction recently reported by Mills and Kneizys<sup>1</sup> was experimentally demonstrated to exhibit an "excess heat effect" according to which the output energy exceeds the input energy to a significant extent. The reaction involves the electrolysis of potassium carbonate in light water, employing a nickel foil cathode and a spiraled platinum wire anode. The reported energy gains for the reaction [i.e.,  $(\text{total heat output} - \text{total energy input})/(\text{total energy input})$ ] range from  $\sim 1.5$  to an impressive 3.8. The maximum ratio of peak excess power out to the input power is claimed to have been  $>37$ . Thus, considering mankind's

need for inexpensive, safe, and nonpolluting energy, the interest in their reaction transcends that of pure science. Their experiment has been independently verified by Noninski,<sup>2</sup> a highly regarded calorimetrist, so their reaction and excess heat effect should be taken seriously. However, efforts conducted by Ontario Hydro to reproduce the Mills and Kneizys results have been unsuccessful.<sup>3</sup>

Bush and Eagleton, of California State Polytechnic University (Cal Poly), have conducted successful electrolytic experiments employing a nickel cathode, a platinum anode, and a light water-based 0.57 M potassium carbonate electrolytic solution. With this setup, which is very similar to that of Mills and Kneizys, we have achieved excess power with current

densities ranging from  $\sim 2$  to  $\sim 40$  mA/cm<sup>2</sup>. The peak excess power reached was  $\sim 4$  W, and the total excess heat is estimated to have been  $\sim 0.3$  MJ. A detailed presentation of these experiments will be reported in a future paper.

Mills and Kneizys based their reaction on a novel chemistry of Mills and Farrell<sup>4</sup> with which the latter replace quantum mechanics. It can readily be shown that this novel chemistry, ingenious though it may be, is flawed. Mills and Kneizys also claim that the novel chemistry of Mills and Farrell can account for the excess heat effect of Fleischmann and Pons.<sup>5</sup> Instead, while the novel chemistry is rejected, it is shown that Mills and Kneizys have made an important discovery, namely, a *light water cold fusion reaction* exhibiting the excess heat effect. The importance of the latter is that it may serve as a prototype allowing us to obtain a better understanding of cold fusion.

At this juncture, it must be strongly emphasized that, far from fading away, the Fleischmann-Pons excess heat effect has gained renewed vigor from reports presented at the Second Annual Conference on Cold Fusion held at Como, Italy, June 29-July 4, 1991. In addition, two rather remarkable reviews of cold fusion research, the earlier one by Srinivasan<sup>6</sup> and the later one by Storms,<sup>7</sup> have recently been circulated. Both contain strong evidence for the excess heat effect. At the Como conference, evidence of the ability of researchers to obtain an enhanced and more robust Fleischmann-Pons excess heat effect was presented by researchers such as Pons and Fleischmann,<sup>8</sup> McKubre et al.,<sup>9</sup> Bush and Miles,<sup>10</sup> and Bush and Eagleton.<sup>11</sup> These researchers had built upon the earlier strong work of experimenters such as Fleischmann and Pons,<sup>5</sup> Huggins et al.,<sup>12</sup> Appleby et al.,<sup>13</sup> Scott et al.,<sup>14</sup> Hutchinsen et al.,<sup>15</sup> Bockris et al.,<sup>16</sup> McKubre et al.,<sup>17</sup> Liebert and Liaw,<sup>18</sup> and Eagleton and Bush.<sup>19</sup>

Thus, it is important to realize that the excess heat effect must now be considered a permanent fixture in any serious scientific considerations, with the two possibilities for its origin being, with the reasonable assumption that we have no violation of the first law of thermodynamics, (a) nuclear energy and (b) a new unknown source of energy. The best bet is nuclear energy because the excess heat effect goes away, or at least becomes too small to measure, when heavy water in the cold fusion reactions is replaced by light water and because the energy is too large to be chemical in origin. In the latter regard, it can be reported that, employing a cathode in the form of a 5-μm thin film of palladium electroplated (at Los Alamos National Laboratory) upon a silver substrate with a surface area of  $\sim 4.5$  cm<sup>2</sup>, Bush and Eagleton<sup>11</sup> obtained  $\sim 15$  MJ of excess heat over a 54-day period with a peak excess power of  $\sim 6$  W and an average excess power of  $\sim 3.2$  W, with the latter being  $\sim 28\%$  of the input power. Normalizing the data to the amount of palladium and assuming that the excess heat effect occurs in the palladium, one can employ this data to estimate a lower limit for the normalized excess heat produced in the thin film of  $\sim 63$  GJ per mole of palladium. Note that this result is at least a factor of a million too large for it to have been of chemical origin.

## II. REJECTION OF THE NOVEL CHEMISTRY OF MILLS AND FARRELL

In their abstract, Mills and Kneizys<sup>1</sup> refer to a new atomic model by Mills and Farrell:

According to a novel atomic model, the predominant source of heat of the phenomenon denoted cold fusion is

the electrocatalytically induced reaction whereby hydrogen atoms undergo transitions to quantized energy levels of lower energy than the conventional ground state. These lower energy states correspond to fractional quantum numbers. The hydrogen electronic transition requires the presence of an energy hole of  $\sim 27.21$  eV provided by electrocatalytic reactants . . . and results in "shrunken atoms" analogous to muonic atoms.

Their fractional quantum numbers are presented in Eq. (3) of Ref. 1 as

$$n = \frac{1}{2}, \frac{3}{2}, \frac{5}{2}, \dots \quad (1)$$

Somehow, for this is not very clear, this series gets truncated at  $\frac{1}{3}$ . Moreover their treatment is immersed in the new framework provided by Mills and Farrell, who have replaced standard quantum mechanics by "a novel theory for which the fundamental laws of nature are shown to be applicable on all scales. Maxwell's equations, Einstein's general and special relativity, Newtonian mechanics, and the strong and weak forces are unified."<sup>1</sup> In seeking to replace the conventional theory, Mills and Farrell and Mills and Kneizys seem unaware of the numerous triumphs of standard quantum mechanics, especially those of its ultimate relativistically correct expression, the Dirac equation. Certainly, Mills and Kneizys have exhibited no counterpart to the latter, and there is no independent evidence supporting their new scheme of quantum numbers in Eq. (1) with its inclusion of fractional quantum numbers. However, dismissing the totality of the work of Mills and Kneizys based on their novel chemistry would be to throw away an inestimable scientific treasure, namely, their light water reaction exhibiting an excess heat. We turn now to what is a more appropriate conclusion, that this is apparently the first light water cold fusion reaction conclusively demonstrated to exhibit an excess heat phenomenon.

[In this connection I am grateful to referee number 2 for calling my attention to an explicit claim in the Fleischmann-Pons patent<sup>20</sup> (first priority date: March 13, 1989) for the production of excess energy during electrolysis of light water with nickel and other metals. Apparently, this is a case of independent discovery with Mills and Kneizys being unaware of the patent claim. Certainly, however, they deserve credit for calling this reaction and their study of it to the attention of the academic community in admirably detailed fashion. In contrast, one notes, with no intention of minimizing the inestimable work of Fleischmann and Pons that they have apparently not published the results of such a light water study in a peer-reviewed journal.]

## III. THE MILLS-KNEIZYS LIGHT WATER REACTION AS A COLD FUSION REACTION

One seeks an alternative explanation for this new excess heat effect to that provided by Mills and Kneizys and Mills and Farrell. One key is that their experimental setup is very similar to that of Fleischmann and Pons for cold fusion: An electrolytic cell contains a platinum anode and a cathode, which, however, is nickel rather than palladium. (Note that nickel, like palladium, also has a face-centered crystalline structure and readily absorbs hydrogen. Protons will enter the nickel lattice as will singly ionized potassium atoms.) Because of this similarity, it makes sense to examine whether this light water reaction could possibly be a nuclear reaction, perhaps related to cold fusion.

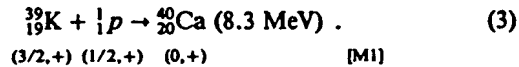
A salient clue is that we have as potential nuclear ingredients potassium (19 protons) and individual protons at interstitial sites in the nickel lattice. And, the addition of a proton to a  $^{39}\text{K}$  nucleus yields the ultrastable  $^{40}\text{Ca}$ , which is a "doubly magic" nuclide. It is this that suggests the possibility of a nuclear reaction and a link to cold fusion. For example,  $^4\text{He}$  is also a doubly magic nuclide, and the recent work of Bush et al.<sup>10</sup> suggests that  $^4\text{He}$  is probably a product of cold fusion. Thus, based on this augmentation of the nuclear stability of the reaction product, it is reasonable to hypothesize that the Mills-Kneizys reaction is a cold fusion reaction, albeit a light water one. (Note in this regard that ~93% of naturally occurring potassium is in the form of  $^{39}\text{K}$ .)

"Doubly magic" here refers to the fact that both the number of protons and the number of neutrons in the nucleus of  $^{40}\text{Ca}$  are equal to the "magic number" of 20. [Recall that the magic numbers were established in connection with the shell model of the nucleus by Mayer<sup>21</sup> and Jensen.<sup>22,23</sup> They are those numbers of protons (neutrons) that produce ultrastable configurations since they are the total number of protons (neutrons) in a configuration just before a large energy gap.] For future reference, we list the magic numbers<sup>24</sup> in bold print for protons (neutrons) along with the total numbers of protons (neutrons) that result in configurations having totally closed shells and, thus, increased stability:

$$\begin{aligned} & \mathbf{2, 6, 8, 14, 16, 20, 28, 32, 38, 40, 50, 58, 64,} \\ & \mathbf{76, 80, 82, 92, 100, 120, 124, 126, \dots} \quad (2) \end{aligned}$$

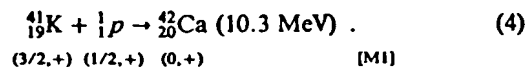
In addition, it is a well-known fact that the energy of a nuclear configuration is minimized by pairing off the protons (neutrons) as much as possible. This is partially reflected by the fact that all of the numbers in Eq. (2) are even. For future reference, an increase in stability produced by pairing two protons (neutrons) is referred to as the "pairing effect."

To explore the ramifications of this hypothesis more fully, consider the Mills-Kneizys light water reaction represented schematically as follows:



Note from the positive  $Q$  value of ~8.3 MeV that this is energetically possible on the basis of nuclear physics. Moreover, we assume that either, or both, of the two reactants, the  $\text{K}^+$  ion and the proton, are an integral part of the metal (nickel) lattice. Since the protons, being more mobile, should fill up interstitial positions fairly quickly, it may be the case that the reaction is one in which a  $\text{K}^+$  ion is incident upon an interstitial proton. On the other hand, another possibility is that of a proton incident upon a substitutional, or interstitial,  $\text{K}^+$  ion.

One cannot, of course, rule out reaction (4) even though  $^{41}\text{K}$  is only ~7% abundant compared to an ~93% abundance for  $^{39}\text{K}$ . In reaction (4), the addition of a proton to a  $^{41}\text{K}$  nucleus produces a more stable  $^{42}\text{Ca}$  nucleus. In this reaction, as in Eq. (3), the proton number becomes magic, going from 19 to 20. The neutron number remains even at 22 in reaction (4):



In fact, the energy release averaged over the nucleons for the  $^{42}\text{Ca}$  nucleus in reaction (4) is given by  $(10.3 \text{ MeV}/42 \text{ nucleons}) = 0.245 \text{ MeV per nucleon}$ , whereas for the  $^{40}\text{Ca}$  nucleus

in Eq. (3), it is given by  $(8.3 \text{ MeV}/40 \text{ nucleons}) = 0.208 \text{ MeV per nucleon}$ . So, both reactions (3) and (4) might be taken to constitute our prototypical reactions. Nevertheless, reaction (3) is generally referred to as the prototype reaction. It would, of course, be interesting to conduct separate experiments employing very high purity  $^{39}\text{K}$  in one and very high purity  $^{41}\text{K}$  in the other to test reactions (3) and (4). In both reactions (3) and (4), the proof that this hypothesis is correct would be the appearance of calcium ( $^{40}\text{Ca}$  and  $^{42}\text{Ca}$ , respectively) as a by-product in an amount correlated with the amount of excess heat generated. Of course, assuming that the hypothesis of a nuclear reaction is correct, it is not clear as to what percentage of the calcium produced would be in the electrolyte and what percentage might remain in the nickel lattice. In addition, an experimental determination might be complicated by the fact that part of the calcium in the electrolytic solution might plate out onto the cathode. Work is currently under way at Cal Poly to correlate calcium production in these reactions with excess heat production. The corroboration of this would be akin to the correlation of excess heat and  $^4\text{He}$  production in the case of cold fusion, and it should be considerably easier to obtain an unequivocal result.

One must also ensure conservation of spin and parity. Thus Eq. (3) cannot express the entire reaction. Below the reactants and the products in the equations are indicated the respective spins (units of  $\hbar$ ) and parities in parentheses. The lowest order electromagnetic multipole radiation (in this case the magnetic dipole [M1]), that would have to be emitted to conserve spin and parity simultaneously is listed in brackets underneath and to the right. As is well known, magnetic dipole radiation is considerably less efficient, in fact by several orders of magnitude, than electric dipole radiation. It is this "radiation frustration factor" implied by a higher multipole than electric dipole [E1] that may provide a clue to a route for the deexcitation energy of the compound  $^{40}\text{Ca}$  nucleus in reaction (3) or the  $^{42}\text{Ca}$  nucleus in reaction (4), constituting an alternative to that of deexcitation via gamma ray or neutron emission. Schwinger<sup>25</sup> points to a similar sort of thing to the author's "radiation frustration factor" in connection with his nuclear energy from an atomic lattice (NEAL) model. The deexcitation route must now be considered.

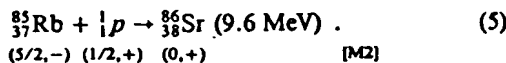
A most serious problem for cold fusion is that of somehow getting the excess energy, in the case of reaction (3) ~8.3 MeV, into the lattice. Thus, if the  $^{40}\text{Ca}$  nucleus were to deexcite to its ground state by the emission of a gamma ray, Mills and Kneizys should have detected the strong resultant radiation field. In fact, without adequate shielding, it would provide a lethal environment, as noted in reference to the oft-stated "dead graduate student problem" associated with cold fusion. Note, also, that there is no boson plasma hypothetically to absorb this radiation since, unlike the case of cold fusion with heavy water, the light water cold fusion case involves a fermion plasma of protons as opposed to a boson plasma of deuterons. (To be sure, some may still argue that the periodicity of the wave function based on crystalline periodicity might yet save the situation for this fermion plasma.) If, on the other hand, the  $^{40}\text{Ca}$  nucleus retains most of the energy in the form of kinetic energy, Coulomb excitation of nickel ions in the lattice should also produce formidable radiation in the form of strong X-ray fields that should be detectable.

A possible solution to this is detailed in Sec. VI. A brief preview must suffice here. The Mössbauer effect is a well-known nuclear effect involving an interaction with the atomic lattice. Thus, for lattice temperatures  $T$  much lower than a

characteristic lattice temperature, the so-called Debye temperature  $\theta_D$ , the energy resulting from a nuclear deexcitation, goes totally into a particle, a gamma-ray photon, serving to conserve energy, while the entire lattice recoils to conserve linear momentum. We take the opposite of the Mössbauer effect to involve the regime of temperatures  $T \geq \theta_D$ : No longer is the lattice infinitely "stiff," and thus, the energy of an emitted gamma ray has the likelihood of being reduced by virtue of phonon formation in the lattice. It is hypothesized that cold fusion involves this opposite process to the Mössbauer effect. In this scheme, a nuclear reaction most likely proceeds by the formation of a compound nucleus between a particle traveling through the metal lattice and a substitutional, or interstitial, particle within the atomic lattice. At a high enough lattice temperature, most, or essentially all, of the deexcitation energy is hypothesized to go directly into the lattice (phonon formation), leaving the particles resulting from the breakup of the compound nucleus with too little energy to produce a readily detectable radiation field outside the electrolytic cell. In the opposite regime of low enough temperatures ( $T \ll \theta_D$ ), it is not clear whether experimenters would encounter cold fusion with associated strong, and therefore dangerous, radiation fields, although the example of titanium deuterioxide tends not to support this. (Another possibility for the deexcitation is the internal conversion hypothesis of Walling and Simons.<sup>26</sup>) It is also shown that the uncertainty principle coupled with special relativity permits the energy to reach the lattice in contravention of the notion of "asymptotic freedom," according to which the time and distance scales involved in the hypothetical nuclear reaction are so small that the nucleus is unaware of the embedding atomic lattice.

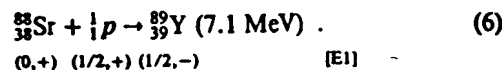
With reaction (3), as in cold fusion, it seems that we have a metal lattice-mediated nuclear reaction. The reaction is a pickup reaction in which the less stable  $^{39}\text{K}$  nucleus becomes an ultrastable  $^{40}\text{Ca}$  nucleus by latching onto a proton. To be sure, it is not clear at what range of depth in the metal lattice the reaction is occurring. An educated guess based on what we know of most cold fusion reactions is that the reaction is probably a near-surface effect, ranging from essentially the surface to a depth of perhaps a few microns into the nickel lattice.

Mills and Kneizys postulate that rubidium carbonate ( $\text{Rb}_2\text{CO}_3$ ) should also be an ideal candidate for their novel chemistry reaction and promise to present work in the near future in this area. They surmise that the replacement of potassium carbonate by  $\text{Rb}_2\text{CO}_3$  in the light water-based electrolyte might also lead to this novel chemical reaction yielding an excess heat effect. Again one can show that as in the case of  $^{39}\text{K}$ , this would make sense from the standpoint of the nuclear physics leading to a stable product nucleus. Arguably then, this is a cold fusion reaction. About 75% of naturally occurring rubidium is in the form of  $^{85}\text{Rb}$  so that the cold fusion reaction takes the form



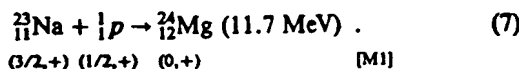
Note, as in the case of  $^{39}\text{K}$  that the nuclear reaction has produced a more stable nuclide,  $^{86}\text{Sr}$ , which, from the ultrastable list [Eq. (2)] is seen to have reached a more stable number of protons, 38, and has maintained its even number of neutrons in this proton pickup reaction. An increase in  $^{86}\text{Sr}$  would be the clue that this reaction is proceeding. (Strontium-86 is only ~10% abundant.) A partial test of this might be to substitute strontium for the rubidium in the electrolyte. Note that ~83% of naturally occurring strontium is in the

form of  $^{88}\text{Sr}$ , which has 38 protons and a magic number 50 of neutrons. However, this reaction, represented schematically by Eq. (6), is energetically possible as seen from the positive  $Q$  value. It would lead to the nuclide  $^{89}\text{Y}$  for which the neutron configuration is unchanged, but having a less stable number, 39, of protons than in the case of  $^{88}\text{Sr}$  with 38 protons. So, based on this logic, the substitution of strontium for rubidium should reduce the excess heat effect, or make it go away:



Note, in contrast to reaction (6), the large radiation frustration factor implied in reaction (5), where [M2] indicates that magnetic quadrupole radiation would be the lowest order of radiation involved were radiation actually to occur in connection with the deexcitation of the compound nucleus. A small radiation frustration factor is implied in reaction (6) for which the radiation would be electric dipole [E1] and therefore extremely efficient.

Mills and Kneizys indicated that they were unable to see an excess heat effect when the potassium carbonate was replaced with sodium carbonate in the light water reaction. Thus, at Bush's suggestion, Bush and Eagleton ran a sodium carbonate cell, expecting to see no excess heat. To our surprise, it gave about twice the excess power as a comparable potassium carbonate cell. To see that this positive result is consistent with the present line of reasoning and inconsistent with the null result of Mills and Kneizys, consider the alternative nuclear reaction to Eq. (3) represented schematically by



Sodium-23 is 100% abundant. The key here is that even though the proton number, 12, of the product,  $^{24}\text{Mg}$ , is not an ultrastable number, the pairing effect is at work since the number of protons has been made even. Moreover, there is a mass defect in the  $^{24}\text{Mg}$  resulting in a released energy of 11.7 MeV, which is greater than the energy release of 8.3 MeV in reaction (3). [In fact, the energy release per nucleon of the product in reaction (7) is more than double the energy release per nucleon of the product in reaction (3).]

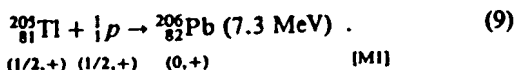
A possible light water cold fusion reaction not indicated by Mills and Kneizys is the following, obtained when the potassium carbonate is replaced by cesium carbonate:



This would have to be considered a borderline possibility. On the one hand, the new number of protons is an even number, but 56 is not on the ultrastable list. However, there is a mass defect in the product relative to the reactants of 8 MeV. In addition, the radiation frustration factor is extremely large, as implied by magnetic octupole radiation [M3] being indicated as the lowest order. In fact, this is the highest multipolarity of any of the possible lowest order radiations found for reactions considered in this paper. So, it would be worth exploring this possibility as a potential light water cold fusion reaction leading to excess heat.

Finally, we arrive at a hypothetical reaction, Eq. (9), which differs from the preceding reactions in that one of the reactant nuclides,  $^{205}\text{Tl}$ , is associated with neither an alkali nor an alkali-type atom. Thus, instead of having a single

s-state electron beyond a closed shell, thallium has three electrons outside a closed shell, but the highest energy electron of these is an unpaired electron in a p-subshell:

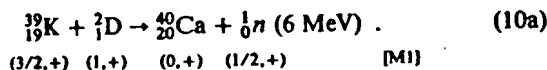


The addition of the proton results in a nuclide,  $^{206}\text{Pb}$ , with a magic number 82 of protons. The neutron number of 124, while not magic is, nevertheless, on the ultrastable list. This should make  $^{205}\text{Tl}$  (70.5% abundant) a likely candidate for a light water reaction. Thallium-203 (29.5% abundant) would also have a good possibility for a light water reaction, although the product,  $^{204}\text{Pb}$ , has a neutron number 122 that is not on the ultrastable list. Great care should be exercised when working with thallium since it is extremely toxic.

#### IV. CANDIDATES FOR ALKALI-DEUTERIUM FUSION AND ALKALI-TRITIUM FUSION

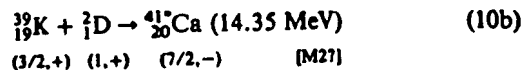
Since the hypothetical nuclear reactions (3) through (8) all involve the fusing of an alkali atom nuclide with a proton, it seems appropriate to coin the term "alkali-hydrogen fusion" for this class of nuclear reactions. This general reaction pattern also applies to the additional reactions considered now, although there are exceptions, such as reaction (9), that are specified in various sections. In this new form of fusion, an alkali atom nuclide, or, in some instances, an alkali-type atom nuclide, fuses with either a proton, deuteron, or triton to form a compound nucleus. The latter then deexcites by losing energy to the atomic lattice, to achieve a more stable nuclear shell-model configuration than was the case for the reactant nuclides. This greater stability is achieved by attaining an even number of protons and/or neutrons (in the case of fusion with a deuteron or triton), the pairing effect, or a magic number of protons and/or neutrons or one of the other numbers for either protons (neutrons) on the ultrastable list. We now consider hypothetical reactions for the subclasses alkali-deuterium fusion and alkali-tritium fusion.

Returning to the potassium reaction in Eq. (3), one might guess that the substitution of heavy water for light water in the electrolyte might lead to  $^{40}\text{Ca}$  plus neutrons as shown schematically by the following proton-stripping reaction:

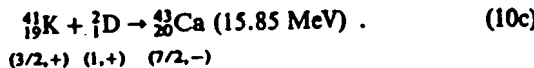


A possibility here is that a reaction between the compound nucleus and the lattice will result in the 6 MeV being given to the lattice (phonon formation) rather than going into the neutron. Thus, one would want to search for slow neutrons suggested by reaction (10a). Bush<sup>27</sup> and Bush and Eagleton<sup>28</sup> recently reported seeing such slow neutrons in conjunction with a search for excess heat with a cathode consisting of a 5-μm-thick film of palladium electroplated on a silver substrate but emphasize that the experiment must be repeated. Marshall<sup>29</sup> has also told the author that he believes that slow neutrons may be generated in some of the cold fusion reactions. This aspect is treated again in Sec. VI, where it is hypothesized that cold fusion involves a nucleus-lattice effect essentially opposite to the well-known Mössbauer effect. For additional reactions in this paper where the energy is listed next to a light particle, it is to be assumed that there is also the possibility that much of the energy was given essentially directly to the lattice in the deexcitation process.

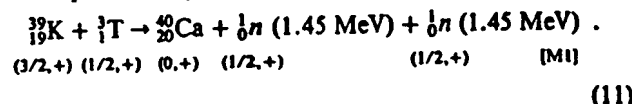
Mills and Kneizys also reported achieving excess heat using an electrolyte with potassium carbonate in heavy water. In addition, Noninski and Noninski<sup>30</sup> also obtained excess heat with a heavy water-based electrolyte with  $\text{K}^+$  ions and a nickel electrode. A problem, then, for reaction (10a) is that it would have produced a large number of neutrons accompanying the excess heat, and this was clearly not observed. Thus, two more likely reactions to account for the excess heat found are provided as follows:



and

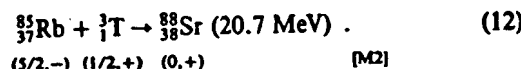


A possible superheavy water reaction for potassium based on the proton-stripping prototype might be the following:

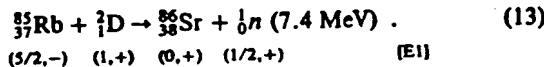


This would be the superheavy water analog of reaction (3).

Another reaction based on this logic that might produce excess heat would be the superheavy water reaction involving a tritium-based  $\text{Rb}_2\text{CO}_3$  electrolyte with the nuclear reaction schematically represented by Eq. (12), since this leads to a nuclide,  $^{88}\text{Sr}$ , which has a magic number 50 of neutrons and a very stable number 38 of protons:

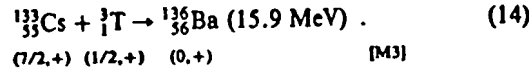


Still a third possibility would be to employ a heavy water-based electrolyte to yield a  $^{86}\text{Sr}$  nucleus and a neutron as follows:

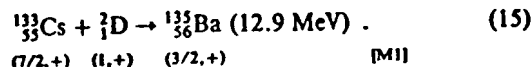


We note that the radiation frustration factor implied by [E1] is very low for reaction (13), which suggests that it may not be highly favored.

Possible alkali-hydrogen reactions for cesium with tritium and deuterium, respectively, appear to be as follows:



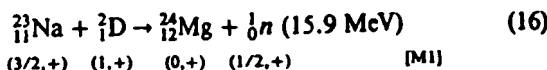
For  $^{136}\text{Ba}$ , the number of neutrons has become 80, which is not magic but is on the ultrastable list, while the number of protons, though not on the ultrastable list, has been made even at 56, which takes advantage of the pairing effect. In addition, [M3] implies one of the larger radiation frustration factors.



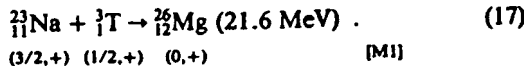
However, this reaction seems less likely than reaction (14) since neither of the nucleon numbers in  $^{135}\text{Ba}$  are on the ultrastable list, and the proton pairing effect in going from 55 protons to 56 must be somewhat compensated by an unpairing of neutrons in going from 78 to 79 neutrons.

\*Half-life =  $7.7 \times 10^4$  yr.

Similarly, hypothetical alkali-deuterium and alkali-tritium reactions for sodium are, respectively,



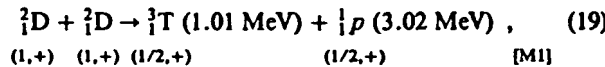
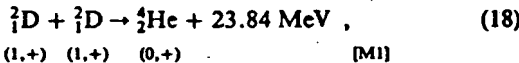
and



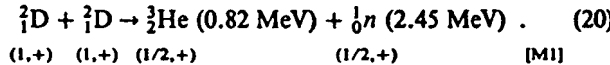
One notes that the term "cold fusion" has become an emotionally charged one for many, especially those whose work involves high-temperature fusion reactions. It must be admitted that there is a possible semantic difficulty here that may be impeding an objective hearing for new and startling nuclear phenomena associated with hydrided metals. Thus, to the extent that "cold fusion" suggests that these new phenomena involve the familiar high-temperature reactions simply duplicated at a relatively low temperature, the term is extremely misleading. For one thing, as many have noted, this could hardly be, since cold fusion laboratories do not show the lethal radiation fields that a simple low-temperature duplication of the familiar high-temperature nuclear reactions would entail. The nuclear reactions presented in this study so far, with one of the reactants in each reaction most likely an integral part of an atomic lattice at a relatively low temperature, serve to underscore this crucial difference: Alkali-hydrogen fusion is a new nuclear process, and it contains, as is shown in Sec. V, the hypothetical cold fusion reactions that have received the most attention from researchers. Perhaps the adoption of the term "alkali-hydrogen fusion," suggesting a genuinely new nuclear process, might help to reduce the unfortunate hostility generated by the term "cold fusion."

#### V. ALKALI-HYDROGEN FUSION FOR HYDROGEN AND LITHIUM

A characteristic of all of the reactions considered in this paper, with the exception of those in Sec. VI, is that one of the reactants is an alkali atom and the other is the alkali-type hydrogen atom in one of its three varieties. In these cases, the relatively easy removal of the sole electron outside the inner core of closed shells by the metal lattice guarantees a much smaller entity, a singly ionized atom. This should permit it to travel through the metal lattice (e.g., nickel, palladium, etc.) much more readily than the larger neutral atom. The deuterium-deuterium (D-D) reaction schematized in Eqs. (18), (19), and (20) could, of course, be a key example of alkali-hydrogen fusion, with Eq. (18) a strong candidate for a prime source of excess heat:



and

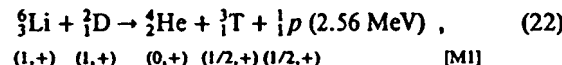
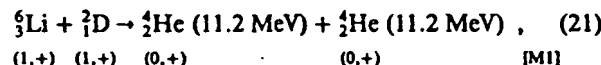


Reasoning along the lines of the prototypical reaction in Eq. (3), reaction (18) should be favored over reactions (19) and (20) based on the stability argument, in that the  ${}^4\text{He}$  nucleus is doubly magic with two neutrons and two protons. Reactions (19) and (20) are favored to a lesser extent, leading as they do to the singly magic nuclides  ${}^3\text{T}$  and  ${}^3\text{He}$  with two neutrons and two protons, respectively.

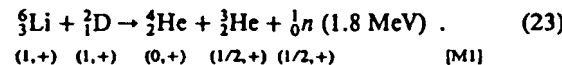
It must be emphasized again that reactions (18), (19), and (20) are hypothesized to involve the lattice, also. Thus, they differ from the familiar D-D reactions in a thermonuclear plasma. It is nevertheless useful to assume a rough correspondence between them for purposes of comparison. For the reactions in the thermonuclear plasma, reactions (19) and (20) have essentially the same branching ratio, which is orders of magnitude larger than the branching ratio for reaction (18).

So, what produces an apparent reversal of this situation in the lattice in which reaction (18) is now favored over reaction (19) or (20)? One answer might be as follows: In the lattice, the longer de Broglie wavelength and lower velocities imply a much greater overlap and overlap time for two interacting deuterons so that the stability argument for reactions may make sense. For the thermonuclear plasma, on the other hand, the de Broglie wavelength is much shorter and the velocities much greater so that the overlap and the overlap time of two deuterons is considerably reduced. This poorer overlap favors the stripping reactions corresponding to Eqs. (19) and (20). In addition, in the thermonuclear plasma, the large relative velocity of the deuterons militates against polarization of the positive charge distributions of the two deuterons so that the branching ratios of reactions (19) and (20) are approximately equal. For the lattice reaction, however, the relative approach velocity is so much lower that the resultant positive charge distribution polarization may highly favor neutron exchange over proton exchange. Thus, the branching ratio should be highly in favor of reaction (19) over reaction (20), implying the much larger tritium yield over neutron yield that researchers see. Employing this hypothesis, the author<sup>31</sup> derived a theoretical lower limit for the branching ratio between reactions (20) and (19) in terms of two independently determined parameters, the electromagnetic charge radius of the proton and that for the deuteron. The result,  $\sim 2 \times 10^{-9}$ , is essentially equal to the lowest experimental value that has been obtained. Storms<sup>32</sup> indicates that he believes the author's calculation to be correct and points out that empirical deviations from the author's value can probably be explained on the basis of there being at least one other neutron-yielding reaction and experimental difficulties in establishing the branching ratio.

As is well known, Fleischmann and Pons, and other researchers in cold fusion following their lead, employ the alkali atom lithium in the electrolyte, typically in the form of a 0.1 M solution of LiOD. Employing reaction (3) as our prototypical reaction, we can explore the best candidates for the lithium reactions. Thus, the alkali-hydrogen fusion reaction counterparts for  ${}^6\text{Li}$  to the deuterium reactions (18), (19), and (20) are shown in Eqs. (21), (22), and (23), respectively, with reaction (21) as the best candidate for an excess heat reaction of the three:



and



Thus, in line with the prototypical reaction (3), one sees in reaction (21) the production of two ultrastable doubly magic nuclides (two  ${}^4\text{He}$  nuclei) in which both the proton and neutron numbers have become magic at 2. In addition, reaction

(21) might be the "stripping reaction" counterpart of the pickup reaction (3). Thus, in reaction (21), the  $^6\text{Li}$  might be thought of as roughly an association of an ultrastable  $^4\text{He}$  nucleus and a much less stable deuteron. In this picture, the deuteron might be thought of as stripping the deuteron away from the  $^4\text{He}$  within the  $^6\text{Li}$  nucleus to produce two  $^4\text{He}$  nuclei. Moreover, reaction (21), like reaction (18), produces  $^4\text{He}$  in agreement with the recent findings of Bush, et al.<sup>10</sup> that show a strong positive (negative) correlation, albeit not totally quantitative, between the presence (absence) of  $^4\text{He}$  in the effluent gases and the occurrence (nonoccurrence) of excess heat in connection with the cathode operation in the case of palladium cathodes.

If lithium is key to the heat reaction, for example, via reaction (21), then the extent to which the heat reaction is near surface or bulk, might depend on the degree of "lithiation" of the palladium cathode that exists prior to charging the cathode. In this connection, one recalls the apparent ease with which Huggins et al.<sup>12</sup> were able to achieve the excess heat reaction and the fact that Huggins was convinced that his cathode material had been prelithiated. On the other hand, Appleby et al.<sup>13</sup> witnessed a near-surface excess heat reaction and established that the depth of lithium penetration prior to the onset of observable excess power was  $\sim 5 \mu\text{m}$  or so. In Appleby's case, this was about the depth of  $^6\text{Li}$  penetration prior to the onset of an observable excess heat effect. Because of the more rapid diffusion of deuterons, as compared with lithions, it seems that prelithiation could lead to more of a bulk reaction should it turn out that reaction (21) is a key heat-producing reaction. On the other hand, the lack of bulk lithiation should lead to a near-surface effect, which may be more desirable in some cases. For example, because of the cost of palladium, it may be that a near-surface effect "reactor" would be more desirable than a bulk effect reactor.

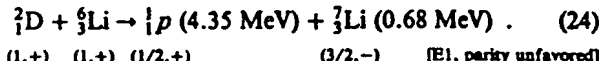
Until recently, it might have been argued that the time delay between the beginning of electrolysis and the first observance of excess heat might have been geared to the diffusion time for lithium. Certainly, the time lag is greater than could be accounted for on the basis of the diffusion time for deuterons, although advocates of "superloading" might argue that this long time lag of days or weeks might be necessary to acquire a high ratio of deuterons to palladium atoms (stoichiometry  $\geq 1$ ). The author, however, on the basis of his transmission resonance model<sup>31</sup> (TRM), has argued that this time lag may actually be associated with a surface conditioning reaction in which the deposition of platinum black (in the case of a platinum anode) creates a condition according to which there is a low enough "hydrogen overvoltage" (i.e., hydrogen activation potential) and yet a high enough current density to observe the excess heat effect. [In the TRM (Ref. 31), the hydrogen overvoltage for an electrolytic cell with a palladium cathode should be less than  $\sim 340 \text{ mV}$  to see an excess heat reaction. On the other hand, it is known empirically that the excess heat effect disappears for current densities less than  $\sim 60$  to  $100 \text{ mA/cm}^2$ .]

Strong support for this portion of the TRM has now come from Szpak et al.,<sup>33</sup> who reported on the use of palladium chloride to enable one to obtain the Fleischmann-Pons excess heat reaction within hours after the initiation of electrolysis. Palladium chloride functions to put down a layer of palladium black on the palladium cathode, which would function in much the same way as platinum black by increasing the active surface area. This was quickly corroborated by Bush and Miles.<sup>34</sup>

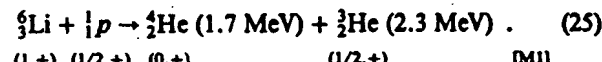
The author previously asked Storms about conducting

such an experiment at Cal Poly to test a portion of the TRM, and Storms<sup>35</sup> suggested using palladium chloride to produce a layer of palladium black. So, it appears that the diffusion time argument in favor of reaction (21) being the key heat reaction has now been vitiated.

Another possible branch of the D- $^6\text{Li}$  reaction in addition to reactions (21), (22), and (23) is the following:

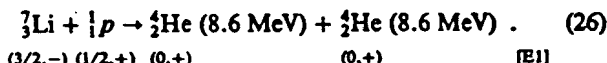


Is a light water cold fusion reaction or a reaction involving  $^7\text{Li}$  suggested by the prototype? One possibility is the light water- $^6\text{Li}$  reaction in Eq. (25) producing the doubly magic  $^4\text{He}$  and the singly magic (two protons)  $^3\text{He}$ :



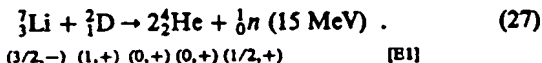
It is this reaction that may be responsible for the fact that in some cases the excess heat reaction dies out gradually over time as heavy water is replaced by light water in the electrolyte.

A possible  $^7\text{Li}$  reaction with light water, the  $^7\text{Li}$  counterpart to reaction (21), is given by Eq. (26), which leads to two doubly magic nuclei:

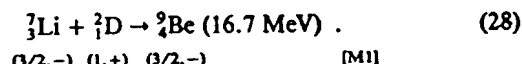


This reaction may also contribute to the effect mentioned in connection with reaction (25), in which the excess heat effect dies away slowly when light water is substituted for heavy water in the electrolyte. Note that the radiation frustration factor might favor the light water reaction (25) for  $^6\text{Li}$  over this light water reaction for  $^7\text{Li}$ . At any rate, experiments with light water should be conducted to test both reactions (25) and (26). If excess heat is found in connection with reaction (25), an attempt should be made to correlate the  $^4\text{He}$  and  $^3\text{He}$  produced with the amount of excess heat. In the case of reaction (26), one would be attempting a correlation of excess heat and  $^4\text{He}$  production. Clearly, however, these correlation attempts are probably considerably more difficult than in the light water reactions hypothesized to produce calcium or strontium.

The  $^7\text{Li}$  counterpart to reaction (23) is



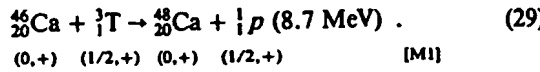
Reaction (27) might account for Matsumoto's claim<sup>36</sup> of observing neutron emission but no excess heat effect with light water and  $^6\text{LiOH}$ . Thus, a small contamination of the electrolyte with  $^7\text{LiOH}$  and  $\text{D}_2\text{O}$  might allow reaction (27) to account for this claim, based on the fact that neutron detection is so much more sensitive than that of heat. A second branch of the D- $^7\text{Li}$  reaction might be the following:



## VI. NEUTRON EXCHANGE REACTIONS: TRINT AND OPPL

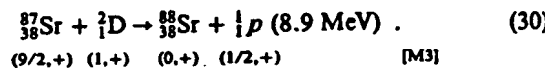
If there are reactions in a hydrided metal such as nickel or palladium in which a proton is added to a nucleus to produce a more stable nucleus, it makes sense that there should be corresponding reactions involving neutron addition. Reactions (12), (14), (15), (17), (18), (21), and (24) are cases for

which both neutrons and protons are added. Reactions in which neutrons alone are added to achieve greater stability may include the following, in which one of the reactants is neither an alkali atom nuclide nor an alkali-type atom nuclide:



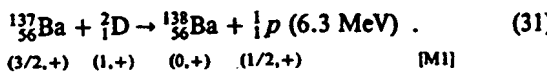
This reaction in which two neutrons are transferred from the triton to the heavier nuclide is hypothesized since the  $^{48}\text{Ca}$  nucleus is doubly magic with 28 neutrons and 20 protons.

Reaction (30), a neutron-stripping reaction, results in a nuclide,  $^{88}\text{Sr}$ , having a magic number 50 of neutrons:

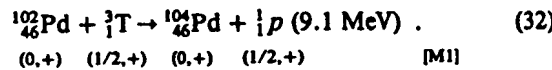


Note, also, that this reaction has a large radiation frustration factor as implied by [M3].

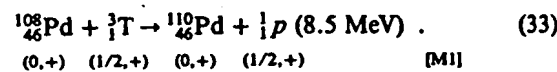
The neutron-stripping reaction in reaction (31) is suggested since  $^{138}\text{Ba}$  has achieved a magic number 82 of neutrons as indicated by the ultrastable list:



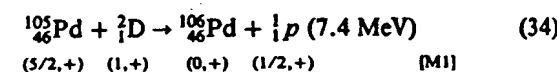
Neutron transfer reactions involving the metal nuclides of palladium and nickel might be as follows:



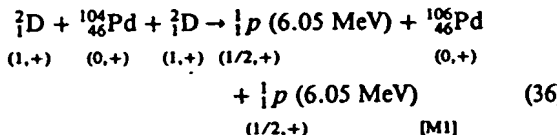
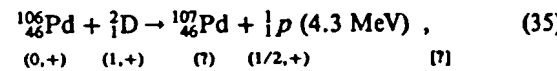
In reaction (32), the addition of two neutrons leads to  $^{104}\text{Pd}$  with a number of neutrons 58 on the ultrastable list. In the next reaction, the addition of two neutrons leads to  $^{110}\text{Pd}$  with a number of neutrons 64 on the ultrastable list:



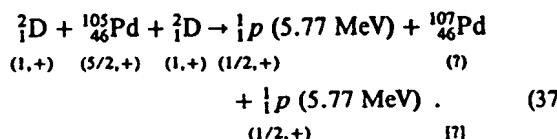
The author<sup>31</sup> has hypothesized the two single-neutron transfer reactions (34) and (35) and the two three-body reactions (36) and (37), which result in double-neutron transfers:



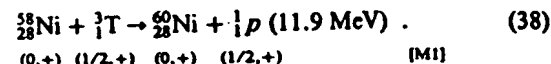
and



and



Finally, in reaction (33) we have a two-neutron transfer reaction to produce  $^{60}\text{Ni}$  with a number of neutrons 32 on the ultrastable list. The number of protons 28 for nickel is, of course, magic:



Now, the general pattern of all of the reactions studied so far is that of the transfer of one to three nucleons from a light nucleus (e.g.,  $^2\text{D}$  or  $^3\text{T}$ ) to a heavier one. If the TRM (Ref. 31) is correct with its suggestion of the transmission resonance-induced neutron transfer (trint) reaction, then it might be consonant with this pattern to generalize this to a transmission resonance-induced nucleon transfer (TRINT) reaction.

Another possibility is that the general pattern of nucleon transfer in a lattice may be modeled analogously to the well-known Oppenheimer-Phillips process. In this connection, we note that Ragheb and Miley,<sup>37</sup> Paolo,<sup>38</sup> Bush,<sup>31,39</sup> and Bush and Eagleton<sup>40</sup> have all suggested the Oppenheimer-Phillips-type reaction as a strong possibility for cold fusion. If this description for the general pattern turns out to be correct, perhaps the designation OPPL (Oppenheimer-Phillips process in a lattice) would be appropriate for these reactions.

## VII. A HYPOTHESIS: COLD FUSION INVOLVES AN EFFECT ESSENTIALLY OPPOSITE TO THE MÖSSBAUER EFFECT

A serious difficulty in the acceptance of cold fusion has been the problem of how to dispose of the excitation energy of the compound nucleus to account for the fact that cold fusion laboratories are not flooded with lethal gamma rays or neutrons. The explanation that this does not occur because the energy has simply been carried away as the energy of the charged-particle products is, of course, a possibility, but appears to lack credibility. Thus, the effects of bremsstrahlung and Coulomb excitation of the metal nuclei of the lattice that this should entail would still result in readily detectable radiation fields outside the electrolytic cell.

Previously it has been suggested by Walling and Simons<sup>26</sup> that this deexcitation energy is given directly to the electrons via internal conversion. With the electron-rich environments involved, this possibility cannot be dismissed. Nevertheless, it seems that detectable levels of X rays should arise from this.

The author's hypothesis is that cold fusion (alkali-hydrogen fusion) involves a nucleus-lattice effect that is essentially the opposite of the well-known Mössbauer effect. In the latter effect, for a lattice temperature  $T$  that is significantly lower than a characteristic temperature, the so-called Debye temperature  $\theta_D$ , there is a significant probability of the "recoilless emission" of an excited nucleus embedded in the lattice, that is, emission in which all of the deexcitation energy goes into the emitted gamma-ray photon because the entire crystalline lattice, rather than the nucleus, recoils to conserve the linear momentum. Because of the large mass of the crystal relative to the nuclear mass, the lattice requires essentially zero kinetic energy for this recoil. The probability  $f$  for such recoilless emission is given by Segré<sup>41</sup> as

$$f = \exp \left\{ -\frac{3}{2} \frac{(\hbar^2 \omega^2 / 2mc^2)}{k\theta_D} \left[ 1 + 4 \left( \frac{T}{\theta_D} \right)^2 \int_0^{\theta_D/T} \frac{x dx}{e^x - 1} \right] \right\} \quad (39)$$

$$= \exp \left\{ -\frac{3}{2} \frac{(\hbar^2 \omega^2 / 2mc^2)}{k\theta_D} \left[ 1 + \frac{2}{3} \left( \frac{\pi T}{\theta_D} \right)^2 \right] \right\} \quad (T \ll \theta_D) \quad (40)$$

Thus, for a temperature low enough compared with the Debye temperature, the crystal acts as though it is stiff, whereas for increasingly higher temperature, the probability of phonon formation in the crystal (1-f), with subsequent loss of deexcitation energy to the gamma ray increases, as seen from Eq. (39). So, in the extreme opposite effect to the Mössbauer effect, most of the energy of deexcitation would actually go to the crystalline lattice leaving relatively little energy in the gamma-ray or neutron component. This primary heat reaction would lead to  ${}^4\text{He}$  (assuming that this is the nuclear "ash") and probably also some neutrons, born as slow particles. This suggests looking also for thermal neutrons in conjunction with a search for excess heat. In support of this hypothesis is the fact that the Debye temperature of palladium is 274 K, and most of the best excess heat results in cold fusion research have been obtained with palladium with room temperature ( $\sim 300$  K) and higher. However, experiments with titanium, which has a Debye temperature of  $\sim 420$  K, have been relatively unsuccessful in achieving an excess heat effect. An exception, which seems to support this thesis, is that Liebert and Liaw<sup>18</sup> have recently achieved a large excess heat effect in titanium by employing the electrolysis of molten salts at  $\sim 400^\circ\text{C}$  (673 K). Also, Schoessow<sup>42</sup> claims to have demonstrated the excess heat effect at around room temperature for both zirconium (Debye temperature of 291 K) and uranium (Debye temperature of 207 K). A bit of a mystery here would be the Mills-Kneizys use of nickel as a lattice (Debye temperature of 450 K) since they ran at temperatures of only up to  $\sim 350$  K. (Referee 1 suggested that the answer here may lie in the alteration of the Debye temperature by the presence of the hydrogen.)

Preparata<sup>43</sup> previously stressed the possible significance of the Mössbauer effect for the interpretation of cold fusion, emphasizing that it could hold the key to dispelling the so-called problem of asymptotic freedom. According to the latter, the time and distance scales are too small for a deexciting nucleus to even be aware of its embedding lattice. Preparata insisted that the Mössbauer effect requires the phenomenon of "superradiance" for its explanation. In opposition to this, the solid-state physicist S. Chubb<sup>44</sup> has insisted that the Mössbauer effect is associated with the well-known "umklapp process" from solid state and therefore hardly requires a superradiant explanation. Schwinger<sup>25</sup> in his NEAL model attempts to get the deexcitation energy directly into the lattice as phonons. Recently, Jones<sup>45</sup> argued that the uncertainty principle and special relativity combine to prevent the chance of excitation energy from the compound nucleus reaching the atomic lattice on a time scale that would provide an energy loss mechanism to compete with deexcitation via gamma decay or neutron emission. Jones' argument in favor of asymptotic freedom is as follows.

Consider the hypothetical transfer of  $\sim 1$  MeV from a compound nucleus to the lattice. The following form of the uncertainty principle is applicable to this situation, where  $\Delta E$  is taken to be 1 MeV:

$$\Delta E \Delta t \gtrsim h . \quad (41a)$$

So,  $\Delta t = 0.65 \times 10^{-21}$  s. During this time, the maximum range of transfer of the 1 MeV would be given by

$$r = c \Delta t . \quad (41b)$$

Substitution of the value for  $\Delta t$  thus yields

$$r \approx 0.002 \text{ \AA} . \quad (41c)$$

which appears to guarantee asymptotic freedom, i.e., independence of the nuclear and atomic regimes, and end the argument. However, as Puthoff<sup>46</sup> indicates, there is no reason why the transfer could not be in the form of a large number of energy packets, each of which is small compared to 1 MeV. Phonons, after all, would be expected to have much smaller energies. For example, taking phonons of the size of 0.1 eV following Schwinger,<sup>25</sup> the combination of Eqs. (41) and (42) now gives

$$r = 20000 \text{ \AA} . \quad (41d)$$

Thus, the problem of asymptotic freedom is not necessarily a problem for cold fusion.

Finally, the pedagogical point is often made that "zero" energy is required in connection with the crystal recoil to conserve linear momentum in the Mössbauer effect. In point of fact, the energy is not identically zero. Rather, the energy is very small compared with the transition energy, but it is finite and not zero. So, even with the Mössbauer effect, it can hardly be argued that we are observing asymptotic freedom.

### VIII. IMPLICATIONS OF ALKALI-HYDROGEN FUSION FOR THEORETICAL MODELS FOR COLD FUSION

The wider vista for cold fusion suggested by the existence of light water excess heat reactions should prove useful for efforts to construct theoretical models. The pattern suggested by alkali-hydrogen fusion and nucleon transfer in a lattice does not appear to eliminate any of the well-known models for cold fusion such as the TRM (Ref. 31), the Chubbs' lattice-induced nuclear chemistry (LINC) model,<sup>47</sup> Hagelstein's coherent neutron transfer model,<sup>48</sup> Mayer's hidron model,<sup>49</sup> Preparata's superradiance model,<sup>43</sup> or Schwinger's NEAL model.<sup>25</sup> (This list is intended to be representative rather than exhaustive, and I apologize in advance for any models not included.)

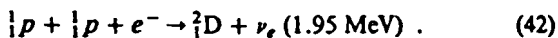
One should not forget that the presence of heavier nuclides in some of these hypothetical reactions helps to enrich an already rich electronic environment provided by the metal ions of the lattice. Electrons can pass right through any nucleus, as is well known from the case of *s*-electrons possessing zero angular momentum, which are forced to pass through the nucleus. They can, therefore, get as close as required to any nucleon or part of the nucleus. Thus, an *s*-electron can spend a certain fraction of its time inside a proton or a deuteron. During this time, the entity of proton plus electron, or deuteron plus electron, would be charge neutral and see no Coulomb barrier. Now, for the case of neutron transfer, there is no Coulomb barrier. Proton transfer is quite another story, with a reaction such as Eq. (3) having no chance of a finite measurable cross section in an ordinary thermonuclear plasma because of an insuperable Coulomb barrier based on two-body forces. Perhaps in the lattice, however, protons are able to get near enough to the centers of these nuclides to undergo a nuclear reaction by virtue of such *s*-electrons providing screening. This, of course, would have the flavor of Mayer's model, but would not require the formation of "hidrons."<sup>49</sup> (Preparata<sup>43</sup> previously stressed the importance of the electron plasma with regard to screening.)

It was suggested in Sec. V that the TRINT reaction or OPPL seem to have the right feel to them to account for alkali-hydrogen fusion. At low energies in a lattice, the de Broglie wavelengths of particles would appear to be important. Thus, in both neutron and proton exchange, it is important that the de Broglie wavelengths of these particles,

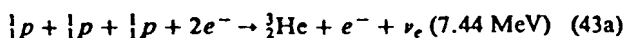
or those of the deuterons and tritons, overlap with the nuclei with which they are going to react. (McNally<sup>50</sup> employed the concept of a de Broglie wavelength interaction of very low energy nuclei.) This appears then to give a positive nod to those models for cold fusion that depend on the de Broglie wavelength either explicitly or implicitly, such as the TRM (Ref. 31), Bass' quantum resonance triggering (QRT) model,<sup>51</sup> or the Chubb's LINC model.<sup>47</sup> (Bass' QRT model<sup>51</sup> combines the TRM with Schwinger's NEAL model,<sup>25</sup> using the former to provide the "trigger" for Schwinger's  ${}^4\text{He}$ -producing oscillations.)

If reaction (3) is a valid cold fusion reaction (or alkali-hydrogen reaction), it appears to affect the aspect of the boson nature of the nuclear reactants in cold fusion. For should there be one cold fusion reaction employing a fermion, e.g., a proton or triton, as a reactant, it calls into question whether the basic nature of bosons is necessary for the excess heat reaction. The changes that this might entail for model builders may not be major. For example, Bush<sup>31</sup> cites boson properties as one of the features of his TRM, but never explicitly employs this feature. The Chubbs in their LINC model<sup>47</sup> appear to make more explicit use of boson properties, even coining the phrase "Bose-Bloch condensate" to describe the fluid of deuterons within a hydrided metal crystal. Of course, even they emphasize the periodic lattice, or "Bloch," aspect, in referring to Lattice-Induced Nuclear Chemistry. (Certainly, bosons would remain important in the scheme of things if only because of the potential significance to cold fusion of phonon formation in the lattice indicated in Sec. VII.) While we cannot, at this early juncture, rule out the possibility of several different nuclear processes being involved, it appears that the broader perspective provided here suggests that cold fusion is not the result of a boson condensation (Bose-Einstein condensation). And, if the boson nature of the deuteron turns out not to be crucial, as suggested by an application of Occam's razor in view of the probable existence of a light water cold fusion reaction, then this study serves to magnify even more the importance of the periodic lattice (Bloch aspect) for models attempting to describe the new reactions.

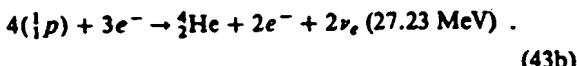
Finally, the author is well aware that the hypothesis of the combination of a heavy nucleus with a proton at the surface of the metal cathode seems unlikely in the extreme from the standpoint of conventional nuclear physics because of the factor  $\exp(-Z_1 Z_2 e^2/\hbar v)$  associated with the Coulomb barrier, where  $Z_1$  and  $Z_2$  are the atomic numbers of the colliding nuclei. Certainly, if a fusion of a rubidium nucleus ( $Z = 37$ ) with a proton ( $Z = 1$ ) could be demonstrated, it would make the problem of fusing two deuterons in the lattice seem almost trivial by comparison. Thus, an alternative hypothesis for the light water reaction would be the fusion of two protons and an  $s$ -electron to produce a deuteron and an electron neutrino:



Thus, an enrichment of the electrolyte with heavy water would be a partial signature, as would the observation of 1.95-MeV deuterons. In addition, it would be interesting to run a light water electrolytic cell at a place like the Kamiokande facility in Japan to see if neutrinos can be detected from such a light water cell. Other reactions that may occur are as follows:



and



In all three cases, it is the presence of  $s$ -electrons inside the protons for a certain fraction of the time that would take care of the problem of the Coulomb barrier. In the case of the principal reaction in Eq. (42), the electron is destroyed in the reaction. Likewise, the secondary reactions represented by Eqs. (43a) and (43b) each involve the destruction of one of the  $s$ -electrons. However, the secondary reactions involve one and two additional  $s$ -electrons, respectively, that are catalytic in the reaction in that they can emerge afterwards with part of the released energy. In this connection, then, it is interesting that researchers at Bhabha Atomic Research Centre have reported seeing fluxes of  $10^7$  to  $10^8$  electrons per second in the electron-volt to several kilo-electron-volt energy range emerging from palladium and titanium samples that had been gas loaded or electrolytically loaded with hydrogen or deuterium.<sup>52</sup> This flux is smaller by a factor of  $\sim 10^{-5}$  than the number of electrons per second that would be involved in the primary reaction, Eq. (42), to produce excess power at the 1-W level. However, it may not be too large a flux to account for the accompanying secondary reactions (43a) and (43b). Note that these electrons would ordinarily not be energetic enough to get outside an electrolytic cell with its electrolyte. However, such electrons would contribute to bremsstrahlung that might be observed indirectly via the fogging of dental film placed against cells. Reactions such as (42), (43a) and (43b) might also occur in heavy water cells because of contamination with light water.

#### IX. A NEW TRM AVOIDS THE CRITICISM OF THE ONE-DIMENSIONAL TRM AND SUGGESTS A SOLUTION TO THE SURFACE, OR NEAR-SURFACE, EXCESS HEAT REACTION

Recently, Jändel<sup>53</sup> calculated the fusion rate for the one-dimensional TRM and found it to be far too low to account for the empirical fusion rates for cold fusion. To take this criticism into account, the author has arrived at a new three-dimensional form of the TRM that avoids Jändel's criticism and yet manages to incorporate the predictive features for cold fusion data that were a hallmark of the original one-dimensional TRM. Thus, it is shown for the new three-dimensional TRM that we can continue to employ the one-dimensional transmission resonance condition as though the model were in fact one-dimensional, provided that we make an important reinterpretation of the transmission resonance condition in terms of an ansatz for treating particle diffraction by a lattice known as Duane's rule. This new TRM will be presented in detail in a future paper. Here it must suffice to provide a brief sketch of those aspects of the model that are useful for present purposes. Finally, it is shown that the new TRM combined with the hypothesis of alkali-hydrogen fusion suggests a solution to the mystery of the surface, or near-surface, excess heat reaction in the form of an alkali-deuterium fusion reaction between  ${}^6\text{Li}$  and a deuteron to produce essentially  ${}^4\text{He}$ .

In 1923, Duane provided an ansatz (later known as Duane's rule) for particle diffraction by a crystal lattice that is an alternative to the much better known treatment employing the de Broglie wavelength of the particle. (I am grateful to R. Bass for reminding me of Duane's rule.) According to Duane, the periodicity of the crystal lattice itself leads to the

quantization of the linear momentum of the crystal in a direction normal to the lattice planes expressed by

$$(P_{lat.})_z = nh/L, \quad n = 0, 1, 2, \dots \quad (44)$$

The changes in the lattice's linear momentum in the  $z$  direction can be expressed by

$$\Delta(P_{lat.})_z = \Delta n(h/L). \quad (45)$$

Equations (44) and (45) can be considered to be an expression of Duane's rule. The author showed<sup>54</sup> that Duane's rule can be theoretically based on phonon emission in a periodic lattice as an alternative to the well-known treatment employing the de Broglie wavelength of a diffracting particle. Indeed, the author<sup>55</sup> and, earlier, Lande<sup>56</sup> showed that the popular treatment employing the de Broglie wavelength for particle diffraction is inconsistent with the special theory of relativity. We now employ Duane's ansatz to provide a significant reinterpretation of the transmission resonance condition that, until now in the TRM, has employed the de Broglie wavelength.

In Ref. 31, the transmission resonance condition in the TRM was expressed as

$$(2n + 1)\lambda/4 = L, \quad n = 0, 1, 2, \dots \quad (46)$$

It was pointed out in Eq. (7e) of Ref. 31 that Eq. (46) is a consequence of the Bragg law of diffraction, expressed as

$$n\lambda = 2L \sin \theta, \quad n = 0, 1, 2, \dots \quad (47)$$

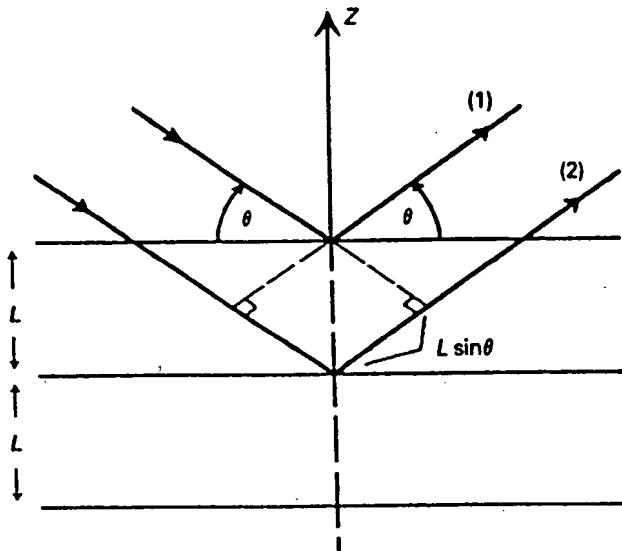
Figure 1 shows that Eq. (47), which allows one to predict the diffraction angle  $\theta$  for a diffraction maximum, expresses the familiar fact that a diffraction maximum occurs when an integral number  $n$  of de Broglie wavelengths  $n\lambda$  fit into the difference in path  $(2L \sin \theta)$  between paths 1 and 2. Eliminating  $\lambda$  by substituting  $\lambda = h/p$  into Eq. (47) allows us to rewrite it in the form

$$2p \sin \theta = 2n(h/2L) \quad (48)$$

or

$$2p_z = 2n(h/2L), \quad (49)$$

where  $p_z$  is the component of the particle's momentum in the  $z$  direction, i.e., transverse to the lattice planes. In the colli-



Diffraction Maxima:  $n\lambda = 2L \sin \theta$

Fig. 1. Diagram for the Bragg law of diffraction.

sion with the lattice, the particle's  $z$  component of momentum is changed from  $+p_z$  to  $-p_z$ . To conserve momentum, the lattice must increase its momentum by the amount given in Eq. (49):

$$\Delta(P_{lat.})_z = 2p_z = 2n(h/2L). \quad (50)$$

Note that this is consistent with Eq. (44) in that the new lattice momentum is still an integral multiple of  $(h/L)$ . Thus, the Bragg law in Eq. (47) can alternatively be derived as a simple consequence of Duane's rule without employing the de Broglie wavelength  $\lambda$ . (In conserving momentum, the lattice takes zero energy away from the particle in the collision, so that the latter is elastic. This is an umklapp process, which was previously mentioned in connection with the Mössbauer effect.) From Eq. (49), we see that the  $z$  component of the particle momentum is quantized:

$$p_z = n(h/2L) = 2n(h/4L) \quad (51)$$

or,

$$p_z = 0, 2(h/4L), 4(h/4L), 6(h/4L), \dots \quad (52)$$

Substituting  $\lambda = h/p_z$  into Eq. (46) provides the nonreflection condition in the Duane treatment, or the Duane's rule equivalent of the transmission resonance condition in Eq. (46):

$$p_z = (2n + 1)(h/4L), \quad n = 0, 1, 2, \dots, \quad (53)$$

which gives the condition that must be satisfied by the  $z$  component of the momentum of a particle for it to be transmitted resonantly, in contrast to Eq. (52), as

$$p_z = (h/4L), 3(h/4L), 5(h/4L), \dots \quad (54)$$

Note the contrast between Eqs. (53) and (51) and between Eqs. (54) and (52).

We hypothesize that it is Duane's treatment that is meaningful for particle diffraction by a lattice. If so, then it is only the  $z$  component of a particle's momentum (the component normal to the lattice planes) that must be utilized, and the de Broglie wavelength need not be employed for particle diffraction. (We are not throwing away the de Broglie wavelength for purposes other than diffraction but are hypothesizing with regard to particle diffraction that it is the Duane treatment that is physically meaningful.) Thus, from here on, the transmission resonance condition is hypothesized to be expressed by Eqs. (53) and (54) rather than by Eq. (46). Moreover, since it is the  $z$  component (normal to the lattice planes) of the momentum that is quantized, without regard for the remaining component in the  $(x, y)$  plane, we have the flexibility to turn the one-dimensional TRM into a new three-dimensional TRM. One does not have this flexibility employing the de Broglie wavelength form of the transmission resonance condition in Eq. (46) since one cannot, for example, employ a  $z$  component of the scalar de Broglie wavelength. That is, the two formulations of the transmission resonance condition are not equivalent. The difference may seem subtle but is in fact monumental. Upon this distinction the new three-dimensional TRM is built.

It is interesting to note, too, that the new TRM is now essentially an "energy band" model. This is easy to see since we have already indicated that it is the component of the particle's momentum in the  $z$  direction that must be quantized, as shown in Eq. (54), to ensure resonant transmission in that direction. But this means that the particle also has its kinetic energy associated with the  $z$  direction motion quantized, while the energies associated with its component motions in the  $x$  and  $y$  directions are essentially unrestricted. In essence, then,

we have energy bands built upon the quantized  $z$  direction kinetic energies. In this connection, it is interesting to note that Chubb and Chubb have insisted for some time that the TRM is undoubtedly closely related to their LINC model, an extremely interesting energy band model.

In the new three-dimensional TRM, we take the direction at right angles to interstitial lattice planes ( $z$  direction) as physically significant with regard to the transmission resonance process. Thus, the  $x$  and  $y$  momentum components of a particle are of no consequence. It is the  $z$  component that produces elastic reflections in the case of  $p_z$  satisfying Eqs. (51) and (52) or produces resonant transmission in the case of  $p_z$  satisfying Eqs. (53) and (54). That we can ignore the particle's momentum in the  $(x, y)$  plane means that the new three-dimensional TRM has effectively been reduced to an equivalent one-dimensional model. This means that all of the positive features (e.g., nonlinear fine structure in a graph of excess power versus current density) discovered for the previous one-dimensional model should still be valid.

We hypothesize that a certain fraction of the resonantly transmitted ions are involved in collisions with particles located at interstitial sites. As we show, the more likely situation is that of a heavy ion incident upon an interstitial proton or deuteron, and we shall see that the kinetics of this is reasonable. Moreover, the new formulation in terms of Duane's rule with its contrast between the behavior of the particles obeying Eq. (52) in a collision with the lattice with the behavior of those obeying Eq. (54) may unravel another mystery, namely, how the energy in the nuclear reaction gets into the lattice. Thus, particles obeying Eq. (52) undergo elastic collisions with the lattice, and the lattice recoils to conserve momentum via an umklapp process with no phonons being created in the lattice. In contrast, suppose a particle obeying Eq. (54) relative to the lattice undergoes an inelastic collision with a proton or deuteron in an interstitial lattice site. It seems that the opposite of an umklapp process by the lattice should now occur with a maximum of phonons created in the lattice. So, it is this process, opposite to the umklapp process, that suggests itself as the likely mechanism for producing phonons in the lattice during a lattice-induced nuclear reaction. Recall that we previously associated the umklapp process with the Mössbauer effect. So, in essence, with the formulation suggested by Duane's rule, we have hypothesized an effect that is the opposite of the umklapp effect and provides a means of escaping the apparent jaws of asymptotic freedom. Moreover, the process emerges in a natural way within the framework of the new TRM. In addition, and very importantly, we take into account Jändel's criticism<sup>53</sup> of the previous one-dimensional TRM. Thus, in the new three-dimensional model, a diffusion such as a deuteron is no longer envisioned as tunneling through Coulomb barriers on the order of a mega-electron-volt. Rather, its fulfilling of the condition of Eq. (53) enhances its chances of either being transmitted resonantly across a lattice plane or of being involved in an inelastic collision, the opposite of the umklapp process engaged in by a deuteron obeying the elastic collision condition of Eq. (51). Thus, in one scenario (Bass' quantum resonance triggering hypothesis<sup>51</sup>), energy is transferred from this deuteron in the inelastic collision to an interstitial deuteron, whose amplitude of oscillation in the lattice is accordingly enhanced, inducing it to undergo a nuclear reaction according to Schwinger's NEAL Model.<sup>23</sup> In a second scenario, the Born-Oppenheimer approximation breaks down: Electronic motions are now correlated with the motions of oscillating deuterons within the lattice. The enhancement

of their vibration of one of these deuterons produces an enhancement in the motions of nuclear reaction-catalyzing  $s$ -electrons. A third scenario envisions that the inelastic collision results in the transfer of a neutron to a palladium nucleus to leave a heavier palladium nucleus and a proton. (The new TRM still does not contain a detailed mechanism for the nuclear reaction, but the previous one-dimensional model also suffered from this defect.)

Within this new interpretive framework, there appears to be the same advantage as before in the transmission resonance process in favor of heavy ions over light ones. Thus, in treating the light water nuclear reactions in a lattice, we can show that there is an advantage to having potassium ions incident upon protons in the nickel lattice rather than vice versa: Consider  $^{39}\text{K}$  ions transmitted resonantly through an interstitial lattice of protons in the nickel crystal by virtue of satisfying the transmission resonance condition given in Eq. (46):

$$(2n + 1)\lambda/4 = L, \quad n = 0, 1, 2, \dots \quad (55)$$

Following our interpretation, based on Duane's rule,  $h/p_z$  should be employed in Eq. (55) instead of  $\lambda$ . The term  $p_z$  can now be written as

$$p_z = (2n + 1)h/4L = (2mE_z)^{1/2}, \quad (56)$$

where  $E_z$  is the kinetic energy associated with the motion in the  $z$  direction and  $m$  is the mass of the particle. Thus, the problem of a proton of energy  $E$  incident upon a  $^{39}\text{K}$  ion, with the latter at a site in the lattice (interstitial or substitutional), is not equivalent to the reverse situation with the  $^{39}\text{K}$  ion of energy  $E$  incident upon an interstitial proton. Because of the differences in masses, ~4.4 times as many orders of transmission resonance are brought into play for the potassium ions as diffusons as for the protons as diffusons. To see this, we substitute Eq. (56) into Eq. (55) and consider the energy  $E_z$  to be the same for species 1 (potassium ions) and species 2 (protons) having respective masses  $m_1$  and  $m_2$ :

$$(2n_1 + 1)(m_1)^{-1/2} = (2n_2 + 1)(m_2)^{-1/2} \quad (57)$$

or

$$(2n_1 + 1) = (m_1/m_2)^{-1/2}(2n_2 + 1). \quad (58)$$

Substituting  $m_1 = 19.3m_2$  leads to

$$n_1 = 4.4n_2. \quad (59)$$

This effect would also favor lithium ions over deuterons in the standard heavy water cold fusion reaction. A group at Oak Ridge National Laboratory discovered that lithium had migrated much deeper into a piece of deuterated palladium than would be anticipated from the migration time and the known diffusion coefficient of lithium.<sup>57</sup> This incident might very well be accounted for on the basis of the resonant transmission of lithium ions through the deuterated palladium lattice. Such resonant transmission of ions is definitely suggested by the TRM and might be studied as an additional means of partially corroborating the new three-dimensional TRM.

A mystery dispelled by the TRM is the disparity between the current densities employed to achieve excess power in cold fusion and those used in the light water Mills-Kneizys process. Thus,  $2 \text{ mA/cm}^2$  is a typical current density for the light water excess heat reaction, whereas  $200 \text{ mA/cm}^2$  is typical of the heavy water excess heat reaction. This might be thought to point to the fact that they are dissimilar processes as opposed to the thesis here that they are both examples of alkali-hydrogen fusion. The situation with regard to the current densities is best understood with reference to Fig. 2, which is

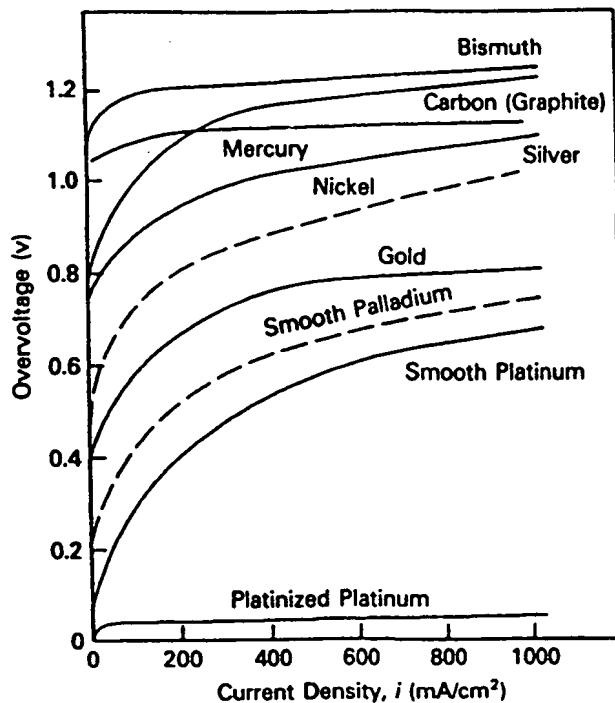


Fig. 2. Activation overpotential for hydrogen on various metals ( $2\text{NH}_2\text{SO}_4$  at  $25^\circ\text{C}$ ) versus applied current density.

essentially Fig. 9 of Ref. 31. Figure 2 differs from Fig. 9 of the earlier paper by the addition of curves for smooth palladium and nickel, shown approximately by the dashed curves. An error in the figure caption of the earlier paper that is corrected here is the substitution of "concentration overpotential" for "activation potential." Thus, the "overvoltage" of the y axis in that figure should be thought of as an activation overpotential. (I am grateful to E. Pye<sup>38</sup> of the Cal Poly Chemistry Department for pointing out this error.) The figure portrays the experimental realization for hydrogen of the well-known Butler-Volmer equation, Eq. (37) of Ref. 31:

$$i = i_0 \exp[(1 - \beta)F\eta/RT]. \quad (60)$$

This relation is incorporated in the derivation of the formula for the relative excess power presented in Ref. 31. It relates the applied current density  $i$  to the equilibrium current density, or exchange current density  $i_0$ , the hydrogen overvoltage  $\eta$ , and the kelvin temperature  $T$ . The term  $F$  is the Faraday,  $R$  is the gas constant, and  $\beta$  is the "symmetry factor," which can be taken as  $\sim \frac{1}{2}$  for our purposes. Equation (60) can be rewritten by employing the relation  $F/R = q/k$ , where  $q$  is the charge on a proton and  $k$  is Boltzmann's constant:

$$i = i_0 \exp(q\eta/2kT). \quad (61)$$

Reference 31 gives examples of exchange current densities for the hydrogen reaction on different metal surfaces at  $\sim 300\text{ K}$ . Relevant exchange densities for the present purposes are platinum:  $i_0 = 10\text{ mA/cm}^2$ ; palladium:  $0.1\text{ mA/cm}^2$ ; gold:  $10^{-3}\text{ mA/cm}^2$ ; nickel:  $10^{-4}\text{ mA/cm}^2$ ; and mercury:  $10^{-10}\text{ mA/cm}^2$ . Note that typical currents for the light water and heavy water experiments are  $160\text{ mA}$  and  $1\text{ A}$ , respectively. For the heavy water experiment, substitution of  $\eta = 0.28\text{ V}$ ,  $i_0 = 1\text{ mA/cm}^2$  (partial platinization of the cathode surface should lead to a compromise between the  $i_0$  values given for

platinum and palladium), and  $T = 312\text{ K}$  into Eq. (61) leads to a current density of  $\sim 182\text{ mA/cm}^2$ . A typical cathode area of  $6\text{ cm}^2$  then implies a total current of  $\sim 1\text{ A}$ . For a typical light water experiment, on the other hand, Fig. 2 shows that  $\eta = 0.65\text{ V}$  would be reasonable. In addition, employing  $i_0 = 10^{-4}\text{ mA/cm}^2$  and  $T = 312\text{ K}$  in Eq. (61) yields a current density of  $i = 2\text{ mA/cm}^2$ . Multiplying this by a typical cathode area of  $\sim 80\text{ cm}^2$  yields  $\sim 160\text{ mA}$ .

In the absence of precise knowledge of the nuclear cross sections, it is nevertheless interesting to compare the  $^{39}\text{K}$  (light water) and  $^6\text{Li}$  (heavy water) reactions with regard to relative weighting factors regarding stoichiometry, kinetics, and energy and to obtain total weighting factors for purposes of comparison by multiplying the respective weighting factors together: [The first-quoted relative factor in each statement refers to  $^{39}\text{K}$  or reaction (3), and the second to  $^6\text{Li}$  or reaction (21).] The relative weights based on the molarities of the respective electrolytes are 0.57 and 0.1. The potassium reaction also receives an extra weighting factor of 2 because there are two potassium atoms in potassium carbonate and only one lithium atom in lithium deuterioxide. The percent abundances give weights of  $\sim 0.931$  and  $0.074$ . Relative weights of 6 and 39 can be assigned for the relative mobilities in the electrolyte based on the inverses of the masses. The currents employed in typical experiments are  $\sim 1$  to  $6$  in favor of the heavy water reaction. The respective energies released in the two nuclear reactions are 8.3 and 22.4 MeV, leading us to assign relative weighting factors of 8.3 and 22.4. From the previous considerations on the density of transmission resonance energy levels per unit energy level [Eq. (58)], we obtain a relative factor in favor of  $^{39}\text{K}$  given by  $(39/6)^{1/2} = 2.55$ . Finally, the respective widths of the transmission resonance energy "windows" can be calculated from Eq. (18) of Ref. 31 as 1 and 16.6. The two products of the respective relative weights then turn out to be  $\sim 135$  and  $645$  and have a ratio  $R_{PWF}$  of the products of the respective weighting factors given by

$$R_{PWF} = (645)/(135) = 4.8. \quad (62)$$

It is interesting then that, in Bush and Eagleton's laboratory, the typical excess power yields from the heavy water experiments are about the same as those from the light water experiments. Thus, in the absence of knowledge of the nuclear cross sections, the agreement is rather good. Rough agreement of the two nuclear cross sections based on the mechanisms being the same might account for this agreement.

While the door has been left open for the alkali-deuterium D-D reaction shown schematically in Eq. (18) to be a contributing reaction, or even the principal reaction, we strongly suggest, based on the new perspective afforded by the alkali fusion hypothesis, that the alkali-deuterium D- $^6\text{Li}$  reaction shown in Eq. (21) is most likely the prime source of the excess heat in Fleischmann-Pons-type experiments. In that case, the by-product, as in the case of the D-D reaction in Eq. (18), would be  $^4\text{He}$ . It seems likely, then, that the other two branches of the D- $^6\text{Li}$  reactions given in Eqs. (22) and (23) might account, respectively, for the lower level tritium production noted by Bockris<sup>39</sup> and the very low level yields of neutrons noted by the author<sup>28</sup> and others. [Note that the D- $^7\text{Li}$  reaction of Eq. (27) appears to be ruled out by the fact that so few neutrons are observed in cold fusion reactions.] In addition, there are no branches of the D- $^7\text{Li}$  reaction as counterparts to the D- $^6\text{Li}$  reactions (22) and (23). (We must be cautious here, however, because we have also hypothesized the successful experiment of Noninski and

Noninski<sup>30</sup> to involve  $^{39}\text{K}$  on deuterium to give  $^{40}\text{Ca}$  and a neutron.) Let us briefly summarize the arguments in favor of the D- $^6\text{Li}$  reaction (21) being the prime source of the excess heat from the standpoint of the new hypothesized framework of alkali-hydrogen fusion:

1. The  $^6\text{Li}$  reaction involving a heavier ion ( $^6\text{Li}$  as opposed to deuterium) seems to fit the pattern of the potassium reaction in Eq. (3) involving an ion,  $^{39}\text{K}$ , that is relatively heavy compared with deuterium.

2. The  $^6\text{Li}$  reaction fits the pattern of the  $^{39}\text{K}$  reaction as suggested by the ratio of the product of their respective weighting factors given in Eq. (62) as compared with the ratio of typical excess power yields.

3. The  $^{39}\text{K}$ - $p$  reaction shows that bosons are probably not important for the reaction, nor is it important that the reaction involve two identical particles as in D-D fusion.

4. The experiment of Appleby et al.<sup>13</sup> provides strong support for the D-Li reaction hypothesis. Thus, when Appleby et al.<sup>13</sup> replaced LiOD with NaOD in the electrolytic cell, the excess heat reaction diminished to the point of not being detectable. The fact that substitution of LiOH for LiOD also made the reaction go away in this case shows that the reactions involving lithium on protons specified in Eqs. (24), (25), and (26) have lower cross sections than their heavy water counterparts. A complicating factor would also seem to be that we need enough deuterons replaced by protons in the interstitial lattice to see a light water reaction. Experiments should be performed with relatively pure  $^6\text{LiOD}$  and  $^7\text{LiOD}$  in an attempt to distinguish between these two possibilities.

Finally, it is interesting, and important, to explore the requirements placed on the new TRM by the combination of the empirically known reaction rate and the known surface flux of  $^6\text{Li}$  ions satisfying the transmission resonance condition now taken to be Eq. (53). [As previously discussed, all of the equations of the old TRM can be retained if we simply replace the de Broglie wavelength of the old TRM by  $h/p_z$ , i.e., Planck's constant divided by the component of the particle's momentum in the  $z$  direction, which is taken to be at right angles to the interstitial lattice planes. Also, the energy  $E$  must be replaced by  $E_z = p_z^2/2m$ , the kinetic energy of the particle associated with motion in the  $z$  direction. (Even the considerations involving absolute temperature  $T$  in Ref. 31 can then be retained since it was shown for the one-dimensional TRM that  $E = E_n = (\frac{1}{2})kT$  creates a special physical condition, where  $E_n$  is a transmission resonance energy and  $T$  is the ambient temperature at the surface of the crystal.)] Thus, in their recent thin-film work, Bush and Eagleton<sup>11</sup> achieved an average of  $\sim 3 \text{ W}$  of excess power for a period of 54 days employing an electrolytic cell in which the cathode consisted of a 5- $\mu\text{m}$ -thick layer of palladium electroplated upon a substrate of silver. The total surface area was  $\sim 4 \text{ cm}^2$  and the total current was  $\sim 1 \text{ A}$ . For the D- $^6\text{Li}$  reaction of Eq. (21) the average fusion rate thus works out to be given roughly by

$$N = 8.4 \times 10^{11} \text{ fusion/s}. \quad (63)$$

For a 1-A total current, the number of  $^6\text{Li}$  ions incident upon the surface would be given approximately by

$$\begin{aligned} & (1 \text{ A}/1.60 \times 10^{-19} \text{ C})/(1836 \times 6) \\ & = 5.7 \times 10^{14} \text{ }^6\text{Li ion/s hitting the palladium surface} \end{aligned} \quad (64)$$

Calculation based on the equations of Ref. 31 show that the fraction of these incident  $^6\text{Li}$  ions that have  $p_z$  values placing them in the transmission resonance energy windows is  $\sim 2.5\%$ . Then multiplying 0.025 times the total number of  $^6\text{Li}$  ions incident per second upon the cathode surface in Eq. (64) yields

$$1.4 \times 10^{13} \text{ }^6\text{Li ion/s hitting the cathode that obey the transmission resonance condition}. \quad (65)$$

The ratio of the number in Eq. (65) to that in Eq. (63) gives the average ratio of the eligible  $^6\text{Li}$  ions hitting per second that must be involved in these alkali-deuterium fusions as  $\sim 1$  in 17. Or, alternatively expressed, the number of incident  $^6\text{Li}$  ions per second involved in nuclear reactions at the surface is  $\sim 1$  in every 700 of the total number of  $^6\text{Li}$  ions incident per second. If we take the reaction to be right at the surface and assume a surface area of  $4 \text{ cm}^2$  and a relatively modest stoichiometry of 0.8 interstitial deuterons per palladium atom, this amounts to a reaction each second at only  $\sim 1$  out of every 10000 deuteron-filled interstitial sites.

## X. EXPERIMENTAL INVESTIGATIONS

### X.A. Introduction

Since the main part of this technical note was written, four new electrolytic cells (44, 45, 47, and 48) employing nickel cathodes, platinum anodes, and a light water-based 0.57 M electrolyte have been successfully run at Cal Poly by Bush and Eagleton. Cells 44, 45, and 47 employed a light water-based 0.57 M potassium carbonate electrolyte. The detection of excess heat quantitatively correlated with calcium in cells 44 and 45 provides support for the hypothesis of a light water reaction expressed by Eq. (3) and alkali-hydrogen fusion set forth by the author before any experimental work had been done at Cal Poly to investigate the claims of Mills and Kneizys. (Cell 47 was run for too short a period to have real hope of calcium detection.)

Cell 48 employed a light water-based 0.57 M sodium carbonate electrolyte. From the work of Mills and Kneizys,<sup>1</sup> we had anticipated that this would be a blank cell evidencing no excess heat. To the contrary, we discovered that it achieved a greater excess power-to-input power ratio for comparable input powers and current densities than the essentially identical cell 47, which differed only by virtue of employing a 0.57 M potassium carbonate electrolyte rather than sodium carbonate. It may be possible to ascribe the fact that we were able to observe excess heat for a sodium cell, whereas Mills and Kneizys did not detect any, to the difference in cathode. Mills and Kneizys employed nickel plate, whereas we employed a different alloy of nickel. In fact, when we employed the nickel plate described in Ref. 1, we were unable to see excess heat in the case of the one potassium cell we tried. Because of our greater success with our cathode material, we have not yet made another attempt with the nickel plate. This excess heat can be accounted for on the basis of the nuclear reaction in Eq. (7) in which a  $^{23}\text{Na}$  nucleus (odd-even) gains a proton to become a  $^{24}\text{Mg}$  nucleus (even-even) with an accompanying energy release to the lattice of 11.7 MeV. It is shown here that the new TRM gives a good theoretical prediction for the observed ratio of respective excess powers for the sodium carbonate cell (48) and the potassium carbonate cell (47). The detection of excess heat for a sodium carbonate cell had been ruled out by Mills and Kneizys based on the

novel chemistry of Mills and Farrell. So, this finding contradicts the Mills model and is additional support for the hypothesis of a light water nuclear process and the alkali-hydrogen fusion scenario.

A dilution experiment suggested by the author and carried out in the Cal Poly laboratory by Bush and Eagleton demonstrates that the excess power effect is real. Moreover, the fairly rapid adjustment of the excess power level to the lowered sodium concentration (cell 48) and the excellent agreement of the experimental value for the decrease in the percentage of the excess power to the input power with the theoretical prediction for this value based on the dilution of the sodium concentration in the electrolyte provides evidence that the reaction is a surface reaction and supports the new TRM, as is shown here.

A later section provides initial evidence for the production of strontium correlated with excess heat production in a  $\text{Rb}_2\text{CO}_3$  cell. Because strontium background concentrations are generally much lower in the environment than that of calcium, this finding provides stronger supporting evidence than did the apparent finding of calcium production in two potassium carbonate cells.

Thus, the preliminary experimental work in our laboratory at Cal Poly provides strong support for the hypothesis of the light water excess heat reactions as cold fusion and for cold fusion as alkali-hydrogen fusion. In addition, the new TRM appears to be on the right track. On the basis of this model a cold fusion reaction might more aptly be termed a TRINT reaction. Another possibility would be OPPL.

### X.B. Experimental Results

It has proven possible to get a reasonably good quantitative correlation between the amount of excess heat detected in the case of cells 44 and 45 and the respective amounts of calcium generated. Consider the excess heat first: When corrections are made for the results of recalibration, the excess heat yields were  $-0.35$  and  $0.75$  MJ, respectively, for cells 44 and 45, corresponding to average powers for the respective cells (13-day run for cell 44 and 15-day run for cell 45) of  $(0.31 \pm 0.08)$  and  $(0.58 \pm 0.15)$  W. Thus, the ratio of the excess heat of cell 45 to that for cell 44 is given by

$$\text{ratio of excess heat} = 2.16 \pm 0.52 . \quad (66)$$

The amount of calcium in the electrolyte was gauged via flame photometry analysis (atomic absorption) performed in the Cal Poly Chemistry Department. This analysis provided the following raw numbers for the calcium content of the electrolyte samples:

Virgin electrolyte (employed in both cells 44 and 45):

$-0.002$  and  $-0.002$

Postrun electrolyte (cell 44):

$0.027, 0.023, 0.024$ , and  $0.026$

Postrun electrolyte (cell 45):

$0.052, 0.046$ , and  $0.045 . \quad (67)$

Based on Eq. (67), the virgin electrolyte could not be a significant source of calcium contamination. Solutions for calibration standards for the flame photometry test were made up for  $0.5, 1.0, 2.0, 3.0$ , and  $5.0$  ppm of calcium. The raw numbers from the flame photometry test corresponding to these respective calibration standards were  $0.031, 0.067,$

$0.138, 0.205$ , and  $0.340$ . (Floyd Howell, a stockroom manager for the Cal Poly Chemistry Department, is thanked for carrying out all of the flame photometry tests, and Carolyn Forrester, the other stockroom manager, is thanked for making up the calcium standards for these tests.) Comparing these with the raw numbers in Eq. (67) allows deduction of the approximate concentrations of calcium in parts per million for the electrolytes of Eq. (67):

Postrun electrolyte (cell 44):  $0.40$  ppm

Postrun electrolyte (cell 45):  $0.75$  ppm .  $(68)$

Here,  $0.75$  ppm implies that there are  $0.75 \mu\text{g}$  of calcium per millilitre of electrolyte. Employing these concentrations in Eq. (68) and the fact that the volumes of electrolyte in 45 and 44 were  $42.5$  and  $35$  ml, respectively, it is now possible to obtain an approximate ratio of the respective amounts of calcium appearing in the two postrun electrolytes:

$$\text{ratio of calcium amounts} = (0.75/0.40)(42.5/35)$$

$$= 2.28 \pm 0.14 . \quad (69)$$

Note that the ratios in Eqs. (69) and (66) compare quite favorably.

A stronger condition is, of course, that the respective amounts of excess heat and calcium produced correlate quantitatively for the respective cells: For cell 44, a concentration of  $0.4$  ppm translates to a mass of  $14 \mu\text{g}$  of calcium in the  $35\text{-ml}$  volume of electrolyte, or  $2.11 \times 10^{17} {}^{40}\text{Ca}$  nuclei produced. For a yield of  $8.3$  MeV of heat per nuclear reaction, the average excess power over a 13-day run would be  $0.25$  W, which compares reasonably well with the average excess power of  $(0.31 \pm 0.08)$  W found experimentally for cell 44. For cell 45, the correlation is also fairly good: A  $0.75$  ppm concentration of calcium in the postrun electrolyte translates to  $31.9 \mu\text{g}$  of calcium, or  $4.8 \times 10^{17} {}^{40}\text{Ca}$  nuclei. Again taking an excess heat yield of  $8.3$  MeV per reaction, based on Eq. (3), the 15-day run of cell 45 would have an average associated excess power of  $0.49$  W, which compares favorably with the  $(0.58 \pm 0.15)$  W of average excess power experimentally determined for cell 45. So the stronger condition of respective correlations between excess heat produced and calcium produced is met quite well. Again, however, it is important to emphasize that these are preliminary results.

The issue of possible calcium contamination of the electrolyte by the nickel material of the cathode is an important one. This is especially true since the manufacturer has indicated that the "as-received" material, which we mechanically fabricate into cathodes, contains from  $0.04$  to  $0.08$  wt% calcium, which is enormous for our considerations. The author originally suggested running the sodium carbonate cell 48 for the dual purposes of seeing what amount of calcium might be contributed to the electrolyte by the cathode and to have an excess energy blank. Before the postrun electrolyte was collected from this cell, we were careful to run the same amount of charge ( $\sim 0.26 \text{ A}\cdot\text{days}$ ) through it as was run through cell 44. In both cases, the cells were kept at a temperature of  $39^\circ\text{C}$ . Flame photometry analysis produced the following data:

Raw data for the known calcium standards:

0.5 ppm (calcium):	0.032
1.0 ppm:	0.067
2.0 ppm:	0.133
3.0 ppm:	0.196
5.0 ppm:	0.324

(70)

Raw data for the samples:

Sodium carbonate prerun (i.e., virgin) electrolyte:

0.048, 0.044, 0.049, and 0.051

Cell 48: postrun electrolyte:

0.011, 0.010, 0.016, 0.018, and 0.018

Deionized water employed in solutions and for rinsing:

-0.006 . (71)

Based on the raw data from the calcium standards, the raw data for the postrun electrolyte of cell 48 translate into 0.23 ppm of calcium. However, this is considerably less than the 0.72 ppm of calcium in the virgin (prerun) electrolyte for the sodium cell 48. Thus, it seems that the calcium originally in the cathode makes no contribution to that of the postrun electrolyte in a positive sense. If, on the other hand, corrections are made to the respective postrun electrolyte calcium concentrations for cells 44 and 45 assuming uptake by the cathode of part of the calcium produced at its surface, then this is clearly a complicating issue. Nevertheless, the evidence appears unambiguous from the sampling of the virgin and postrun electrolytes of cell 48 that the electrolysis process with the nickel material as the cathode tends to lower the calcium concentration of the virgin electrolyte. This fact and a comparison of the virgin and postrun electrolytes for cells 44 and 45 offer strong evidence for the production of calcium during the electrolytic process. It seems most likely that the calcium was produced by reaction (3) in which a  $^{39}\text{K}$  ion incident upon the nickel cathode manages to add an interstitial proton in a way that is as yet poorly understood, but appears to involve the transmission resonance phenomenon discussed earlier.

It was found that the excess power levels of the sodium cell (cell 48) normalized to the input power all exceeded those for the potassium cell (cell 47) for cases of comparable current density and input power and that the average ratio of these respective normalized power values was approximately

$$1.90 \pm 0.33 . \quad (72)$$

Interestingly enough, the new TRM gives a very close prediction to this if we make the interesting simplifying assumption that the cross sections for the nuclear reactions of Eqs. (7) and (3) are approximately the same. Then, the only difference in the excess powers is based on the difference in the energy yields per reaction of 11.7 MeV for the sodium reaction [Eq. (7)] and 8.3 MeV for the potassium reaction [Eq. (3)] and mass factors involving the mass values of 23 and 39 for sodium and potassium, respectively. (Other factors, such as the surface temperature, molarity of the electrolyte, surface areas of the cathodes, fractional hydrogen loading of the cathodes, etc. etc. are assumed to be the same.) According to the new TRM, the formulas for the old TRM are still valid in the three-dimensional case. [The sole exception is that the limitation to transmission resonance states below a certain order (established empirically as about  $n = 17$ ), which was based on thermal disruption (phonon exchange), is no longer considered valid by the author.] The TRM expression for relative excess power is given by Eq. (41) of Ref. 31:

$$P_r = i^3 i_0^{-2} T^{-1} \Sigma_n [(T_n - 2T \ln(i/i_0))^{1/2} T_n \exp(-T_n/T)] , \quad (73)$$

where

$i$  = applied current density

$i_0$  = equilibrium current density

$T$  = temperature of the electrolyte near the surface of the cathode

$T_n$  = transmission resonance energy in temperature units given in Eq. (3) of Ref. 31 as

$$T_n = (2n + 1)^2 T_0 , \quad (74a)$$

where

$$T_0 = h^2 / 32mL^2 , \quad (74b)$$

where

$h$  = Planck's constant

$m$  = mass of the ion incident upon the lattice

$L$  = lattice spacing of the crystal.

The term  $T_n$  is related to the quantized energy  $E_z$  in Eq. (56) by Boltzmann's constant:

$$E_z = kT_n . \quad (75)$$

For purposes of comparing the sodium and potassium cell excess powers, the mobilities must be accounted for by dividing all factors of  $i$  and  $i_0$  in  $P_r$  in Eq. (73) by the mass  $M$ . This results in simply dividing  $P_r$  by  $M$ . [Previously, Eq. (73) was employed in practice by the author only to compare excess powers for two cases involving the same species of ion, namely, the deuteron.] According to the TRM, the ratio of excess powers should be given by

$$R_{\text{Na}/\text{K}} = \{[(P_r)_{\text{Na}}/M_{\text{Na}}]/[(P_r)_{\text{K}}/M_{\text{K}}]\} (E_{\text{Na}}/E_{\text{K}}) , \quad (76)$$

where  $(P_r)_{\text{Na}}$  and  $(P_r)_{\text{K}}$  are, respectively, the relative excess power factors from Eq. (73) for the sodium and potassium cells. The second factor is the ratio of the energy yield in the sodium-on-proton nuclear reaction of Eq. (7) to that of the potassium-on-proton nuclear reaction of Eq. (3). The respective energies are 11.7 and 8.3 MeV. For nickel,  $i_0 = 10^{-4}$  mA/cm<sup>2</sup> (Ref. 31) is employed as an approximate value for purposes of this calculation, and the applied current density will be taken to be  $i = 2$  mA/cm<sup>2</sup>. For deuterons as the incident ions, the value of  $T_0$  in Eq. (74b) is taken to be

$$(T_0)_D = 3.98 \text{ K} . \quad (77a)$$

Then, since  $T_0$  in Eq. (74b) scales inversely as the mass of the incident ion, the  $T_0$  values follow immediately for the cases of sodium, potassium, and rubidium as incident ions with respective approximate masses of 23, 39, and 85:

$$(T_0)_{\text{Na}} = (T_0)_D(2/23) = 0.346 \text{ K} , \quad (77b)$$

$$(T_0)_{\text{K}} = 0.204 \text{ K} , \quad (77c)$$

and

$$(T_0)_{\text{Rb}} = 0.0936 \text{ K} . \quad (77d)$$

Employing Eqs. (73), (77b), and (77c) yields

$$[(P_r)_{\text{Na}}/M_{\text{Na}}] = 1.812 \times 10^{-5} \quad (78a)$$

and

$$[(P_r)_K/M_K] = 1.426 \times 10^{-5} . \quad (78b)$$

Then, from Eqs. (76), (78a), and (78b), the TRM's theoretical prediction for the ratio of the excess powers for sodium and potassium cells is given by

$$\begin{aligned} R_{Na/K} &= (1.812 \times 10^{-5}/1.426 \times 10^{-5})(11.7 \text{ MeV}/8.3 \text{ MeV}) \\ &= 1.8 . \end{aligned} \quad (78c)$$

Note that this is in good agreement with the experimental result in Eq. (72) of  $1.9 \pm 0.3$ . While this good agreement might simply be fortuitous, it seems more likely that it evidences an underlying simplicity associated with the transmission resonance phenomena discussed in Sec. VIII. (Recall, also, that the transmission resonance phenomenon was previously employed in the attack on so-called asymptotic freedom.)

Not only does this provide support for the new TRM, it also provides support for the TRM's scenario in which sodium and potassium ions are incident upon the interstitial protons (contributed by the light water) in the nickel lattice at, or extremely near, the surface. Note that there is no problem of a surface reaction in the new TRM since the de Broglie wavelengths of the ions are no longer involved in the transmission resonance aspect of the model. Rather, it is the Duane rule that is employed for the transmission resonance and that receives its theoretical justification from previous theoretical work.<sup>54,55</sup> Moreover, the energy shift employed in the original TRM, and which has been carried over to the new TRM, now makes sense as an energy shift produced by the hydrogen activation potential (hydrogen overvoltage), as surmised earlier. The overall picture, then, is one in which the nuclear reaction is between an ion obeying the transmission resonance condition and a proton, deuteron, or triton at an interstitial lattice site. The reaction should occur in any matrix in which a hydrogen lattice (protons, deuterons, or tritons) can be set up and with ions for which the addition of a nucleon, or small cluster of nucleons, yields a nuclear reaction in which energy is released. Of course, the reaction need not occur right at the surface but would probably be reasonably near, with the Duane rule simply requiring the existence of a periodic lattice.

In another experiment suggested by the author, Bush and Eagleton carried out a dilution experiment involving cell 48, in which 10 ml of deionized light water was substituted at regular intervals for the electrolyte of the sodium cell for the purpose of studying the effect on the excess power level normalized to the input power as a function of decreasing ion concentration. As anticipated, the excess power normalized to input power decreased with increasing dilution, evidencing the fact that the excess power was real and not simply due to a calibration offset or other artifact. More than that, however, was the fact that the excess power percentage decreased relatively quickly and the decline could be accurately predicted from the theoretical decrease in the sodium concentration produced by the known dilution. Thus, for the 45-ml volume of sodium carbonate electrolyte (light water, 0.57 M) the substitution of 10 ml deionized light water reduces the relative sodium concentration from 100% to  $(35/45 \text{ ml}) \times 100\% = 77.8\%$ , which implies a theoretical decrease of 22.2% in the excess power. Experimentally it was observed that  $(\text{excess power}/\text{input power}) \times 100\%$  for the cell went from  $(0.55/0.64 \text{ W}) \times 100\% = 86.0\%$  before the first 10-ml substitution to  $(0.40/0.625 \text{ W}) \times 100\% = 64\%$  in ~40 min, which is a decrease of 22.0%, in excellent agreement with the

theoretical decrease in the sodium concentration. After the second 10-ml substitution the theoretical sodium concentration should have been  $(27.23/45 \text{ ml}) \times 100\% = 60.5\%$  for a decrease of 17.3%. In agreement with this, the normalized excess power level was observed to decrease by 17.7%. [After the third 10-ml substitution, the system went somewhat haywire with the power level actually increasing. We later discovered that this was more than likely due to a problem with the magnetic stirrer whose operational mode was apparently upset in the mechanical process of opening the cell and making the third dilution. (Future cell designs will incorporate a feature making it possible to substitute a chemical without turning off the cell's input power or physically opening it up. The dilutions here required that the cell current be turned off for ~3 min.) Another distinct possibility is that the current density prior to the dilution may have placed the sample close to a relative minimum (cusp) associated with the TRM. A small change either way in the current density would then be sufficient to produce a net increase in the excess power.] Even though the experiment covered only 2 h and involved only two dilutions, the results give strong support to a surface reaction and also support the TRM scenario in which a heavy ion is incident upon a lattice of interstitial protons created by the metal lattice. (The dilution experiment results would also fit into a scenario of a purely chemical reaction at the lattice surface. The nuclear nature is guaranteed by the fact that cell 48 produced a total excess heat of ~0.1 MJ.)

Clearly, then, there appears to be strong preliminary support for the hypothesis of light water excess heat reactions and for cold fusion as alkali-hydrogen fusion or TRINT.

### X.C. Additional Results

Since the original experimental section was written, two cells, 49 and 50, employing a light water-based  $\text{Rb}_2\text{CO}_3$  electrolyte (0.57 M) have been tried at the author's suggestion, as well as another sodium carbonate (0.57 M) cell, cell 51.

In the case of cell 51, which was found to produce excess heat, an experiment was performed in which heavy water was added to the cell to note its effects on the excess power. (While this was an experiment that we had planned to perform, it was carried out in time for this technical note because of the urging of E. Mallove. I thank him for this and for his general encouragement of my work.) Prior to the addition of heavy water the excess power was ~1.02 W for an input power of 15.628 W, which represents a "gain" of ~6.5%. Ten minutes after the addition of 1 ml of  $\text{D}_2\text{O}$  to the original electrolyte volume of 45 ml, the corresponding values were 0.90 W and 15.726 W for a reduced gain of 5.7%. Another millilitre of heavy water was now added, bringing the total electrolyte volume to 47 ml. After ~15 min, the excess power began to climb and reached ~1.99 W, which represented a gain of ~12.3%, after ~25 min following the addition of the second millilitre. However, 24 h later, it was observed that the power had climbed to ~5.89 W, representing a gain of ~27.3%.

An immediate observation is that these preliminary results apparently rule out models in which light water excess heat effects are the result of a small heavy water contamination of the light water. (Recall that ~1 out of every 8000 molecules in ordinary distilled water is  $\text{D}_2\text{O}$ .) Thus, if the contamination hypothesis were correct, the excess power should have risen much more with the huge percentage increase in the number of deuterons in the electrolyte than it eventually did.

Of course, that is barring some exotic saturation effect, which appears highly unlikely.

There is a difficulty in attempting to apply the TRM to provide a theoretical explanation for these results as in the previous case of applying it to explain the ratio of the excess powers for the sodium and potassium cells. Thus, in the latter instance, the simplifying assumption was made that the nuclear cross sections are very nearly the same for reactions (3) and (7). The likely candidate reaction initially in the present case, since we have an interstitial lattice of protons from the light water, is represented by



It is too much to expect that the cross section for this reaction would be the same as the other two, since the number of protons in the nucleus is 1 here, as compared with 11 for the case of sodium and 19 for potassium. We can, however, work backward employing a calculation such as Eq. (78c) to compare the cross section for Eq. (79) with that for Eq. (7). The value of  $(P_r)_D/M_D$  is readily calculated from Eq. (73) to be  $4.53 \times 10^{-5}$  as compared with  $1.81 \times 10^{-5}$  for the corresponding value from Eq. (73) for sodium. The ratio of the concentrations of ions for deuterium and sodium is readily shown to be ( $0.0426/0.546 M$ ) after the addition of the 2 ml of  $D_2O$  to the original 45 ml of electrolyte. The ratio of the energy yields in the two nuclear reactions is given by ( $5.45/11.7 \text{ MeV}$ ). To find the ratio of the cross sections for the two reactions, the ratio of the  $P_r/M$  factors is multiplied by the two latter ratios and the ratio of the cross sections  $R_{cr}$ , and then this product is equated to the experimentally determined ratio of the excess power associated with the deuterium reaction to that associated with the sodium reaction given by ( $0.97/1.02 \text{ W}$ ):

$$0.0908(R_{cr})_{D/Na} = 0.97/1.02 \text{ W} = 0.95 \text{ W} . \quad (80a)$$

Thus,

$$(R_{cr})_{D/Na} = 10.5 . \quad (80b)$$

(The decrease in excess power immediately after the addition of the first millilitre of heavy water can perhaps be attributed to the decrease in the concentration of sodium ions and the input energy to separate oxygen and deuterium ions at the cathode surface.)

To account, however, for the much higher average excess power level of 5.89 W observed when the cell was checked 24 h after the addition of 2 ml of  $D_2O$ , we invoke the  ${}^4\text{He}$  reaction as the dominant heavy water reaction now since there is a sizable number of deuterons at this stage in lattice interstitial sites, represented by



To see that this makes sense in terms of the experimentally observed excess powers reported previously, note first of all that the ratio of excess powers observed shortly after the second millilitre of  $D_2O$  was added for the hypothesized heavy water reaction in Eq. (79) and the light water reaction for sodium in Eq. (7) is given by

$$0.95 \pm 0.11 . \quad (82a)$$

On the other hand, after 24 h this ratio had become

$$4.77 \pm 0.52 . \quad (82b)$$

Note now that the ratio of Eq. (82b) to Eq. (82a) is given by

$$5.02 \pm 1.17 , \quad (82c)$$

which is reasonably close to the ratio of the energy yields of the  ${}^4\text{He}$  and  ${}^3\text{He}$  reactions of Eqs. (81) and (79), respectively, given by

$$(23.8 \text{ MeV}/5.45 \text{ MeV}) = 4.37 . \quad (83)$$

Of course, a key assumption in these highly simplistic considerations is that the cross sections for reactions (81) and (79) are about the same. This does not appear terribly unreasonable from our previous considerations in that both reactions (81) and (79) involve the same number of protons, namely, 1, in each of the nuclear reactants, and 2 protons in each of the nuclear products. While this may all be overly simplistic, it is, nevertheless, intriguing that this is consistent with the counterpart of the calculation in Eqs. (80a) and (80b) for the ratio of the cross section of Eq. (81) to that for the sodium reaction in Eq. (7). All of the factors are the same in calculating  $(R_{cr})_{D/Na}$  except that the ratio of the energy yields on the right side (not shown) in Eq. (80a) should be replaced by ( $23.8 \text{ MeV}/11.7 \text{ MeV}$ ) and the ratio of the empirical excess powers should be replaced by ( $4.87 \text{ W}/1.02 \text{ W}$ ). With these changes, Eq. (80b) is replaced by

$$(R_{cr})_{D/Na} = 12 . \quad (84)$$

It follows from Eqs. (84) and (80b) that the ratio of the cross sections for the reaction (81) producing  ${}^4\text{He}$  to that in Eq. (79) producing  ${}^3\text{He}$  is  $\sim 1$  and given by

$$(R_{cr})_{D/D} = 12/10.5 = 1.1 . \quad (85)$$

That these cross sections are almost the same seems reasonable in view of the fact that the deuteron and proton both contain the same amount of positive charge. Also, the fact that the cross section is slightly larger for the D-D reaction than for the D-p reaction seems reasonable in view of the relatively loose nuclear structure of the deuteron with two neutrons able to "reach out" in the former reaction more than one neutron in the latter reaction.

Cells 49 and 50 contained a light water-based  $Rb_2CO_3$  electrolyte ( $0.57 M$ ) that was tried at the author's suggestion to test the model.

While cell 50 exhibited no excess power, the other rubidium cell, cell 49, did evidence excess power. The excess powers in this case were lower than for the sodium or potassium cells, which seems reasonable in view of the fact that a calculation for rubidium as the incident ion along the lines of that in Eq. (73) for sodium shows that the latter should yield 2.4 times the excess power as compared to an otherwise identical rubidium cell. On correction for recalibration, cell 45 was calculated to have produced an approximate excess heat of

$$(37 \pm 17) \text{ kJ} . \quad (86)$$

An atomic absorption analysis was then conducted to check for strontium in the postrun electrolyte. Because of the Christmas vacation, Cal Poly Chemistry Department's atomic absorption machine was unavailable. The author was fortunate, then, to locate a state-of-the-art Hitachi flame photometer (model Z8100) at Geo-Monitor, Inc., in Hesperia, California, that also had a strontium lamp. The author is grateful to Mary Ann Lucas of Geo-Monitor for performing the strontium analysis and to the company for contributing this fine work to our research program at Cal Poly. The following results were attained in parts per million of strontium ("Parts per million" here refers to a concentration in terms of micrograms per millilitre of solution.):

Postrun electrolyte (cell 49) [treated with lanthanum. A "puratronic grade" of rubidium carbonate from Aesar (Johnson-Matthey) was employed for the electrolyte.]	(0.07 ± 0.01) ppm
Prerun electrolyte (cell 49) (treated with lanthanum)	(0.01 ± 0.00) ppm
Prerun electrolyte (cell 49) (not treated with lanthanum)	(0.00 ± 0.00) ppm
Prerun electrolyte that had been heated for 5 days to between 39 and 60°C in a sealed glass jar (cleaned with chromic acid) with pieces of prerun nickel cathode of the same mass and composition as the nickel cathode employed in cell 49. (I am thankful to N. J. Kertamus of Southern California Edison for suggesting this.) (treated with lanthanum)	(0.00 ± 0.00) ppm
Postrun electrolyte (cell 50) (treated with lanthanum)	(0.00 ± 0.00) ppm
Postrun electrolyte (cell 50) (not treated with lanthanum)	(0.00 ± 0.00) ppm

(87)

Treatment of the solution with lanthanum is prescribed to suppress interfering absorption lines from other elements that might have contributed to a false reading for strontium. I am grateful to Phrosty Chimiklis of the Cal Poly Chemistry Department and of the Chemistry Department at Victor Valley Community College for preparing the solutions with lanthanum and for arranging to have the atomic absorption analysis performed at Geo-Monitor.

An unsatisfactory aspect was that the postrun cathode for cell 49 was unavailable for any strontium testing since it had been used up in an attempt at a mass spectroscopic analysis that was thwarted by the large amount of rubidium compared with potential strontium and the inability of the spectroscope to obtain sufficient separation of the strontium and rubidium isotopes in the solubilized material. Nevertheless, it is felt that potential strontium contamination of the electrolyte by the cathode should have shown up in the solution achieved by "cooking" prerun cathode material in prerun electrolyte. As seen in the fourth item in Eq. (87), this achieved a concentration of (0.00 ± 0.00) ppm of strontium.

Now, the concentration of (0.07 ± 0.01) ppm of strontium in the postrun electrolyte of cell 49, as seen from Eq. (87), translates into (3.2 ± 0.4) µg of strontium for the 45-ml volume of electrolyte of cell 49. Based on the Rb-*p* reaction, Eq. (5), as the excess heat reaction, this strontium production should have been associated with an excess heat production of about

$$(37 \pm 6) \text{ kJ}, \quad (88)$$

which is in good agreement with the empirically determined value for the total excess heat generated by cell 49 given in Eq. (86).

This must be seen as stronger evidence for the present hypothesis than the previous calcium findings correlated with potassium cell operation since potentially contaminative background concentrations of strontium in the environment are small compared with background concentrations of calcium. Future studies are planned in which the amount of strontium produced is sufficient or is separated chemically from the rubidium to permit a mass spectrometric analysis. It is this, in the long run, that will be most convincing: Thus, if the ratio of the amount of  $^{86}\text{Sr}$  to that of  $^{88}\text{Sr}$  is the same as the ratio of the natural abundances of these isotopes (~0.12) we will know that the strontium was undoubtedly contaminative. On the other hand, if the ratio is closer to the order of magnitude of the ratio of the natural abundances of the hypothesized "parent" isotopes,  $^{85}\text{Rb}$  and  $^{87}\text{Rb}$  (~2.6), it will be a convincing signature of the present hypothesis. Not only is this experiment much easier than the outstanding

$^4\text{He}$  correlation experiment of Bush et al.,<sup>10</sup> but its potential for achieving this isotopic signature that would prove beyond the shadow of a doubt that the purported nuclear product is not the result of contamination guarantees that it could be a more definitive experiment.

Most recently, two independent attempts to see strontium in the postrun electrolyte of cell 49 have been unsuccessful. West Coast Analytical Service conducted a mass spectrometric study and saw no strontium of any sort down to a level of ~5 ppm. Similarly, Los Alamos National Laboratory was unable to detect elemental strontium in the postrun electrolyte of cell 49 down to a concentration of 50 ppb employing arc spectroscopy. (I am grateful to E. Storms for arranging this test.) So, perhaps proton fusion reactions of the sort schematized by Eqs. (42a), (42b), and (43c), rather than the rubidium (potassium)-proton reaction, is the basis for the excess heat in the light water case.

However, Miles and Bush<sup>60</sup> have indicated to the author that the strontium, if it is the nuclear product, should be found in the postrun cathode, and this is now being investigated via SIMS and Auger spectroscopy. Also, with regard to the possibility of calcium as the nuclear product in the operation of a potassium cell, Srinivasan<sup>61</sup> has apprised the author of the recent findings of a company in India that employs nickel cathodes, potassium salts, and heavy water in its commercial operation. Intrigued by a preprint of this manuscript via Srinivasan, they compared postrun electrolyte to prerun and found an otherwise inexplicably large concentration of calcium in the former, as compared to the latter, and have submitted a note for publication. If this is not via contamination, it could be accounted for on the basis of the author's reactions (10b) and (10c) in which a deuteron is added to a nucleus of potassium to yield a nucleus of calcium.

Finally, just before this manuscript was being sent to the printer, the preliminary SIMS analysis for the postrun electrode of cell 53 (light water-based 0.57 M rubidium carbonate electrolyte, platinum anode, and nickel cathode) and the prerun nickel material employed to fabricate the cathode became available. According to the analysis, two substances of weights 86 and 87, tentatively identified as "rubidium hydride" ( $^{85}\text{RbH}$  and  $^{87}\text{RbH}$ ), were found in the postrun cathode but not in the prerun nickel cathode material. The ratio of these substances were the same as that of the ratio of  $^{85}\text{Rb}$  to  $^{87}\text{Rb}$ . In addition, the ratio of "rubidium hydride" in the postrun electrode to rubidium was determined to be  $6.2 \times 10^{-5}$ . Note that the mass spectrograph associated with the SIMS is unable to distinguish between two substances having the same weight, so that  $^{86}\text{Sr}$  would look the same as  $^{85}\text{RbH}$  and  $^{86}\text{Sr}$ .

would appear the same as  $^{87}\text{RbH}$ . Now, in the author's estimation, the so-called "rubidium hydride" is very likely the strontium associated with the author's hypothesis of the light water excess heat reaction being a cold nuclear reaction. In support of this are the following. First, it would not be surprising on the basis of the model that the ratio of the amounts of  $^{86}\text{Sr}$  and  $^{88}\text{Sr}$  would be essentially the same as the ratio of the amounts of the parent isotopes of rubidium. Second, a simple calculation shows an intriguing correlation with the ratio  $6.2 \times 10^{-5}$  of the so-called "rubidium hydride" to rubidium: Cell 53 produced  $(3.6 \pm 0.2)$  MJ of excess heat, which for the reaction of Eq. (5) translates into a hypothetical number of strontium nuclei in the electrolyte for purposes of this calculation of  $(2.2 \pm 0.1) \times 10^{18}$ . On the other hand, the actual number of rubidium nuclei in the electrolyte was  $3.4 \times 10^{22}$ . And, the ratio of the former to the latter is then  $(6.5 \times 0.4) \times 10^{-5}$ , which is intriguingly close to the experimental ratio of  $6.2 \times 10^{-5}$ . Finally,  $\text{RbH}$  is very unstable, and the signals for  $\text{RbO}$  and  $\text{RbHO}$  were both much less than for the "rubidium hydride," whereas their greatest ability would imply a larger signal than for  $\text{RbH}$ .

At the low-power end of the calibration curve (0.0 to  $-0.3$  W), we have achieved our most spectacular gains of  $\sim 800$  to  $\sim 5000\%$  with several light water cells. In an effort to assess whether these high gains are meaningful or simply artifacts of the measurement process, the author suggested employing four different calibration curves for the  $\text{RbOH}$  cell corresponding to four different cell temperatures: 30, 33, 36, and  $39^\circ\text{C}$ . It was found in all cases checked that a high gain at one temperature (based on the appropriate calibration curve) translated into a high gain at the other three temperatures (based on their respective calibration curves). Thus, these spectacular gains may be genuine. However, excess powers for these gains never amounted to more than several watts. On the other hand, there seems to be little doubt about the results with our light water cells yielding gains from  $\sim 25\%$  to  $\sim 300\%$  accompanying higher input powers from several tenths of a watt up to  $\sim 15$  W. Certainly, Mills and Kneizys are to be commended for their work. The fact that in our preliminary studies excess powers and higher gains with the Mills-Kneizys-type cells have been much easier to attain and far more reproducible for us than has been the case for the heavy water cells employing palladium cathodes encourages us to recommend light water research to other research groups. It must be emphasized, however, that while gains have been more spectacular for our light water cells, we have not yet exceeded the peak excess powers of  $\sim 10$  W previously achieved in our heavy water work.

## XI. CONCLUSION

It is important to remember that the nuclear reactions presented here, with their dependence on the atomic lattice, are hypothetical at this stage. However, if the excess heat process discovered by Mills and Kneizys<sup>1</sup> and independently corroborated by Noninski<sup>2</sup> and Bush and Eagleton is a light water cold nuclear reaction (alkali-hydrogen reaction or other) in accord with the present thesis, it is of signal importance for this emerging branch of science. The realization of an important new reaction related to the Fleischmann-Pons excess heat effect, but discovered outside the cold fusion community, that can be achieved robustly and in a highly reproducible fashion using essentially ordinary water, could eventually result in a return to greater objectivity concerning cold fusion

on the part of the general scientific community. Additionally, if the light water work constitutes a subrevolution within cold fusion, as the author maintains, the economic ramifications could be immense in view of the relative expense of heavy water (approximately \$1000/gal) to that of deionized, or distilled, water (pennies per gallon).

Finally, it can be concluded that, should this general picture, in which the heavy water excess heat reactions and those of light water are viewed as two sides of a coin of a new realm, hold up under objective examination, it would be another step enroute to the creation of an essentially new branch of science, namely, the physics of low-energy nuclear transmutations.

## ACKNOWLEDGMENTS

I am indebted to H. Fox, editor of *Fusion Facts*, for stimulating this research by asking me privately near the end of the Como conference where I thought the recent work of R. Mills might fit into the scheme of things. G. Miley, editor of *Fusion Technology*, is thanked for his encouragement and interest. The comments of two anonymous referees for *Fusion Technology* have improved the presentation. R. Mills (Mills Technologies) is thanked for a preprint of his *Fusion Technology* paper. R. Bass, S. Chubb (Naval Research Laboratory), and E. Storms (Los Alamos National Laboratory) are appreciated for brief discussions of the novel chemistry of Mills and Farrell and their experimental results. R. Eagleton, my colleague in the Cal Poly cold fusion project (now the alkali-hydrogen fusion project) is appreciated as always for serving as a sounding board for my ideas. Southern California Edison is thanked for the funding that has made the Cal Poly cold fusion project possible over the last two years. Special thanks go to N. J. Kertamus as research coordinator for Southern California Edison for his help with funding and for his encouragement and abiding interest. It is a pleasure to thank Bose Corporation for financing my participation in the Como conference. Special thanks here to J. Veranth, vice president of engineering for Bose, and to D. Yansen, consultant to Bose.

## REFERENCES

1. R. MILLS and K. KNEIZYS, "Excess Heat Production by the Electrolysis of an Aqueous Potassium Carbonate Electrolyte and the Implications for Cold Fusion," *Fusion Technol.*, 20, 65 (1991).
2. H. FOX, Ed., *Fusion Facts*, Private Communication (June 1991); see also V. NONINSKI et al., "Observation of Excess Energy Effect During the Electrolysis of a Light Water Solution of  $\text{K}_2\text{CO}_3$ ," Abstracts for Contributed Papers for 2nd Annual Conf. Cold Fusion, Como, Italy, June 31-July 4, 1991.
3. H. FOX, Ed., *Fusion Facts*, Private Communication (July 1991).
4. R. MILLS and J. FARRELL, *The Grand Unified Theory*, Science Press (1989).
5. M. FLEISCHMANN and S. PONS, "Electrochemically Induced Nuclear Fusion of Deuterium," *J. Electroanal. Chem.*, 261, 301 (1989).
6. M. SRINIVASAN, "Nuclear Fusion in an Atomic Lattice: An Update on the International Status of Cold Fusion Research," *Curr. Sci.* (Apr. 1991).
7. E. STORMS, "Review of Experimental Observations About the Cold Fusion Effect," *Fusion Technol.*, 20, 433 (1991).

8. S. PONS and M. FLEISCHMANN, "Calorimetric Measurements on Palladium-Based Cathodes Polarized in Heavy Water," presented at the 2nd Annual Conf. Cold Fusion, Como, Italy, June 31-July 4, 1991.
9. M. McKUBRE et al., presented at 2nd Annual Conf. Cold Fusion, Como, Italy, June 31-July 4, 1991.
10. B. BUSH et al., "Helium Production During the Electrolysis of D<sub>2</sub>O in Cold Fusion Experiments," *J. Electroanal. Chem.*, 304, 271 (May 1991).
11. R. BUSH and R. EAGLETON, "A Calorimetric Study of the Excess Heat Effect in Thin Films of Palladium," presented at 2nd Annual Conf. Cold Fusion, Como, Italy, June 31-July 4, 1991.
12. R. HUGGINS et al., "Two Fast Mixed Conductor Systems: Deuterium and Hydrogen in Palladium—Thermal Measurements and Experimental Considerations," *Proc. Workshop on Cold Fusion Phenomena*, Santa Fe, New Mexico, May 23-25, 1989.
13. A. APPLEBY et al., "Evidence for Excess Heat Generation Rates During Electrolysis of D<sub>2</sub>O in LiOD Using a Palladium Cathode: A Microcalorimetric Study," *Proc. Workshop on Cold Fusion Phenomena*, Santa Fe, New Mexico, May 23-25, 1989.
14. C. SCOTT et al., "Measurement of Excess Heat and Apparent Coincident Increases in Neutron and Gamma Ray Count Rates During the Electrolysis of Heavy Water," *Fusion Technol.*, 18, 103 (1990).
15. D. HUTCHINSON et al., "Initial Calorimetry Experiments in the Physics Division at ORNL," *Proc. 1st Annual Cold Fusion Conf.*, Salt Lake City, Utah, March 28-31, 1990.
16. J. BOCKRIS et al., "A Review of the Investigations of the Fleischmann-Pons Phenomena," *Fusion Technol.*, 18, 11 (1990).
17. M. McKUBRE et al., "Calorimetry and Electrochemistry in the DPd System," *Proc. 1st Annual Conf. Cold Fusion*, Salt Lake City, Utah, March 28-31, 1990, p. 20.
18. B. LIEBERT and B. LIAW, "Cold Fusion with Molten Salts," *Proc. 8th World Hydrogen Energy Conf. Cold Fusion Supplement*, Honolulu, Hawaii, July 23-24, 1990.
19. R. EAGLETON and R. BUSH, "Calorimetric Evidence Supporting the Transmission Resonance Model for Cold Fusion," *Fusion Technol.*, 20, 239 (1991).
20. M. FLEISCHMANN et al., "Method and Apparatus for Power Generation," International Application Published Under Patent Cooperation Treaty (PCT/US90/01328, International Publication Number WO 90/10935) (Mar. 13, 1989).
21. M. MAYER, "On Closed Shells in Nuclei," *Phys. Rev.*, 74, 235 (1948).
22. J. JENSEN et al., "On the 'Magic Numbers' in Nuclear Structures," *Phys. Rev.*, 75, 1766 (1949).
23. J. JENSEN et al., "Interpretation of the 'Special' Nucleon Numbers of Nuclear Structure in Terms of a Shell Model," *Naturwiss.*, 36, 155 (1949).
24. P. TIPLER, *Foundations of Modern Physics*, p. 446, Worth Publishers (1969).
25. J. SCHWINGER, "Nuclear Energy in an Atomic Lattice," *Proc. 1st Annual Conf. Cold Fusion*, Salt Lake City, Utah, March 28-31, 1990.
26. C. WALLING and J. SIMONS, "Two Innocent Chemists Look at Cold Fusion," *J. Phys. Chem.*, 93, 12, 4696 (1989).
27. R. BUSH, "The Transmission Resonance Model (TRM) for Cold Fusion Updated: Explication of Neutron Emission," presented at 2nd Annual Conf. Cold Fusion, Como, Italy, June 31-July 4, 1991.
28. R. BUSH and R. EAGLETON, "Neutron Emission from Electrolytic Cells: Correlation with Current Density," presented at 2nd Annual Conf. Cold Fusion, Como, Italy, June 31-July 4, 1991.
29. J. MARSHALL, *Electrolytic Solutions*, Private Communication (1990).
30. V. NONINSKI and C. NONINSKI, "Determination of the Excess Energy Obtained During the Electrolysis of Heavy Water," *Fusion Technol.*, 19, 364 (1991).
31. R. BUSH, "Cold 'Fusion': The Transmission Resonance Model Fits Data on Excess Heat, Predicts Optimal Trigger Points, and Suggests Nuclear Reaction Scenarios," *Fusion Technol.*, 19, 313 (1991).
32. E. STORMS, Los Alamos National Laboratory, Private Communication (1990).
33. S. SZPAK et al., "Reliable Procedure for the Initiation of the Fleischmann-Pons Effect," presented at 2nd Annual Conf. Cold Fusion, Como, Italy, June 31-July 4, 1991.
34. B. BUSH and M. MILES, presented at 2nd Annual Conf. Cold Fusion, Como, Italy, June 31-July 4, 1991.
35. E. STORMS, Los Alamos National Laboratory, Private Communication (May 1991).
36. T. MATSUMOTO, "Cold Fusion Observed with Ordinary Water," *Fusion Technol.*, 17, 490 (1990).
37. M. RAGHEB and G. MILEY, "On the Possibility of Deuteron Disintegration in Electrochemically Compressed D<sup>+</sup> in a Palladium Cathode," *Fusion Technol.*, 16, 243 (1989).
38. P. PAOLO, *Nature*, 338, 711 (1989).
39. R. BUSH, "A Transmission Resonance Model for Cold Fusion," presented at the Winter Meeting of the American Society of Mechanical Engineers, San Francisco, California, December 12, 1989.
40. R. BUSH and R. EAGLETON, "'Cold Nuclear Fusion': A Hypothetical Model to Probe an Elusive Phenomenon," *J. Fusion Eng.*, 9, 397 (1990).
41. E. SEGRÉ, *Nuclei and Particles*, 2nd ed., p. 381, W. A. Benjamin, Inc., Reading, Massachusetts (1977).
42. H. FOX, Ed., *Fusion Facts*, Private Communication (1990).
43. G. PREPARATA, "Theories of 'Cold' Nuclear Fusion: A Review," Preprint, National Cold Fusion Institute (Oct. 1990).
44. S. CHUBB, Naval Research Laboratory, Private Communication (July 1991).
45. S. JONES, "Current Issues in Cold Fusion Research: Heat, Helium, Tritium, and Energetic Particles," August 1991 (unpublished).
46. H. PUTHOFF, Institute for Advanced Studies, Private Communication (Aug. 1991).

47. S. CHUBB and T. CHUBB, "An Explanation of Cold Fusion and Cold Fusion By-Products Based on Lattice-Induced Nuclear Chemistry," submitted to *Fusion Technol.*

48. P. HAGELSTEIN, "Coherent and Semi-Coherent Neutron Transfer Reactions," presented at 2nd Annual Conf. Cold Fusion, Como, Italy, June 31-July 4, 1991.

49. F. MAYER and J. REITZ, "Nuclear Energy Release in Metals," *Fusion Technol.*, 19, 552 (1991).

50. J. McNALLY, Jr., "Cold Fusion and Grasser Prospects," *Fusion Technol.*, 7, 331 (1985).

51. R. BASS, "QRT: Quantum Resonance Triggering Principle," submitted to *Fusion Technol.*

52. R. ROUT, A. SHYAM, M. SRINIVASAN, and A. BANSAL, "Copious Low Energy Emissions from Pd Loaded with Hydrogen or Deuterium," *Ind. J. Technol.*, 29, 571 (1991).

53. M. JÄNDEL, "The Fusion Rate in the Transmission Resonance Model," *Fusion Technol.*, 21, 176 (1992).

54. R. BUSH, "The DeBroglie Wave Derivation for Material Particle Diffraction Re-Examined: A Re-Derivation Without Matter Waves," *Nuovo Cimento*, 44, 683 (1985).

55. R. BUSH, "A Theory of Particle Interference Based upon the Uncertainty Principle," *Nuovo Cimento*, 34, 363 (1982).

56. A. LANDE, *New Foundation of Quantum Mechanics*, Cambridge University Press (1965).

57. L. MICHELS, Oak Ridge National Laboratory, Private Communication (Fall 1989).

58. E. PYE, California State Polytechnic University, Private Communication (1991).

59. J. BOCKRIS, *Proc. NSF/EPRI Workshop*, 1989.

60. M. MILES and B. BUSH, China Lake Naval Air Weapons System Command, Private Communication (May 1992).

61. M. SRINIVASAN, Bhabha Atomic Research Centre, Private Communication (May 1992).

## Faradaic Efficiencies Less Than 100% during Electrolysis of Water Can Account for Reports of Excess Heat in "Cold Fusion" Cells

Jonathan E. Jones, Lee D. Hansen,\* Steven E. Jones, David S. Shelton, and James M. Thorne

Departments of Physics and Chemistry, Brigham Young University, Provo, Utah 84602

Received: September 30, 1994; In Final Form: December 23, 1994\*

The purpose of this study is to evaluate claims of excess heat generation during water electrolysis. Several cells were constructed and operated similarly to low-current-density cells described in the literature. All produced excess heat as defined and calculated in the literature reports, but the production of excess heat could be readily terminated by the introduction of various barriers to the migration of hydrogen and oxygen. Remarkably, published reports of excess heat fail to disprove the presence of decreased faradaic efficiency (e.g., current that oxidizes H<sub>2</sub> or reduces O<sub>2</sub>) or systematic calorimetric errors. Illustrative examples of both problems are given. Thus, failure to rule out prosaic explanations probably invalidates all the currently available reports of excess heat in both light water-Ni/Pt and heavy water-Pd/Pt cells. There is no compelling evidence that excess heat is of a nuclear origin in such electrolytic cells.

### Introduction

Since Fleischmann and Pons' <sup>1</sup> announcement of the generation of excess heat by electrolysis with a Pd cathode in D<sub>2</sub>O, many experiments have been done in an attempt to duplicate or even improve upon their results. More recently, excess heat has also been observed during electrolysis of light water with K<sub>2</sub>CO<sub>3</sub> electrolyte, a Ni cathode, and a Pt anode. The purpose of this study is to evaluate these literature reports to determine the source of the reported excess heat.

The excess heat rate in an open cell is given by eq 1

$$\% \text{ excess heat rate} = 100(q_{\text{meas}} - q_{\text{cell}})/q_{\text{cell}} \quad (1)$$

where  $q_{\text{meas}}$  is the heat rate measured in a calorimeter. The value of  $q_{\text{cell}}$ , assuming 100% faradaic efficiency, is calculated by eq 2

$$q_{\text{cell}} = I(E_{\text{cell}} - E_b) \quad (2)$$

where  $I$  is the cell current,  $E_{\text{cell}}$  is the total voltage across the cell, and  $E_b$  is the thermoneutral potential.  $E_b$  is given by eq 3

$$E_b = \Delta H/F \quad (3)$$

where  $\Delta H$  is the enthalpy change for formation of water and  $F$  is the Faraday constant. Calculations using  $\Delta H$  values from ref 2 give  $E_b = 1.48$  V for light water and 1.53 V for heavy water. The assumption of 100% faradaic efficiency, required for eq 2 to be valid, means that the electrical current is consumed by the reaction  $2\text{H}_2\text{O} \rightarrow 2\text{H}_2 + \text{O}_2$  and by no other reaction.

To date, no compelling evidence has been presented for any clear explanation of the origin of the excess heat observed. The excess heat could come from unsuspected chemical reactions, mechanical or electrical work, experimental error, nuclear fusion, or new chemistry. This paper will present the results of experiments showing that reactions of hydrogen and oxygen at the electrodes probably account for many previous observations of excess heat. Other reports of excess heat are shown to result from systematic calorimetric error. Thus, no new physics or

chemistry is warranted to explain calorimetric measurements on such cells.

Information in the papers reviewed for this study is insufficient to determine whether the reports of excess heat can definitely be attributed to the reactions associated with eq 4



but neither do any of the papers give compelling evidence that it cannot be. For example, some papers do not include the cell voltage and/or current, and therefore the total input power cannot be calculated. An excess heat rate greater than the total input power, i.e.,  $I E_{\text{cell}}$ , cannot be attributed to a faradaic efficiency <100%. Mills et al.<sup>3</sup> make the only clear claim to such an excess heat rate, but their use of pulsed power and uncertainty about calorimetric accuracy complicates interpretation of their work. Neither can faradaic efficiency explain excess heat generated in a closed cell with the recombiner inside the calorimeter. Bush et al.<sup>4</sup> make claim to observing excess heat this way, but the description of their calorimeter, although recently published, remains incomplete. Most of the papers reviewed have addressed the issue of faradaic efficiency, and all assumed 100% for various reasons, but without compelling experimental evidence. To provide compelling evidence against reactions of H<sub>2</sub> and O<sub>2</sub> as the source of excess heat, the faradaic efficiency must be measured simultaneously with excess heat.

In considering the possible reactions of H<sub>2</sub> and O<sub>2</sub>, Srinivasan et al.<sup>5</sup> suggest "...if the applied voltage is more than 2.96 V (as in most of our experiments) in order to generate apparent excess power of say 50% the recombination fraction has to be more than 50%. Thus excess heat margins of 50% or more measured in some of our experiments, particularly in the low input power range, cannot be explained away on the basis of recombination effects." This argument is based on the assumption that the faradaic efficiency cannot be less than 50% under any condition and ignores problems inherent in eq 1 when  $E_{\text{cell}}$  is near  $E_b$ . Noninski<sup>6</sup> argues that nickel is a poor catalyst for recombination, but in fact, nickel, platinum, and palladium are among the best catalysts for the combination of hydrogen and oxygen.<sup>7</sup> Srinivasan et al.,<sup>5</sup> Mills et al.,<sup>3</sup> Noninski,<sup>6</sup> and Miles et al.<sup>8</sup> all measured the faradaic efficiency of cells similar to those used in their heat measurements, but none measured heat and gas production rates simultaneously. Their evidence against

\* Corresponding author: Dr. Lee D. Hansen, Chemistry, BYU, Provo, Utah 84602. Phone 801-378-2040. FAX 801-378-5474.

<sup>†</sup> Abstract published in *Advance ACS Abstracts*, April 1, 1995.

reaction 4 occurring is thus not compelling. After arguing that recombination could not be the source of excess heat in his experiments, Nonniski<sup>6</sup> says "The problem of recombination is a crucial one ... , and it deserves special attention in any further experiments." In an attempt to increase the production of excess heat, Mallove<sup>9</sup> assembled a list of "Protocols for Conducting Light Water Excess Energy Experiments." Many of these protocols enhance the rate of reactions of H<sub>2</sub> and O<sub>2</sub> at the electrodes.

Experimental error also cannot be ruled out as the source of apparent excess heat because most papers do not give enough experimental detail to fully assess the methods used. Most continue to use "freshman-level"<sup>10</sup> home-built calorimeters with all their inherent uncertainties rather than switch to proven, commercially available designs. It is often impossible for the reader to detect an error from simply reading a paper even when the author tries very hard to give explicit details. Experimenters have frequently failed to follow normal protocols for accurate calorimetric measurements.<sup>11</sup> For example, Notoya's demonstration at the Third International Conference on Cold Fusion in Nagoya, Japan, in 1992 showed a Ni-light water cell running approximately 10 °C warmer than a resistor-heated control cell with supposedly the same input of thermal power (i.e., power equaled  $I(E_{heater})$  in the control cell and  $I(E_{cell} - E_h)$  in the electrolysis cell with  $E_{heater} = E_{cell} - E_h$ ). By measurement of the voltage drop in a portion of exposed heater lead wire, it was discovered that a resistance of 2.0 Ω in the heater leads accounted for 36% of the total resistance in the control cell heater circuit. In contrast, power loss was negligible in the leads to the electrolysis cell. Thus, 36% of the total power going to the control cell was being dissipated from the leads into the air, and not into the control cell, making it appear cooler than the electrolysis cell. The temperature difference in this demonstration did not clearly indicate excess heat but rather experimental error. A reader of the resulting publication<sup>12</sup> could not detect this problem, however, because the heater leads were not described. None of the publications by Mills et al.,<sup>3</sup> Bush et al.,<sup>4</sup> or Miles et al.<sup>8</sup> contain details on the design and construction of their calibration heaters. Electrical calibration of calorimeters is notoriously difficult, particularly at high power.<sup>13</sup>

We will not attempt to prove that all observations of excess heat are due to either a reduced faradaic efficiency or experimental error. Evaluating all reports of excess heat in sufficient detail would, in fact, be impossible because critical information is missing from the published reports. Furthermore, the burden of providing adequate evidence that the reactions of H<sub>2</sub> and O<sub>2</sub>, or calorimetric errors, are not the source of reported excess heat rests on the experimenters. The results reported in this paper support the hypothesis that reaction 4 can explain most available reports to date of excess heat in both Pd/LiOD(D<sub>2</sub>O)/Pt and Ni/K<sub>2</sub>CO<sub>3</sub>(aq)/Pt cells when running at low current densities. Compelling evidence against a null hypothesis must be presented before considering new theories that propose other origins for excess heat. We also note that none of the claims that excess heat is of nuclear origin have been confirmed by unequivocal detection of equivalent amounts of nuclear byproducts formed during excess heat production.<sup>14</sup>

## Experimental Section

The first two experiments used the cell and circuit shown in Figure 1. This cell uses the same materials and current density typical of light water cells where excess heat has been reported. In experiment 1, the cell had no glass tubes (K) surrounding the electrodes, and the mixed gas was vented in a single tube

rather than through tubes A and F as shown. Experiment 2 was designed to hinder reactions of hydrogen and oxygen as much as possible. To accomplish this, a glass tube closed at the bottom and open at the top was placed around the Pt anode. The top was open to the electrolyte to allow electrical conductivity but minimal transport of dissolved gases. A second tube open at the bottom enclosed the nickel cathode to conduct evolved oxygen gas to vent-tube F. These tubes, constructed from ordinary borosilicate glass, serve as a barrier to inhibit migration of evolved gases between the electrodes. The tubes around the electrodes were vented through separate tubes, A and F, so the gases could not mix before leaving the calorimeter. Since the increased electrolytic path length resulted in increased cell resistance, the voltage was adjusted to keep the current density, and therefore the expected excess heat rate, constant during the experiment.

Figure 2 shows the cell configuration for experiments 3 and 4. The cell circuitry was the same as that used for experiments 1 and 2. The glass frit at the bottom of the cell was used to bubble dry oxygen or nitrogen through the cell at a constant flow rate. This rate was controlled by a two-stage pressure regulator and a fixed length of glass capillary tubing as a flow restrictor: in experiment 3, 60 cm of 30 μm i.d.; in experiment 4, 12 cm of 15 μm i.d.

The cathodes for experiments 1–3 were flat, 1 cm<sup>2</sup> pieces of sintered Ni, and for experiment 4, a 4 cm<sup>2</sup> piece of sintered Ni was curled in a semicircle around the Pt anode. The sintered Ni used in these experiments was 1 mm thick. Sintered Ni is made by hot pressing a mat of Ni wire or powder. It is commonly used for filtration of gases and liquids and has a very high surface area compared with Ni foil.

In experiments 1–3, the nickel was stored in an airtight container and handled with plastic gloves to avoid contamination of the electrode surfaces. In experiment 4, the electrodes were cleaned with a solution of 0.1 M HCl in methanol and then rinsed in distilled water.

Two further experiments (beyond 1–4) were done using the cell in Figure 2. In experiment 5, the electrolyte was replaced with 0.6 M Na<sub>2</sub>CO<sub>3</sub>. In experiment 6, the Ni electrode was replaced with a 1 cm<sup>2</sup> piece of Pd foil, and the electrolyte was replaced with 0.3 M LiOD in heavy water.

Data were collected on a near-continuous basis over a 6 month period during the performance of these six experiments.

In experiments 3 and 4 with gas flowing through the electrolysis cell, the base line was established both by (a) measuring the calorimeter output signal as a function of gas flow rate with no electrolysis occurring and (b) calculating the expected heat rate at different gas flow rates with eq 5.

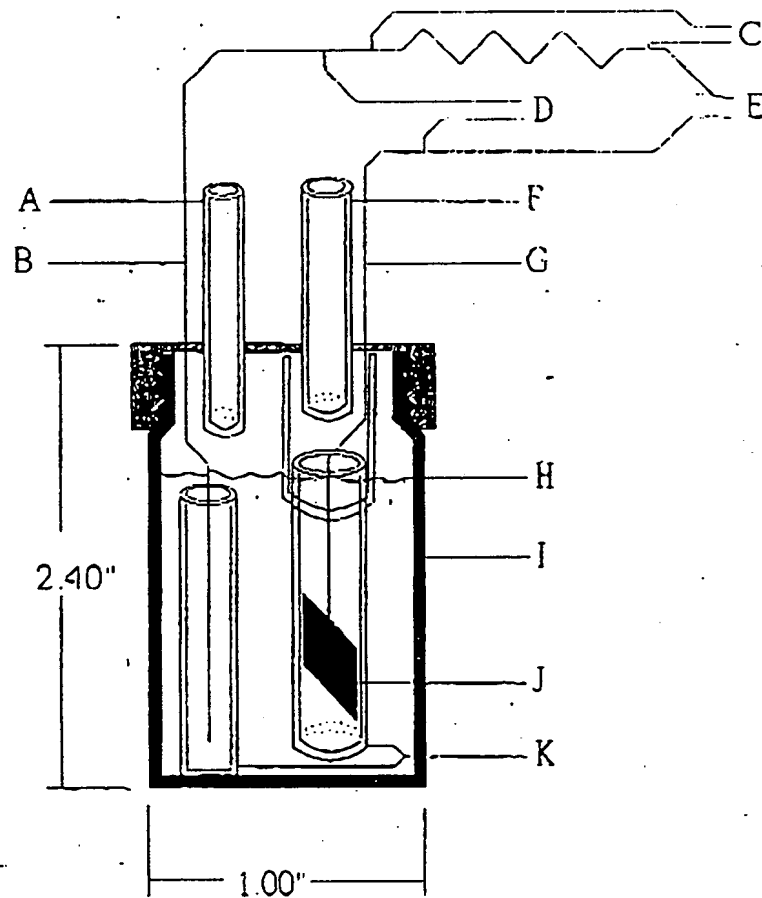
$$q_{\text{gasflow}} = I(r_{\text{gas}})(\text{vapor pressure of H}_2\text{O}/RT)\Delta H_{\text{vap}} \quad (5)$$

In eq 5,  $q_{\text{gasflow}}$  is the heat rate resulting from gas flowing at the volumetric rate  $r_{\text{gas}}$ .  $R$  is the gas constant,  $T$  is the Kelvin temperature, and  $\Delta H_{\text{vap}}$  is the enthalpy change for vaporization of water. The vapor pressure over 0.6 M K<sub>2</sub>CO<sub>3</sub> was assumed to be the same as the vapor pressure over pure water. Vapor pressure data were taken from ref 15 and  $\Delta H_{\text{vap}}$  from ref 2. The base lines calculated with eq 5 agreed with measured base lines to within ±100 μW, as shown in Figure 3. The measured base line was the same for flowing either nitrogen or oxygen.

## Apparatus

The cells were powered by a Tenmars Model 72-420 dc power supply operated in constant voltage mode. The cell voltage,

## Accounting for Excess Heat in "Cold Fusion" Cells

*J. Phys. Chem., Vol. 99, No. 18, 1995 6975*

**Figure 1.** Cell used for experiments 1 and 2. (A) Tube for evolved oxygen, (B) no. 24 Pt wire, (C) 10 kΩ wire-wound potentiometer adjusted to either 2 kΩ (experiments 1–3) or 5 kΩ (experiment 4) and calibrated for voltage measurements to determine current, (D) cell voltage, (E) leads to power supply—no. 32 Cu wire, (F) tube for evolved hydrogen, (G) no. 22 Ni wire, (H) 0.6 M K<sub>2</sub>CO<sub>3</sub> level, (I) glass vial, (J) 1 cm × 1 cm sintered Ni, and (K) glass tubes. Tubes A and F and wires E extend out of the boundaries of the calorimeter.

calorimeter output, and voltage across the calibrated resistor (Figure 1) were recorded with a strip chart recorder and Keithley Model 195 digital multimeter for experiments 1 and 2. For the rest of the experiments, data were recorded at 60 s intervals using the digital multimeter and a computerized data acquisition system.

A Hart Scientific Model 4225, isothermal, differential, heat conduction calorimeter was used to make the heat rate measurements. It was operated at 25.0 °C for experiments 1 and 2 and at 30.4 °C for the remainder of the experiments. Both sides of the calorimeter were calibrated electrically with the heaters in each calorimeter cell. The calorimeter cells consist of nickel-plated aluminum blocks with a cylindrical cavity 32 mm in diameter and 75 mm deep. The calibration heaters are 1 kΩ wire-wound, low-temperature-coefficient resistors cemented into holes drilled in the corners of the blocks. Separate pairs of matched leads are used to measure current and voltage and deliver power to the heater. Further details of heater construction and calibration test data are available from the manufacturer, Hart Scientific. The calorimeter cell and cover completely surround the electrolysis cell, so the distribution of heat generated by the electrolysis cell closely duplicates heat generated by the calibration heater, and thus systematic errors in heat rate measurement are negligible. The base line of this calorimeter is reproducible to <0.5 μW. The absolute accuracy in the configuration used for these experiments with several wires and tubes connected through the cell lid is probably better than 10 μW when no gas is flowing through the electrolysis cell. When gas is flowing through the cell from an external

source, fluctuations in gas flow rate cause a 100 μW uncertainty in the base line (see Figure 3). In the experiments described here, the calorimetric time constant is determined by the time constant for heat flow from the sample to the detectors. This time constant was experimentally established to be between 5 and 10 min and therefore was short compared to the time period of data gathering.

### Results

Table I shows the results for experiments 1a and 1b with the cell operating at 0.96 and 1.66 mA, respectively. The excess heat rate ( $q_{ex} = q_{ex,ex} - q_{cell}$ ) increased 153 μW with the increase in current, but the input power ( $q_{in}$ ) increased 377 μW.

Figure 4 and Table I show the results obtained in experiment 2 with the cell shown in Figure 1: first, with the glass tubes in place (Table I, expt 2a), then with the tubes off (Table I, expt 2b), and again with the tubes on (Table I, expt 2c). When the tubes were off, the input power was lower, but the heat rate measured by the calorimeter was higher. The increase in heat rate, along with the decrease in input power, gave up to 114% excess heat while the tubes were off. While the tubes were on, the excess heat was only ±17%, which is consistent with no measurable excess heat at the accuracy of this experiment.

In experiment 3a, nitrogen was bubbled through the cell at 1.7 mL min<sup>-1</sup> for several hours while measurements were made. Then the gas was changed to oxygen. The results with nitrogen (experiment 3a) and with oxygen flowing at 1.2 mL min<sup>-1</sup> (experiment 3b) are given in Table I. When nitrogen was

TABLE 1: Representative Results from Experiments 1-6

expno.	$q_{\text{max}} (\mu\text{W})$	I (mA)	$E_{\text{cell}} (\text{V})$	$q_{\text{cell}} (\mu\text{W}) = [I(E_{\text{cell}} - E_b)]$	$q_{\text{ex}} (\mu\text{W}) = [q_{\text{max}} - q_{\text{cell}}]$	% excess	glass tubes or gas	cathode size ( $\text{cm}^2$ )
1a	743	0.96	1.83	336	407	121	none	1
1b	1,274	1.66	1.91	713	560	78	none	1
2a	732	1.02	2.09	622	110	18	glass tubes	1
2b	803	1.04	1.86	395	407	103	none	1
2c	656	1.01	2.18	707	-51	none	glass tubes	1
3a	278	1.04	1.84	374	-96	none	$N_2$	1
3b	1,609	1.08	1.61	140	1,468	1049	$O_2$	1
4a	3,861	4.17	2.04	2,335	1,526	65	none	4
4b	10,756	8.08	2.61	9,130	1,626	18	none	4
4c	6,588	5.73	2.62	6,532	55.8	1	$N_2$	4
4d	7,415	5.68	2.72	7,043	372	5	$N_2$	4
6a	2,395	1.65	2.70	1,931	464	24	none	1
6b	2,071	1.60	2.81	2,048	23	1	$N_2$	1
6c	2,651	1.60	2.81	2,048	603	29	none	1

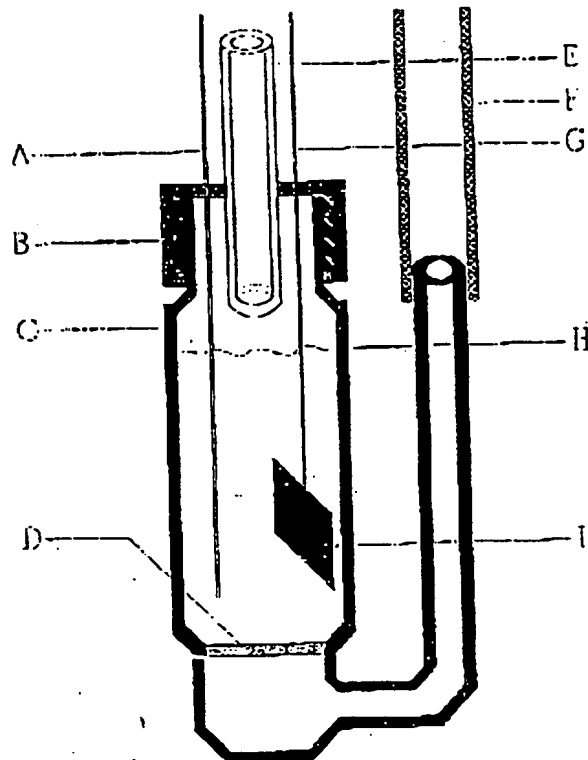


Figure 2. Cell used in experiments 3 and 4. (A) no. 24 Pt wire, (B) plastic cap, (C) glass test tube, (D) fine glass frit, (E) tube for exiting gases, (F) tube for incoming gases—attached to 30 (or 15)  $\mu\text{m}$  i.d. glass tubing and gas system, (G) no. 22 Ni wire, (H) 0.6 M  $K_2CO_3$  level, (I) 1 cm  $\times$  1 cm sintered Ni. Wires A and G are attached to no. 32 Cu wire leads and the circuit shown in Figure 1. Wires A and G and tubes E and F extend beyond the boundaries of the calorimeter.

flowing through the cell, the calculated heat rate was within the uncertainty of the measured heat rate under these conditions, i.e.,  $\pm 100 \mu\text{W}$ . Thus no excess heat was found. The results obtained with  $O_2$  flowing are shown graphically in Figure 5. Initially (at time = 15 min in Figure 5) the oxygen flow rate was started at 2.0  $\text{mL min}^{-1}$ . At this flow rate, the cell voltage dropped below 1.48 V, resulting in a negative  $q_{\text{cell}}$ , as shown in Figure 5, at  $15 < t < 30$  min. At 30 min the  $O_2$  flow rate was decreased to 1.2  $\text{mL min}^{-1}$ , and at 100 min it was increased to 2.2  $\text{mL min}^{-1}$  for a short time. Again the cell voltage dropped below 1.48 V. When the flow rate was again decreased to 1.2  $\text{mL min}^{-1}$  (at  $t = 130$  to 1100 min, Figure 5) and left constant, the cell voltage fluctuated between 1.42 and 1.84 V. The calorimeter output does not show these fluctuations because the calorimeter time constant is too long. The calculated excess heat rate ranged up to 750% when  $O_2$  was flowing through the

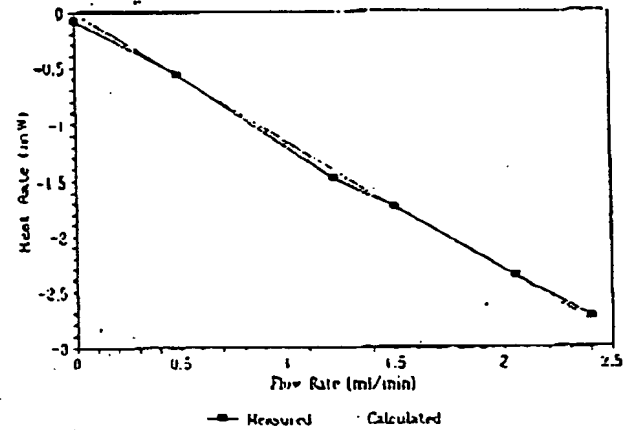


Figure 3. Measured and calculated (see eq 1) base lines with dry  $N_2$  or  $O_2$  gas flowing through the cell.

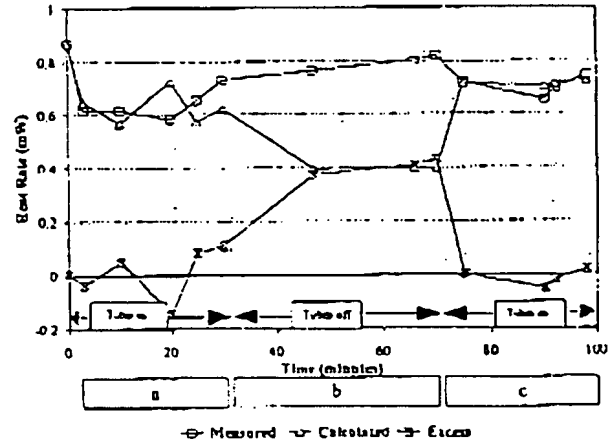


Figure 4. Results of experiment 2.

cell. When the cell voltage equals 1.48 V, note that eq 1 predicts infinite excess heat rate if  $q_{\text{max}}$  is not exactly zero.

Experiment 4 was done to determine the effect of electrode surface area by replacing the 1  $\text{cm}^2$  Ni electrode with a 4  $\text{cm}^2$  Ni electrode cut from the same piece of sintered Ni. Table 1 shows an excess heat rate of 1526 and 1626  $\mu\text{W}$  (65 and 18%), respectively, for experiments 4a and 4b with no gases flowing. This result can be compared with that of experiment 2b at the same current density, which showed an excess heat rate of 407  $\mu\text{W}$  (103%) (see Table 1). Thus, the absolute excess heat rate observed increased by nearly a factor of 4. Comparing experiments 4a and 4b shows that the absolute excess heat rate increased slightly, if at all (i.e., by  $100 \pm 100 \mu\text{W}$ ), when the current was doubled and the input power was increased by 6795

## Accounting for Excess Heat in "Cold Fusion" Cells

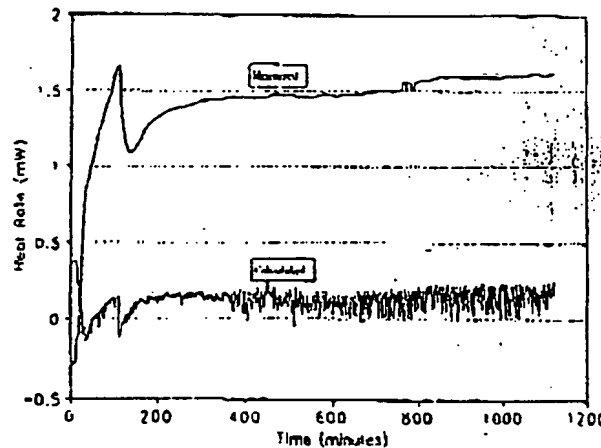
*J. Phys. Chem., Vol. 99, No. 18, 1995 6977*

Figure 5. Results of experiment 3 with oxygen flowing. The calculated heat rate is equal to  $I(E_{cell} - 1.18 \text{ V})$ .

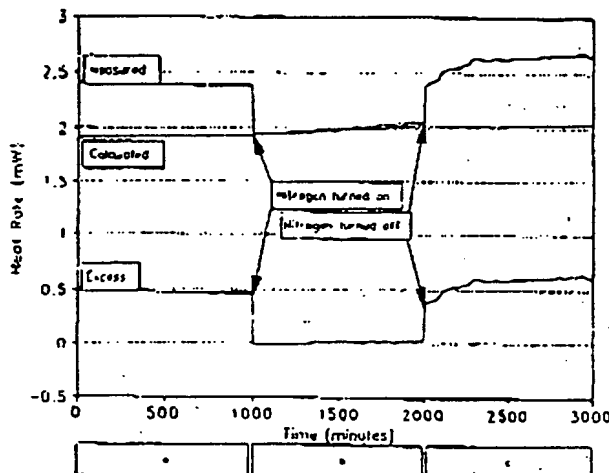


Figure 6. Results of experiment 6 using Pd foil in 0.3 M LiOD.  $\mu\text{W}$ . The excess heat rate dropped below  $400 \mu\text{W}$  when the cell was purged with nitrogen to reduce the concentrations of dissolved  $\text{H}_2$  and  $\text{O}_2$ . (See Table 1, expts 4c,d.)

With  $\text{Na}_2\text{CO}_3$  as the electrolyte in the cell, only a small amount of excess heat was observed. A small drop of liquid detergent was then added to the electrolyte, after which the observed excess heat rate increased to the same range as that observed in cells using  $\text{K}_2\text{CO}_3$  as the electrolyte. Because the measured heat rate showed large fluctuations, no numerical data are given in Table 1.

In experiment 6, the Ni electrode was replaced with Pd foil and the electrolyte was replaced with 0.3 M LiOD in  $\text{D}_2\text{O}$ . The observed excess heat was about  $500 \mu\text{W}$  (25%) at  $0.8 \text{ mA/cm}^2$  (see Table 1). The excess heat was readily eliminated by flowing  $\text{N}_2$  gas through the cell (see Figure 6). This experiment was performed with a variety of sizes of Pd foil and wire. Higher percentages of excess heat were obtained at lower current densities while at higher current densities, excess heat was completely eliminated.

Notably, these results are expressed in  $\mu\text{W}$  quantities due to the limited size of the cells that can be accommodated in the calorimeter. It is important to realize that current density is the same magnitude as in the reviewed literature (except refs 1, 8, 16, and 17), as is also the percent excess heat.

#### Discussion

Excess heat was observed with all the cells tested in this study, but the results clearly show it was due solely to reaction

of  $\text{H}_2$  (or  $\text{D}_2$ ) and  $\text{O}_2$  to produce  $\text{H}_2\text{O}$  (or  $\text{D}_2\text{O}$ ) in the cell. During electrolysis, the solution around the cathode becomes saturated with hydrogen while the solution around the anode becomes saturated with oxygen. In cells without separators, dissolved oxygen is free to migrate to the cathode and hydrogen can migrate to the anode. If hydrogen is oxidized at the anode and oxygen is reduced at the cathode or if hydrogen and oxygen simultaneously come in contact with a catalytic surface, reaction 4 takes place and the faradaic efficiency is <100%. Experiment 2 demonstrates that by restricting the migration of gases between electrode surfaces the production of excess heat can be effectively quenched.

The heat rate from reaction 4 can be obtained from eq 6

$$q_{\text{ex}} = I\Delta H_i f_{\text{gas}}/F \quad (6)$$

where  $f_{\text{gas}}$  is the fraction of evolved gas reacted. The value of  $f_{\text{gas}}$  depends on several factors, including the cathode and anode materials, geometry of the cell, current density, and mixing in the cell. Assuming that 50% of the evolved gas reacts in a typical light water cell ( $I = 1 \text{ mA}$ ,  $E_{\text{cell}} = 1.8 \text{ V}$ ), eqs 1 and 3 predict a measured heat rate 2.3 times the expected heat rate. This is consistent with results reported by Srinivasan et al.,<sup>3</sup> Bush,<sup>4</sup> Mills et al.,<sup>5</sup> and Nonnisski.<sup>6</sup> Oriani has reported faradaic efficiencies of 50 to 78% from measured gas flow rates of  $\text{Ni}/\text{K}_2\text{CO}_3$  in light water/Pt cells.<sup>18</sup>

One of the most common configurations of light water cells reporting large excess heat rates has a Pt anode wound in a spiral around a Ni cathode, a configuration that probably reduces the resistance of the cell, lowers  $E_{\text{cell}}$  for a given current, and increases the chance of reaction of  $\text{H}_2$  and  $\text{O}_2$ . Both the reduced cell voltage and increased rates of  $\text{H}_2$  and  $\text{O}_2$  reactions would increase the excess heat calculated by eq 1. Experiment 3 showed that faradaic efficiency could be reduced to less than 5% by bubbling oxygen through the cell. The flowing gas thoroughly mixes the cell contents and brings oxygen to the surface of the nickel cathode. This experiment shows that some cell configurations would substantially increase the reaction rate of the evolved gases. The rate of reaction 4 and hence the excess heat rate should scale with electrode surface area at any fixed steady-state concentration of dissolved  $\text{H}_2$  and  $\text{O}_2$  gases. Experiment 4 demonstrated that it does scale as predicted.

If the rate of reaction 4 increases and cell resistance decreases with temperature as expected from kinetic theory, the numerator of eq 1 will increase and the denominator will decrease with increasing temperature, thus causing the calculated percent excess heat to increase substantially with temperature. This may answer the question posed by Fleischmann and Pons<sup>19</sup> in connection with Pd/ $\text{D}_2\text{O}$  cells: "How can it be that the temperature of the cell contents increases whereas the enthalpy input decreases with time?" We expect precisely this relationship if reported excess heat in these cells is due to reaction 4.

An optimum in current density versus percent excess heat was observed by Mills et al.<sup>5</sup> and Nonnisski.<sup>6</sup> This optimum accounts for the observation in experiments 1 and 4 that the excess heat rate does not scale linearly with current. Once the electrolyte is saturated with hydrogen and oxygen, the observed excess heat rate from their reactions should remain approximately constant. Again, the location of the maximum will depend on details of cell configuration. Also, typical of all our runs, the higher the current density (beyond a certain point), the lower the calculated percent excess heat, suggesting that purging of the solution near the electrode surface by evolved  $\text{H}_2$  is effective in reducing the degree to which  $\text{O}_2$  can penetrate to the electrode surface. This study did not experimentally examine the question of the excess heat source in cells operated

at high current density, e.g., Fleischmann et al.<sup>1</sup> Accurate examination of such cells will require a different experimental design than used here. However, we note the lack of compelling evidence for the assumption of 100% faradaic efficiency or for the accuracy of calorimetric measurements on cells operated at high current density (e.g., refs 1, 8, 16, and 17).

Excess heat has been observed in Ni/Na<sub>2</sub>CO<sub>3</sub>(aq)/Pt cells by some workers,<sup>4,5</sup> but others have used such cells as a control.<sup>3,6</sup> In agreement with a recent report<sup>20</sup> showing that different electrolytes produce differing bubble sizes in aqueous solution, our experiments show that the difference between Na<sub>2</sub>CO<sub>3</sub> and K<sub>2</sub>CO<sub>3</sub> as electrolytes probably is due to differences in interfacial properties of the solutions at the electrodes. The H<sub>2</sub> bubbles were smaller when K<sub>2</sub>CO<sub>3</sub> was the electrolyte than when Na<sub>2</sub>CO<sub>3</sub> was the electrolyte in the same cell. Smaller bubbles allow better mobility of gases in the electrolyte and contact between the electrolyte and the electrode surface, thus allowing more frequent reaction of dissolved gases. When detergent was added to the Na<sub>2</sub>CO<sub>3</sub> electrolyte, the bubbles became much smaller, did not adhere to the electrode, and resulted in about the same rate of apparent excess heat as was observed with the K<sub>2</sub>CO<sub>3</sub> electrolyte.

Of all the results reviewed, only Mills et al.<sup>3</sup> claim  $q_{ex}$  is greater than the input power. Mills' use of several different, low-resistance calibration heaters and the paucity of experimental detail fails to rule out calorimetric error, e.g., loss or generation of heat in the heater lead wires, as an explanation of these results.

Ni, Pt, and Pd are effective catalysts for reaction 4. One measure of catalytic efficacy for this reaction is the exchange current density ( $\eta_0$ ). The value of  $\eta_0$  depends on solution composition, temperature, and electrode geometry and surface area as well as electrode material.<sup>7</sup> Ni, Pt, and Pd have much higher  $\eta_0$  values than the other metals in their periods when compared under similar conditions.

Another consequence of the high  $\eta_0$  values of Ni, Pt, and Pd is a minimal overvoltage required to drive electrolysis: the higher the  $\eta_0$ , the lower the overvoltage. The overvoltage is equal to  $E_{cell} - 1.23$  V, where 1.23 V is the reversible cell potential for light water. If the overvoltage decreases,  $E_{cell}$  will approach, and may go below, the thermoneutral potential of 1.48 V, as shown in experiment 4. The excess heat rate given by eq 1 approaches ±infinity or becomes undefined as  $E_{cell}$  approaches 1.48 V. In such cases, very small absolute errors in calorimetry will result in large values of apparent percent excess heat as calculated by eq 1. Thus, some of the extraordinary claims made by Mills et al.<sup>3</sup> and others may be due to the effects of small measurement errors or noise in a cell operating near 1.48 V. If  $q_{meas}$  does not equal zero when  $E_{cell} = 1.48$  V,  $q_{ex}$  goes to ±infinity. For examples of this condition, see experiments 2 and 3 in ref 3 and Figure 5 in this study. Because time constants of heat conduction calorimeters are typically quite long, oscillating signals such as those seen in Figure 5 are not present in the calorimetric signal. This mismatch in time constants can result in an incorrect calculation of apparent excess heat. Also, because heat losses from electrical calibration heaters are an ever present problem in calorimetry, positive systematic errors are much more likely in calorimetric measurements than negative errors, thus giving positive, but incorrect, excess heat values. Failure to account for even a small amount of exothermic heat from reaction 4 in a cell operating near 1.48 V can cause an apparent very large excess heat rate. Thus, reports of very large, exothermic excess heat rates on cells with low overvoltage are probably an artifact

arising from a combination of small experimental errors and the way excess heat rate is defined.

## Conclusions

This study was designed to determine the sources of excess heat in electrolysis cells operated at low current densities. Pitfalls that can occur with electrical leads, with blockage of electrode surfaces by bubbles, and, more importantly, with decreased faradaic efficiency are demonstrated. Less than 100% faradaic efficiency was shown to occur in both Ni/light water cells with alkali metal carbonate electrolyte and in a Pd/LiOD cell using heavy water. Excess heat was seen in all of these cells unless they were configured or operated in such a way so as to avoid contact between dissolved hydrogen and oxygen and the electrode surfaces.

If compelling evidence for sources of excess heat other than reaction of H<sub>2</sub> (or D<sub>2</sub>) and O<sub>2</sub> is to be obtained, faradaic efficiency must be accurately determined and calorimetric accuracy must be demonstrated while the cell is producing excess heat. In the absence of confirmatory nuclear products, calorimetric measurements must be beyond reproach. Better calorimetric methods than typically used for "cold fusion" studies are in common usage and compatible instrumentation is commercially available. Until such studies have been carefully done, there is no compelling reason for not adopting the hypothesis that calorimetric errors or failure to account for reactions of hydrogen and oxygen during electrolysis of water account for all reports of excess heat to date. Compared with other hypotheses,<sup>3,4</sup> this is much simpler and requires no changes in well-established scientific principles. Thus, Occam's razor places the burden of proof on those postulating "new science". Such proof requires adequate experimentation to establish that a reduced faradaic efficiency or calorimetric errors cannot explain the excess heat effect.

**Acknowledgment** We appreciate the support of Brigham Young University in contributing supplies and student salaries. We thank Dr. J. Ward Moody for help in setting up the data acquisition system and Doug Davidson for helping with preliminary experiments.

## References and Notes

- (1) Fleischmann, M.; Pons, S. *J. Electroanal. Chem.* 1989, 261, 301.
- (2) Wagman, D. D.; Evans, W. H.; Parker, V. B.; Schuman, R. H.; Halow, I.; Bailey, S. M.; Churney, K. L.; Nierlak, R. L. *The NBS Tables of Chemical Thermodynamic Properties*; National Bureau of Standards: Washington, DC, 1982; pp 2-38.
- (3) Mills, R. L.; Good, W. R.; Farrell, J. J. *Unification of Spacetime, the Forces, Matter and Energy*; Science Press: Ephrata, PA, 1992; pp 173-208.
- (4) Bush, R. T. *Fusion Technol.* 1992, 22, 301.
- (5) Srinivasan, M.; Shyam, A.; Sankaranarayanan, T. K.; Bajpai, M. B.; Ramamurthy, H.; Mukherjee, U. K.; Krishnan, M. S.; Nayak, M. G.; Naik, Y. P. In *Nagoya Conference Proceedings, Frontiers of Cold Fusion*; Ikegami, H., Ed.; Universal Academy Press: Tokyo, 1993; pp 123-138.
- (6) Nonniski, V. C. *Fusion Technol.* 1992, 21, 163.
- (7) McDougall, A. *Fuel Cells*; Macmillan: London, 1976; p 54.
- (8) Miles, M. H.; Hollins, R. A.; Bush, B. F.; Lagowski, J. J.; Miles, R. E. *J. Electroanal. Chem.* 1993, 346, 99.
- (9) Mallove, E. F.; Rotliwell, J. Private communication.
- (10) University of Utah press release, March 23, 1989.
- (11) Bucher, D. R.; Hansen, I. D.; Jones, S. E.; Rees, L. B. In *Nagoya Conference Proceedings, Frontiers of Cold Fusion*; Ikegami, H., Ed.; Universal Academy Press: Tokyo, 1993; pp 248-251.
- (12) Notoya, R.; Enyo, M. In *Nagoya Conference Proceedings, Frontiers of Cold Fusion*; Ikegami, H., Ed.; Universal Academy Press: Tokyo, 1993; pp 421-426.
- (13) Hinca, L. D.; Han, R. H.; Chen, D. M.; Gibbard, H. F. *Rev. Sci. Instrum.* 1982, 53, 503.

## Accounting for Excess Heat in "Cold Fusion" Cells

*J. Phys. Chem., Vol. 99, No. 18, 1995 6979*

(14) Jones, S. E.; Hansen, L. D. Examination of Claims of Miles et al. in Pons-Pleischmann-Type Cold Fusion Experiments. *J. Phys. Chem.* 1995, 99, 6966.

(15) Wenzl, R. C., Ed. *Handbook of Chemistry and Physics*, 55th ed.; CRC Press: Cleveland, OH, 1974; D-159.

(16) McKubre, M. C. H.; Crouch-Baker, S.; Riley, A. M.; Smalley, S. I.; Tanzella, F. L. In *Nagoya Conference Proceedings, Frontiers of Cold Fusion*; Ikegami, H., Ed.; Universal Academy Press: Tokyo, 1993; pp 51-191.

(17) Stoirns, E. *Fusion Technol.* 1993, 23, 230.

(18) Oriani, R. A. Private communication.

(19) Pleischmann, M.; Pons, S. *Phys. Lett. A* 1993, 176, 118.

(20) Craig, V. S. J.; Ninham, B. W.; Pashley, R. M. *Nature* 1993, 364, 317.

IP9426561

Notoya, R., Enyo, M., Proceedings of the International Conference on Cold Fusion, October 21-25, 1992, (H. Ikegami, Editor), Universal Academy Press, Inc., Tokyo, Japan.

421

## Excess Heat Production in Electrolysis of Potassium Carbonate Solution with Nickel Electrodes

Reiko NOTOYA and Michio ENYO  
Catalysis Research Center, Hokkaido University  
Kita-11, Nishi-10, Kita-ku, Sapporo 060  
JAPAN

### ABSTRACT

With the aim of realizing the potassium-proton cold fusion, the electrolysis of light water solution of potassium carbonate was carried out by means of porous nickel cathode. The cell was cooled by a constant rate air stream and maintained at 20°C during all the electrolysis. Typical results indicated that the excess heat production rate was proportional to the input power in the range of measurements(up to 2W) and the excess heat observed was 3 to 4 times greater than the input power, after corrected for the thermo-neutral potential.

After the electrolysis, the calcium ion concentration in the electrolytes was measured by flame photospectrometry and the increases of calcium concentration in the electrolytes due to the electrolysis were found to be 3.2 to 4.4 ppm. These amounts are comparable to the amounts of the excess heat calculated within the same order of magnitude.

### 1. Introduction

It was a shocking news that nuclear reactions of deuterium occurred on palladium cathode at room temperature<sup>1</sup>. The study of "cold fusion" has burst into flame throughout the world. Moreover, the novel type of the cold fusion in light water was suggested by Mills et al<sup>2</sup>, last year. The majority of scientists still are doubtful about them, because of little reproducibility and consistence among the amounts of

## Excess Heat Production in Electrolysis of Potassium Carbonate Solution with Nickel Electrodes

Reiko NOTOYA and Michio ENYO  
Catalysis Research Center, Hokkaido University  
Kita-11, Nishi-10, Kita-ku, Sapporo 060  
JAPAN

### ABSTRACT

With the aim of realizing the potassium-proton cold fusion, the electrolysis of light water solution of potassium carbonate was carried out by means of porous nickel cathode. The cell was cooled by a constant rate air stream and maintained at 20°C during all the electrolysis. Typical results indicated that the excess heat production rate was proportional to the input power in the range of measurements(up to 2W) and the excess heat observed was 3 to 4 times greater than the input power, after corrected for the thermo-neutral potential.

After the electrolysis, the calcium ion concentration in the electrolytes was measured by flame photospectrometry and the increases of calcium concentration in the electrolytes due to the electrolysis were found to be 3.2 to 4.4 ppm. These amounts are comparable to the amounts of the excess heat calculated within the same order of magnitude.

### 1. Introduction

It was a shocking news that nuclear reactions of deuterium occurred on palladium cathode at room temperature<sup>1</sup>. The study of "cold fusion" has burst into flame throughout the world. Moreover, the novel type of the cold fusion in light water was suggested by Mills et al<sup>2</sup>, last year. The majority of scientists still are doubtful about them, because of little reproducibility and consistence among the amounts of

their products, heat emission and radiation. However, these systems are essentially the most popular ones for hydrogen evolution reaction. Matsuda's group had shown in their works<sup>3</sup> that several active metals for hydrogen evolution reaction, for example, nickel, formed considerable amounts of the alkali metallic intermediates during electrolysis of alkaline solutions. On the basis of them<sup>3</sup>, the nuclear reaction of potassium was sufficiently likely and therefore warranting further investigation. The aim of this work was to obtain the unequivocal evidence of this nuclear reaction.

## 2. Experimentals

An electrolytic cell made of Pyrex glass was used for the experiment and equipped with 3 electrodes, these being, a 1 x 0.5 x 0.1 cm sintered nickel test-electrode, platinum counter and platinum reference electrodes. A 20 milli-liter light water's solution of potassium carbonate with a concentration of 0.5 mol per liter was used as the electrolyte, and stirred by bubbling hydrogen gas, with gas stream rate of 1.5 ml/min during the electrolysis. The nickel electrode was cathodically polarized by a stationary constant current from 0.01 to 0.70 ampere and the temperature of the electrolyte was measured. A standard nichrome heating wire with a resistance of 15 ohm was put in the cell for comparison. The electrolysis was carried out using the twin celles simultaneously, in order to confirm that the heat discharged was only by electrolysis. The twin cells were placed a thermostat chamber of the temperature held at  $20.00 \pm 0.01^{\circ}\text{C}$  during the electrolysis by air convection.

## 3. Results and Discussion

Figure 1 shows the typical relationship between the input power,  $W_{\text{input}}$ , given by electrolysis and the increase of electrolyte temperature,  $T$ . The input power,  $W_{\text{input}}$  is given by the following equation:

$$W_{\text{input}} = I(E - 1.482 \text{ V}), \quad (1)$$

where  $I$  and  $E$  denote the current and the potential difference between the test electrode and the counter electrode. The 1.482 V value is due to the enthalpy change for  $\text{H}_2\text{O} + \text{H}_2 + (1/2)\text{O}_2$ . Figure 1 shows the electrolyte temperature increase for the standard resister(2) and that for electrolysis. It was found that the electrolyte temperature increased up to

$54.2^{\circ}\text{C}$  from the initial temperature of  $20^{\circ}\text{C}$  with the input power of  $2.70$  joule/sec and this temperature rise was proportional to the input power  $W_{\text{input}}$ , within the input power range of  $0$  to  $2.7$  joule/sec. The figure shows a linear relationship between the temperature increase and the input power  $W_{\text{input}}$  with a correlation coefficient of more than  $0.999$  for both lines. The line gradient for the cell is remarkably greater than that for the standard resister.

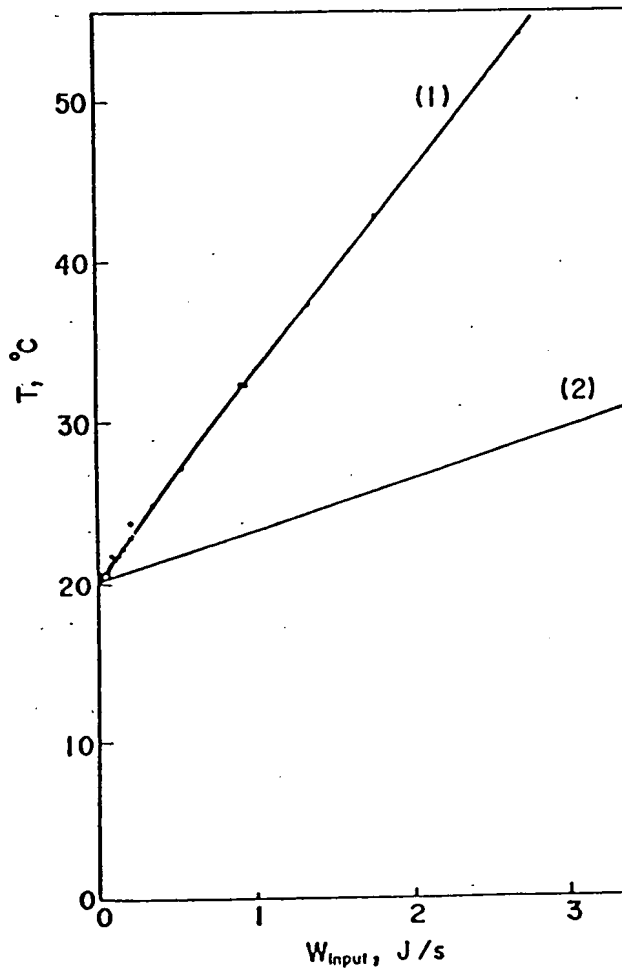


Figure 1. a. Relationship between temperature increase of electrolyte and input power  $W_{\text{input}}$  in the cell-(1) and as compared with the standard resister-(2).

The difference in the value of input power  $W_{\text{input}}$  between two lines at a given temperature, shown in this figure, can be defined as the excess heat. Figure 2 shows the relationship between the excess heat  $\Delta W_{\text{output}}$  and the input power  $W_{\text{input}}$  observed in the cell. The excess heats determined from ten time-repeated experiments were found to be from 2.7 to 3.4 times more than  $W_{\text{input}}$ .

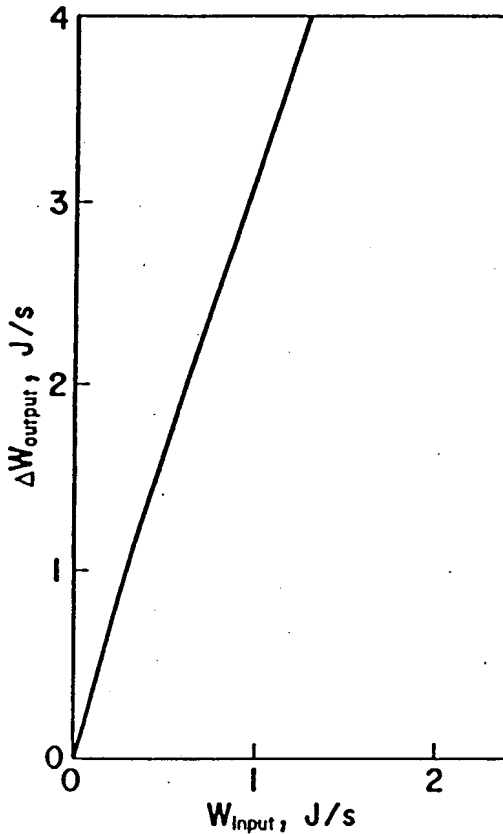


Figure 2. Amount of excess heat  $\Delta W_{\text{output}}$  evolved during the electrolysis with input power  $W_{\text{input}}$  in 0.5 M  $\text{K}_2\text{CO}_3$ .

The calcium ion concentration in the electrolyte was measured by flame photospectrometry with an accuracy of  $\pm 0.02$  ppm. In the same solution of 0.5 mol per liter potassium carbonate as the electrolyte, calcium ion was not detected, before use. In order to determine the background value, the calcium ion concentration in the solution of 20ml was poured into the electrolytic cell vessel equipped with the three

electrodes and the standard heater and put at 20°C without electrolysis, during the electrolysis of the working cell, which was made exactly the same as the former. The calibration line of the intensity of the spectrum for calcium plotted against its concentration is shown in Figure 3. On the basis of this line, the calcium concentrations in the three samples of electrolyte after different conditions of electrolysis were found to be 24.7, 25.1 and 26.2 ppm when the background values, to be 21.5, 21.5 and 22.0. The increases of calcium concentration in the samples of electrolyte due to the electrolysis were determined to be 3.2, 3.6 and 4.2 ppm by use of these data. These increases of calcium concentration in the electrolytes are comparable to the total amounts of excess heats evolving in these electrolytes, within the same order of magnitude.

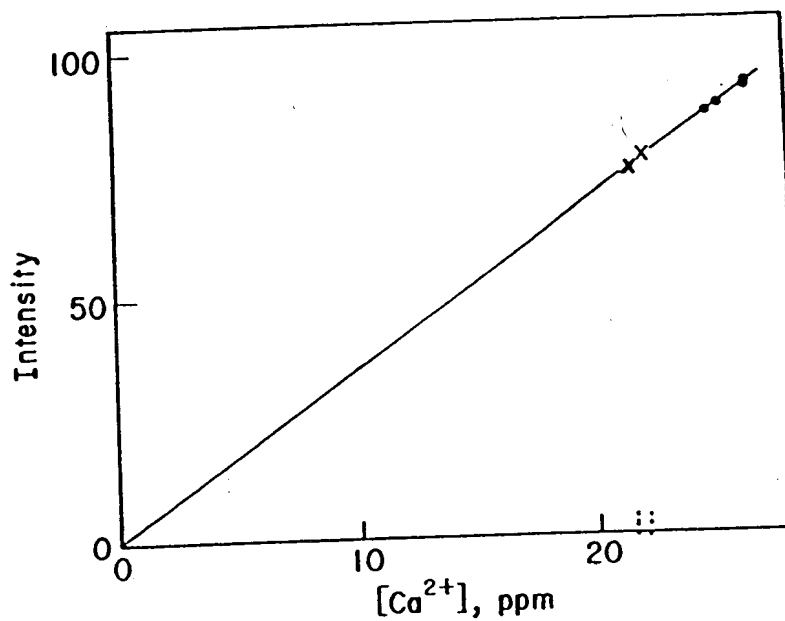
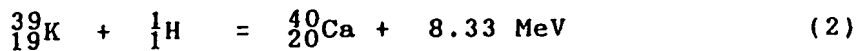
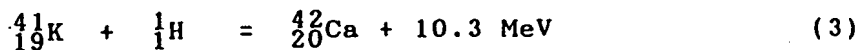


Figure 3. Intensities of flame photospectra of calcium with concentrations of calcium ion in the electrolytes after electrolysis (•) and in electrolytes put in cell without electrolysis (x). A line shown in this figure is the calibration line for the calcium ion concentration.

Brown et al<sup>4</sup> proposed the possibility of nuclear reactions between potassium and proton as follows,



and



From the present work, it is not clear which of the 2 reactions, (2) or (3), was predominant in this system. A further investigation is being conducted at present to verify this.

#### 4. List of Symbols

$W_{\text{input}}$  = Input power, joule/sec

I = Current, amp

E = Potential difference, volt

T = Temperature, °C

$\Delta W_{\text{output}}$  = Excess Heat, joule/sec

#### 5. References

1. Fleischmann, M. and Pons, S., 1989, J.Electroanal Chem., 261, 301.
2. Mills, R. and Kneizys, K., 1991, Fusion Technol., 19, 65.
3. Notoya, R. and Matsuda, A., 1966, J.Research Inst. Catal., Hokkaido Univ., 14, 198.
4. Bush, R.T, 1991, Fusion Technol., 22, 301.

# Substantial Doppler broadening of atomic-hydrogen lines in DC and capacitively coupled RF plasmas

Kamran Akhtar<sup>1</sup>, John E. Scharer<sup>2</sup>, and Randell L. Mills<sup>1</sup>

<sup>1</sup> BlackLight Power, Incorporated  
493 Old Trenton Road, Cranbury, New Jersey 08512

<sup>2</sup>Department of Electrical and Computer Engineering  
University of Wisconsin-Madison, Wisconsin 53706

The mechanism of extraordinary broadening of the Balmer lines of hydrogen admixed with Ar or He as opposed to Xe in a DC glow discharge and a capacitively coupled rf discharge is studied over a wide range of pressure and gas compositions. High-resolution optical emission spectroscopy is performed parallel to the electrode axis (end-on) and perpendicular to the electrode axis (side-on) along with Langmuir probe measurements of plasma density and electron temperature for the capacitive discharge case. An excessively broad and symmetric (Gaussian) Balmer emission line corresponding to 20-60 eV of hydrogen atom energy is observed in Ar/H<sub>2</sub> and He/H<sub>2</sub> plasmas when compared to the majority species atom temperatures. Energy is transferred selectively to hydrogen atoms whereas the atoms of admixed He and Ar gases remain cold (<0.5 eV). In the field acceleration model that has recently been put forth to explain the broadening [Cvetanovic et. al. J. App. Phys., Vol. 97, 033302-1, 2005], there is neither a preferred ion nor atom and according to this model, one should observe enhanced temperature hydrogen and helium atoms in He/H<sub>2</sub> discharges where the atomic mass is more comparable (4:1). The absence of hot H atoms in Xe/H<sub>2</sub> plasmas also challenges the paradigm of the field acceleration model since Xe is also a noble gas and electronically similar to He. The model of an energetic chemical reaction of hydrogen [Mills et. al *IEEE Trans. Plasma Sci.*, 31, p.338, 2003] as the source of broadening can explain the observation that only the selective heating of hydrogen atoms in certain plasmas exhibits the selective extraordinary broadening and isotropic emission profiles.

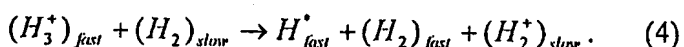
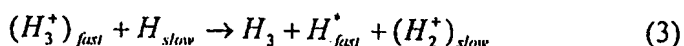
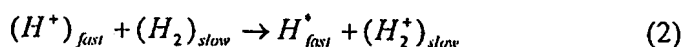
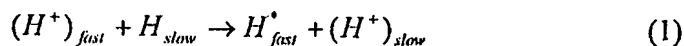
## I. INTRODUCTION

Substantial Doppler broadening of hydrogen Balmer lines has been observed in pure hydrogen and specific gaseous mixtures of hydrogen with certain heavier atom plasmas produced by DC and capacitively coupled 13.56 MHz radio frequency waves [1-17]. This broadening is caused by the presence of excited hydrogen atoms. In all these instances, energy is transferred selectively to the hydrogen atom whereas the H<sub>2</sub> molecules as well as the He and Ar atoms remain cold. Historically, most mechanisms proposed for excessive H<sub>a</sub> broadening in pure hydrogen and mixtures of hydrogen with inert gases [1-14] are explained in terms of energetic ions (H<sup>+</sup>, H<sub>2</sub><sup>+</sup> and H<sub>3</sub><sup>+</sup>) that are accelerated in the cathode fall region followed by energy transfer to the matrix gas (H and H<sub>2</sub>) through charge exchange collisions. However, there are variations in the proposed theoretical explanations of the mechanisms that provide energy to atomic H and cause the observed enhanced blue-shifted H<sub>a</sub> spectra width that is symmetric with respect to the red-shifted portion of the emission profile. It should be noted, however, that none of these mechanisms explains the selective transfer of energy to the hydrogen atomic state with the atoms of the admixed gases remaining cold (<0.5 eV).

In a pure hydrogen discharge, the Doppler-broadened profile exhibits the presence of a bimodal (or a tri-modal) distribution of neutral species temperatures [14]. The profile consists of a central peak that corresponds to slow thermal hydrogen atoms with kinetic energies in the range 0.25 to 1.0 eV. The population of warm H atoms (10-20 eV) is evident in the plateau of the Doppler broadened profile along with a population of fast hydrogen atoms (> 40 eV). There is general agreement on the mechanisms proposed for the production of slow H (~0.1-1.0 eV) atoms in the excited n=3 state through the process of dissociative excitation,  $H_2 + e^- \rightarrow H_2^+ + e^- \rightarrow H^+(n=3) + H$ , and dissociative ionization,

$H_2 + e^- \rightarrow 2e^- + H_2^+ \rightarrow H^*(n=3) + H^+$ , of hydrogen molecules and electron impact excitation of H atoms,  $H + e^- \rightarrow e^- + H^*(n=3)$  [1-2].

There are significant variations in the literature describing the mechanisms proposed to explain the production of hydrogen atoms with energies greater than 20 eV. These were originally proposed to be the result of dissociation of  $H_2^+$  ions in vibrationally excited molecular ground states [2-3]. Recently, the mechanism of charge exchange between ions accelerated in the sheath and neutrals and ion impact on electrodes has been proposed as the source of energetic hydrogen atoms in these discharges. In this model, henceforth called the Collisional Model (CM) [5 and references therein], sheath accelerated  $H^+$  and  $H_3^+$  ions in a hydrogen plasma are proposed to either transfer charge directly to the hydrogen atom or dissociate the  $H_2$  molecule followed by charge exchange collisions to explain the energy spectrum of hydrogen atoms [1-15]. The processes are governed by the following reactions [5-7] where the \* indicates excited n=3 atomic state:



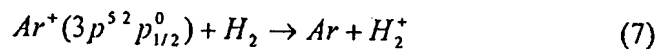
Since the particle acceleration due to the electric field is directional, the energy gained by a positive ion as it travels towards the cathode will maintain that directionality along with the directed energy of the excited hydrogen atom as long as ion-neutral collision rates are small. This mechanism can only account for the red portion of the spectrum when viewed optically towards the ion accelerating electrode sheath. The observed symmetry in the Gaussian profile of the

hydrogen Balmer line is explained in terms of the sputtered fast H atoms and the back-reflected fast H atoms from the cathode surface [5]. It is argued that this will give rise to a symmetric distribution of energetic H atoms leaving the cathode compared to those accelerating towards the cathode.

In the presence of inert gases, the additional process of charge transfer has been proposed to explain the symmetric  $H_{\alpha}$  broadening [3,12-13]. The introduction of Ar in a pure  $H_2$  plasma increases the Balmer line emission intensity that implies that the concentration of excited hydrogen atoms in the excited  $n=3$  state is also increased. In addition, the fractional population of hot hydrogen atoms obtained from the area under the Gaussian curve implies a concentration in excess of 80 percent of the population in the  $n=3$  state. It has been suggested in the above articles that energetic  $Ar^+$  ions dissociate and ionize  $H_2$  to form  $ArH^+$  that enhances the population of  $H_3^+$  that is proposed as the primary source of atomic hydrogen as shown below when Eq. (6) is combined with Eq. (4).



The role of metastable argon ions in the enhanced production of  $H_3^+$  ions through the formation of molecular hydrogen ions has also been emphasized [6].



It has been suggested in the above articles that the contribution of these pathways to the significant production of  $H_3^+$  in Ar/ $H_2$  results in an enhanced population of energetic  $H_{fast}$  atoms through the processes described in Eqns. (3-4).

However, some of the recent observations [17-26] in DC and capacitively coupled rf discharges are in contrast to the field acceleration based Collisional Models described earlier. For example, it is important to note that, to the best of our search of the scientific literature, no experimental observation has ever been reported, including results in this paper where equally energetic atoms of admixed gases have been found even when the plasma is collisional and mass ratios are comparable. The energy is transferred selectively only to the hydrogen atom whereas the electron energy is less than few eV and admixed gas atoms remain cold (<0.5 eV). It is also very intriguing that no hot H atoms are observed when the admixed gas is xenon. In the CM, the energy of the hot H atom should be independent of the nature of the background gases except for differing collision cross-sections with the background gas. Therefore, it is not possible to readily explain the presence of broadening in argon/hydrogen and helium/hydrogen plasmas along with the absence of broadening in xenon/hydrogen plasmas using this model. In addition, the observation of comparably hot hydrogen atoms in regions outside the plasma sheath requires the local creation of energetic H atoms. As discussed later, the rapid thermalization of H atoms with the background gas due to short ion-neutral collision mean free paths should also confine fast H near the region where it is formed. Therefore, only a process where hot H is produced locally can explain the comparable energies of hot H observed well outside the plasma sheath regions.

It should be noted however, that these observations demonstrate that the source of these hot H atoms is a process fully consistent with the Mills' model of energy production known as Resonance Transfer Model (RTM) [17-26]. The RTM predicts excessive broadening due to a novel energetic chemical reaction of H with certain catalysts involving a two-step energy transfer. First, resonant energy transfer occurs from H to a catalyst and then a second radiative emission or a resonant energy transfer to another H atom that serves as a third body to take away

the remaining reaction energy [19-20]. In this model, it is postulated that the electron in the hydrogen atom that undergoes a ‘catalytic’ reaction that allows decay from the ‘conventional’ ground state (principal quantum number,  $n=1$ ) to a ‘fractional’ quantum state (e.g.  $n=1/2$ ). Since the ionization energy of hydrogen is 13.6 eV, two hydrogen atoms can also provide a net enthalpy equal to the potential energy of the hydrogen atom, 27.2 eV—the necessary resonance energy, for a third hydrogen atom to form H ( $n=1/2$ ).

In order to clarify the underlying mechanism of hydrogen Balmer alpha broadening in hydrogen plasmas and plasmas of hydrogen admixed with noble gases and test the validity of field acceleration based Collisional Model (CM) [5], a comprehensive experiment that covers a wide range of gas pressure and plasma parameters has been performed. A DC glow discharge with pin electrodes and a capacitively coupled radio frequency plasma over a wide pressure range (three orders of magnitude – 10 mTorr to 10 Torr) along with different gas mixture ratios are used to test the ability of the CM to explain the unusual nature of the observed hydrogen broadening. As suggested by the CM, the degree of symmetry of the plasma emission profile should be a function of the electron-neutral and ion-neutral collision frequency and, therefore, should depend on the neutral gas pressure. The CM mandates that observations parallel and perpendicular to the electric field lines yield different emission profiles if the collisional scattering rate is sufficiently small. The experimental setup allows observations both parallel and perpendicular to the electrode axes to test this property. In addition, the presence of hot H atoms was examined in regions far away from the high electric field plasma sheath region near the electrodes. The CM also implies that the energy of hot H atoms is independent of the nature of admixed gases. In contrast, the RTM proposes that the nature of admixed gases will be critical to the broadening mechanism that results in the observed hydrogen emission profile. This aspect is

tested by mixing different gases with hydrogen and observing broadening in the plasma emission profile. In addition to plasma emission spectroscopy, a Langmuir probe is also used to diagnose the capacitive discharge plasma. It should be noted here that the experiments were designed and parameter regimes were considered primarily to test the field acceleration based Collisional Model (CM). In this process, however, the Resonance Transfer Model (RTM) is also tested in light of these new observations.

## II. EXPERIMENTAL SYSTEM

The experimental arrangement of the DC discharge is shown in Figure 1. In this configuration, the discharge is created between fine tips of 2% thoriated tungsten electrodes of diameter 1/8 inch spaced 2 cm apart inside either a ½ inch or 1 inch diameter quartz tube. Very fine electrode tips (Fig.1) that are tapered over the last ½ inch to a point are used to minimize the surface area perpendicular to the face of the electrodes. The high E-field near the sharp electrode tip will reduce rapidly as one moves away from it. High-resolution plasma emission spectroscopy is performed through an annulus parallel to the electrode axis along the electric field lines (end-on) and perpendicular to the field lines (side-on). For the end-on observation, plasma emission can be sampled looking towards the anode or cathode. For the side-on observation, an axial scan of the plasma emission is observed in a region adjacent to the cathode rod. Here the cathode tip is located at  $z=0$  cm. The DC plasma setup is placed on an X-Y motion table so that an accurate axial measurement can be carried out without changing the position of the fiber optic bundle. The discharge pressure is maintained in the range of 10 mTorr to 10 Torr. A stabilized negative DC power supply (Kaiser System Inc., Beverly, MA) with voltage and current in the range 0-2000 V and 0-500 mA, respectively, is used to create the plasma. A high

wattage ballast resistor of  $20\text{ k}\Omega$  is used in series with the power supply to limit the discharge current. Once the discharge is created, the glow discharge is maintained with cathode-anode voltages of 300-400 volts and results in discharge currents in the range of 10-100 mA depending upon the gas pressure, gas flow and discharge configuration.

The capacitively driven radio frequency plasma system consists of a large cylindrical (14 cm ID  $\times$  36 cm length) quartz plasma chamber with two electrodes (stainless steel plates of diameter 8.25 cm) placed 1 cm apart at the center (Figure 2). Radio frequency power (13.56 MHz, RF Power Products Inc. NJ, Model RF 5, 500 Watts) is coupled to the electrode using a commercially available impedance matching network (RF VII Inc., Glassboro, NJ). Radio frequency power from the source is fed through the impedance matchbox to the capacitive electrodes using a 1/2-inch diameter steel tube that also facilitates the end-on (parallel to the electric field) observation of plasma through holes in the center of the electrodes. One of the electrodes is permanently grounded. A common ground is maintained for the grounded electrode, rf shield and vacuum system. Two ports in the center of the plasma chamber (Position 2) permit side-on observations of plasma emission  $90^\circ$  and  $45^\circ$  to the electric field. Another side port at the same position allows insertion of a Langmuir probe for plasma density and electron temperature measurements. Plasma emission far away (15 cm) from the high-field plasma sheath region is sampled at Positions 1 and 2. In order to ensure that the plasma emission sampled at positions 1 and 2 have no contribution from the reflected light, the inside of the rf shield enclosure is made non-reflecting.

A helium leak detector (QualyTest, Model: HLT 260, Pfeiffer Vacuum) is utilized to leak test the evacuated plasma chamber. The plasma chamber is maintained with a leak rate below  $10^{-7}$  Torr-L/s. Independent mass flow controllers (MKS) were used to introduce UHP grade

(99.999%) H<sub>2</sub>, Ar, He and Xe gases into the plasma chamber through Ultratorr fittings at one end. The chamber pressure for all gas compositions is maintained between 10 mTorr and 10 Torr. An MKS Baratron gauge is used to read the chamber pressure.

### III. DIAGNOSTICS

#### A. Plasma Emission Spectroscopy

Plasma emission from the glow discharge passes through a high-quality UV (200-800 nm) fiber-optic bundle into a monochromator through a 220F matching fiber adapter that is detected either by a photomultiplier tube (PMT) with a stand-alone power supply of 995 volts or by a high quality scientific grade liquid nitrogen cooled CCD arrays. The numerical aperture of the fiber optic bundle is 0.12 and the corresponding acceptance angle is 12°. The spectrometer utilizes a 1250 mm focal length spectrometer (Jobin Yvon Horiba: Model 1250M Research Spectrometer) with a 2400 g/mm grating and a high resolution of ± 0.006 nm. The spectrometer is rated for an accuracy of ±0.05 nm and repeatability of ±0.005 nm. The spectrometer was scanned through emission profiles of Balmer lines with a step size of 0.01 nm. The entrance and exit slits were set at 20 μm. The liquid nitrogen cooled Symphony model CCD detectors are a family of array detectors from Jobin Yvon with 16 bit ADC with 20 KHz and 1 MHz read out. A back illuminated 2048×512 CCD of 13.5 μm × 13.5 μm size provides very high-resolution capability.

The Doppler-broadened line shapes for atomic hydrogen have been used to calculate the energy of the atomic hydrogen. The motion of a radiating particle moving towards or away from an observer results in a wavelength shift of the emitted line. This broadening is related to the random thermal motion of the emitting atoms and for a Maxwellian velocity distribution it

depends only on the translational (kinetic) temperature. Full half-width,  $\Delta\lambda_G$ , of the Gaussian profile results from the Doppler ( $\Delta\lambda_D$ ) and instrumental ( $\Delta\lambda_I$ ) half-widths are  $\Delta\lambda_G = \sqrt{\Delta\lambda_D^2 + \Delta\lambda_I^2}$ . The instrumental half-width  $\Delta\lambda_I$  is 0.006 nm and is negligible. The temperature of atomic hydrogen in terms of Doppler ( $\Delta\lambda_D$ ) half-width is given as [27]

$$\Delta\lambda_D = 7.16 \times 10^{-7} \lambda_0 \left( \frac{T}{\mu} \right)^{1/2} \text{ nm.}$$

Here  $\lambda_0$  is the line wavelength in nm, T is the temperature in K, and  $\mu$  is atomic mass number (=1 for hydrogen). It can be seen that Doppler broadening is more pronounced for lighter elements at high temperatures. For high densities  $> 10^{13}/\text{cc}$ , Doppler broadening competes with Stark broadening. In addition, a contribution to the broadened profile may arise from the mass motion of the plasma. However, for these glow discharges where the plasma density is low ( $< 10^{11}/\text{cc}$ ), the contribution of Stark broadening to the line shape profile can be neglected without loss of accuracy. We checked the contribution from the mass motion of the plasma by sampling the plasma emission side-on as well as end-on. The absence of line shift shows that the line broadening is primarily due to the thermal motion. In each case, the error in the average Doppler half-width over 10 scans was about  $\pm 5\%$  that is attributed to the fluctuations in the plasma. The half-width of the Doppler broadened emission profile was obtained using a multi-Gaussian curve fit utilizing the curve fitting software GRAMS from Jobin Yvon Horiba.

#### B. Plasma Density Measurement

In the present work, Langmuir probe (LP) data has been used for obtaining the bulk plasma density and bulk electron temperature in the capacitive discharge [28-29]. The cylindrical Langmuir probe is a tungsten tip of radius 1 mm and length 5 mm enclosed in an alumina tube.

The LP is placed between the electrodes at position 2 where most of the plasma heating occurs. In order to characterize the capacitively coupled radio frequency plasma, an rf compensated LP is utilized that allows accurate measurement of bulk electron temperature. The probe filtering does not allow time varying, non-Maxwellian properties of the electron energy distribution to be readily observed. Thus, the possible presence of a small population of hot electrons ( $E_e > 20$  eV) in such low-density capacitive discharges at gas pressures above 10 mTorr is not considered in this paper. Data acquisition software written in Lab View is used for automatic transfer from the oscilloscope to the computer. The entire LP data analysis in the present work was undertaken using an interactive graphics based software package developed in MatLab.

#### IV. EXPERIMENTAL RESULTS

##### A. DC Discharge

The axial profile of the Balmer  $H_\alpha$  line (near 656.3 nm) observed perpendicular (side-on) and parallel to the electrode axis (end-on) looking towards anode as well as cathode is obtained for 1 Torr of Ar/H<sub>2</sub> (95/5%), He /H<sub>2</sub> (95/5%), and Xe/H<sub>2</sub> (95/5%) 300-400 V DC plasmas produced between fine tipped electrodes spaced 2 cm apart. The DC discharge is produced over a wide pressure range (and ion mean free path) of 10 mTorr-10 Torr. Significant broadening was observed for Ar/H<sub>2</sub> and He/H<sub>2</sub> plasmas whereas no broadening was observed for Xe/H<sub>2</sub> plasmas.

Axial profiles of the  $H_\alpha$  line for side-on as well as for end-on observations for 1 Torr argon mixed with 5% hydrogen plasma are shown in Fig. 3 and Fig. 4, respectively. The emission profile is isotropic and symmetric. The axial scan is performed parallel to the cathode pin axis with the tip located at  $z=0$ . The fiber optic cable entrance aperture is placed perpendicular to the surface of the quartz tube. The sampled plasma volume with an acceptance

angle of  $12^0$  for 1 inch and  $\frac{1}{2}$  inch diameter tubes is  $30 \text{ mm}^3$  and  $4 \text{ mm}^3$ , respectively. The  $H_\alpha$  line profiles clearly exhibit a two-component Doppler-broadened profile corresponding to two populations of hydrogen atoms. The central narrow part corresponds to slow hydrogen atoms with temperatures in the range of 0.4-0.5 eV. The broad component of the profile corresponds to fast hydrogen atoms with an average temperature of  $\sim 40$  eV. The fractional concentration of the slow part as obtained by curve fitting is 20-25% and the fast hydrogen component corresponds to 80-75 % indicating that the production of fast hydrogen atoms is substantial. Similar emission profiles are obtained for  $\text{He}/\text{H}_2$  plasmas where the fast hydrogen atoms have temperatures in the range of 30-40 eV. In contrast, only the slow component ( $\sim 0.5$  eV) of the hydrogen population is observed for  $\text{Xe}/\text{H}_2$  plasmas (Fig. 5). The axial temperature and population profiles of both fast and slow hydrogen atoms corresponding to the emission profiles in Fig.3 are shown in Fig. 6. It can also be seen from Figs. 3 and 6 that the average width of the two Gaussians of the Doppler broadened profile and hence the average temperature does not change appreciably along the axis. Even though the potential drops primarily near the cathode tip, the population of fast hydrogen atoms (area under the curve) peaks at a distance 2 cm away from the cathode tip. Moreover, the population of fast hydrogen atoms as a fraction of the total population is a minimum (82%) at the cathode tip ( $z=0$ ) and it increases to 94% at  $z = 2$  cm and remains nearly uniform up to  $z = 8$  cm (Fig. 6). It is noted that the intensity and corresponding plasma density decreases away from the cathode tip (Fig. 3) although the hot hydrogen component increases.

Figure 7 shows the normalized emission profile for an end-on observation in  $\text{Ar}/\text{H}_2$  and  $\text{He}/\text{H}_2$  plasmas looking towards the anode. A similar symmetrical emission profile is also obtained when the emission is sampled looking towards the cathode. Reflection of field-accelerated ions in equal measure to the accelerated direction is required by the CM to explain

the absence of either a predominant red or blue wing in the emission profile for the end-on observation. Furthermore, the symmetrical profile cannot be explained by the gas matrix collision effect as no change in the normalized profile symmetry is observed as the gas pressure is varied from 10 mTorr to 10 Torr resulting in a variation of electron-neutral collision frequency by three orders of magnitude (Fig. 8).

The average thermal energy of hot hydrogen atoms as catalytic (Ar, He) and non-catalytic (Xe) gases are added to a 100 mTorr hydrogen plasma DC discharge is shown in Fig. 9. As the fractional concentration of the catalyst gas is increased, the thermal energy of hot hydrogen atoms increases. In contrast, the hot H atom thermal energy decreases sharply with increasing Xe concentration. The absence of  $H_{\alpha}$  broadening with a non-catalyst such as Xe cannot be explained on the basis of the collisional model since the acceleration mechanism should be independent of the ion mass.

In addition, the transfer of energy from the electric field in these admixed plasmas is selectively to hydrogen atoms. Since the mass ratio of He to atomic hydrogen is 4:1, especially for highly collisional plasmas at higher gas pressures, it is expected from the Collisional Model [5] that a correspondingly energetic concentration of helium atoms (Doppler broadened profile) will be present. The Doppler half-width of the 667.82 nm He I line as shown in Fig. 10 is 0.012 nm and it can be accurately resolved by the high-resolution spectrometer with an instrumental half-width of only 0.006 nm. The He atoms' average thermal energy corresponding to a 0.012 nm Doppler half-width is 0.2 eV. No change in Doppler broadening of the 667.82 nm He I line was observed for all pressure and composition ranges studied in these experiments. The absence of hot helium atoms in He/H<sub>2</sub> plasmas where the hydrogen atoms have 30-40 eV energies also contradicts the Collisional Model because the atomic mass ratios are comparable (4:1).

## B. Capacitively Coupled RF Discharge

The capacitively coupled radio frequency discharge is characterized using Langmuir probe (LP) and plasma emission spectroscopy diagnostics. The LP is employed to measure electron bulk plasma density ( $n_e$ ) and electron temperature ( $T_e$ ) and to determine if a bulk population of high temperature ( $>5$  eV) electrons, not detectable by spectroscopic techniques, exists in our capacitively coupled RF plasmas. A side port at position 2 (Fig. 2) allows the insertion of the LP between the rf electrodes. The on-axis LP measurements are summarized in Table 1 for different noble gases admixed with 10% hydrogen at constant pressure of 100 mTorr. The coupled radio frequency power is maintained constant at 100 W for all the cases. In general, a low-density plasma ( $\sim 10^{10} \text{ cm}^{-3}$ ) with bulk electron temperatures of 2-3 eV is observed for all plasma conditions. There is a slight drop (~15-20%) in  $n_e$  as well as in  $T_e$  as hydrogen is added to the pure noble gas plasmas. It should be noted, however, that we did not observe any high-energy ( $>5$  eV) electron population obtained from the LP measurements. A single temperature bulk electron population characterizes these plasmas. The absence of higher-energy electrons in the higher-field regions between the electrode plates implies that there also are no fast electrons in low field regions far away from the electrodes.

Plasma emission from capacitively coupled rf discharges varied over a wide pressure range is sampled perpendicular to the electric field between the large disc electrodes (Position 2 in Fig. 2) and along the electric field through the 1 cm holes in the electrode plates (end-on). In addition, observations are also made at locations far way from the electrode plates (Positions 1 and 3 in Fig. 2). Isotropic and symmetric  $H_\alpha$  line profiles are observed for all three locations, independent of the observation angle relative to the electric field direction. The line profile also

remains symmetric as the gas pressure is varied over a wide range from 10 mTorr to 10 Torr. Line broadening is observed only for Ar/H<sub>2</sub> and He/H<sub>2</sub> plasmas and there is no broadening in comparable control mixtures of Xe/H<sub>2</sub>. The energy of the hot H atoms increases with increasing concentration of Ar and He gases whereas it decreases with Xe concentration. For the Ar/H<sub>2</sub> and He/H<sub>2</sub> plasmas the energy is selectively transferred to hydrogen atoms. In addition, the temperature of fast H atoms is quite uniform throughout the plasma chamber.

The average thermal energy of hot hydrogen atoms as a function of Ar, He and Xe concentrations [H<sub>2</sub>(x sccm); Ar, He, Xe (y=1-x sccm)] is shown in Fig. 11. A pure hydrogen plasma at 150 mTorr with a 20 sccm flow rate is produced at a coupled rf power level of 200 W. The corresponding thermal energy of the fast hydrogen atoms in this hydrogen plasma is ~ 13-15 eV. Noble gases are introduced into the plasma chamber and the total chamber pressure and flow rate are maintained at 150 mTorr and 20 sccm, respectively, by adjusting the hydrogen and noble gas flow rates. As shown in Fig. 11, the average thermal energy of the hydrogen atom, obtained from symmetric emission profiles, increases from ~13-15 eV to 25-30 eV as the Ar and He fraction is increased. In contrast, the average energy of the hydrogen atom decreases with increasing concentration of Xe.

Figures 12 and 13 show the energy and fractional population of fast hydrogen atoms in Ar/H<sub>2</sub> (95/5%) plasmas as the chamber pressure is varied from 10 mTorr to 10 Torr. Plasma emission is sampled perpendicular to the field between the electrodes and along the field lines through holes in the powered and grounded electrodes. As shown in the figures, the fast hydrogen energy (20-25 eV) and their fractional population (70-80%) in n=3 states remains nearly constant as the gas pressure is varied over three orders of magnitude. Very similar profiles

of fast hydrogen energy (Fig. 14) and fractional population (Fig.15) as a function of pressure are obtained for (95/5%) He/H<sub>2</sub> plasmas.

The presence of hot hydrogen far away from the high field sheath region is in contradiction with the Collisional Model. The plasma emission is sampled at Position 1 and Position 3 (Fig. 2) and angular variation is obtained by rotating the optical probe. The reference is normal to the chamber axis and as the observation angle is varied, plasma emission far away (~ 6 cm) from the electrode region is sampled. As shown in Fig. 16, there is a very small influence of the tilt angle on the hot hydrogen energy for both Ar/H<sub>2</sub> and He/H<sub>2</sub> plasmas. It should be noted here that the symmetry of the emission profile is independent of the angle of observation.

## V DISCUSSION

The observations and implications resulting from this study contradict the Collisional Model [5] where excessive H<sub>α</sub> broadening in pure hydrogen and mixtures of hydrogen with noble gases is explained primarily in terms of energetic ions (H<sup>+</sup>, H<sub>2</sub><sup>+</sup> and H<sub>3</sub><sup>+</sup>) accelerated in the cathode fall region followed by energy transfer to the matrix gas (H and H<sub>2</sub>) through charge exchange collisions. The character of atomic hydrogen broadening, namely the fast component temperature and the fractional population of the fast hydrogen atoms is quite different for different gas mixtures. In all variations of the collisional model [5], one consistent aspect is that the energy required for selective heating of the hydrogen atoms in plasmas consisting of hydrogen and hydrogen admixed with other gases is locally absorbed by ions from the electric field in the cathode fall region. In the CM at low pressures and collisionality, the emission profile should be dependent on the observation angle relative to the electric field direction. In order to explain the observed symmetry in the emission profile, they have argued that sputtered fast H

atoms and the back-reflected fast H atoms from the cathode surface give rise to fast H concentrations leaving the cathode in the same abundance as that moving towards the cathode.

We summarize the significant results of our experimental observations that are inconsistent with the field acceleration based Collisional Model [5]: 1) Hot hydrogen atoms are observed only for pure hydrogen and specific mixtures such as Ar/H<sub>2</sub> and He/H<sub>2</sub> plasmas whereas no hot H atoms are found when hydrogen is admixed with electronically similar Xe [36]. 2) In the Ar/H<sub>2</sub> and He/H<sub>2</sub> cases, energy is transferred selectively to hydrogen atoms where molecular hydrogen and the admixed gas atoms remain colder (<0.5 eV). 3) The population of neutral H atoms is much hotter (15-40 eV) than any of the charged species ( $T_e \sim 2-3$  eV in capacitive discharge). 4) The emission profile is symmetric over a wide pressure and mean free path range (three orders of magnitude) and is independent of the observation angle relative to the electric field direction. 5) Comparably hot hydrogen atoms are observed in field-free regions far away (up to 15 cm) from the high-field sheath region. In the following sections we discuss the inconsistency of the field acceleration based Collisional Model to account for these results and demonstrate that the Resonance Transfer Model is consistent with these observations.

Let us consider the presence of hot hydrogen atoms that occur only for pure hydrogen and hydrogen admixed with Ar and He plasmas and the absence of hot hydrogen atoms in electronically similar Xe/H<sub>2</sub> plasmas for the entire pressure range from 10 mTorr to 10 Torr. In the field acceleration based Collisional Model, the energy of hot hydrogen atoms should be independent of the nature of the electronically similar background gas except for differing collision cross sections of their ions with H. In order to test the collisional effect of background gases, we consider the cross section data for Balmer alpha and beta line emission from H and H<sup>+</sup> impact reactions on hydrogen (H<sub>2</sub>) and our other reacting gases [31-36]. It should be noted that

cross-section data for low energy ( $< 100$  eV) H and  $H^+$  impact on all three reacting gases considered in this paper are not available. Therefore,  $H_\alpha$  emission cross-sections from the impact of 100 eV H atoms on noble gas targets  $H + X(X = Ar, He, Xe) \rightarrow H_\alpha$  are considered. These are  $7 \times 10^{-17}$  cm $^2$ ,  $2 \times 10^{-18}$  cm $^2$ , and  $5 \times 10^{-18}$  cm $^2$  for Ar, He, and Xe, respectively, [31,33,35]. Similarly, the  $H_\alpha$  emission cross-sections from 100 eV  $H^+$  impact  $H^+ + X(X = Ar, Xe) \rightarrow H_\alpha$ , are  $2 \times 10^{-19}$  cm $^2$  and  $1 \times 10^{-17}$  cm $^2$  for Ar and Xe, respectively [32,36]. The emission cross-section data for  $H^+ + He \rightarrow H_\alpha$  reaction is not available for  $H^+$  energies below 1.25 keV because of the small magnitude of the photon signals [36]. The cross section for  $H^+ + He \rightarrow H_\alpha$  collisions at  $H^+$  energies of 1.25 keV is given as  $0.6 \pm 0.3 \times 10^{-20}$  cm $^2$  and it will be much smaller for lower  $H^+$  energies [36].

The CM argues that  $H^+$  ions will travel and be accelerated over longer distances and gain more energy before interacting with the target gas if the cross-section of  $H^+$  impact on the target gas is smaller. As a result, increasingly energetic  $H^+$  ions and, therefore via charge exchange, more energetic H atoms should be observed when the target gas is changed from Xe to Ar to He. Hence, following these arguments, we should observe the most energetic H atoms in the presence of He gas at low pressure. In addition, the  $H_\alpha$  emission intensity should be similar for both He and Xe since the H impact cross-sections on He and Xe are similar. However, we observe H atoms of comparable energy (30-40 eV in the DC discharge and 20-25 eV in the capacitive discharge) with either He or Ar as the background gas whereas the H atom energies are only 1-2 eV with Xe. The  $H_\alpha$  line intensity is also sharply reduced in Xe/H<sub>2</sub> discharges indicating low atomic hydrogen concentrations in non-RT plasmas. It can be concluded,

therefore, that the collisional model fails to explain the absence of fast H in Xe/H<sub>2</sub> discharges in contrast to its presence in Ar/H<sub>2</sub> and He/H<sub>2</sub> discharges.

These observations are consistent with the RTM which mandates that hot hydrogen atoms will be observed in Resonance Transfer (RT) plasmas where an ion is present that can provide a net enthalpy of reaction of an integer multiple of the potential energy of atomic hydrogen. Hence He<sup>+</sup>, and Ar<sup>+</sup> can act as ‘catalysts’ for the process since the electron ionization energies are an integral multiple of 27.2 eV [24]. Furthermore, as predicted by the RTM, Xe species are incapable of acting as catalysts since the ionization energy for Xe is not an integral multiple of 27.2 eV. As a result we do not observe hot hydrogen atoms in Xe/H<sub>2</sub> plasmas. In addition, the atomic hydrogen concentrations in non-RT plasmas are also low as evidenced by the emission line intensity.

We now consider the observation that the energy is transferred selectively primarily to hydrogen atoms (15-40 eV) whereas the atoms of admixed gases remain cold (<0.5 eV). In the Collisional Model there are neither preferred ions nor atoms and, therefore, one should observe correspondingly hot atoms of the admixed gases along with the hot hydrogen atoms. To our knowledge, no measurement has ever been made where equally hot atoms of admixed gases have been found. In collision dominated plasmas at higher gas pressures where an ion is bound to suffer many collisions with the background gas as it moves towards the cathode and where the mass ratios of the constituent gases are comparable, the presence of correspondingly hot atoms of admixed gases is inferred from the Collisional Model. Let us consider a He/H<sub>2</sub> plasma at 10 Torr with the electron-neutral collision frequency of  $3 \times 10^{10} \text{ s}^{-1}$  [30]. If in gas mixtures where only a trace amount of hydrogen (~1%) is added to the helium plasma, plasma hydrogen and helium ions will undergo many collisions with the background helium gas as they travel towards

cathode. It should be noted that the recombination rate coefficients of helium and hydrogen ions with energy in the range  $\approx 20\text{-}30$  eV is given by the reaction  $\text{He}^+ + e \rightarrow \text{He}$  and  $\text{H}^+ + e \rightarrow \text{H}$ . The two-body recombination rates for these two processes are comparable ( $\alpha_c = 10^{-13} \text{ cm}^3/\text{s}$ ) [37-38]. Therefore, the survival probability of both  $\text{He}^+$  and  $\text{H}^+$  ions as they travel towards the cathode is comparable. It should be noted, however, that with an atomic mass ratio of 4:1 in helium-atomic hydrogen plasmas, we observe hydrogen atoms with average energies of 30-40 eV whereas helium atoms are cold and have energies less than 0.5 eV (Fig. 10). In contrast, this selective transfer of energy to hydrogen atoms even though other comparable mass ratio ions are present is a cornerstone of the RTM prediction.

As shown in Fig. 16, there is a significant presence of comparably hot hydrogen atoms far away from the high-field plasma sheath regions where most of the potential variation occurs. It is well known that outside the sheath region, where the plasma is largely quasi-neutral, the plasma potential variation is very small. Therefore, in a field free region, the field acceleration CM cannot explain the existence of hot hydrogen up to 15 cm from the electrode. In order to explain the presence of hot H atoms in low field regions, the modified CM [5] requires the presence of fast electrons that produce hot atomic hydrogen with an energy comparable in magnitude to that obtained in the high field region where the source of these atoms are accelerated ions in the sheath. The measured electron temperature using the Langmuir probe located between the rf plates, where most of the electron heating takes place, is  $\approx 2\text{-}3$  eV (Table 1). It is reasonable, therefore, to argue that the bulk of the plasma well away from the electrodes region is cold. Moreover, the tail of the electron energy distribution function comprising high-energy electrons is not observed in the LP measurements for up to  $-70$  V applied voltages and is definitely negligible in the region far away from the electrodes. Hence, these electrons cannot

produce energetic ions that recombine to form H atoms with energies > 15-20 eV. The cross sections for resonant charge exchange transfer ( $Ar_{fast}^+ + Ar_{slow} \rightarrow Ar_{fast} + Ar_{slow}^+$  and  $He_{fast}^+ + He_{slow} \rightarrow He_{fast} + He_{slow}^+$ ) can be utilized to estimate the distance traveled by an ion produced in the cathode fall region without suffering a charge exchange collision that reduces the maximum energy it can obtain. At 20 eV, the resonant charge exchange transfer cross sections ( $\sigma_i$ ) for Ar and He ions are comparable at  $2.2 \times 10^{-15} \text{ cm}^2$  and  $1.5 \times 10^{-15} \text{ cm}^2$ , respectively [39].

The mean free path is given as  $\lambda_i = \frac{1}{n_g \sigma_i}$  cm, where  $n_g$ , the neutral particle density, is a function

of gas pressure. At 10 mTorr, the mean-free path for charge transfer,  $\lambda_i$ , is 0.06 cm. Therefore, the ions produced in the cathode fall region will not maintain their energy over a distance of 15 cm without suffering a charge exchange collision in these plasmas [39]. These ions cannot be the source of hot H atoms in a region far away from the electrodes. Moreover, the radiative lifetime of the hydrogen n=3 state is  $10^{-8}$  s [15] and with an assumed average velocity of  $10^6\text{-}10^7 \text{ cm/s}$  corresponding to hydrogen energies of 1-100 eV, it can only travel a distance of 0.01-0.1 mm before emission and reduced energy. This implies that the observed H<sub>a</sub> emission is a result of local excitation. The rapid thermalization of H atoms with the background gas will also localize fast H concentrations to the region where it is formed. Therefore, a mechanism that explains the localized production of hot H over the larger plasma chamber is required. Mills' hypothesis of a catalytic reaction of hydrogen is consistent with the observation of hot H atoms far way from the high field region.

In order to explain the symmetric line emission profile, the CM model mandates the presence of a reflector or divertor. In this model a Gaussian distribution is achieved either by the scattering of hydrogen atoms by the electrode surface or by collisional excitation of H<sub>f</sub> on H<sub>2</sub>

with large angle scattering [6], where  $H_f$  represents the hot hydrogen atoms that have previously collided with the electrode. This implies that the sputtered fast H atoms and the back-reflected fast H atoms from the cathode surface are produced in equal measure to produce a symmetric profile. This requires an “ideal isotropic reflector” to reverse the momentum of a positive ion gained from the electric field to give rise to fast H leaving the cathode in the same abundance as that moving towards the cathode. In addition, according to their model, a “divertor” must also exist such that the ratio of fast H at any given energy towards and away from the cathode remains equal and this must be the case in all directions including the direction perpendicular to the electric field. The interaction of an H atom with a metal surface is quasi-elastic for a large range of targets and energies. The particle and energy reflection coefficients for hydrogen atoms to be reflected back in the energy range of 20-30 eV are only 50% [40]. Therefore, the possibility that backscattered H atoms produced with a comparable distribution to those of the incident H atoms with comparable energy distributions so as to yield a symmetric profile is not feasible. In addition, it is well known that the effective cross section for many small-angle ion-neutral collisions to produce an equivalent deflection is larger than that for single large-angle collision [41]. Hence, this argument is not viable as a mechanism to explain the symmetry of the plasma emission profile.

Electron-ion, electron-neutral, and ion-neutral collision frequencies are a complex function of not only the gas pressure but also of the energy of the colliding particles. Therefore, in order to obtain a better insight into the energy transfer through the collision and charge exchange process, an estimate of the collision frequencies at the pressure and energies of interest is discussed. For a flux of incident electrons with velocities  $v$  colliding with a background neutral gas, the collision frequency is given approximately as  $\nu_{cn} = n_g \sigma v = n_g K \sim 3 \times 10^9 \times P(\text{Torr})s^{-1}$

where  $n_g$  is the neutral number density given by Loschmidt's number and  $\sigma$  is the collision cross-section and  $K$  is the rate constant [41-42]. At 10 mTorr and 10 Torr, the electron-neutral collision frequencies are  $3 \times 10^7 \text{ s}^{-1}$  and  $3 \times 10^{10} \text{ s}^{-1}$ , respectively, a variation of three orders of magnitude. Therefore at 10 mTorr, the electron-neutral collision frequency is comparable to the rf frequency and the electron can travel to the anode in one rf period of 73 ns. The LP measured electron temperature is 2-3 eV and the electron can travel a distance of about 8 cm during one rf period without suffering collisions with the background neutral gas. Therefore, in low-collision-rate plasmas compared to the ion transit time between the electrodes, based on the CM, fast H atoms produced by the charge exchange process will continue to move towards the direction of the accelerated ions and will yield a predominant red or blue wing in the emission spectrum relative to the direction of observation. However, the data presented in this paper are contrary to the prediction of the CM field acceleration mechanism of energy transfer to hydrogen atom. The symmetric line profile is independent of the angle of observation.

## VI CONCLUSION

The mechanism of extraordinary broadening of the hydrogen Balmer lines in hydrogen admixed with noble gases has been studied in two different discharge systems over a wide parameter range to examine highly collisional and weakly collisional regimes. Experiments were performed to test the validity of the field acceleration based Collisional Model. The field acceleration based Collisional Models were formulated to explain the energy gained by hydrogen atoms in experiments where only hydrogen plasmas and plasmas of hydrogen admixed with much heavier noble gases (Ar) were considered. As a result, the selective transfer of energy only to the hydrogen atom was not considered while theories were formulated to explain the

extraordinary broadening. However, we have found that energy is transferred only to hydrogen atoms and not to the admixed gases even when the admixed gas is helium with a mass ratio of 4:1. It was also realized that this energy transfer is not the same even when the admixed gases are electronically similar. For example, hot H atoms are absent when He and Ar are replaced with an electronically similar noble gas Xe. The directionality of energy gained according to the field acceleration based CM mechanism was tested by using sharp tipped electrodes in a DC discharge, thus minimizing the electrode surface area perpendicular to the axis. The plasma emission parallel and perpendicular to the electric field lines was sampled over a wide pressure range. The  $H_{\alpha}$  line profiles were observed to be symmetric in all cases. As discussed earlier, this symmetry can not be explained by the field acceleration based CM model, including its variations where it is argued that equally hot H atoms in equal measure are produced by backscattering with the cathode surface.

Moreover, the Collisional Model utilizes the presence of a plasma sheath where most of the ions are accelerated and these then transfer energy to hydrogen atoms through the charge exchange process. It has been shown in this paper that hot hydrogen atoms are observed far away from the cathode fall regions in plasmas. The presence of hot H in a region where the plasma potential variation is low and plasma electrons are cold ( $T_e < 2$  eV), is clearly in contrast to the CM. It is concluded that these observations are consistent with the RT-plasma mechanism.

References:

1. A.L. Cappelli, R.A. Gottscho, and T.A. Miller, "Doppler-broadened line shapes of atomic hydrogen in a parallel-plate radio frequency discharge," *Plasma Chem. Plasma Process*, vol. 5, pp. 317-331, 1985.
2. G. Baravian, Y. Chouan, A. Ricard, and G. Sultan, "Doppler broadened H<sub>a</sub> line shapes in a rf low pressure H<sub>2</sub> discharge," *J. Appl. Phys.*, vol. 61, pp. 5249-5253, 1987.
3. S. Djurovic and J.R. Roberts, "Hydrogen Balmer alpha line shapes for hydrogen-argon mixtures in a low-pressure rf discharge," *J. Appl. Phys.*, vol. 74, pp. 6558-6565, 1993.
4. C. Barabeau and J. Jolly, "Spectroscopic investigation of energetic atoms in a DC hydrogen glow discharge," *J. Phys. D, Appl. Phys.*, vol. 23, pp. 1168-1174, 1990.
5. N. Cvetanovic, M. M. Kuraica, and N. Konjevic, "Excessive Balmer line broadening in a plane cathode abnormal glow discharge in hydrogen," *J. Appl. Phys.*, vol. 97, pp. 33302-33309, 2005.
6. M.R.G. Adamov, B.M.Obradovic, M.M. Kuracia, and N. Konjevic, "Doppler spectroscopy of hydrogen and deuterium Balmer alpha line in an abnormal glow discharge," *IEEE Trans. Plasma Sci.*, vol. 31, no. 3, pp. 444-454, 2003.
7. E. L. Ayers and W. Benesch, "Shapes of atomic-hydrogen lines produced at cathode surface," *Phys. Rev. A, Gen. Phys.*, vol. 37, pp. 194, 1988.
8. W. Benesch and E. Li, "Line shapes of atomic hydrogen in hollow cathode discharge," *Opt. Lett.*, vol. 9, no. 8, pp. 338-340, 1984.
9. M. Kuraica and N. Konjevic, "Line shapes of atomic hydrogen in a plane-cathode abnormal glow discharge," *Phys. Rev. A*, vol. 46, no. 7, pp. 4429-4432, 1992.
10. M. Kuraica, N. Konjevic, M. Platisa, and D. Pantelic, "Plasma diagnostics of the Grimm-

type glow discharge," *Spectrochim. Act*, vol. 47, pp. 1173, 1992.

11. S. Alexiou and E. Leboucher-Dalimier, "Hydrogen Balmer- $\alpha$  in dense plasmas," *Phys. Rev. E*, vol. 60, no. 3, pp. 3436-3438, 1999.
12. S. B. Radovanov, J. K. Otthoff, R. J. Van Brunt, and S. Djorovic, " Ion kinetic-energy distribution of Balmer-alpha ( $H_{\alpha}$ ) excitation in Ar-H<sub>2</sub> radio-frequency discharges," *J. Appl. Phys.*, vol. 78, pp. 746-757, 1995.
13. A. V. Phelps, "Collisions of H<sup>+</sup>, H<sup>+</sup><sub>2</sub>, H<sup>+</sup><sub>3</sub>, ArH<sup>+</sup>, H<sup>-</sup>, H, and H<sub>2</sub> with Ar and of Ar<sup>+</sup> and ArH<sup>+</sup> with H<sub>2</sub> for Energies from 0.1 eV to 10 keV," *J. Phys. Chem. Ref Data*, vol. 21, pp. 883-897, 1992.
14. S. B. Radovanov, K. Dzierzega, J. R. Roberts, and J. K. Olthoff, "Time resolved Balmer-alpha emission from fast hydrogen atoms in low pressure, radiofrequency discharges in hydrogen," *Appl. Phys. Lett.*, vol. 66, no. 20, pp. 2637-2639, 1995.
15. A. Bogaerts and R. Gijbels, "Effects of adding hydrogen to an argon glow discharge: Overview of some relevant processes and some quantitative explanations," *J. Anal. At. Spectrom.*, vol. 15, pp. 441-449, 2000.
16. R. L. Mills, P. Ray, B. Dhandapani, R. M. Mayo, and J. He, "Comparison of excessive Balmer  $\alpha$  line broadening of glow discharge and microwave hydrogen plasmas with certain catalysts," *J. Appl. Phys.*, vol. 92, pp. 7008-7022, 2002.
17. R. L. Mills, P. C. Ray, M. Nansteel, X. Chen, R.M. Mayo, J. He, and B. Dhandapani, "Comparison of excessive Balmer  $\alpha$  line broadening of inductively and capacitively coupled RF, microwave, and glow discharge hydrogen plasma with certain catalysts", *IEEE Trans. Plasma Sci.*, vol. 31, pp. 338-355, 2003.
18. R. L. Mills and P. Ray, "Extreme ultraviolet spectroscopy of helium-hydrogen plasma," *J.*

*Phys. D: Appl. Phys.*, vol. 36, pp. 1535-1542, 2003.

19. R. L. Mills, P. Ray, B. Dhandapani, M. Nansteel, X. Chen, and J. He, "New power source from fractional quantum energy levels of atomic hydrogen that surpasses internal combustion," *J Mol. Struct.*, vol. 643, no. 1-3, pp. 43-54, 2002.
20. R. Mills and P. Ray, "Spectral emission of fractional quantum energy levels of atomic hydrogen from a helium-hydrogen plasma and the implications for dark matter," *Int. J. Hydrogen Energy*, vol. 27, no. 3, pp. 301-322, 2002.
21. C. Chen, T. Wei, L. R. Collins, and J. Phillips, "Modelling the discharge region of a microwave generated hydrogen plasma." *J. Phys. D: Appl. Phys.*, vol. 32, pp. 688-698, 1999.
22. R. L. Mills and P. Ray, "Substantial changes in the characteristics of a microwave plasma due to combining argon and hydrogen," *New J. Phys.*, www.njp.org, vol. 4, pp. 22.1-22.17, 2002.
23. R. Mills, M. Nansteel, and P. Ray, "Argon-hydrogen-strontium discharge light source," *IEEE Trans. Plasma Sci.*, vol. 30, no. 2, pp. 639-652, 2002.
24. R. Mills, M. Nansteel, and P. Ray, "Bright hydrogen-light source due to resonant energy transfer with strontium and argon ions", *New J. Phys.*, vol. 4, pp. 70.1-70.28, 2002.
25. R. Mills, "Spectroscopic identification of a novel catalytic reaction of atomic hydrogen and hydride ion product", *Int. J. Hydrogen Energy*, vol. 26, pp. 1041-1058, 2001.
26. R. Mills and P. Ray, "Vibrational spectral emission of fractional-principal-quantum-energy-level hydrogen molecular ion, *Int. J. Hydrogen Energy*, vol. 27, pp. 533-564, 2002.
27. W.L. Wiese, "Line Braodening", in *Plasma Diagnostic Techniques*, R. H. Huddleston and S. L. Leonard, Eds., Academic Press, NY, (1965)

28. F. F. Chen, "Electric Probes", in *Plasma Diagnostic Techniques*, R. H. Huddleston and S. L. Leonard, Eds., Academic Press, NY, (1965).
29. A. Ganguli, M.K. Akhtar, and R.D. Tarey, "Investigation of microwave plasmas produced in a mirror machine using ordinary-mode polarization", *Plasma Sources Science & Technol.* 8, pp. 519, 1999.
30. Kamran Akhtar, John E. Scharer, Shane Tysk and Enny Kho," Plasma interferometry at high pressures", *Rev. Sci. Instrum.*, 74, pp. 996, 2003.
31. B. Van Zyl, H. Neumann, H.L. Rothwell, Jr., and R.C. Amme, "Balmer- $\alpha$  and Balmer- $\beta$  emission cross sections for H + Ar collisions", *Phys. Rev. A* , Vol. 21, pp. 716, 1980.
32. B. Van Zyl, H.L. Rothwell, Jr., and H. Neumann, "Balmer- $\alpha$  and Balmer- $\beta$  emission cross sections for H<sup>+</sup> + Ar collisions", *Phys. Rev. A* , Vol. 21, pp. 730, 1980.
33. B. Van Zyl, M. W. Gealy, and H. Neumann, " Balmer- $\alpha$  and Balmer- $\beta$  emission cross sections for low-energy H collisions with He and H<sub>2</sub>", *Phys. Rev. A*, Vol. 28, pp. 176, 1983.
34. B. Van Zyl, M. W. Gealy, and H. Neumann, "Excitation of low-energy H atoms in H+Ne collisions", *Phys. Rev. A* , Vol. 31, 5, pp. 2922, 1985.
35. B. Van Zyl, H. Neumann, and M. W. Gealy, "Balmer-line emission from low-energy H impact on Kr and Xe", *Phys. Rev. A* , Vol. 33, pp. 2093, 1986.
36. B. Van Zyl, M. W. Gealy, and H. Neumann, "Balmer-line emission from low-energy H<sup>+</sup> impact on rare-gas atoms", *Phys. Rev. A* , Vol. 33, 4, pp. 2333, 1986.
37. M. Arnaud and R. Rohenflug, *Astron. & Astrophys. Suppl.* 60, 425 (1985),
38. T. Kato and E. Asano, " comparison of recombination rate coefficients given by empirical formulas for ions from hydrogen through nickel", NIFS-DATA-54, National Institute of Fusion Science (NIFS), Nagoya, Japan, 1999.

39. E.W. McDaniel, J.B.A. Mitchell, and M.E. Rudd, *Atomic Collision: Heavy Particles Projectiles*, Wiley, New York, 1993.
40. D.E. Post and R. Behisch, Physics of Plasmas-Wall Interactions in Controlled Fusion, NATO ASI series B, 131, 423, (1986)
41. M.A. Lieberman and A.J. Lichtenberg, "Principles of plasma discharges and material processing", 2<sup>nd</sup> edition, Hoboken, New Jersey: John Wiley & Sons, Inc., 2005.
42. V. Vahedi, R. A. Stewart, and M. A. Lieberman, "Analytic model of the ion angular distribution in a collisional sheath," *J. Vac. Sci. Technol. A*, vol. 11, pp. 1275-1282, 1993.

TABLE I

Langmuir probe measurement of plasma density and electron temperature in capacitively coupled radio frequency plasmas at 100 mTorr and 100 W coupled rf power.

Gas Composition	Bulk Plasma Density ( $\text{cm}^{-3}$ )	Bulk Electron Temperature (eV)
Ar	$2-3 \times 10^{10}$	2.1-2.4
Ar/10%H <sub>2</sub>	$5-8 \times 10^9$	1.8-2.0
He	$6-9 \times 10^9$	2.5-3.0
He/10%H <sub>2</sub>	$3-5 \times 10^9$	1.9-2.3
Xe	$2-5 \times 10^{10}$	1.7-2.0
Xe/10%H <sub>2</sub>	$7-9 \times 10^9$	1.7-1.9

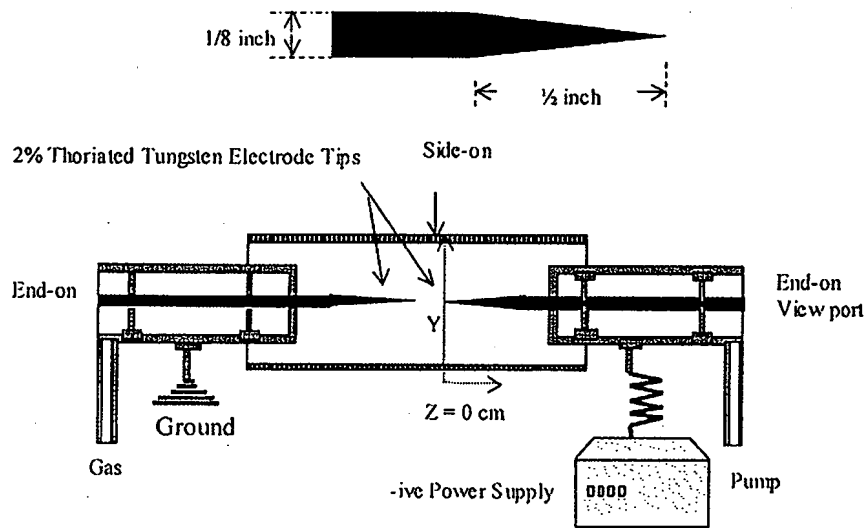


Fig 1. Schematic of the DC discharge created between the fine tips of 2% thoriated tungsten electrodes with the direction of axial scans defined. The cathode tip is taken as  $z=0$  cm for side-on observations measured along the axis of the cathode from its tip to its electrical connection.

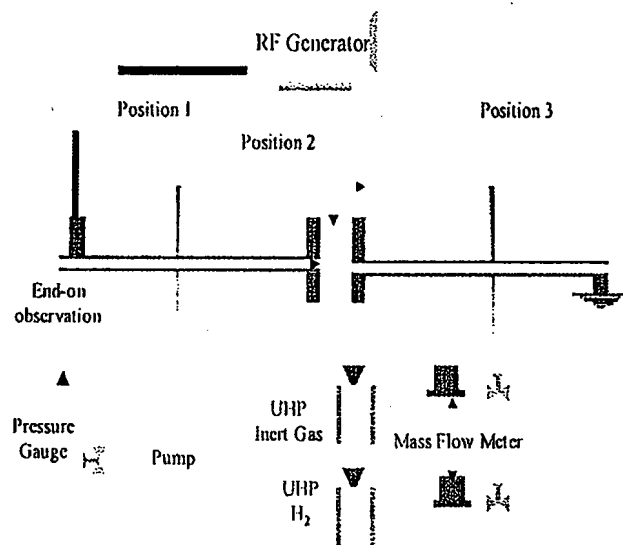


Fig.2: Schematic of the capacitively coupled radio frequency plasma system. Optical emission spectroscopy is performed perpendicular to the electric field (Position 2) and parallel to the field (end-on observation).

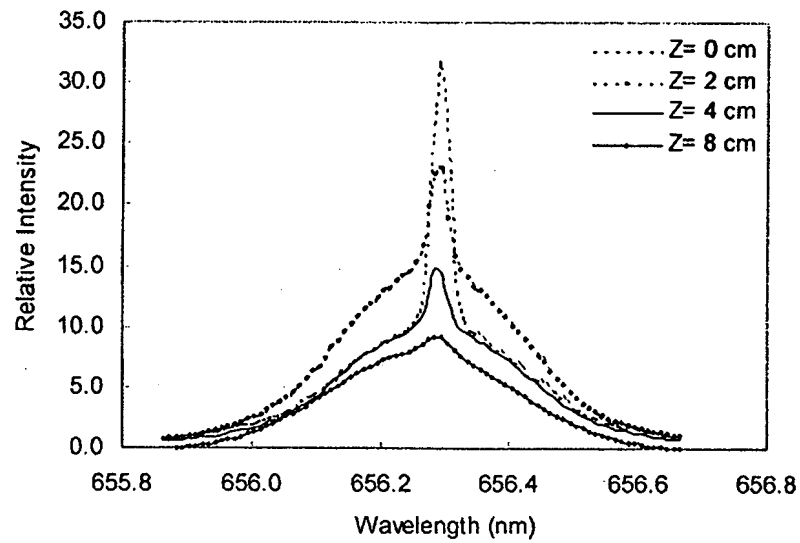


Fig. 3. Axial scan of the 656.3 nm Balmer  $\alpha$  line width recorded on a 1 Torr  $Ar/H_2$  (95/5%) DC plasma discharge with needle-like electrodes at 400 V and 20 mA showing 80% of the hydrogen was 'hot' with an average hydrogen atom energy of 40 eV, compared to < 0.5 eV for the slow population.

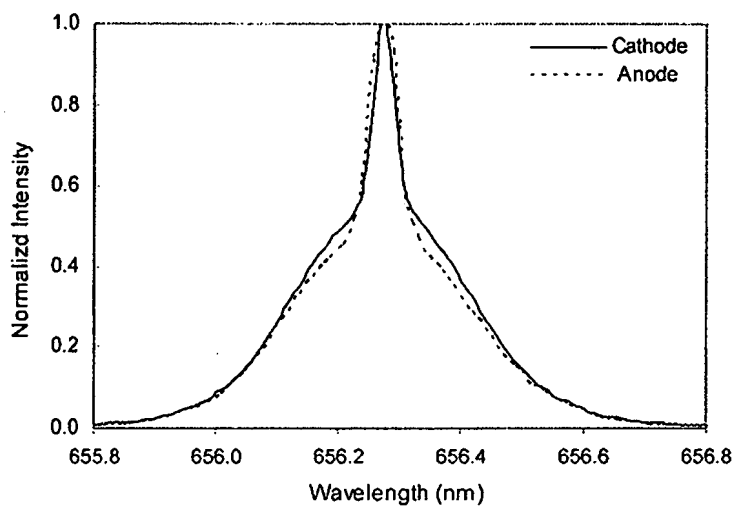


Fig. 4. The 656.3 nm Balmer  $\alpha$  line width recorded end-on (parallel to the electric field) on a 1 Torr  $Ar/H_2$  (95/5%) DC plasma discharge with needle-like electrodes at 400 V and 20 mA. Both views looking towards the cathode as well as the anode show a symmetrical emission profile. The temperature of hot hydrogen atoms is in the range of 38-40 eV.

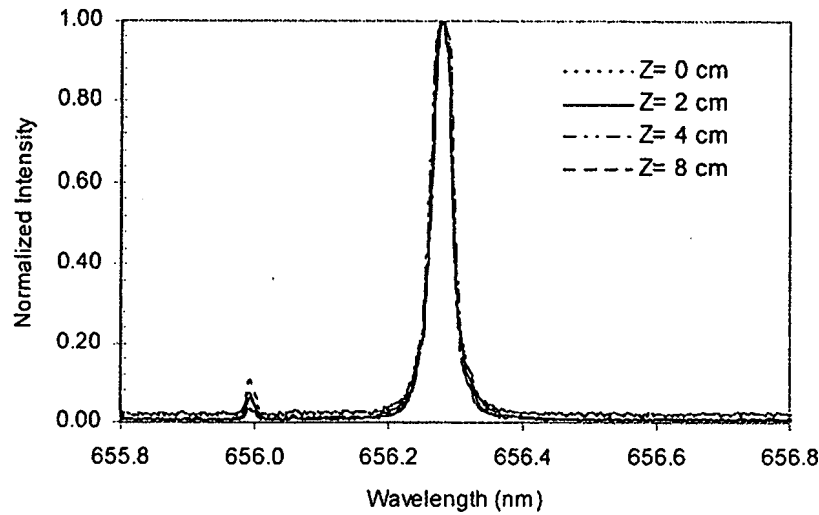


Fig. 5. Axial scan of the 656.3 nm Balmer  $\alpha$  line width recorded on a 1 Torr  $Xe/H_2$  (95/5%) DC plasma discharge with needle-like electrodes at 400 V and 20 mA showing only a cold population of <1 eV with a decrease in intensity along the cathode due to a decrease in electron density and energy.

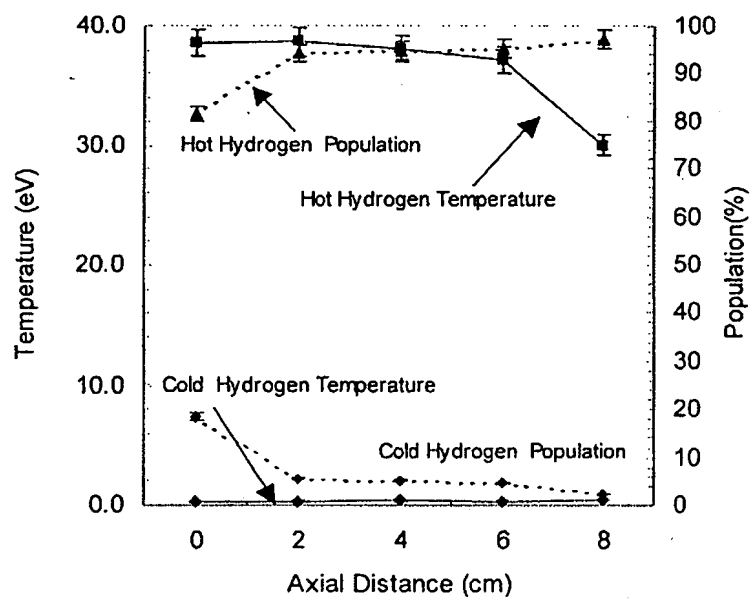


Fig. 6. Axial plots of hot hydrogen atoms temperature and population (given by area under the curve) corresponding to the spectrum in Figure. 3. A hot hydrogen population is present even at a distance of 8 cm away from the cathode tip where most of the potential falls.

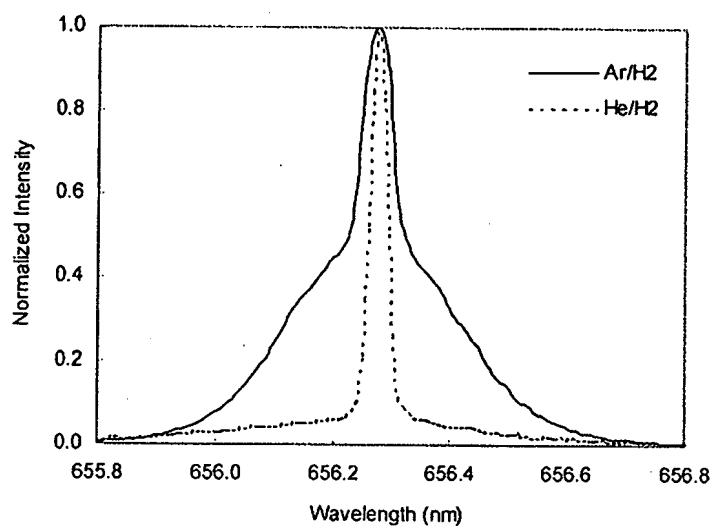


Fig. 7 Normalized end-on emission spectrum of 1 Torr Ar/5%H<sub>2</sub> and He/5%H<sub>2</sub> plasma looking towards the anode. Note the symmetrical emission profile.

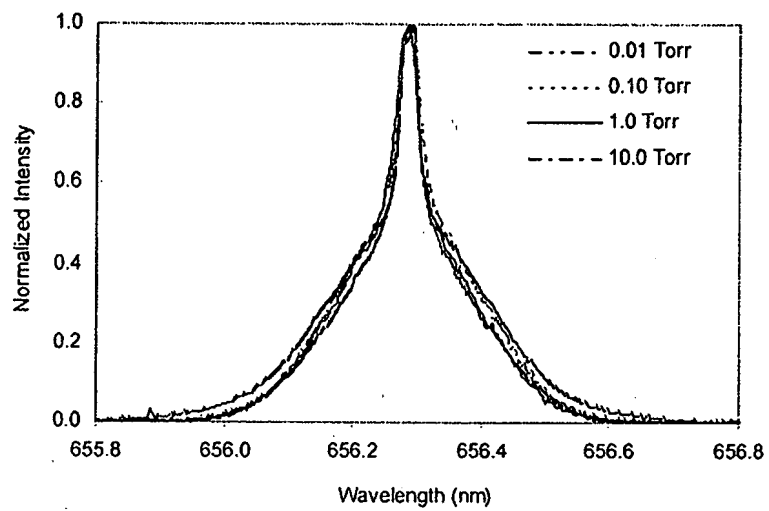


Fig. 8 Normalized end-on emission spectrum of Ar/5%H<sub>2</sub> plasma looking towards cathode as the gas pressure is varied over three-orders-of magnitude from 10 mTorr to 10 Torr. Note the symmetrical emission profile.

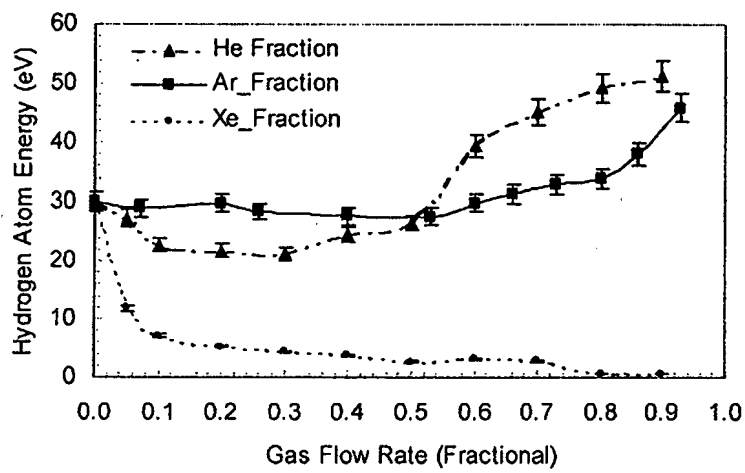


Fig.9 Energy of hot hydrogen atoms as a function of fractional concentration of admixed gases in a DC discharge at 100 mTorr. Note the increase in the energy of hot H as Ar and He concentration increases and decrease in energy with the addition of Xe.

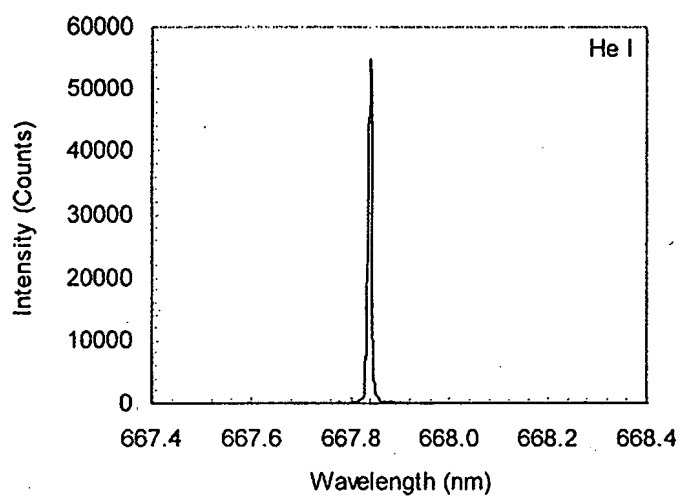


Fig. 10

Fig. 10 The 667.816 nm He I line width for 1 Torr He/H<sub>2</sub> (95/5%) at 400 V and 20 mA . No broadening was observed,

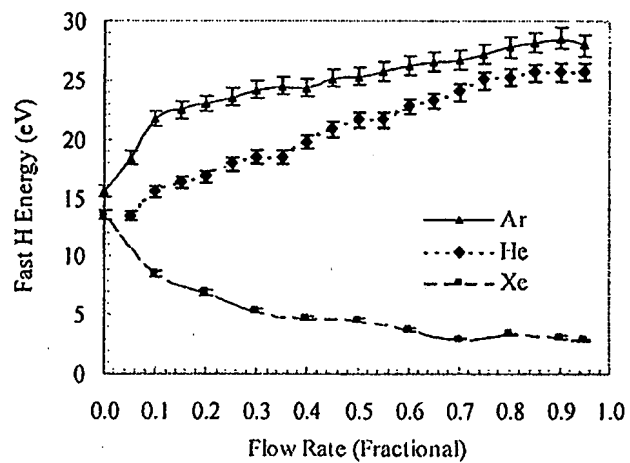


Fig.11. Energy of hot hydrogen atom in  $\text{Ar}/\text{H}_2$ ,  $\text{He}/\text{H}_2$  and  $\text{Xe}/\text{H}_2$  plasmas as a function of the noble gas concentration [ $\text{H}_2(x)$  Ar, He, Xe( $y=1-x$ )] in capacitively coupled rf discharge. The plasma chamber is maintained at 150 mTorr with a total flow rate of 20 sccm. The coupled rf power is 200 Watt.  $\text{H}_\alpha$  emission is sampled perpendicular to the electric field between the capacitive plates.

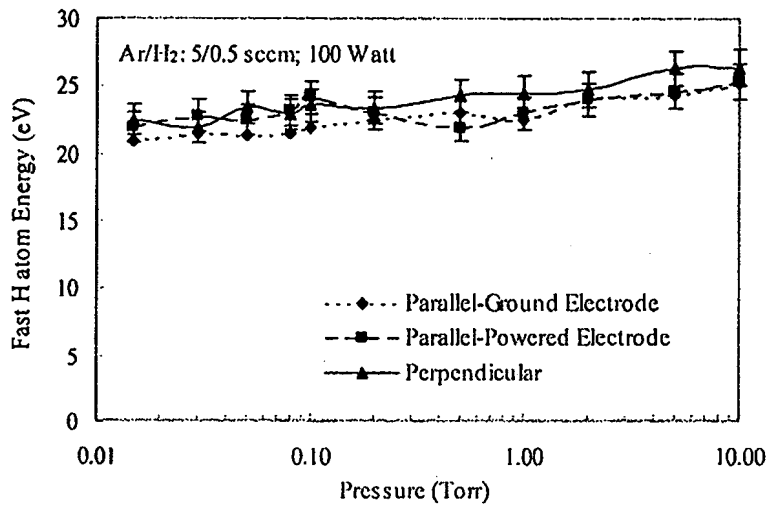


Fig. 12: Hot hydrogen atom temperature for capacitively coupled Ar/H<sub>2</sub> discharge at different gas pressures. Observations are made perpendicular to the field between the electrodes and parallel to the field lines through holes in both powered and grounded electrodes.

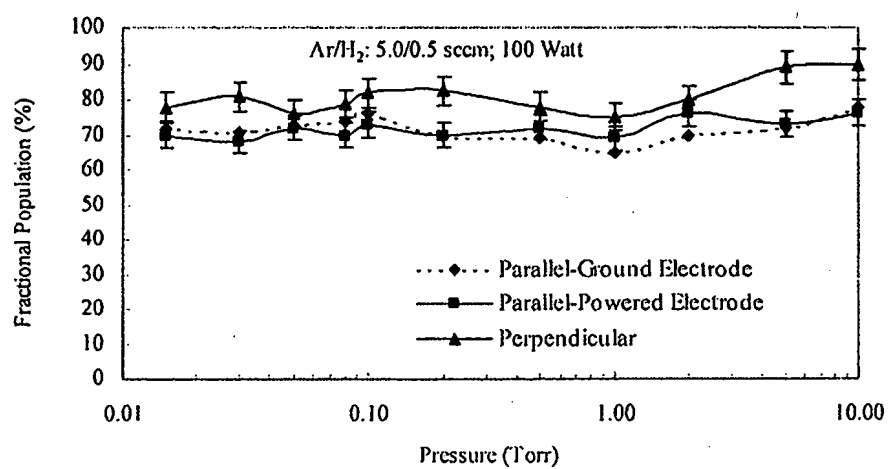


Fig.13. Fractional population of hot hydrogen atoms in  $n=3$  excited state in a capacitively coupled Ar/H<sub>2</sub> discharge at different gas pressures.

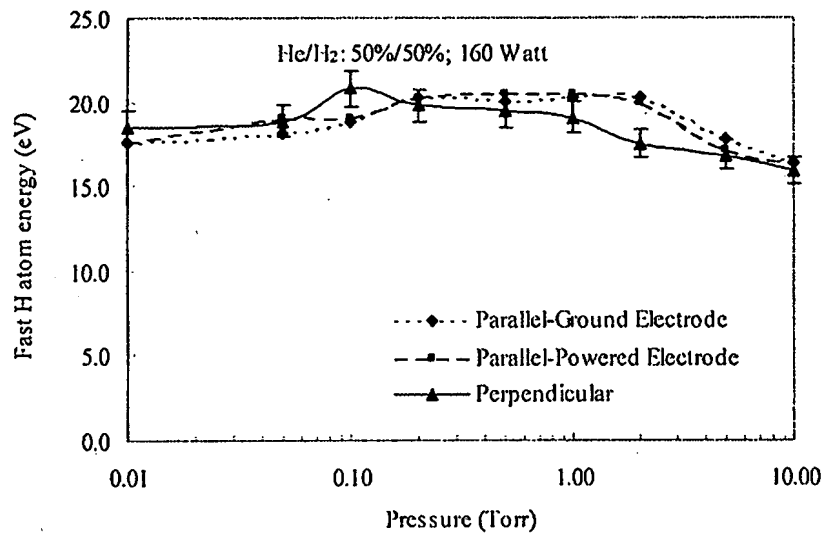


Fig.14. Hot hydrogen atom energy in a capacitively coupled He/H<sub>2</sub> discharge at different gas pressures.

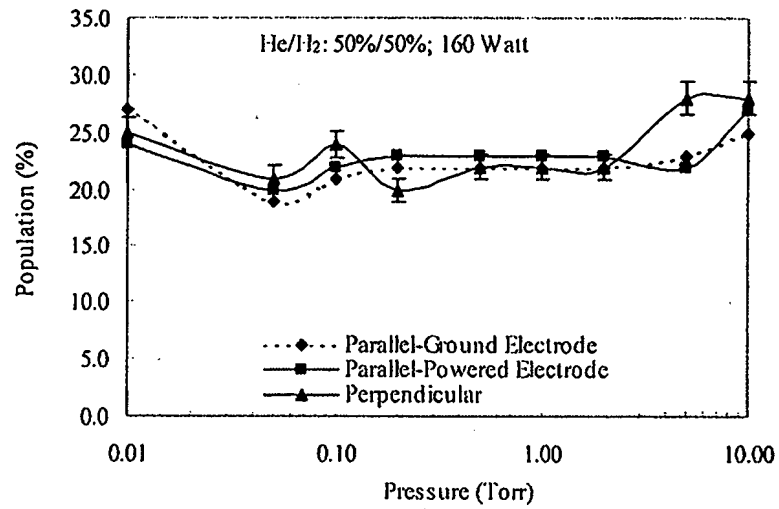
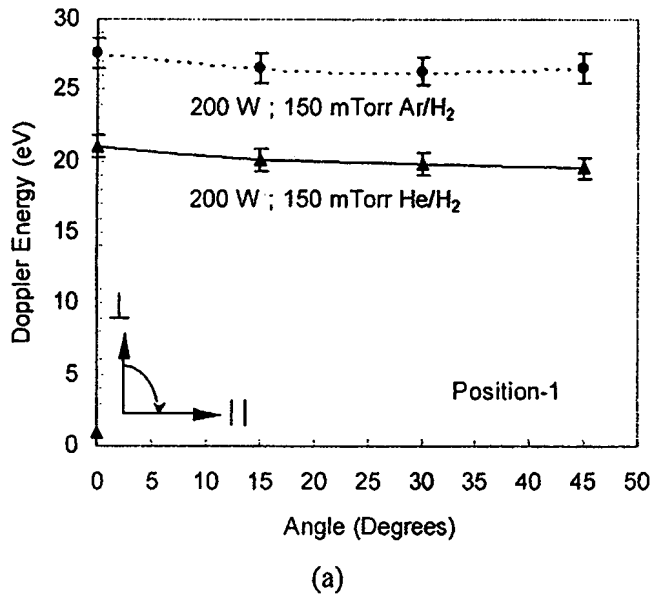
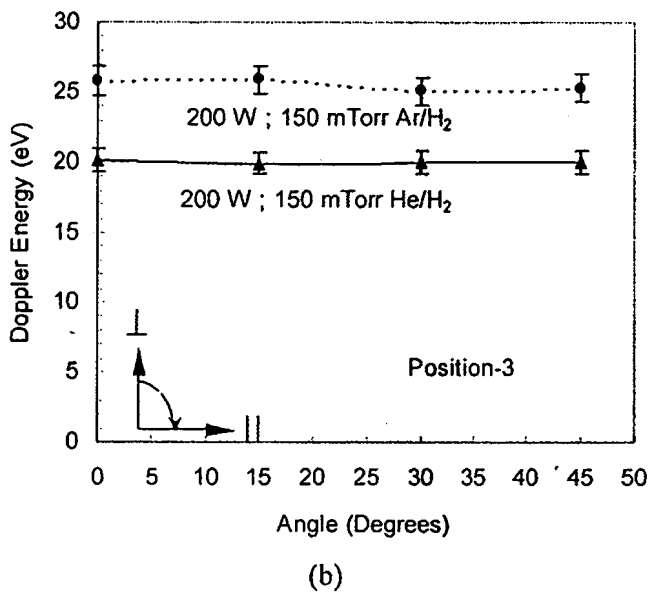


Fig.15. Fractional population of hot hydrogen atoms ( $n=3$  state) in a capacitively coupled He/H<sub>2</sub> discharge at different gas pressures.



(a)



(b)

Fig.16. Angular variation of Doppler energy of hot hydrogen atom in a capacitively coupled radio frequency discharge at 150 mTorr 50%Ar/50%H<sub>2</sub> and 50%He/50%H<sub>2</sub> plasma at 200 W. Plasma emission is sampled at Position 1 (Fig. a) and Position 3 (Fig. b) far away from the region of high field in plasma sheath. Reference is normal to the chamber axis.

## Water Bath Calorimetry on a Catalytic Reaction of Atomic Hydrogen

R. L. Mills\*, H. Zea, J. He, B. Dhandapani

BlackLight Power, Inc.

493 Old Trenton Road

Cranbury, NJ 08512

### ABSTRACT

Plasmas of certain catalysts such as  $Sr^+$  and  $Ar^+$  mixed with hydrogen were studied for evidence of a novel energetic reaction. These hydrogen plasmas called resonant transfer or rt-plasmas were observed to form at low temperatures (e.g.  $\approx 10^3 K$ ) and extraordinary low field strengths of about 1-2 V/cm when argon and strontium were present with atomic hydrogen. Time-dependent line broadening of the H Balmer  $\alpha$  line was observed corresponding to extraordinarily fast H (25 eV). When an argon-hydrogen hollow-anode glow discharge plasma with strontium metal contained in the cell was optimized for  $Sr^+$  emission, an average hydrogen hot atom temperature of 50.2 eV with a 83.5% population and an excess power of 28.5% of the input power were observed. Using water bath calorimetry, an excess power of 2.85 W was measured on rt-plasmas with  $Sr^+$  and  $Ar^+$  as catalysts and atomic hydrogen as a reactant, compared with controls with no hydrogen and no catalyst present. The energy balance was high. Given an argon-hydrogen (95/5 %) flow rate of 1.0 sccm and an average excess power of 2.85 W and energy balances of over  $-7.7 \times 10^4 kJ/mole H_2$  were measured.

Keywords: catalysis, rt-plasma, fast H, excess power

\* To whom correspondence should be addressed. Phone: 609-490-1090; Fax: 609-490-1066;  
E-mail: [rmills@blacklightpower.com](mailto:rmills@blacklightpower.com)

## 1. Introduction

A new chemically generated or assisted plasma source has been developed that is based on a resonant energy transfer mechanism (rt-plasma). One such source operates by incandescently heating a hydrogen dissociator and a catalyst to provide atomic hydrogen and gaseous catalyst, respectively, such that the catalyst reacts with the atomic hydrogen to produce a plasma. It was extraordinary that intense EUV emission was observed by Mills, et al. [1-4] at low temperatures (e.g.  $\approx 10^3$  K) and an extraordinary low field strength of about 1-2 V/cm from atomic hydrogen and certain atomized elements or certain gaseous ions, which singly or multiply ionize at integer multiples of the potential energy of atomic hydrogen, 27.2 eV. A number of independent experimental observations [1-26] confirm that the rt-plasma is due to a novel reaction of atomic hydrogen which produces as chemical intermediates, hydrogen atoms in fractional quantum states that are at lower energies than the traditional "ground" ( $n=1$ ) state. Power is released, and the final reaction products are novel hydride compounds. The supporting data include EUV spectroscopy [1-7, 10, 14-20, 23], characteristic emission from catalysts and the hydride ion products [1-4, 14, 16-20], lower-energy hydrogen emission [5-7, 23], chemically formed plasmas [1-4, 14-20], Balmer  $\alpha$  line broadening [1-6, 8-14, 16, 19-20, 23], population inversion of H lines [19-21], elevated electron temperature [6, 8-9], anomalous plasma afterglow duration [14-15], power generation [6, 10, 14, 22-23], and analysis of novel chemical compounds [14, 24-26].

The theory given previously [27-29] is based on applying Maxwell's equations to the wave equation. The familiar Rydberg equation (Eq. (1)) arises for the hydrogen excited states for  $n > 1$  of Eq. (2).

$$E_n = -\frac{e^2}{n^2 8\pi\epsilon_0 a_H} = -\frac{13.598 \text{ eV}}{n^2} \quad (1)$$

$$n = 1, 2, 3, \dots \quad (2)$$

An additional result is that atomic hydrogen may undergo a catalytic reaction with certain atoms and ions, which singly or multiply ionize at integer multiples of the potential energy of atomic hydrogen,  $m \cdot 27.2 \text{ eV}$ , wherein  $m$  is an integer. The reaction involves a nonradiative energy transfer to form a hydrogen atom that is lower in energy than unreacted atomic hydrogen that corresponds to a fractional principal quantum number. That is

$$n = \frac{1}{2}, \frac{1}{3}, \frac{1}{4}, \dots, \frac{1}{p}; \quad p \text{ is an integer} \quad (3)$$

replaces the well known parameter  $n = \text{integer}$  in the Rydberg equation for hydrogen excited states. The  $n=1$  state of hydrogen and the  $n=\frac{1}{\text{integer}}$  states of hydrogen are nonradiative, but a transition between two nonradiative states, say  $n=1$  to  $n=1/2$ , is possible via a

nonradiative energy transfer. Thus, a catalyst provides a net positive enthalpy of reaction of  $m \cdot 27.2 \text{ eV}$  (i.e. it resonantly accepts the nonradiative energy transfer from hydrogen atoms and releases the energy to the surroundings to affect electronic transitions to fractional quantum energy levels). As a consequence of the nonradiative energy transfer, the hydrogen atom becomes unstable and emits further energy as  $q \cdot 13.6 \text{ eV}$  emission [5-7] or  $q \cdot 13.6 \text{ eV}$  transfer to H to form extraordinarily hot, excited-state H [8-13] until it achieves a lower-energy nonradiative state having a principal energy level given by Eqs. (1) and (3). Processes such as hydrogen molecular bond formation that occur without photons and that require collisions are common [30]. Also, some commercial phosphors are based on resonant nonradiative energy transfer involving multipole coupling [31].

Certain atoms, excimers, and ions which provide a reaction with a net enthalpy of an integer multiple of the potential energy of atomic hydrogen,  $E_h = 27.2 \text{ eV}$  where  $E_h$  is one hartree. Specific species (e.g.  $\text{He}^+$ ,  $\text{Ar}^+$ ,  $\text{K}$ , and  $\text{Sr}^+$ ) identifiable on the basis of their known electron energy levels are required to be present in plasmas with atomic hydrogen to catalyze the process. In contrast, species such as atoms or ions of  $\text{Mg}$  or  $\text{Xe}$  do not fulfill the catalyst criterion—a chemical or physical process with an enthalpy change equal to an integer multiple of  $E_h$  that is sufficiently reactive with atomic hydrogen under reaction conditions.

$\text{Ar}^+$  may serve as a catalyst since its ionization energy is about  $27.2 \text{ eV}$ . Also, since the ionization energy of  $\text{Sr}^+$  to  $\text{Sr}^{3+}$  has a net enthalpy of reaction of  $2 \cdot 27.2 \text{ eV}$ ,  $\text{Sr}^+$  may serve as catalyst alone or with  $\text{Ar}^+$  catalyst. It was reported previously that an rt-plasma formed with a low field ( $1\text{V/cm}$ ), at low temperatures (e.g.  $\approx 10^3 \text{ K}$ ), from atomic hydrogen generated at a tungsten filament and strontium which was vaporized by heating the metal [1-4]. Strong VUV emission was observed that increased with the addition of argon, but not when sodium, magnesium, or barium replaced strontium or with hydrogen, argon, or strontium alone. Characteristic emission was observed from a continuum state of  $\text{Ar}^{2+}$  at  $45.6 \text{ nm}$  without the typical Rydberg series of Ar I and Ar II lines which confirmed the resonant nonradiative energy transfer of  $27.2 \text{ eV}$  from atomic hydrogen to  $\text{Ar}^+$  [2, 4, 18]. Predicted  $\text{Sr}^{3+}$  emission lines were also observed from strontium-hydrogen plasmas [2, 4] that supported the rt-plasma mechanism.

Significant Balmer  $\alpha$  line broadening corresponding to an average hydrogen atom temperature of  $14 \text{ eV}$  and  $24 \text{ eV}$  was observed for strontium and argon-strontium rt-plasmas and  $23\text{-}45 \text{ eV}$  for discharges of strontium-hydrogen, helium-hydrogen, argon-hydrogen, strontium-helium-hydrogen, and strontium-argon-hydrogen, compared to  $\approx 3 \text{ eV}$  for pure hydrogen, krypton-hydrogen, xenon-hydrogen, and magnesium-hydrogen. To achieve that same optically measured light output power, sodium-hydrogen, magnesium-hydrogen, and barium-hydrogen mixtures required 4000, 7000, and 6500 times the power of the strontium-

hydrogen mixture, respectively, and the addition of argon increased these ratios by a factor of about two. A glow discharge plasma formed for strontium-hydrogen mixtures at an extremely low voltage of about 2 V compared to 250 V for hydrogen alone and sodium-hydrogen mixtures, and 140-150 V for magnesium-hydrogen and barium-hydrogen mixtures [1-2, 4]. These voltages are too low to be explicable by conventional mechanisms involving accelerated ions with a high applied field.

To further characterize argon-strontium rt-plasmas, plasma formation was studied relative to mixtures of hydrogen and a chemically similar control that does not have electron ionization energies which are a multiple of 27.2 eV, and the Balmer lines were recorded by visible spectroscopy to confirm that an energetic hydrogen plasma was present having H energy states greater than 12 eV corresponding to  $n \geq 3$  in Eqs. (1-2). The broadening of the Balmer  $\alpha$  line was also recorded as a function of time, and thermal power balance measurements were performed. The cell comprised a titanium or tungsten filament to heat and vaporize some strontium as a source of catalyst and to dissociate molecular hydrogen to atomic hydrogen. The addition of argon to the plasma further provided the catalyst  $Ar^+$ .

Since a conventional discharge power source was not present, the formation of a plasma would require an energetic reaction. The origin of Doppler broadening is the relative thermal motion of the emitter with respect to the observer—in this case the spectrometer. Line broadening is a measure of the atom temperature, and a significant increase was expected and observed for catalysts from strontium or argon with hydrogen. The observation of a high hydrogen temperature with no conventional explanation would indicate that an rt-plasma must have a source of free energy. An energetic chemical reaction was further indicated since it was found that the broadening is time dependent. Therefore, the thermal power balance was measured calorimetrically. To maintain a constant level of ionized argon and strontium as catalysts, a DC glow discharge of plasma of argon-hydrogen (97/3%)-strontium was maintained using a hollow anode. The energy balance was measured by water bath calorimetry. We report the results of these characterizations and discuss the implications regarding the rt-plasma mechanism in Secs. 3A-C.

## 2. Experimental

**Balmer Line Broadening.** An argon-hydrogen (97/3%)-strontium rt-plasma was generated in the experimental set up (Figure 1) described previously [1-4] comprising a thermally insulated quartz cell with a cap that incorporated ports for gas inlet, and outlet. A titanium filament (55 cm long, 0.5 mm diameter) that served as a heater and hydrogen dissociator was in the quartz tube. 2.5 g of magnesium or strontium metal (Alfa Aesar 99.95%) was placed in the center of the cell under one atmosphere of dry argon in a glovebox.

The cell was sealed and removed from the glovebox. The cell was maintained at 50 °C for four hours with helium flowing at 30 sccm at a pressure of 0.6 Torr. The filament power was increased to 120 W in 20 increments every 20 minutes. At 120 W, the filament temperature was estimated to be in the range 800 to 1000 °C. The external cell wall temperature was about 700 °C. The cell was then operated with and without an argon-hydrogen (90/10%) flow rate of 5.5 sccm maintained at 0.6 Torr. Additionally, the cell was operated with hydrogen and argon-hydrogen (90/10%) gas flow and no metal. Each metal was vaporized by the filament heater. The presence of a hydrogen plasma was determined by recording the visible spectrum over the Balmer region with a Jobin Yvon Horiba 1250 M spectrometer with a PMT detector described previously [8-9] using entrance/exits slits of 200/100  $\mu\text{m}$ , 0.1 Å step size, and a 3 s integration time. The width of the 656.3 nm Balmer  $\alpha$  line emitted from the argon-hydrogen (90/10%)-strontium rt-plasma having a titanium filament was measured initially and periodically during operation. The Balmer profile was also recorded on the air-gap, glow discharge reactor described in the next section with an input power of 20 W (V=200; I=0.1A).

**Power balance measurements.** The power balance of a rt-plasma of strontium with argon-hydrogen mixture (95/5%) maintained in an air-gap, glow discharge reactor shown in Figure 2 was measured by water bath calorimetry using the experimental setup shown in Figure 3. Excess power was observed from argon-hydrogen-strontium plasmas compared to calibration control experiments with the same input power.

The reaction cell comprised a cylindrical stainless steel case of 5.1 cm OD and 17.2 cm in length welded to a set of high vacuum, 8.6 cm diameter Con-flat flanges, as shown in Figure 2. A silver plated copper gasket was placed between a mating flange and the cell flange. The two flanges were clamped together with 10 circumferential bolts. The top-mating flange had a radial centered stainless steel hollow feed through that extended 8.6 cm into the cell and was partially covered by a 3.6 cm long ceramic sleeve, measured from the flange. Gas was fed into the cell by a 1 cm OD stainless steel tube welded to the top-mating flange. Gas flow was controlled by a 0-20 sccm range mass flow controller (MKS model M100B21CS1BV). The cell pressure was monitored by a 0-10 Torr MKS Baratron (model 626A11TEE) absolute pressure gauge. Additionally, the top-mating flange had a drilled thermo well that housed a stainless steel thermocouple (0.3 cm OD). Two 1 cm OD stainless steel tubes were welded to the bottom wall of the reaction cell. One carried the exhaust gas, and the other served as a connection port for a 0.6 cm OD and 16.5 cm long quartz rod to perform optical emission spectroscopy studies. In an oxygen free environment (glove box), 4 grams of strontium distributed in 15 pieces was loaded into the reaction cell and placed below the hollow electrode

as shown in Figure 2, the reaction cell was transferred into the stainless steel jacket, and all the gas and electrical connections were fitted and checked for leaks.

The reaction cell was housed inside a cylindrical stainless steel jacket of 15.2 cm OD and 30.5 cm in length with a removable front flange having welded Ultratorr connectors that fit the reaction cell gas line and the thermocouple. The bottom wall of the stainless steel jacket had two welded Ultratorr connections that fitted the reaction cell exhaust gas and the quartz rod connection port. Two 0.41 cm OD copper power feed-throughs were welded on the side wall and that provided electrical connectors for the reaction cell when it was placed inside the stainless steel jacket. The jacket housing containing the reaction cell was placed inside the drained water bath container, the gas inlet and outlet tubes were connected to the gas/vacuum manifold, as shown in Figure 3.

The water bath (Figure 3) comprised an insulated reservoir filled with 41 liters of deionized water. The water was agitated with a paddle driven by a stirring motor. A high precision linear response thermistor probe (Omega OL-703) recorded the temperature of the water bath as a function of time for the stirrer alone to establish the baseline. The water bath was calibrated by a high precision heater (Watlow LGEX17B Type CR-1, with a Xantrex XDC power supply 0-6000  $\pm$  0.01 W). Each experiment comprised three distinctive periods: pre-period, heating period, and post period. The pre-period was performed with no power applied to the electrode or to the heater during the reaction test or calibration test, respectively. During the heating period, power was applied through the electrode or through the heater. In the post period, the power applied during the heating period was turned off. The water of the bath was agitated with a stirrer spinning at constant speed throughout all three periods.

The heat capacity was determined for several input powers, 10, 20, 30, 40, and 50 W  $\pm$  0.01 W, and was found to be independent of input power over this power range within  $\pm$  1.8 %. The temperature rise of the reservoir as a function of time gave a slope in  $^{\circ}\text{C}/\text{s}$ . This slope was baseline corrected for the stirrer power and loss to ambient. The constant known input power (J/s), was divided by this slope to give the heat capacity in J/ $^{\circ}\text{C}$ . Then, in general, the total power output from the cell to the reservoir was determined by multiplying the heat capacity by the rate of temperature rise ( $^{\circ}\text{C}/\text{s}$ ) to give J/s.

The power balance for a plasma system consisting of the contents of the water bath calorimeter is [23]

$$\dot{H} = \dot{M} (\hat{H}_{in} - \hat{H}_{out}) + \dot{Q}_{plasma} + \dot{Q}_{power\ cable} + \dot{Q}_{stirrer} + \dot{Q}_{heat\ exchange} \quad (4)$$

where  $H$ 's are enthalpy values (inlet and outlet gases as indicated by the subscripts in and out, respectively, and the hat designates per mole),  $\dot{M}$  is the molar flow rate, and the  $\dot{Q}$ 's are heat flow rates. It is clear from Eq. (4) that a correction must be considered both for the gas flow term (first term, right side), ' $\dot{Q}_{power\ cable}$ ' which represents the input of the section (approx. 80 cm long) of the power cable that passes through the water bath as it brings power to the discharge, for the work of the stirrer, and for the heat exchange between the insulated water bath and its surroundings.

The values of ' $\dot{Q}_{power\ cable}$ ' and the heat carried out with the gas were small, as determined by appropriate temperature readings. Thermocouples were employed to measure the temperature of the input and output gas, as well as the temperature of the power cable just outside the water bath. Given that the temperature of the power cable was the same as the water bath,  $\dot{Q}_{power\ cable}$  was taken as zero. The gas temperature change between input to the plasma and output from the water bath was never more than 1 K. Heat transfer from cell containing the flowing gas to the water in the bath was clearly very efficient. Given the flow rate was 1 sccm, this requires a maximum correction of less than  $10^{-6}$  W, a trivial correction. The stirrer and heat exchange terms were found to be the most significant correction, but its value was readily determined by measuring the temperature rise with only the stirrer operating. This correction can be accurately calculated from the slope of the pre- and post-heating periods and was found to be constant, 5.0 W for all experiments. Once these relatively trivial corrections are made, the 'effective' energy balance becomes:

$$\dot{H} = \dot{Q}_{plasma} \quad (5)$$

The calibration procedure resulted in a linear change in temperature for constant power inputs. This is expected, given the nearly constant heat capacity of water over small changes in temperature (<14 K in all cases). Thus, changes in enthalpy can be readily equated with change in temperature of the bath. In short:

$$\dot{H} = C_p \dot{T} = \dot{Q}_{plasma} \quad (6)$$

Thus, one must only multiply the calibration constant by the rate of change of bath temperature to obtain the plasma's heating power of the water bath. In the event that the change in temperature is nearly linear with time, as it was in all cases in this study, the rate (W) of heat input from the plasma to the bath can be readily determined, and compared with the input power. The rt-plasma results were compared with the results of the calibration control experiment determined using the same analytical procedure.

Since the cell and water bath system were adiabatic, the general form of the power balance equation with the possibility of excess power is:

$$P_{in} + P_{ex} - P_{out} = 0 \quad (7)$$

where  $P_{in}$  is the input discharge or heater power,  $P_{ex}$  is the excess power generated from the hydrogen catalysis reaction, and  $P_{out}$  is the thermal power loss from the cell to the water bath.

The plasma voltage and current reached steady state in about 5 to 10 minutes after the heating period started, and the temperature measured at the wall of the cell typically reached a steady state in about 1 to 2 hrs after the heating period was started. At this point, the power lost from the cell  $P_{out}$  was equal to the power supplied to the cell,  $P_{in}$ , plus any excess power  $P_{ex}$ .

$$P_{in} + P_{ex} = P_{out} \quad (8)$$

Since the cell was surrounded by water that was contained in an insulated reservoir with negligible thermal losses as discussed above, the temperature response of the thermistor  $T$  as a function of time  $t$  was modeled by a linear curve

$$\dot{T}(t) = a^{-1} P_{out} \quad (9)$$

where  $a$  is the heat capacity ( $J/\text{°C}$ ) for the least square curve fit of the response to power input for the control experiments ( $P_{ex} = 0$ ). The slope was recorded for about 25 hours after the cell was started, to achieve an accuracy of  $\pm 1.8\%$ .

The slope of the temperature rise as a function of time was recorded for each run and baseline corrected for the stirrer power and loss to ambient, then the output power was calculated from the corrected slope. After the calorimeter was calibrated,  $T(t)$  was recorded with a selected power to the plasma and compared to the results of identical input to the heater in a separate run of the identical system. The higher slope produced with argon-hydrogen-strontium plasma, having  $Sr^+$  and  $Ar^+$  as catalysts and atomic hydrogen as a reactant, compared with controls with no hydrogen and no catalyst present was representative of the excess power. In the case of the catalysis run, the total output power  $P_{out}$  was determined by solving Eq. (9) using the measured  $\dot{T}(t)$  and the heat capacity  $a$ . The excess power  $P_{ex}$  was determined from Eq. (8).

### 3. Results and discussion

#### A. RT-plasma emission

An argon-hydrogen (90/10%)-strontium rt-plasma formed with a low field ( $1\text{V/cm}$ ), at low temperatures (e.g.  $\approx 10^3 K$ ), from atomic hydrogen generated at a titanium filament and strontium which was vaporized by heating the metal. H Balmer emission corresponding to population of a level with energy  $> 12 eV$  was observed as shown in Figure 4 which also requires that Lyman emission was present. No plasmas formed when magnesium replaced strontium or with hydrogen, argon/hydrogen, or strontium alone. This result indicates that the

emission was due to a reaction of hydrogen with vaporized strontium. No possible chemical reactions of the titanium filament, the vaporized strontium, and 0.6 Torr argon-hydrogen mixture at a cell temperature of 700°C could be found, which accounted for the Balmer emission. In fact, no known chemical reaction releases enough energy to excite Balmer and Lyman emission from hydrogen. In addition to known chemical reactions, electron collisional excitation, resonant photon transfer, and the lowering of the ionization and excitation energies by the state of "non ideality" in dense plasmas were also rejected as the source of ionization or excitation to form the hydrogen plasma [15]. The formation of an energetic reaction of atomic hydrogen was consistent with a source of free energy from the catalysis of atomic hydrogen by  $Sr^+$  and  $Ar^+$ .

### B. Balmer $\alpha$ line widths

The energetic hydrogen atom energies were calculated from the Doppler width of the 656.3 nm Balmer  $\alpha$  line emitted from RF rt-plasmas [8-9]. The full half-width  $\Delta\lambda_G$  of each Gaussian results from the Doppler ( $\Delta\lambda_D$ ) and instrumental ( $\Delta\lambda_I$ ) half-widths:

$$\Delta\lambda_G = \sqrt{\Delta\lambda_D^2 + \Delta\lambda_I^2} \quad (10)$$

$\Delta\lambda_I$  in our experiments was 0.006 nm. The temperature was calculated from the Doppler half-width using the formula:

$$\Delta\lambda_D = 7.16 \times 10^{-7} \lambda_0 \left( \frac{T}{\mu} \right)^{1/2} \quad (11)$$

where  $\lambda_0$  is the line wavelength,  $T$  is the temperature in K ( $1\text{ eV} = 11,605\text{ K}$ ), and  $\mu$  is the molecular weight (=1 for atomic hydrogen). In each case, the average Doppler half-width that was not appreciably changed with pressure varied by  $\pm 5\%$  corresponding to an error in the energy of  $\pm 10\%$ .

The 656.3 nm Balmer  $\alpha$  line widths recorded on the argon-hydrogen (90/10%)-strontium rt-plasma having a titanium filament initially and after 70 hours of operation are shown in Figure 4. Significant broadening was not observed initially. However, the Balmer  $\alpha$  line profile of the plasma emission after 70 hours comprised two distinct Gaussian peaks, an inner, narrower peak corresponding to a slow component with an average hydrogen energy of 1 eV and an outer broader peak corresponding to a fast component of 20 eV. Only the hydrogen lines were broadened. These results are consistent with the catalysis of hydrogen to lower-states followed by subsequent transitions with increasing energy release by an autocatalytic mechanism previously reported with spectroscopic evidence [7-8].

We have assumed that Doppler broadening due to thermal motion was the dominant source to the extent that other sources may be neglected. This assumption was confirmed

when each source was considered. In general, the experimental profile is a convolution of two Doppler profiles, an instrumental profile, the natural (lifetime) profile, Stark profiles, van der Waals profiles, a resonance profile, and fine structure. The contribution from each source was determined to be below the limit of detection [1-6, 8-14, 16, 19-20, 23].

The emission spectrum from the hollow anode, glow discharge of argon-hydrogen (95/5%)-strontium (Figure 5a) showed an intense  $Sr^+$  (407.77 nm) line. The selectively Doppler-broadened 656.3 nm Balmer  $\alpha$  line width recorded with a high resolution visible spectrometer corresponding to an average hydrogen hot atom temperature of 50.2 eV with a 83.5% population is shown in Figures 5b and 5c. The independence of the broadening and the peak shape with position in the cell or the dependence on applied voltage or pressure over a broad range excludes the only conventional explanation of a field acceleration mechanism as discussed previously [1-6, 8-14, 16, 19-20, 23].

The formation of fast H can be explained by a resonant energy transfer from hydrogen atoms to  $Sr^+$  or  $Ar^+$  ions of two and one times the potential energy of atomic hydrogen, respectively, followed by a collisional energy transfer to yield fast  $H(n=1)$ , as well as the emission of  $q \cdot 13.6\text{ eV}$  photons reported previously [5-7]. For example, the exothermic chemical reaction of  $H + H$  to form  $H_2$  does not occur with the emission of a photon. Rather, the reaction requires a collision with a third body,  $M$ , to remove the bond energy  $H + H + M \rightarrow H_2 + M^*$  [30]. The third body distributes the energy from the exothermic reaction, and the end result is the  $H_2$  molecule and an increase in the temperature of the system. In the case of the catalytic reaction with the formation of states given by Eqs. (1) and (3), the temperature of H becomes very high.

### C. Power balance of the rt-plasma cell

The thermogram,  $T(t)$  response of the air-gap reactor with an input power of 10 W to maintain an argon-hydrogen (95/5%)- $Sr^+$  plasma compared to the heater calibration with stirring only and with a constant input power to the high precision heater of 10 W is shown in Figure 6a. It is evident that the value of the heating slope of the calibration experiment (heater) is smaller than the value of the reaction test, implying that for the same experimental conditions and input power, the rt- plasma transferred more heat to the water than the control performed using the high precision heater. According to Eq. (6), the water bath temperature is a direct indication of the amount of heat generated inside the reaction cell and transferred to the system; therefore, the results of this study show that the argon-hydrogen (95/5%)-strontium plasma generated heat in excess of the input power.

The average baseline corrected least squares fit of the slope,  $\dot{T}(t)$ , for several calibrations was  $5.23 \times 10^{-5} \text{ }^{\circ}\text{C}/\text{s}$ , and the heat capacity determined from Eqs. (8-9) with  $P_{ex} = 0$ , and  $P_m = P_{out} = 10 \text{ W}$  was  $1.911 \times 10^5 \text{ J}/\text{ }^{\circ}\text{C}$ . Then the temperature response of the calorimeter for any case (Eq. (9)) was determined to be

$$\dot{T}(t) = (1.911 \times 10^5 \text{ J}/\text{ }^{\circ}\text{C})^{-1} \times P_{out} \quad (12)$$

Also a plot of the evolution of excess heat as a function of time can be obtained by using the same heat capacity multiplied by the delta temperature between the reaction and calibration test profiles and further dividing by the time increment:

$$P_{ex}^i = \frac{C_p(T_r^i - T_c^i)}{t_i - t_0} \quad (13)$$

where  $P_{ex}^i$  is the excess heat,  $T_r^i$  and  $T_c^i$  are the water bath temperature of the reaction test and the calibration test at time  $t_i$ , respectively, and  $t_0$  is the time at which the heating period started. The excess power obtained for the plasma reaction as a function of time determined by using the measured  $\dot{T}(t)$ , the input power of 10.0 W, and Eqs. (8) and (9), is shown in Figure 6b. The typical excess heat observed was 2.85 W. These results agree with those obtained using Eq. (13). Sources of error were the error in the calibration curve ( $\pm 0.05 \text{ W}$ ) and the measured input power ( $\pm 0.01 \text{ W}$ ). The propagated error of the calibration and power measurements was  $\pm 0.05 \text{ W}$ .

Given an argon-hydrogen (95/5%) flow rate of 1.0 sccm and an average excess power of 2.85 W, energy balances of over  $-7.7 \times 10^4 \text{ kJ/mole H}_2$  ( $471 \text{ eV/H atom}$ ) were measured. The reaction of hydrogen to form water, which releases  $-241.8 \text{ kJ/mole H}_2$  ( $1.48 \text{ eV/H atom}$ ) is about 320 times less than that observed. The results indicate that once an atom given by Eqs. (1) and (3) is formed by a catalyst, further catalytic transitions  $n = \frac{1}{3} \rightarrow \frac{1}{4}, \frac{1}{4} \rightarrow \frac{1}{5}$ , and so on, occur to a substantial extent. This is consistent with the series of lower-energy hydrogen lines with energies of  $q \cdot 13.6 \text{ eV}$  where  $q = 1, 2, 3, 4, 6, 7, 8, 9, \text{ or } 11$  [5-7], the previously given theory [1-7, 27-29], and previous studies which show very large energy balances [6, 10, 14, 22-23]. These results were confirmed by Calvet and water-flow calorimetry.

#### **4. Conclusion**

An rt-plasma formed with a low field ( $1\text{V/cm}$ ), at low temperatures (e.g.  $\approx 10^3\text{ K}$ ), from argon and atomic hydrogen generated at a titanium filament with strontium which was vaporized by heating the metal. Strong Balmer emission was observed that indicated an energy source of  $> 12\text{ eV}$ . The energetic reaction of atomic hydrogen was anticipated to form energetic hydrogen atoms. Significant Balmer  $\alpha$  line broadening corresponding to an average hydrogen atom temperature of  $20\text{ eV}$  was observed. The time-dependence of the appearance of fast H supported an energetic chemical reaction as the source. The power balance of a rt-plasma with  $\text{Sr}^+$  and  $\text{Ar}^+$  as catalysts was measured by water bath calorimetry. An average excess power of  $2.85\text{ W}$  was observed. The enthalpy of formation  $\Delta H_p$  of strontium hydride is  $-199.1\text{ kJ/mole}$  ( $1.0\text{ eV/H atom}$ ) [32]. Thus, the energy for hydriding all of the  $4\text{ g}$  (46 immoles) of strontium would be  $9.2\text{ kJ}$  compared to the energy released over the 25 hours of reaction time of  $257\text{ kJ}$ . Thus, an excess power of  $2.85\text{ W}$  measured calorimetrically on rt-plasmas with  $\text{Sr}^+$  and  $\text{Ar}^+$  as catalysts and atomic hydrogen as a reactant, compared with controls with no hydrogen and no catalyst present was representative of the excess power. This observation supported the rt-plasmas mechanism since there is no known chemistry which could account for the observed power.

#### **Acknowledgments**

Special thanks to M. Nansteel for the calorimetric design and analysis.

#### **References**

1. R. Mills and M. Nansteel, P. Ray, "Argon-Hydrogen-Strontium Discharge Light Source", IEEE Transactions on Plasma Science, Vol. 30, No. 2, (2002), pp. 639-653.
2. R. Mills, M. Nansteel, and P. Ray, "Excessively Bright Hydrogen-Strontium Plasma Light Source Due to Energy Resonance of Strontium with Hydrogen", J. of Plasma Physics, Vol. 69, (2003), pp. 131-158.
3. R. Mills, J. Dong, Y. Lu, "Observation of Extreme Ultraviolet Hydrogen Emission from Incandescently Heated Hydrogen Gas with Certain Catalysts", Int. J. Hydrogen Energy, Vol. 25, (2000), pp. 919-943.
4. R. Mills and M. Nansteel, P. Ray, "Bright Hydrogen-Light Source due to a Resonant Energy Transfer with Strontium and Argon Ions", New Journal of Physics, Vol. 4, (2002), pp. 70.1-70.28.
5. R. L. Mills, P. Ray, "Extreme Ultraviolet Spectroscopy of Helium-Hydrogen Plasma", J. Phys. D, Applied Physics, Vol. 36, (2003), pp. 1535-1542.

6. R. L. Mills, P. Ray, B. Dhandapani, M. Nansteel, X. Chen, J. He, "New Power Source from Fractional Quantum Energy Levels of Atomic Hydrogen that Surpasses Internal Combustion", *J Mol. Struct.*, Vol. 643, No. 1-3, (2002), pp. 43-54.
7. R. Mills, P. Ray, "Spectral Emission of Fractional Quantum Energy Levels of Atomic Hydrogen from a Helium-Hydrogen Plasma and the Implications for Dark Matter", *Int. J. Hydrogen Energy*, Vol. 27, No. 3, (2002), pp. 301-322.
8. R. L. Mills, P. Ray, B. Dhandapani, R. M. Mayo, J. He, "Comparison of Excessive Balmer  $\alpha$  Line Broadening of Glow Discharge and Microwave Hydrogen Plasmas with Certain Catalysts", *J. of Applied Physics*, Vol. 92, No. 12, (2002), pp. 7008-7022.
9. R. L. Mills, P. Ray, B. Dhandapani, J. He, "Comparison of Excessive Balmer  $\alpha$  Line Broadening of Inductively and Capacitively Coupled RF, Microwave, and Glow Discharge Hydrogen Plasmas with Certain Catalysts", *IEEE Transactions on Plasma Science*, Vol. 31, No. (2003), pp. 338-355.
10. R. L. Mills, P. Ray, "Substantial Changes in the Characteristics of a Microwave Plasma Due to Combining Argon and Hydrogen", *New Journal of Physics*, [www.njp.org](http://www.njp.org), Vol. 4, (2002), pp. 22.1-22.17.
11. R. Mills, K. Akhtar, B. Dhandapani, "Tests of Features of Field-Acceleration Models for the Extraordinary Selective H Balmer  $\alpha$  Broadening in Certain Hydrogen Mixed Plasmas", submitted.
12. J. Phillips, C. Chen, "Evidence of Energetic Reaction Between Helium and Hydrogen Species in RF Generated Plasmas", submitted.
13. J. Phillips, C-K Chen, K. Akhtar, B. Dhandapani, R. Mills, "Evidence of Catalytic Production of Hot Hydrogen in RF Generated Hydrogen/Argon Plasmas", submitted.
14. R. Mills, P. Ray, B. Dhandapani, W. Good, P. Jansson, M. Nansteel, J. He, A. Voigt, "Spectroscopic and NMR Identification of Novel Hydride Ions in Fractional Quantum Energy States Formed by an Exothermic Reaction of Atomic Hydrogen with Certain Catalysts", *European Physical Journal-Applied Physics*, Vol. 28, (2004), pp. 83-104.
15. H. Conrads, R. Mills, Th. Wrubel, "Emission in the Deep Vacuum Ultraviolet from a Plasma Formed by Incandescently Heating Hydrogen Gas with Trace Amounts of Potassium Carbonate", *Plasma Sources Science and Technology*, Vol. 12, (2003), pp. 389-395.
16. R. L. Mills, P. Ray, "A Comprehensive Study of Spectra of the Bound-Free Hyperfine Levels of Novel Hydride Ion  $H^- (1/2)$ , Hydrogen, Nitrogen, and Air", *Int. J. Hydrogen Energy*, Vol. 28, No. 8, (2003), pp. 825-871.

17. R. Mills, P. Ray, "Spectroscopic Identification of a Novel Catalytic Reaction of Potassium and Atomic Hydrogen and the Hydride Ion Product", *Int. J. Hydrogen Energy*, Vol. 27, No. 2, (2002), pp. 183-192.
18. R. Mills, "Spectroscopic Identification of a Novel Catalytic Reaction of Atomic Hydrogen and the Hydride Ion Product", *Int. J. Hydrogen Energy*, Vol. 26, No. 10, (2001), pp. 1041-1058.
19. R. Mills, P. Ray, R. M. Mayo, "CW HI Laser Based on a Stationary Inverted Lyman Population Formed from Incandescently Heated Hydrogen Gas with Certain Group I Catalysts", *IEEE Transactions on Plasma Science*, Vol. 31, No. 2, (2003), pp. 236-247.
20. R. L. Mills, P. Ray, "Stationary Inverted Lyman Population Formed from Incandescently Heated Hydrogen Gas with Certain Catalysts", *J. Phys. D, Applied Physics*, Vol. 36, (2003), pp. 1504-1509.
21. R. Mills, P. Ray, R. M. Mayo, "The Potential for a Hydrogen Water-Plasma Laser", *Applied Physics Letters*, Vol. 82, No. 11, (2003), pp. 1679-1681.
22. J. Phillips, R. L. Mills, X. Chen, "Water Bath Calorimetric Study of Excess Heat in 'Resonance Transfer' Plasmas", *Journal of Applied Physics*, Vol. 96, No. 6, pp. 3095-3102.
23. R. L. Mills, X. Chen, P. Ray, J. He, B. Dhandapani, "Plasma Power Source Based on a Catalytic Reaction of Atomic Hydrogen Measured by Water Bath Calorimetry", *Thermochimica Acta*, Vol. 406/1-2, (2003), pp. 35-53.
24. R. Mills, B. Dhandapani, M. Nansteel, J. He, T. Shannon, A. Echezuria, "Synthesis and Characterization of Novel Hydride Compounds", *Int. J. of Hydrogen Energy*, Vol. 26, No. 4, (2001), pp. 339-367.
25. R. Mills, B. Dhandapani, N. Greenig, J. He, "Synthesis and Characterization of Potassium Iodo Hydride", *Int. J. of Hydrogen Energy*, Vol. 25, Issue 12, December, (2000), pp. 1185-1203.
26. R. Mills, B. Dhandapani, M. Nansteel, J. He, A. Voigt, "Identification of Compounds Containing Novel Hydride Ions by Nuclear Magnetic Resonance Spectroscopy", *Int. J. Hydrogen Energy*, Vol. 26, No. 9, (2001), pp. 965-979.
27. R. Mills, *The Grand Unified Theory of Classical Quantum Mechanics*, May (2006) Edition posted at [www.blacklightpower.com](http://www.blacklightpower.com).
28. R. L. Mills, "The Nature of the Chemical Bond Revisited and an Alternative Maxwellian Approach", *Physics Essays*, Vol. 17, No. 3, (2004), pp. 342-389.
29. R. L. Mills, "Exact Classical Quantum Mechanical Solutions for One- Through Twenty-Electron Atoms", in press.
30. N. V. Sidgwick, *The Chemical Elements and Their Compounds*, Volume 1, Oxford, Clarendon Press, (1950), p.17.

31. M. D. Lamb, *Luminescence Spectroscopy*, Academic Press, London, (1978), p. 68.
32. W. M. Muller, J. P. Blackledge, G. G. Libowitz, *Metal Hydrides*, Academic Press, New York, (1968), p 201.

### Figure Captions

Figure 1. The experimental setup for generating an argon-hydrogen-strontium rt-plasma.

Figure 2. Air-gap reactor comprising a hollow anode DC glow discharge cell and a stainless steel jacket for maintaining an argon-hydrogen (95/5%)- $Sr^+$  plasma.

Figure 3. Water bath calorimetric system for measuring the power balance on an argon-hydrogen (95/5%)- $Sr^+$  plasma.

Figure 4. The 656.3 nm Balmer  $\alpha$  line width recorded with a high-resolution visible spectrometer on the initial emission of a hydrogen-strontium rt-plasma and the emission at 70 hours of operation. Significant broadening was observed over time corresponding to an average hydrogen atom temperature of 20 eV.

Figure 5. (a) The emission spectrum from a hollow anode, glow discharge of argon-hydrogen (95/5%)-strontium showing an intense  $Sr^+$  (407.77 nm) line. (b) The high resolution spectrum (653.0-659.0 nm) of the argon-hydrogen (95/5%)-strontium plasma emission showing selective broadening of the Balmer  $\alpha$  line relative to the argon and strontium atomic lines. (c) The selectively broadened 656.3 nm Balmer  $\alpha$  line width recorded with a high-resolution visible spectrometer corresponding to an average hydrogen hot atom temperature of 50.2 eV with a 83.5% population.

Figures 6. (a) Water bath temperature profiles of the air-gap reactor with an input power of 10 W to maintain an argon-hydrogen (95/5%)- $Sr^+$  plasma compared to the heater calibration. (b) Excess power obtained for the plasma reaction as a function of time.

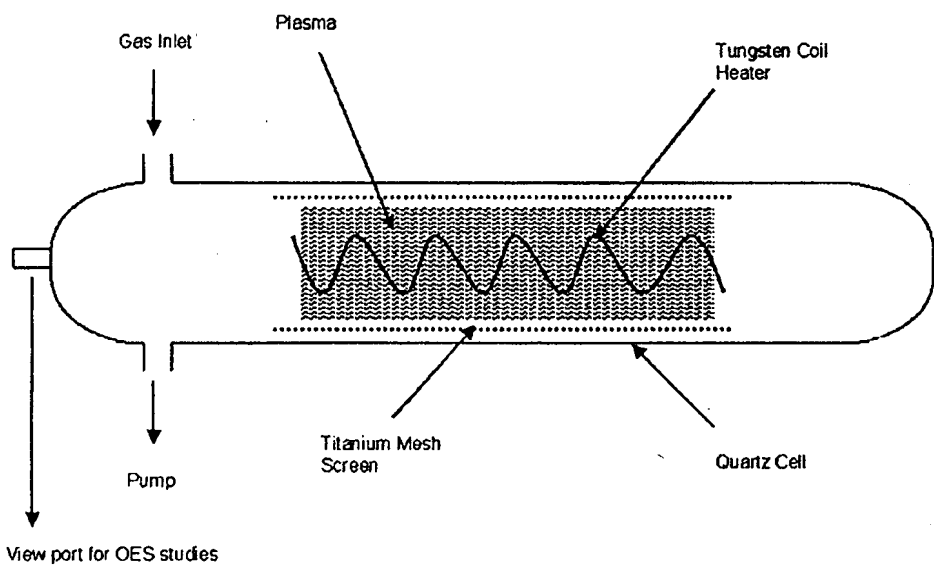


Fig. 1

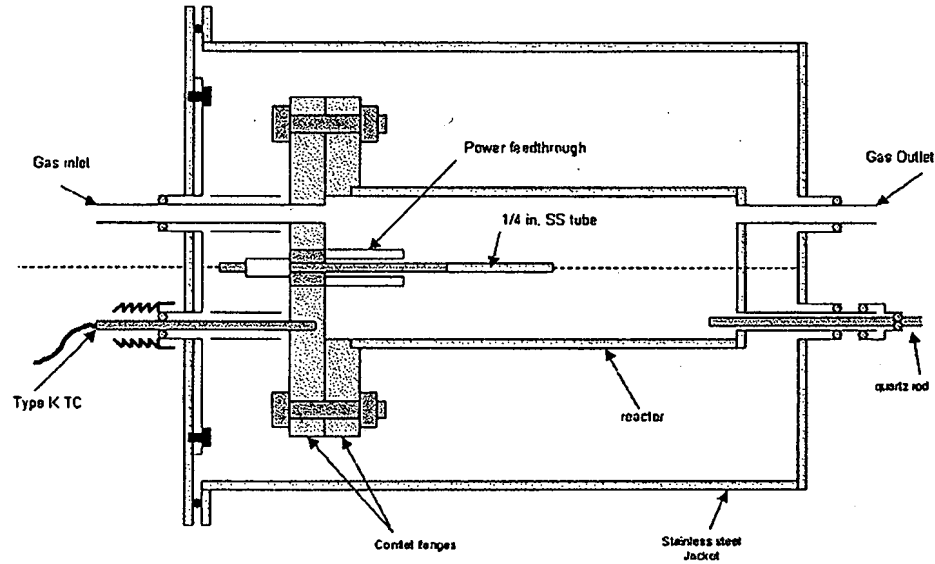


Fig. 2

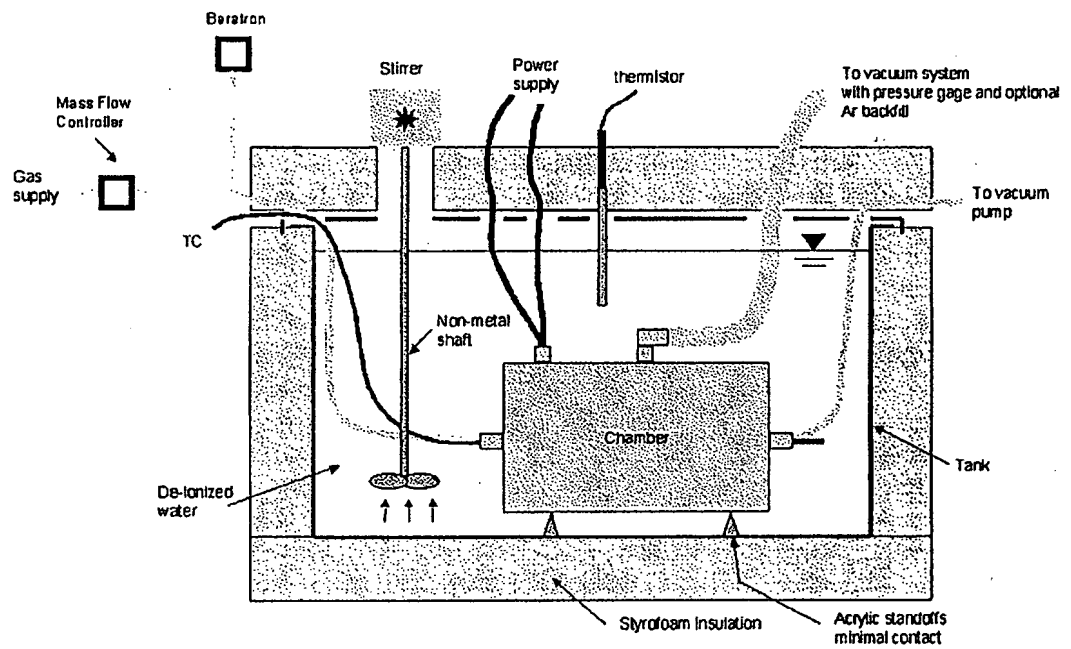


Fig. 3

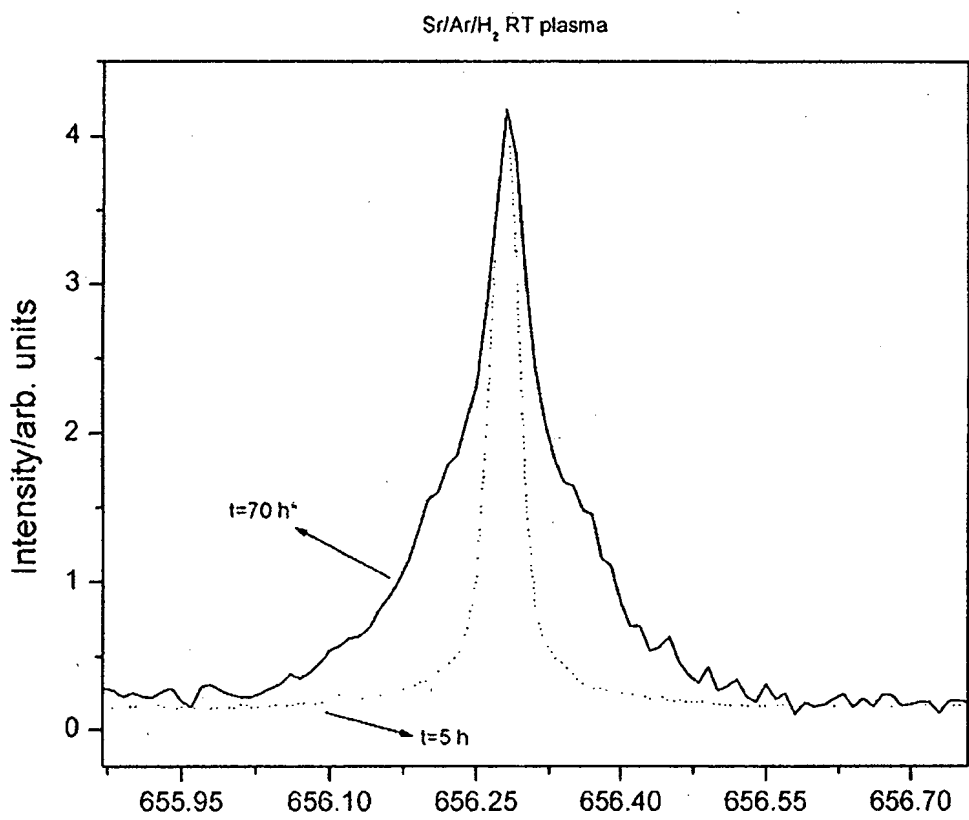


Fig. 4

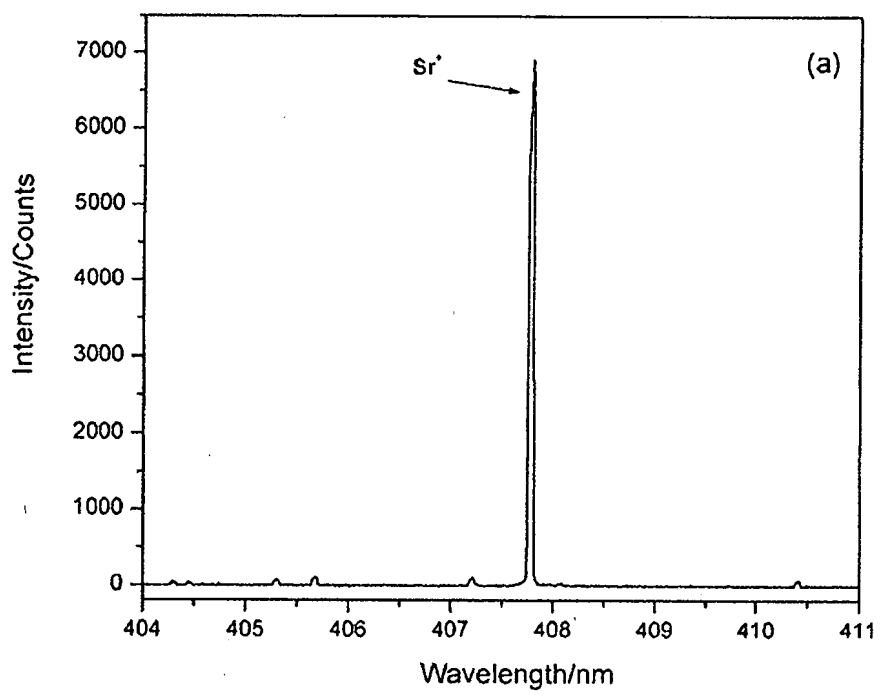


Fig. 5a

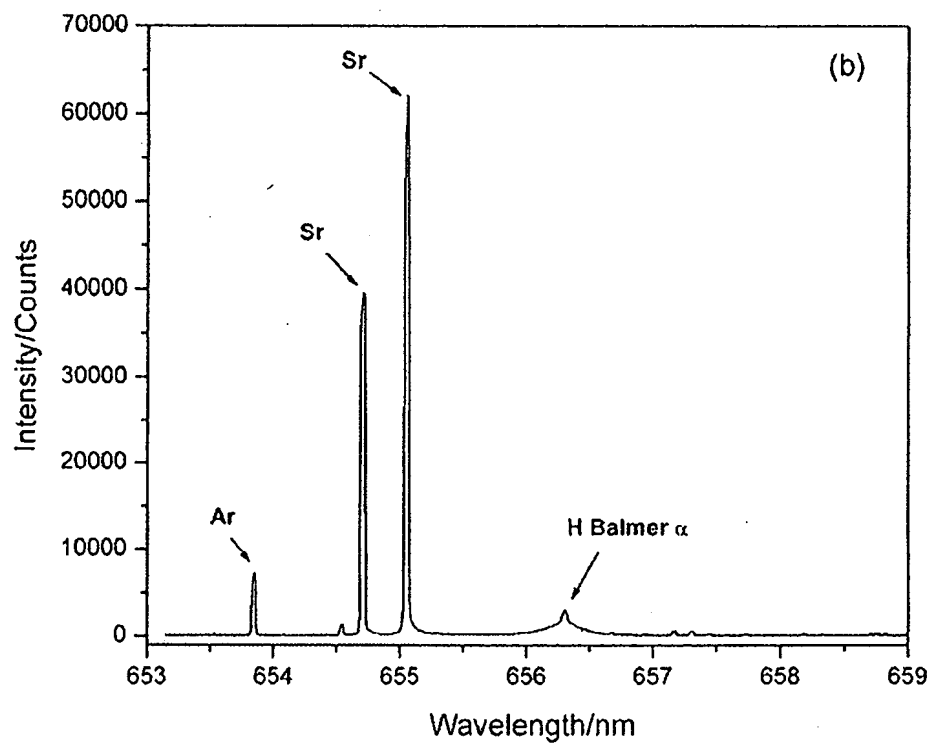


Fig. 5b

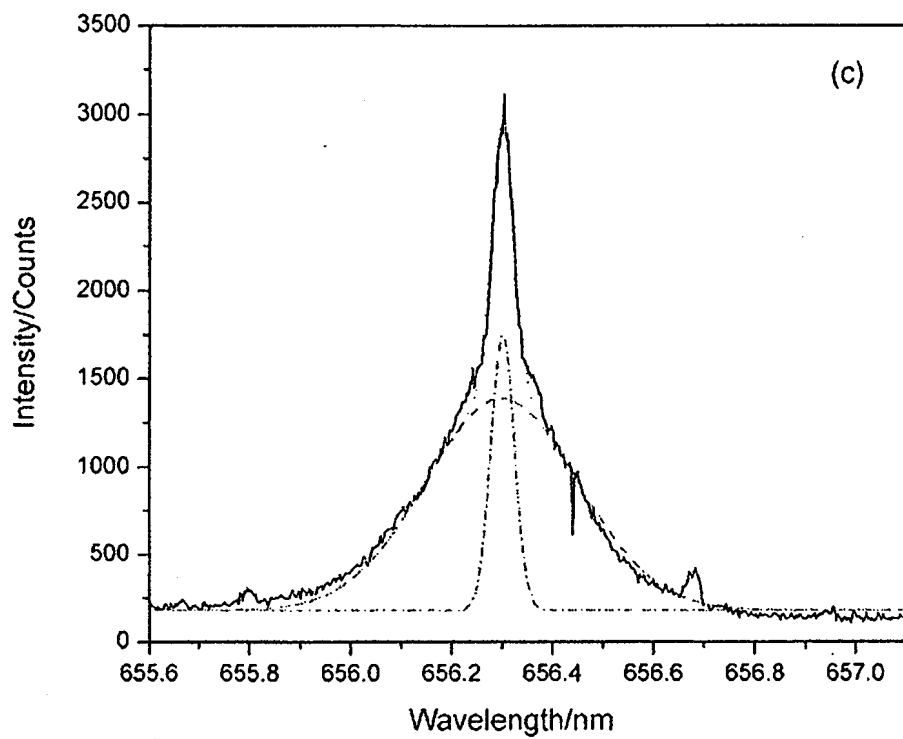


Fig. 5c

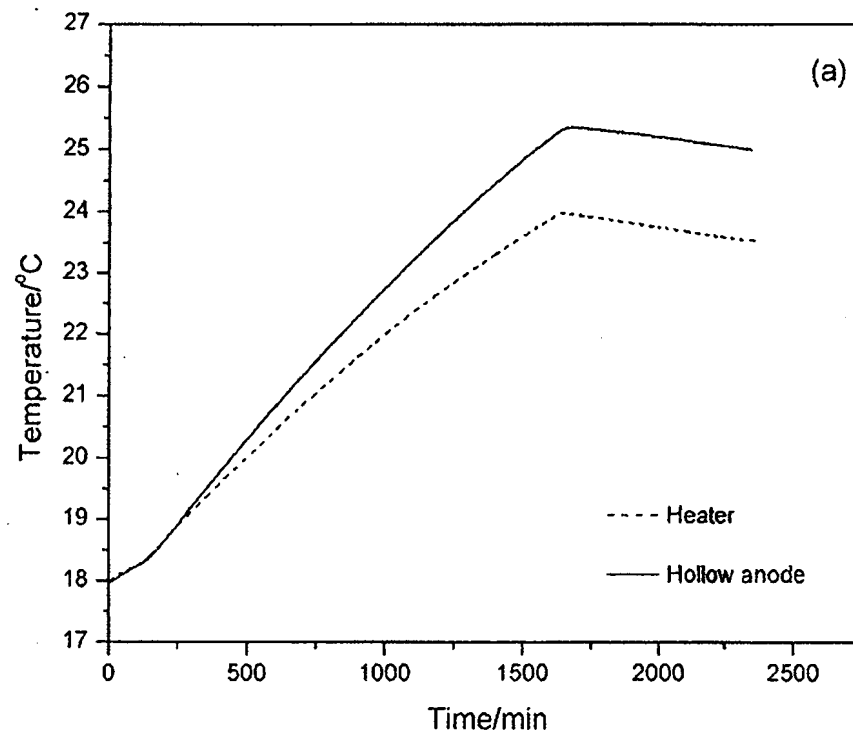


Fig. 6a

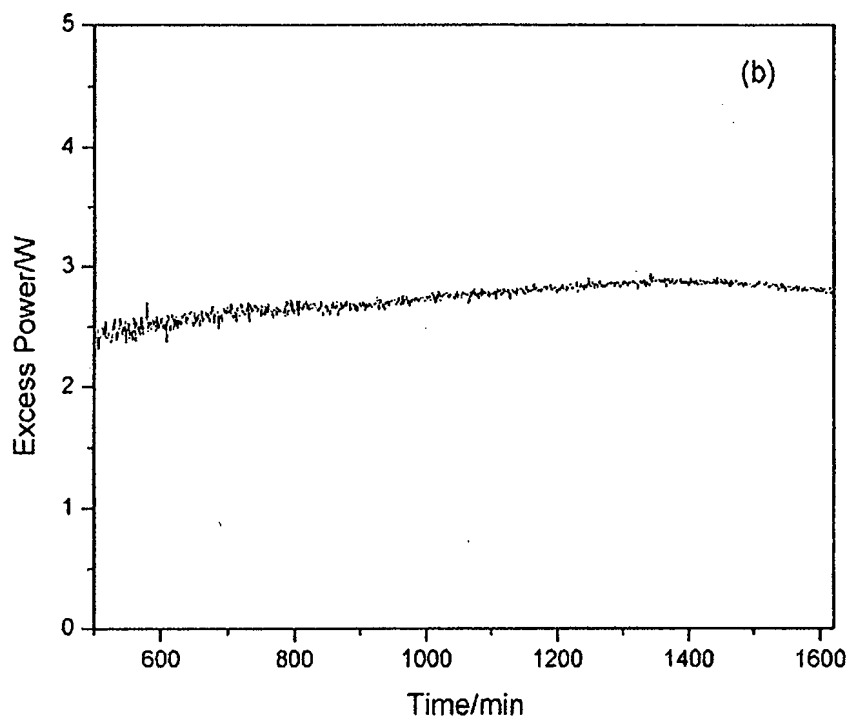


Fig. 6b